AFCRL 67-0512

RESEARCH IN ENERGY CONVERSION

by

Welville B. Nowak

Karl Weiss

Robert N. Wiener

Photochemistry and Spectroscopy Laboratory

Northeastern University

Boston, Massachusetts 02115

Contract No. AF19(628)-3836

Project No. 8659

Task No. 865901

Work Unit No. 01

FINAL REPORT

1 October 1963 — 30 September 1966

Prepared for

AIR FORCE CAMBRIDGE RESEARCH LABORATORIES

OFFICE OF AEROSPACE RESEARCH

UNITED STATES AIR FORCE

BEDFORD, MASSACHUSETTS 01730

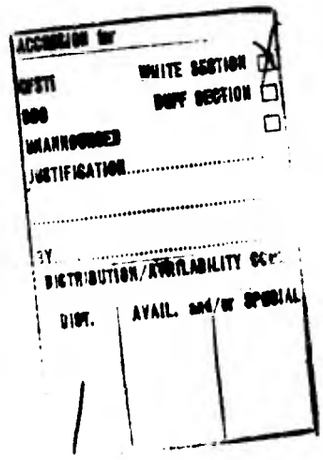

Qualified requestors may obtain additional copies from the Defense Documentation Center. All others should apply to the Clearinghouse for Federal Scientific and Technical Information.

AFCRL -67-0512

RESEARCH IN ENERGY CONVERSION

by

Welville B. Nowak

Karl Weiss

Robert N. Wiener

Northeastern University

360 Huntington Avenue

Boston, Massachusetts 02115

Contract No. AF 19(628)-3836

Project No. 8659

Task No. 865901

Work Unit No. 01

FINAL REPORT

1 October 1963 - 30 September 1966

Contract Monitor: Nicholas F. Yannoni
Space Physics Laboratory

Prepared for

AIR FORCE CAMBRIDGE RESEARCH LABORATORIES
OFFICE OF AEROSPACE RESEARCH
UNITED STATES AIR FORCE
BEDFORD, MASSACHUSETTS

TABLE OF CONTENTS

TABLE OF CONTENTS (continued)

PERSONNEL

Senior Investigators

Welville B. Nowak	Professor of Mechanical Engineering
Karl Weiss	Professor of Chemistry
Robert N. Wiener	Associate Professor of Chemistry

Research Associates

E. Wall	J. Babakian	K. Bar-Eli

Research Assistants

D. N. Mitra	Y. P. Pilette	K. P. Smith
J. J. Bohning*	T. A. Tyler	D. Cameron
S. N. Singh	W. M. Moreau	R. Sonoff
L. I. Rubin	H. P. Wolf	R. French
G. P. Rabold**	R. M. Danziger***	E. Steeves
A. M. Halpern	E. Reid	N. Barnett
C. L. Adam	D. H. Lambert	S. Rizvi

Technicians

W. Kuchar	J. Surette	W. Goddard

Secretary

S. Robinson

---

* Northeastern University Research Fellow

** National Science Foundation Cooperative Research Fellow, 1963-1965

*** Supported by U. S. Public Health Service, Grant RH 00302

PERSONNEL (continued)

Undergraduate Cooperative Students

F. Connolly	E. McGrath	R. Sidor
J. Fischer	L. Santoro	C. Walker
V. Fricke	A. Giordano	M. Doyle
D. Furman	P. Schnieper	

General Introduction

This report presents the results of investiations dealing with a broad spectrum of topics in energy conversion. The studies fall into two main categories: (1) Those dealing with thermionic and photovoltaiv phenomena, and (2) Efforts related to photochemical energy conversion.

The first category includes subjects such as the response characteristics of silicon solar cells, the fabrication of silicon single crystal films, energy conversion applications of heterojunction diodes, the thermodynamic aspects of photovoltaic devices, the properties of cathodes, and diffusion effects in silicon.

The studies pertaining to photochemical energy conversion deal with the spectroscopy and photolysis of a variety of molecular systems including ketones, nitro compounds, charge transfer complexes, and sulfur compounds. Experimental and theoretical information was gathered on energy levels and energy transfer, thermodynamic properties, photosensitization, and multiphoton processes.

The work described was directed by three senior investigators, and the report is presented in three sections, the titles of which follow. Detailed summaries of the individual studies which constitute these sections are to be found at the beginning of each section.

LIST OF FIGURES

LIST OF FIGURES (continued)

LIST OF FIGURES (continued)

LIST OF FIGURES (continued)

LIST OF FIGURES (continued)

LIST OF FIGURES (continued)

LIST OF FIGURES (continued)

LIST OF FIGURES (continued)

LIST OF FIGURES (continued)

LIST OF FIGURES (continued)

LIST OF FIGURES (continued)

LIST OF FIGURES (continued)

LIST OF TABLES

LIST OF TABLES (continued)

LIST OF TABLES (continued)

LIST OF TABLES (continued)

A. INVESTIGATIONS IN THERMIONIC AND PHOTOVOLTAIC ENERGY CONVERSION

BLANK PAGE

1. Techniques for Fabrication of Large, Thin, Silicon Single Crystals

Welville B. Nowak, Robert D. French, Earl C. Steeves, and Raymond J. Sonoff.

2. Cathodes for Thermionic Energy Conversion

Welville B. Nowak, Jacob Babakian.

3. Carnot-Limitation on Efficiency of Photovoltaic Energy-Converters

Welville B. Nowak, David H. Laananen.

4. Transient Photoresponse of Solar Cells from Reverse to Zero Bias

Welville B. Nowak, Raymond J. Sonoff.

5. Electric Field Effects on Diffusion in Silicon

Welville B. Nowak, David H. Laananen.

6. Heterojunction Photovoltaic Energy-Converters

Welville B. Nowak, K. Paul Smith.

ABSTRACT

1. TECHNIQUES FOR FABRICATION OF LARGE, THIN, SILICON SINGLE CRYSTALS

The growth of large (1 cm x 1 cm) silicon single crystal films about 1μ thick on amorphous quartz has been achieved. A novel technique of planar-edge-growth (PEG) in the solid state using vacuum deposition through a moving, slotted mask has been employed to obtain these films. The technique is described, and approximate values for the salient parameters are given.

Application of the PEG technique using chemical vapor deposition was less successful in producing silicon single crystals.

2. CATHODES FOR THERMIONIC ENERGY CONVERSION

The conversion efficiency of thermionic energy converters is maximized when emitter and collector surfaces have optimum work functions that are uniform over the surfaces. This implies a surface consisting of a single type of crystallographic plane. A review of the literature has been made with respect to surface structures of the refractory metals and the treatments producing these structures. There is direct evidence that single crystals, properly treated, and that well-oriented, properly-treated polycrystalline material can provide surfaces with relatively uniform work functions. There is reason to believe that, with suitable chemi-thermal treatments and induced material transport, one could produce a uniform work function surface on randomly oriented, polycrystalline material. An x-ray back reflection Laue technique was developed for obtaining the orientation of the surfaces of exposed grains, provided the grain size is 1 to 4

mm. Because efforts to obtain such a grain size in tungsten, tantalum, and rhenium sheets were unsuccessful, the program aimed at investigating the effects of chemi-thermal treatments on surface orientations was not carried out.

3. CARNOT-LIMITATION ON EFFICIENCY OF PHOTOVOLTAIC ENERGY-CONVERTERS

Because of conflicting statements in the literature, a short study was made of the conditions under which the efficiency of a photovoltaic energy-converter is subject to the Carnot limit. If the photocell receives radiation from a source at thermal equilibrium (emitting radiation that follows the Planck distribution law), the energy influx is heat and the photocell operates as a heat engine, thereby being Carnot-limited. Conversion of non-equilibrium radiation is not subject to the Carnot-limitation. Solar cells at room temperature have a Carnot-limitation on efficiency of about 95% when receiving sunlight.

4. TRANSIENT PHOTORESPONSE OF SOLAR CELLS FROM REVERSE TO ZERO BIAS

The forward transient response of a momentarily reverse-biased silicon solar cell has been studied as a function of reverse-bias, load resistance, and steady light intensity. A substantial decrease was observed in the time for discharge under illumination as compared with the discharge time in the dark. Photoconductive effects are insufficient to explain this observation. However, an accounting can be made for all electrical charges including those originally stored in the junction capacitance and those photogenerated. An increase in overall energy conversion efficiency by application of momentary reverse-bias is shown to be not feasible.

5. ELECTRIC-FIELD EFFECTS ON DIFFUSION IN SILICON

An investigation has started concerning the effects of electric fields on the diffusion process in silicon. Differences in diffusion coefficients reported in the literature may be attributed, at least in part, to internal fields which exist during diffusion. The I-V curves for diodes heat-treated with a concurrently applied bias showed certain reversible trends, depending on the direction of the bias.

6. HETEROJUNCTION PHOTOVOLTAIC ENERGY-CONVERTERS

The recent fabrication of heterojunction diodes has raised interest in their possible use as devices. The existence of a "window" in the photovoltaic spectrum of the diodes suggests use as solar cells. A heterojunction of silicon and gallium phosphide combines the desirable properties of heterojunctions with the known high solar cell efficiency of silicon. Attempts have been made to manufacture these diodes, and a limited theoretical study has been made. Techniques for analyzing the heterojunctions have been studied by measuring the properties of silicon solar cells. GaAs-GaP graded-gap diodes were obtained and analyzed to further refine the techniques as applicable to heterojunctions.

1. TECHNIQUES FOR FABRICATION OF LARGE, THIN, SILICON SINGLE CRYSTALS

Introduction

The growth of large area, single crystal, semiconductor films of device quality would be a useful accomplishment. For solar cell applications, it could lead to more economical fabrication and to systems sufficiently thin as to possess some degree of mechanical flexibility (which would increase the possible methods for packaging solar energy conversion systems aboard satellites).

Most large area, semiconductor, single crystal films are grown epitaxially on single crystal substrates of the same (homoepitaxy) or of different (heteroepitaxy) materials. The maximum extent of the area depends on the size of these substrates, and is usually limited to about 7 cm^2. Unsupported (no substrate) single crystal films are difficult to grow. Films grown on amorphous or polycrystalline substrates are usually amorphous, or polycrystalline, or have a preferred orientation, depending upon the growth conditions.

If a single crystal film could be grown on an amorphous or polycrystalline substrate, the size restriction imposed by single crystal substrates would be removed.

Some success has been achieved in growing single crystals on amorphous substrates. In the 1850's Herapath grew large thin plates of iodosulphate of quinine, as a substitute for tourmaline, by flotation on a solution of ethyl alcohol and acetic acid. Rasmanis and Cline[1] have obtained rather small areas of single crystal silicon on a fluid glass. The silicon was deposited both by chemical vapor deposition (CVD) of $SiCl_4$ and by vacuum evaporation onto alumina substrates glazed

with a special glass that is fluid at the deposition temperature (about 1100°C) and that has a thermal expansion coefficient close to that of silicon.

Single crystal films of germanium have been produced[2-5] non-epitaxially by microzone melting of a film with a scanning electron beam. Sapphire, glass, and polycrystalline tungsten substrates were employed. Crystals as large as 1 mm across were produced; perhaps larger crystals would be possible with larger beam deflections. Attempts to apply this process to silicon were frustrated by failure to find a suitable non-reactive substrate of appropriate thermal expansion.

Single crystallites as large as 0.5 to 3.0 mm were grown in a silicon film on 96% and 99% Al_2O_3 alumina ceramic substrates by Doo[6] using a melting-and-recrystallization technique. The silicon films (12-15μ thick) were formed by chemical vapor decomposition (CVD). No attempt was made to control the growth of the crystallites. The regrown film was contaminated by the substrate, and it was postulated that some intermediate compounds existed between substrate and film which prevented cracking of the film despite the large difference in their thermal expansion coefficients.

Silicon single crystallites up to 3 x 7 mm in size were produced by McAleer, et al[7] by zone melting a CVD silicon film on a graphite substrate (United Carbon - UT1) of moderate density. Here also, as is usually the situation with molten silicon, the substrate reacted with and contaminated the film. No attempts were made to control the crystallite growth. These authors carried out the zone melting steps in argon using an rf generator.

Single crystal grains as large as 0.3 mm were obtained in silicon films on amorphous quartz substrates by Filby and Nielsen[8]. Prior to

the deposition of these films (which were up to 20μ thick; formed by vacuum evaporation or sublimation), a gold film about 3000 Å thick was evaporated onto the quartz. Silicon deposition rates were 2-50 μ/hr and substrate temperatures 700-900°C. The presence of the gold modified the nucleation and growth mechanisms of the silicon so as to yield the relatively large grains. A high proportion of these crystallites had their (111) planes parallel to the surface, but were randomly rotated with respect to one another. It seems likely that a vapor-liquid-solid (VLS) mechanism[9] was operating here.

From the above referenced literature one may conclude that realization of very large area single crystal silicon films is feasible, but that much greater control must be exercized over the nucleation and growth process. In bulk (3-dimensional) crystal growth a seed is usually provided for greatest control; at the very least, provision is made for selecting a preferred nucleus by commencing growth from a point. For some of their experiments on the growth of germanium single crystal films on tungsten (from molten germanium), Weinreich and Dermit[4] did provide a seed.

In the summer of 1962 we conceived a novel technique for controlled growth of films. This technique has been named "planar-edge-growth", or PEG. It departs from previous techniques by its controlled extension of the film from a seed edgewise across a substrate surface with the growing edge epitaxial at least to itself (autoepitaxial). Early work on this concept was reported in Ref. 10.

We have applied the PEG technique to the growth of silicon films on amorphous quartz films, the latter being on single crystal silicon substrates for convenience. Single crystals about 1 cm x 1 cm x 1μ

have been achieved with vacuum deposition of the silicon. An account of the progress in this work was given at the American Vacuum Society Meeting, New York, N. Y., September 1965[11]. Attempts to achieve PEG single crystal silicon films using CVD for the silicon were relatively unsuccessful.

In contrast to our results, an independent effort[12] using an edge growth technique was more successful with CVD then with vacuum evaporation. These investigators obtained oriented epitaxial growth of {110} silicon along a $\langle\bar{1}10\rangle$ direction on the {001} of hexagonal SiC, producing crystallites up to 0.5 mm x 1.5 mm. They used the pyrolysis of silane in hydrogen at 1250°C, but did not optimize the growth conditions. Their attempts to obtain large crystals by vacuum evaporation of silicon onto SiC, Si_3N_4, and glazed ceramic substrates were unsuccessful, possibly because of inadequate masking procedures. Failure to obtain larger crystals with the CVD approach may have been due to the lack of controlled growth from a seed, since heteroepitaxy with the substrate was being utilized and since there are two equivalent {111} orientations of the silicon (trigonal symmetry of Si (111) and hexagonal symmetry of SiC (001).

Figure 1 illustrates schematically the basic geometry of PEG. Figure 2 shows a possible edge profile of the film. The steps should provide preferred sites for adding atoms to the film and should lead to unique 3-dimensional orientations of crystal nuclei, in contrast to the 2-dimensional misorientations possible with the usual whole-surface deposition. It may be possible, therefore, to produce more perfect films by PEG than with whole-surface deposition (which involves the nucleation, growth, impingement, coalescence and "reorientation" of film crystallites[13]).

PEG can be utilized for films either epitaxial or non-epitaxial to the substrate, the latter through autoepitaxy with the leading edge of the film.

For successful autoepitaxy, the bonding forces and propensity for crystal growth should be stronger in the film than between substrate and film-producing atoms.

The remainder of this report describes our investigations into the PEG technique for producing large area single crystal silicon films on amorphous quartz.

Experimental Techniques and Results

Because of the successful oxidation of single crystal silicon wafers, it was hypothesized that silicon dioxide would make a suitable substrate for the PEG of silicon. A further advantage of this substrate is the fact that, at the somewhat elevated temperatures (about 900-1200°C) required for silicon homoepitaxy in vacuum (about 10^{-6}-10^{-5} Torr) or in CVD systems using $SiCl_4$, the silicon reacts with the SiO_2 to form volatile SiO. This should, then, provide a clean surface and ensure tighter bonding of the film to itself than to the substrate. A concomitant disadvantage is the obvious dynamic balance that must be obtained (and that might in fact be very delicate) between removal of incident atoms via substrate reaction and sticking of incident atoms to the film edge. Since the thermal expansion of SiO_2 is very different from silicon, only films of SiO_2 can be used. Supporting substrates for the SiO_2 films should have expansion coefficients similar to that of silicon. Thus, tungsten, tantalum, molybdenum or silicon are examples of candidates among the elements. For convenience, silicon was chosen, and Fig. 3 shows a cross section of the specimen geometry used for the PEG of silicon on amorphous quartz.

The specimen geometry indicated in Fig. 3 is obtained by (1) coating a polished silicon slice with SiO_2, and then (2) etching away a portion

of the SiO_2 to reveal the silicon and leave a more or less gradual transition from silicon to SiO_2. The SiO_2 was produced either by thermal oxidation of the silicon at 1000°-1100°C in flowing wet oxygen, or by CVD of an organometallic compound. The former was carried out in our laboratory; and the resulting thickness was about 1.0 micron. Slices coated with at least 5 microns of CVD SiO_2 were purchased from Semimetals, Inc., Westbury, L. I., N. Y.

The program was divided into two portions: one employing vacuum evaporation of the silicon, and the other employing CVD of silicon from $SiCl_4$ in H_2.

A. Vacuum Evaporation

A number of investigators have reported upon the vacuum evaporation of silicon[14-19]. References 15-19 are specifically concerned with the epitaxial deposition of silicon onto silicon. These investigations show that homoepitaxial silicon can be obtained at pressures of 10^{-6} - 10^{-5} Torr with substrate temperatures about 1100°-1250°C and deposition rates between 01. μ/min and 3.0 μ/min. In most cases, electron beam evaporation of the silicon was employed. Best results were obtained with fast deposition rates (>1.0 μ/min) and substrate temperatures over 1125°C.

The evaporated silicon films can be amorphous, or polycrystalline with either random or preferred orientation, or single crystalline with or without an epitaxial relationship to the substrate. Amorphous silicon is only produced at relatively low substrate temperatures. At the temperatures employed in this work, generally 1100-1250°C, either polycrystalline or single crystal films will be formed. The crystallinity was judged by one or more of several methods:

(1) visual appearance
(2) optical microscope metallographic features
(3) x-ray back reflection Laue photograms
(4) electron reflection diffraction.

(1) Single crystal (SX) films are relatively smooth and shiny compared to the matte surface of polycrystalline (PX) films. Occasionally it is possible, at the lower temperatures and at high evaporation rates, to produce a very smooth microcrystalline film. (2) When examined in a metallograph at 80X to 400X, occasional very small flaws are observed in the films, often near the end of the deposited area. In PX films these flaws have no specific shape and are often round or oval. In SX films, on the other hand, the flaws are polygonal with angles characteristic of the cubic structure (i. e. 30^{o}, 45^{o}, 60^{o}, 90^{o}, 120^{o}, etc.) and with sides that can be related to the major crystallographic directions of the seed (i. e. [[110]] and [[211]] in the (111) plane). (3) Back reflection Laue (BRL) photograms are useful for identifying most PX films because of the positive evidence afforded by the presence of rings. These rings appear along with the spots characteristic of the (111) silicon substrate. Spots from a film whose orientation is the same as the seed substrate are coincident with those of the substrate. If a film is very thin ($\frac{1}{2}$ μ or less), or if the film is microcrystalline (very fine grain size), no BRL spots or rings will appear. Consequently, the absence of rings does not necessarily indicate a SX film. However, reasonably accurate estimates of the general crystalline nature of a film can often be made from sample weight gain, metallography, appearance, and the BRL photograms. More definitive judgements can usually be made by use of electron reflection diffraction. This is especially true for thin films, for microcrystalline films, and for positive identification of epitaxial films.

Prior to installation of our electron beam gun, a few experiments were performed with silicon evaporated from an electron-bombarded SiC crucible. Polycrystalline silicon deposits several microns thick on tantalum and molydenum had the following characteristics:

(a) for substrate temperatures $<500^{o}C$, deposits were flaky and non-adherent,

(b) for substrate temperatures $>500^{o}C$, deposits were smooth and adherent,

(c) for substrate temperatures $>1000^{o}C$, deposits reacted with the substrates to form silicides, as evidenced by x-ray diffractometer traces. Whole-surface deposition of silicon was carried out on (111) silicon and on pyrolytic boron nitride (BN). PEG was attempted on (111) Si-SiO_2 substrates (Fig. 3). The PEG mask was of pyrolytic BN (0.010-in. thick) containing a slot about 3 mm wide in the direction of motion. In the PEG experiments, deposits about ½ in. long were produced; unfortunately, during the time required for this deposition, the pressure rose to $2X10^{-4}$ Torr. Table 1 is a summary of the results of this early work. All the films contain silicon and SiO_2, the latter in the form of tetragonal low-crystobolite. The silicon is polycrystalline. The SiO_2 is polycrystalline where little chance for single crystal growth existed, i. e. surface growth on pyrolytic BN. However, the SiO_2 is monocrystalline on the (111) silicon where epitaxial surface-growth may occur, and on the amorphous SiO_2 where PEG was used. These results are probably a consequence of the relatively poor vacua. However, they apparently constitute the first time that a single crystal film of low-crystobolite has been grown.

Figure 4 is a schematic representation of the PEG bell-jar geometry with an electron beam gun installed (Consolidated Vacuum Corporation,

TABLE 1

Silicon Films Evaporated From Electron-Bombarded SiC Crucible

Specimen No.	Deposition Conditions	Electron Diffraction Results[1]
12S	(111)Si substrate; 1200°C; 5×10^{-5} Torr; whole-surface grown; 10 min. exposure; 0.1-0.2 μ/min.	strong SiO_2 spots[2]; weak Si and SiO_2 rings.
27S	(111)Si-SiO_2 substrate; 1250°C; 2×10^{-4} Torr; PEG; 0.13 cm/min. mask speed; 2 min./mask opening; 0.1-0.2 μ/min.	SiO_2 spots; Si rings.
28S	same as 27S, but 0.80 cm/min. mask speed.	strong Si rings; weak SiO_2 rings and spots.
30S	pyrolytic BN substrate; 1250°C; 5×10^{-5} Torr; 20 min. exposure; whole-surface grown.	SiO_2 rings; Si rings (?).
33S	same as 12S, but 20 min. exposure.	SiO_2 spots, Si rings.

Notes:

(1) Electron diffraction results through the courtesy of Dr. Lee Tanner, Ledgemont Laboratories, Kennecott Corporation, Lexington, Mass.

(2) SiO_2 is low-crystobolite (tetragonal). All but 30S is single crystal SiO_2 with (101) SiO2 // (111) Si. Unanalyzed fine structure is present in the patterns.

Rochester, N. Y., 1.5kW, 10kV). Figures 5 and 6 are photographs of the equipment. A schematic exploded-view of the substrate heater assembly is shown in Fig. 7.

The substrate temperature was monitored by a micro-optical pyrometer focussed on the substrate through the slot in the PEG moving mask. Shields were installed to prevent silicon from depositing on the bell-jar window used as pyrometer sight port. Furthermore, the pyrometer was sighted directly at the substrate at an angle such as to avoid nearly specular reflection from the silicon source. Pyrometer temperature corrections were made on a nearly absolute basis by calibration runs wherein the silicon substrate was melted. It is estimated that substrate temperatures are known to about $\pm 15^{\circ}C$ during the course of a deposition run.

Silicon deposition rates in excess of 5 μ/min on silicon substrates at about $1100^{\circ}C$ were obtained with the electron beam gun using SiC crucibles. Unfortunately, these crucibles cracked easily. Evaporation rates are a sensitive function of crucible design (for heat flow from the melt) and of focal spot size of the electron beam. Containment of the silicon directly in a water cooled copper crucible produced very low evaporation rates. Consequently, a ½-in. thick, very pure, reactor grade graphite insert was placed in the copper crucible. This insert reduced the heat loss and lead to an increased volume of molten silicon and a hotter focal spot. Deposition rates as high as 2 μ/min on silicon substrates at about $1200^{\circ}C$ were achieved with this graphite insert. However, after many remeltings, the resistivity of a silicon charge that was originally 50 ohm-cm n-type would fall to about 0.4 ohm-cm n-type, presumably due to contamination from the graphite.

For the PEG technique to be successful, an epitaxial relationship must exist with the seed crystal, in our case a (111) silicon surface. To establish the conditions for obtaining epitaxy, silicon was evaporated onto bare, chemically polished (111) silicon substrates. Homoepitaxial films, 5-20 microns thick, were produced in pressures of 1-5 x 10^{-5} Torr, at substrate temperatures of 1210-1270°C, and at deposition rates as high as 1.8 μ/min. These results conform to those of Unvala and Booker[15, 17]. The electrical resistivities of these films, as measured with a 4-point probe, are from 2 to 5 ohm-cm n-type, and are considered representative of the silicon melt.

Figure 8 is a photograph of a PEG silicon film several microns thick (specimen geometry similar to Fig. 3) produced under conditions approximating those that yielded homoepitaxial films with whole-surface deposition. Mask speed was 1-in./hr. and slot length was 1/16-in. Growth direction is from bottom to top of the Figure, and is slightly off from a [[211]] direction. The edge between seed silicon and thermal-oxidation SiO_2 is clearly visible, running parallel to the scale at about the level of the mm markings, with the SiO_2 region at the top. Extent of the film from left to right is governed by a slot dimension in the moving mask. The bottom, homoepitaxial portion of the film is shiny, and this shiny film extends onto the SiO_2 in the left hand region. On the right hand region of the SiO_2 the film has a matte appearance. BRL photograms indicate only spots of the substrate pattern from the left region (and from the homoepitaxial region) and spots plus coarsely-spotted rings from the right region. This is good evidence that the left region has a single crystal film of silicon on the amorphous SiO_2, whereas the film on the

right region was nucleated into polycrystallinity by unknown causes just after surmounting the oxide layer. The interface between SX and PX portions is the feathery edge between light and dark regions.

Figure 9 is a photograph of another PEG silicon film on thermal-oxidation SiO_2. The growth conditions approximated those of Fig. 8 and the growth direction is [[211]] , i. e. left to right on the Figure. The edge of the SiO_2 is at the notch and is parallel to the left side of the specimen. The transition from silicon tc SiO_2 is so gradual that it is not noticeable in the Figure. The silicon film is shiny and smooth.

Figure 10 is a photograph of another PEG silicon film on thermal-oxidation SiO_2. Growth conditions and direction are similar to those for the sample of Fig. 8. The homoepitaxial region is at the top of the Figure with the SiO_2 edge approximately parallel to the end of the scale. The film is smooth and shiny as it extends from the homoepitaxial region a distance of about 7 mm along the SiO_2. At this point in the deposition the mask was jumped ahead about 3 mm and the deposition then continued for another 2 mm. The final 2 mm of silicon film has a very matte appearance, quite unlike that of the first portion. (The two bright bands of light separated by a darker band are not part of the sample, but are the reflection of a double flourescent-tube room-lighting fixture.)

In many of the experiments with PEG using thermal-oxidation SiO_2, very little oxide remained on some of the areas not coated with silicon. Therefore, a few samples of PEG silicon on this type of SiO_2 substrate were broken to isolate the deposit grown over the oxide. It was discovered that the films were not insulated from the silicon substrate. Examination of a small-angle bevel-cut confirmed that only a very thin oxide layer

existed. This indicates that pinholes were formed in the SiO_2 layer. These pinholes did not interfere with the PEG. However, to insure more perfect electrical isolation, thicker SiO_2 layers were mandatory. The upper limit of thickness for thermal-oxidation SiO_2 films is about 1 μ, so that CVD films, of thickness greater than 5 μ, were subsequently used.

Evidence that the SiO_2 layer is substantially present, and that only pinholes and random thinning cause the lack of electrical isolation of deposited film from underlying silicon, is found from two sources. One, a very thin oxide layer of varying thickness can be seen metallographically after a small-angle bevel cut. Two, the four-point probe measurement of resistivity gives very high apparent values, and only after the necessary correction for silicon film thickness do the values become reasonable. If there were no SiO_2 layer of substantial extent, the resistivities would fall into the expected range with no thickness correction needed.

To reduce the time necessary for growing a relatively thick PEG film, a hybrid process was sometimes employed. This consisted of depositing the usual PEG film and then following with a whole-surface homoepitaxial deposition. If epitaxial growths are being achieved, then only a thin PEG film should be needed to provide the substrate for a thicker film.

Table 2 lists the results of the best PEG depositions on CVD SiO_2. The required substrate temperature, aside from being fairly critical for homoepitaxy and autoepitaxy, is intimately related to the silicon evaporation rate because of the vapor pressure of SiO. SiO is readily formed by reaction of arriving silicon vapor with the SiO_2. At temperatures

TABLE 2

Results of Silicon PEG Deposition Upon Pyrolytically Oxidized Silicon

Sample	Electron Beam Current (mA)	Substrate Temp. (°C)	Slot Speed (in./hr.)	Growth Direction	Crystallinity
140R	85	1210+	2 1/2, spl.	10° off {211}	SX and PX regions
151R	75;100	1150	2 1/2, 2 1/2	10° off {211}	SX
152R	100	1160	2 1/2, spl.	4° off {110}	PX
153R	85	1160	2 1/2, spl.	1° off {110}	PX
154R	100	1220	2 1/2	{110}	PX
156R	85	1220	1	{211}	PX
158R	85	1140	1	3° off {211}	PX
162R	75	1150	2 1/2	8° off {211}	SX
163R	75	1150	2 1/2	{110}	SX
164R	75	1150	2 1/2	9° off {110}	SX

Note: 2 1/2, spl. = PEG with slot speed of 2 1/2 in./hr. followed by a whole-surface splash deposition.

above 1200°C and with low silicon evaporation rates, no silicon will be deposited and the substrate will lose weight by loss of SiO_2. Because of the unknown extent of the weight loss, deposition rates could not be calculated from gravimetric measurements. Since the film thickness monitor (quartz crystal oscillator) was not operable during these runs, the deposition rate may only be estimated. However, a relative indication is given in Table 2 by the electron beam current, assuming that the beam spot size was constant. From previous experience, evaporation rates of 1 to 2 μ/min. are estimated. Resulting film thicknesses were about 5 microns. Electrical resistivity of these films varied from 0.15 to 5.0 ohm-cm, and probably reflect the resistivity of the melt.

Figures 11 and 12 are photographs of samples 151R and 156R, respectively, listed in Table 2. The visual appearance of 156R is matte compared to the relatively smooth and shiny 151R. The other single crystals listed in Table 2 were smaller in extent; the silicon ceased to deposit during the run. Reasons for this are not known, but perhaps the substrate temperature increased or the evaporation rate decreased. The former could have occurred, even with constant monitoring, if the sight glass became slightly filmed (and the temperature is critical). The latter might occur if the electron beam focal spot increased.

Electron reflection diffraction patterns were obtained* on two of the PEG silicon films deposited on CVD SiO_2, and grown in the [[211]] .

---

* One set of electron reflection diffraction pictures were taken through the courtesy of Dr. Lee Tanner, Ledgemont Laboratory, Kennecott Copper Co., Lexington, Mass., and another set through the courtesy of Richard Cornelisson, Air Force Cambridge Research Laboratory, Bedford, Mass.

These films (specimens 163R and 164R) measured about 1 cm x 0.3 cm and were probably about 0.5-1 μ thick. The silicon film on specimen 163R was single crystalline with the orientation relationship:

Substrate	Deposit
$[\bar{1}10]$	$[\bar{1}\bar{1}2]$
[111]	[111]
$[\bar{1}\bar{1}2]$	$[\bar{1}10]$

The homoepitaxial and autoepitaxial portions (on the silicon substrate and on the SiO_2, respectively) were both single crystals with the above orientation. Therefore, although the film is epitaxial, it does not have the same orientation as the underlying silicon: the (111) planes are parallel, but the film is rotated 30° about the [111] with respect to the substrate.

Figures 13, 14, and 15 are electron reflection diffraction patterns from the PEG specimen 164R-1. Figure 13 is from the hemoepitaxial ("seed") region; Figures 14 and 15 are both from the autoepitaxial region, but at different specimen position and orientation with respect to the electron beam. Both homoepitaxial and autoepitaxial regions of the silicon film have a (111) deposit plane, but again the film is rotated 30° about the [111] with respect to the substrate, i. e. the $[\bar{1}10]$ is interchanged with the $[\bar{1}\bar{1}2]$. The rings (faint relative to the spots) in Fig. 15 may be due either to a small amount of polycrystalline silicon or to multiple scattering of the reflection diffracted electrons from the very slight roughness of the surface, although the surface was considered smooth rather than matte.

In summary, very large area single crystal silicon films can be produced in a potentially controllable manner on amorphous SiO_2 by the

planar-edge-growth technique using vacuum evaporation. Crystals up to approximately 1 cm x 1 cm x 1μ have been fabricated. The size was limited by convenience of equipment, except in those cases where deposition ceased completely for unknown reasons. Table 3 summarizes the values of parameters associated with the PEG crystals in this exploratory effort.

TABLE 3

Some Parameters for Vacuum PEG of Silicon Single Crystal Films

Substrate: Amorphous SiO_2
Seed: (111) Si Surface

Vacuum:	$\sim 10^{-5}$	Torr
Substrate Temperature:	~1150-1200	^{o}C
Deposition Rate:	$\approx$0.5	μ/min
Slot Speed (1.5 mm aperture):	2-6	cm/hr
Growth Direction: (a) [[110]] (b) [[211]]		
Resistivity (Room T): (Similar to melt)	0.15-5.0 n-type	Ω-cm

Further work should be carried out on PEG silicon films to determine the parameter values or technique modifications that will result in a better control and higher yield of single crystals. Extensive evaluation of the crystal films needs to be done, examining, for example, the crystallographic perfection, electrical, galvanomagnetic, and photoelectric properties. Devices should be fabricated in the film and evaluated.

B. Chemical Vapor Deposition

During the early portions of the CVD work, considerable difficulty was experienced with obtaining a consistently leak-tight system. Teflon stopcocks proved inadequate, and even the use of Kel-F grease with glass

stopcocks required a constant maintenance. Reaction chambers of complex design with multiple feed-throughs also proved troublesome. Eventually, a consistently workable, flexible system was constructed using stainless steel solenoid-operated valves with teflon seats, copper tubing with "Koncentrik" fittings and teflon-tape-sealed screw threads, and a relatively small, cylindrical, horizontal reaction chamber with tapered input. This system was reliable and required only a minimum of maintenance. The substrates were indirectly heated from a susceptor that was itself induction heated by a 10kW, 100kHz RF generator.

All of the CVD experiments utilized $SiCl_4$ in a carrier gas of H_2, with the usual reaction[20] $SiCl_4 + 2H_2 \rightarrow Si + 4HCl$. Values usually set for the deposition parameters were:

H_2 flow	1-2 liters/minute
$SiCl_4$ temperature	-30 to -50°C
Substrate temperature	900-1200°C
Mask movement (PEG)	1 inch/hour; 3/8 inch total.

The susceptors were made from high purity, high density graphite (obtained through the courtesy of Paul Ahearn of the Army Materials Research Agency, Watertown, Mass.). Prior to use, the susceptors were ultrasonically cleaned in alcohol for 30 minutes and then vacuum outgassed to 3-4 x 10^{-5} Torr at 1400-1500°C for one hour. The incoming hydrogen gas was passed through a platinum catalyst to convert any oxygen to water vapor and then passed through a U-tube filled with Linde Type 4A Molecular Sieve and immersed in liquid nitrogen to trap water vapor.

Prepatory to attempting PEG depositions with this apparatus, several runs were made with a stationary, slotted mask of pyrolytic BN

placed over a (111) silicon slice. The slice rested on a fused quartz disc that was slightly recessed into a graphite susceptor, ¼-in thick and 1 1/8-in diameter. With close contact bewtween mask and slice, a sufficiently well defined bar of epitaxial silicon was deposited as to warrant proceeding with PEG experiments.

Requisite to the PEG technique is some form of motion. For CVD this could be movement of a mask, of a hot zone, or of a directed stream of reactants, relative to the substrate. Toward this requirement a technique was developed for producing relatively smooth linear motion of a quartz rod within the reaction chamber. The quartz rod was pulled by a wire, external to the chamber, attached to a gear-reducer and motor. The rod passed through a teflon tube inside a copper tube which was brazed to the end plate of the chamber. Kel-F grease was used to seal the small spaces between the tubes and between the quartz rod and the teflon; the Kel-F also provided lubrication for the sliding motion of the rod. This arrangement was successful in providing the required motion while maintaining a contaminant-free chamber. Counterbalancing springs, external to the chamber, were added to promote uniform motion.

In one series of experiments, the substrate (a (111) silicon slice) was uniformly heated and a thin, slotted, BN mask was either held stationary of moved slowly over the substrate. When the mask was more or less in contact with the substrate, the motion was somewhat errotic. This behaviour was attributed to material deposited under the mask, including some silicon that bridged the small, irregular gaps between substrate and mask. To obviate this difficulty, a small spacing between substrate and mask was deliberately introduced. This arrangement was tested

with the mask stationary. An epitaxial hump of silicon was formed beneath the slot, but polycrystalline silicon deposited over the remaining area of the substrate. The hump was thickest under the center of the slot and became thinner at the edges. Unsuccessful attempts were made to eliminate the polycrystalline deposits by deflecting the vapor stream downwards through the slot by means of small vanes placed in the stream. From these experiments it appeared that the moving mask technique would require a much more sophisticated and accurate construction to provide gas-tight masking of the slice. Consequently, a different approach was used in another series of experiments.

In the second set of experiments a narrow hot zone was produced on (111) silicon substrates. A stationary, graphite susceptor was shaped to provide a narrow hot strip, and the substrate was moved over the hot strip. Many trials with tungsten and tantalum wire and strip heaters led to the conclusion that for efficient heating and reproducible geometry graphite was the best choice of susceptor material. Tests made with the narrow hot zone (about 1/16-in) and a stationary substrate yielded clean, uncontaminated substrates with an epitaxial silicon deposit over the hot zone, but with polycrystalline regions on either side. In these regions the temperature fell rapidly between epitaxial temperatures and no-deposition temperatures, thus presenting opportunity for deposition of polycrystalline silicon. By suitable placement of BN radiation shields, the temperature gradient on each side of the hot zone was increased considerably. Since this reduced the extent of the polycrystalline regions to fairly small values, PEG experiments on (111) silicon were conducted with the narrow hot zone and a moving substrate. Here,

however, the entire slice eventually became sufficiently hot so that polycrystalline silicon deposited after about 1/16-in of movement.

In the above arrangement, to prevent deposition on the portions of the slice not over the hot zone itself, a slotted BN mask was positioned over the substrate with the slot over the hot zone. With this improvement, a PEG deposit of silicon on a (111) silicon substrate was obtained that was epitaxial over a large area (about 5 mm x 5 mm), although the small remaining portion of the deposit was polycrystalline. This sample encouraged us to pursue the technique further.

A more refined masking and susceptor arrangement was built to provide a narrow hot zone on the substrate with a fairly uniform temperature across the portion of this zone that was to be open to the gaseous reactants, see Fig. 16. Half-slices of silicon were used for convenience and economy. This arrangement was still inadequate for preventing contamination of the areas supposedly masked. It was suspected that, among other possible problems, the gas flow might be turbulent. An inspection of the gas flow by means of a smoke generator confirmed this suspicion. Therefore, the outlet of the reaction tube was increased in diameter from 1/4-in. to 3/4-in. and this reduced the turbulence considerably. Although some substrates were possibly epitaxial via PEG with this arrangement there was still difficulty with depositions on supposedly masked areas.

Consequently, the arrangement of Fig. 17 was constructed. This graphite susceptor-mask resembled the slider used for coin insertion in many coin-operated machines. It provided a fairly tight box around the substrate (to eliminate unwanted depositions) and a very smooth trans-

lation of the slice. In contrast to the previous fixture, the entire substrate was heated. Several runs with this apparatus, after initial "bake-out" runs, indicated that the desired isolation from unwanted depositions was achieved, but no weight gains (indicating deposition) were observed. The reasons for this may have been (1) a temperature somewhat too low and (2) insufficient amounts of reactants reaching the substrate. Both of these reasons point to the need for further modifications of the susceptor-mask geometry. The edges of the slot exposing the substrate could be tapered; reactant gas flow could be led in and directed downwards onto the slot; slits or heavier sections could be added to the susceptor to control the eddy current distribution and raise the temperature.

In view of the more successful vacuum deposition PEG experiments, we have not pursued the CVD method any farther. However, it is our opinion that the CVD method could be successful if a suitable masking arrangement were found. It has recently been brought to our attention that United States Patents[21] has been issued covering the equivalent of the PEG method as carried out with CVD.

Conclusions

The planar-edge-growth technique for growing single crystal films in the solid state by vacuum evaporation onto amorphous substrates has been demonstrated for the interesting case of silicon on amorphous quartz (silica). The deposition parameters that seem most critical for these materials are substrate temperature and incident flux of silicon atoms. Appropriate values are about 1150°C and 2×10^{16} atoms/cm^2-sec, respectively.

The silica substrate should be sufficiently thin so that differential thermal contraction will not crack the silicon film, and yet must be thick enough to avoid local penetrations that can electrically short the silicon film to the substrate underlying the silica. A silica thickness of 5 microns appears to be satisfactory.

Mask slot dimensions and mask speed do not seem critical, and values used for these parameters were 1.5 mm and 2 to 6 cm/hr.

Growth direction of the silicon film was close to [[110]] or [[211]], and also appears uncritical at the present state of development.

Additional investigations should be made into the reasons for the low yields of these films, with greater control of the silicon evaporation rate and substrate temperature.

The initial success of this program warrants further examination of the properties of vacuum deposited, planar-edge-growth, single crystal silicon films.

Chemically vapor-deposited, planar-edge-growth, silicon single crystal films could perhaps be obtained with better control over

masking than was achieved in this investigation. However, it is not recommended that efforts be made in this direction until more information is available concerning experimental results obtained in connection with the U. S. Patents granted on this process.

References

1. E. Rasmanis and J. Cline, "Active Thin-Film Techniques Micromin Program", DDC Reports No. AD286177 (Oct. 12, 1962) and AD294715 (Jan. 14, 1963).

2. J. Maserjian, Solid-State Electronics, 6, 477 (1963).

3. S. Namba, J. Appl. Phys., 37, 1929 (1966).

4. O. A. Weinreich and G. Dermit, J. Appl. Phys., 34, 225 (1963).

5. T. O. Poehler and G. B. Gilbert, Jr., in "Single Crystal Films", Pergamon Press Ltd., Oxford, England (1964), p. 129.

6. V. Y. Doo, J. Electrochem. Soc., 111, 1196 (1964).

7. W. J. McAleer, M. A. Kozlowski, and P. I. Pollak, J. Electrochem. Soc., 111, 877 (1964).

8. J. D. Filby and S. Nielsen, J. Electrochem. Soc., 112, 957 (1965).

9. R. S. Wagner and W. C. Ellis, Appl. Phys. Letters, 4, 89 (1964).

10. W. B. Nowak, R. D. French, and E. C. Steeves, "Techniques for Fabrication of Large, Thin Silicon Single Crystals", Contract AF19(604)-7358 for the Air Force Cambridge Research Laboratories, Bedford, Mass., Section I of Report No. AFCRL-63-940, November 22, 1963, entitled "Research in Energy Conversion".

11. W. B. Nowak, J. Vac. Sci. Technol., 2, 276 (A), (1965). Paper presented at the 12th National Symposium of the American Vacuum Society, Thin-Film Division, September 29, 1965, New York, N. Y.

12. T. L. Chu, M. H. Francombe, G. A. Gruber, J. J. Oberly, and R. L. Tallman, "Deposition of Silicon on Insulating Substrates", Contract AF19(628)-4220 for the Air Force Cambridge Research Laboratories, Bedford, Mass., Report No. AFCRL-65-574, July 27, 1965.

13. D. W. Pashley, "The Growth and Structure of Thin Films", Pg 59-98 in "Thin Films", American Society for Metals, Metals Park, Ohio, 1964. (Papers presented at an ASM Seminar, October 1963.)

14. F. M. Collins, Trans. of the 8th National Vacuum Symposium (1961), Pergamon Press Inc., New York, 1962, Pg 899.

15. B. A. Unvala, Nature, 194, 966 (1962).

16. A. P. Hale, Vacuum, 13, 93 (1963).

17. B. A. Unvala and G. R. Booker, Phil. Mag., 9, 691 (1964).

18. G. R. Booker and B A. Unvala, Phil, Mag., 11, 11 (1965).

19. H. Widmer, Appl. Phys. Letters, 5, 108 (1964).

20. H. C. Theurer, J. Electrochem. Soc., 108, 649 (1961).

21. W. Heywang, et al. U. S. Pat. No. 3,157,541, Nov. 17, 1964.
G. Ziegler, et al. U. S. Pat. No. 3,160,521, Dec. 8, 1964.
W. Heywang, et al. U. S. Pat. No. 3,160,522, Dec. 8, 1964.
These patents are assigned to Siemens and Halske Co., Germany.

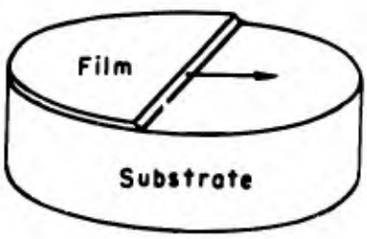

Fig. 1. Simplified PEG schematic.

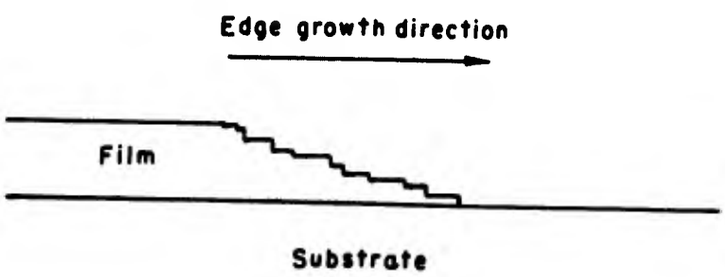

Fig. 2. An edge configuration.

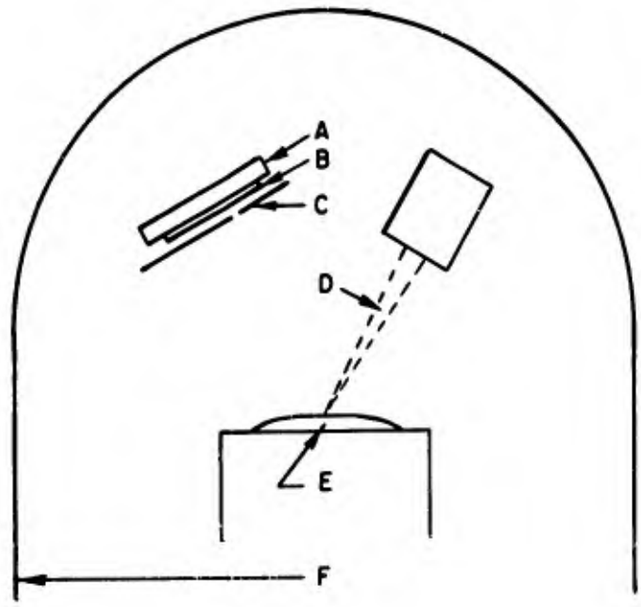

Fig. 3. Schematic of PEG experimental geometry. A - specimen heater; B - specimen; C - slotted, movable mask; D - focussed electron beam; E - molten pool of silicon; F - vacuum bell jar.

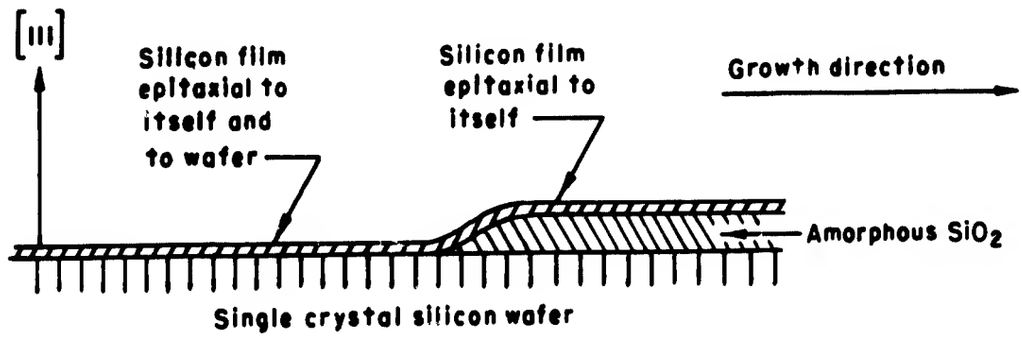

Fig. 4. Cross section of PEG demonstration specimen - geometry.

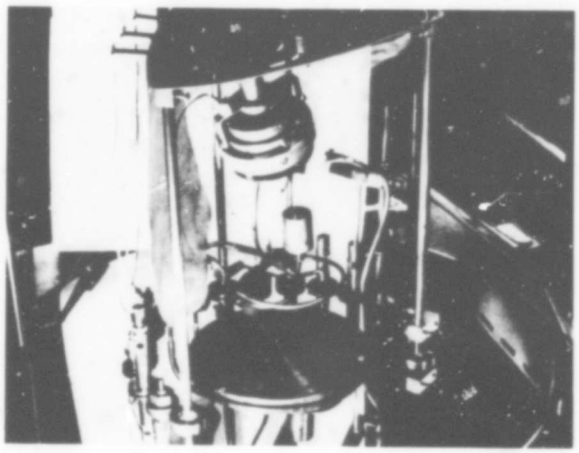

Fig. 5. Photograph of Interior of Vacuum Chamber Showing Overall Position of Components for PEG.

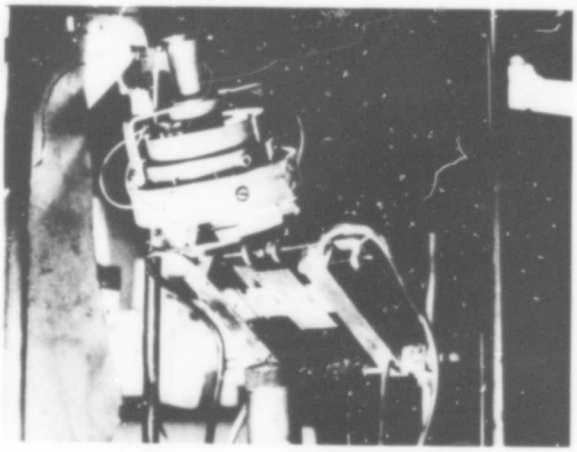

Fig. 6. Photograph of PEG Apparatus Showing Electron Beam Gun, Graphite Insert on Water-Cooled Copper Crucible, Substrate Heater-Holder (in Water-Cooled Clamp), and BN Slotted Mask with Pulley Arrangement for Motion.

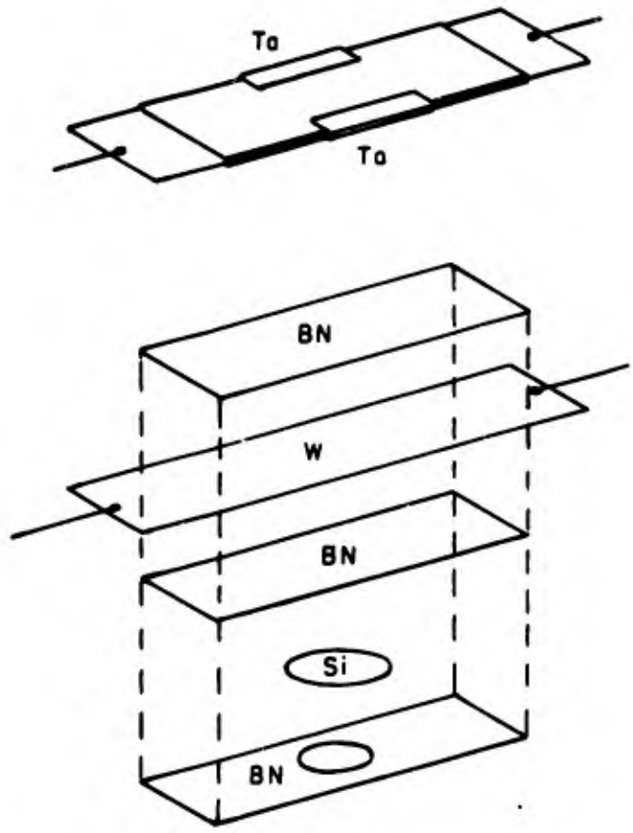

Fig. 7. Exploded view of Substrate heater-holder assembly

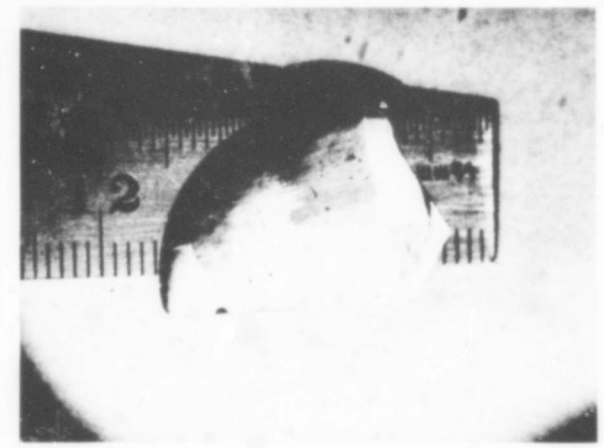

Fig. 8. PEG Silicon Film on (111) Silicon-SiO_2. Sample 32F.

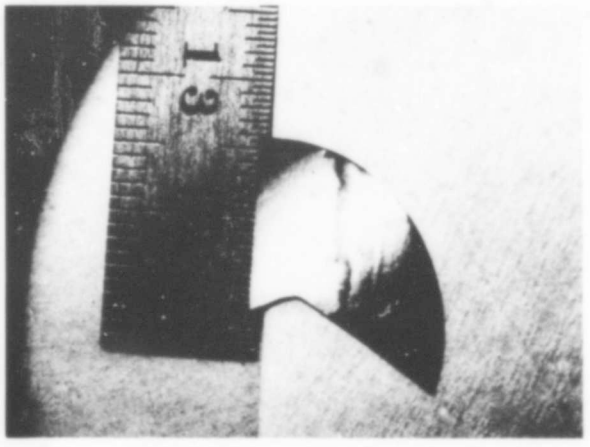

Fig. 9. PEG Silicon Film on (111) Silicon-SiO_2. Sample 132R.

Fig. 10. PEG Silicon Film on (111) Silicon-SiO_2. Sample 138R.

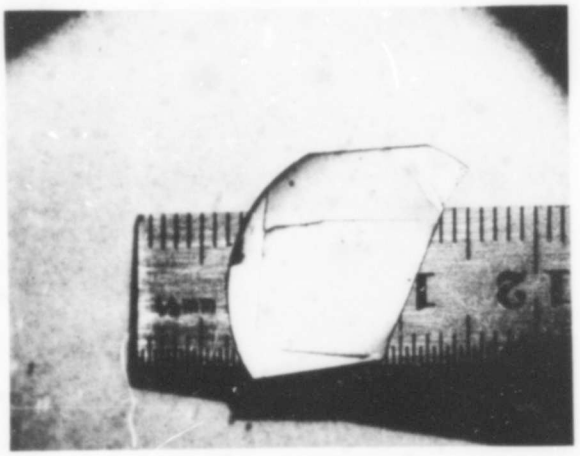

Fig. 11. PEG Silicon Film on (111) Silicon-SiO_2. Sample 151R.

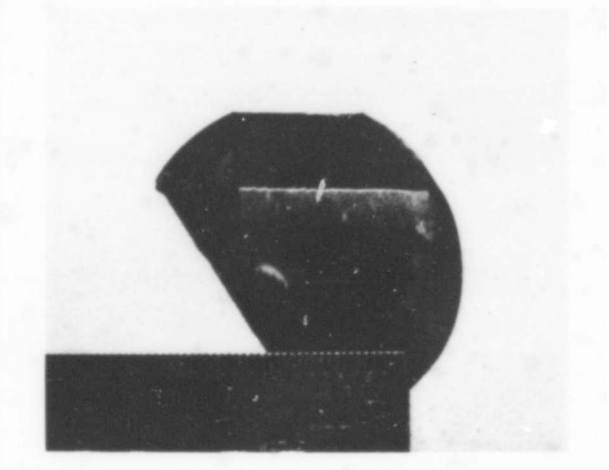

Fig. 12. PEG Silicon Film on (111) Silicon-SiO_2. Sample 156R.

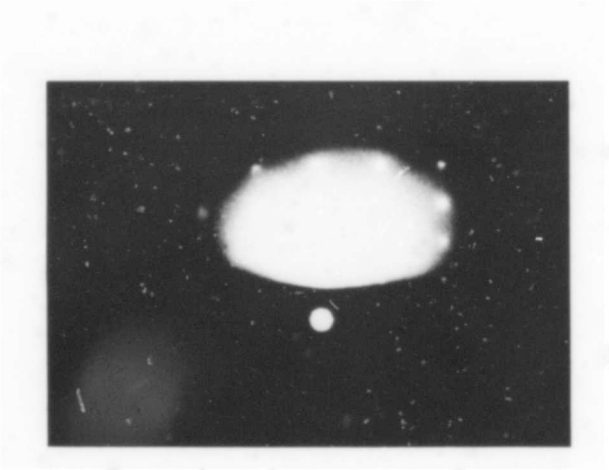

Fig. 13. Electron Reflection Diffraction Pattern from PEG Specimen 164R-1, Homoepitaxial Region. (Plate No. 2304).

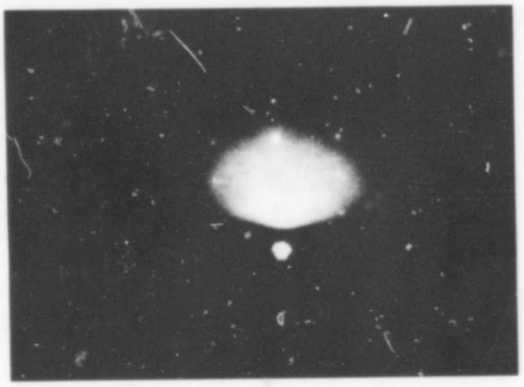

Fig. 14. Electron Reflection Diffraction Pattern from PEG Specimen 164R-1, Autoepitaxial Region. (Plate No. 2305).

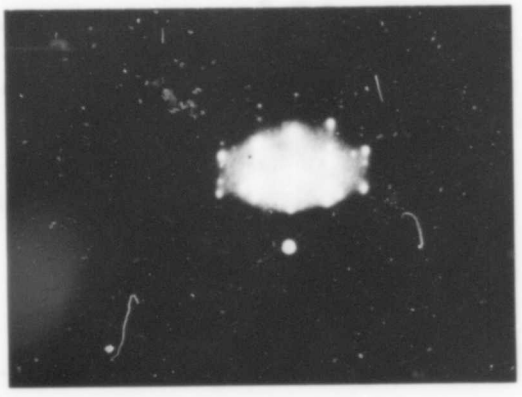

Fig. 15. Electron Reflection Diffraction Pattern from PEG Specimen 164R-1, Autoepitaxial Region Different from that of Fig. 14. (Plate No. 2303).

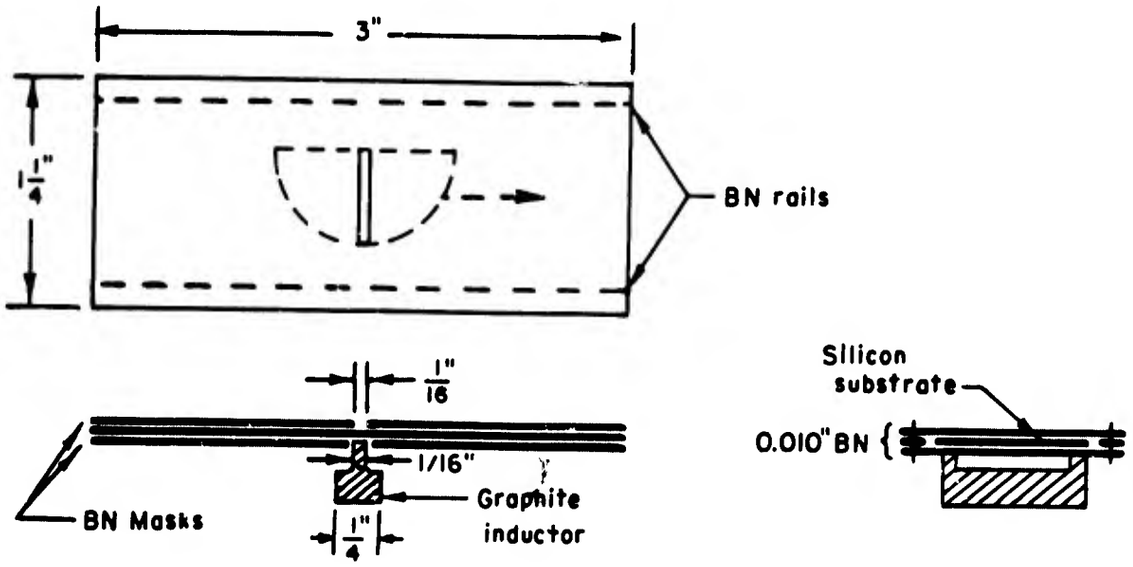

Fig. 16. Schematic Diagram of a Masking and Susceptor Arrangement for Attempted PEG of Silicon by the CVD Method.

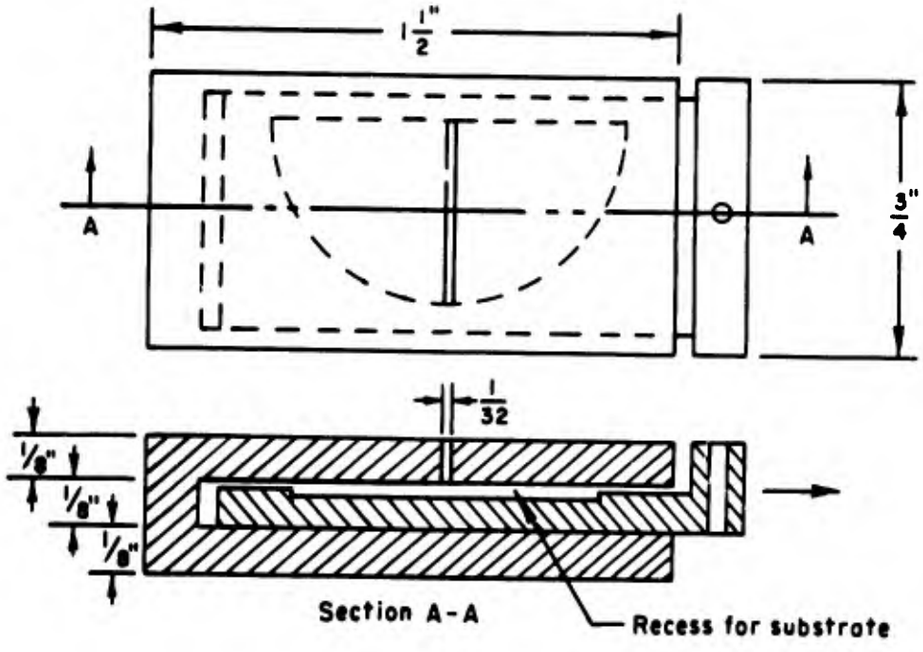

Fig. 17. Graphite Susceptor-Mask Apparatus for Attempted PEG of Silicon by the CVD Method.

2. CATHODES FOR THERMIONIC ENERGY CONVERSION

Introduction

Investigations[1,2] on the relationship of thermionic energy converter efficiency to the uniformity of cathode and anode work functions have shown that substantial increases in efficiency can be obtained by using surfaces of uniform work function. Such surfaces may be achieved by use of single crystals[1], by preferred textures obtained through chemical vapor deposition[2,3], or by suitable heat treatment[4] of polycrystalline material. However, single crystal surfaces may be non-uniform emitters under some conditions[1]. Although empirical procedures may be found that will transform a material with a given metallurgical history into a uniform emitter, very little is known about the nature of the transformation or the product.

It is well known that, after elevated temperature heat treatment, the surfaces of metals change markedly not only through bulk grain growth but through local differences in evaporation rates, and through surface migration. Characteristic surface markings have often been noticed after such treatment. Modification of the ambient atmosphere during the high temperature treatment from a pressure of 10^{-7} Torr to over 10^{-4} Torr with oxygen, water vapor, halogen gas, etc. can cause large differences in the resulting surface. In particular, a non-uniform polycrystalline emitter can be transformed to a uniform polycrystalline emitter[4]. Since the work function is dependent upon crystallographic direction, the previous statement implies that the exposed crystal faces are of the same family, for example ((100)), regardless of the orientation of the corre-

sponding grains. That is to say, surface tension and surface mobility at elevated temperatures, promoted by chemical interaction with certain atmospheres, can alter the original exposed faces of a surface so that preferred facets are exposed. In such an alteration, an originally flat surface will become rumpled.

It was originally intended to study these effects on flat, polycrystalline tungsten surfaces by direct observation of the crystallographic surfaces. However, inability to obtain suitable samples of tungsten, tantalum, or rhenium, frustrated this intention. The following section describes some of the experiments and techniques used in this work.

Concurrent with the initial experiments, a literature survey was started. There are very few papers dealing directly and solely with the subject. Many interesting observations have been reported in the "Experimental Technique" portions of papers devoted principally to other topics, especially thermionic emission. This literature survey covered the period from 1923 to 1965. A critical review and summary of the literature has been issued[5].

Experimental Results

In order to watch the evolution of the crystallography of a surface, an adequate means for identifying the exposed crystal faces must be available. Several techniques were examined for tungsten: anodization, heat-tinting, and x-ray back-reflection Laue photograms.

Anodization of a tungsten single crystal cylinder, 1/8-in in diameter, was carried out in nitric and in sulfuric acid solutions. Prior to anodization the crystal was electropolished to insure a smooth surface.

The anodization resulted in a uniform color and so could not serve to identify crystal faces.

Heat-tinting also was unsuccessful. Exposures of five minutes to temperatures up to 500°C in air resulted in surfaces with a uniform brownish color. During attempts to remove these oxide films by electropolishing in 10% NaOH solution, some preferential attack of film was noted. However, it is doubtful that this technique would be definitive enough to permit identification of crystal faces.

A combination of optical alignment and x-ray back-reflection Laue (BRL) photograms was successful in identifying individual exposed crystal faces provided the grain size was at least one millimeter in diameter. A microscope mechanical stage was adapted to mount in the goinometer of a standard BRL x-ray camera (Norelco). The specimen was mounted on the X-Y mechanical stage and the desired grain selected by sighting through the camera frame with the collimator removed. The collimator was then replaced and a strong light (from a microscope illuminator) sent down the collimator. The light was reflected from the shiny surface of the grain, nd the sample was rotated by the goniometer until the reflection was centered at the collimator. This insured that the x-ray beam was perpendicular, within a few degrees, to the grain surface. A BRL photogram would then reveal the orientation of the grain surface.

A previously unreported phenomenon was observed during some early work on tungsten wires. The tungsten wire specimen, 0.006-in in diameter, was stretched between copper electrodes in a vacuum system. To maintain tension on the wire and eliminate stresses due to differential

thermal expansion between wire and electrodes, the wire consisted of a straight portion and a helical portion. After 10-20 minutes at 4×10^{-5} Torr and 2300°C (ac heating), the wire material redistributed itself so as to form ellipsoidal lumps more or less regularly spaced along the wire and separated by straight portions of cross section considerably reduced from that of the original wire. This "lumping" occurred over the entire hot section including the helix portion. A possible explanation for the lumping, and one that is consistent with the premature failure of wires at higher temperatures in vacua, is the degenerative cycle inherent in resistive self-heating. Should a portion of wire become hotter than the adjacent regions, tungsten will migrate to the cooler regions; the reduced and increased cross-sections will then become hotter and cooler, respectively, thus leading to further action of a similar nature.

Unsuccessful efforts were made to grow medium-sized (1-4 mm) grains in tungsten sheet. Vacuum ac heat treatments ranging from 6 min. at 3000°K (burnout) to 85 min. at 2900°K produced recrystallized grains up to only 0.2 mm diameter in 0.002-in sheet (Plansee tungsten obtained from the National Research Corp., Newton, Mass.).

No appreciable grain growth was induced in cold-worked rhenium strip (Chase Brass Co.) by vacuum ac heating up to burnout, and at 2500°K, for one hour.

A few experiments with the strain-anneal technique also failed to produce the required grain size for application of the BRL analysis of orientation. Because of its lack of ductility at room temperature, tungsten must be strained at an elevated temperature, which in turn requires a vacuum or inert gas environment. Accordingly, apparatus was

constructed to heat the strip samples (approximately 2-in x 1/8-in x 0.002-in cut from Plansee sheet) with 60 cycle current to about 400°C and load them to about 55,000 psi in a helium atmosphere. This temperature and pressure were selected from the tensile data on tungsten given in Ref. 6. No yielding up to fracture was observed for these specimens. This tungsten is fabricated by a powder metallurgy process. Apparently, the microstructure and purity of this material is sufficiently different from the tungsten materials reported in Ref. 6 that a redetermination of the values for temperature and stress for yielding would have to be made in order to carry out a strain-anneal technique.

The strain-anneal method was also tried with tantalum. Strips, 0.002-in thick, were vacuum annealed (3×10^{-5} Torr and 2070°C) and strained to 2.5% in a Young's tensile-testing machine. Small pieces were cut from the strained strip and their edges etched to remove the heavily cold-worked region adjacent to the cut. These pieces were then annealed between tungsten strips heated by 60 cycle current in a vacuum bell jar at about 10^{-5} Torr. The longest anneal was 14 hours at 2300°C. Grain growth to about 0.5 mm was observed. These grains were again too small, and were also striated as though heavily twinned. As in the case of tungsten, it was evident that much empirical work would be required to achieve the necessary grain size.

Attempts were made to obtain tungsten, tantalum, or rhenium with a grain size of 1-4 mm through commercial suppliers or their research and development laboratories. Such material was not available.

Conclusions

Although this small program was not able to proceed towards its objective by its chosen route, we still feel that there is a reasonable chance for obtaining a uniform work function surface on polycrystalline material by suitable thermo-chemical treatments.

References

1. N. S. Rasor, S. S. Kitrilakis, D. P. Lieb, "Proceedings of the Thermionic Specialist Conference", Gatlinburg, Tenn., October 1963.

2. I. Weissman and N. L. Kinter, J. Appl. Phys., 34, 3187 (1963).

3. M. N. Huberman and R. A. Holzl, "Proceedings of the Thermionic Specialist Conference", Gatlinburg, Tenn., October 1963.

4. J. B. Taylor and I. Langmuir, Phys. Rev., 44, 423 (1933).

5. W. B. Nowak and J. Babakian, "Literature Survey on the Surface Structures of Refractory Metals with Reference to Thermionic Emission and Energy Converters", Air Force Cambridge Research Laboratories, Bedford, Mass., Report No. AFCRL-66-362, June 1966.

6. G. E. Gazza, "Survey of the Deformation Characteristics of Tungsten", Report No. AD610658, July 1963, Clearinghouse for Federal Scientific and Technical Information, U. S. Department of Commerce.

3. CARNOT-LIMITATION ON EFFICIENCY OF PHOTOVOLTAIC ENERGY-CONVERTERS

A short study has been made of the conditions under which the efficiency of a photovoltaic energy-converter is subject to the Carnot limit. This study was initiated because of conflicting statements in the literature to the effect that solar cells are Carnot-limited[1,2], photovoltaic cells may be Carnot-limited[3,4], and photovoltaic cells are not Carnot-limited[5,6].

Whether a solar cell is so limited or not is academic for practical purposes, since the temperature of the sun (the source) is about $6000^{o}K$ and the temperature of the cell and its surroundings is about $300^{o}K$ thereby establishing a Carnot limit of (6000 - 300)/6000 = 95%. Present solar cells are limited by the mechanisms of the energy conversion process. However, as a matter of principle for the solar cell, and perhaps as a practical matter for photovoltaic converters in other applications, it is desirable to clarify the situation regarding a thermodynamic limit of efficiency.

Rose[3] developed an expression for the maximum power delivered from any photovoltaic device in terms of the incident light intensity measured in units of black body radiation. He assumed that the added incident radiation is characterized by Planck's law for a source temperature T_2, and he simply states that the useful output power is Carnot-limited. The choice of a Planck distribution for the incident radiation implies that the radiation is <u>in equilibrium</u> with the source at T_2, and that the radiative transfer constitutes heat. Under these special conditions, the photovoltaic converter is Carnot-limited. It should be noted that

the title of Ref. (3) is "Photovoltaic Effect Derived from the Carnot Cycle" and the paper has no statements regarding non-Carnot-limited operation of photovoltaic converters.

Miser[4] makes assumptions similar to, but more restrictive than, Rose[3]. Angrist[5], on the other hand, in the introduction to his Chapter 5, states, "In this chapter we consider a method [photovoltaic generation] that does not involve heat but converts electromagnetic radiation directly to electrical power. By eliminating the intermediate step of conversion to heat, we bypass the Carnot limitation on efficiency of heat engines." In view of the analyses presented in Refs. (3) and (4) it appears that Angrist's statement is only partially true.

When, then, is the photovoltaic converter Carnot-limited? The answer may be obtained from re-examination of thermodynamic fundamentals. The generalized approach of Hatsopoulos and Keenan[7] will be adopted.

The efficiency of a device is the ratio of useful effect produced to principal expenditure incurred. For a work-producing heat engine, the useful effect produced is work, and the principal expenditure incurred is the consumption of energy delivered from a heat source. Such a reversible heat engine has the Carnot-limitation $(T_1 - T_2)/T_1$, where T_1 and T_2 are the source and sink temperatures, respectively, between which the engine is operating.

The Carnot-limit applies only to a heat engine, which is a system operating in a cycle while only heat and work cross its boundaries. Therefore, a device must fit this definition in order to be subject to the limitation. Some energy converters, such as thermoelectric generators, obviously are heat engines. The fuel cell is not a heat engine,

since chemical reactants enter the system and products leave as work is produced. In the case of photovoltaic converters, the transfers of energy between devices and their environments must be investigated in order to determine whether they fit the thermodynamic definitions of heat and work.

Work is an interaction between two systems such that the occurrences in each at the interaction boundary could be repeated while the sole effect external to each system was the change in level of a weight. Electrical work fits this definition as well as the obvious mechanical work.

Heat is an interaction which may occur between two systems, originally isolated and in stable states, when they are brought into communication without altering their allowed states and without work being done by the environment.

Heat is the only kind of interaction between systems that are in stable equilibrium, or nearly so. A work interaction cannot occur unless at least one of the two interacting systems is not at a stable state. Otherwise, if two systems are initially in stable states, in order for work to be done, at least one of the systems must be changed to a state which was not initially an allowed state. In other words, a constraint must be relaxed and a system must be thrown out of stable equilibrium to have work.

In order to insure that an interaction is solely a heat interaction, it is necessary that at each instant during the process the two systems would be in stable states if they were suddenly isolated. Since such a system is in a stable state, no change to another allowed state will occur spontaneously while the system is isolated.

If the departure from equilibrium is so great that isolation of the parts of the systems, with or without changes in constraints, results in substantial spontaneous change in the states of the parts, then interactions other than heat and work may be involved. Such interactions may be some type of light or other radiation with a frequency distribution unlike that of heat. They usually occur while the interacting systems are far from equilibrium. For example, the interaction between a fluorescent lamp and a photocell cannot be called either heat or work. Interactions of this type may result in an exchange of energy between the two interacting systems. The energy exchanged, in turn, can be computed by evaluating the work involved in an adiabatic process (a process involving only work interactions) through quasistatic states which would have the same final effects on the system. A photocell operating under such conditions is not a heat engine and is, therefore, not subject to the Carnot limit of efficiency.

Suppose, however, that a photocell receives radiation from an equilibrium source which has the temperature-dependent frequency distribution of thermal radiation as predicted by Planck. The energy influx is heat, electrical work is produced, and heat is rejected to the surroundings. A photocell operating in this manner is a heat engine and must be less efficient than the corresponding Carnot engine.

References

1. W. Shockley and H. J. Queisser, "Detailed Balance Limit of Efficiency of p-n Junction Solar Cells", J. Appl. Phys., 32, 510 (1961).

2. B. D. Wedlock "Spectral Response and Conversion Efficiency of p-n Junctions", D.Sc. Thesis, 1962, Department of Electrical Engineering, Massachusetts Institute of Technology, Cambridge, Mass.

3. A. Rose, "Photovoltaic Effect Derived from the Carnot Cycle", J. Appl. Phys., 31, 1640 (1960).

4. H. A. Müser, "Thermodynamische Behandlung von Electronenprozessen in Halbleiter-Randschichtne", Z. Physik, 148, 380 (1957).

5. Stanley W. Angrist, "Direct Energy Conversion", Allyn and Bacon Inc., Boston, 1965, Chapter 5.

6. F. Daniels, American Scientist, 55, 15 (1967), esp. Pg. 34.

7. George N. Hatsopoulos and Joseph H. Keenan, "Principles of General Thermodynamics", John Wiley and Sons, Inc., New York, 1965.

4. TRANSIENT PHOTORESPONSE OF SOLAR CELLS FROM REVERSE TO ZERO BIAS*

Introduction

The purpose of this investigation was to assess experimentally the possibility of obtaining an increased photovoltaic energy conversion efficiency in silicon solar cells through momentary applications of a reverse bias.

Application of a reverse bias to an illuminated p-n junction has two principal effects. First, an increase in the width of the depletion-layer region is produced. Second, a collection occurs of photo-generated carriers which are within a diffusion length of the now-widened p-n junction[1].

Since majority carriers see an increased barrier due to reverse bias, an effective charge-storage condition is established across the junction region[2]. This situation is analogous to the charge storage which occurs on the plates of a capacitor when a DC potential is impressed on it.

Upon the removal of the reverse bias, the device will relax to the state which existed before the application of the bias. The p-n junction would become forward-biased in the presence of light. For the dark case, equilibrium is reached at zero-bias conditions.

The momentary application of the reverse bias, therefore, serves to stimulate the collection of a greater number of carriers across the

---

* A major portion of this work has been incorporated in the thesis entitled "The Transient Photoresponse of a P-N Homojunction and the Relationship of this Response to the Overall Photovoltaic Energy Conversion Efficiency" submitted by Raymond J. Sonoff to the Graduate School of Northeastern University in partial fulfillment of the requirements for the Master of Science Degree in Electrical Engineering.

junction region. This could be considered as an enhanced field effect. And since conversion efficiency is directly related to the collection efficiency[3,4,5,6], the possibility exists for obtaining an overall increase in energy conversion efficiency by this method.

For an increase in the overall energy conversion efficiency to be realized, several factors have to be offset. Assuming that an enhanced field effect occurs, the transient discharge portion of the solar cell response must contain sufficient energy to more than account for the energy supplied by the reverse bias source. In addition, compensation is required for the energy lost due to the fact that the solar cell does not supply the steady-state value of power during the reverse-biased interval.

Questions to be answered regarding the transient photoresponse include the following: How long will the transient condition exist for the charging cycle? for the discharging cycle? What are the magnitudes of the transient voltages and currents? Will the time of application of the reverse bias be much less than the duration time of the forward transient? Or, in terms of one concise question, "Is it possible to produce, on the average, an enhanced field and widened depletion region at a p-n junction which will result in an increased energy conversion efficiency after all factors are considered?"

The transient response of semiconductor diodes has received considerable attention for nearly two decades. A survey of the literature quickly attests to this fact[7-18]. However, we have uncovered no reported investigations of the forward transient photoresponse of a semiconductor diode from a reverse-biased state.

Three types of measurements were conducted on solar cells: (1) the static reverse I-V characteristics, (2) the transient response from a reversed bias condition with and without illumination for various values of initial bias and for various load resistances, and (3) the small-signal equivalent-circuit values of capacitance, shunt (P-N junction) resistance, and series resistance.

Component Descriptions

A. Solar cells

Two solar cells, both commercially manufactured silicon homojunction units, are subjected to experimental measurement. Cell #E is a p-on-n, three-grid cell having flexible leads and a nominal efficiency of eight (8) per cent as reported by the manufacturer. Cell L-22 is a n-on-p, five-grid cell specified as having a 12½ per cent efficiency.

B. Electronic equipment

The power supply used for the constant DC voltage source of reverse bias was a Thornton Model 201D.

The transient response was observed on a Fairchild/Dumont Model 766 DC-25 MHz oscilloscope used in a triggering mode.

The source of illumination was a Bausch & Lomb microscope illuminator. #0 position of the selector switch is off. #1 position places 5 volts across a GE 1630 tungsten bulb mounted within a prefocussed assembly. Adjustment of the lamp-to-solar-cell distance was established to produce an illumination of 100 foot-candles on the cell, as calibrated with a Weston Model 614 foot-candle meter.

The General Radio Capacitance Bridge Type 1615-A used in conjunction with a General Radio Audio Oscillator Type 1311-A and a General

Radio Tuned Amplifier Type 1232-A provided the means for establishing the small-signal values of the equivalent circuit components shown in Fig. 7 of the section of this report on Heterojunctions. The two-frequency method of measurement for C, R_p, and R_s was employed (refer to the Heterojunction section).

Experimental Results

Figure 1 illustrates schematically the simple circuit used to collect the transient response data. Both charging and discharging responses were measured. The behaviour was observed for load resistances of 200, 1000, and 10,000 ohms, for reverse biases of 2, 5, 10, and 15 volts, and for zero and 100 foot-candles illumination.

Figures 2 and 3 show the reverse I-V characteristics of solar cells E and L-22, respectively. A maximum reverse bias of 15 volts was used for the transient response experiments because beyond this value the current increased substantially.

The charging responses were independent of the value of load resistance (except for short circuit termination). Figures 4 and 5 display the transient charging current of cell E for the various bias voltages in the dark and under illumination. The departures from exponential behaviour, and the marked differences between dark and illuminated conditions are evident. L-22 had a similar response although the rate of current decay was faster.

The discharging responses were, of course, very dependent upon load resistance and also upon the presence of illumination. Figures 6 and 7 display the transient discharging voltage of cell E at 1000 ohm load resistance for various bias voltages in the dark and with illumination.

Although one may draw straight lines of moderate fit through the data points over limited regions, consideration of all the data favors departure from exponential behaviour. The large increase in voltage decay-rate when illumination is present should be noted.

Figures 8 and 9 present the discharging transient voltage response of cell E at 10 volts reverse bias, with and without illumination, and for load resistances of 200 and 10,000 ohms. These curves are plotted linearly rather than semilogarithically to show the general nature of the overall behaviour of all the discharging transients. Since the voltage decays to zero in the dark and to a small positive value under illumination, the whole curve cannot be depicted on a semilog plot, although such a plot is useful in revealing deviations from exponential behaviour.

For reference purposes, the discharging transient voltages for cell E with open circuit termination, with and without illumination, for various biases, are given linearly and semilogarithically in Figs. 10-13, inclusive.

If the initial portions of the discharging voltage transients are considered as exponential, then one can compute a time constant in the usual way. Summaries of such time constants are given for a variety of parameters in Fig. 14 and in Table 1.

Less extensive data was taken on cell L-22. However, the same general behaviour was observed but at more rapid rates. Figure 15 shows this for case of 5 volts reverse bias, 1000 ohm load, and both with and without illumination. This figure should be compared with the appropriate curves in Figs. 6 and 7, allowing for the difference between linear and logarithmic ordinates.

TABLE 1

Comparison of voltage and current discharge time constants

Reverse bias (volts)	Light intensity (foot-candles)	Load resistance (ohms)	$TC_{volt.}$ (μs)	$TC_{curr.}$ (μs)
-5	0	200	9.0	10.0
-5	100	200	7.2	6.0
-5	0	1000	32.0	32.0
-5	100	1000	15.0	15.0
-5	0	10,000	180.0	200.0
-5	100	10,000	30.0	20.0
-10	0	200	6.5	8.0
-10	100	200	5.6	6.5
-10	0	1000	36.0	38.0
-10	100	1000	15.0	20.0
-10	0	10,000	132.0	145.0
-10	100	10,000	37.0	30.0
-15	0	200	6.0	6.5
-15	100	200	5.2	6.0
-15	0	1000	20.0	27.0
-15	100	1000	13.0	15.0
-15	0	10,000	100.0	110.0
-15	100	10,000	33.0	25.0

Note that the tabulated values for the time constants were observed independently and are presented in tabular form to illustrate the expected degree of reproducibility of the experimental data. To explain, the time constants under ideal conditions should agree for each specified reverse bias, load resistance, and light intensity.

In order to assess the magnitudes and nature of the capacitance, series resistance and parallel resistance in the equivalent circuit model of the solar cell diode, capacitance and dissipation factor of cell E were measured at several frequencies as a function of reverse bias, both with and without illumination.

Figure 16 presents the capacitance-voltage data plotted as $(\text{capacitance})^{-2}$ versus reverse voltage. Since at low voltages (where the reverse current is small) there is a linear relation, it is deduced that there is probably an abrupt junction in the diode. Values for the capacitance, C, and parallel resistance, R_p, are listed in Table 2, and it may be seen that illumination produces only slight changes in C and that photoconductivity effects reduce R_p. The series resistance, R_s, could not be measured accurately, but was in the range of 10 to 100 ohms.

Figure 17 presents the dissipation factor, DF, versus $(\text{frequency})^{-1}$ at several reverse voltages. As expected, the DF and R_p increase with reverse bias because of the corresponding increase in reverse current in the static I-V characteristic. Since $R_p >> R_s$, and $\omega R_p C >> 1$ (where $\omega = 2\pi \times$ frequency), then $DF \doteq (\omega R_p C)^{-1}$, which is verified by the data in Fig. 17.

Power transients were calculated from the product of the corresponding voltage and current transients. Typical results are given in Figs. 18 and 19, where the charging and discharging power transients are plotted for cell E at 1000 ohms load, 5 volts reverse bias, with and without illumination. It may be seen that the charging power is increased and the discharging power decreased in the presence of light.

TABLE 2

Junction capacitance and resistance of cell #E

Bias voltage (volts)	Light intensity (foot-candles)	C (uf)	R_p (ohms)
-2	0	0.0353	very high*
-2	100	0.0356	very high*
-5	0	0.0241	14,800
-5	100	0.0243	14,800
-10	0	0.0162	4,000
-10	100	0.0164	3,800
-15**	0	-	-
-15**	100	-	-

* Such a value occurs (see Appendix for equations) as a consequence of the measured capacitance at the two frequencies of measurement remaining unchanged.

** The dissipation factor exceeded unity and measurements could not be made with the bridge.

Discussion

Two major facts stand out:

(1) the time of transient decay of the reverse voltage is markedly decreased by the presence of light, and

(2) more energy is put into the charging cycle than is recovered on the discharging cycle.

The effect of light in shortening the discharge time cannot be explained on the basis of photoconductivity. The parallel resistance is changed only about 10 per cent by the illumination, whereas the "time constant" may be decreased by a factor as large as 5.

On the other hand, an explanation based on Charge Balance for the charge "lost" in the shortened discharge transient appears to be consistent with the data. A constant current source of infinite impedance must be added in parallel to the R_p - C equivalent circuit model of the illuminated solar cell. The photocurrent partially discharges the junction capacitance internally (within the depletion region) producing a shorter discharge time through the external load resistor.

Integrating under the voltage dependent junction capacitance curve yields the value of the total stored charge. Neglecting small losses, this stored charge equals the total charge which enters the cell terminals. This equality holds both with and without illumination, and correlates with the fact that the values of capacitance and time for charging are nearly the same for both light and dark cases. That is, all the charge entering the cell from the external circuit appeared on the capacitor; but all the charge leaving the capacitor during the relaxation transient did not enter the external circuit.

The circuit model for the illuminated photocell contains a constant current source which forward biases the cell under no external bias conditions. Assigning the proper polarities to the reverse-biased capacitor and to the current source, it may be seen that the current source discharges the capacitor internally as the capacitor is discharging externally through the load resistance. The essence of the Charge Balance theory is that the difference between total charge leaving the cell with and without illumination is equal to the amount of charge generated by the current source during the relaxation transient.

Table 3 presents charge balance calculations for solar cell E. ΔQ_o is the difference between charge on the capacitor and charge leaving the cell during the relaxation transient with no illumination. ΔQ_o is thus due to "inherent" losses. ΔQ_I is the corresponding difference with the cell under illumination. Subtracting the loss mechanisms implied by ΔQ_o from ΔQ_I should then leave the net "lost" charge attributable to cancellation by the photon-produced charge. This assumes that the "inherent" losses are the same with and without illumination. The last column in Table 3 is the total charge, Q_g, produced by the current generator. This is calculated by multiplying I_g (the photon-produced current source) by the total relaxation time. Agreement between the last two columns is considered satisfactory.

No new mechanisms need be invoked to explain the shortened discharge transient, so the complete discharge curve may be reproduced by considering the relaxation of a non-linear capacitance. This description of the curve has not yet been completed.

Table 3

Charge Balance for Solar Cell E

V_B (volts)	Ill. (ft-c.)	R_L (ohms)	ΔQ_o (μcoul)	Q_{ch} (μcoul)	Q_{dch} (μcoul)	ΔQ_I (μcoul)	Q_{lost} (μcoul)	Q_g (μcoul)
-5	100-110	200	0.025	0.250	0.135	0.115	0.090	0.095
-5	100-110	1000	0.020	0.250	0.055	0.195	0.175	0.150
-5	70-80	200	0.025	0.245	0.120	0.125	0.100	0.085
-5	70-80	1000	0.020	0.245	0.088	0.157	0.137	0.135
-5	50-60	200	0.025	0.235	0.150	0.095	0.070	0.060
-5	50-60	1000	0.020	0.235	0.095	0.140	0.120	0.110
-5	30-40	200	0.025	0.220	0.145	0.075	0.050	0.040
-5	30-40	1000	0.020	0.220	0.115	0.105	0.085	0.100

Consider the power transient curves of Figs. 18 and 19 . Integration under these curves gives the following approximate energies and relative transient efficiencies:

Case	Integration Limit (μ sec)	Energy (μ J)	Transient Efficiency
input, dark	17	0.33	
output, dark	30	0.31	0.94
input, light	15	0.48	
output, light	25	0.14	0.29

From the above table it may be seen that the application of a reverse bias for sufficient time to adequately charge the junction capacitance leads to an overall loss of energy compared to no application of reverse bias. Accounting for the incident photon energy not converted into electrical energy during the charging cycle will result in a further loss in overall energy conversion. That is, not only is the charging energy only partially recovered, but the opportunity is lost for energy conversion during charging. Aside from small "inherent" losses, and even with a shortened charging cycle, the momentary reverse bias will not result in an overall increase in energy conversion. This is because the photo-generated current in the depletion region of the junction decreases the recoverable stored energy by an amount greater than any possible increase in conversion efficiency due to the enhanced field across the junction.

Conclusions

Photo-generated current in the depletion region of the junction in a solar cell shortens the transient decay by as much as a factor of 5 from an initial condition of externally-imposed reverse bias to normal

photovoltage forward bias. This effect eliminates the possibility of an increase in energy conversion efficiency by momentary application of reverse bias to enhance the electron-hole collection efficiency.

REFERENCES

1. Shockley, W., Electrons and Holes in Semiconductors, D. Van Nostrand Company, Inc., New Jersey, 1950.

2. Steele, Earl L., "Charge Storage in Junction Diodes", Journal of Applied Physics, 25, 7, pp. 916-918, 1954.

3. Queisser, H. J., "Forward Characteristics and Efficiencies of Silicon Solar Cells", Solid-State Electronics, 5, pp. 1-10, 1962.

4. Tauc, J., Photo and Thermoelectric Effects in Semiconductors, Pergamon Press, New York, 1962.

5. Shockley, W. and Queisser, H. J., "Detailed Balance Limit of Efficiency of p-n Junction Solar Cells", Journal of Applied Physics, 32, 510, 1961.

6. Angrist, S. W., Direct Energy Conversion, Allyn and Bacon, Inc., Boston, 1965.

7. Ko, W. H., "The Forward Transient Behavior of Semiconductor Junction Diodes", Solid-State Electronics, 3, pp. 59-69, 1961.

8. Hartman, T. E., "Transient Photovoltaic Response of Diffused-Junction Silicon Photodiodes", Solid-State Electronics, 3, pp. 127-133, 1961.

9. Gossick, B. R., "On the Transient Behavior of Semiconductor Rectifiers", Journal of Applied Physics, 26, 11, pp. 1356-1365, 1955.

10. Jones, N. T., Kingston, R. H., and Neustadter, S. F., "Anomalous Forward Switching Transient in p-n Junction Diodes", Journal of Applied Physics, 26, 2, pp. 210-213, 1955.

11. Ko, W. H., "The Reverse Transient Behavior of Semiconductor Junction Diodes", IRE Transactions on Electron Devices, Vol. ED-8, pp. 123-131, March 1961.

12. Armstrong, H. L., "On the Switching Transient in the Forward Conduction of Semiconductor Diodes", IRE Transactions on Electron Devices, Vol. ED-4, pp. 111-113, April 1957.

13. Kano, K., and Reich, H. J., "Forward Transient Behavior of P-N Junction Diodes at High Injection Levels", IRE Transactions on Electron Devices, Vol. ED-11, pp. 515-523, Nov. 1965.

14. Lax, B. and Neustadter, S. F., "Transient Response of a p-n Junction", Journal of Applied Physics, 25, 9, pp. 1148-1154, 1954.

15. Shulman, R. G. and McMahon, M. E., "Recovery Currents in Germanium p-n Junction Diodes", Journal of Applied Physics, 24, 10, pp. 1267-1272, 1953.

16. Fink, H. J., "Reverse Recovery Time Measurements of Epitaxial Silicon p-n Junctions at Low Temperatures", Solid-State Electronics, 7, pp. 823-831, 1964.

17. Chang, Y. F., "Switch-On Transients in p-n Junctions", Journal of Applied Physics, 34, 7, pp. 2056-2060, 1963.

18. Dorn, C. G., "Forward Transients in Point Contact Diodes", IRE Transactions on Electron Devices, Vol. ED-3, pp. 153-156, July 1956.

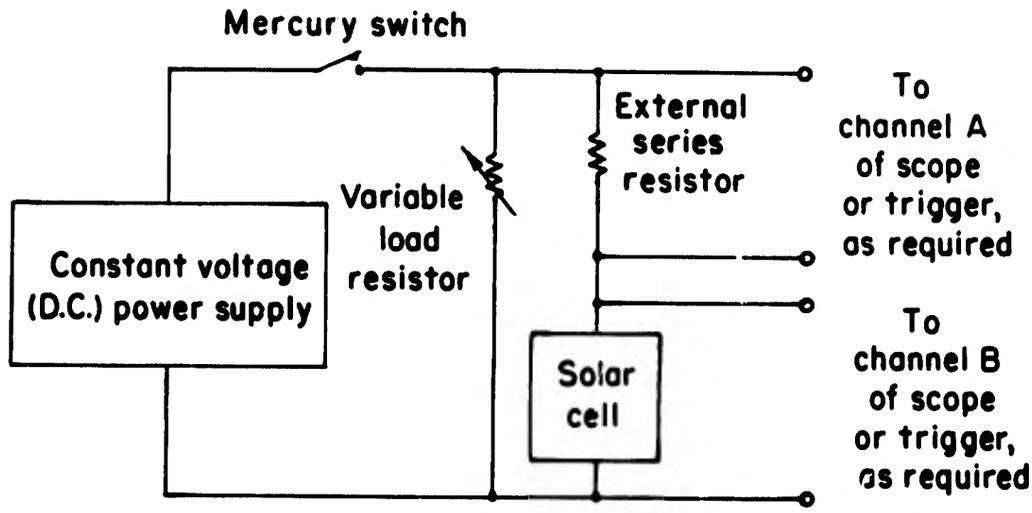

Fig. 1. Transient Response Circuitry.

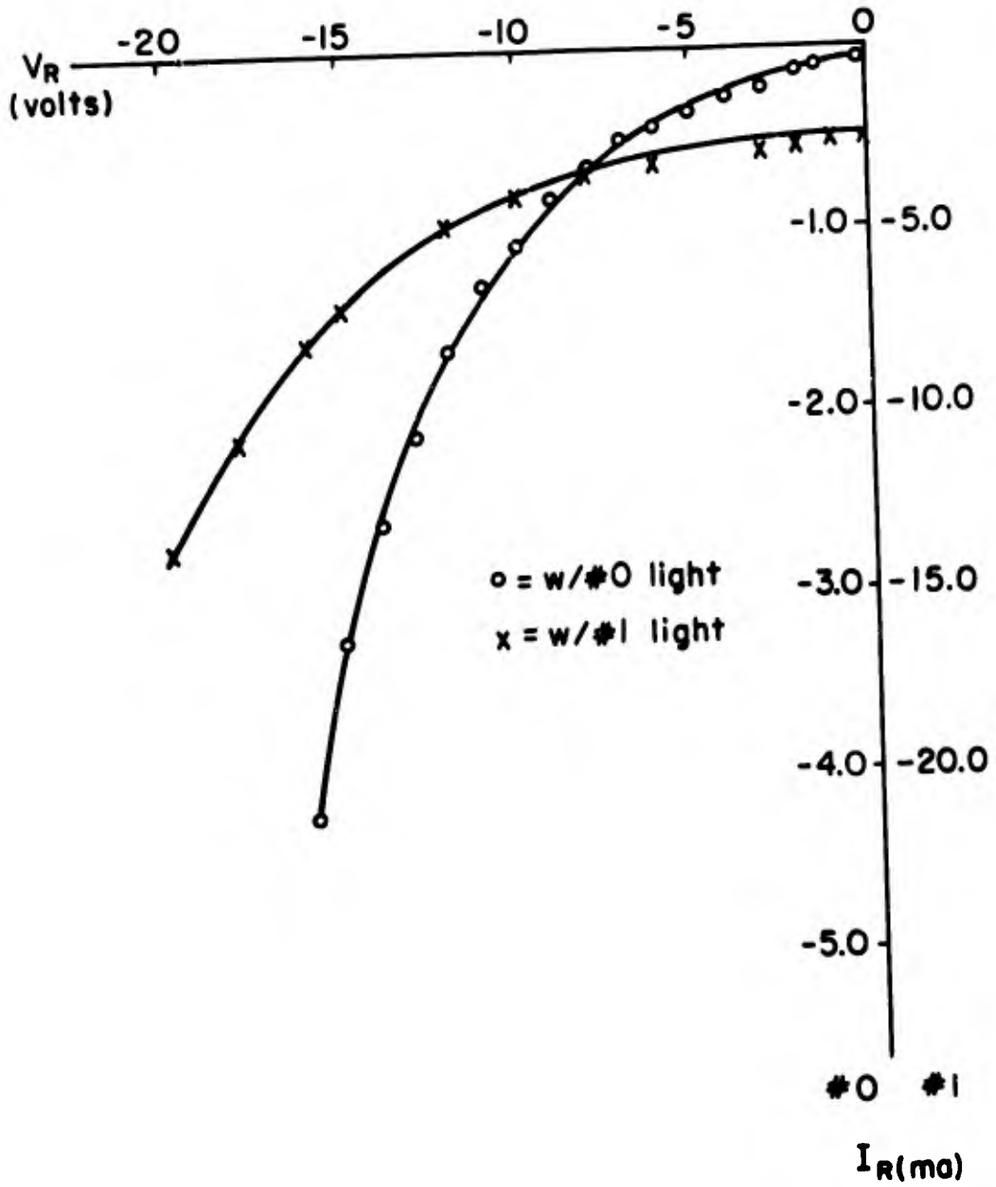

Fig. 2. Reverse I-V Characteristics for Solar Cell #E.

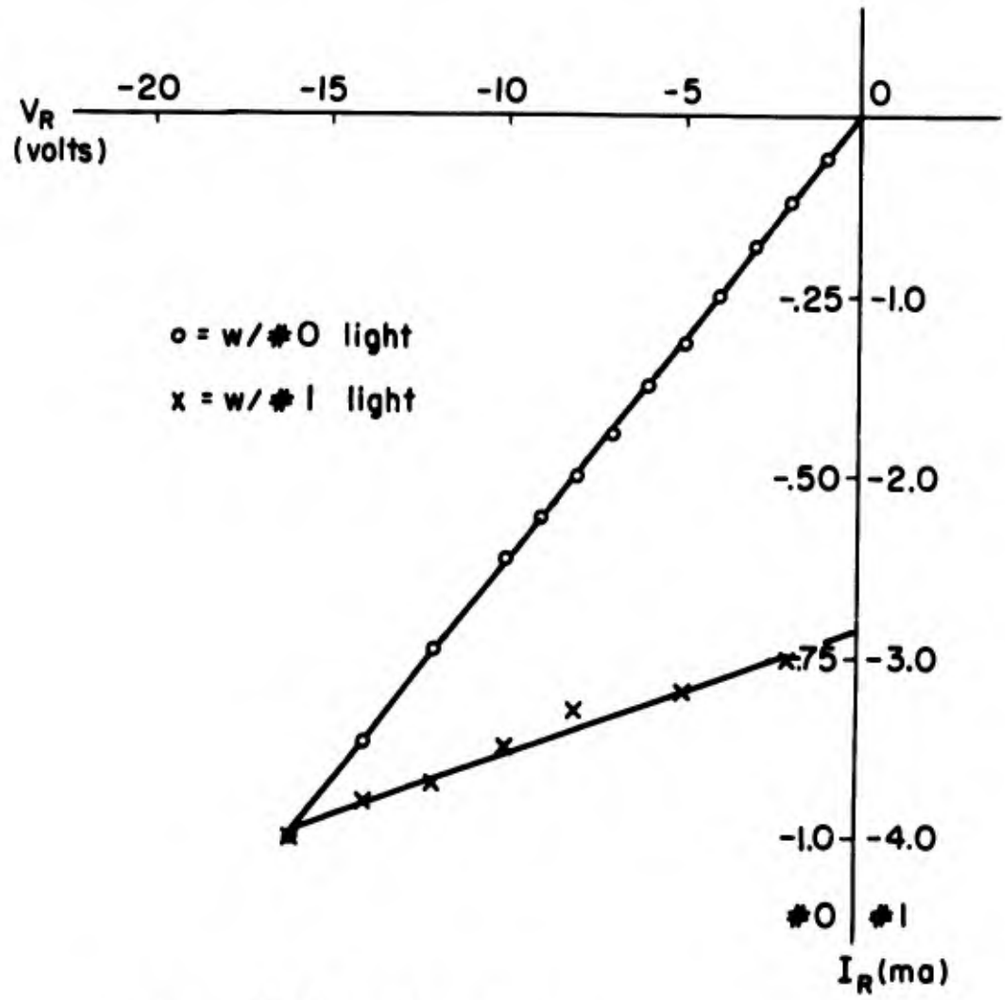

$$\frac{1}{\text{Slope}} = \frac{16-0}{1-0} \times 10^3 = 16\text{k ohms}$$

$$\frac{1}{\text{Slope}} = \frac{16-2}{4-3} \times 10^3 = 14\text{k ohms}$$

Fig. 3. Reverse I-V Characteristics for Solar Cell L-22.

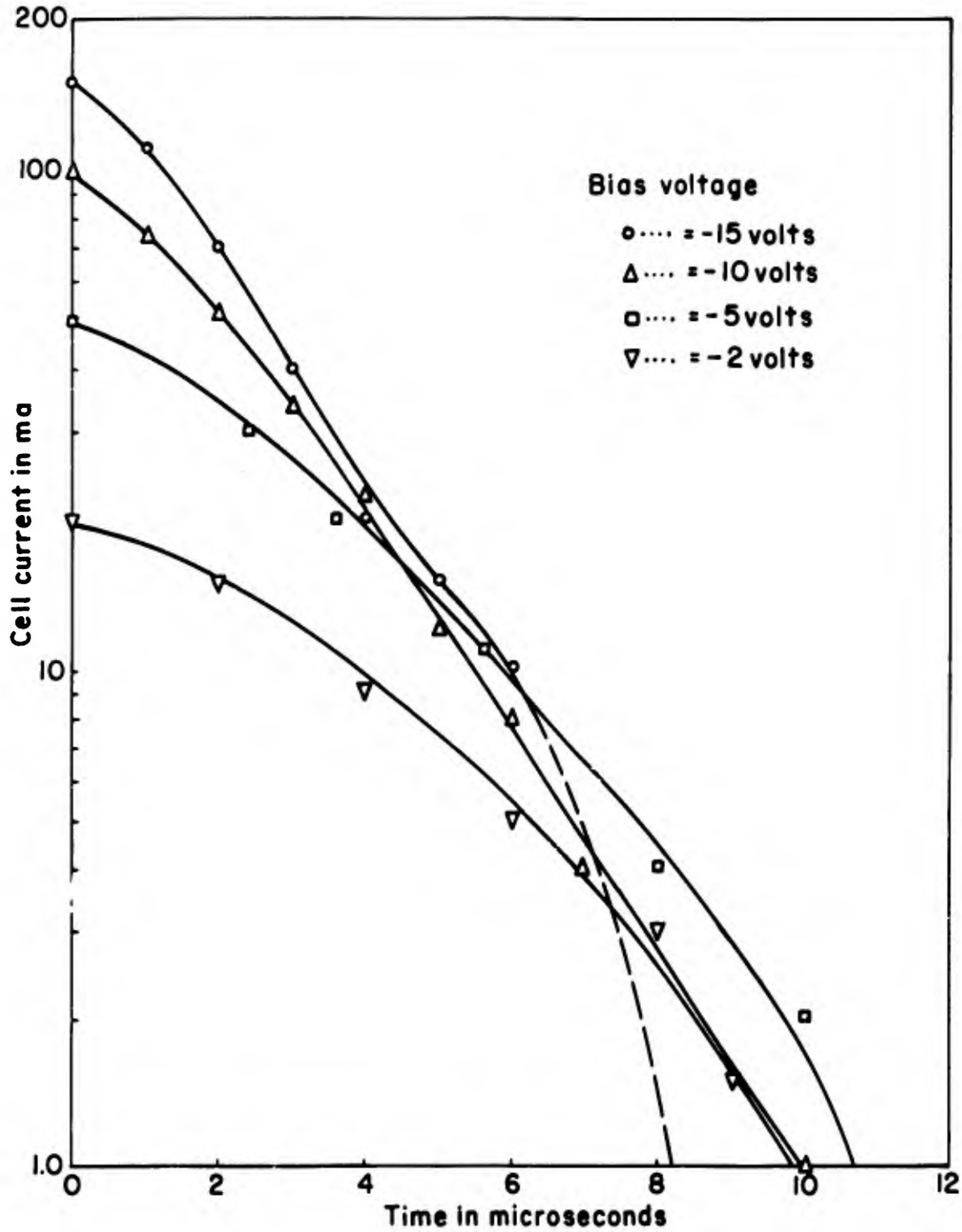

Fig. 4. Charging Transient Current vs. Time. Cell #E. Dark (#0 Light).

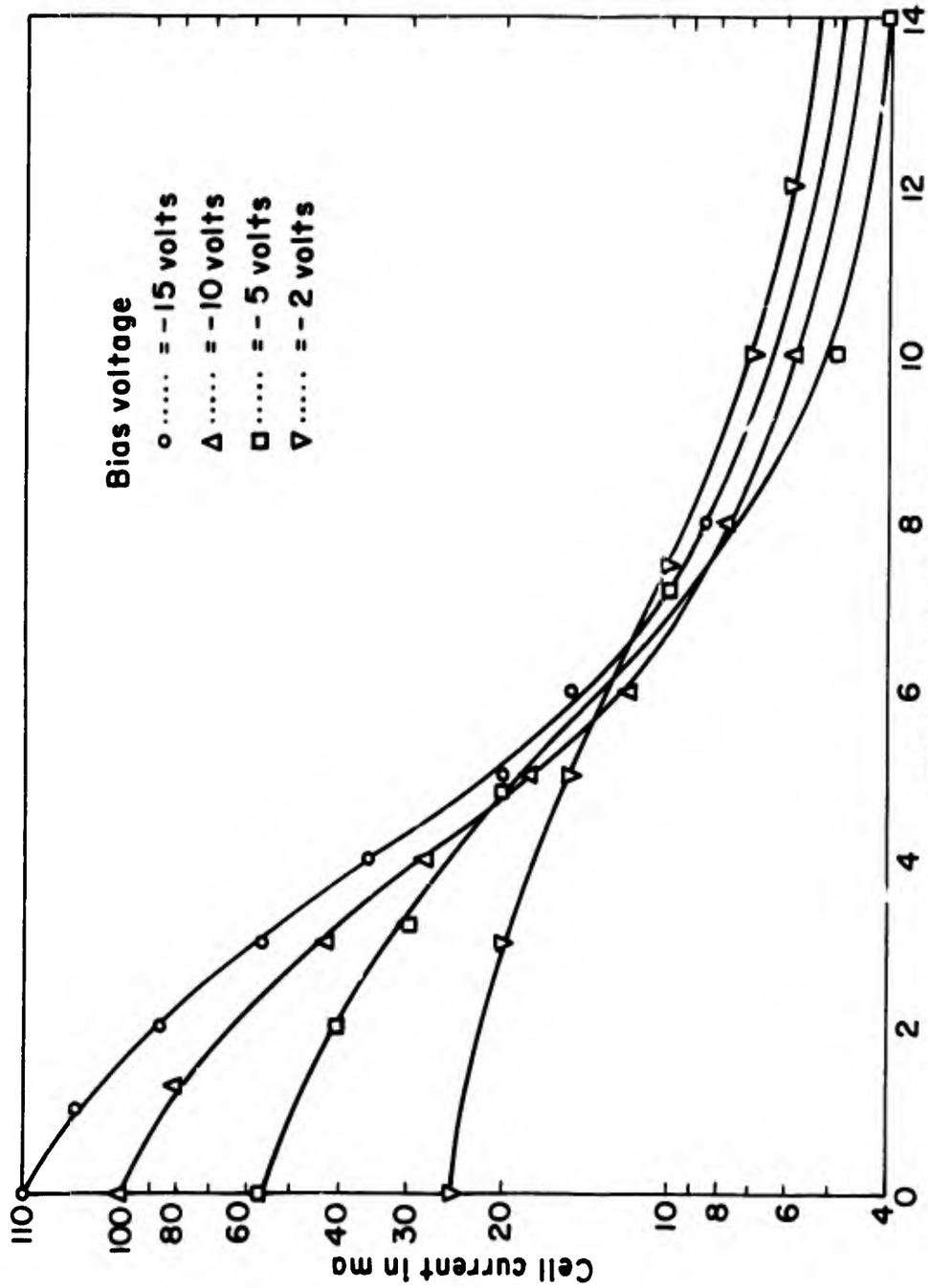

Fig. 5. Charging Transient Current vs. Time. Cell #E. 100 Foot-Candles, Tungsten (#1 Light).

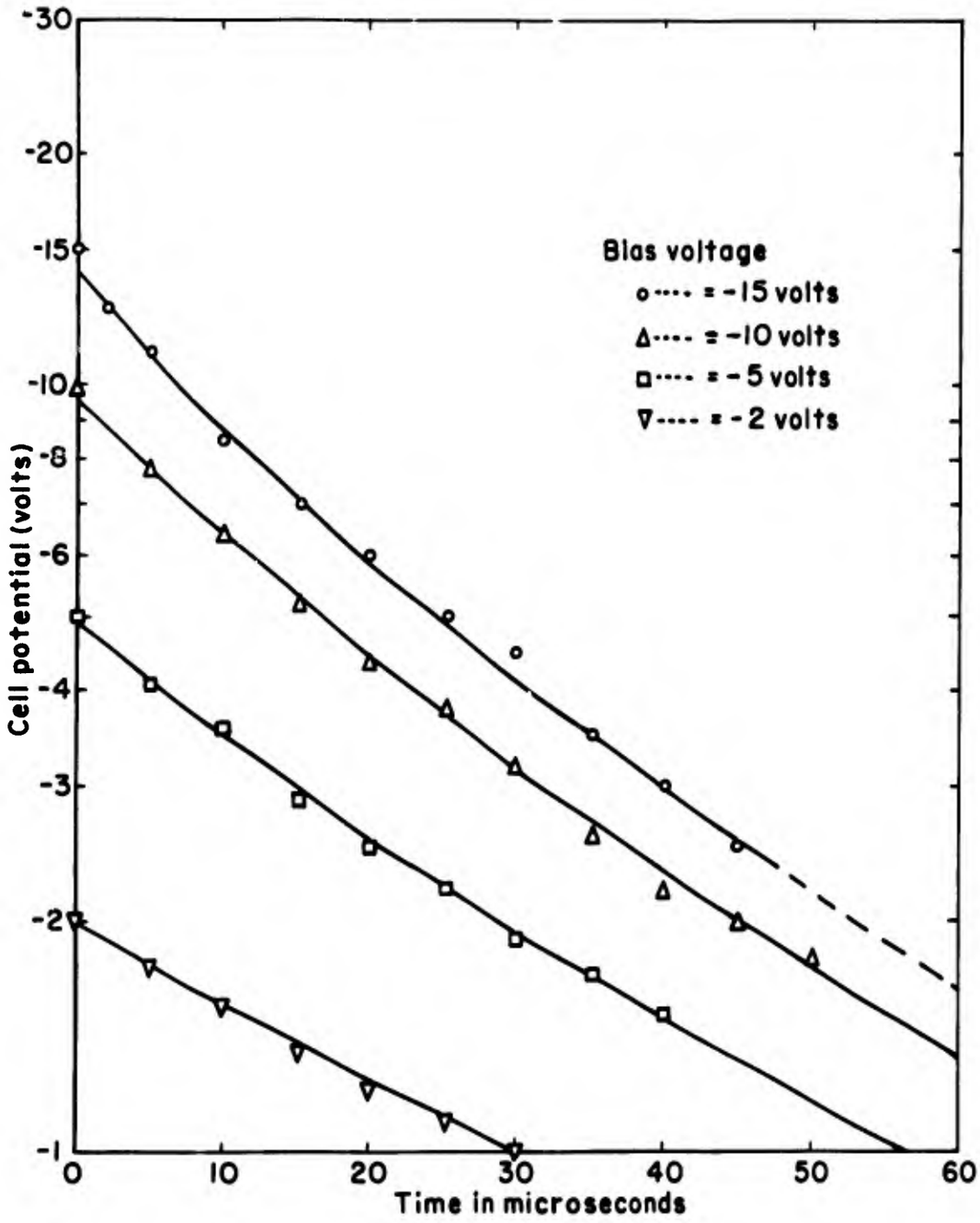

Fig. 6. Discharging Transient Voltage vs. Time.
Cell #E. R_L = 1000 ohms. Dark.

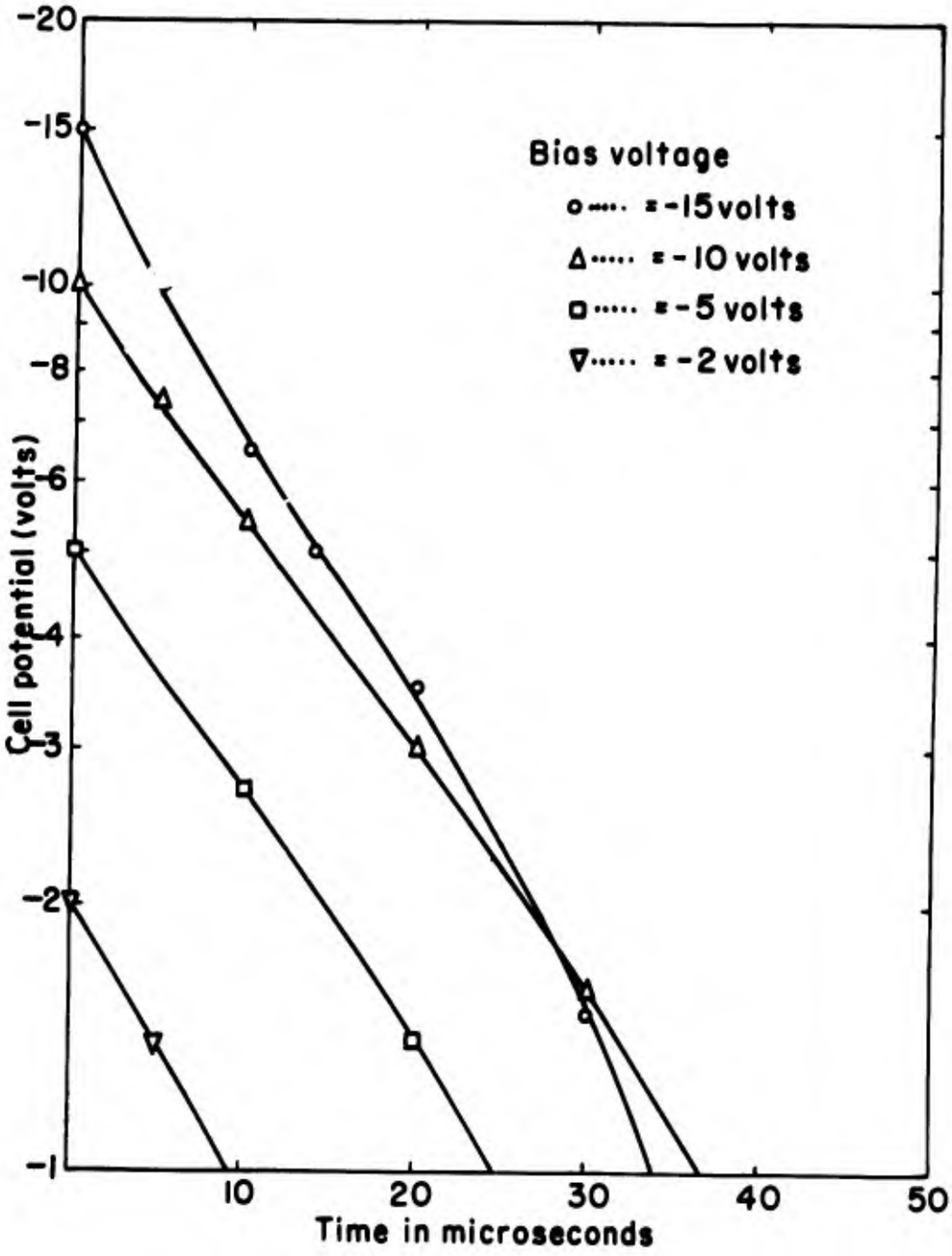

Fig. 7. Discharging Transient Voltage vs. Time. Cell #E. R_L = 1000 ohms. #1 Light.

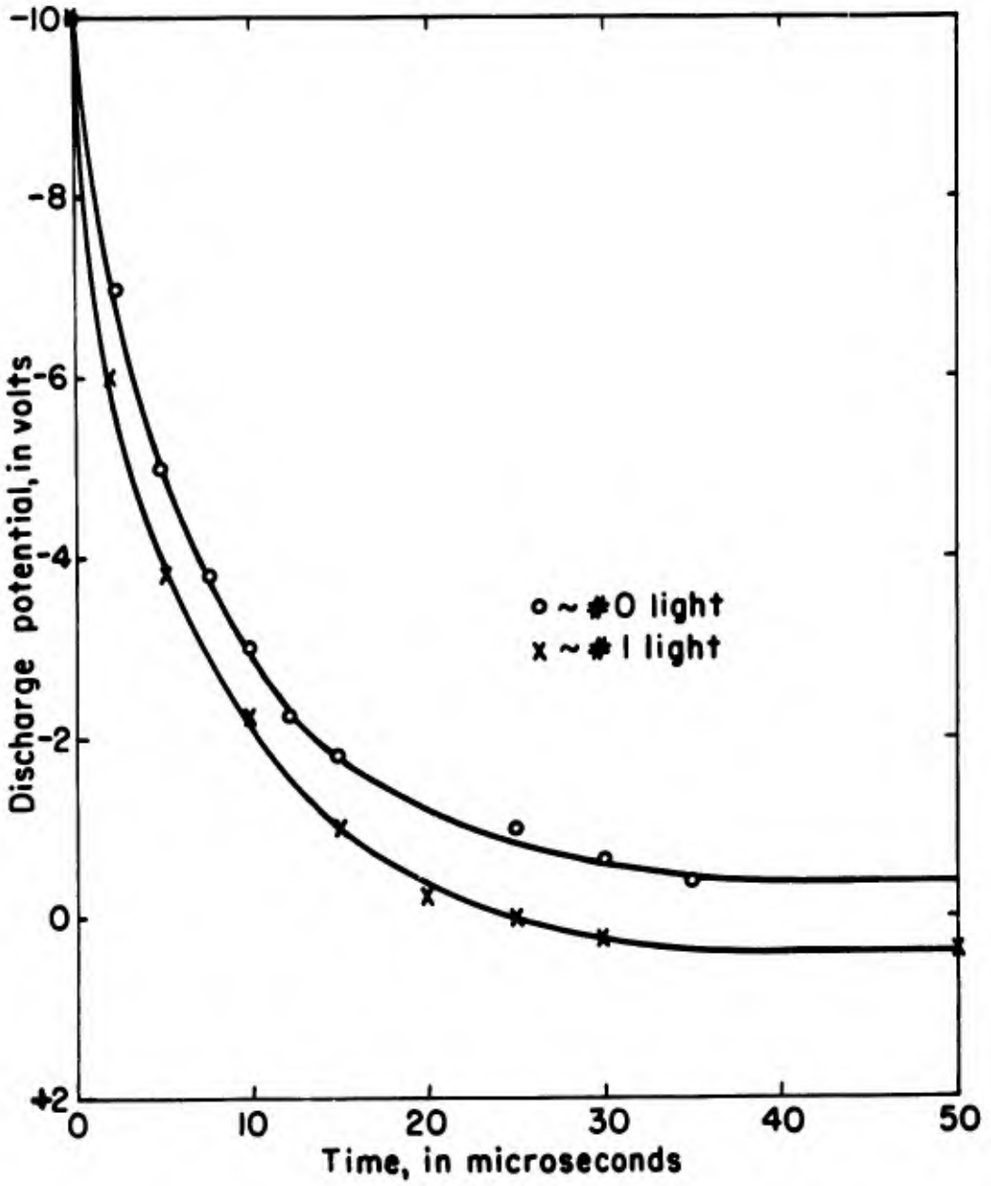

Fig. 8. Discharging Transient Voltage vs. Time. Cell #E. R_L = 200 ohms. Reverse Bias of -10 Volts.

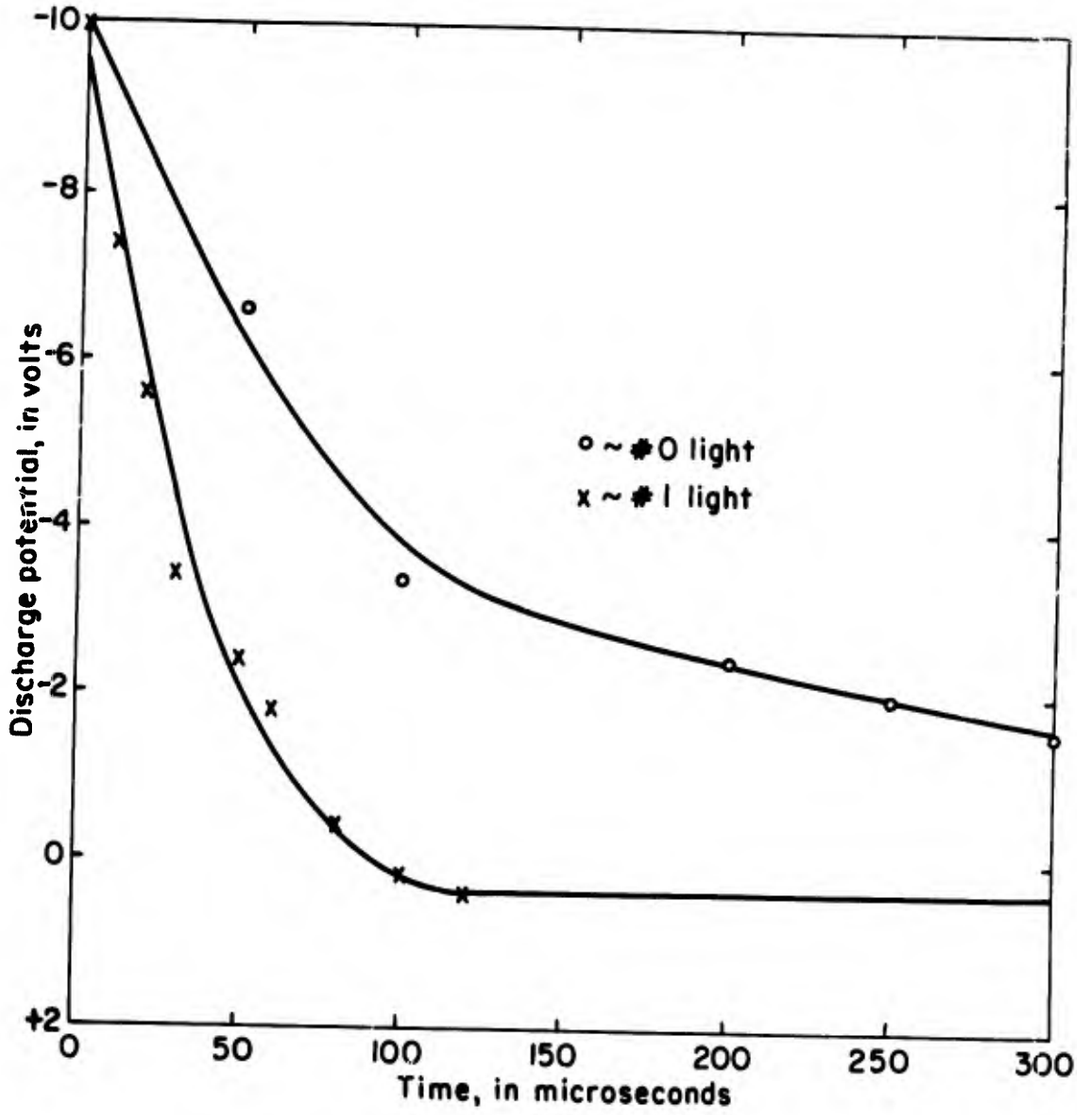

Fig. 9. Discharging Transient Voltage vs. Time. Cell #E. R_L = 10,000 ohms. Reverse Bias of -10 Volts.

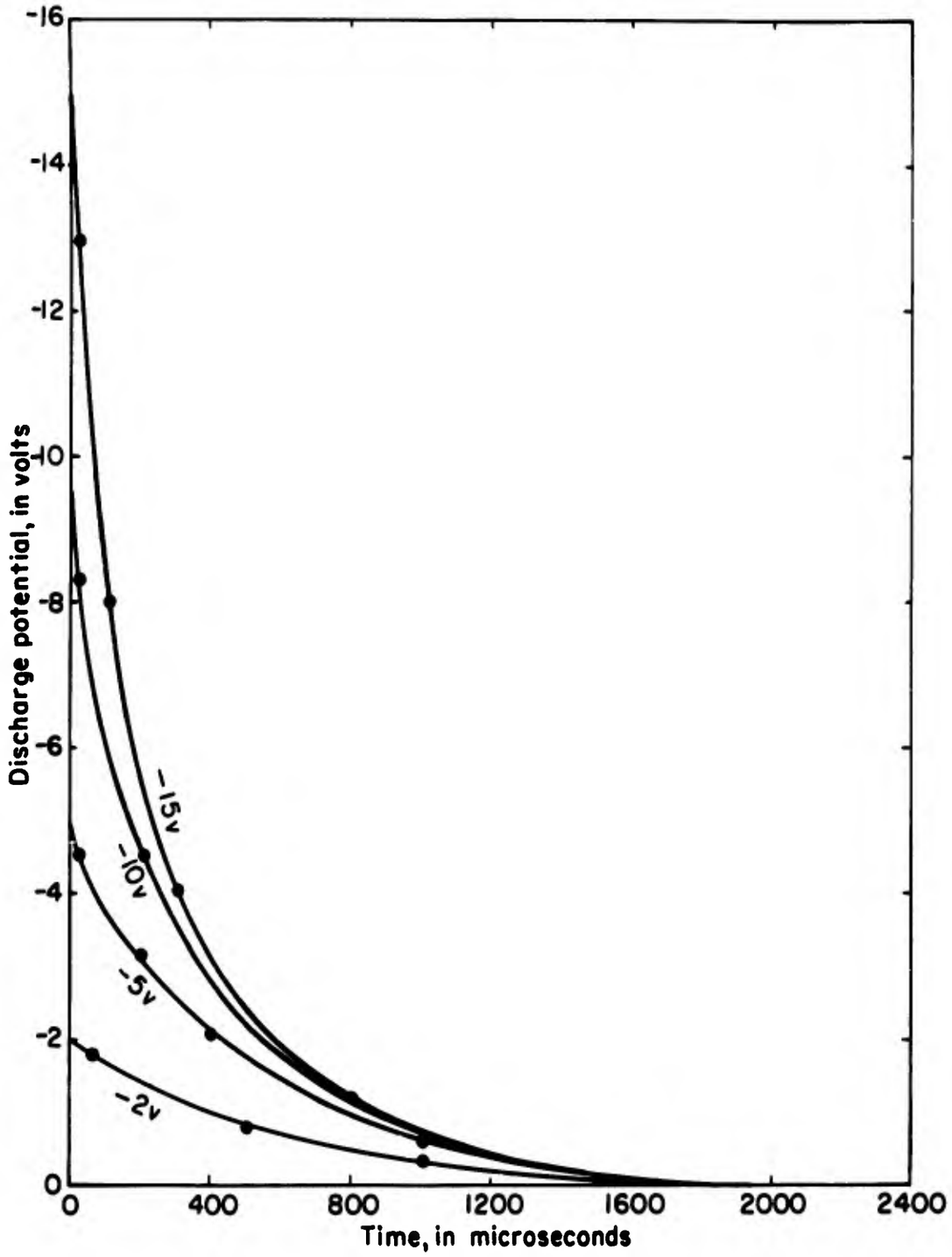

Fig. 10. Discharging Transient Voltage vs. Time.
Cell #E. No-Load (Open-Circuit). Dark.

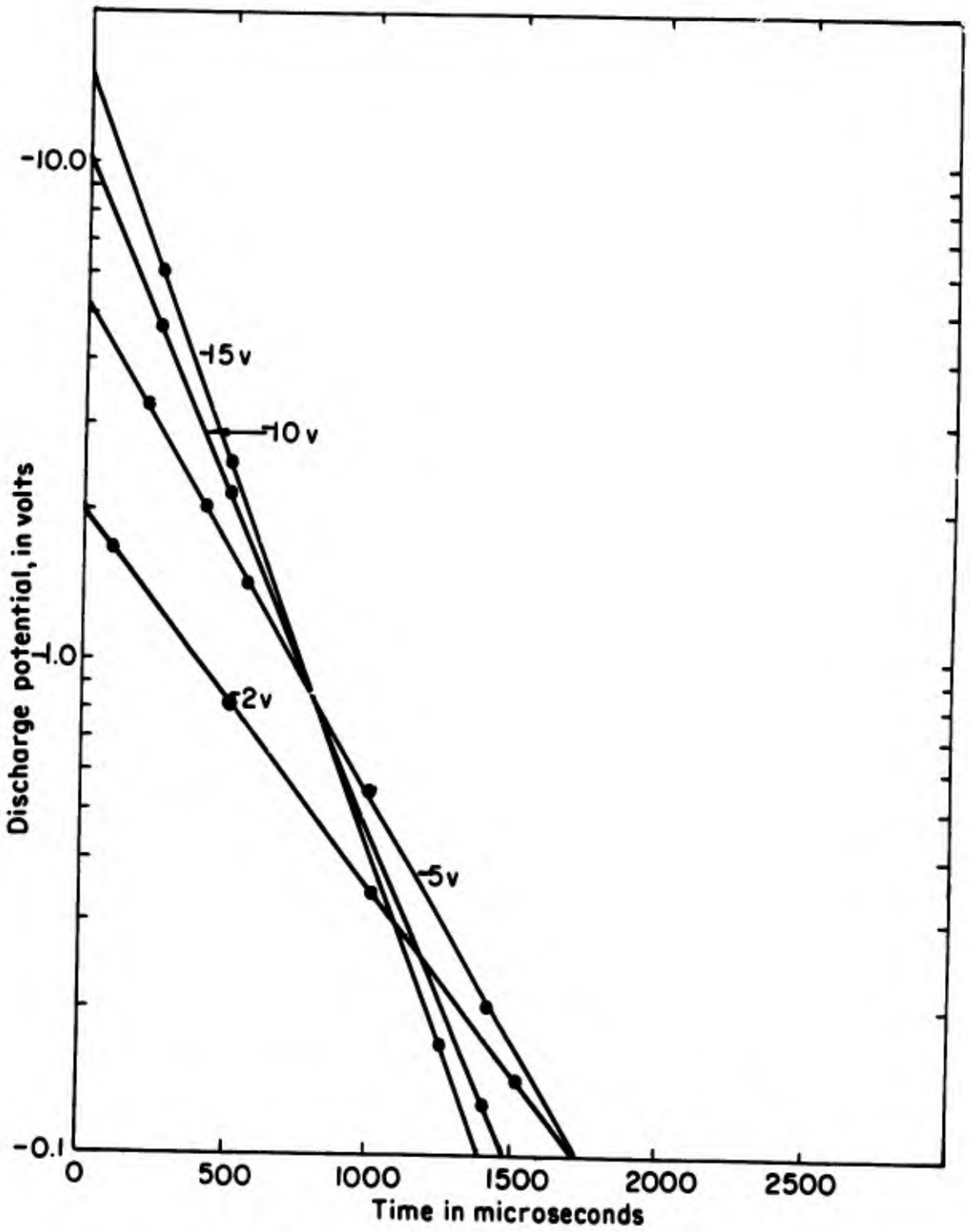

Fig. 11. Discharging Transient Voltage vs. Time. Cell #E. No-Load (Open-Circuit). Dark.

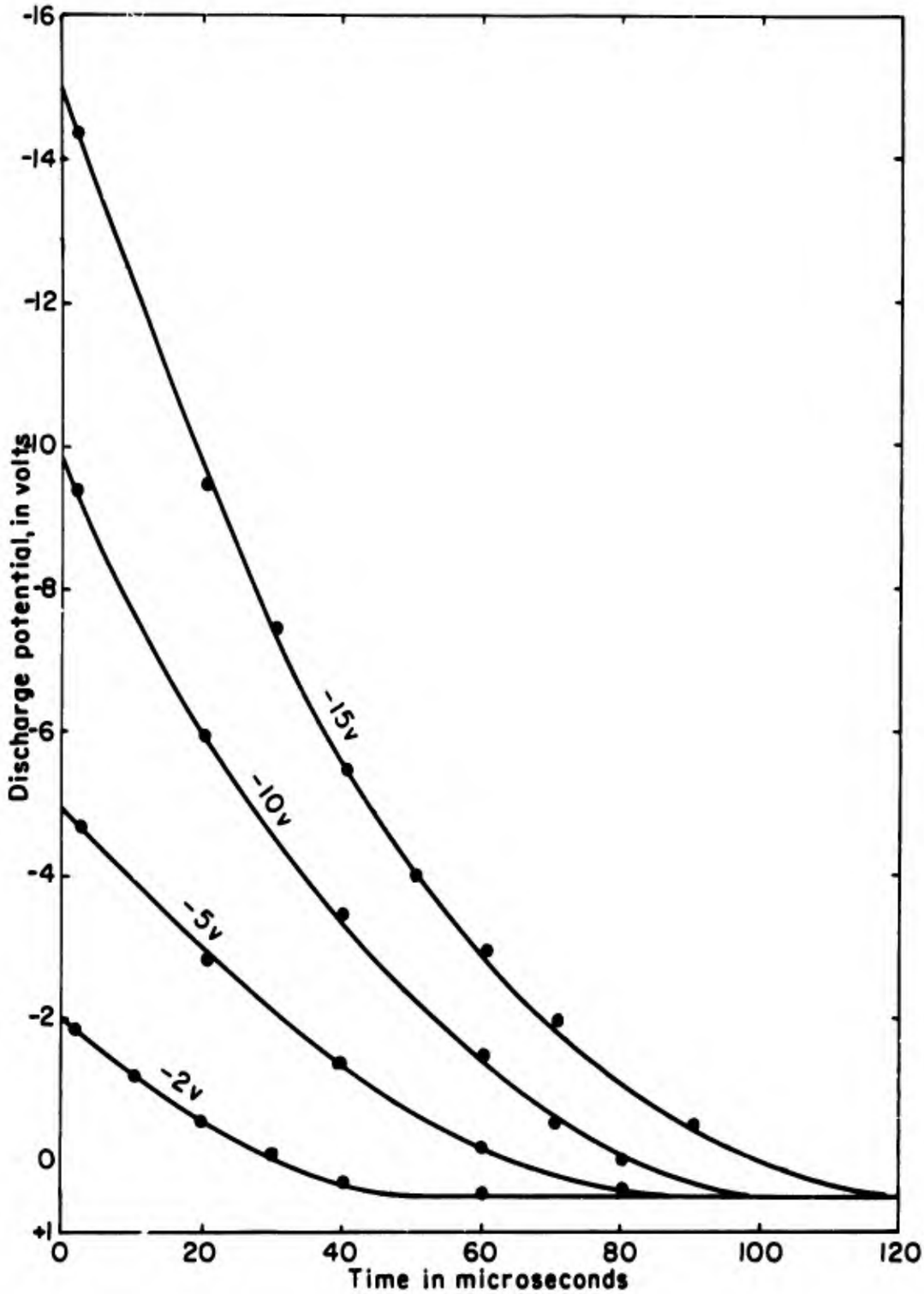

Fig. 12. Discharging Transient Voltage vs. Time. Cell #E. No-Load (Open-Circuit). #1 Light.

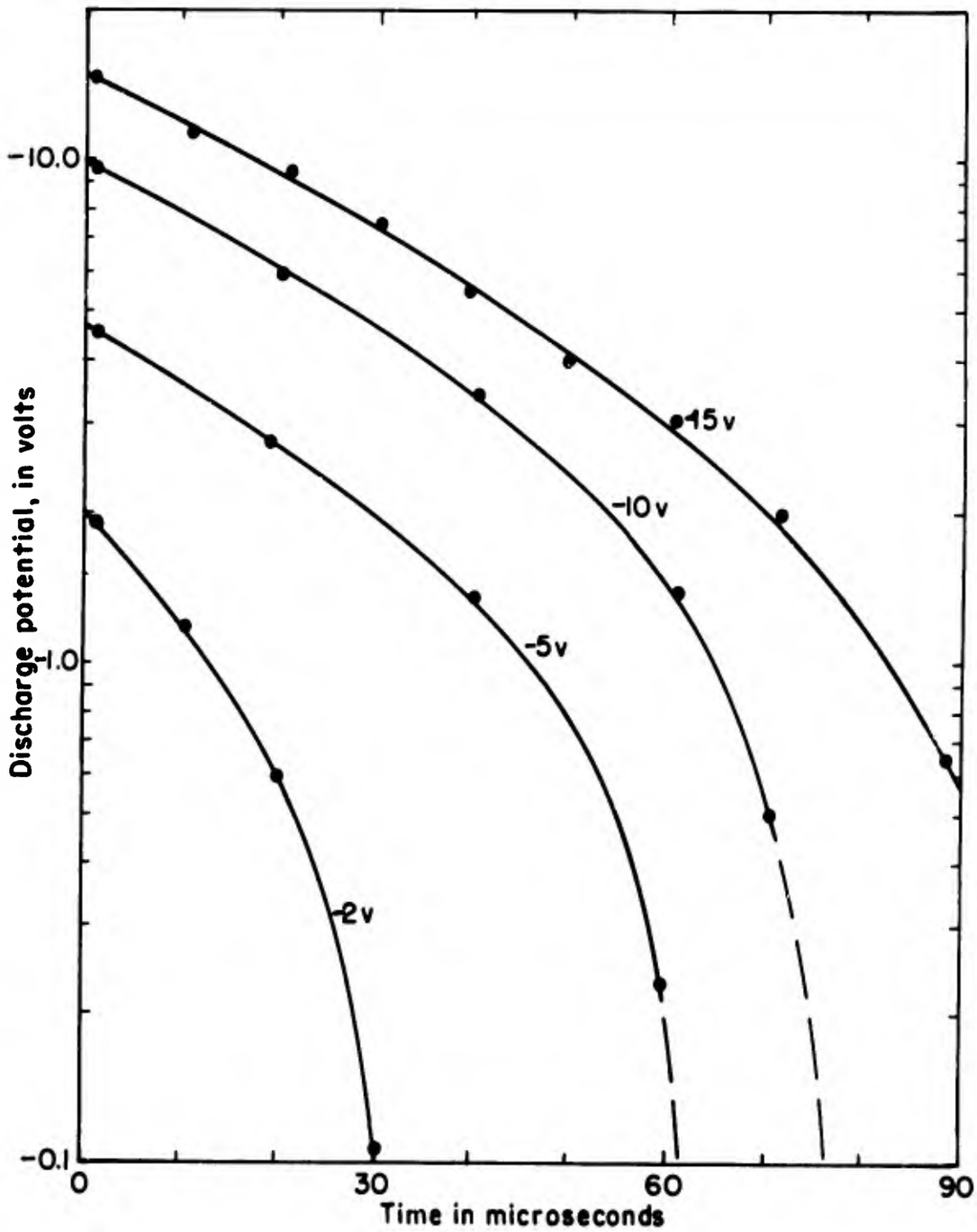

Fig. 13. Discharging Transient Voltage vs. Time. Ceil #E. No-Load (Open-Circuit). #1 Light.

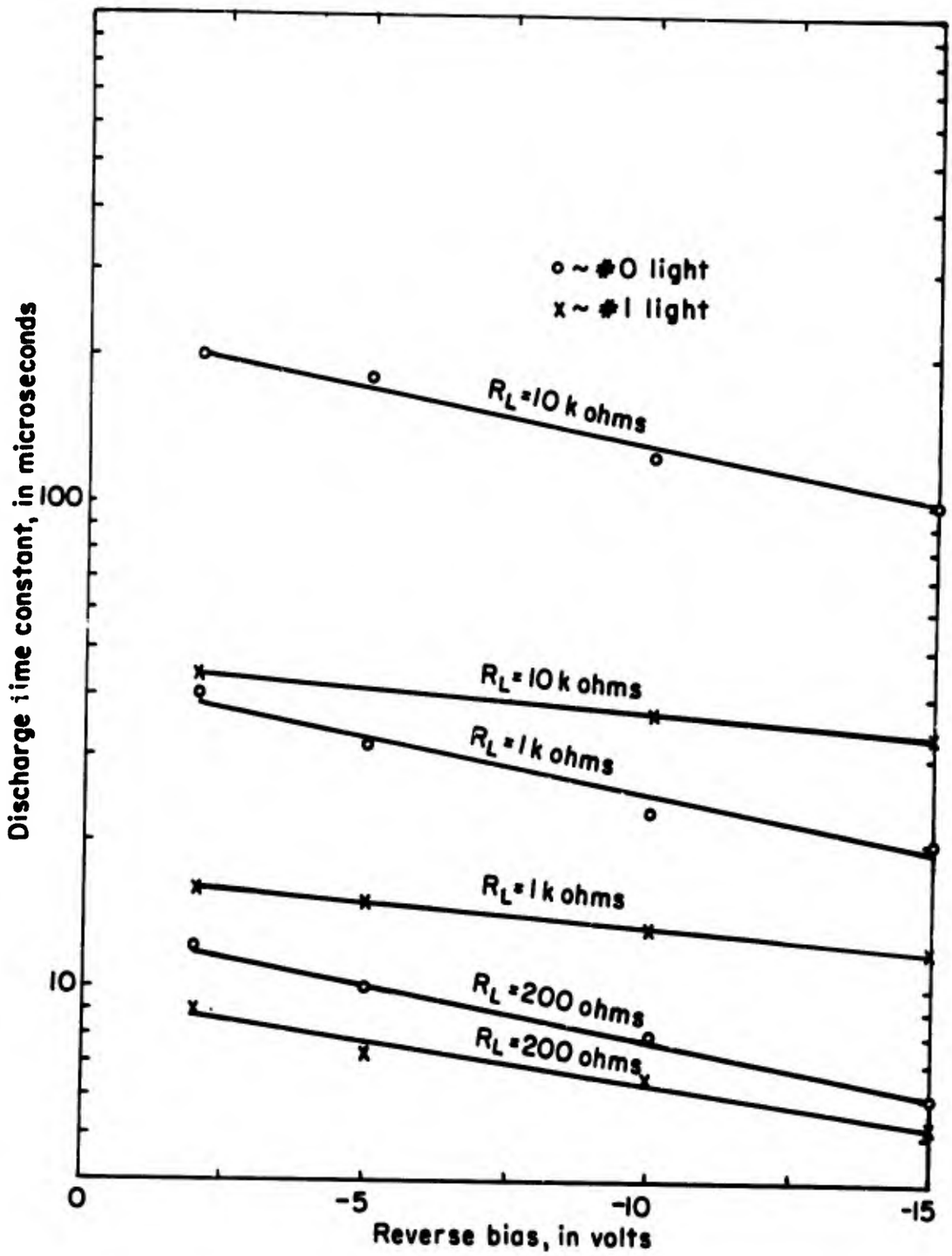

Fig. 14. Transient Discharge Time Constant vs. Reverse Bias. Cell #E.

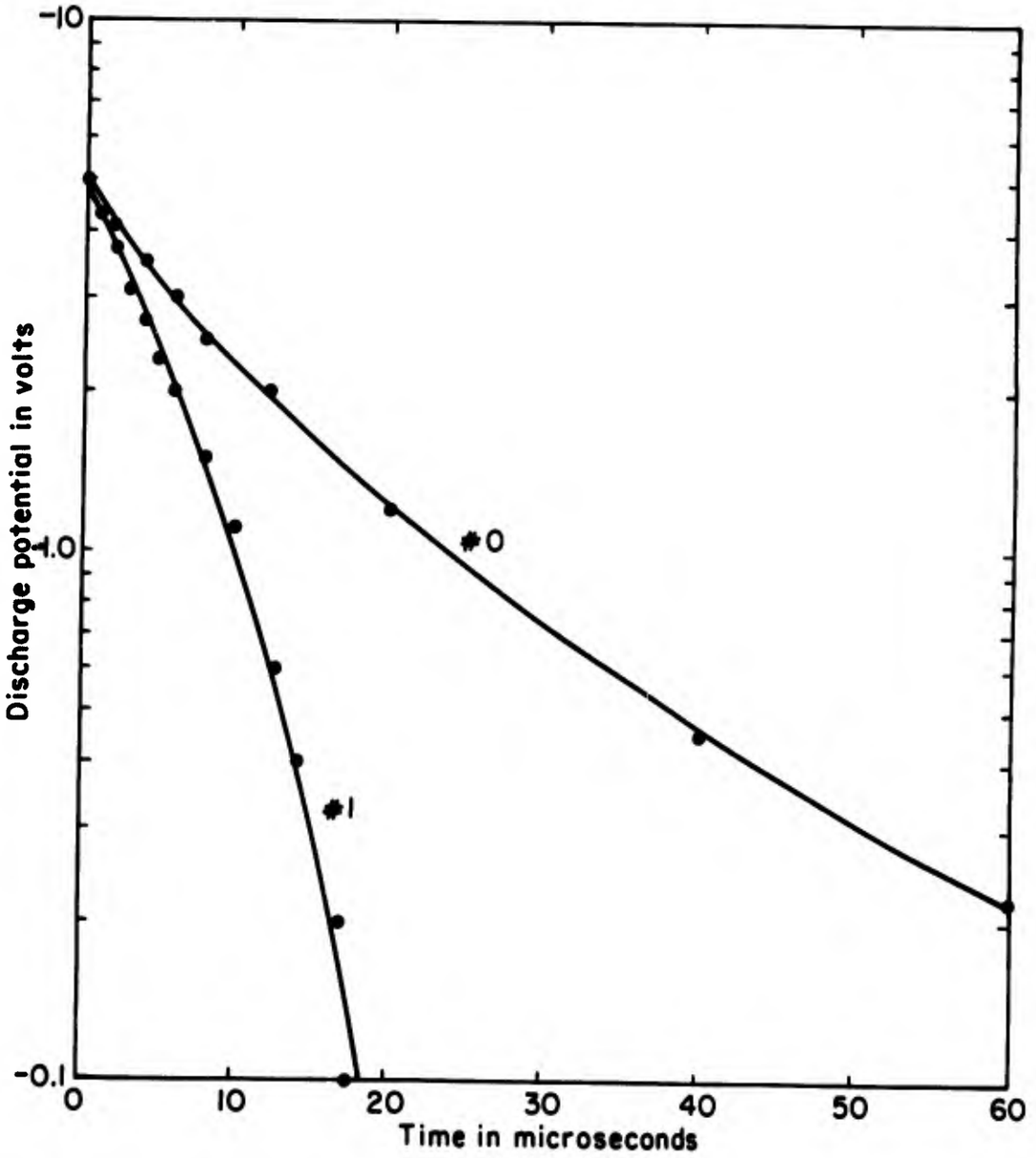

Fig. 15. Discharging Transient Voltage vs. Time. Cell L-22. R_L = 1000 ohms. Reverse Bias of 5 Volts.

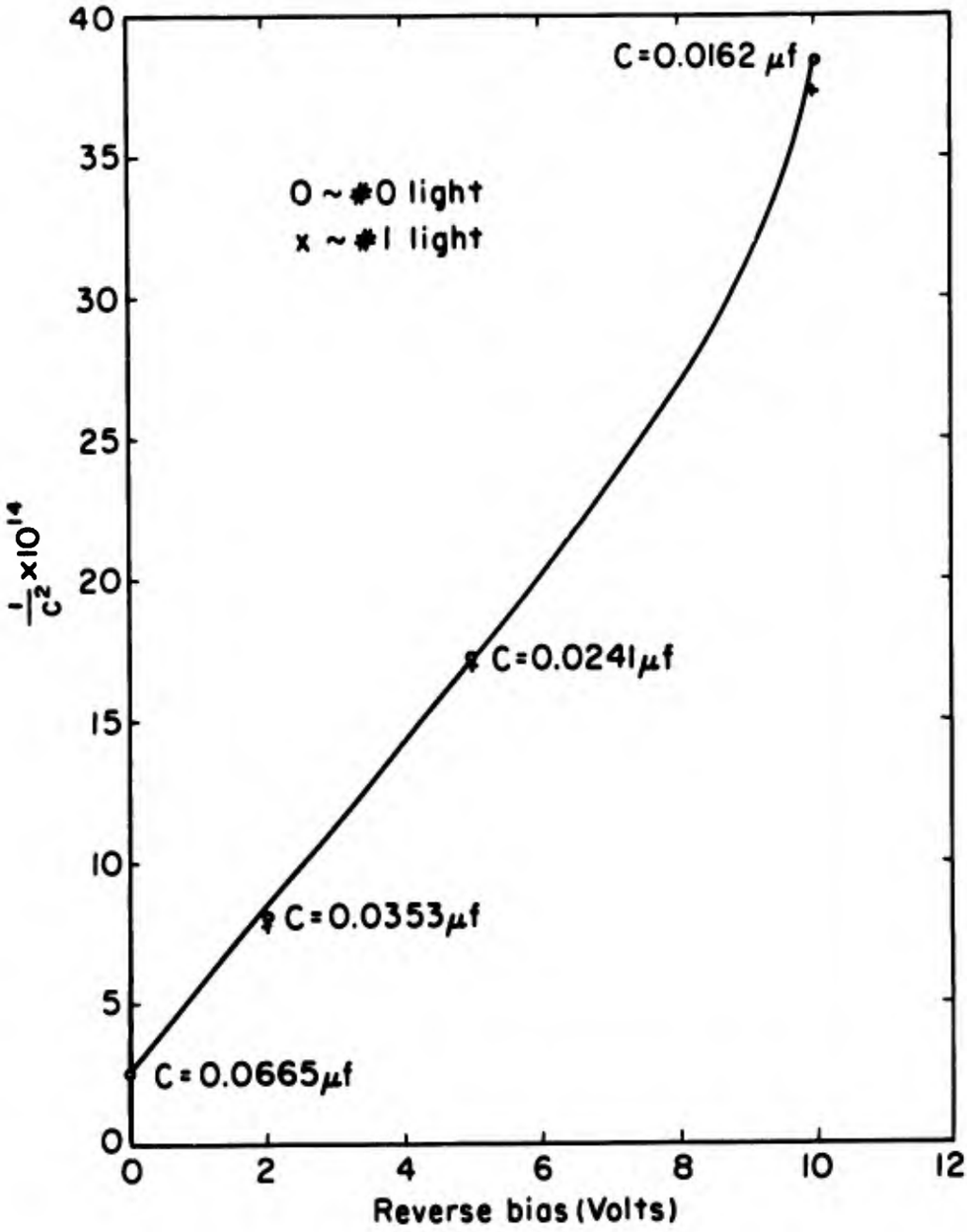

Fig. 16. Junction Capacitance Dependence Upon Reverse Bias. Cell #E.

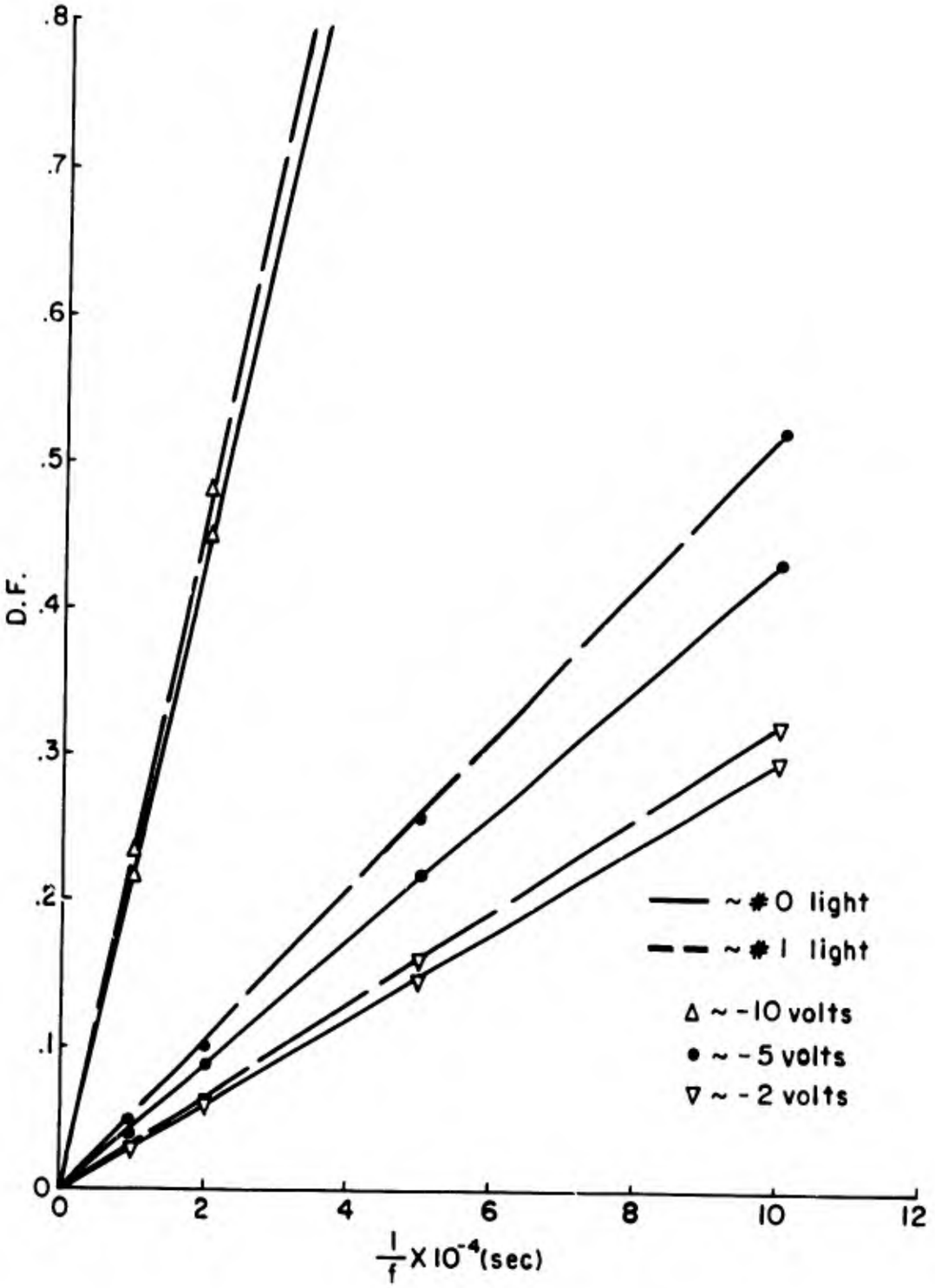

Fig. 17. Dissipation Factor vs. Reciprocal Frequency. Cell #E.

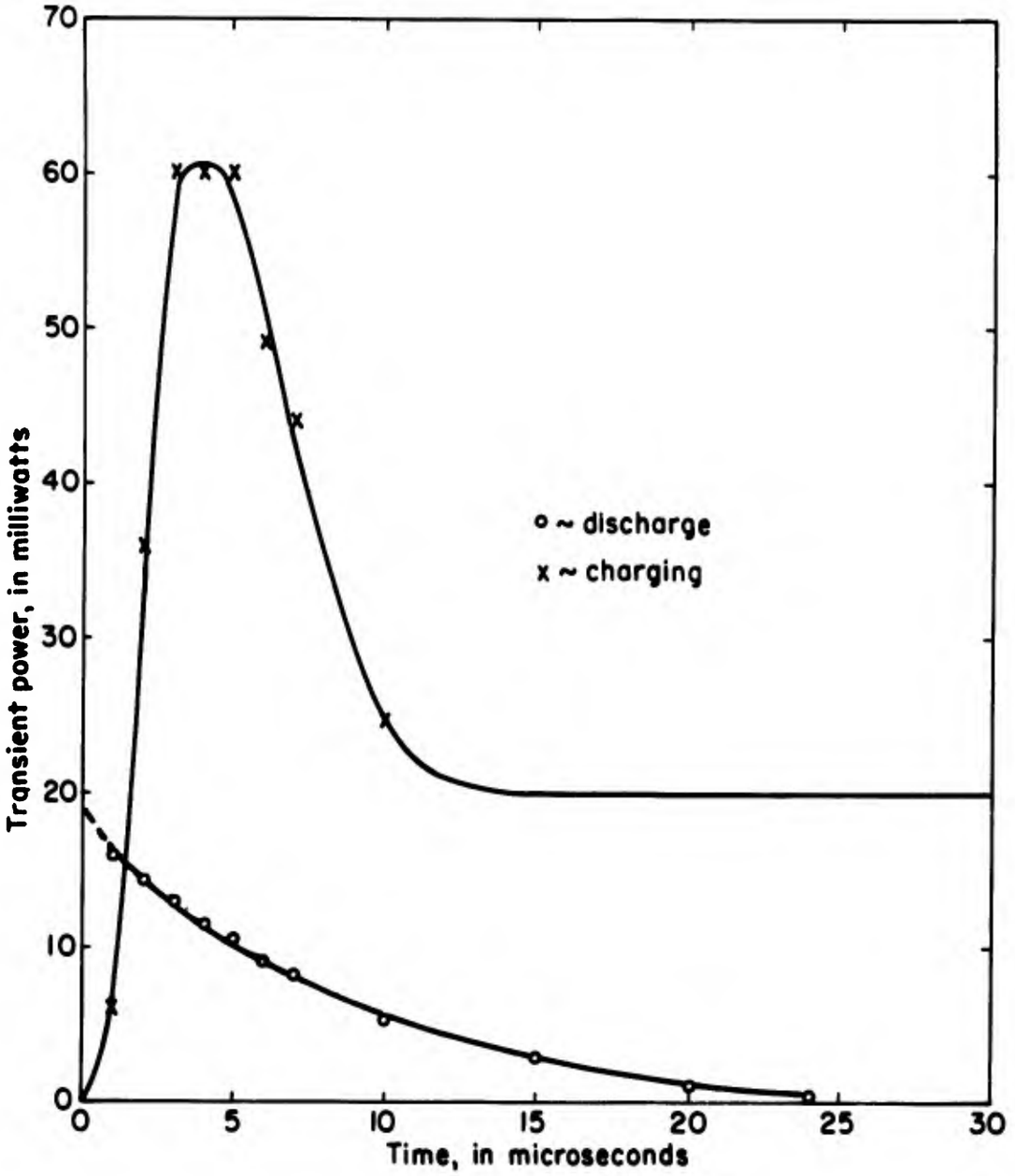

Fig. 18. Transient Power vs. Time. Cell #E.
R_L = 1000 ohms. Reverse Bias of -5 Volts.
#1 Light.

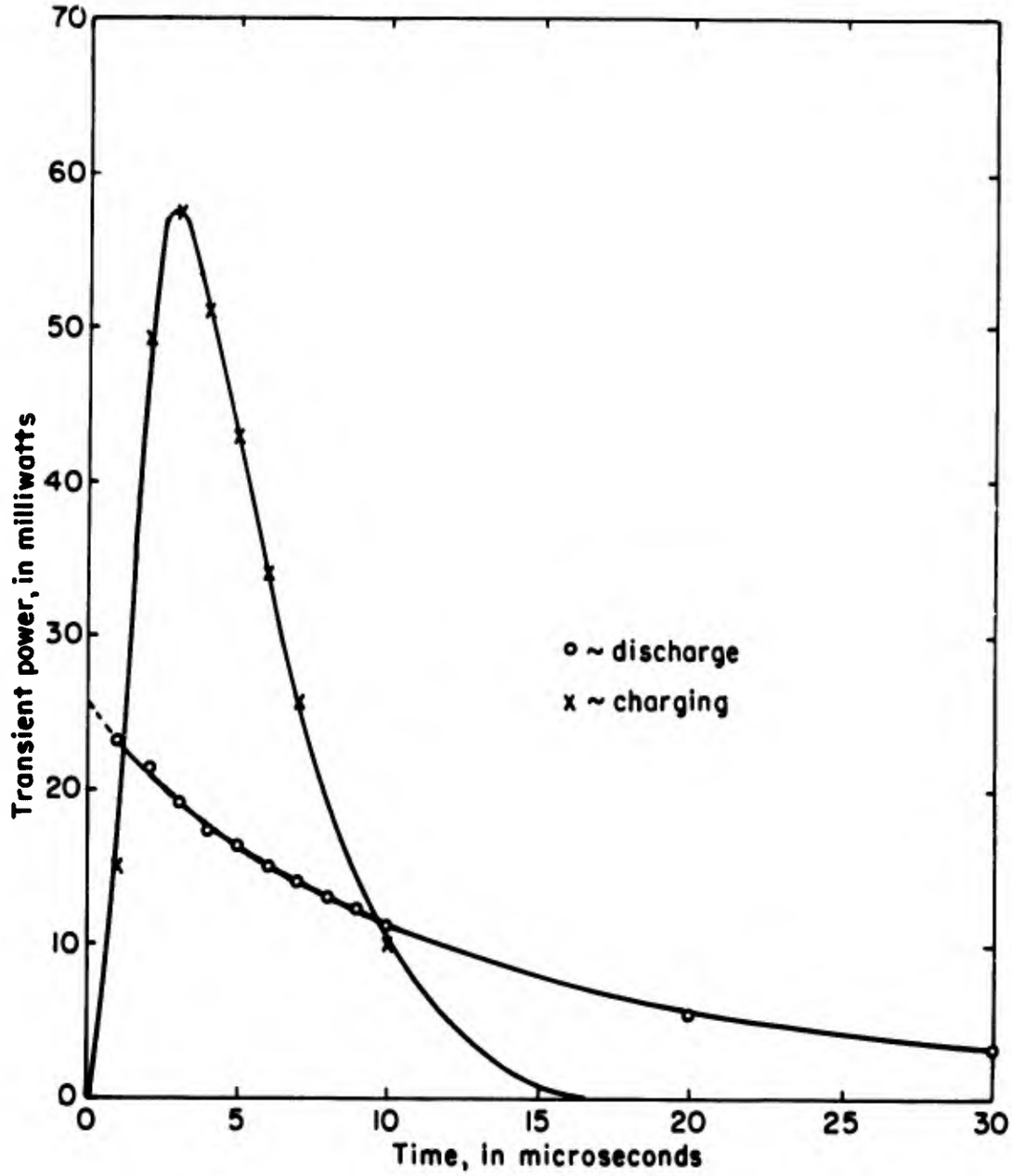

Fig. 19. Transient Power vs. Time. Cell #E.
R_L = 1000 ohms. Reverse Bias of -5 Volts.
Dark.

5. ELECTRIC-FIELD EFFECTS ON DIFFUSION IN SILICON*

Introduction

A study is being made of the effects of an electric field on diffusion in semiconductors. There is a possibility that p-n junction profiles may be altered to obtain slightly larger energy conversion efficiencies in solar cells than are achieved by ordinary diffusion techniques.

Results of Literature Survey

Numerous studies have been made of the diffusion of impurities in semiconductors. Discrepancies in the results have often been left unexplained or attributed to experimental error. It has usually been assumed that the diffusion rate is governed by Fick's laws, without consideration of dependence on concentration, compound formation, or electric fields generated during diffusion of charged impurities.

Zaromb[1], by use of Onsager's equations for isothermal diffusion, demonstrated that interactions between donors and acceptors, particularly covalent compound formation may have significant effects on impurity diffusion. Millea[2] found that the diffusion coefficients for phosphorus and antimony are twice as large in n-type as in pure silicon and half as large in p-type as in pure silicon. Rates of diffusion in semiconductors are increased by the presence of another impurity of like charge and decreased when the second impurity carries opposite charge. Examining the effects of the internal field generated during diffusion, Lehovec and

---

* Partially supported by AF19(628)-3836

Slobodskoy[3] considered the field to be proportional to the gradient of impurity concentration and represented the field current as an additional diffusion current. Solutions of their differential equation which included a concentration-dependent diffusion coefficient yielded results different from those of the usual complementary-error-function solution.

Vas'kin et al[4] theoretically analyzed the internal field on the basis of an approximate solution of the diffusion equation, including the electric field term, with the aid of the Poisson equation. After investigation of impurity distribution for various levels of doping, it was found that the erfc law is valid only in the case where the original homogenous concentration of donors or acceptors (before diffusion process) is much less than the intrinsic electron-hole concentration. If the concentration is higher, the effect of the internal electric field is important and the erfc law can not be used.

In a further analysis of the "build-in" field Klein and Beale[5] made use of a modified diffusion coefficient which included the impurity and intrinsic carrier concentrations. Results showed that a considerable modification of diffusion profiles can be caused by the field when donors and acceptors are diffusing simultaneously. The modification is greatest when a slow-moving impurity is present in excess of a faster one. They demonstrated that the erfc law yields a good approximation when impurity concentrations are low, e. g. less than 5×10^{17} atoms/cm^3 boron in silicon.

Boltaks and Dzhafarov[6] investigated the effect of the local electric field created by a concentration gradient of indium or gallium on the diffusion of antimony in germanium. Their work verified that if donor and acceptor concentration gradients are directed oppositely, the dif-

fusion is retarded by the field.

An external electric field may be used to control the diffusion of impurities in semiconductors. Gallagher[7] found that at temperatures around 1100°C, copper diffuses through the silicon lattice as a positive ion. In his work, a source of radioactive copper Cu^{64} was placed between two silicon samples, and the arrangement was clamped between two electrodes. The field was produced by d.c. which also served to heat the samples. A substantially greater amount of copper was found to migrate toward the cathode than toward the anode.

Boltaks et al[8], in a similar experiment with gold in silicon, found that gold was transported predominantly to the cathode below 1280°C, suggesting existence as positive ions. However, at higher temperatures, the gold moved toward the anode, due to either a change in the nature of ionization or due to the electron drag, according to a theory derived by Fiks[9]. Boltaks, after comparing his results on the temperature dependence of effective mobility of gold in silicon with Fiks' calculation, concluded that electron drag plays an important role in electrical transport of impurities in semiconductors.

Experimental

Diode Heat Treatments

Several experiments were carried out on UT-238 diode rectifiers manufactured by Unitrode Corporation, Watertown, Mass. Two diodes were heated at various temperatures in a furnace consisting of a quartz tube surrounded by a resistance heating element. A protective atmosphere was maintained by a flow of nitrogen through the furnace at a rate of 1 lpm. A voltage was applied to one of the diodes (no. 1) from an external power

supply, and the other diode (no. 2) had no applied voltage (open terminals) and was used as a control.

After each run at an elevated temperature, the diodes were cooled to room temperature ($\sim 25^{\circ}C$) and I-V measurements were taken with forward and reverse bias. The control diode (no. 2) showed little change after each run. However, the diode with bias applied during heating showed changes in both forward and reverse characteristics.

With forward voltage, two parameters were determined from plots of $\ln I_f$ *vs* V_f. The ideal rectifier equation is

$$I = I_s \left[\exp \left(\frac{eV}{kT}\right) - 1 \right]$$

or approximately

$$I_f = I_s \exp \left(\frac{eV_f}{kT} \right)$$

For real diodes, however, a closer representation has been found to be

$$I_f = I_s \exp \left(\frac{eV_f}{\eta kT} \right)$$

with η greater than unity.

From the plots of $\ln I_f$ *vs* V_f, one can determine I_s and η for a given temperature. Table I summarizes the experimental results, and Fig. 1 gives a condensed summary of the $\ln I_f - V_f$ plots. The parameter I_s was found to increase from one run to the next. The η factor varied between high and low values, but showed the greatest increase after heating with forward bias applied.

The reverse I-V characteristics yielded more clearly defined changes, as shown in Fig. 2. The increase in reverse current with voltage was

Table 1

Room Temperature I-V Characteristics

of Control and of Biased Diodes after Heat Treatments

Diode	η	I_s (μa)	I_r at V_r=600v (μa)
UT-238-1 (Initial)	1.42	3.85×10^{-4}	3.27
UT-238-1, Run 1 (½ hr, V_r=14-50v, T=300°C)	1.49	6.2×10^{-4}	6.75
UT-238-1, Run 2 (½ hr, V_r=14v, T=350°C)	1.29	1.1×10^{-4}	21.1
UT-238-1, Run 3 (½ hr, V_r=10v, T=375°C)	1.45	4.0×10^{-4}	13.7
UT-238-1, Run 4 (5 hr, V_r=15v, T=350°C)	1.49	5.0×10^{-4}	19.0
UT-238-1, Run 5 (½ hr, V_f=0.5v, T=350°C)	1.57	1.1×10^{-3}	5.04
UT-238-1, Run 6 (½ hr, V_r=15v, T=350°C)	1.47	3.5×10^{-3}	20.0
UT-238-2 (Initial)	1.39	2.1×10^{-4}	3.15
UT-238-2, Run 1	1.40	1.9×10^{-4}	3.27
UT-238-2, Run 2	1.39	1.7×10^{-4}	3.33
UT-238-2, Run 3	1.34	1.0×10^{-4}	3.35
UT-238-2, Run 4	1.34	1.1×10^{-4}	3.75
UT-238-2, Run 5	1.35	1.4×10^{-4}	3.77
UT-238-2, Run 6	1.30	5.8×10^{-4}	3.60

more rapid after heating with an applied reverse bias. One deviation occurred in run 3 at the highest temperature used (375°C), where the current rose less rapidly than after the previous runs.

However, after heating with forward bias (run 5) the current curve dropped so as to almost approach the initial case. The following run was carried out with reverse bias, and the I_r - V_r curve became quite steep, as it had been before, thus exhibiting an apparently reversible behaviour.

Solar Cell Heat Treatments

A number of heat-treatment experiments similar to those made on diodes, were carried out on silicon solar cells. Heliotek cells of approximately 10% efficiency were used in the first series of tests. Later experiments used higher efficiency cells manufactured by Heliotek and by Hoffman.

For each run, two cells were heated in a furnace consisting of a quartz tube surrounded by a resistance heating element (used previously for the diode heat treatments). Protective atmosphere in the furnace was maintained by a flow of dry nitrogen at a rate of 1 lpm. The cells were supported in nickel-plated copper clamps. Bias was applied to one of the diodes from an external power supply, and the other, used as a control, had no applied bias. Temperature was measured by means of a chromel-alumel thermocouple clamped to the control cell.

In the first series of experiments (A-1, A-2), Heliotek cells A and B were heated with reverse bias on cell A. Before and after the runs, measurements were made of current vs. bias voltage (in the dark) and of photocurrent vs. photovoltage for various values of load resistance.

Listed in Table 2 are the values of the parameter η that appears in the forward-bias current equation for a real diode

$$I_f = I_s \exp\left(\frac{eV_f}{\eta kT}\right)$$

as discussed in the previous section. Also included are values of short-circuit current (I_{sc}), open-circuit voltage (V_{oc}), and maximum power output (P_{max}).

From the photo-current and photo-voltage data for various loads, values of photopower output were calculated and are plotted vs load resistance in Figs. 3 and 4. (Light source for this data was a 750 watt projector lamp, positioned 47 inches from the cell, providing 120 foot-candles illumination.) Slight increases in the maximum power and in the optimum load resistance may be noted as a result of these heat treatments.

The next series of experiments concerned the effects of heat treatment with and without applied bias on a few high-efficiency silicon solar cells manufactured by Heliotek and by Hoffman. The results are summarized in Table 3.

Runs B-1, B-2, and B-3 were evaluated using a 750 watt projector lamp, positioned 29 inches from the cell. Maximum power output was observed to decrease for all cells heated with bias and for all but one of those heated without bias. The one exception was Heliotek cell 2, used as a control in run B-1 at 250°C for ½ hr.; here, P_{max} increased by about 16 percent.

The results of runs B-4, B-5, B-6 and B-7 were evaluated using light from a 750 watt projector lamp positioned 20 inches from the cell. The light was passed through 3 cm. of water that served as an infrared filter.

Table 2

Room Temperature Characteristics

of Control and of Biased Solar Cells after Heat Treatments

Cell Identification	η	I_R at V_R=10v (mA)	I_{sc} (mA)	V_{oc} (volts)	P_{max} (mW)
Heliotek A (Initial)	2.69	17.4	1.71	0.327	0.31
Heliotek A (Run A-1: T=250°C, ½ hr, V_R=1.5V, I_R = 40mA)	2.46	16.8	1.70	0.317	0.31
Heliotek A (Run A-2: T=350°C, ½ hr, V_R=0.04-0.05V, I_R=50mA)	3.09	29.8	1.67	0.383	0.345
Heliotek B (Initial)	3.26	3.53	1.78	0.375	0.35
Heliotek B(Run A-1: T=250°C, ½ hr) (control)	2.57	2.80	1.68	0.380	0.36

Table 3

Room Temperature Characteristics

of Control and of Biased Solar Cells after Heat Treatments

Cell Identification	η	750W proj. lamp (tungsten fil) at 29" I_{sc} (mA)	V_{oc} (volts)	P_{max} (mW)	Heliotek Data;Solar Spectrum, A.M.O. 140 mW/cm^2 I_{sc} (mA)	V_{oc} (volts)	P_{max} (mW)
Heliotek 1 (Initial)	2.39	3.46	0.463	1.09	75.3	0.566	31.5
Heliotek 1 (Run B-1, 250°C, 1 hr, V_K = 5V, I_R=30mA)		3.49	0.453	1.05			
Heliotek 1 (Run B-2, 300°C, 1 hr, V_R=0.5V, I_R=40mA)		3.27	0.448	0.932			
Heliotek 2 (Initial)	3.32	3.10	0.447	0.838	73.6	0.569	30.7
Heliotek 2 (Run B-1) /Control		3.39	0.450	0.972			
Heliotek 2 (Run B-2)		2.98	0.443	0.845	72.6	0.567	30.1
Heliotek 3 (Initial)		3.46	0.471	1.110	75.2	0.571	31.7
Heliotek 3 (Run B-3,300°C, 1hr, V_F=0.025V, I_F=40mA		3.01	0.451	0.915	74.4	0.569	30.4
Heliotek 4 (Initial)		3.47	0.462	1.058	75.0	0.565	30.8
Heliotek 4 (Run B-3)/Control		3.11	0.459	0.943			
		750w proj. lamp (tungsten fil) at 20", 3cm. water as infrared filter					
Heliotek 5 (Initial)		7.53	0.480	2.60	75.0	0.563	31.0
Heliotek 5 (Run B-4,325°C, 1 hr, I_R=40mA)		8.17	0.489	2.96	74.2	0.560	30.6
Heliotek 6 (Initial)		7.55	0.484	2.63	74.3	0.563	30.8
Heliotek 6 (Run B-4)/Control		8.18	0.492	2.98	74.0	0.563	30.5
Hoffman 86 (Initial)		6.07	0.473	2.06			

Table 3 (Cont.)

Cell Identification	η	750W proj lamp (tungsten fil) at 20", 3cm. water as infrared filter			Heliotek Data; Solar Spectrum, A.M.O. 140mW/cm^2		
		I_{sc} (mA)	V_{oc} (volts)	P_{max} (mW)	I_{sc} (mA)	V_{oc} (volts)	P_{max} (mW)
Hoffman 86 (Run B-5, 300°C 1 hr, I_R=40mA)		5.63	0.470	1.88			
Hoffman 91 (Initial)		5.78	0.473	2.00			
Hoffman 91 (Run B-5)/Control		5.88	0.467	1.88			
Heliotek 4 (From Run B-3)	2.79	8.14	0.486	2.87			
Heliotek 4 (Run B-6, 325°C, 2 hr, I_R=40mA)	2.99	8.30	0.489	2.94	74.0	0.561	30.4
Heliotek 7 (Initial)	2.18	8.27	0.487	2.91	75.9	0.565	31.2
Heliotek 7 (Run B-6)/Control	1.99	8.30	0.483	2.91	74.9	0.565	30.6
Hoffman 93 (Initial)	2.54	6.64	0.482	2.37			
Hoffman 93 (Run B-7, 325°C, 2 hr, I_F=40mA)	2.96	5.92	0.473	1.99			
Hoffman 96 (Initial)	1.85	6.56	0.473	2.26			
Hoffman 96 (Run B-7)/Control	5.54	5.87	0.412	1.11			

In addition, a fixture was used to maintain a constant distance (20 inches) between the lamp and the cell. The load curves were plotted on a Moseley 2D-2A X-Y recorder.

In run B-4, maximum power output of Heliotek cells 5 & 6 appeared to increase by approximately 14 percent over the initial values (Figs. 5 & 6 and Table 3) but decreased or remained constant in all other runs.

Heliotek cells 2 through 7 were returned to the manufacturer for testing in his solar simulator at air-mass zero conditions. When these load I-V curves were compared with the initial curves received with the cells, small decreases (1 to 2 percent) in power output were observed in every case (see Table 3, Figs. 7 - 10).

It is concluded that, whereas definite changes occurred in the diodes as a result of heat treatment under bias, no trends were observed in the data from solar cells heat treated under bias. While many of the changes are larger than our estimated error of several percent, no coherent picture has emerged.

A systematic investigation of the diffusion of impurities in silicon in the presence of externally applied fields and currents has been started.

Conclusions

It can be concluded from the literature search that the application of an electric field during diffusion can greatly affect the diffusion rates for certain interstitial impurities in silicon such as gold, silver, and copper. However, the extent to which an externally applied field can affect the diffusion of substitutional impurities (which are of greatest interest in semiconductor devices) has not been determined. As long as the impurity is ionized, there should be some effect, and further investigations with Groups III-A and V-A elements are planned to determine its magnitude.

It has been shown[2,5] that, when the concentration of the diffusing impurity is sufficiently high (e. g. > 5×10^{17} atoms/cm^3 boron in silicon) concentration profiles do not agree with solutions of Fick's laws. This modification is particularly significant during simultaneous diffusion of donors and diffuses much more slowly than the other and is present in excess of the faster impurity. It is believed that field effects account for this difference[5].

The solar cell heat treatments carried out in this work have demonstrated no conclusive evidence concerning field effects. Variations in the line voltage to the lamp, as well as the X-Y recorder, may have accounted for the observed changes in cell output. However, in the case of the diodes, the reversible changes in electrical characteristics for those heated with bias in contrast to those heated without bias indicate that the field had a definite effect which could not be attributed to the effects of heat on contacts or on the glass envelope. The changes

may have resulted from the redistribution of the impurity elements in the silicon, but without an analysis of concentration profile or junction depth, a definite statement cannot be made.

References

1. S. Zaromb, IBM J. Res. Dev., 1, 57, (1957).

2. M. F. Millea, Semiconductor Electronics, 316, 3271, (1959).

3. K. Lehovec and A. Slobodskoy, Sol. St. Elec., 3, 45, (1961).

4. V. V. Vas'kin, V. A. Uskov, and M. Ya. Shirobakov, Fiz. Tver. Tela, 7, 3356, (1965).

5. T. Klein and J. R. A. Beale, Solid St. Elec., 9, 59, (1966).

6. B. I. Boltaks and T. D. Dzhafarov, Fiz. Tver. Tela, 5, 2061, (1964).

7. C. J. Gallagher, J. Phys. Chem. Solids, 3, 82, (1957).

8. B. I. Boltaks, G. S. Kulikov, and R. Sh. Malkovich, Fiz. Tver. Tela, 2, 2134, (1960).

9. V. B. Fiks, Fiz. Tver. Tela, 1, 14, (1959).

10. B. Goldstein, Bull. Amer. Phys. Soc., Ser. 2, 145 (1956).

11. R. C. Miller and A. Savage, J. Appl. Phys., 27, 1430 (1956).

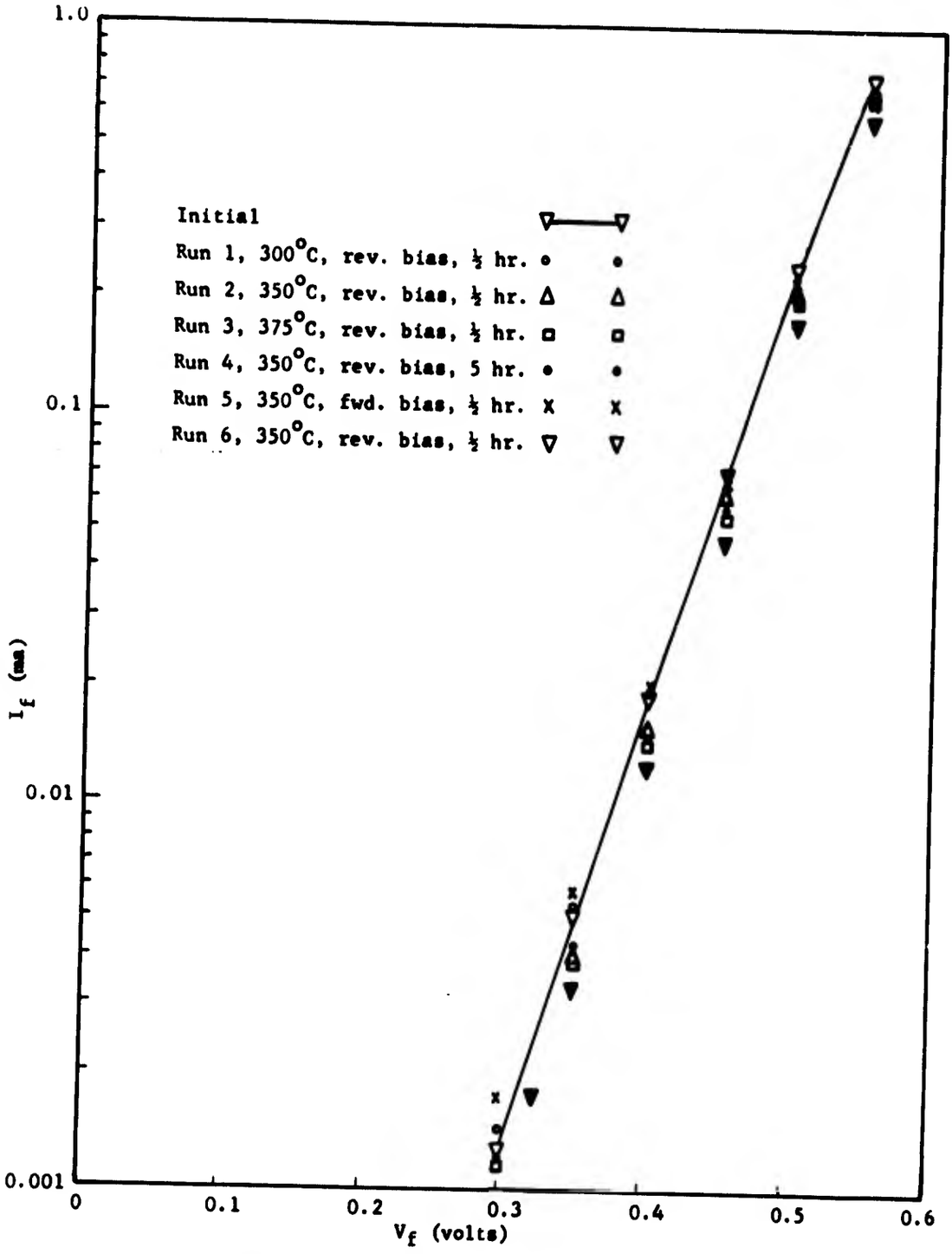

Fig. 1. Forward Bias I-V (25°C) for Unitrode UT-238 #1 after Heat Treatments with Bias Applied

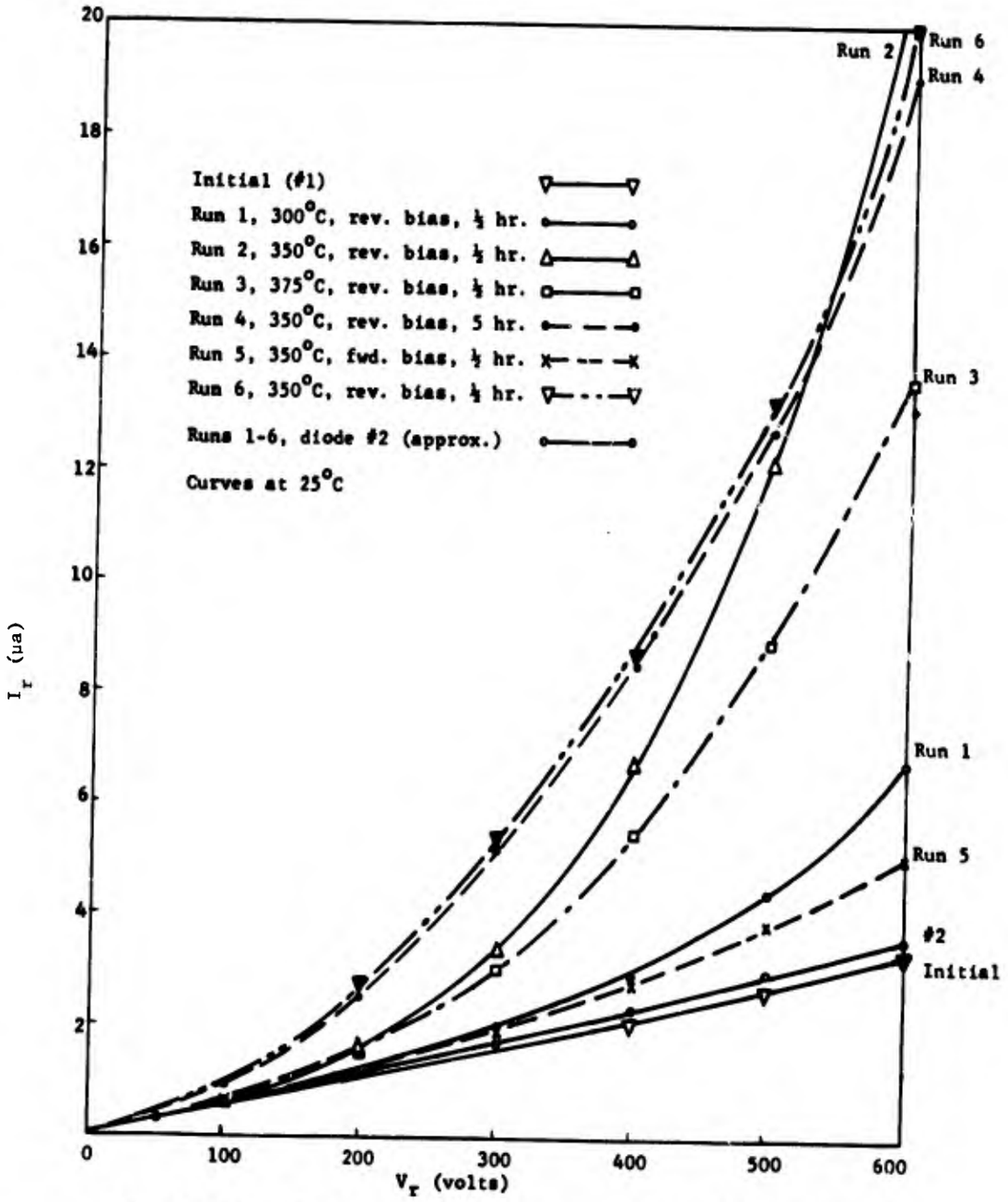

Fig. 2. I-V in Reverse Bias for Unitrode UT-238 #1 and #2 after Heat Treatments with Bias on #1

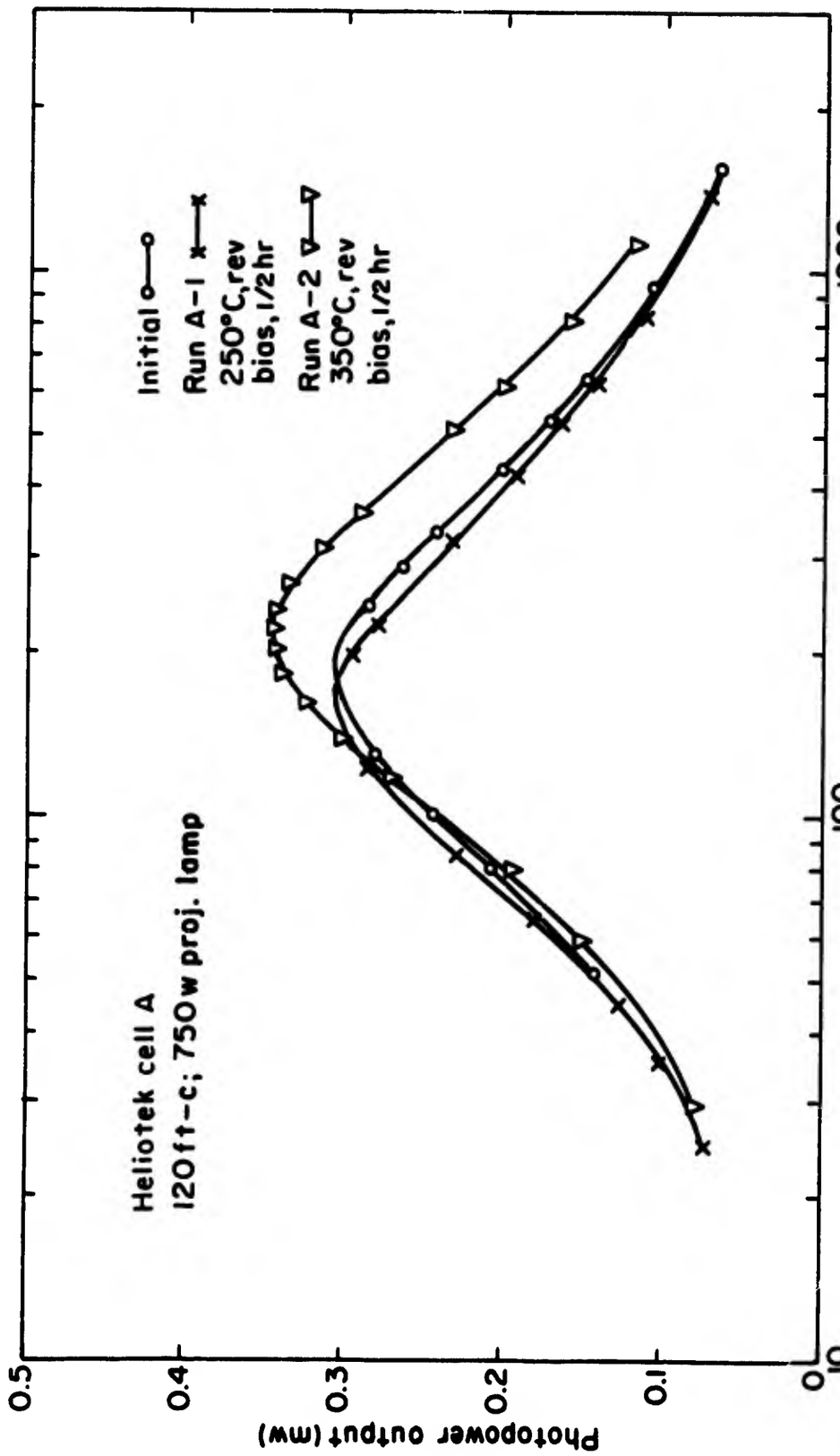

Fig. 3. Photopower Output vs. Load Resistance. Heliotek Cell A.

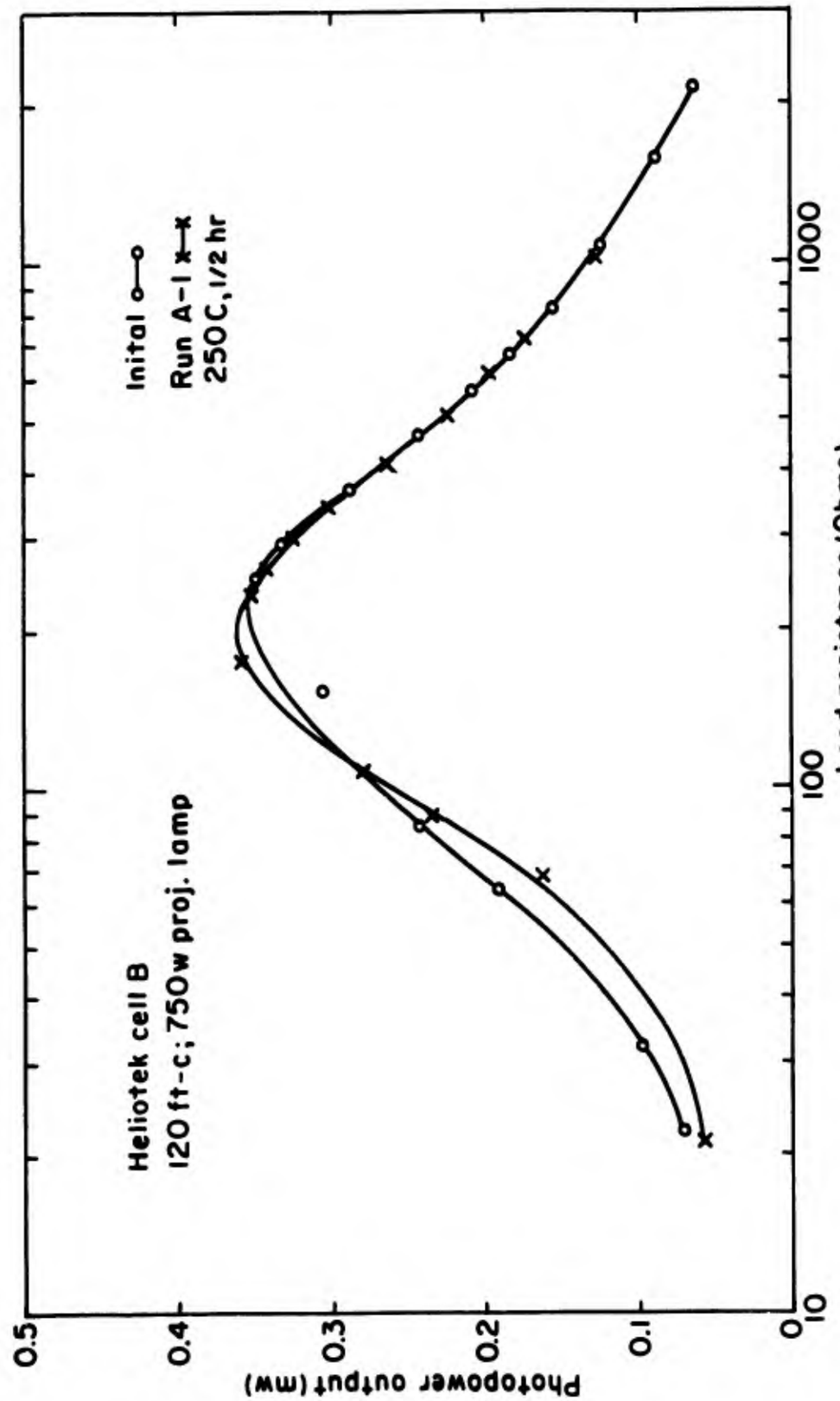

Fig. 4. Photopower Output vs. Load Resistance. Heliotek Cell B.

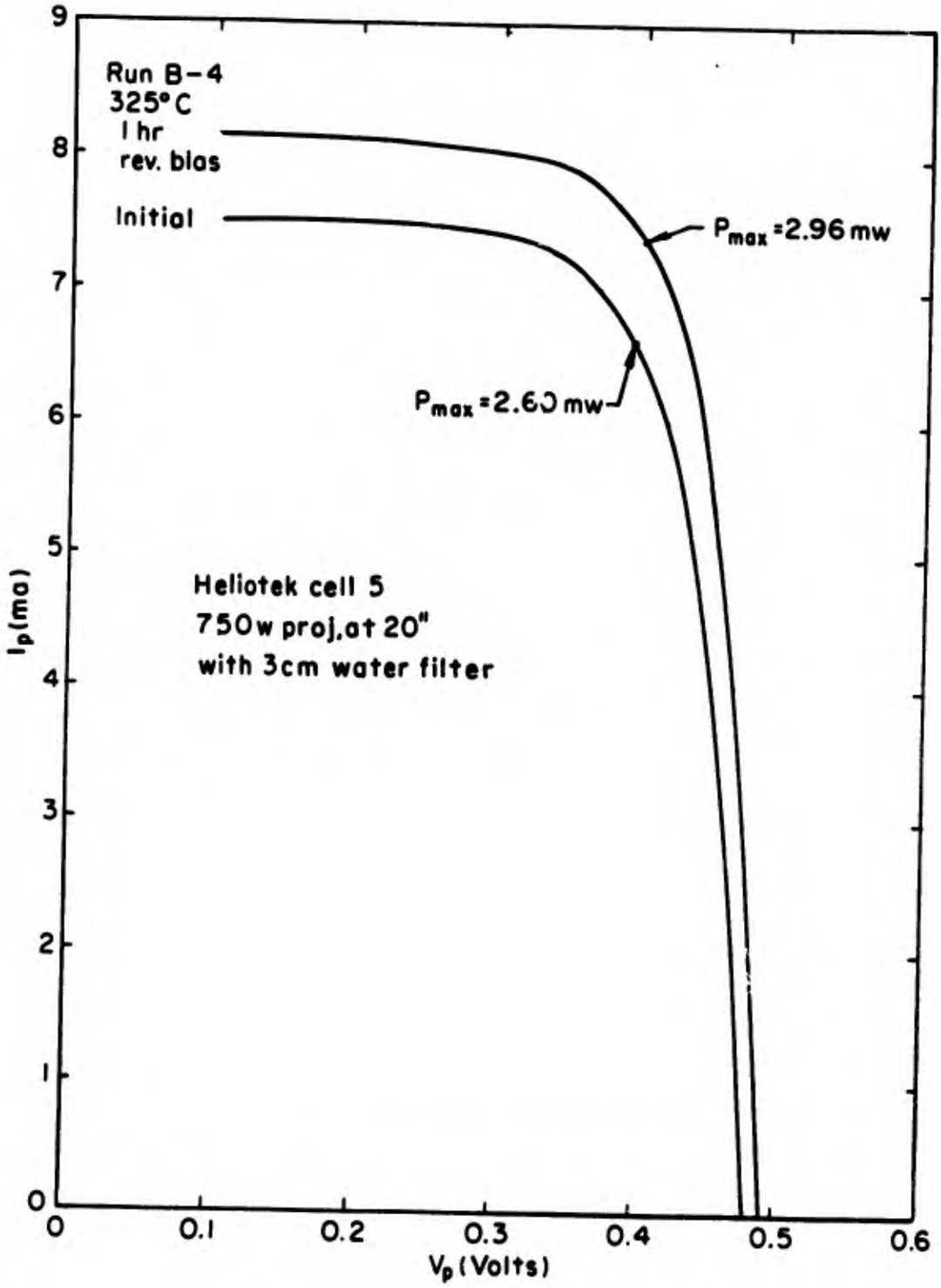

Fig. 5. Load I-V Curves for Heliotek Cell 5 Before and After Heat Treatment of 1 Hour at 325°C with mA Reverse Current.

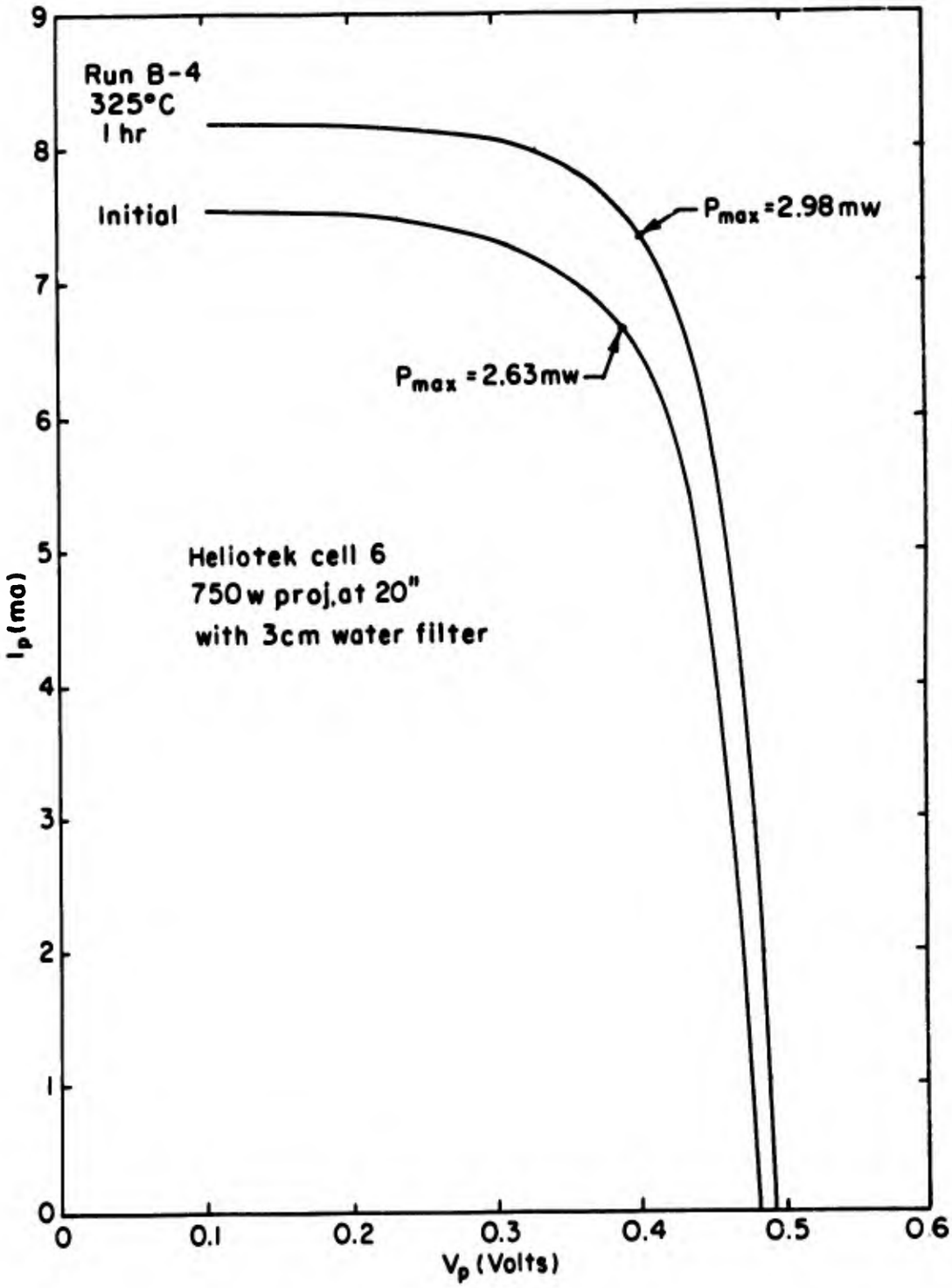

Fig. 6. Load I-V Curves for Heliotek Cell 6 Before and After Heat Treatment of 1 Hour at 325°C, Control Specimen.

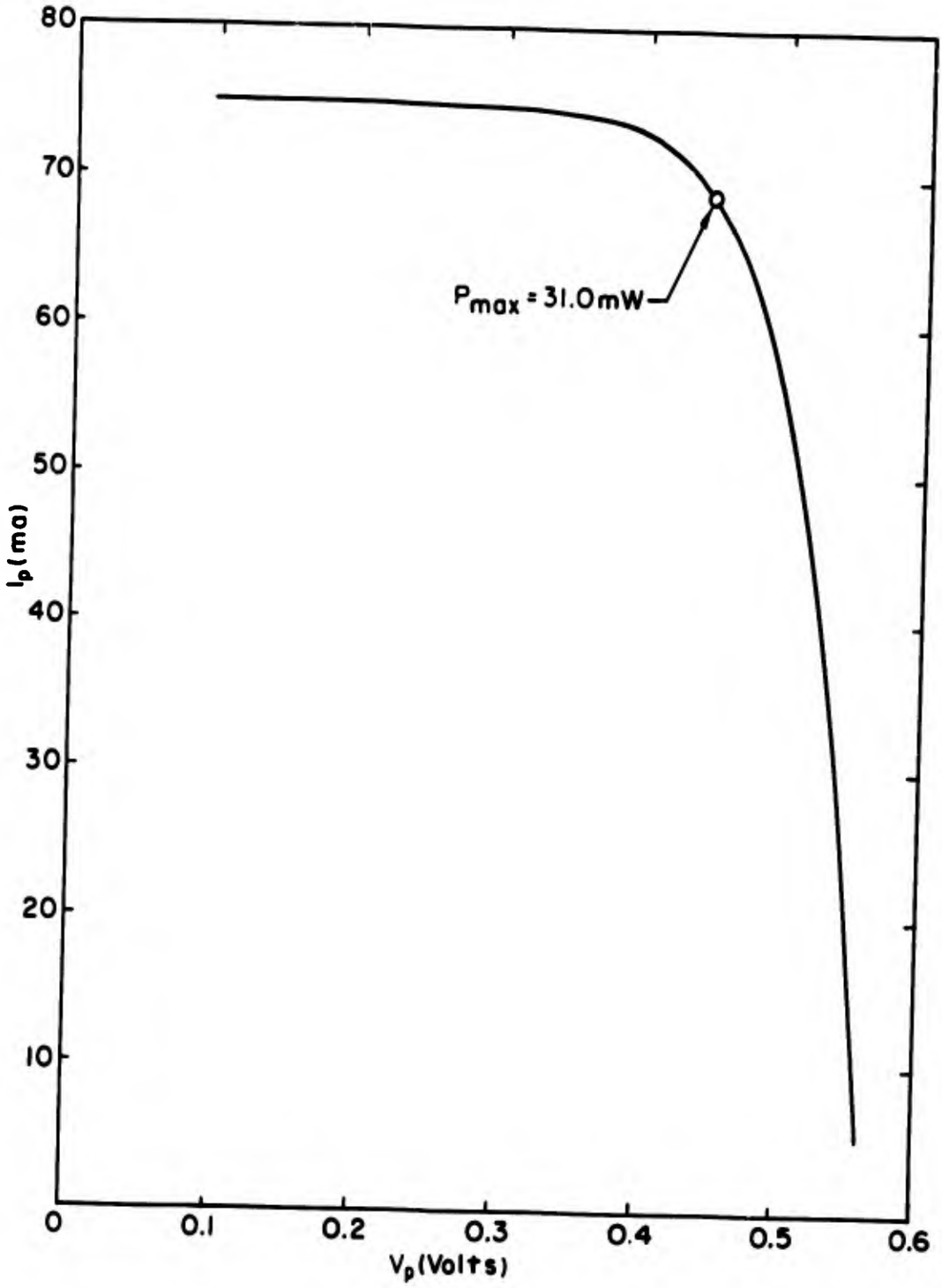

Fig. 7. Load I-V Curve for Heliotek Cell 5, Initial Condition. (Solar Simulator, 140 mW/cm^2, Air Mass = 0.)

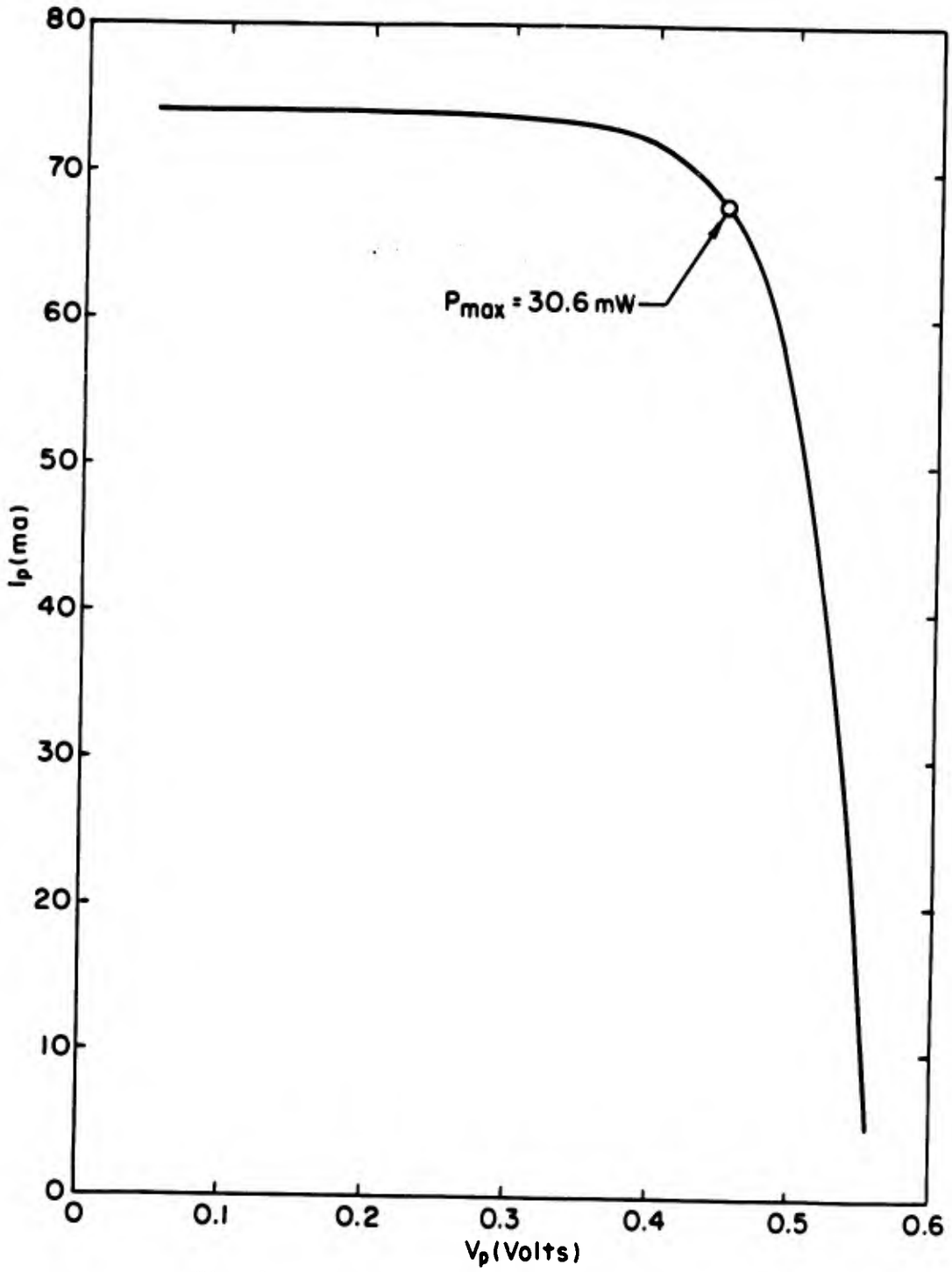

Fig. 8. Load I-V Curve for Heliotek Cell 5, After Run 8-4. (Solar Simulator, 140 mW/cm^2, Air Mass = 0.)

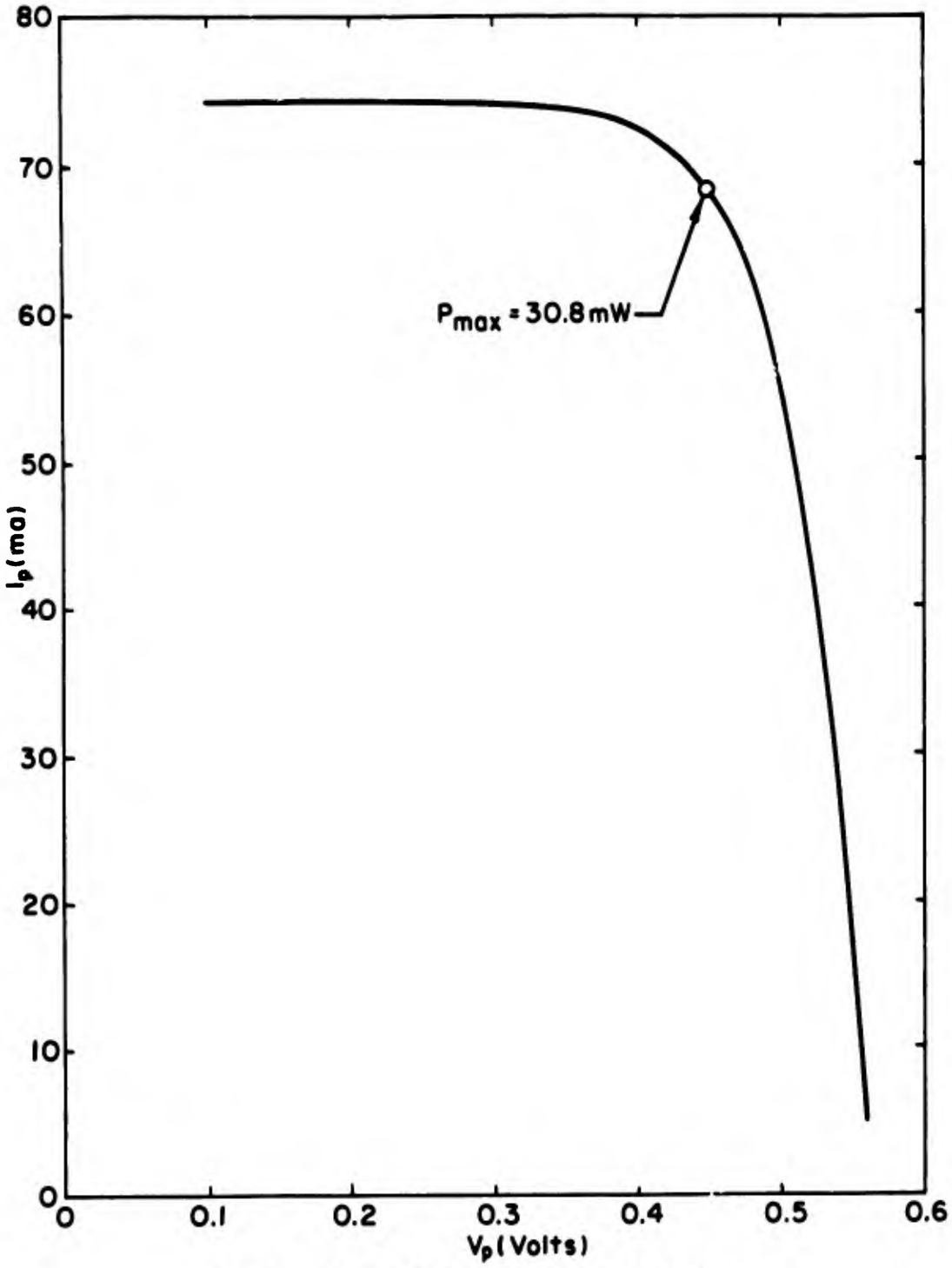

Fig. 9. Load I-V Curve for Heliotek Cell 6, Initial Condition. (Solar Simulator, 140 mW/cm^2, Air Mass = 0.)

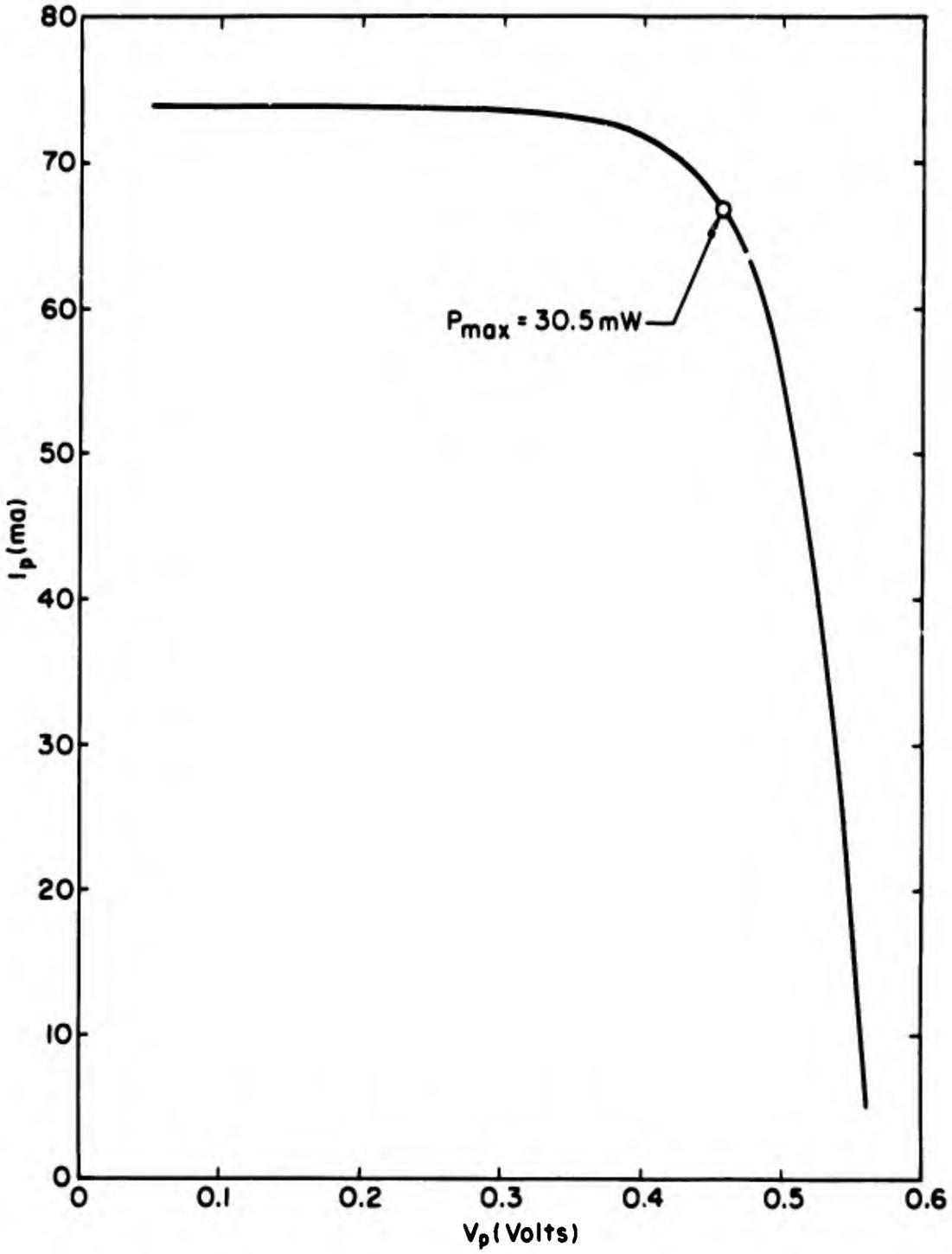

Fig. 10. Load I-V Curve for Heliotek Cell 6, After Run$_2$B-4. (Solar Simulator, 140 mW/cm^2, Air Mass = 0.)

6. HETEROJUNCTION PHOTOVOLTAIC ENERGY-CONVERTERS

Introduction

A heterojunction diode is a rectifier formed by the junction of two different semiconductor materials. The basic difference between a heterojunction and a homodiode (one material) arises from the abrupt change in electron affinities at the junction of the materials. This change in electron affinity creates discontinuties in the energy band diagram. A typical energy band diagram for a heterojunction where the small energy gap material is n-type and the large energy gap material is p-type (nsp1) is shown in Figure 1. This type of diagram, originally proposed by Anderson[1], has been substantially verified experimentally.

Several theories have been proposed to explain the charge carrier transport mechanisms of heterojunction diodes. Anderson[1] coupled the discontinuities in the energy band diagram with the Shockley diffusion theory to describe the current. Perlman and Feucht[2] modified Anderson's theory by coupling the Shockley metal-semiconductor model with the diffusion theory. Riben[3] added a tunnelling model to fit experimental data that he obtained on Ge-GaAs heterojunctions. Other work has been done on effects such as interface states, crystal orientation, photon and polaron interaction, and electro-optical effects. At the present time no theory will explain all the measurements and each theory will only partially explain a given set of measurements.

Primary applications considered for heterojunctions have been wide band-gap emitter transistors and photocells. Our concern here is with the photocell application.

Photocell Operation

The heterojunction diode has several inherent advantages over the homojunction diode for photovoltaic applications. The mechanism of photon absorption results in the so-called "window" effect. Anderson[4], Lopez and Anderson[5], and Augusta and Anderson[6] have investigated this effect. Perlman[7], using his combination of the diffusion and metal-semiconductor model, has presented a theoretical discussion of heterojunction photocells.

In a suitably constructed heterojunction, a spectral response curve such as in Figure 2 is obtained. E_{gs} and E_{gl} are the band gap energies of the small gap and large gap materials respectively. The "window" effect can be explained by looking at the energy band diagram of Figure 3. Photons with energy $h\nu > E_{gl}$ are absorbed in material II exciting hole-electron pairs. The majority of these pairs are produced near the surface of material II and contribute to the photocurrent if they reach the junction. The statistics involved are much the same as in a homodiode photocell.

Photons with energies $E_{gs} < h\nu < E_{gl}$ pass through material II and are absorbed in material I near the junction. Since the pairs are produced near the junction, nearly all are collected and contribute to the photocurrent. The advantage of a heterojunction over a homodiode comes mainly from current produced in this photon region. As is shown in a later figure, the spectral response of a homojunction photodiode decreases rapidly at photon energies higher than approximately 1.5 times the energy gap. Absorption near the surface of the diode, but outside the collection region causes this loss. In a heterojunction, as long as $h\nu < E_{gl}$, the

photons pass through the large gap material essentially unattenuated and are collected near the junction. The spectral response is nearly flat between E_{gs} and E_{gl}. Since the pairs are produced close to the junction, reductions in surface recombinations and sheet resistance can be obtained. Higher collection efficiencies than a homodiode are expected for photons in this range. Efficiency is also enhanced by the collection of photons with energies much higher than E_{gl} which would normally contribute little in a homodiode.

Photons with energies $h\nu < E_{gs}$ do not excite hole-electron pairs and do not contribute to the photocurrent.

A heterojunction photocell with the energy gaps of the two materials selected to bracket the spectrum of the incident light source should be more efficient than an equivalent homodiode. Problems arise however in the manufacture of the exact heterojunction desired. At present, a heterojunction cell has not been made which is more efficient than the standard silicon homodiode cell for solar radiation.

Our work has been divided roughly into two portions: (1) an initial phase wherein measurement techniques were tested and perfected, and (2) a second phase comprising the fabrication and characterization of heterojunctions. The initial phase examined standard silicon-homodiode solar cells and experimental GaAs-GaP graded-gap cells made by the Eagle-Picher Co. as a result of their contracts with the U. S. Army Signal Research & Development Laboratories, Fort Monmouth, N. J. The second phase has thus far only investigated the fabrication of Si-GaP heterojunctions.

I. Initial Phase

Measurements

As stated before, a number of models exist for describing heterojunction diodes. The current densities calculated from the various models

differ by orders of magnitude. Different heterojunction cells made from the same two materials have exhibited the properties of each of the models. There also have been serious discrepancies between theoretical and experimental data giving evidence that either another model is needed or a combination of models is involved.

There are two purposes in measuring the properties of the junctions: (1) to characterize the diodes according to a model, and (2) to ascertain its usefulness. The previous paragraph indicated difficulties in modelling the junctions. It is somewhat easier to ascertain the usefulness of the junctions, but it may be easier to maximize this usefulness if its operation is both qualitatively and quantitatively understood.

A. Preliminary measurements.

Commercial silicon solar cells were measured to check equipment and techniques and to help in later interpretation of the heterojunction data. A description of these measurements and their results are given below.

Current-voltage (I-V) curves are important for determining the current transport mechanism of the diode. The temperature variation of the I-V curves yields information as to which is pertinent: diffusion model, tunnelling model, or some other model. Diodes which follow the Shockley diffusion model exhibit the familiar exponential 1/T temperature dependence. Tunnel diodes exhibit different characteristics depending on the type of barrier and tunnelling path.

Room temperature I-V curves of two silicon cells are reproduced in Figure 4. Energy conversion efficiencies of these cells were alleged to be about 8%. The diodes in reverse bias have a constant resistance characteristic instead of the predicted saturation current. The equiva-

lent circuit model is a parallel capacitor-resistor combination. The D. C. series resistance is high enough so that it cannot be neglected as is the case with a "good" junction. Linear extrapolation of the current at high forward bias to I = 0 should give the value of the diffusion potential. Normal silicon diodes have a value in the vicinity of 0.7 volts. Figure 4 shows a value of about 0.6 volts. The lower value can be explained with the addition of a series resistance to the equivalent circuit model. Capacitance measurements have confirmed this assumption. Figure 5 is a logarithmic plot of the forward bias I-V curve. The expected exponential behavior is shown, i. e.

$$I = I_o \exp \frac{qV}{\eta kT}$$

Capacitance versus reverse bias measurements give information on the character of the junction region, the abruptness of the junction, and the uniformity of doping. In a heterojunction, where interface states, trapping sites, multiple junctions, etc., may exist, the capacitance data can help to clarify the operation of the diode.

An abrupt, uniformly doped diode exhibits a linear dependence of the reciprocal capacitance squared $\frac{1}{C^2}$ on reverse bias voltage (V_R). The extrapolated value of the voltage at $\frac{1}{C^2} = 0$ is another, and more accurate, indication of the diffusion potential. Figure 6 shows $\frac{1}{C^2}$ versus reverse bias for the two silicon solar cells. These data were obtained with a General Radio 1615-A Impedance Bridge. The strictly linear dependence is verified as expected for a silicon cell. The diffusion potential for both diodes extrapolates to 0.72 volts. This is in good agreement with values expected from silicon solar cells.

Most available commercial capacitance bridges measure the capacitive reactance and the dissipation constant (the ratio of the real impedance to the imaginary impedance). If the diode could be described by a parallel resistor-capacitor combination as shown in Fig. 7a, the measurements could be interpreted as they stand.

$$C = C_{MEAS} \tag{1}$$

$$R = \frac{D_{MEAS}}{WC} \tag{2}$$

$W = 2\pi \times$ frequency.

However, nearly all solar cells exhibit the circuit properties shown in Fig. 7b. The parameters measured by the bridge are now no longer directly related to circuit parameters. There are three unknowns with measurement of only two quantities.

The impedance of the circuit in Fig. 7b is

$$Z = R_S + \frac{R_p}{1 + W^2 R_p^2 C^2} + \frac{WR_p^2 C}{j(1 + W^2 R_p^2 C^2)} \tag{3}$$

$$Z = R' + \frac{1}{jWC'} \tag{4}$$

The bridge measures C' and $D_{MEAS} = R'/1/WC' = WR'C'$. Therefore

$$C_{MEAS} = C' = C + \frac{1}{W^2 R_p^2 C} \tag{5}$$

$$D_{MEAS} = WR'C' = \left(R_S + \frac{R_p}{1 + W^2C^2R_p^2}\right)\left(WC + \frac{1}{WR_p^2C}\right) \qquad (6)$$

Since we are primarily interested in the capacitance C, the measurements will be valid if

$$C >> \frac{1}{W^2R_p^2C} \qquad (7)$$

The condition implicit in equation (7) does not hold for the values of R_p and C of the cells measured and at the maximum frequency (10 kcps) of the bridge used (General Radio 1615-A).

The easiest method to obtain a valid condition for the inequality of equation (7) is to raise the frequency of measurement. The highest frequency of any bridge available to us is 20 kcps, which is not sufficiently high. A method of calculating the capacitance from the bridge measurements at two frequencies was chosen for its convenience and applicability. Measurements are taken of the overall capacitance at the two frequencies, and the dissipation constant at the higher frequency. The dissipation constant at the lower frequency is not necessary, but since it has to be measured in order to balance the bridge, it is taken and used as a check. The equations used to calculate C, R_S, and R_p are as follows, with subscripts 1 and 2 to denote the frequencies, and with $W_2 > W_1$.

$$C = \frac{W_2^2 C_{2\ MEAS} - W_1^2 C_{1\ MEAS}}{W_2^2 - W_1^2} \qquad (8)$$

$$R_p^2 = \frac{1}{W_2^2\, C(C_{2\ MEAS} - C)} \tag{9}$$

$$R_S = \frac{D_{2\ MEAS}}{W_2\, C_{2\ MEAS}} - \frac{R_p}{1 + W_2^2\, R_p^2\, C^2} \tag{10}$$

The two frequency method assumes the frequency invariance of the three equivalent circuit parameters. While this is expected to be true for the two frequencies used (10 kc/sec and 5 kc/sec), measurements were taken at a third frequency (1 kc/sec) as a check. Agreement was within the experimental accuracy. A further check was also made by placing a pre-calibrated resistor in series with the diode and obtaining similar data. The difference between the series resistances R_S with and without the resistor agreed with the value of the resistor.

The method has provided a simple and satisfactory solution to the capacitance measurement problem without the modification of existing equipment or the addition of other equipment.

B. Measurements on graded-gap cells.

I-V, capacitance, and photoelectric measurements have been carried out on several graded-gap diodes made by the Eagle-Picher Co. (EP429, EP438, EP455, and EP467). These are graded band gap structures produced from the pseudo-binary solid solutions of GaAs-GaP[8].

The room-temperature I-V curves of the EP cells are shown in Figs. 8, 9, and 10. Figure 8 is the semi-log plot of the diodes under forward bias. All follow the normal non-ideal diode equation

$$I = I_S \left[\exp\left(\frac{qV}{\eta kT}\right) - 1\right]$$

The values of η for these diodes range from two to three. Etas of a GaAs homodiode normally are around 2.5, and the values of the EP cells are as might be expected.

Figure 9 is a linear plot of the reverse I-V characteristics. Different characteristics arise among the diodes. A semi-log plot of these curves, as in Fig. 10, while not normally informative in the reverse bias case, here shows these different characteristics more clearly. EP438 and EP467 are nearly exponential in behavior. EP429 has a strict exponential behavior while EP455 is nearly exponential at low bias and then has a resistive characteristic at higher reverse bias corresponding to 2500 ohms. Commercial solar cells exhibit a resistive characteristic (see Fig. 4). The mechanisms giving rise to these characteristics are not fully understood as yet.

A fundamental problem exists with the description of the graded band gap of the diodes. Near the metallurgical junction the compound is of the form $GaAs_{1-x}P_x$. Therefore the band gap at that point would be between the band gaps of GaAs and GaP, depending on the value of x. Interpretation of the effects of the junction are difficult since the composition of the solid solution, its variation with distance, and the location of the p-n junction in this region are not known. Metallurgical studies of the junction region should clarify this problem. However, the junction is located within one micron of the surface, and techniques for measuring composition versus distance and the location of the electrical junction have not yet been worked out.

The remarks of the previous paragraph also apply to the problem of interpreting the data of capacitance vs. reverse bias obtained on the diodes.

The capacitance is dependent, among other things, on the value of the dielectric constant of the material. In the miscible system, the dielectric constant is expected to change as a function of composition. On the whole, the junction must be fairly well described in order to predict the capacitance variation.

Figure 11 is a plot of the reciprocal capacitance squared $\frac{1}{C^2}$ versus reverse bias voltage for cells EP429 and EP438. The extrapolated voltage at $\frac{1}{C^2} = 0$ is a measurement of the diffusion voltage, V_D. In this case the values are 2.43 volts and 1.58 volts for EP429 and EP438, respectively. The values of the diffusion voltage will depend on the band gap characteristics and the doping levels in the junction region, and could easily be far apart. The curve shows a constant slope, normally understood to arise from an abrupt junction between uniformly doped regions. This suggests that for the reverse bias voltages measured (> 0.1 volt) the doping is uniform and the depletion region encompasses the graded-band-gap region. Therefore, changes in depletion width versus reverse voltage would occur outside the graded-gap region and would not show any effects due to a graded-gap. An alternative possibility is that the p-n junction lies entirely outside the graded-gap region. Significant data about the junction region could also come from capacitance measurements at lower voltages and at low temperatures.

One of the more important characteristics determining the effectiveness of the heterojunction photodiodes is the photocurrent spectrum. This spectrum can prove the existence and partially measure the effectiveness of the "window". Figure 12 shows the relative short circuit photo-

current (normalized for constant incident light intensity) versus wavelength of the incident monochromatic light for the silicon solar cell "A" and the GaAs-GaP cells EP429 and EP467.* It should be understood that the current amplitudes are relative only for each diode, and the values have been normalized to present them clearly on the Figure. The high-wavelength cutoff should occur at the minimum energy gap of the cells, the 1.1 eV band gap of silicon and 1.40 eV band gap of GaAs. The values calculated from Fig. 12 give 1.07 eV for silicon cell A and 1.38 eV for the Eagle-Picher cells. The peak photocurrent occurs at 7300 Å for EP429 and 8500 Å for EP467. The majority of the absorption is occurring in the GaAs for EP467 on the basis of the spectrum shape. The "window" effect has been more nearly obtained in the EP429 cell. The peak photocurrent output comes roughly midway between the band gap of GaP (2.24 eV) and GaAs (1.40 eV) and a flatter peak is observed than in a homodiode. Figure 13 is a reproduction of Fig. 1 from Zh. I. Alferov, et al, Soviet Physics-Solid State, 7, 990 (1965), and illustrates the "window" obtained by these authors with an epitaxial GaAs-GaP p-n heterojunction. This diode has an abrupt metallurgical junction.

Photocurrent and photovoltage of these cells under zero bias were measured for varying loads and for three light intensities. These measurements determine the cells' usefulness for delivering power to a load and give a relative measure of the efficiency of each.

---

* These measurements were made on a special spectrophotometer located at the Air Force Cambridge Research Laboratories, and the data was obtained through the courtesy of Hervey Gauvin and Joseph Grenier.

The light source used was a standard 500 W photoprojector bulb at distances from the cell face of 36, 50 7/8, and 72 inches. These distances were large enough so that the bulb acted as a point source, and the light intensities varied inversely with the square of the distance. Light-meter measurements gave intensities of approximately 120, 60, and 30 foot-candles respectively.

Figures 14 and 15 show the photocurrent (I_p) versus photovoltage (V_p) under varying loads and for the three light intensities for the silicon cells A and B. These curves are as expected. The slopes of the curves as the photocurrent approaches zero (photovoltage approaches V_{oc}) give a measurement of the total resistance (sheet + bulk + contact) of the cell. This resistance, primarily sheet resistance, is large enough to seriously affect the efficiency. Increasing the light intensity decreases this resistance and should improve the efficiency of the cell.

Figures 16 - 18 show similar curves for the GaAs-GaP graded band gap cells. Again, the sheet resistance decreases as the light intensity increases.

Figures 19 and 20 are plots of the power (P_o) delivered by the silicon cells versus the resistive load on the cell. P_o is the product $V_p \times I_p$ from Figures 14 and 15 at its particular value of load resistance.

Figures 21 - 23 are similar plots for the GaAs-GaP graded band gap cells. Table 1 lists the maximum power output per cm^2 of illuminated area of each cell and the load at which this maximum occurs. The maximum power output of the graded gap cells occurs in the kilohm range while the silicon cells' best efficiency is in the low hundreds of ohms.

TABLE 1 - MAXIMUM POWER DELIVERED AND THE CORRESPONDING LOAD

Illumination Intensity	120 ft-candles		60 ft-candles		30 ft-candles	
Cell	Load at Max P_o (Ω)	Max Po_2 (w/cm^2)	Load at Max P_o (Ω)	Max Po_2 (w/cm^2)	Load at Max P_o (Ω)	Max Po_2 (w/cm^2)
A	190	246	330	102	520	40
B	250	328	450	147	750	68
EP429	3.2 K	93	5.6 K	41	9 K	17
EP438	2.4 K	48	3.9 K	17	7.4 K	5.3
EP467	5.4 K	48	9.5 K	22	17.5 K	9.2

The EP429 graded gap cell is approximately 40% as efficient as silicon cell A under the illumination used, while the EP438 and EP467 cells are only 20% as efficient. Silicon cell A is taken as a reference against which to compare the heterojunction cells. Both silicon cells were to be used for this purpose, but cell B was accidentally cracked during a low temperature experiment. The EP438 cell's relative efficiency (to the silicon cell) increases from 13% to 20% as the illumination intensity increases. However, the I_p versus V_p curves for this cell show a very high value of sheet resistance at 30 foot-candles light intensity that decreases substantially under higher light intensity. The gain in relative efficiency is probably due to the reduction in sheet resistance. None of the other cells exhibit this gain nor have as large a sheet resistance. The photocurrent (I_p) for all the cells is proportional to the illuminating intensity, see Table 2, coincident with solar cell theory, and therefore the gain cannot be accredited to an increase in collection efficiency or similar phenomenon.

The factor of 2 difference in the efficiencies between EP429 and either EP467 or EP438, as well as an insight into the structure of the diode, can be deduced from their short-circuit-current spectral response and from the diffusion voltages deduced from the capacitance measurements. The peak in the spectral response for EP429 occurs between the band-gaps of GaAs and GaP suggesting that the p-n junction is in the graded band-gap region. The spectral response for EP467 peaks near the band-gap of GaAs and decreases rapidly as the incident photon energy is increased. EP429 collects more of the incident light over a larger spectral range than does EP467. The data suggests that the p-n junction of EP467 is deep

TABLE 2 - SHORT-CIRCUIT CURRENT AND OPEN-CIRCUIT VOLTAGE VS. LIGHT INTENSITY

Predicted V_{oc} in Parenthesis

Illumination Intensity	120 ft-candles		60 ft-candles		30 ft-candles	
Cell	V_{oc} (V)	I_{sc} (mA)	V_{oc} (V)	I_{sc} (mA)	V_{oc} (V)	I_{sc} (mA)
A	.390 (.389)	2.05	.336 (.335)	1.04	.281 (.282)	.521
B	.469 (.490)	1.78	.440 (.445)	.900	.406 (.405)	.469
EP429	.523 (.531)	.147	.471 (.480)	.0729	.420 (.431)	.0357
EP438	.390 (.388)	.166	.332 (.333)	.0825	.258 (.277)	.0402
EP467	.471 (.456)	.0810	.440 (.417)	.0400	.393 (.376)	.0190

in the GaAs side of the diode and does not use the advantage of the graded band-gap. The photocurrent spectrum for EP438 was not taken, but it has a much lower diffusion voltage (1.58 volts vs. 2.43 volts) than EP429 and in view of the similarity in efficiency to EP467, a suggestion of similar properties to EP467 can be entertained.

Table 2 gives the values of open-circuit voltage (V_{oc}) and short-circuit current (I_{sc}) for the four cells at the three illuminating intensities. A successful attempt was made to calculate V_{oc} from I_{sc} or vice-versa. The figures in parenthesis are the calculated values of V_{oc} as predicted by the following theory.

A short-circuited photodiode produces a current (I_{sc}) proportional to the intensity of the light received. In the open-circuit condition, this current is still being generated, but recirculates through the diode and in the forward direction sets up the open-circuit photo-emf (V_{oc}). This circulating current and V_{oc} must satisfy the I-V relationship for the diode. The circuit model is shown in Figure 24a. The photo-generated current (I_p) must equal the circulating current density (I).

$$I_p = I \tag{1}$$

Since the diode is in forward bias, ideal diode theory predicts

$$I = I_s \left[\left(\exp \frac{qV}{nkT}\right) - 1\right] \tag{2}$$

but for the four cells discussed here, recombination currents and other anomalies lead to an I-V relationship

$$I = I_s' \exp \left(\frac{qV}{\eta kT}\right) \tag{3}$$

at significant forward bias. Therefore

$$I_p = I = I_s' \exp\left(\frac{qV}{\eta kT}\right) \tag{4}$$

Assume now that the light generated current (I_p) is constant regardless of load and depends only on intensity. This is generally a valid assumption. Extrapolating to the short-circuit condition,

$$I_p = I_{sc} \tag{5}$$

and to the open-circuit condition

$$I_p = I_s' \exp\left(\frac{qV_{oc}}{\eta kT}\right) \tag{6}$$

Equating (5) and (6)

$$I_{sc} = I_s' \exp\left(\frac{qV_{oc}}{\eta kT}\right) \tag{7}$$

or

$$V_{oc} = \frac{\eta kT}{} \ln \frac{I_{sc}}{I_s} \tag{8}$$

The figures in parentheses in Table 2 are the calculations of V_{oc} from I_{sc} from this theory. The agreement is very good except for cell EP467.

An extension of the above theory has been made to the case where a load is applied to the diode. The circuit diagram of Fig. 24b is assumed, where I_p is the generated photocurrent and is equal to I_{sc}, I_j is the current which circulates through the diode in the forward direction, and I_L is the current through the external load R. From the model,

$$I_p = I_{sc} = I_j + I_L \tag{9}$$

The junction current must follow the I-V curve, therefore:

$$I_j = I_s' \exp \frac{qV_j}{\eta kT} \tag{10}$$

and

$$I_L = \frac{V_L}{R} = \frac{V_j}{R} \tag{11}$$

Substituting (10) and (11) into (9);

$$I_{sc} = I_s' \left(\exp \frac{qV}{\eta kT}\right) + \frac{V_L}{R} \tag{12}$$

Most of the I-V curves follow (10) over the region of interest, however the values of I_j used in the calculations were taken directly from the I-V measurements for better accuracy. In Figs. 14 - 23, the calculated values of V_L are plotted for the 120 ft-candle light intensity. The additional relation

$$P_o = I_L V_L \tag{13}$$

was used for Figs. 19 - 23.

Again, the agreement is as good as should be expected except for diode EP467. The reason for this deviation is not understood. This method can be used to predict fairly accurately the photo-electric characteristics of a photocell from its I-V curve and its short-circuit current (or open circuit voltage) at any light intensity.

Conclusions

Measurement techniques have been refined for the study of heterojunctions. A basis for comparison of heterojunction solar cells with high efficiency silicon solar cells has been set up which will allow a determination of the relative efficiencies. A method for low temperature (liquid nitrogen) measurement of I-V and possibly capacitance curves should be found to complete the desired set of electrical and electro-optical parameters.

One of the GaAs-GaP graded-gap cells was shown to be approximately 40% as efficient as a silicon cell. These cells are not believed to have been maximized for highest available efficiencies and had no anti-reflection coating. Interpretation of the measurements lead to the conclusion that the graded portions of the diodes are very small and that in some cases the p-n junction is well outside the metallurgical junction. In the latter case, the desirable properties of a heterojunction diode are not realized. The "window" of the short circuit photocurrent spectrum has been shown to exist. Efficiency gains over a silicon cell can be obtained by bracketing the solar spectrum with the "window" of a suitable heterojunction.

II. Si-GaP Heterojunction Photovoltaic Cells

Materials

Silicon and gallium arsenide are the only two materials from which relatively high efficiency solar cells have been made. Many studies of Ge-GaAs and GaAs-GaP heterojunctions have been made, but, except for Ge-Si, no heterojunctions using Si as one of the materials have been extensively studied. An excellent start towards a more thorough exploration of heterojunctions with silicon has been made by R. L. Anderson, et al[9] using Si-GaP. As detailed below, this pair is much more promising than Ge-Si, especially for solar cells. The availability of relatively inexpensive, very high quality, silicon single crystals is an additional reason for using silicon as a base-line material.

A primary factor in the choice of material pairs is the requirement of epitaxy. This essentially limits the number of semiconductors to those of the diamond cubic structure (similar to silicon) and with lattice mismatch* to less than 7%.

Other limiting factors in the choice of materials come from consideration of the operation of a heterojunction as a solar cell. The spectrum of solar radiation peaks at about 1.4 eV. Proper utilization of the "window" effect of a heterojunction requires that the energy gaps be above and below 1.4 eV. This "window" effect is the basic property of heterojunctions that holds promise for higher efficiency solar cells than have presently been achieved.

---

* Lattice mismatch between semiconductors of lattice constants a_1 and a_2 is defined as $2(a_2 - a_1)/(a_1 + a_2)$.

While epitaxy is relatively uninhibited with lattice mismatches of less than 7%, mismatches of more than about 2% produce undersirable electrical characteristics, as in the case of the Ge-Si heterojunction. With any mismatch, bonding deficiencies exist at the interface. Dislocations and interface states act as fast recombination centers nullifying the possible output of any hole-electron pairs they trap. Serious degradation of the photocell efficiency occurs if the interface state density is sufficiently high.

A semiconductor pair which has considerable promise is silicon-gallium phosphide. The energy gap of GaP is 2.25 eV. Its lattice constant is 5.4505 Å compared to silicon's 5.4307 Å, the mismatch being 0.18%. This should produce negligible interface states due to lattice mismatch effects.

Another semiconductor pair that might be useful for solar cells is germanium-zinc selenide. Exploratory work with this pair has been carried out by Feucht and Milnes[10]. However, the mobilities are smaller in ZnSe than in GaP and, in general, it is more difficult to produce excellent quality II-VI compounds than III-V compounds.

Theory of the Si-GaP Heterodiode

The materials readily available and suitable for making the Si-GaP heterojunctions were 1 ohm-cm and 0.1 ohm-cm p-type boron-doped silicon and $10^{17}/cm^3$ tellerium-doped gallium phosphide. A model has been constructed for these materials and evaluated for photodiode performance.

The model is based on the energy band profile theory proposed by Anderson[1] and substantially verified for a number of different heterojunctions.

This model proposes discontinuities in the valence and conduction band edges arising from the difference in electron affinities of the materials. Since these discontinuities are in general different, the barrier to electrons does not equal the barrier for holes. The minority carrier transport theory has to be modified to take this into account.

The Fermi level in the materials was calculated from the Fermi distribution function analysis given by Kittel[11].

$$e^{-E_F/kT} = \frac{-1 + \left[1 + 4\frac{N_a}{N_v} e^{E_a/kT}\right]^{\frac{1}{2}}}{2e^{E_a/kT}} \qquad (1)$$

$$e^{E_F/kT} = \frac{-1 + \left[1 + 4\frac{N_d}{N_c} e^{(E_g-E_d)/kT}\right]^{\frac{1}{2}}}{2e^{-E_d/kT}} \qquad (2)$$

where

$$N_v = 2(2\pi\, m_h^*\, kT/h^2)^{3/2}$$

$$N_c = 2(2\pi\, m_e^*\, kT/h^2)^{3/2}$$

The derivation assumes complete thermal ionization of donors and acceptors and defines the valence band edge as zero energy. Using the values

E_a = 0.046 eV above the valence band edge (Ref. 12)

(E_g-E_d) = 0.11 eV below the conduction band edge (Ref. 13)

m_e^* (GaP) = 0.35 m_e (Ref. 14)

m_h^* (Si) = 0.39 m_h

E_g (Si) = 1.10 eV

E_g (GaP) = 2.25 eV

the Fermi levels with respect to the relevant band edge are

E_F (GaP) = 0.11 eV below the conduction band edge

E_F (1 Ω -cm Si) = 0.151 eV above the valence band edge

E_F (.1 Ω -cm Si) = 0.068 eV above the valence band edge

The electron affinities, χ , for silicon and gallium phosphide are 4.15 eV respectively. The room temperature energy band diagrams for the materials before epitaxy are given in Fig. 25.

The equilibrium energy band profile for the 1 Ω -cm silicon case is given in Fig. 26. The following equations were used to derive the diagram[15]:

$$\Delta E_c = \chi_{Si} - \chi_{GaP}$$

$$\Delta E_v = E_{g\ GaP} - E_{g\ Si} - \Delta E_c$$

$$V_D = \phi_{Si} - \phi_{GaP}$$

$$V_D = \chi_{Si} + E_{g\ Si} - \delta_{Si} - \chi_{GaP} - \delta_{GaP}$$

The diffusion voltage (V_D) is equal to the sum of the partial voltages across each of the materials. Applied voltages will also divide unequally between the two materials. The diffusion voltages across each of the materials are

$$V_{D\ Si} = \frac{\epsilon_{GaP}\ N_{GaP}}{\epsilon_{Si}\ N_{Si} + \epsilon_{GaP}\ N_{GaP}}\ V_D$$

$$V_{D\ GaP} = \frac{\epsilon_{Si}\ N_{Si}}{\epsilon_{Si}\ N_{Si} + \epsilon_{GaP}\ N_{GaP}}\ V_D$$

$$V_D = V_D - V_{Si}$$

In the case considered, $V_{D\ Si}$ = 0.52 eV and $V_{D\ GaP}$ = 0.12 eV.

The depletion widths in the materials will also be different. Assuming an abrupt, uniformally doped junction, they are given by

$$\ell_{Si} = \left[\frac{2\ \varepsilon_{Si}\ \varepsilon_{GaP}\ N_{GaP}\ V_D}{q\ N_{Si}\ (\varepsilon_{Si}\ N_{Si} + \varepsilon_{GaP}\ N_{GaP})}\right]^{1/2}$$

$$\ell_{GaP} = \left[\frac{2\ \varepsilon_{GaP}\ \varepsilon_{Si}\ N_{Si}\ V_D}{q\ N_{GaP}\ (\varepsilon_{Si}\ N_{Si} + \varepsilon_{GaP}\ N_{GaP})}\right]^{1/2}$$

Again for the case of Fig. 26, ℓ_{Si} = 1950 Å and ℓ_{GaP} = 351 Å.

The 0.1 Ω -cm silicon case has the same energy band diagram as Fig. 26 except for the values

$$V_D = 0.73 \text{ eV}$$

$$V_{D\ Si} = 0.09 \text{ eV}$$

$$V_{D\ GaP} = 0.64 \text{ eV}$$

$$\ell_{Si} = 155 \text{ Å}$$

$$\ell_{GaP} = 775 \text{ Å}.$$

In this case the GaP has more control of the parameters because of its larger partial diffusion voltage and depletion width. This case should be useful in determining the transport and electro-optical properties of heterojunction, but is not expected to be as efficient a photocell as the Si-dominated case.

These band diagrams point out another advantage of the pSi-nGaP heterojunction over other possibilities. In contrast to most heterojunctions (see Ref. 1, for example), the pSi-nGaP does not have a notch in either the conduction or valence band edges. These notches become step barriers for the carriers to penetrate and frequently become tunnelling

barriers, which are undesirable in a high efficiency photocell. If the barrier is large enough, the notches may create trapping sites which are especially undesirable.

The transport theory for the pSi-nGaP heterodiode has not been attempted because, as stated in the introduction, it is difficult to decide beforehand which transport model to use.

Experimental Results

For convenience, and in the hope that epitaxy could be achieved at a relatively low temperature (thus promoting coincidence of physical and electrical interfaces), vacuum evaporation of GaP onto Si was the fabrication technique chosen for initial study.

However, many of the III-V compounds dissociate when heated in a vacuum. One of the components evaporates more readily than the other, producing a vapor that is deficient in the less volatile component. The deposit resulting from these vapors is not stoichiometric. GaP is one of the compounds that dissociate this way, the phosporous being more volatile than the gallium.

Flash evaporation[16] is a technique used to maintain the correct composition of the vapor. Small grains of the III-V compound are evaporated by a heater whose temperature is high enough to vaporize rapidly the least volatile component. If the grains are small enough so that each grain vaporizes almost instantaneously and completely, the vapor will have the same composition as the source material. Many III-V and other compounds have been successfully deposited using this method.

The GaP powder is placed in a trough and vibrated so that the GaP particles fall into a cylindrical tantalum evaporator. The temperature of the evaporator, approximately 1600°C, is measured by an optical

pyrometer sighted through a small hole in the radiation shield surrounding the evaporator. The silicon substrate is held against a tungsten strip by a nickel block. The temperature of the substrate is set primarily by the tungsten strip heater and secondarily by radiation from the tantalum evaporator, and is measured by a thermocouple welded to the nickel block.

Prior to placing in the vacuum system, the silicon (111) wafer is lapped with 600 SiC grit, cleaned in trichloroethylene and isopropyl alcohol with ultrasonic agitation, heavily chemically polished in White Etch with bromine added, rinsed in deionized water, and finally rinsed in ultrasonically agitated isopropyl alcohol.

Out of 38 depositions, six were proven to be either polycrystalline or oriented-polycrystalline deposits of GaP on silicon. The thinner deposits are shiny and red-orange, whereas the thicker deposits are matte and gray-white. The crystalline nature of the films is partially determined by Laue back reflection x-ray photograms. The substrate temperature is very critical, oriented polycrystalline deposits being obtained over a range of 20°C at about 670°C.

Several of the deposits do not show any x-ray reflection patterns, but appear to be micro-polycrystalline from an examination of the deposit by optical microscopy. These deposits were produced at substrate temperatures lower than those that yield x-ray patterns consisting of either spotted or continuous rings. At higher substrate temperatures the phosphorous evaporates from the substrate surface leaving an excess of gallium.

The fact that oriented polycrystalline GaP deposits were obtained suggests strongly that single crystal deposits can be obtained under appropriate conditions. The problems seem to be determination of the proper

substrate and evaporator temperatures, and proper preparation of the silicon surface. In particular, the major problem is to keep the surface of the silicon substrate free of silicon dioxide.

As a generalized check on our equipment, the epitaxial deposition of GaP on (111) germanium was attempted by flash evaporation, duplicating the work of Richards, et al[16]. Eight runs were made yielding deposits about five microns thick, as determined gravimetrically. Laue back reflection x-ray photograms gave no negative indications, i. e. no rings were observed, only the spots from the germanium substrate were visible. However, electron diffraction plates* displayed intense spots or spots plus faint rings (which might be due either to polycrystalline regions or to multiple diffraction from the matte surface). It was concluded that the GaP was substantially single crystalline.

A possible method to circumvent the formation of SiO_2 on silicon substrates is to cleave the silicon in vacuo while evaporating GaP. A fixture has been designed and is under construction which will support, cleave, and heat the silicon substrate. In operation, the GaP source will first be activated, and then the silicon cleaved. The GaP vapor should deposit on the silicon before any oxide is formed, and it is hoped that epitaxial single crystal films will be achieved.

---

* Electron diffraction plates were taken at the Ledgemont Laboratory of the Kennecott Copper Company, Lexington, Mass., through the courtesy of Dr. K. Chopra.

Summary

Silicon and gallium phosphide have been chosen as the most promising materials for a heterojunction photocell. An energy band model for this pair is proposed. Attempts to fabricate diodes are being made by flash evaporation of GaP on silicon substrates. Silicon slices were originally used as substrates; however, silicon dioxide on the surface of the slices prevented epitaxy. A fixture is now being used that cleaves the silicon under deposition conditions, the GaP forming a deposit (hopefully epitaxial) before the formation of silicon dioxide.

Depositions of GaP on germanium were carried out as a check on the equipment. Electron diffraction pictures showed that these deposits were single crystal when formed under temperature conditions similar to those used by other investigators.

References

1. R. L. Anderson, "Ge-GaAs Contacts" Thesis, Syracuse University, 1960.

2. S. S. Perlman and D. L. Feucht, "p-n Heterojunctions", Solid-State Electronics, 7, 911, (1964).

3. Arthur R. Riben, "n Ge-p GaAs Heterojunctions" Thesis, Carnegie Institute of Technology, 1965.

4. R. L. Anderson, "Experiments on Ge-GaAs Heterojunctions", Solid-State Electronics, 5, 341, (1962).

5. A. Lopez and R. L. Anderson, "Photocurrent Spectra of Ge-GaAs Heterojunctions", Solid-State Electronics, 7, 695, (1964).

6. B. Agusta and R. L. Anderson, "Opto-Electric Effects in Ge-GaAs p-n Heterojunctions", Journal of Applied Physics, 36, 206, (1965).

7. S. S. Perlman, "Heterojunction Photovoltaic Cells", Advanced Energy Conversion, 4, 184, (1964).

8. Eagle-Picher Research Laboratories, under Government Contracts DA-36-039-SC-85246 (1960) and DA-36-039-SC-87408 (1961).

9. R. L. Anderson, G. Zeidenbergs, S. Yawata, T. Huang, D. Boyce, and M. Reutlinger, "Heterojunction Devices", Defense Documentation Center Report No. AD 635026, 1966.

10. D. L. Feucht and A. G. Milnes, "Semiconductor Heterojunction Structure Studies", Air Force Cambridge Research Laboratories Report No. AFCRL-66-447, June 1966.

11. C. Kittel, "Introduction to Solid State Physics", John Wiley & Sons, Inc., New York, 1962, p. 358-361.

12. T. S. Moss, "Optical Properties of Semiconductors", Butterworth & Co., London, 1961.

13. D. N. Nasoldov et al, "Electrical Properties of Gallium Phosphide Doped with Tellerium", Soviet Physics-Solid-State, 7, 1549, (1965).

14. T. S. Moss and B. Ellis, Proc. Phys. Society (London), 83, 217, (1964).

15. J. R. Donnelly, "Studies of Ge-GaAs and Ge-Si Heterojunctions", Defense Documentation Center Report No. AD 623842, 1965.

16. J. L. Richards et al, J. Appl. Phys., 35, 3418, (1964).

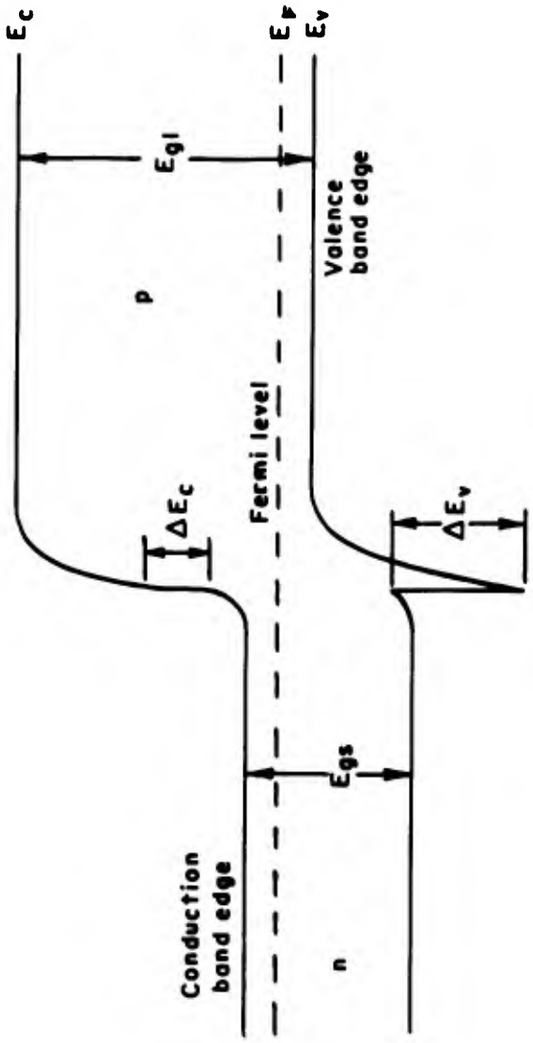

Fig. 1. Equilibrium Energy Band Diagram For A nspl Heterojunction

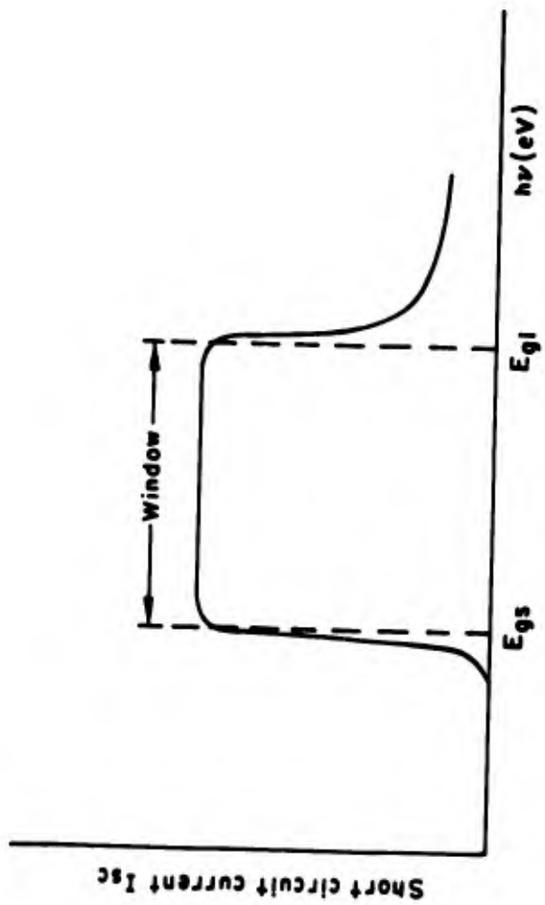

Fig. 2. Spectral Response of a Heterojunction Photocell

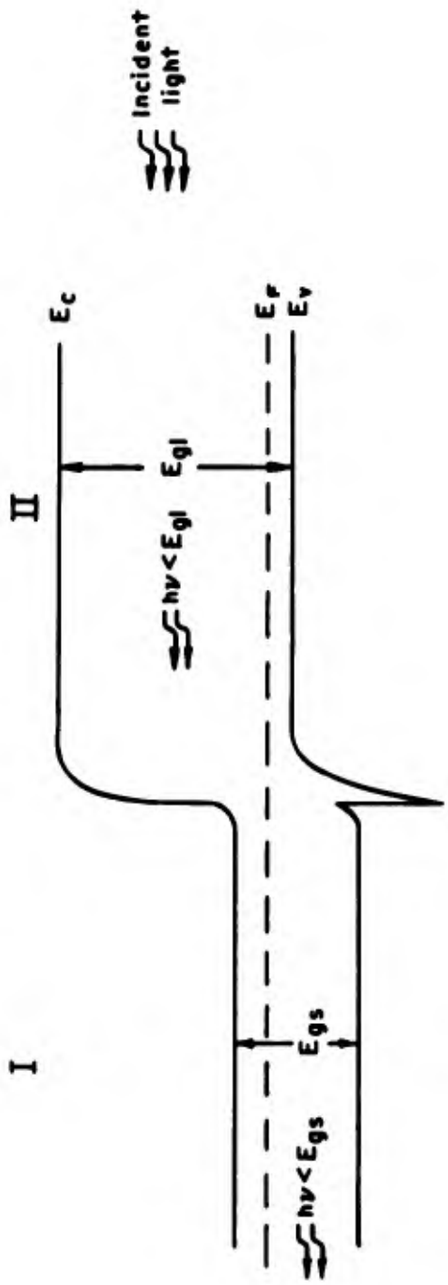

Fig. 3. Energy Band Diagram of Heterojunction

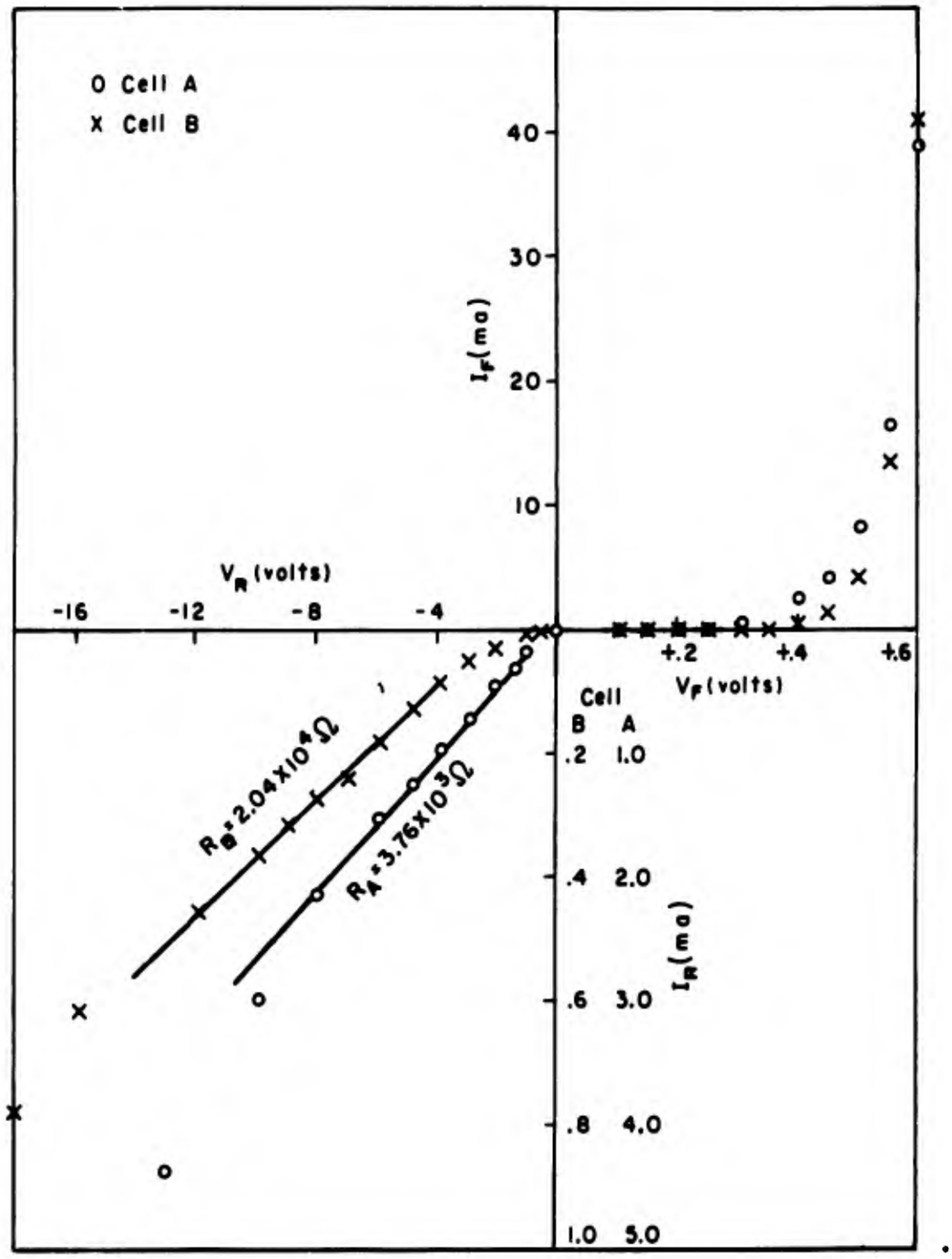

Fig. 4 - I-V Curves, Silicon Cells A & B, @ 80°F, in the Dark.

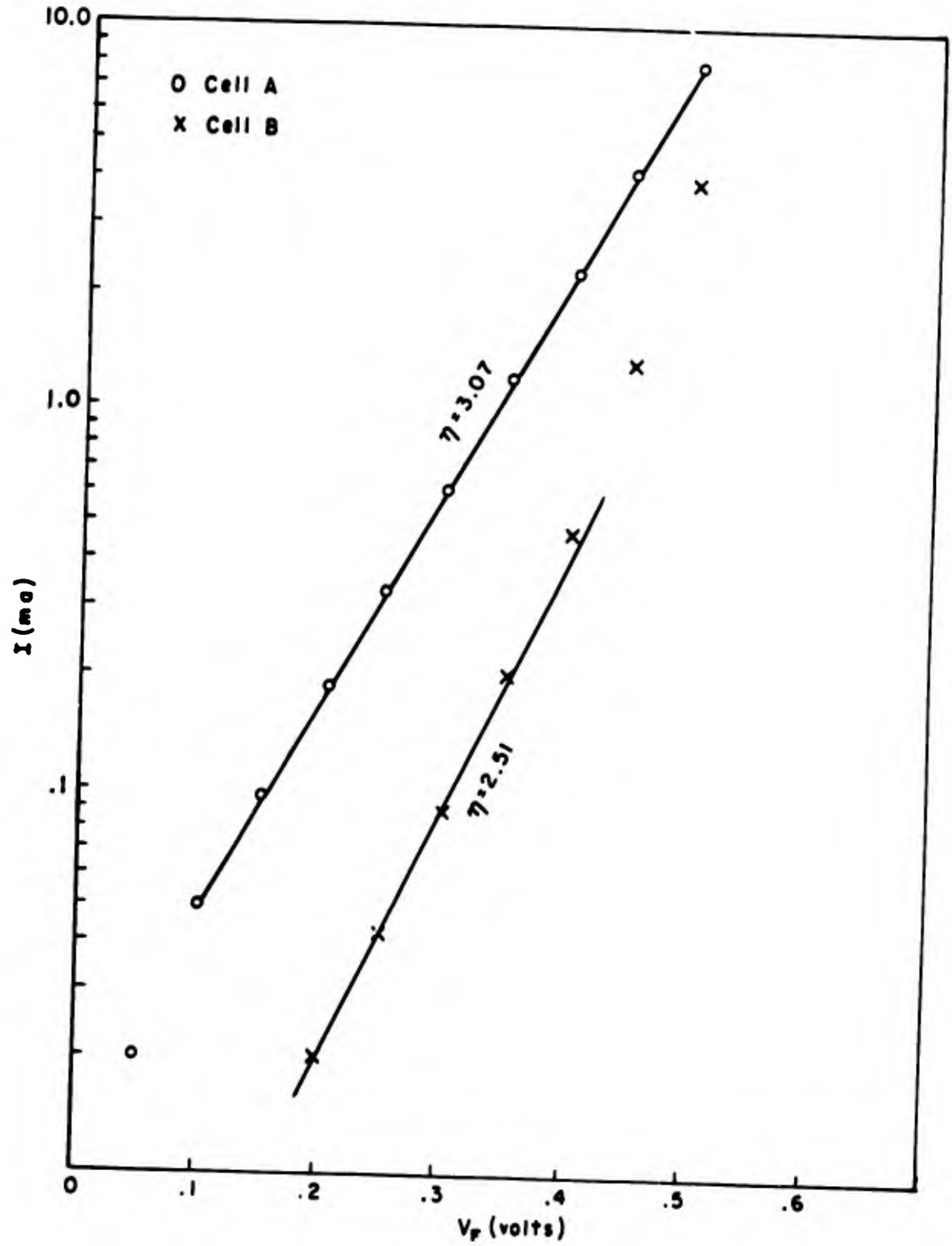

Fig. 5 - Forward Bias I-V Curve Silicon Cells A & B

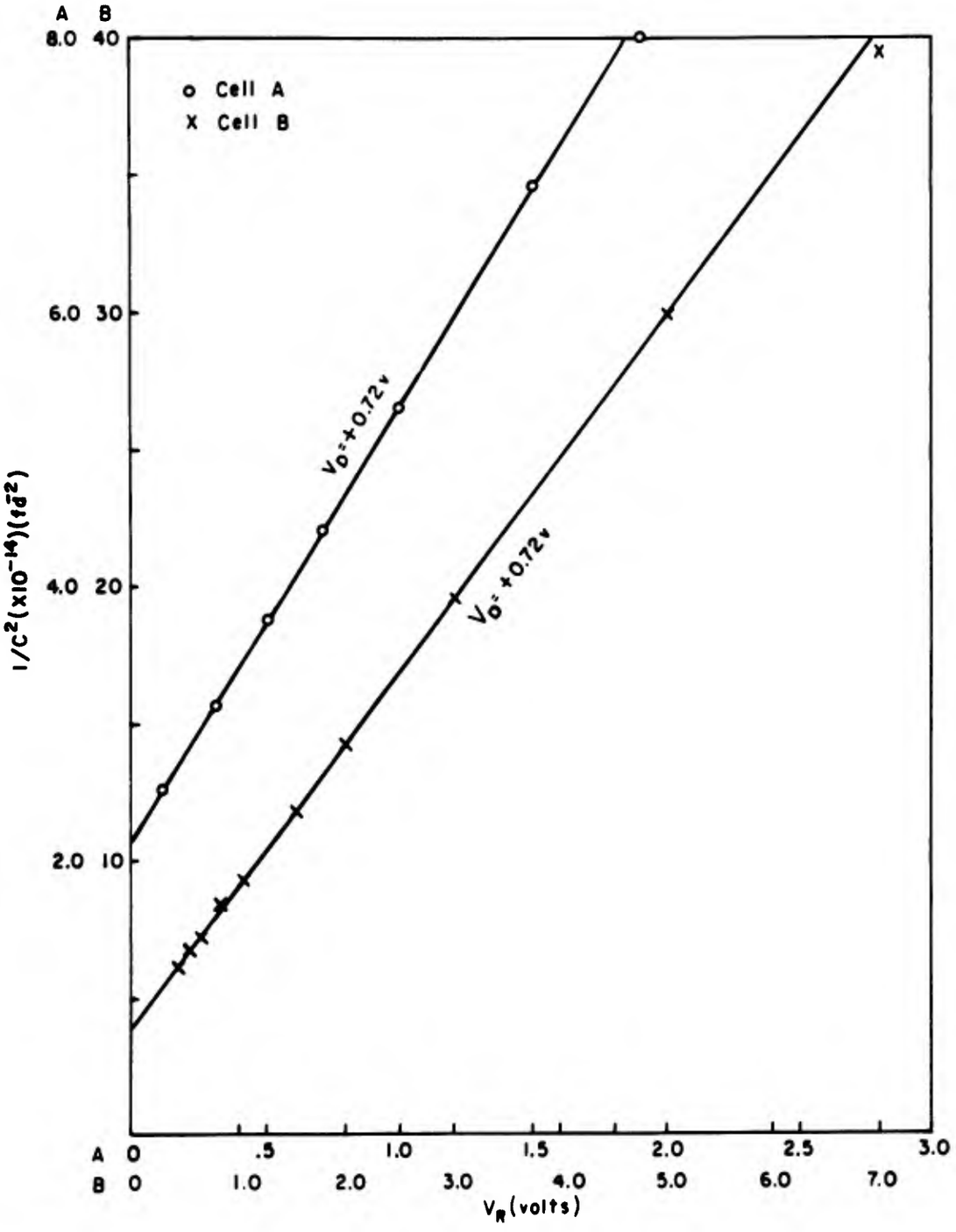

Fig. 6 - $1/c^2$ vs. Reverse Bias, Silicon Cells A & B, @ 80°F, in the Dark.

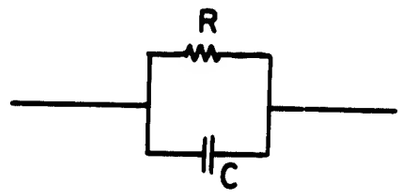

(a) Ideal

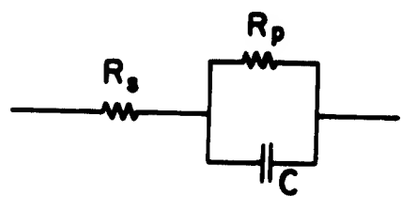

(b) Actual

Fig. 7. Small Signal Equivalent Circuit Model of Solar Cell in the Dark.

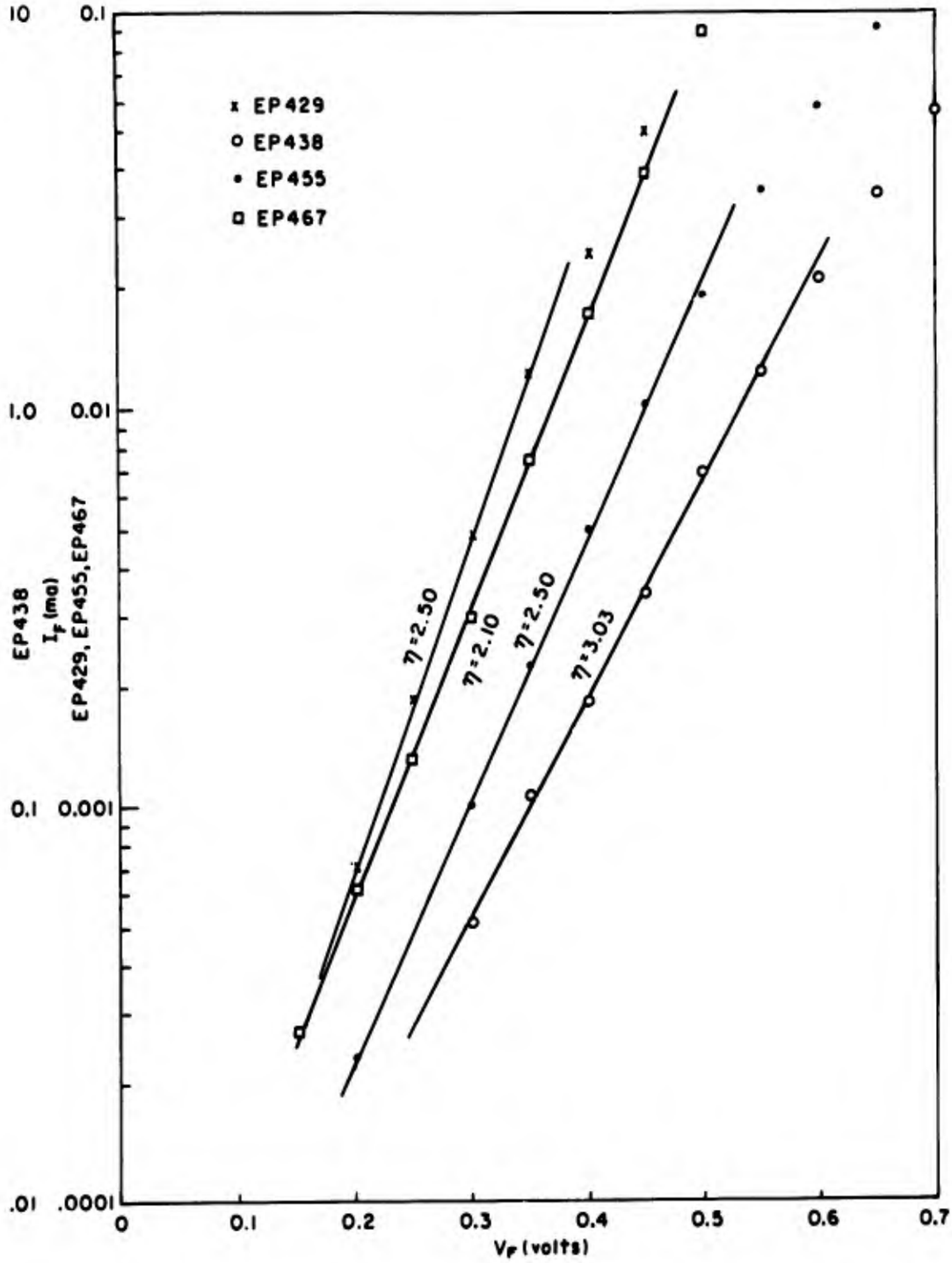

Fig. 8. Room Temperature Forward-Bias I-V Curves for GaAs-GaP Graded-Gap Solar Cells.

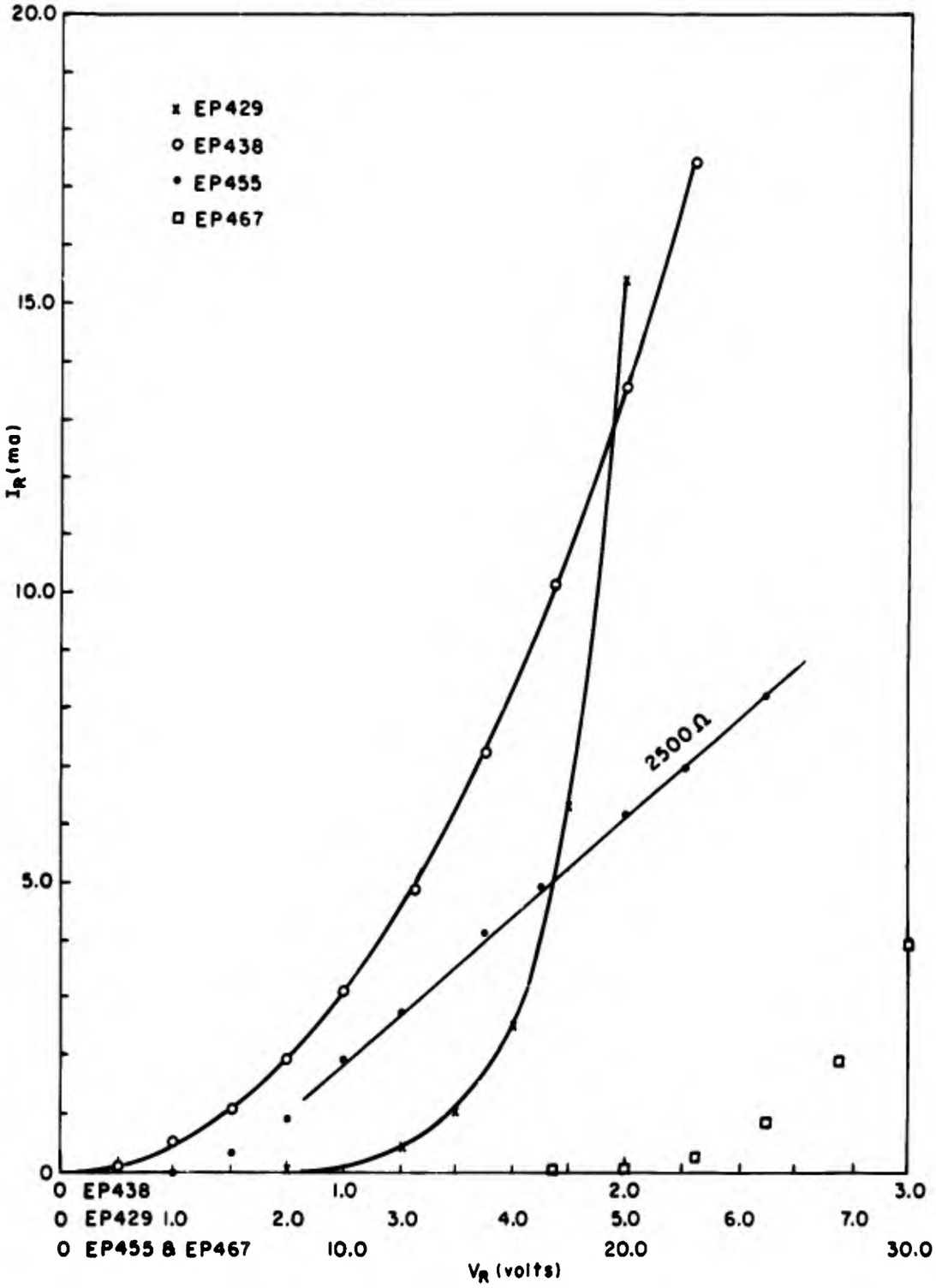

Fig. 9. Room Temperature Reverse-Bias I-V Curves for GaAs-GaP Graded-Gap Solar Cells.

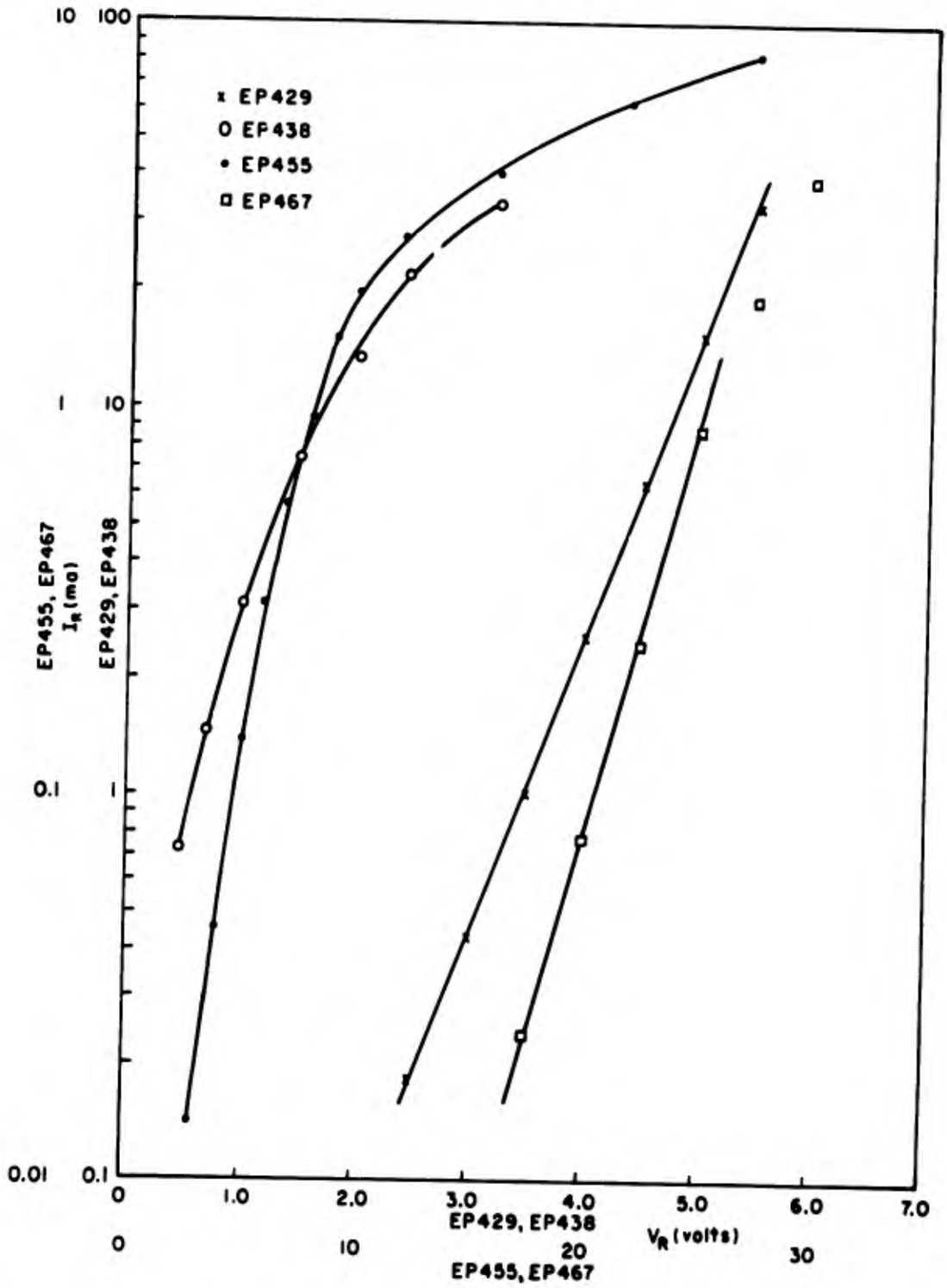

Fig. 10. Room Temperature Reverse-Bias I-V Curves for GaAs-GaP Graded-Gap Solar Cells.

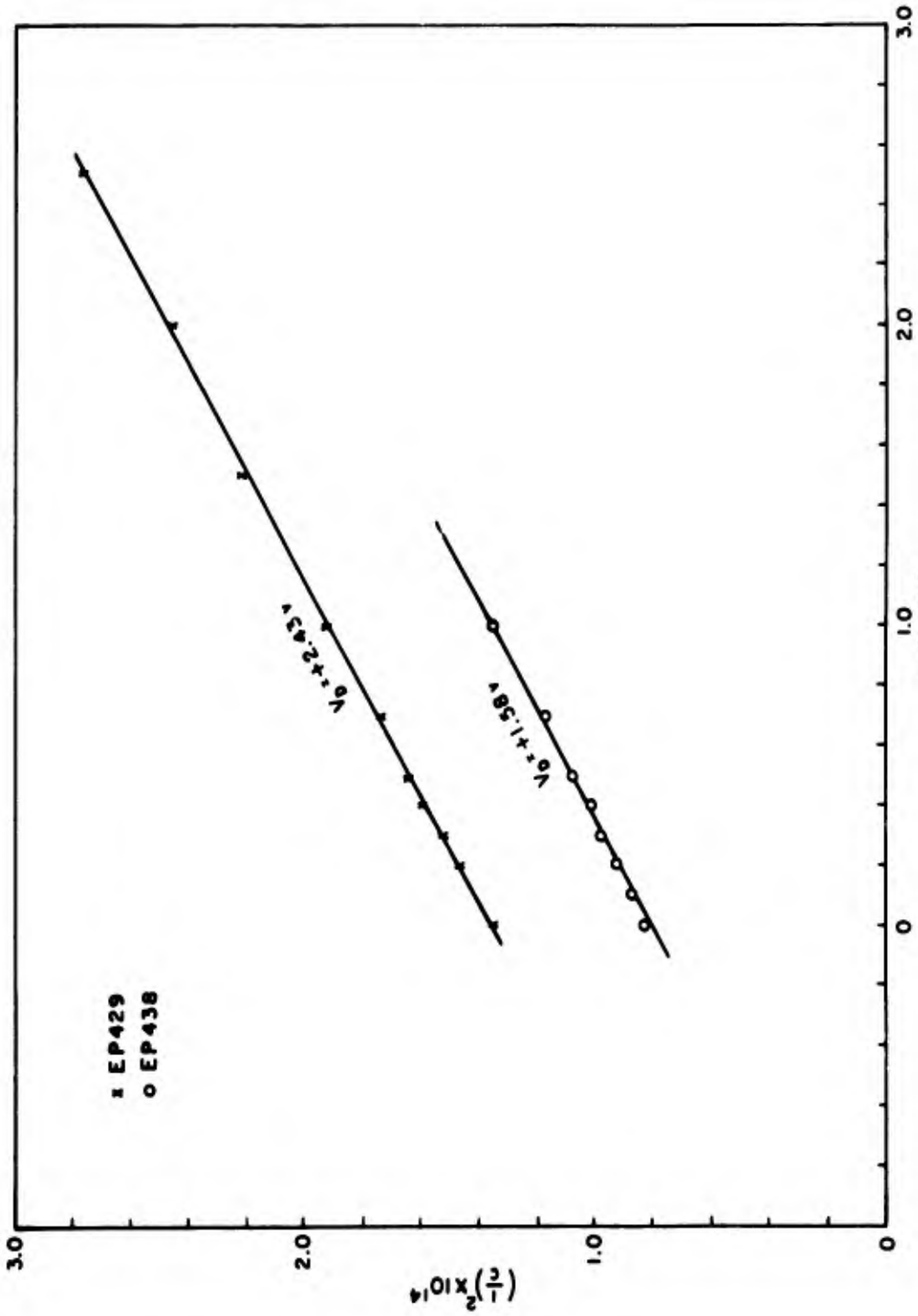

Fig. 11. $(\frac{1}{C})^2$ Versus Reverse-Bias for GaAs-GaP Graded-Gap Solar Cells.

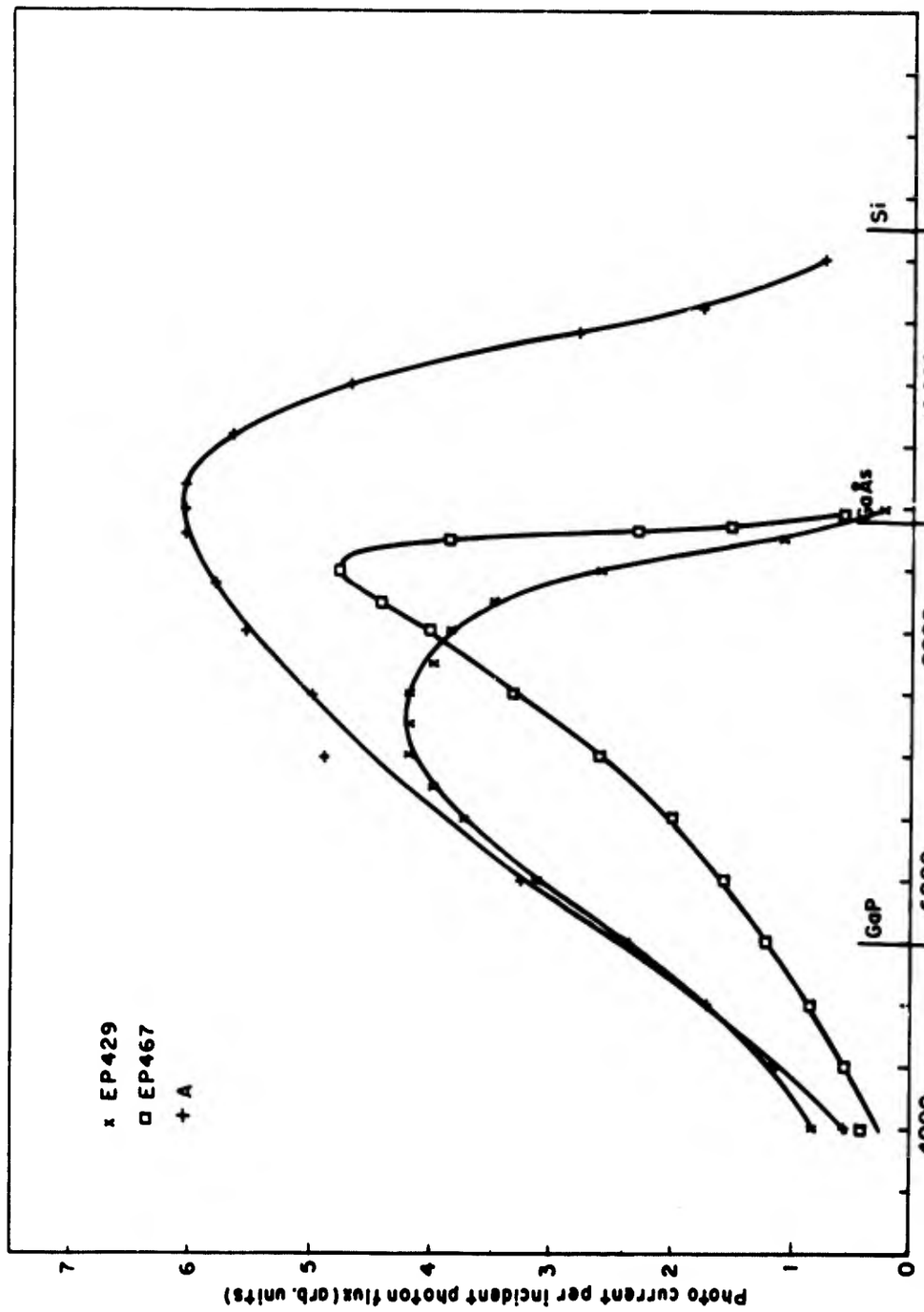

Fig. 12. Photocurrent Spectral Response of Silicon and GaAs-GaP (Graded-Gap) Solar Cells.

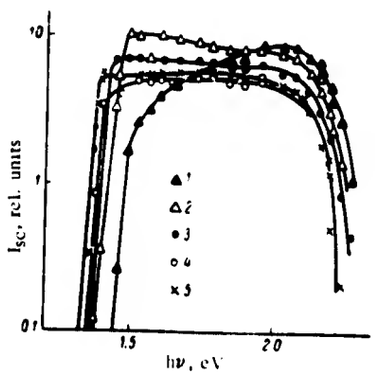

Fig. 13. Spectral Dependence of the Photo-emf at Various Temperatures T (in °K): 1) 80; 2) 215; 3) 240; 4) 320; 5) 350. (Alf̈erov, et al, Soviet Physics - Solid State, 7, 990 (1965)).

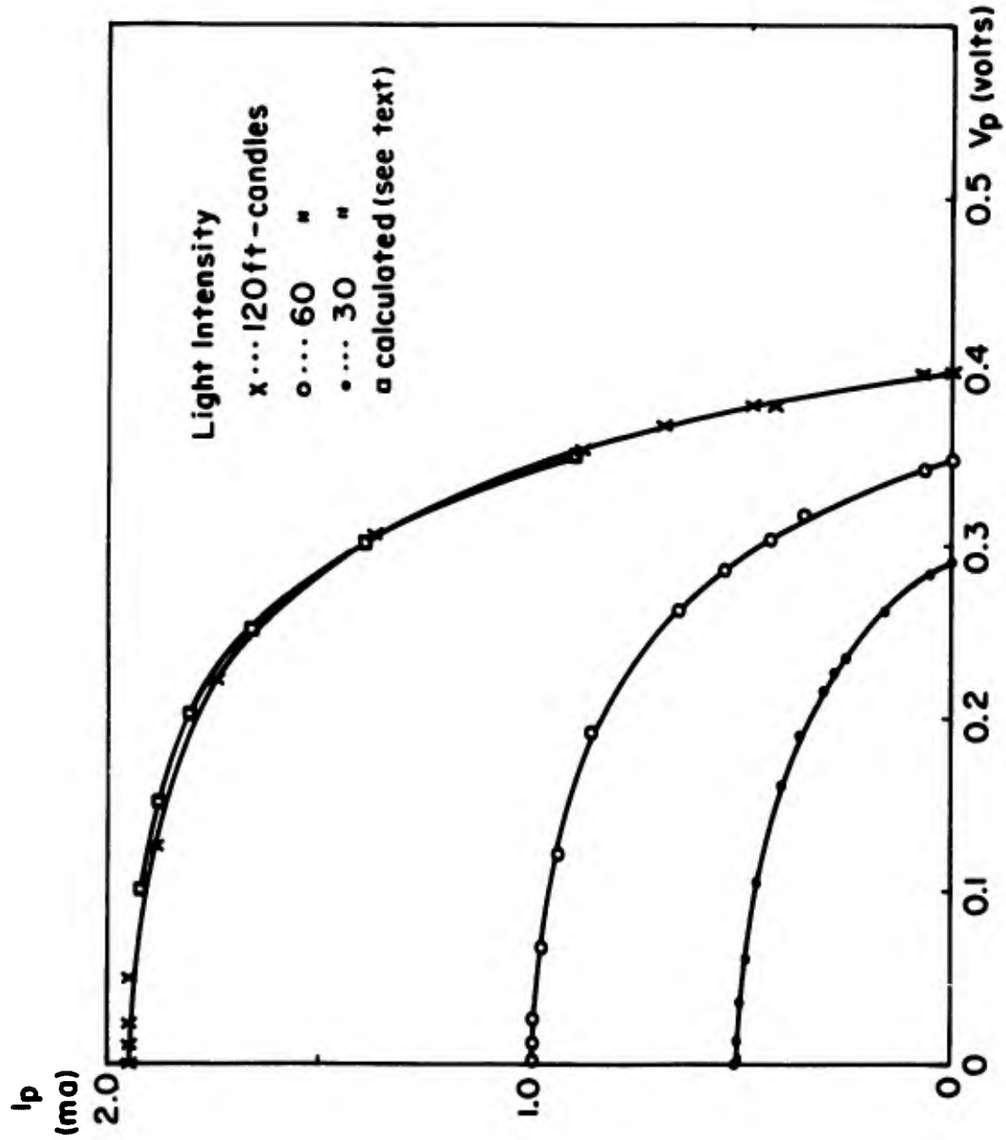

Fig. 14. Photocurrent vs Photovoltage; Varying Loads at Three Light Intensities, Silicon Cell A.

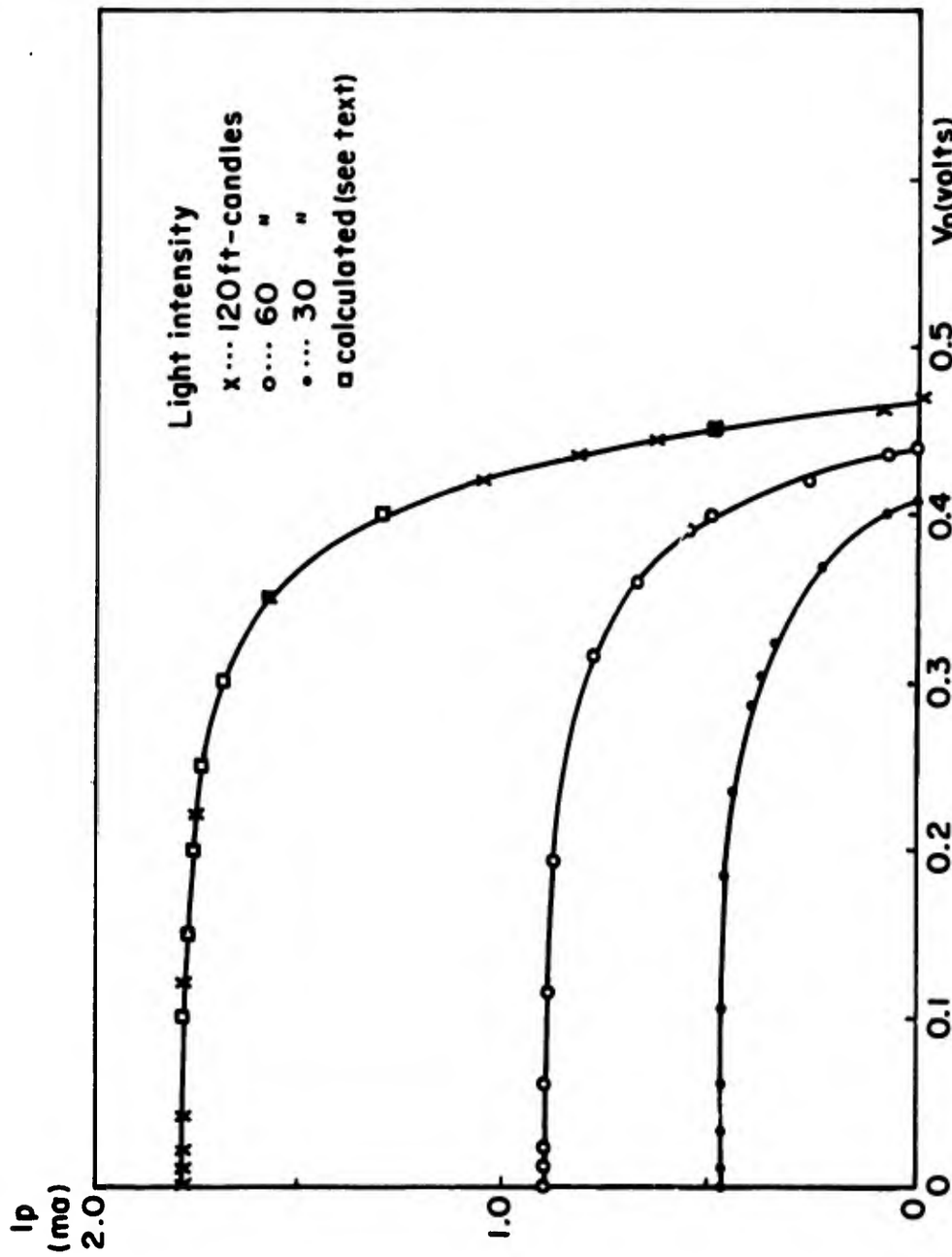

Fig. 15. Photocurrent vs Photovoltage; Varying Loads at Three Light Intensities, Silicon Cell B.

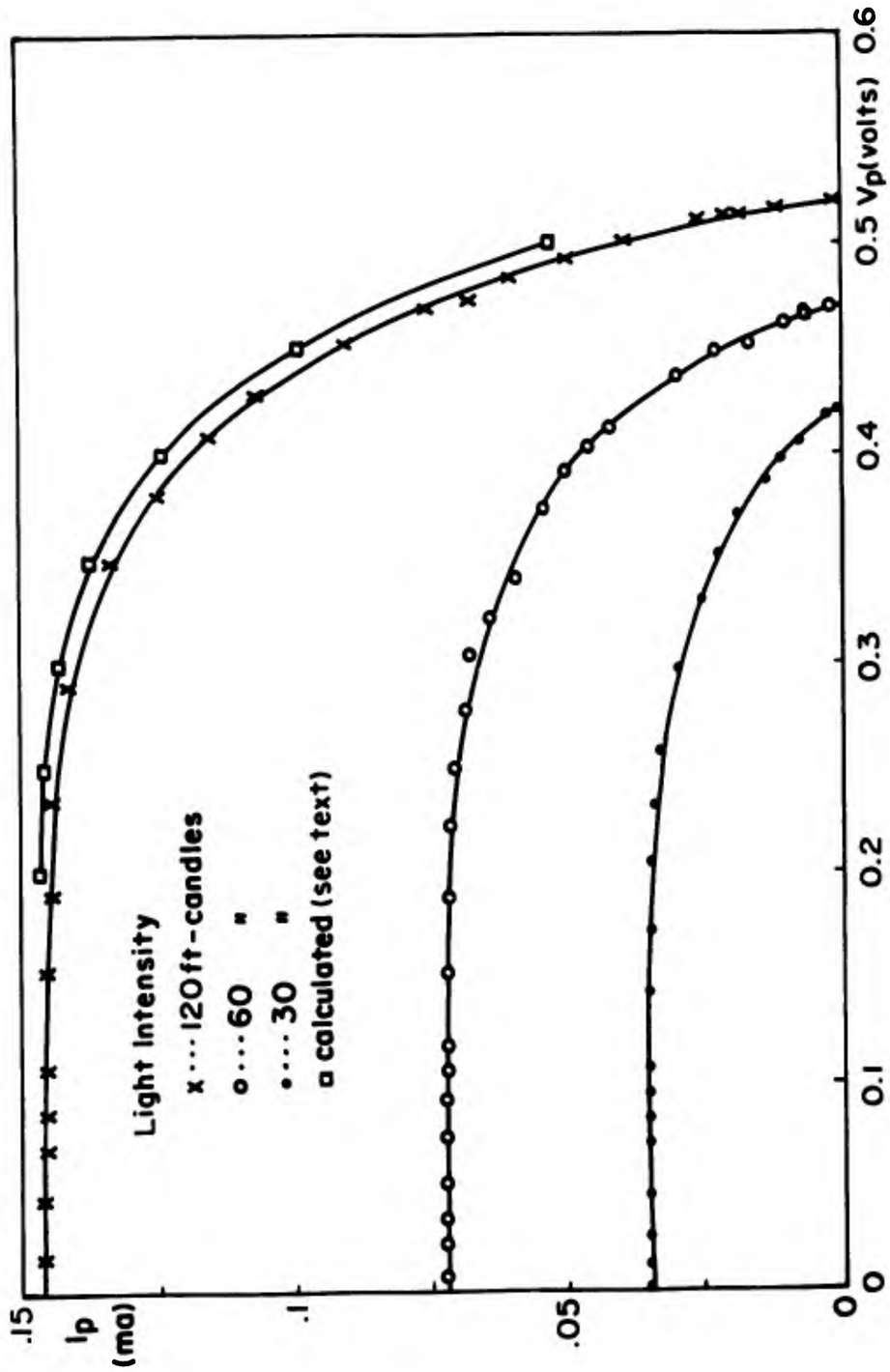

Fig. 16. Photocurrent vs Photovoltage; Varying Loads at Three Light Intensities, EP429 GaAs-GaP Graded Gap Cell.

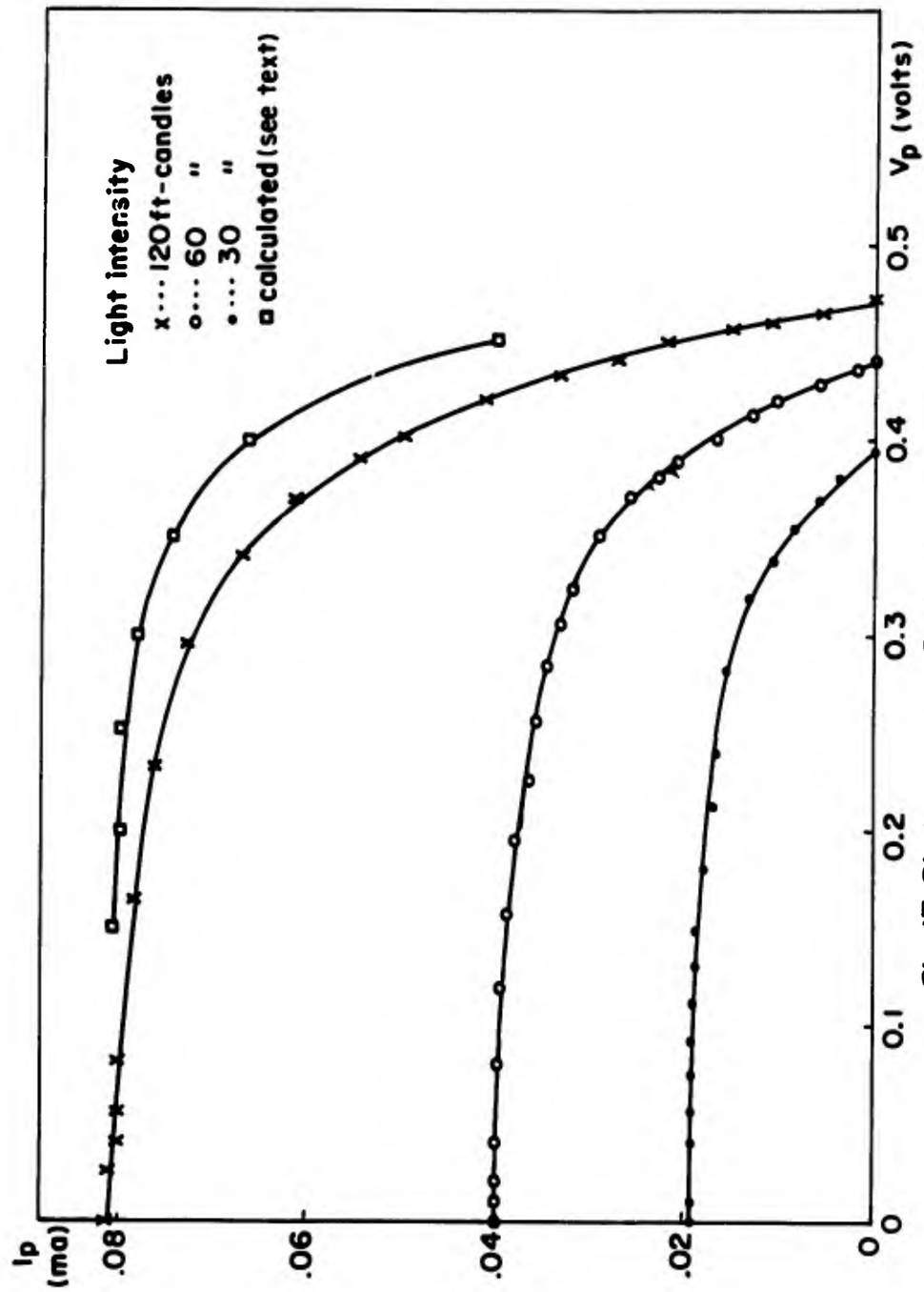

Fig. 17. Photocurrent vs Photovoltage; Varying Loads at Three Light Intensities, EP467 GaAs-GaP Graded Gap Cell.

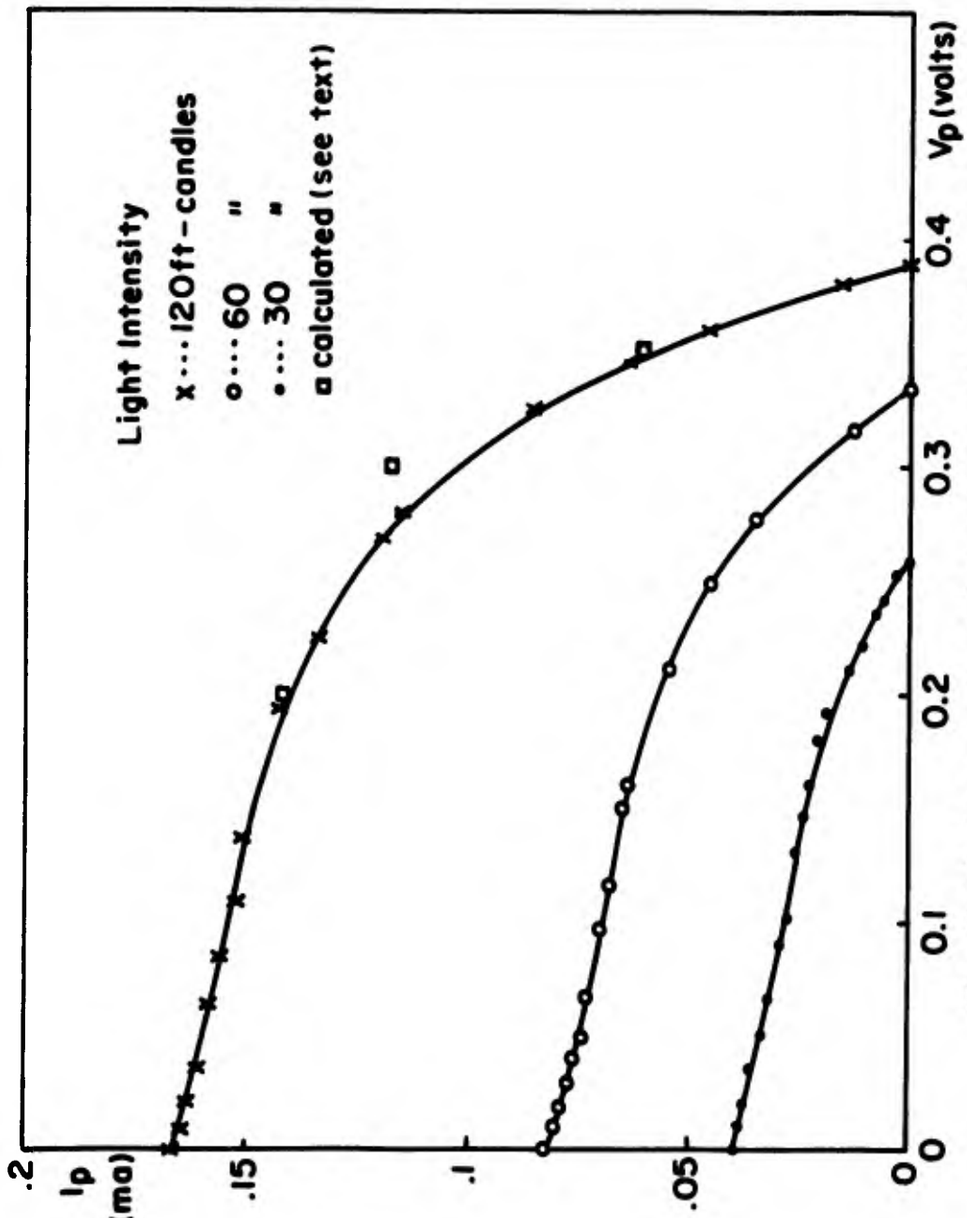

Fig. 18. Photocurrent vs Photovoltage; Varying Loads at Three Light Intensities, EP438 GaAs-GaP Graded Gap Cell.

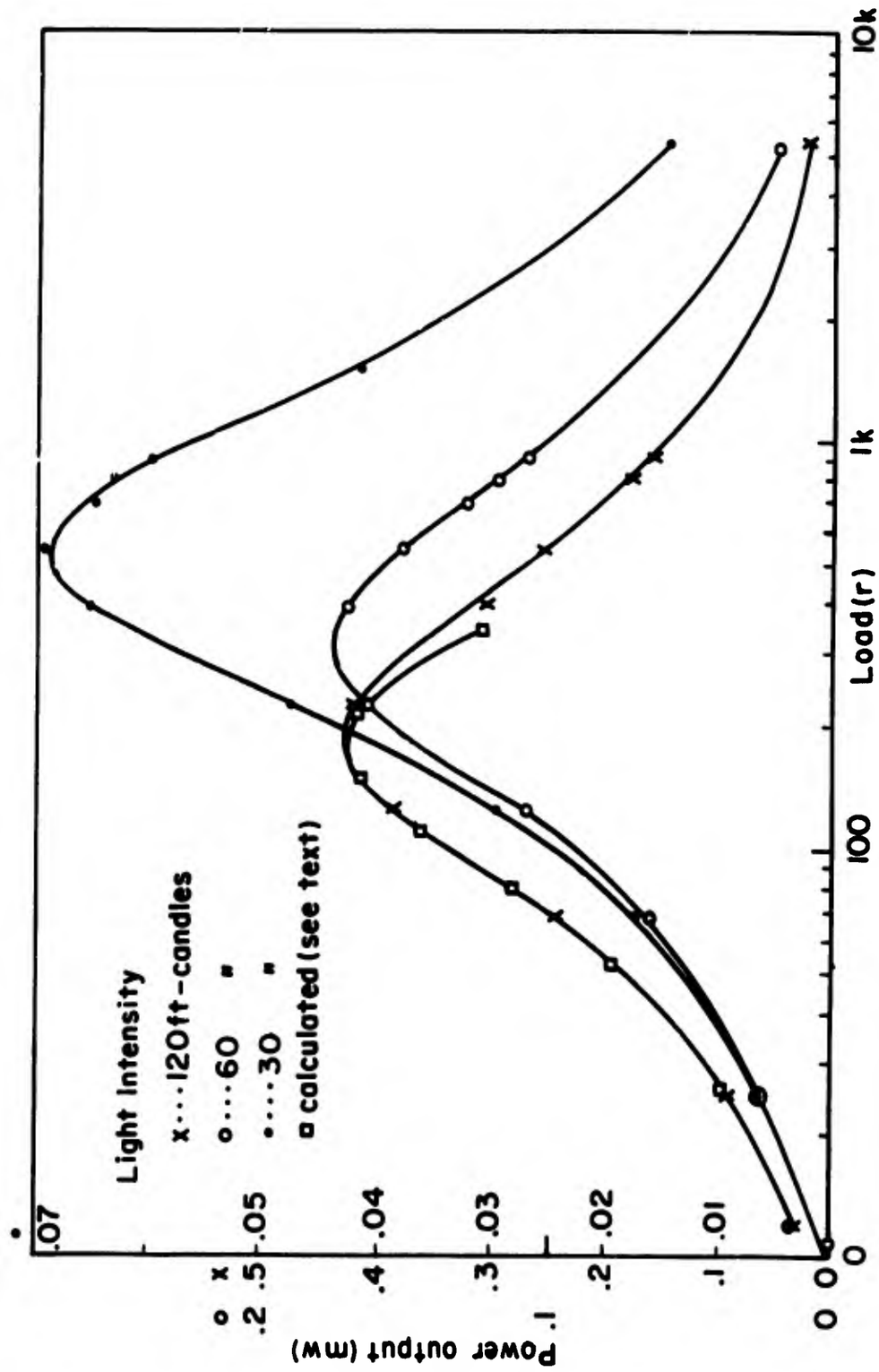

Fig. 19. Photocell Power Output vs Load for Three Light Intensities, Silicon Cell A.

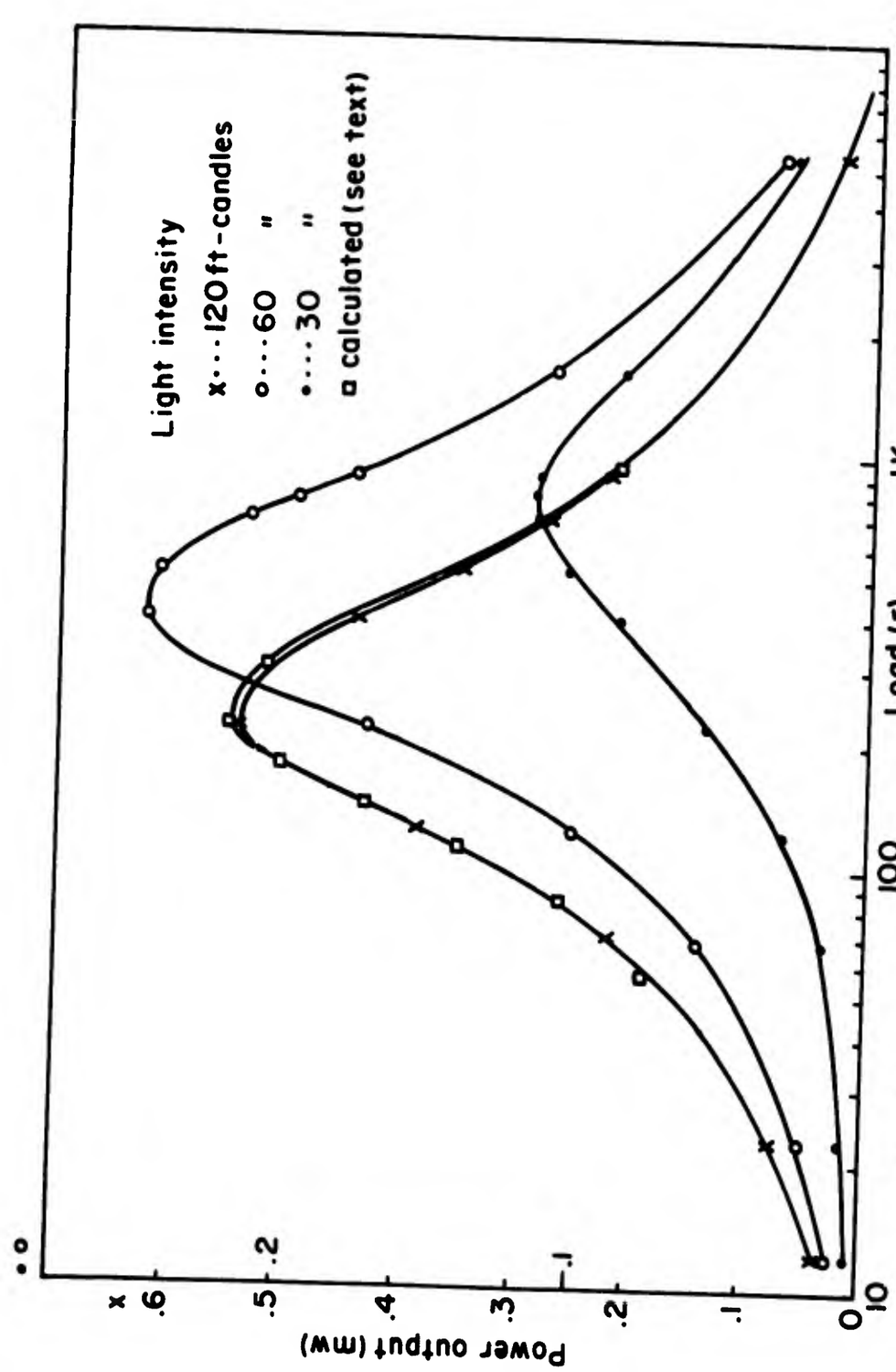

Fig. 20. Photocell Power Output vs Load for Three Light Intensities, Silicon Cell B.

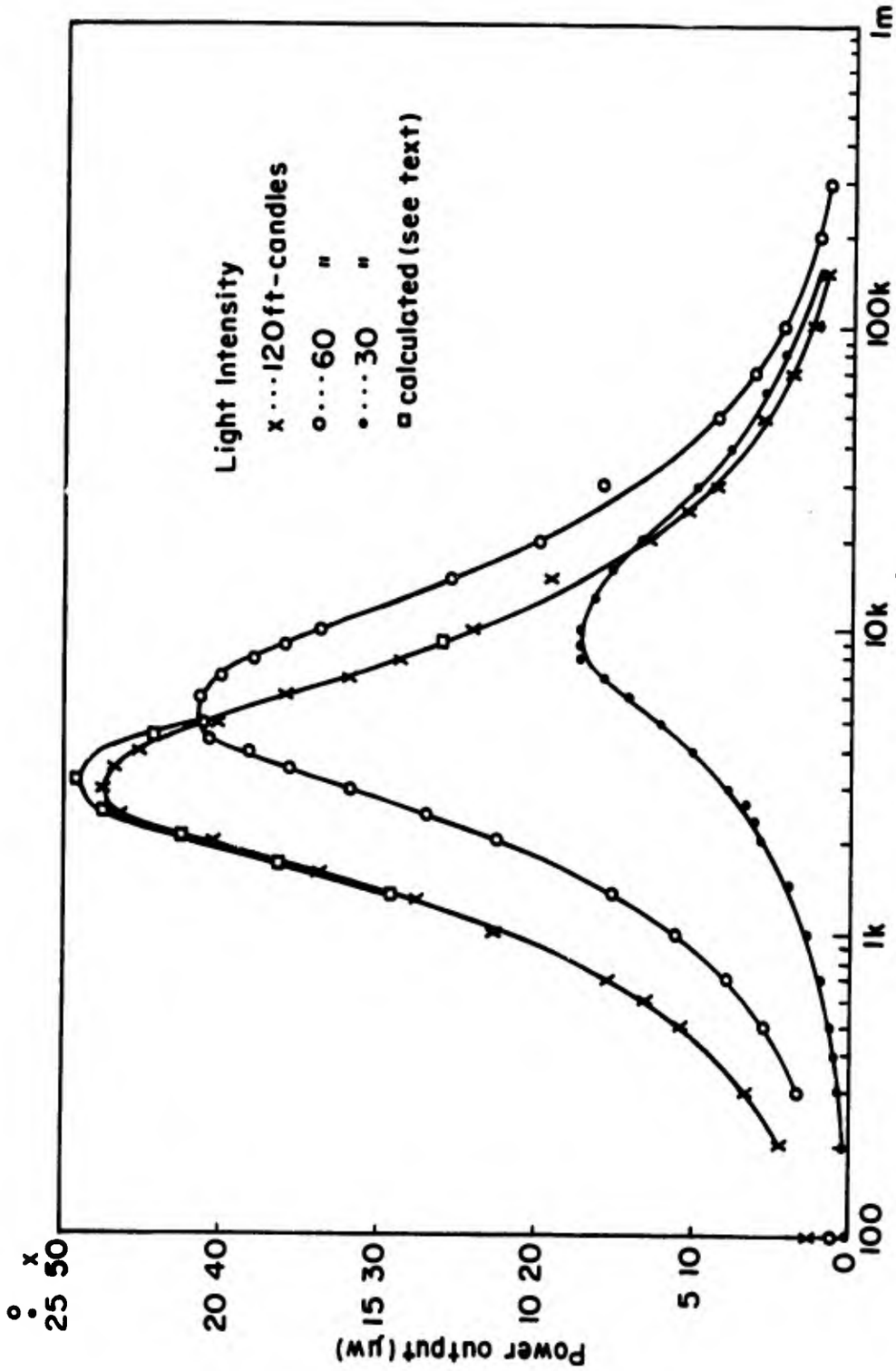

Fig. 21. Photocell Power Output vs Load for Three Light Intensities, EP429 GaAs-GaP Graded Gap Cell.

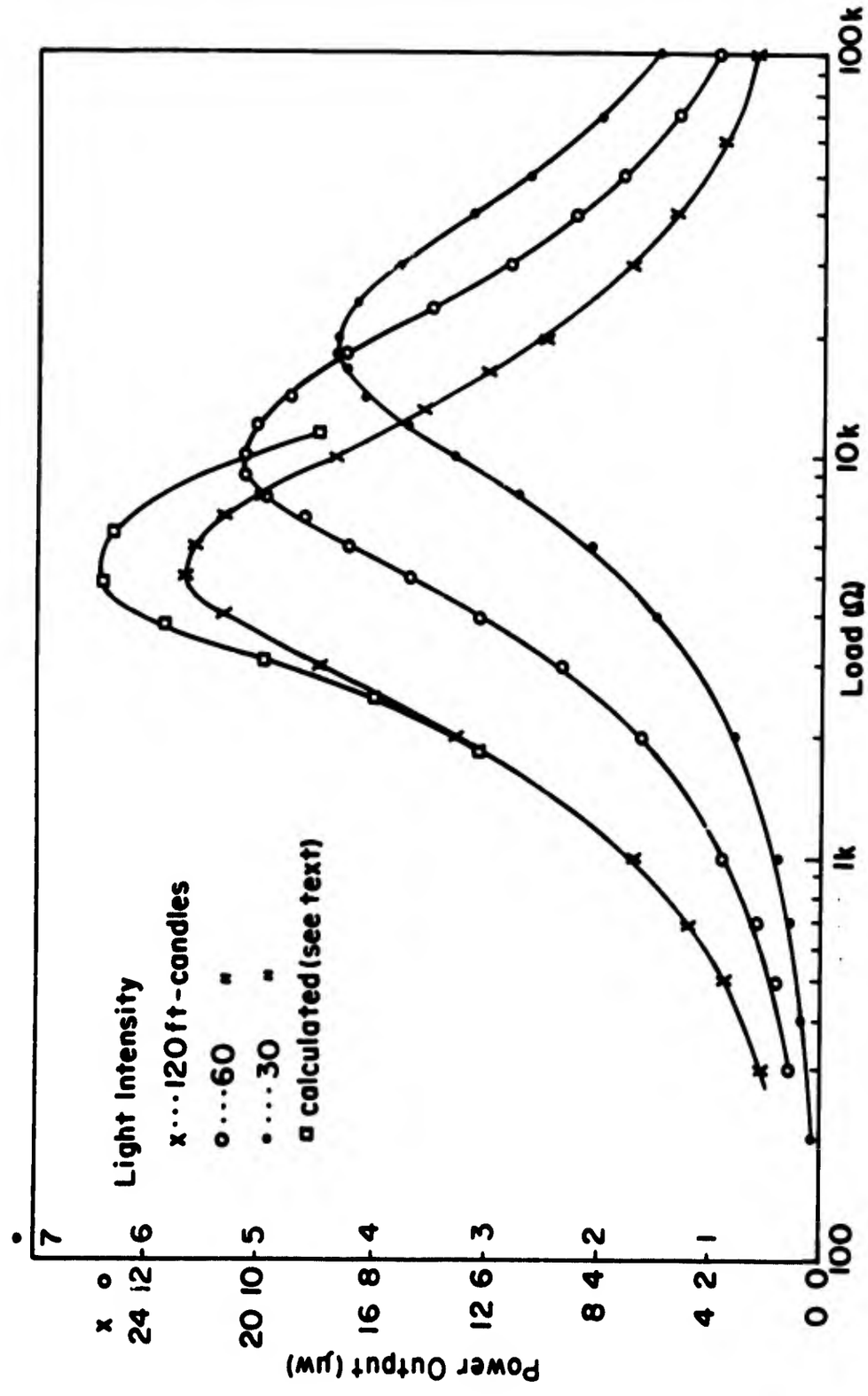

Fig. 22. Photocell Power Output vs Load for Three Light Intensities, EP467 GaAs-GaP Graded GaP Cell.

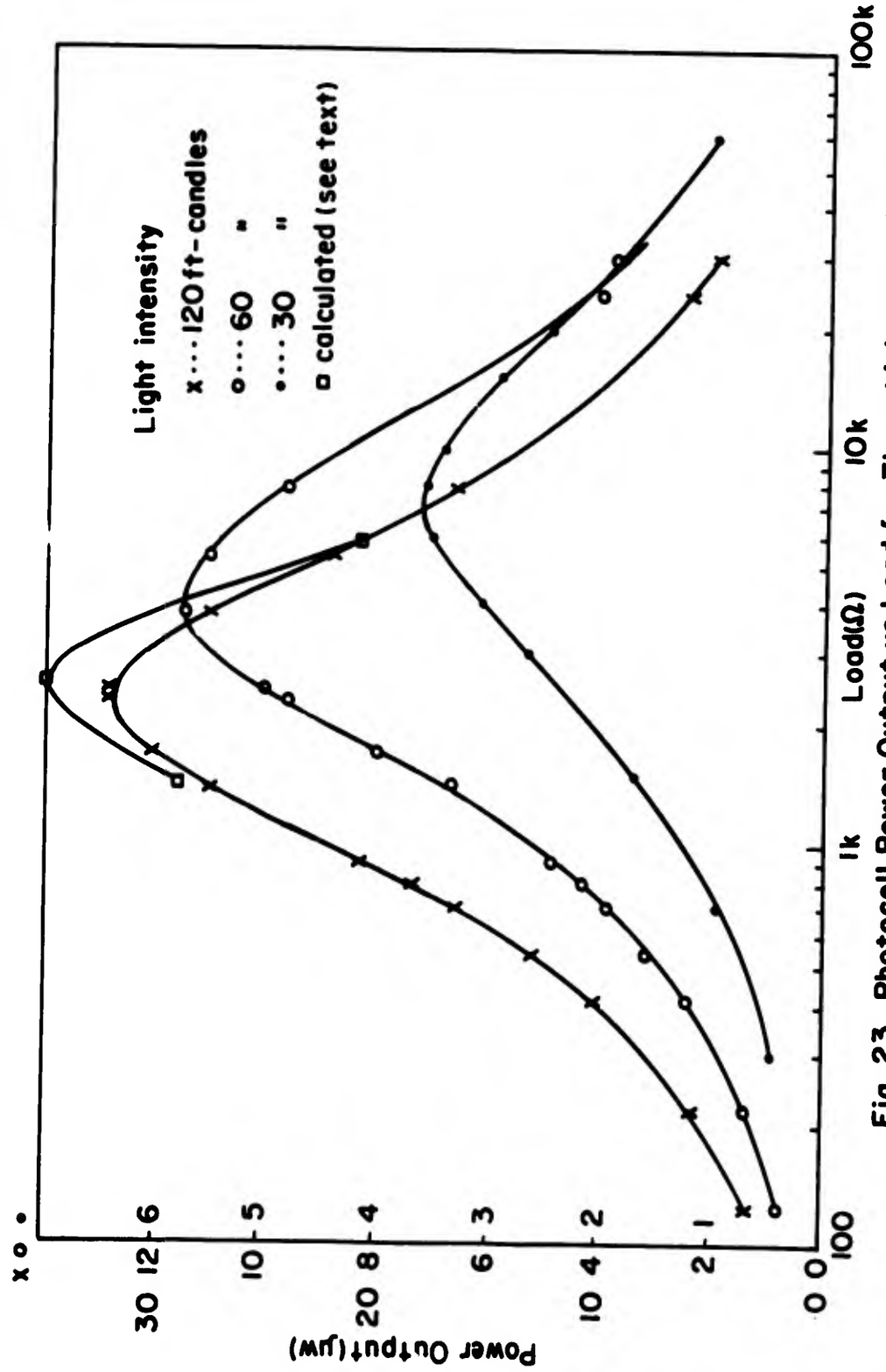

Fig. 23. Photocell Power Output vs Load for Three Light Intensities, EP348 GaAs-GaP Graded Gap Cell.

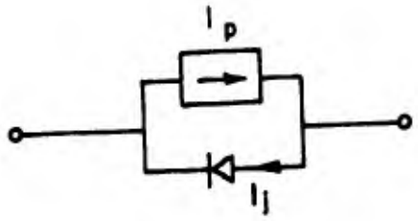

(a)

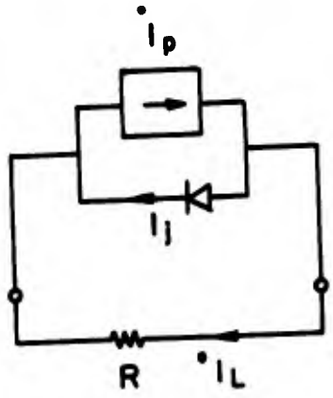

(b)

Fig. 24. Photodiode Circuit Models:
(a) No Load,
(b) Resistive Load.

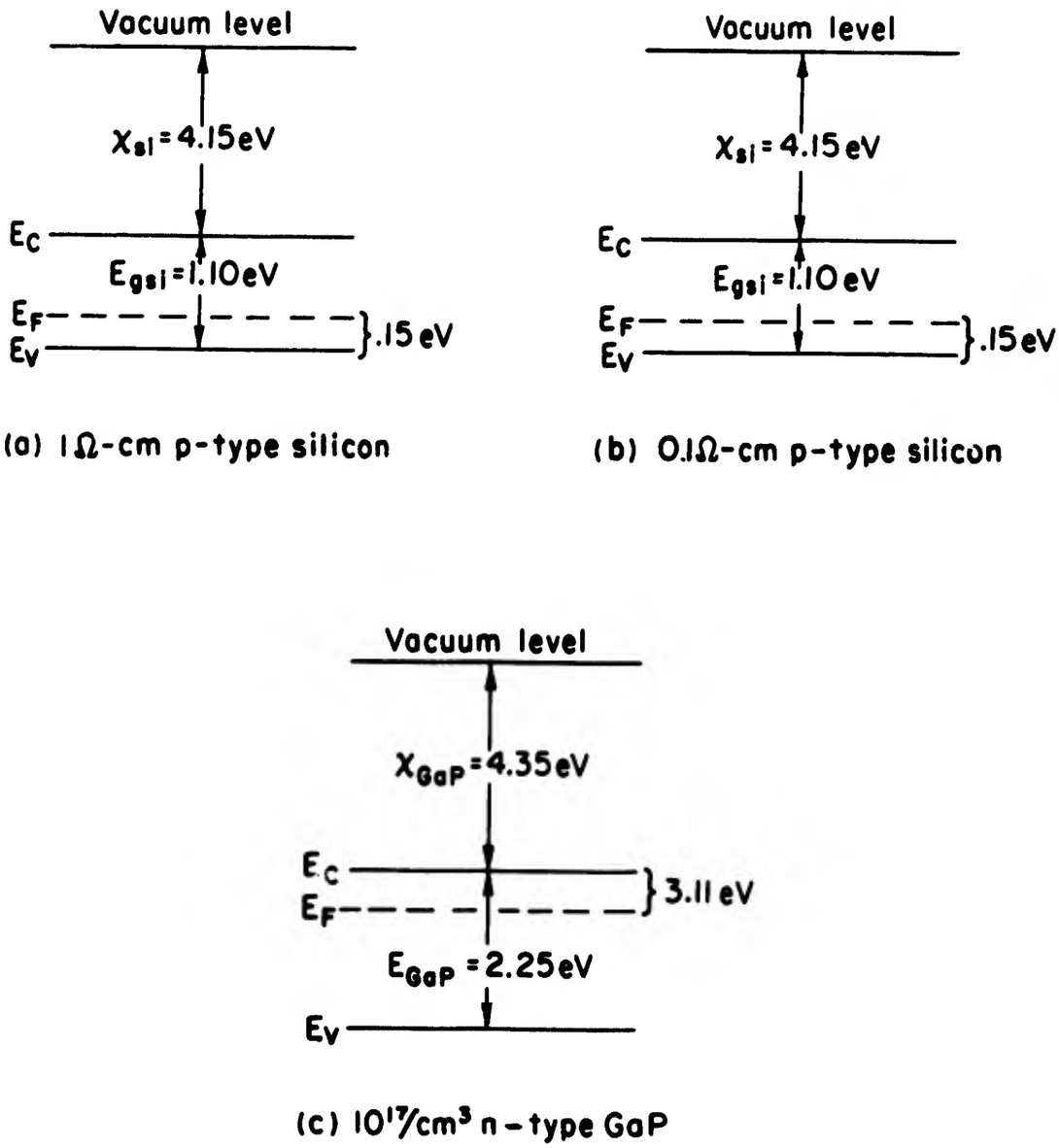

Fig. 25. Energy Band Diagrams at Room Temperature Before Epitaxy.

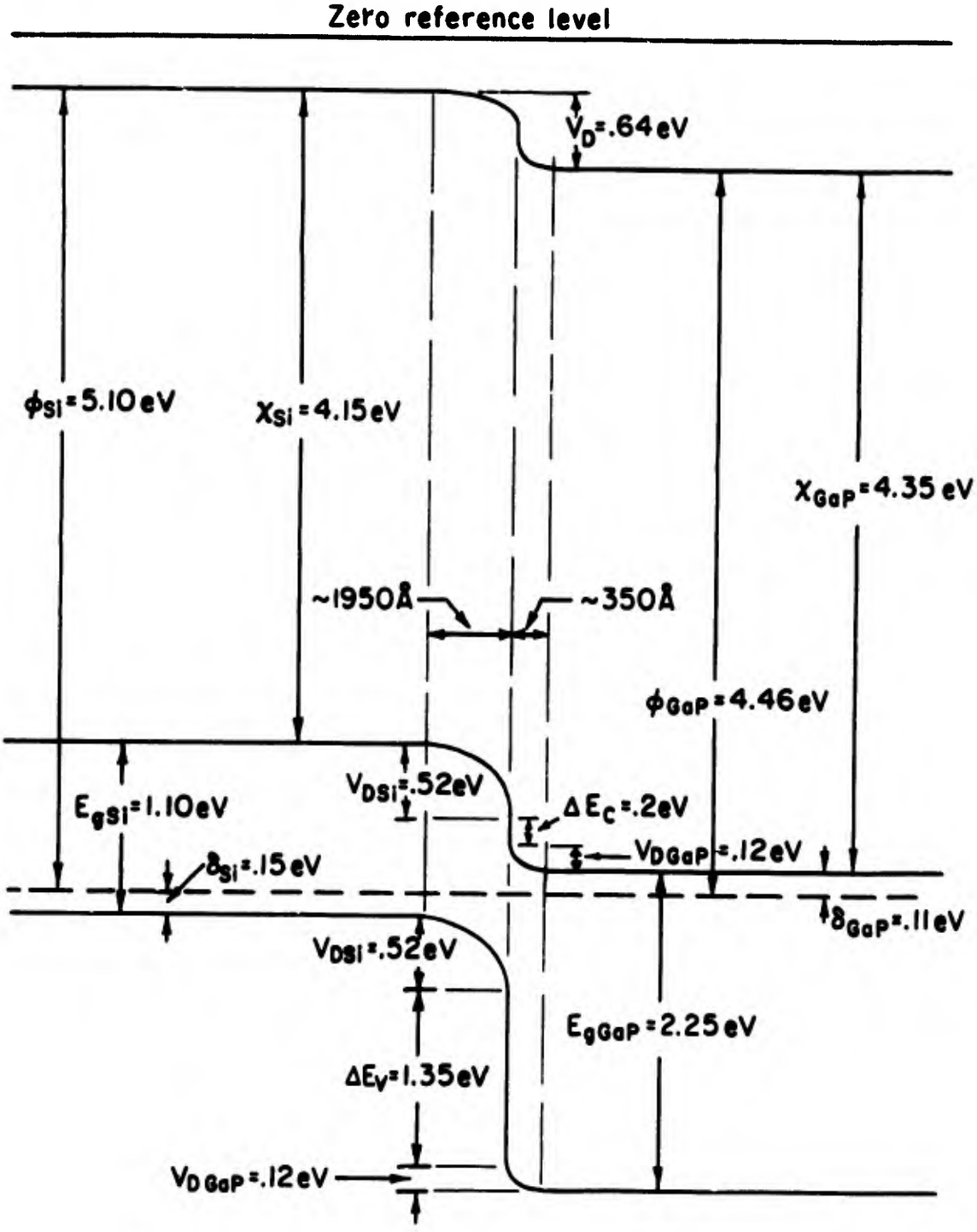

Fig. 26. Equilibrium Energy Band Profile at Room Temperature for the Heterojunction Between Si (1 Ω -cm, p-type) and GaP ($10^{17}/cm^3$, Te Doped).

ACKNOWLEDGEMENTS

The authors are indebted to William Kuchar and James Surette for their able assistance in the laboratory. Thanks are also extended to Dr. L. Tanner, Dr. K. Chopra, and M. R. Randlett of the Ledgemont Laboratory, Kennecott Copper Company, and to R. Cornelissen of the Air Force Cambridge Research Laboratories for their assistance in obtaining electron diffraction pictures. The following gifts are gratefully acknowledged: graded band gap GaAs-GaP photodectors from Eagle-Picher Industries, Inc.; Si-Ge heterojunctions from Prof. R. L. Anderson of Syracuse University, New York; GaP from Dr. Ronald Enstrom, RCA Laboratories, Princeton, New Jersey; and silicon solar cells from Texas Instruments, Solar Systems, and the International Rectifier Corp.

BLANK PAGE

B. PHOTOCHEMICAL STUDIES OF MOLECULAR SYSTEMS

1. Apparatus for Photochemical Investigations

K. Weiss, J. J. Bohning, P. A. Schnieper, H. P. Wolf, M. Doyle, E. Wall, K. H. Bar-Eli, Y. Pilette, T. A. Tyler, W. M. Moreau, and E. Reid.

2. The Photochemistry of Perinaphthenone

K. Weiss, G. P. Rabold, H. Koller, T. A. Tyler, and K. H. Bar-Eli.

3. The Photochemistry of Phenanthrenequinone

K. Weiss, J. J. Bohning, and H. P. Wolf.

4. The Unsensitized and Sensitized Photoreduction of Disulfides

H. P. Wolf and K. Weiss.

5. The Photochemistry of 1,3,5-Trinitrobenzene

W. M. Moreau and K. Weiss.

6. Studies of Charge Transfer Systems

K. Weiss, W. M. Moreau, A. M. Halpern, and Y. P. Pilette.

7. Laser Photochemistry

K. Weiss, R. M. Danziger, and K. H. Bar-Eli.

8. Diphenylpicrylhydrazil as a Calibration Standard in Electron Spin Resonance Spectroscopy

K. Weiss and K. H. Bar-Eli.

ABSTRACTS

1. Apparatus for Photochemical Investigations

The following apparatus and techniques for photochemical work are presented. (a) Apparatus for the measurement of quantum yields and rates of photochemical reactions. This unit provides monochromatic radiation with a photon flux of *ca.* 10^{15} photons/second; (b) Flash photolysis apparatus which can be used with photographic and photoelectric detection. Input energies may be varied in the range 10 to 5600 joules. Flash duration is 20 μseconds. A ruby laser flash assembly and a flash unit for use with ESR detection are also described; (c) An assembly for measurement of fluorescence quantum yields by the relative method; (d) Computer data processing techniques for flash photolysis, ESR, and spectroscopic data are described. Three publications based on this work are cited.

2. The Photochemistry of Perinaphthenone

The photolysis of perinaphthenone in solvents from which a hydrogen atom can be abstracted generates the hydroxyperinaphthenyl radical and an unstable intermediate which absorbs at 650 mμ. The ESR spectra of this radical and some related radicals have been measured and interpreted with the aid of molecular orbital calculations. Data are presented on the products of the photolysis of perinaphthenone and on the properties and factors influencing the formation of the 650 mμ transient. The mechanistic implications of the results are discussed, and a tentative structure for the 650 mμ intermediate is presented. Three publications have thus far resulted form this study.

3. The Photochemistry of Phenanthrenequinone

The photochemical reaction of phenanthrenequinone with stilbenes, 1,1-diphenylethylene, and triphenylethylene has been studied. Quantum yields for the addition of the diketone to these olefins are in the range 0.14 to 0.035. With the stilbenes, sensitized *cis-trans* isomerization occurs for which the quantum yields *cis* → *trans* and *trans* → *cis* are equal (0.45). Measurements with α,α'-stilbene-d_2 indicate a kinetic isotope effect for the addition and isomerization. The results are consistent with the formation of spectroscopic triplet of *trans*-stilbene and of a short-lived common association complex between the triplet quinone and the *cis*- or *trans*-olefin which is partitioned between decay to a non-spectroscopic excited state of the olefin and collapse to adduct. The publication based on this work is included.

The phenanthrenequinone/2-propanol photoreducing system was studied in relation to the possibility of generating intermediates capable of reducing disulfides. The reduction produces 9,10-phenanthrenediol and acetone. The quantum yield for the disappearance of phenanthrenequinone exhibits a complex dependence on the alcohol concentration, tending to an upper limit 2 at high concentrations and zero at low concentrations. The rate of phenanthrenequinone disappearance is directly proportional to the absorbed light intensity. The mechanism proposed invokes the phenanthrenequinone triplet state as the photochemically active species, and involves the formation of a dimeric species of finite lifetime from two semiquinone radicals. This photoreduction is not quenched by naphthalene, but is quenched by

disulfides. With *t*-butyl disulfide, collisional quenching of the phenanthrenequinone triplet state is indicated, but no thiol could be detected.

4. The Unsensitized and Sensitized Photoreduction of Disulfides

The direct and sensitized photolysis of thioctic acid in 2-propanol has been studied. A mechanism is proposed which predicts the observed linear dependence of the rate of disappearance of disulfide on absorbed intensity, and the lack of dependence of the quantum yield of disulfide disappearance and of the quantum yield of appearance of titratable thiol on the disulfide concentration. These quantum yields increase with decreasing wavelength of the exciting light. The major products of the reaction are the dithiol and pinacol which appear in *ca.* equivalent amounts. There are indications of side reactions leading to polymers, which become important at very low alcohol concentrations.

A number of compounds have been screened as sensitizers for this reduction. 3,4-Benzopyrene and benzanthrone were investigated in detail. A mechanism is presented which accounts for the observed behavior of benzanthrone, a non-sensitizer, and of 3,4-benzopyrene, a sensitizer. Fluorescence measurements indicate collisional quenching of the excited singlet state of 3,4-benzopyrene by the disulfide. These data indicate a lifetime of *ca.* 50×10^{-9} sec. for the excited state of the sensitizer, which is in reasonable agreement with the lifetime deduced from the sensitization data.

5. The Photochemistry of 1,3,5-Trinitrobenzene

The photochemistry of 1,3,5-trinitrobenzene in ethanol was studied under a variety of conditions. It was confirmed that 3,3',5,5'-tetranitroazoxybenzene and acetaldehyde are the major products under continuous photolysis conditions. 3,5-Dinitroaniline was identified as a minor product. Low temperature irradiation in ethanol generates the radical $3,5\text{-}(NO_2)_2C_6H_3NO_2H$, which was identified by its ESR spectrum. Flash excitation produces a single product in very low yield which absorbs in the visible region. Further photolysis of this product produces the azoxy compound. Several observations indicate that the flash product incorporates two molecules of trinitrobenzene.

Transient spectra and kinetics were measured, and are interpreted in terms of two transients which decay by consecutive reactions. The first transient is proposed to be the radical $3,5\text{-}(NO_2)_2ArNO_2H$, and the second transient is formulated as a diamagnetic species resulting from the addition of two hydrogen atoms to 1,3,5-trinitrobenzene was flashed in solvents which are poor hydrogen donors. The excited state of trinitrobenzene evidently abstracts hydrogen form the alcohol during the lifetime of the flash.

In unbuffered aqueous ethanol, while in buffered solutions at pH 2 and pH 8.5, additional transient species are generated.

6. Studies of Charge Transfer Systems

Spectroscopic and photochemical studies have been made of three systems: (a) Disulfide-tetracyanoethylene complexes; (b) Amine-iodine complexes; (c) Complexes derived from hydrocarbon donors.

The association constants and extinction coefficients have been measured for a number of disulfide-TCNE complexes. In the series n-alkyl disulfides, t-butyl disulfide, and thioctic acid, K_c at 25° increases from *ca.* 0.1 to 1 ℓ/mole and ΔH decreases from -0.41 to -7.2 kcal/mole. The charge transfer transition energies decrease in the same order. The spectral results are interpreted with the aid of a semiempirical molecular orbital theory. The calculated and observed spectral transitions were in good agreement. Two publications have resulted from this investigation.

A method has been developed for measuring the formation constants of the 1:1 and 1:2 complexes of diamines with iodine. The method may have general validity for equilibria involving multifunctional components. Constants have been measured for six diamines. In general, it was found that $K_1 > K_2$, indicative of the operation of intramolecular perturbations which cause the complexed donor site to influence the complexing ability of the uncomplexed site. The effect can be rationalized in terms of charge transmission from the polarized complexed site through σ-bonds.

The TCNE complexes of diphenylacetylene, 2-iodanaphthalene, and *cis*- and *trans*-stilbene are photochemically inert. No *cis-trans* isomerization occurs with the stilbene complexes. Photolysis causes a small increase in absorption in the charge transfer region which is slowly reversed in the dark. It is proposed that this change is due to a structural isomerization of the complex as a whole. Flash photolysis of the complexes of pyromellitic anhydride with triphenylene and with anthracene produces transients which absorb in the visible

region. Conversion into transients in extensive, and the changes are completely reversible. The transient decay is complex and follows no simple rate law. It is clear that these transients are uniquely associated with the complex, but their identity remains to be elucidated.

7. Laser Photochemistry

The giant ruby laser pulse photolysis of plain aqueous methylene blue solutions revealed three transients, A, B, and C, with half-lives of 2, 30, and 140 μsecs, respectively. These intermediates are generated in proportion to the equilibrium mole fractions of monomer and dimer in the dye solution. Transients A and B are assigned as the triplets of dimer and monomer, respectively, on the basis of their lifetimes and their behavior with oxygen. Transient C, whose decay is insensitive to oxygen, is postulated to be formed from A. Evidence is presented for the dimeric nature of transient C, which is formulated as a charge-transfer state. The kinetic results indicate further that the establishment of the ground state equilibrium $M_2 \rightleftarrows 2\ M$ is slow relative to the decay of the transient species. The results of the laser photolysis and conventional flash photolysis are compared. The publication based on this work is included.

Exploratory experiments in solution indicate the feasibility of observing multiphoton-generated transients by kinetic spectroscopy. With anthracene, transient absorption was observed in the triplet-triplet absorption region. The transient absorption observed in concentrated naphthalene solution does not correspond to reported triplet-triplet transition for this compound. With benzophenone in

2-propanol, the integrated effect of a large number of laser pulses produced a chemical change, although no transient absorption could be detected.

8. Diphenylpicrylhydrazyl as a Calibration Standard in Electron Spin Resonance Spectroscopy

Diphenylpicrylhydrazyl (DPPH) admixed with inert solids is widely employed as a standard for the estimation of spin concentrations. In this study it was found that interactions leading to the loss of spins can occur even with materials considered to be inert. The extent of spin loss depends on the nature of the diluent material and on the method of sample preparation. It is proposed that the deterioration is due to a reaction of DPPH with water on the surface of the diluent particles. The data indicate that freshly prepared, ground mixtures of DPPH with potassium chloride are useful standards for a wide concentration range. The publication based on this study is included.

Introduction

General Considerations - Solar cells are based on photochemical energy conversion. There is currently much interest in complex molecular systems for applications of this nature. The development of useful devices based on complex molecules requires detailed knowledge of the radiative, radiationless, and chemical changes which occur as the result of the absorption of light. The phase of project discussed in this section is concerned with the study of such basic aspects of photochemical energy conversion. Detailed investigations were made of model systems which promised to provide the maximum amount of generally pertinent information about photochemical behavior. The number of potentially useful systems is vast, and the knowledge gained in these studies aids in the optimization of variables for particular applications.

The studies described here involve the identification and characterization of excited states and intermediates, the elucidation of kinetic behavior, and the measurement of how the absorbed energy is partitioned between various decay models. Our approach has been to utilize as many pertinent experimental techniques as possible. These include absorption and emission spectroscopy, continuous and flash photolysis, and electron spin resonance spectroscopy. The apparatus designed and constructed for this work consists of a monochromatic irradiation assembly for the measurement of quantum yields and rates of photochemical reactions, a continuous flash photolysis unit, a laser flash photolysis unit, and a calibrated fluorescence assembly.

The investigations dealt exclusively with organic compounds in solution, in particular with members of these classes:

Aromatic Ketones

Sulfur Compounds

Charge-Transfer Complexes

Aromatic Nitro Compounds

The findings of individual studies are summarized in the following sections, and in the publications of Appendices A to H.

1. Apparatus for Photochemical Investigations

by K. Weiss, J. J. Bohning, P. A. Schnieper, H. P. Wolf, M. Doyle, E. Wall, K. H. Bar-Eli, Y. Pilette, T. A. Tyler, W. M. Moreau, and E. Reid.

(a) Apparatus for Continuous Photolysis

An accurate means of measuring quantum yields is essential for meaningful photochemical work. The apparatus for this purpose must provide reasonably monochromatic radiation, operate at constant temperature, and should be useful over a wide wavelength range. Construction of this equipment constituted one of the earliest efforts on this project. The first version of the apparatus is described in the final report of contract AF19(604)-7358[1], in the doctoral dissertation of J. J. Bohning[2], and in a publication based on that dissertation[3]. It provides monochromatic radiation with a photon flux of *ca.* 10^{15} photons per second and uniform illumination of the sample. A continuous

record may be made of the transmitted intensity during irradiation, thus providing, under the proper conditions, a means for determining the total energy absorbed and the photochemical kinetics of the system being photolyzed.

During work on several photochemical systems, some minor short-comings of the original apparatus came to light. The necessity for correction of the absorbed intensity value for reflections from the cell faces and from the thermopile window focused attention on the problem of stray light reflected from the polished exterior of the thermopile. Masks were installed which confine the light to the sensitive portion of the thermopile and to the open area of the cell holder. Another necessary modification involved construction of a new constant temperature cell holder which allows the reproducible alignment of the sample in the illumination train. A decrease in the sample volume and in the area illuminated insured more effective stirring. Particular care was necessary in choosing the width of the aperture in the cell holder as it was found that "light-piping" by the walls of the cell can cause serious errors in the measurement of the intensity of the transmitted light. Incorporation of the proper limiting aperture into the structure of the sample holder also eliminated problems and uncertainties attendent with the fragile removable masks, which had previously been used. Finally, quartz lenses were substituted for the "Pyrex" lenses of the original irradiation train, thereby increasing the useful range of the apparatus and improving the intensity available from the 313 mμ line.

A complete description of the apparatus in its current form is given in Appendix A. Measurements with the potassium ferrioxalate actinometer provided quantum yield values which are in gratifying agreement with those reported in the literature. As anticipated, the paper fulfilled a real need in the fields of photochemistry and photobiology, and over 100 requests for reprints were received in the first month after publication.

(b) Apparatus for Flash Photolysis

While continuous photolysis studies provide valuable information about the rates of disappearance of reactants and appearance of products, they furnish only indirect evidence about reactive intermediates in photochemical reactions. The evaluation of kinetic data obtained under continuous irradiation conditions invariably involves the application of the steady state approximation, which assumes the concentrations of reactive intermediates to be constant by virtue of the equality of their rates of formation and decay. Mechanisms formulated on this basis yield only ratios of rate constants. Absolute values of rate constants can only be obtained by direct measurements on the reactive species. In photochemistry such data can be obtained by flash photolysis. This technique, when used under the proper conditions and in conjunction with the critical variation of experimental parameters, can provide the identity of the reactive intermediates as well as details regarding their kinetic behavior.

The flash tubes used in this apparatus are constructed in our laboratory. The feature distinguishing them from commercial tubes is an expansion chamber behind each electrode, which connects with the flash chamber by means of holes in the end cap. Tests have indicated these tubes to be vastly superior to commercial tubes for short pulse work. In the tubes described in the original report[4], the quartz tube which constitutes the discharge chamber was cemented permanently to the end caps with epoxy cement. This meant that tubes which had become crazed and hazy by extensive use (~5,000 flashes) had to be broken apart and the end caps remachined for reuse. More recently, the tube design has been changed so that defective quartz jackets can be easily replaced and the electrodes cleaned and reconditioned. Figure 1 shows how this is accomplished. The permanently cemented joint between the quartz tube and the end cap is replaced by a commercial "Swagelok" fitting* with "Teflon" ferrules, which provides a vacuum-tight seal. The modified tubes have proven to be as stable as the original tubes.

In using the flash apparatus, an optical alignment problem is often encountered, which arises from the fact that the cylindrical sample cells are invariably slightly prismatic with respect to a beam of light passing length-wise through the cell. This causes divergence of the monitoring beam so that the light detected at exit slit of the spectrograph does not remain maximized when cells are exchanged. Realignment is tedious and time-consuming when performed by the trial-and-error movement

*Crawford Fitting Company, Cleveland, Ohio

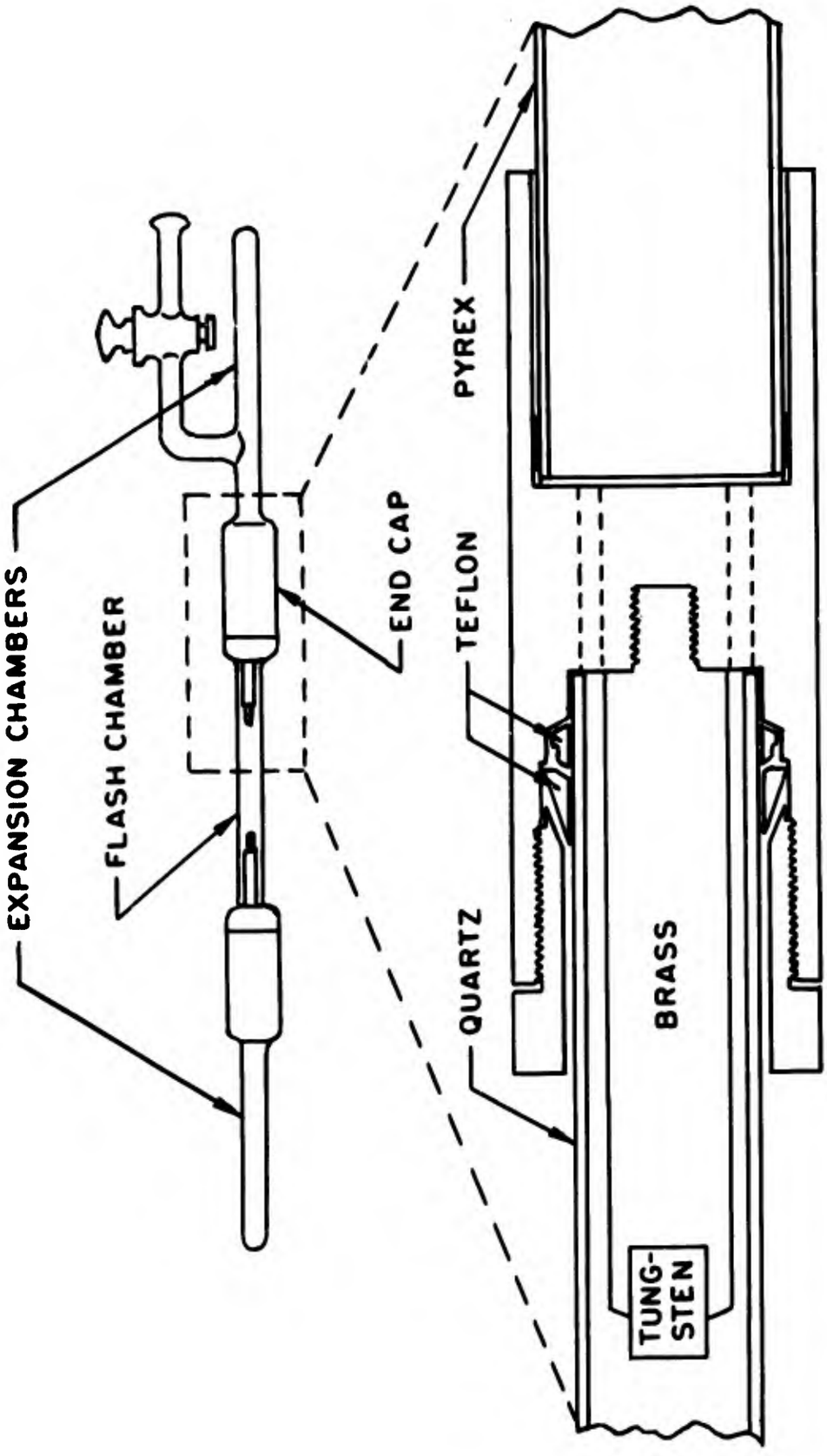

FIGURE 1: Modified End Caps for Flash Tube

The construction of a flash apparatus dates back to the beginning of our photochemical endeavors in 1963. Early versions which suffered from numerous disadvantages, particularly an inordinately long flash duration, are recorded in the final report of contract AF19(604)-7358[1]. The latest conventional flash photolysis apparatus, so designated to distinguish it from the laser flash apparatus which is described later in this section, is described in detail in a report under this contract[4]. An abbreviated version of this report was published in the NEREM Record, 1965, and is included here as Appendix B.

Based on four flash tubes with a distance of 16 cm between electrodes, the apparatus can be operated with input energies spanning the range 10 to 5600 joules. The flash duration is somewhat wavelength dependent; at 440 mμ, the maximum intensity is reached *ca.* 10 μsecs after onset of the flash and it decays to 1/*e* of the maximum value in 10 μsecs. The flash unit can be used with photographic and with photoelectric detection. A high resolution spectrograph (Jarrell-Ash f/6.3) is used for both detection methods. For the photographic method, a secondary flash of 150 joules lasting *ca.* 20 μsecs is actuated at various time intervals after the photolytic flash. This provides a complete transient absorption spectrum spanning a large wavelength range at a predetermined time after excitation. The photoelectric method utilizes a continuous xenon of tungsten filament monitoring light source which provides transient absorption data at constant wavelength as a function of time.

of components. The simple device shown in Figure 2 was developed to solve this alignment problem. It is essentially a water-filled wedge in which the inclination of one window with respect to the other can be adjusted by means of four screws. Its purpose is to compensate for the prismatic action of the sample cell. For use, this beam director is placed in the monitoring beam near the sample cell. Redirection of the beam along the sample-spectrograph slit axis and maximization of the light signal can be achieved in a matter of minutes.

The early flash experiments were carried out with simple cylindrical sample cells. These cells provide no temperature control. They have been replaced by jacketed cells (Figure 3). The rapid circulation of filter solution from a thermostatted bath through the jacket serves not only to keep the temperature constant, but also to confine light absorption by the sample to selected spectral regions.

In most cases, the flash-generated intermediates are sensitive to oxygen and the samples have to be thoroughly outgassed. If the flash-induced changes are completely reversible in the dark, a single sample may be used for many experiments. The preparation of many identical degassed samples is necessary if irreversible changes occur. For this purpose, the simple transfer apparatus described in Appendix C was developed. In this assembly a large quantity of solution is degassed from which aliquots are transferred into the photolysis

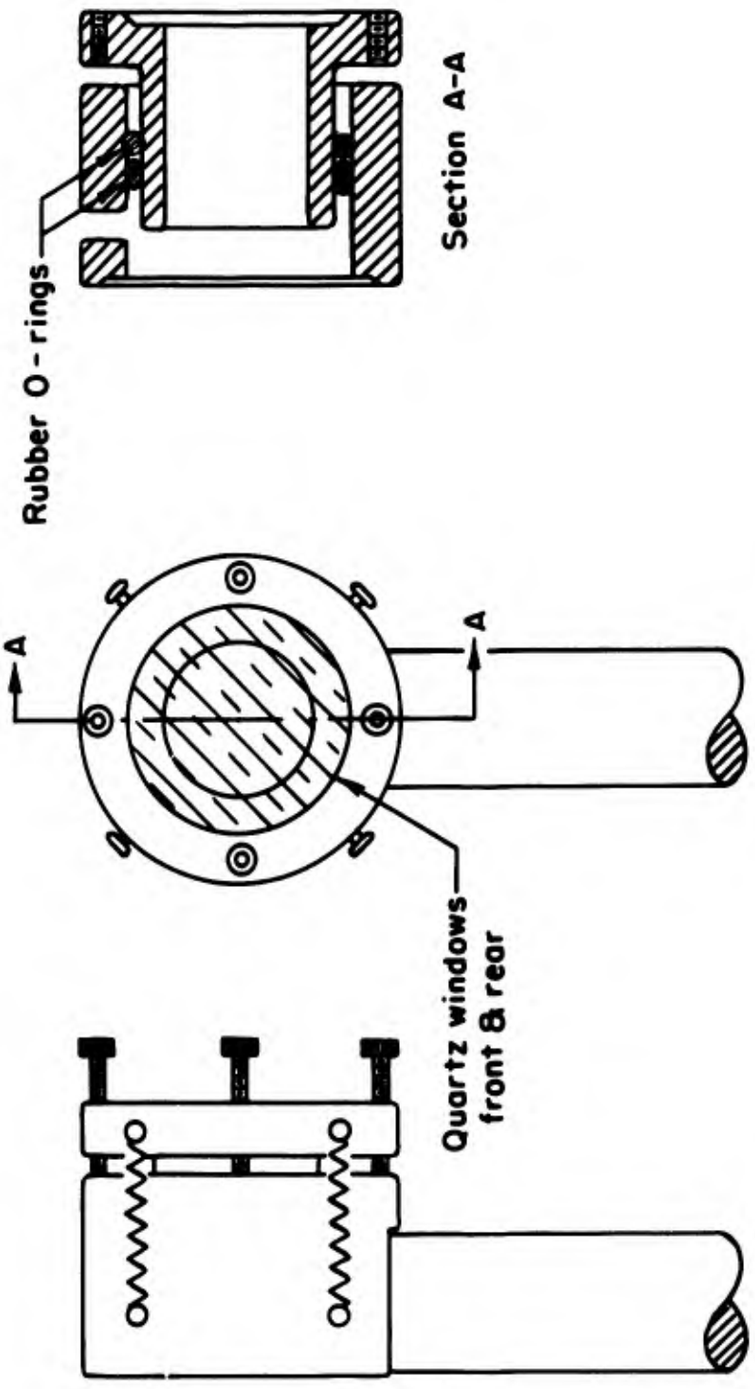

FIGURE 2: Light Beam Director

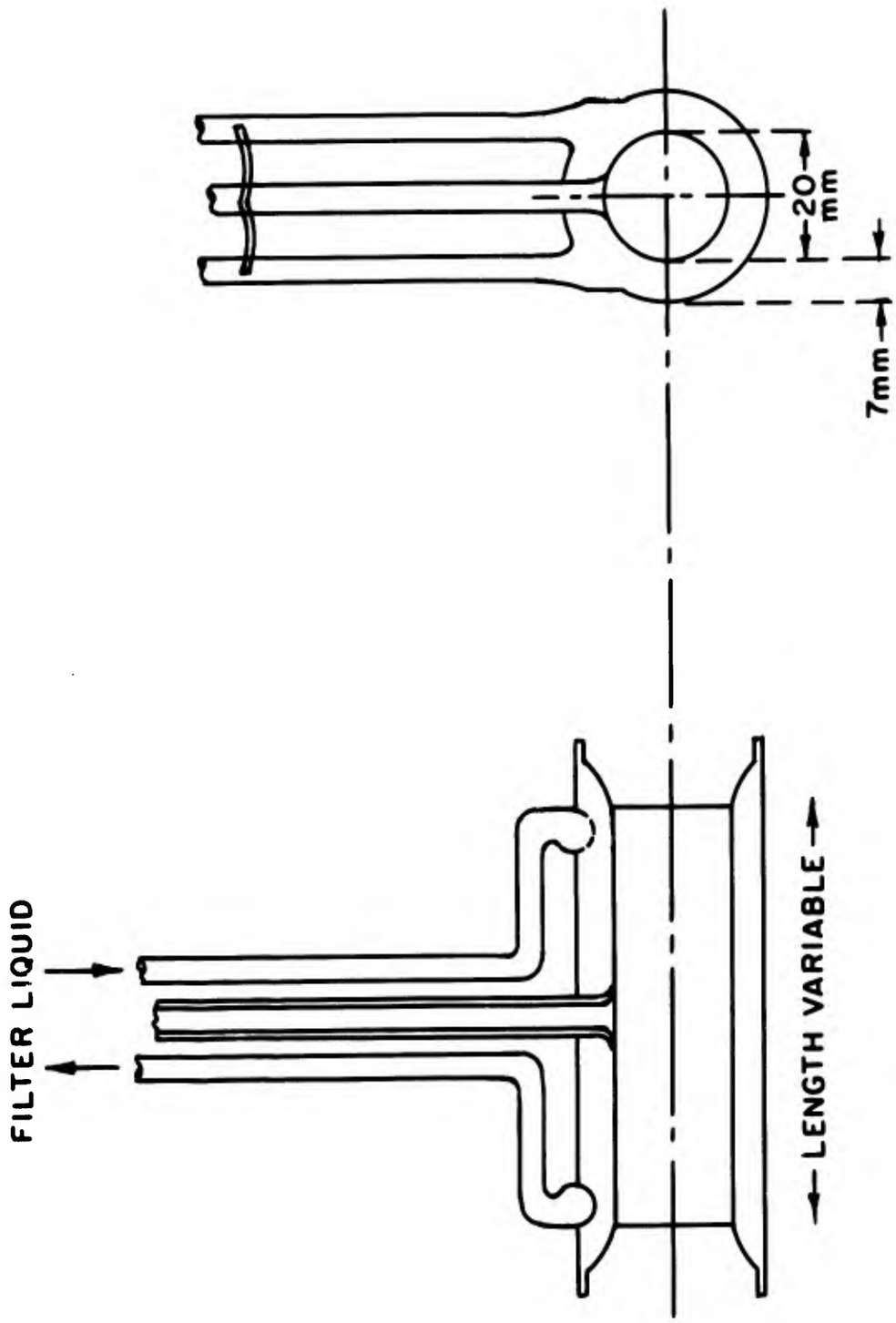

FIGURE 3: Jacketed Flash Cell

cell. This convenient device has been successfully used in several studies.

Efforts to improve the detection circuit used in the photoelectric monitoring method have been made throughout the contract period. It has been possible to prevent saturation of the photomultiplier by stray light with strategically placed baffles and some modifications in the optical train. Use of the switching circuit described in Scientific Report No. 3[4], which renders the photomultiplier tube inoperative during the photolytic flash, is not necessary in most cases. Two tubes, the EMI 9558Q and the DuMont 6911 photomultipliers are used to span the 180 mμ to 1100 mμ wavelength range. The most significant improvement in the signal-to-noise ratio resulted fron incorporation of a specially selected EMI tube in the detection circuit. The latest circuit modifications have made it possible to eliminate the cathode follower. Signal collapse is prevented by employing very short coaxial leads to the oscilloscope.

The flash apparatus just described is classified as "conventional" since it is based on ordinary flash tubes, though these are of unconventional design. In a phase of this photochemical research cosponsored by the U. S. Public Health Service, we have developed a ruby laser photolysis apparatus. The original version of this apparatus is described in Scientific Report No. 3 and in Appendix B. The most important changes in the experimental arrangement are the replacement of the liquid nitrogen-cooled laser by a Maser Optics model 869 water-cooled

head, and the use of shorter reaction cells (1cm path length) for experiments which involve compounds absorbing at the laser wavelength of 6943 Å. The reproducible production of Q-spoiled pulses of constant energy is vastly superior with the new head, which can also be operated at a higher repetition rate. The shorter path length reaction cells were necessary to suppress regular sinusoidal patterns which were superimposed on the decay curves when long cells are employed. The cause of this interesting phenomenon is not yet known.

The apparatus which was used for the study of the photolysis of aqueous methylene blue is shown in Figure 4. The various components and their interrelationships are presented in the block diagram of Figure 5. The duration of the pumping flash is approximately 2.3 msecs, with onset of regular laser action occuring after about 1.2 msecs and the Q-switched pulse appearing after *ca.* 1.6 msecs. The laser beam is at an angle of about 15° to the monitoring beam, and hence also with the axis of the reaction cell. Monitoring light (M, Figure 4) is provided by a General Electric type CPR 108-watt filament projection lamp which is powered by five 6-volt batteries wired in parallel. The monitoring light is focussed at infinity by lens L_1. The beam passes through an 18" long light pipe which terminates in a mask with an opening the size of the laser beam. After passing through the sample cell, the beam enters another 12" long light pipe and is finally focussed on the entrance slit of the monochromator by lens L_2. Changes in the transmission

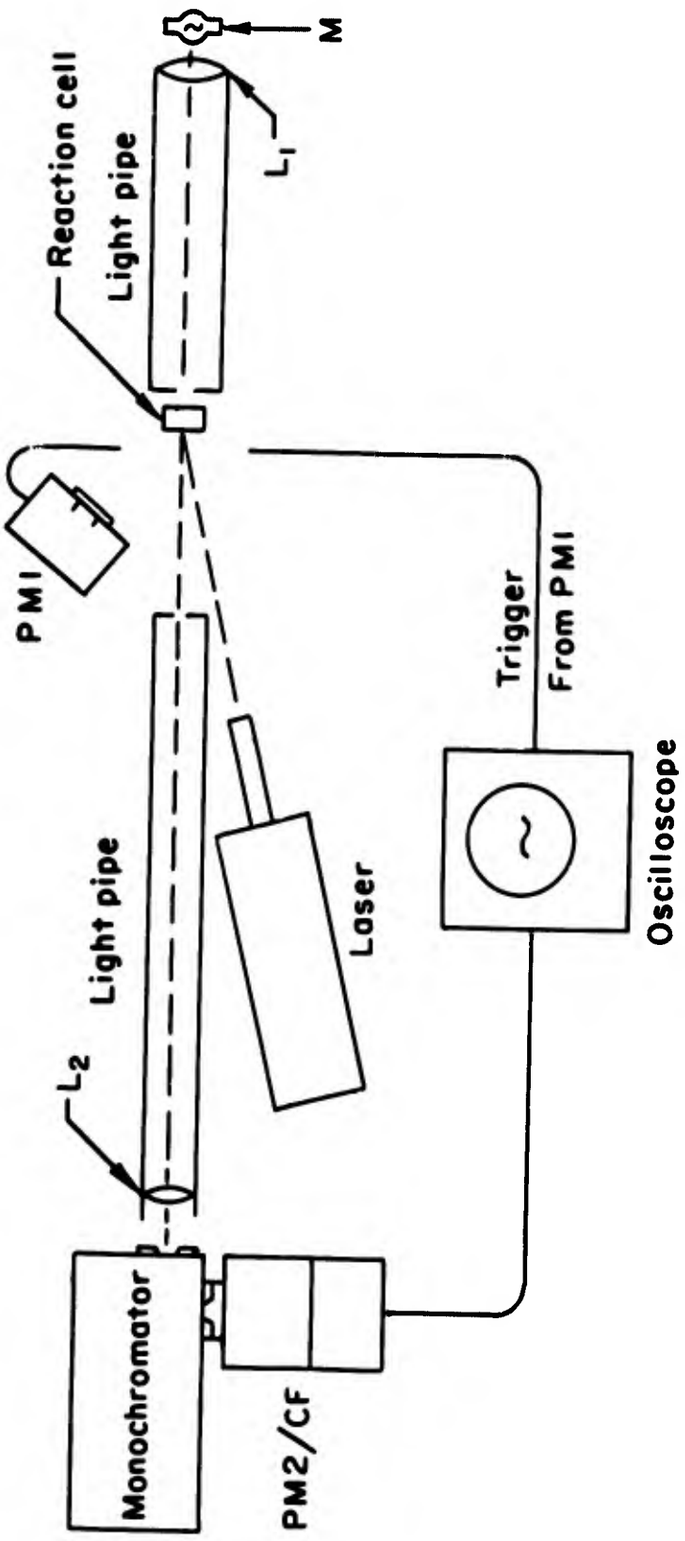

FIGURE 4: Laser Photolysis Apparatus

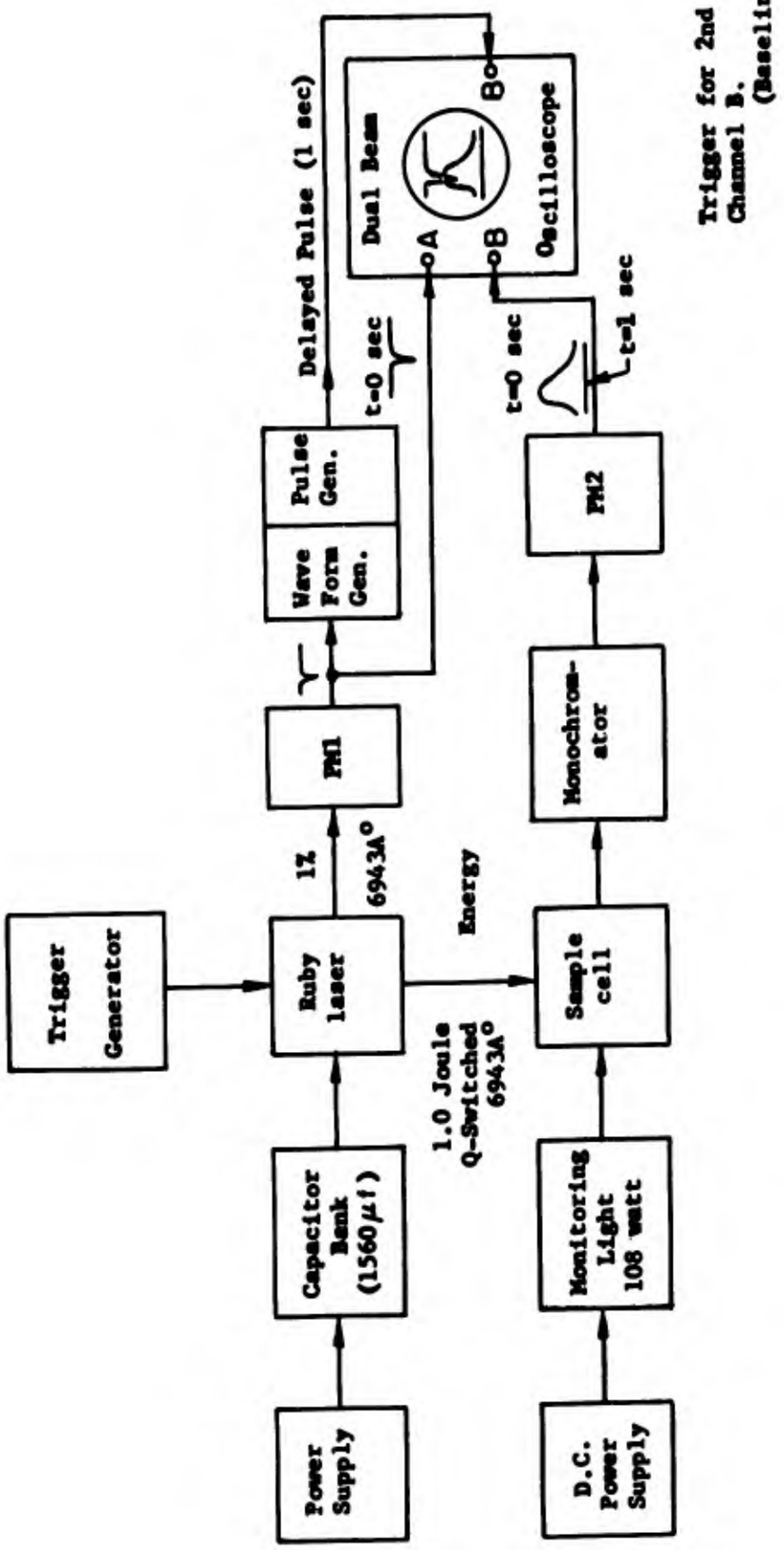

FIGURE 5: Block Diagram of Laser Photolysis Apparatus

of the sample are detected by the photomultiplier-cathode follower circuit (PM2/CF) mounted on the monochromator.

Since the Q-spoiled laser pulse can occur over a sizable time interval, it is necessary for the pulse itself to initiate the oscilloscope trace which records the transient change. This is accomplished by allowing some of the light scattered from the front of the reaction cell to fall on PM1, a photomultiplier-emitter follower circuit. The rising pulse in this tube is fed simultaneously to the trigger input of a Fairchild dual beam oscilloscope and to waveform and pulse generators (Figure 5). Undelayed traces which record the intensity of the laser pulse and the transient absorption change are displayed concurrently. A delayed pulse from the waveform and pulse generators retriggers the lower trace to provide a base line for the transient absorption display.

The arrangement described above suffers from several disadvantages. These are: (1) it is impossible to achieve angle less than 15° between the laser and monitoring beams; (2) the placement of light confining masks is ectremely critical since they can act as sources of scattered light; the diameter of the laser beam cannot be changed. The latest laser photolysis arrangement is illustrated in Figure 6. In this apparatus the laser beam-monitoring beam angle is *ca.* 5°. Confining the monitoring light to the irradiated portion of the solution is achieved by optical means rather than with physical masks. The new arrangement has the added advantage that the monochromator

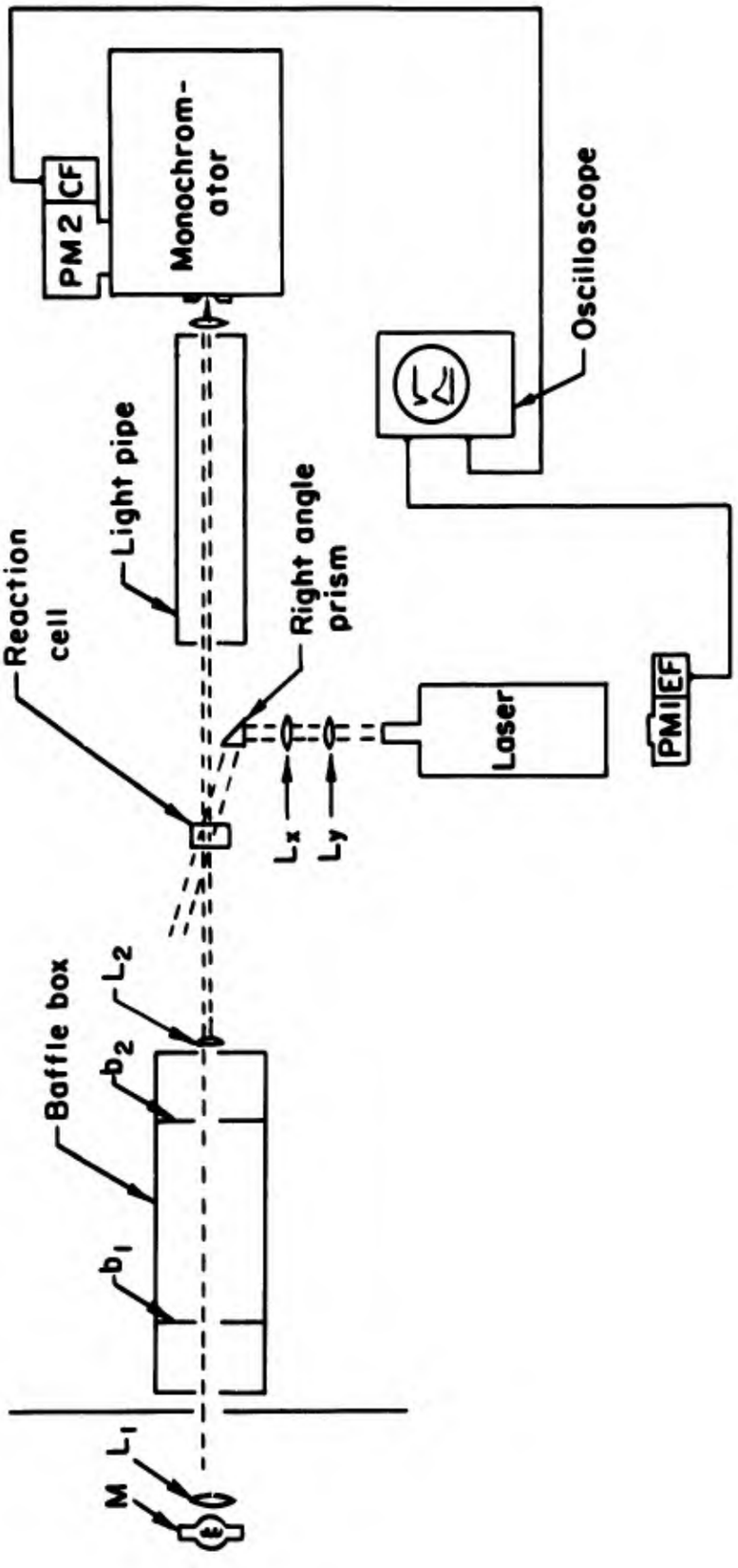

Figure 9 Revised Laser Apparatus

and detection circuit can be placed outside the room which houses the laser.

Referring to Figure 6, M is the monitoring light; lens L_1 (63 mm. diameter, 50 mm. focal length) focusses the filament at lens L_2 (20 mm. diameter, 100 mm. focal length), which acts as a field lens and also reduces the diameter of the light traversing the sample to approximately 0.5 cm. The baffle box defines the beam with baffles b_1 and b_2 having $^1/_4$-ins. diameter holes. Light from the laser is brought to the reaction cell by means of the right-angled prism. Lenses L_x and L_y (both 50 mm. diameter, 60 mm. focal length) can be used to modify the size and intensity of the laser beam. However, their inclusion in the optical train increases the stray light level. A red filter (Corning 2-64, not shown), placed near the laser, serves to eliminate wavelengths shorter than 6943Å from the exciting light. A dielectric filter (Spectrum Systems, Inc., not shown) in front of the monochromator entrance slit rejects 6943 Å stray light. The detection and triggering circuits of PM1/EF and PM2/CF are identical with those described previously.

Alignment procedures for the laser, and sources of difficulties and errors are discussed in detail in the doctoral dissertation of R. Danziger[5]. This thesis also presents the results of some explanatory multiphoton experiments. The laser photolysis of methylene blue is discussed in section 10 and in Appendix K.

Some work was carried out on the development of a technique for using flash photolysis in conjunction with electron spin

resonance (ESR) spectroscopy. For this purpose a focussed flash unit was built[6] with which samples can be photolyzed directly in the ESR spectrometer cavity. Based on an EG&G FX-51 flash tube, the unit operates with an input energy of 600 joules and provides flashes lasting *ca.* 500 μsecs. The apparatus was successfully used to generate hydroxyperinaphthenyl radicals from perinaphthenone[7]. These radicals are relatively long-lived ($t_{1/2}$ 5 mins.) and both the resolved spectrum and the decay can be measured. With radicals as stable as the hydrozyperinaphthenyl radical, flash operation offers no particular advantage. The flash photolysis-ESR technique would be an extremely powerful investigative tool for short-lived radical species, where continuous irradiation furnishes too low a concentration for meaningful measurements.

The photolytically generated radical from chloranil in tetrahydrofuran[8], which appears to decay in less than 1 second at -26°C, was used as the model system for tests with shorter-lived radicals. This lifetime was found to be close to the detection limit for meaningful decay measurements with the standard spectrometer detection circuit. A number of circuit modifications were tried, without success, to measure shorter lifetimes. These involved eliminating the 100 kc modulation frequency and by-passing the Klystron's automatic frequency control. Under these conditions, the flash produced transient signals in the microsecond to millisecond range which were found to be independent of the magnetic field strength.

It is clear that ESR measurements with short-lived radicals produced by a simgle flash represent a formidable problem. Repetitive flashing coupled with signal sampling and storage detection techniqyes has been successfully used by other investigators. However, this method is inapplicable for irreversible photochemical systems with which a single flash accomplishes a substantial change in composition. The problem of measuring the resolved spectrum and decay kinetics of radicals with life-times $\sim 10^{-3}$ second is intriguing and challenging. We believe that it can be solved, and we have recently commenced work on the design of a modified flash assembly and ESR spectrometer.

(c) Emission Measurements

For the study of the sensitized reduction of disulfides which is presented in Section 7, it was necessary to measure fluorescence quantum yields. The relative method described by Parker and Rees[6] was employed. This involves measuring the apparent fluorescence intensity as a function of wavelength for a fluorescence standard and for the compound of interest, and correcting the curves for the sensitivity of the monochromator-photomultiplier combination. The sensitivity of the instrument is determined by measuring the photomultiplier response as a function of wavelength for a lamp of known spectral distribution. The fluorescence intensities corrected in this manner are converted into units of quanta per unit frequency interval. Integration of plots of these values against frequency over the entire emission interval yields areas which are directly proportioned to the quantum yield of fluorescence.

The apparatus used for the emission work is shown in Figure 7. It is limited to measurements with liquid samples near room temperature. The assembly consists of the Beckman DK-1 spectrophotometer with its detection circuitry, a fluorescence attachment (Beckman #22850), and a monochromatic rxcitation source. The latter is an Osram mercury arc lamp (# Hg/3) powered by a Gates Universal Supply (# 125). The Bausch and Lomb f/3.5 high intensity grating monochromator, (catalog# 33-86-25, grating blazed at 5000 Å) is used with entrance optics consisting of lenses A (61 mm. focal length, 35 mm. diameter), B (56 mm. focal length, 35 mm. diameter), and C (81 mm. focal length, 27 mm. diameter), and with exit optics consisting of field lens D (60 mm. focal length, 28.5 mm. diameter) and lens E (78 mm. focal length, 63 mm. diameter). In the arrangement shown, an area of *ca.* 9.0 mm. by 22.0 mm. of the sample is illuminated with an image of the exit slit. The slit widths used are 5.36 mm. for the entrance and 3.00 mm. for the exit.

The spectral response of the fluorescence assembly was measured with a lamp calibrated against a National Bureau of Standards standard lamp.[6,7] The procedure developed involves the substitution of a carefully prepared aluminum blank, the illuminated surface of which is uniformly coated with fresh magnesium oxide, for the sample cell. The reflectance properties of this nearly perfect diffusing surface permit the calibration of the apparatus with no change in the geometry and under

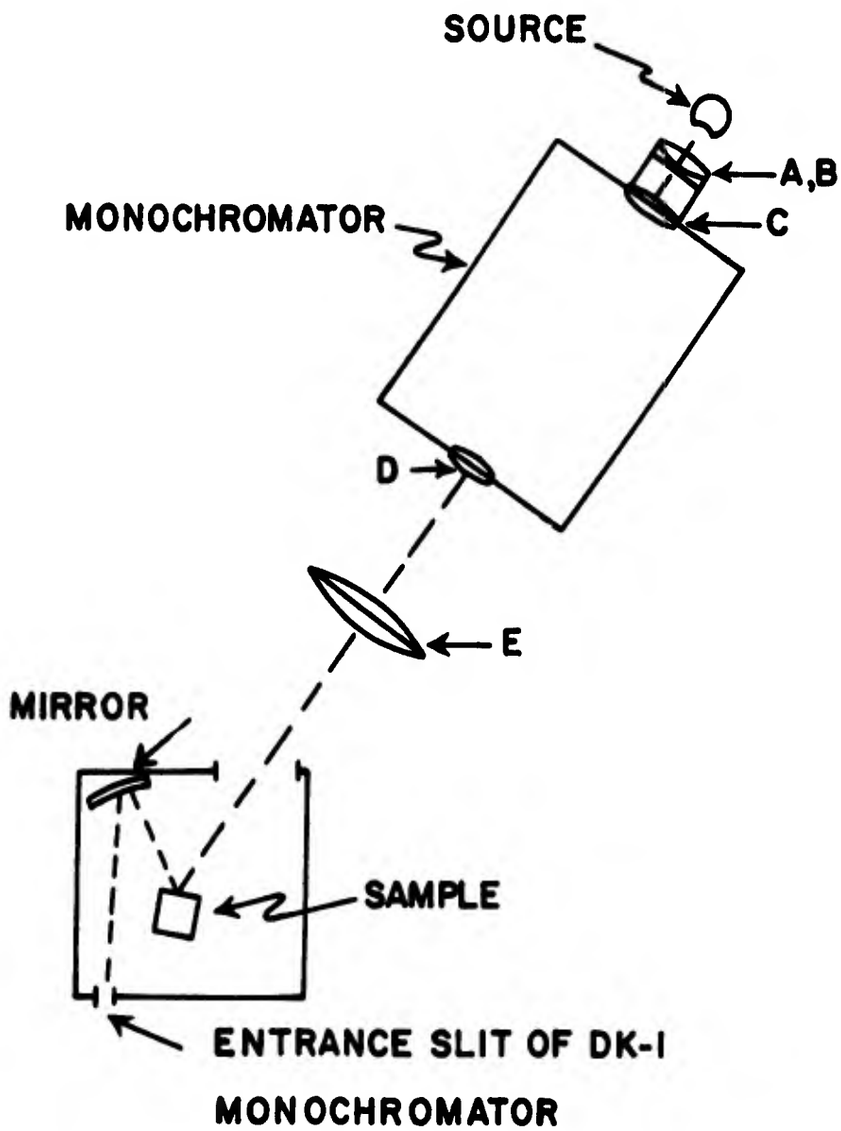

FIGURE 7: Fluorescence Apparatus

conditions which simulate fluorescence. During the course of the measurements, the intensity of the excitation was maintained constant by reference to the fluorescence of a piece of "uranium" glass securely mounted below the sample holder. The solutions were examined in standard Beckman quartz spectrophotometer cells attached to tubes in which degassing oculd be affected.

An aqueous solution of quinine sulfate was used as the fluorescence standard. The quantum yield of fluorescence of this compound under specified conditions is 0.55.[8] The performance of the apparatus was tested with anthracene in ethanol. The values obtained, 0.28 $\pm$ 0.02 with 313 mμ excitation and 0.30 $\pm$ 0.01 with 366 mμ excitation are in good agreement with the values 0.26[6] and 0.28[8] reported by other workers. It should be mentioned that results obtained with 3,4-benzopyrene, which are presented in a later section, indicate that the quantum yield of 0.55 for quinine sulfate on which all the quoted values are based is too high by about 10%.

(d) Data Processing

Photochemical experimentation of the type under way in our laboratory involves a great deal of data evaluation. This often involves tedious and time-consuming operations of a repetitive nature which not infrequently represent the bottleneck of the experiment. We have therefore placed increasing emphasis throughout the contract period on the use of the digital computer. For small problems and to test segments of larger problems, the

IBM 1620 computer at Northeastern University proved to be satisfactory. Large problems have been processed on the IBM 7094 computer at the Massachusetts Institute of Technology.

Much of our raw data is in analog form, i.e., continuous curves representing plots of one parameter against another. For computation purposes these data must be digitized. We have acquired a Gerber Digital Data Reduction System for this purpose. In this unit the curve is aligned on a viewing screen and points are selected by manual positioning of cross hairs. The output is in the form of IBM cards which register the X and Y values to three digits. The maximum resolution is 1/200 inch, which is more than adequate in view of the thickness of pen-drawn curves.

Computer techniques have been used for the following problems.

(1) Flash Photolysis - The raw data consist of photographic records of oscilloscope traces which represent the alternation of the monitoring light at a given wavelength as a function of time. In the course of investigating the behavior of one system, many thousands of such pictures are collected. A computer program converts the digitized traces into values of the change in optical density. Transient spectra, representing the absorption at various times after the flash, are constructed with a Cal-Comp plotter. Other programs have been constructed for elucidating the kinetic behavior of the transients. Various rate laws are tested and appropriate plots are made with the Cal-Comp equipment.

(2) Spectroscopic Measurements - The dissociation constants and extinction coefficients of charge-transfer complexes are generally determined by the Benesi-Hildebrand method.[9] The data consist of optical densities in the charge transfer absorption region at various donor and acceptor concentrations. A program has been constructed for the computation of the spectral and equilibrium parameters and their uncertainties from these data. A new method for determining the equilibrium constants for systems involving multifunctional donors and acceptors from spectral data is presented in Section 6. The calculations for this procedure have also been programmed.

Another fruitful application of the computer is in the evaluation of vacuum ultraviolet spectral data. Our instrument operates with a single beam, and the incident and sample-attenuated intensities are measured separately. The light sources employed have highly structured emissions, and to obtain a highly resolved absorption spectrum closely spaced points must be read. The Gerber data reduction unit is particularly useful for digitizing the recorder output. A program has been written for computing the extinction coefficients as a function of pressure from the intensity values and the pressure of the sample.

(3) Electron Spin Resonance Spectroscopy - An obvious application of the computer in this area, which we have employed extensively, is the quantum mechanical calculation of spin densities in molecules. Further, a program has been

written for the simulation of electron spin resonance spectra from experimentally determined line widths and splitting constants. Both Lorentzian and Gaussian line shapes can be tested. Some effort has been expended, alas unsuccessfully, to solve the difficult problem of gleaning the splitting parameters from the experimental spectra.

(4) Fluorescence Quantum Yield Measurements - Computer programs we have constructed accomplish the following operations for digitized raw data.

i) Conversion of the photomultiploer response for the standard lamp into sensitivity factors and plotting these as a function of frequency.

ii) Conversion of photomultiplier response for the fluorescent samples into relative number of quanta per unit frequency interval using the above-mentioned sensitivity factors.

iii) Calculation of the areas under the relative number of quanta per unit frequency interval *versus* frequency curves for the entire emission spectrum.

The quantum yields are then easily calculated by hand from the areas for the sample and the standard and the corresponding measured optical densities at the exciting wavelength.

References

(1) K. Weiss, H. Koller, D. H. Lambert, G. P. Rabold, W. M. Moreau, P. Schnieper, and H. P. Wolf, "Photochemical Studies of Some Organic Sulfur Compounds and Ketones," in "Research in Energy Conversion," AD 429 505, November, 1963.

(2) J. J. Bohning, "A Kinetic Study of the Photochemical Addition of Phenanthrenequinone to Olefins," Scientific Report #1, Contract AF19(628)-3836, AFCRL 65-714, July, 1965.

(3) J. J. Bohning and K. Weiss, J. Am. Chem. Soc., 88, 2893 (1966).

(4) P. A. Schnieper, "Apparatus for Flash Photolysis," Scientific Report #3, Contract AF19(628)-3836, July 1965.

(5) R. Danziger, "The Giant Pulse Ruby Laser Photolysis of Aqueous Methylene Blue and Some Other Systems," Doctoral Dissertation, Northeastern University, June 1967.

(6) K. Weiss, Quarterly Report No. 1, Contract AF19(628)-3836, December 1963.

(7) K. Weiss, Quarterly Report No. 2, Contract AF19(628)-3836, April 1967.

(8) C. Lagercrantz and M. Yhland, Acta Chem. Scand., 16, 1043 (1962).

(9) C. A. Parker and W. T. Rees, Analyst, 85, 587 (1960).

(10) R. Starr, W. E. Schneider, and J. K. Jackson, Appl. Optics, 2, 1151 (1963).

(11) W. H. Melhnish, N. Z. J. Sci. Tech., 37B, 142 (1955).

(12) H. A. Benesi and J. H. Hildebrand, J. Am. Chem. Soc., 71, 2703 (1949).

2. The Photochemistry of Perinaphthenone

by K. Weiss, G. P. Rabold, H. Köller, T. A. Tyler, and K. H. Bar-Eli.

(a) Introduction

Carbonyl compounds play a central role in photochemistry. The carbonyl group is one of the simplest functional groups, and its incorporation into alkanes shifts the absorption spectrum into the more accessible near ultraviolet region. Studies of carbonyl compounds have contributed much to knowledge about energy transfer, singlet to triplet state intersystem crossing, and the mechanism of photochemical reductions.

Acetone is a key compound for gas phase work; its photochemical reactions are now fairly well understood. In solution, aromatic ketones such as benzophenone have received, and continue to receive, a great deal of attention. The excited states of these ketones generally abstract hydrogen from suitable donors and produce pinacols. Thus the irradiation of benzophenone in the presence of benzhydrol furnishes benzpinacol.[1] The same product is obtained in high yield when a degassed solution of benzophenone in 2-propanol is photolyzed. However, this system also produces a yellow, oxygen-sensitive intermediate which decays only slowly in the dark.[2] This intermediate has been the subject of several investigations.[3,4,5,6] The original suggestion that the colored intermediate is a radical[2] is unacceptable owing to the absence of electron spin resonance absorption.[4] The most recent view is that it is derived from two semibenzpinacol radicals which combine by bond formation

between aromatic rings. The structure remains to be unequivocally established. It has been proposed that, by acting as an inner filter, the intermediate is responsible for the observed rate acceleration of the photo reduction of benzophenone on dilution with inert solvents.[7]

The point of departure for the work reported here was the observation that perinaphthenone (phenalene-1-one, I) exhibits unique behavior on irradiation. A study of this ketone and some of its derivatives was anticipated to provide further

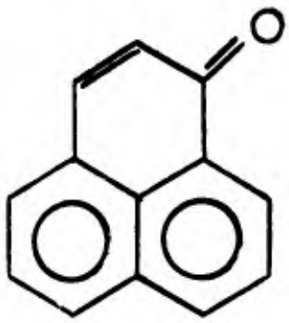

I

information about the photochemical behavior of aromatic ketones, particularly with respect to the nature of intermediates such as that observed with benzophenone. Perinaphthenone incorporates the structural features of α,β-unsaturated ketones and of simple aromatic ketones. It exhibits strong basic properties, having pK_B=0.4.[8] The addition of an electron or of a hydrogen atom to the oxygen atom leads to relatively stable radicals.[9] α,β-Unsaturated ketones generally

dimerize to cyclobutane structures.[10] Consequently, the irradiation of perinaphthenone could be expected to yield a veriety of products.

(b) General Features of the Photochemistry

The results of our initial experiments with perinaphthenone have been summarized in the final report for contract AF19(604)-7358.[11] The three publications which have to date resulted from this study are collected in Appendix D. The most comprehensive account of the perinaphthenone work is contained in Scientific Report No. 2[12] under this contract.

The prolonged irradiation of degassed solutions of perinaphthenone in inert solvemts such as benzene, methylcyclohexane, or carbon tetrachloride results in very little change. However, photolysis in 2-propanol leads to the rapid formation of a deep green color which decays slowly in the dark. The spectrum of the freshly irradiated solution (Appendix D, 1) shows a broad maximum at 650 mμ, a sharp peak at 550 mμ, and some additional structural features toward lower wavelengths. Identical spectra are observed in outgassed solutions of the following solvents:

Methanol

Ethanol

Acetone

Diisopropyl ether

Ethyl acetate

The green intermediate reacts rapidly with oxygen, iodine, and nitric oxide. This behavior is entirely analogous to that of the

yellow color developed during the photolysis of benzophenone under similar conditions. The green solution shows strong electron spin resonance (ESR) absorption due to the hydroxyperinaphthenyl radical (II). It was originally assumed that the 650 mμ absorption band is associated with this radical.

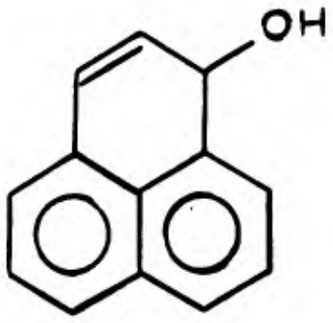

II

Kinetic measurements have shown this not to be the case; the ESR signals and the color decay at distinctly different rates.

(c) Products of Irradiation

The products of the photolysis of perinaphthenone in alcohols are quite revealing. From irradiations in methanol and in 2-propanol, perinaphthanone (III) was isolated as the major product. This is unusual inasmuch as α,β-unsaturated

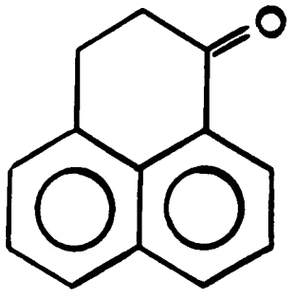

III

ketones generally produce dimers and aromatic ketones give rise to pinacols. It is probable that the saturated ketone III arises from the hydroxyperinaphthenyl radical I which abstracts a second hydrogen atom from the solvent. Other reactions occur since at least five other products were isolated in methanol. Two of these are dimers of perinaphthenone of unknown structure. Although the spectra of the green intermediate in methanol and in 2-propanol are identical, only one of the five additional products formed in the latter solvent is identical with a product from the methanol reaction. This is one of the perinaphthenone dimers which, on the basis of later experiments, appears to be a precursor of the green intermediate. Acetone was also detected in the irradiated 2-propanol solutions.

(d) Electron Spin Resonance Measurements

The ESR study of the radicals generated by photolysis of perinaphthenones is described in Appendix D,2 and D,3. Here, only some highlights and conclusions will be presented. First order analysis of the 24-line spectrum obtained by photolysis of perinaphthenone in 2-propanol clearly shows the absorption to be due to the hydroxyperinaphthenyl radical (Figure 3, Appendix D,3). Under optimized high resolution conditions, the spectrum is further resolved into 100 lines (Figure 4, Appendix D,3). The structure of radical II is consistent with one set of five almost equivalent protons and a second set of three almost equivalent protons. The additional splitting can be ascribed to small differences in the spin densities at the ring positions within each set of protons.

This is born out by molecular orbital calculations. Hückel molecular orbital theory is clearly inapplicable since it assigns totally inadequate spin densities to the ring positions corresponding to the set of three protons. Application of the McLachlan M)-SCF procedure provides a spin density distribution which leads fo six splitting constants. This model accurately reproduces the spectrum, as illustrated in the computer simulation of Figure 1 which is to be compared with Figure 4, Appendix D,3. The observed and calculated spin densities were found to be in good agreement.

A significant piece of information which could be gleaned from the EST spectrum of radical II is an estimate of Q_{OH}, the spin density transmission parameter for the OH σ-bond (Appendix D,2). Hyperfine splitting due to the proton attached to the oxygen atom is clearly evident in the spectrum. Using McConnell's relationship in the form $Q_{OH} = Q_{OH}\rho_O$, where Q_{OH} is the splitting constant, the spin density on oxygen (ρ_O) calculated on the basis of McLachlan MO-SCF theory gives $|Q_{OH}| \approx 7$ gauss. Approximately the same value was obtained by an independent calculation based on McConnell's configuration interaction model for the transmission of spin density. More recently, values of Q_{OH} between -17.5 and -20.5 gauss have been estimated from the spectrum of the hydroquinone cation radical.[13] $Q_{OH} = -17$ gauss has been obtained by Gough[14] *via* simple valence bond considerations. It has been suggested that the lower value reported by us reflects some out-of-plane movement of the C-O-H bond in radical II.

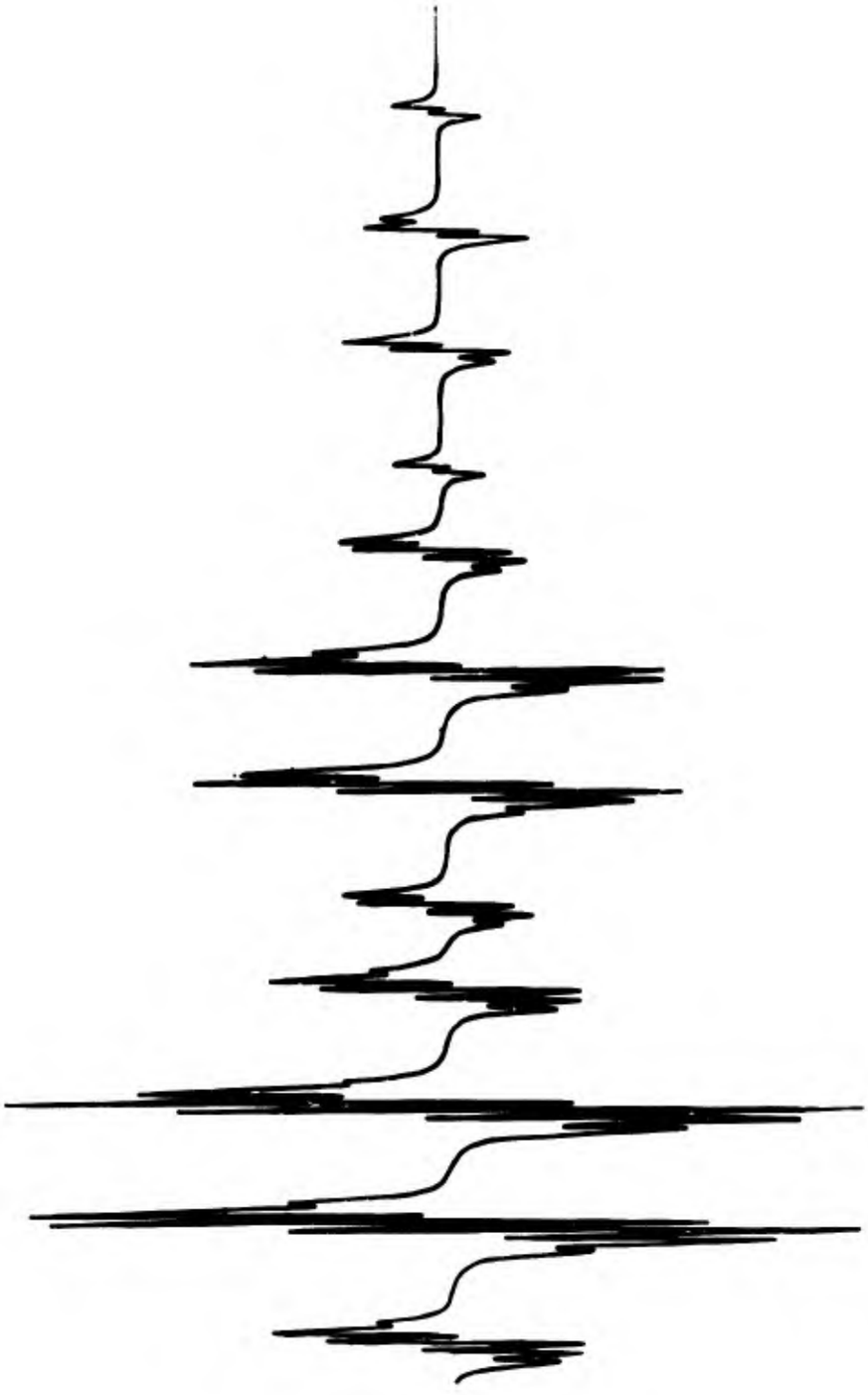

FIG. 1. COMPUTER-SIMULATED ESR SPECTRUM OF HYDROXYPERINAPHTHENENYL.

The ESR spectra of the radicals obtained by photolysis of some substituted perinaphthenones (IVa-IVe) show some interesting features. 2-Bromoperinaphthenone (IVa) gives rise

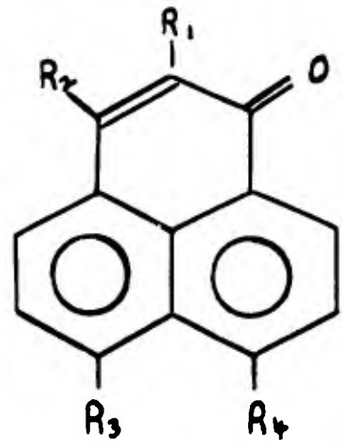

	R_1	R_2	R_3	R_4
IVa	Br	H	H	H
IVb	morpholino	H	H	H
IVc	H	morpholino	H	H
IVd	H	H	OH	H
IVe	H	H	OC—O—CO	

to radical III. This implies that photolysis results in loss of the bromine atom and conversion to perinaphthenone. Compound IVb furnishes a spectrum consistent with the removal of a proton from a low spin density position in perinaphthenone. The 3-morpholino compound (IVc), on the other hand, shows a complicated spectrum. The substituent in this case replaces a proton in a high spin density position, and splitting by the nitrogen nuclear

spin seems plausible. The dihydroxyperinaphthenyl radical derived from ketone IVd is considerably less stable than radical II. Its spectrum of five quartets is consistent with one less proton in a high spin density position. The calculated and observed splitting constants are in reasonable agreement for this radical. Pyrenic anhydride (IVe) evidently reacts with 2-propanol on standing in the dark. Irradiation of a degassed, aged solution gives an ESR spectrum which may be assigned to the radical derived from a half-ester of pyrenic acid, e.g. IV, R_3 = COOH and R_4 = $CO_2CH(CH_3)_2$. The major lines consist of four quartets. Splitting of the terminal lines into two doublets is ascribed to interactions with protons on oxygen. The splitting constants of 0.13 gauss and 0.39 gauss are assigned to the protons on the ring hydroxyl group and on the carbonyl group, respectively. The smaller value compares well with the hydroxyl splitting of 0.14 gauss observed for radical II.

(e) Kinetic Results

The kinetic behavior of radical II and of the green intermediate has been examined in some detail. Most of the measurements with the radical were performed by ESR spectroscopy. With relatively concentrated (10^{-2}M to 10^{-1}M) degassed solutions of perinaphthenone, the rate of formation of radical II follows the simple law

$$\log (R_{SS}-R) = -kt + \text{constant} \qquad \ldots\ldots (1)$$

where R_{SS} and R represent the steady state and instantaneous

concentrations, respectively, of the radical. The constant k is a function of light intensity; under the conditions used it had a value of $\sim 10^{-2}$ sec^{-1}. The decay of the radical in the dark approximately follows a first order rate law. The first order rate constant at room temperature os $2.42 \pm 0.15 \times 10^{-3} sec^{-1}$, corresponding to a half-life of 5 minutes.

Photolysis of perinaphthenone in degassed diphenylmethane generates no green transient. There is no absorption near 650 mμ, although the peak at 550 mμ appears. Radical II is produced and disappears rapidly in a second order decay process. For an experiment in 2-propanol solution it was found that plots of the logarithm of the optical density at 550 mμ *vs.* time and of the logarithm of the ESR signal *vs.* time run parallel within narrow limits. This method of plotting eliminates instrument factors. These results, as well as other observations,[15] leave no doubt that the absorption band at 550 mμ is associated with the hydroxyperinaphthenyl radical.

Perinaphthanone, a product of the photolysis of perinaphthenone in alcohols, can act as a hydrogen donor for excited ketone I. Photolysis of a mixture of these two ketones in benzene generates radical II, which decays by a second order process. The irradiated solutions show absorption at 550 mμ.

Kinetic measurements with the green intermediate have been performed under a variety of conditions. Early experiments were carried out with high concentrations ($\sim 10^{-2}$ M) of perinaphthenone, and relatively long continuous irradiations (> 5 minutes) were

employed to generate optical densities of *ca.* 0.6 at 450 mμ. It was found that the formation of green transient is complex. Plots of the optical density at 650 mμ *versus* time are sigmoid-shaped, suggestive of a consecutive sequence of steps leading to the colored intermediate. The most significant result is that color formation is greatly enhanced in decayed solutions. Thus the first irradiation of a given solution shows an initial formation rate of zero at zero time. On reirradiation after allowing the intermediate to decay completely, there is a finite initial formation rate as well as a substantially increased overall rate. After the third decay cycle, the formation rate remains essentially constant.

The decay kinetics for the green intermediate follow neither first nor second order kinetics exactly, but can be described by concurrent first and second order steps. The first order contribution appears to be predominant. In 2-propanol at 25°C, the first order constant is 8.0×10^{-4} sec^{-1}; based on an estimate of 10^4 for the extinction coefficient of the green transient, the second order constant is 10 ℓ/mole sec. The activation energy for the first order decay is 15.0 $\pm$ 0.5 kcal/mole, and the entropy of activation is -6.6 e.u. at 25°.

More recent optical kinetic studies have been conducted with more dilute solutions of perinaphthenone (10^{-3}M to 10^{-5}M) using short irradiation times (20 to 60 seconds). The conversion into transients is less extensive under these conditions and the optical densities reached are quite small. Meaningful

kinetic measurements are possible by using the spectrophotometer in an expanded transmission measuring mode. In 2-propanol in this concentration range, the decay at 650 mμ is approximately first order and the decay at 550 mμ (radical II) is approximately second order. The decay constants of both species are only slightly changed in rephotolyzed samples. The results in different solvents are informative. In cyclohexanol, no green transient is observed at ketone concentrations which provide significant quantities in 2-propanol. The radical decays slower in the cyclic alcohol. In ethylbenzene, only radical is generated. Using *iso*pentane as diluent 2-propanol solutions, it was found that high concentrations of the alcohol favor radical formation and low concentrations favor green transient formation. Production of the 650 mμ intermediate is also enhanced by low temperature. The decay rate of this transient increases with decreasing alcohol concentration.

(f) Generation of Green Intermediate from Other Compounds

Further information regarding the sequence of events leading to green transient was obtained from product isolation experiments. The isolation of compounds having analyses and molecular weights consistent with their being dimers of perinaphthenone has already been mentioned (Appendix D,1). It was found that photolysis of degassed solutions of these products gives rise to green transient. If a green solution is exposed to air immediately after photolysis, predominantly one product is formed, which is also formed in lesser amount

when the solution is first allowed to decay in the dark. The photolysis of this isolated material produces only green and no radical II.

An attempt to produce the green transient by careful acidification of the sodium ketyl of perinaphthenone failed. The corresponding reaction with benzophenone ketyl has been reported to give the yellow photochemical intermediate of this system.[5] The perinaphthenone ketyl yielded only radical II, which was identified by its absorption spectrum.

(g) Flash Experiments

Flash photolysis of a degassed 5×10^{-5} M solution of perinaphthenone in 2-propanol produces short-lived transient absorption in the 450-550 mμ region, which has a maximum near 500 mμ. The lifetime of this transient is ~100 μsecs; its decay appears to coincide with increasing absorption at 550 mμ due to radical II. Spectral examination of the solution after the flash revealed no absorption at 650 mμ.

(h) Experiments with Some Other Ketones

Benzanthrone (IV) is structurally related to perinaphthenone I; in this ketone a benzene ring replaces the double bond.

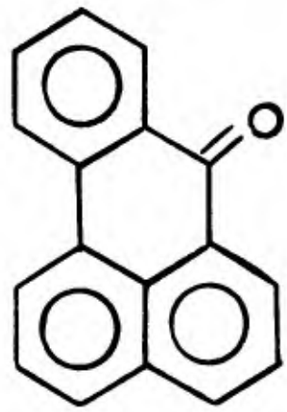

IV

It was found in earlier experiments[11] that benzanthrone is quite inert photochemically. Prolonged photolysis in 2-propanol and other solvents produced no colored imtermediates and conversion into products is extremely small. It therefore appears that the long-lived colored transient from perinaphthenone is related to the presence of a double bond. The generation of radicals from ketone IV was not studied.

1,1-Dimethyl-2-keto-1,a-dihydronaphthalene (V) retains the double bond, but has one less aromatic ring than perinaphthenone. Its photolysis in methanol produces no

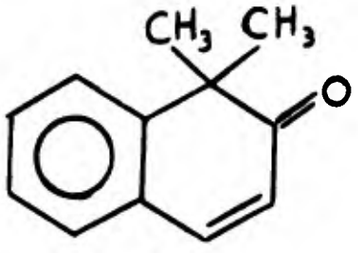

V

colored transients; instead, a dimer is formed in high yield. The NMR spectrum of this dimer clearly indicates it to incorporate a cyclobutane ring. Four structures can be written for this product, namely *cis* and *trans* configurations of head-to-head and tail-to-head dimers, respectively. The NMR data permit the tentative conclusion that the product is a head-to-head dimer. X-ray measurements* showed the crystals

---

*Kindly performed by Dr. J. Silverman, Air Force Cambridge Research Laboratories.

to be monoclinic, and of space group $P2_1/C$. There are 4 molecules per unit cell. Packing considerations were insufficient to distinguish between the *cis* and *trans* forms of the head-to-head structure.

(i) Conclusions

The photochemical behavior of perinaphthenone is dependent on the irradiation conditions. The material is surprizingly inert in solvents which are incapable of donating hydrogen atoms. In reactive solvents, perinaphthenone and substituted perinaphthenones readily produce the corresponding hydroxy-perinaphthenyl radicals. These are readily identified by their electron spin resonance spectra, for which meaningful theoretical interpretations could be developed. Further conclusions pertaining to the photochemistry of the parent ketone I may be summarized as follows.

(1) The short-lived transient absorbing at 550 mμ is tentatively assigned as the lowest triplet state of perinaphthenone. This identification is based primarily on its lifetime and that this transient appears to be the precursor of radical II.

(2) Radical II (R·) is produced by a hydrogen atom abstraction reaction of the triplet ketone (K*) with the solvent, e.g.

$$K^* + (CH_3)_2\,CHOH \rightarrow R\cdot + (CH_3)_2\dot{C}OH \qquad \ldots\ldots (2)$$

(3) The 650 mμ transient (green) arises from the further photolysis of a product. Although the alcohol appears to be necessary for green to have some stability, this solvent is not incorporated in its structure.

(4) The green intermediate is not a radical; it is formed from two molecules of perinaphthenone. The reduction product, perinaphthanone (III) is not involved in its formation.

(5) Radical II is most probably not involved in the production of green.

(6) Perinaphthanone is formed from radical II. Depending on the solvent, this involves either a disproportionation reaction of two radicals or the further reaction of the radical with solvent.

(7) Excited perinaphthenone can abstract hydrogen from perinaphthanone to produce radical II.

Based on the assumption, contrary to points above, that the hydroxyperinaphthenyl <u>is</u> the precursor of the green transient, detailed mechanisms have been developed for the formation and decay of this transient.[12] The key steps in green formation are considered to be the addition of radical II to a ground state perinaphthenone molecule, followed by reaction of the resulting radical with another ketone molecule to furnish the green transient and regenerate radical II. While on the basis of later results this scheme is now viewed as

incorrect, it leads to the formulation of the green transient as a dimer of perinaphthenone, which is consistent with all the evidence at hand. Formula VI represents one of several possible structures. If the green transient arises by photochemical isomerization of its precursor, structure VII is plausible for the latter compound. In concentrated solutions, the reaction of triplet ketone with ground state ketone may represent a significant decay mode, and compounds VI and/or VII could result from the stabilization of an excimer. The decay of green would produce compound VII. The enhanced formation of green on rephotolysis reflects the higher concentration of compound VII in decayed solutions. It is conceivable that green can also be formed by the perinaphthenone-sensitized isomerization of compound VII. These mechanistic views are still speculative. It is hopefully anticipated that work under way will enable us to elucidate the structure of green and to firmly establish its mode of formation and decay.

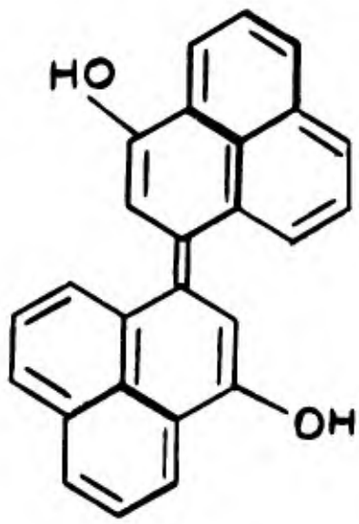

VI

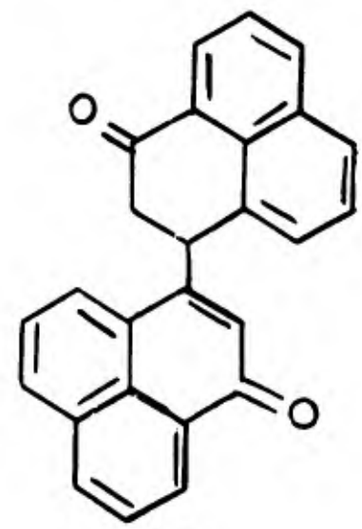

VII

References

(1) A. Schönberg and A. Mustafa, J. Chem. Soc., 276 (1943).

(2) J. N. Pitts, Jr., R. L. Letsinger, R. P. Taylor, J. M. Patterson, G. Recktenwald, and R. B. Martins, J. Am. Chem. Soc., 81, 1068 (1959).

(3) G. O. Schenck, W. Meder, and M. Pape, Proc. of the Second U. N. Internat. Conf. on the Peaceful Uses of Atomic Energy, 29, 352 (1958).

(4) J. H. Sharp, T. Kuwana, A. Osborne, and J. N. Pitts, Jr., Chem. and Ind. (London), 508 (1962).

(5) H. Mauser, U. Sproesser, and H. Heitzer, Chem. Ber., 98, 1639 (1965).

(6) V. Franzen, Ann., 633, 1 (1960).

(7) S. G. Cohen, unpublished observations reported in a talk delivered at Symposium on Radiation and Photochemistry, Northeastern Section of The Am. Chem. Soc., May 11, 1967.

(8) H. Takashi, Bull. Chem. Soc. Japan, 28, 483 (1955).

(9) H. Berg, Preprints, Fifth Internat. Symposium on Free Radicals, Uppsala, Sweden, 1961.

(10) A. Mustafa, Chem. Revs., 51, 1 (1952).

(11) K. Weiss, H. Köller, D. H. Lambert, G. P. Rabold, W. M. Moreau, P. Schnieper, and H. P. Wolf, "Photochemical Studies of Some Organic Sulfur Compounds and Ketones" in "Research in Energy Conversion," AD 429 505, November 1963.

(12) G. P. Rabold, "An Investigation of Photochemically Generated Free Radicals from Perinaphthenones," Scientific Report #2, AFCRL 65-715, July 1965.

(13) A. B. Barabas, W. F. Forbes, and P. D. Sullivan, Can. J. Chem., 45, 267 (1967).

(14) T. E. Gough, Trans. Faraday Soc., 62, 2321 (1965).

(15) K. Weiss, Quarterly Report No. 8, Contract AF19(628)-3836, December 1965.

3. The Photochemistry of Phenanthrenequinone

by K. Weiss, J. J. Bohning, and H. P. Wolf.

In contrast to the efforts expended on monoketones, relatively few investigations have dealt with diketones. Among these, the 1,2-diketones have been the most extensively studied. Photoreduction often accompanies other photochemical reactions of 1,2-diketones in hydrocarbon solvents and, in solvents with "available" hydrogen, it is invariably the major course of reaction.[1-4] Phenanthrenequinone (PAQ), which may be considered as a prototype for non-enolizable 1,2-diketones, is photochemically highly reactive. This diketone adds hydrocarbons to form 9,10-dihydro-9-hydrozy-9-alkyl-10-ketophenanthrenes,[7,8] and olefins to produce substituted dioxenes.[5-7] The photochemical reduction of phenanthrenequinone yields 9,10-dihydroxyphenanthrene, effective reducing agents being tetralin, ethanol, ethyl *ortho*formate, and zinc tetrahydrotetraphenylporphyrin.[8-13]

This report deals with two aspects of phenanthrenequinone photochemistry. A detailed kinetic study of the reaction of PAQ with stilbene and with two other phenyl-substituted olefins was undertaken to firmly establish a mechanism for the addition reaction and to shed light on the role of olefin-sensitizer intermediates in sensitized *cis-trans* isomerization. A second study was concerned with the mechanism of the photochemical reduction of PAQ. This reaction was of interest since it is anticipated to proceed *via* intermediate radicals which could serve as hydrogen donors for the reduction of disulfides.

(a) The Photochemical Reaction of Phenanthrenequinone with Olefins

This study is described in detail in Scientific Report No.1 [14] under this contract. A publication based on this work is reproduced in Appendix E. In comparing the quantum yields listed in the report and publication, it will be noted that the values in the latter are about 10% lower. The published results incorporate reflection corrections which were inadvertently omitted in the original computations. It is further to be noted that the mechanism offered in the publication differs in some details from that given in the report. This change was prompted by a careful reexamination of the quantitative data prior to publication.

The results obtained and conclusions reached in this investigation may be summarized as follows:

1. The quantum yields at 405 mμ for addition of PAQ to the stilbene, triphenylethylene, and 1,1-diphenylethylene are low (0.14 to 0.035). They are independent of the light intensity, and of the olefin concentration over a wide range.
2. *Cis*-stilbene and *trans*-stilbene react at different rates; isomeric adducts are formed.
3. Sensitized *cis-trans* isomerization occurs for which $\Phi_{cis \rightarrow trans}$ $\Phi_{trans \rightarrow cis}$ 0.45.
4. The system reaches a stationary *trans/cis* isomer ratio of 0.7 ± 0.05, which is close to that reported for some photostable, high energy sensitizers, but which in this case represents a balance between the adduct formation and isomerization rates.

5. Measurements with a,a'-stilbene-d_2 indicate a kinetic isotope effect for adduct formation.

The utilization of light energy is seen to be quite efficient for the PAQ-stilbene systems; once absorbed, a quantum leads either co addition or to isomerization. The results are interpreted in terms of the formation of the spectroscopic triplet state of *trans*-stilbene by classical energy transfer and of the short-lived common association complex between triplet PAQ and the *cis*- or *trans*-olefin. The complex is partitioned between collapse to adduct and decay to a non-spectroscopic excited state of the olefin which results to the isomeric ground state. The singlet to triplet intersystem crossing efficiency for PAQ is inferred to be unity.

A potentially highly significant finding of this study is that the PAQ-sensitized isomerization of the stilbene appears to show a deuterium isotope effect. Thus for stilbene-d_2, $\Phi_{cis \rightarrow trans} > \Phi_{trans \rightarrow cis}$ barely within error limits. The possible occurrence of an isotope effect in *cis-trans* isomerization is obviously pertinent to the detailed mechanism of this process, and to the more general problem of radiationless transitions. Further work with deuterated olefins is in progress in our laboratories. These experiments involve unsensitized photolyses, as well as reactions sensitized with photostable compounds.

(b) <u>The Photochemical Reduction of Phenanthrenequinone</u>

<u>Introduction</u> - The interest in this reaction stems from our work in sulfur

photochemistry (*cf.* Section 5 of this report). Atom transfer may prove to be a significant mode of sensitization for the photochemical reduction of disulfides in the sense that the sensitizer could act as a hydrogen atom transfer agent. A possible sequence of steps is shown in Equations 1 and 2, in which RSSR is the disulfide, $R'H_2$ a hydrogen-donating solvent, and S* an excited state of the sensitizer.

$$S^* + R'H_2 \longrightarrow SH\cdot + R'H\cdot \qquad \ldots\ldots (1)$$

$$RSSR + SH\cdot \text{ (or } R'H\cdot) \longrightarrow RSH + S \text{ (or } R') + RS\cdot \qquad \ldots\ldots (2)$$

The photoreduction of ketones and quinones gives rise to intermediate radicals which can function in this manner.[15,16] Benzophenone is illustrative of those non-enolizable ketones which ca affect hydrogen atom transfer. This ketone has been extensively studied.[17-20] Its photoreduction is proposed to proceed *via* intermediate $(C_6H_5)_2\dot{C}OH$ radicals which dimerize to form benzopinacol. Although this mechanism for the reduction is now generally accepted, there are contradictory reports concerning the quantum yield. Further, there is controversy regarding the structure and role of the colored intermediate which is generated during photolysis under reducing conditions.

In analogy to the monoketones, it has been proposed that many of the photochemical reactions of 1,2-diketones proceed *via* triplet states,[1-4] although direct experimental evidence is often lacking. In the case of biacetyl, which represents the simplest member of

this class of compounds, energy transfer experiments involving emission measurements provide direct proof that the triplet level is readily accessible.[21-23] Both biacetyl and benzil bring about the isomerization of suitable olefins.[24] For phenanthrenequinone, the involvement of the triplet state may be inferred from the ability of the photo-excited ketone to similarly induce the *cis-trans* isomerization of olefins.

The study reported here had two objectives. The first one was to establish a mechanism for the photochemical reduction of PAQ in 2-propanol. Secondly, it was desired to establish how the reaction is affected by added disulfides.

Experimental - Spectral measurements were made with a Beckmann DK-1 spectrophotometer. Gas-liquid chromatography (GLC) analyses were performed with an F & M Model 720 gas chromatograph. The purification of the solvents (2-propanol and benzene), of the disulfides (phenyl, mesityl, and t-butyl disulfide), and of naphthalene is described in the experimental part of Section 5 of this report. Phenanthrenequinone was purified by column chromatography on silica gel and recrystallized from benzene. The material had m.p. 208-209° (lit.[25] 208.5-210°).

The amperometric procedure which was used for thiol analysis is described in Section 5. Details regarding the irradiation cell assembly and the preparation of the samples are also given in Section 5. The quantum yield apparatus discussed in Section 2 and described in Appendix A was used for the photolyses.

The results of the photolysis of a 7.46×10^{-4} M solution of phenanthrenequinone in 2-propanol at 435 mμ is shown in Figure 1. The post irradiation spectrum shows maxima at 354 mμ and 368 mμ, which are characteristic of 9,10-phenanthrenediol.

Acetone was detected by GLC as a product of the photolysis (435 mμ) of a 2-propanol solution 7.5×10^{-3} M in PAQ and 8.52×10^{-3} M in t-butyl disulfide. A Triton X-305 on Chromasorb P column was used at 70°C with a helium flow rate of 60 ml./min. The estimated acetone concentration produced was $< 5 \times 10^{-3}$ M.

Regeneration of the characteristic absorption of phenanthrenequinone form photolyzed samples could be effected by several means. Shaking a photolyzed solution exposed to the atmosphere caused a slow regeneration. The addition of a single microcrystal of potassium permanganate to an almost completely photolyzed solution (4.76×10^{-4} M phenanthrenequinone; 0.599 M *t*-butyl disulfide; 1.16 M 2-propanol in benzene; 435 mμ) caused the rapid regeneration of 92% of the density loss.

Results -

1. Products of the Photoreduction

On the basis of the product spectra and oxidative regeneration it is evident that at least 90% of the rapid photobleaching of phenanthrenequinone results in the formation of 9,10-phenanthrenediol. Acetone has been identified by gas-liquid chromatography and appears to be a major product. The latter conclusion is rendered tentative however, as the

FIGURE 1

A TYPICAL PHOTOLYSIS OF PHENANTHRENEQUINONE

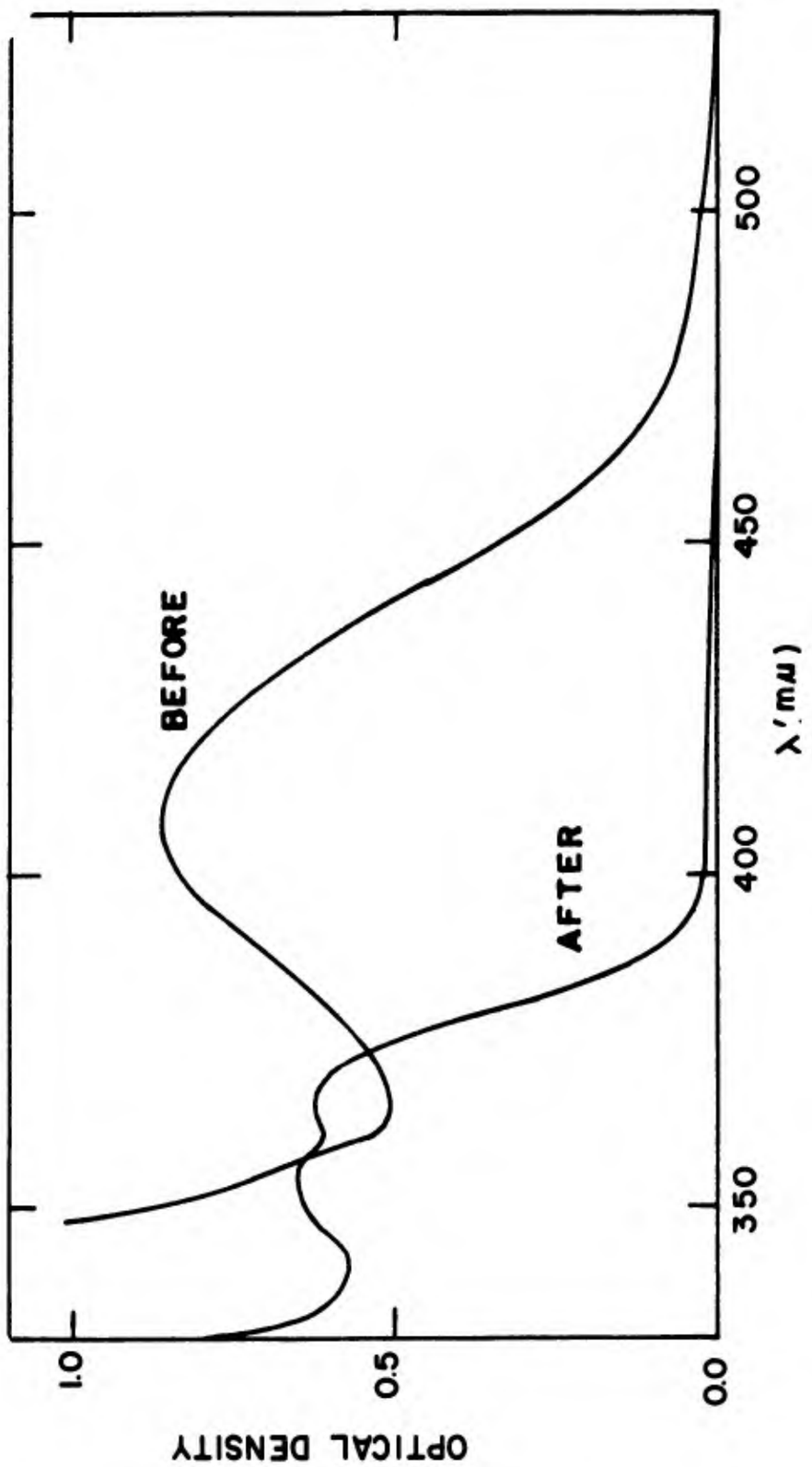

relatively low sensitivity of the thermal conductivity detector did not justify more than approximate estimation.

2. The Rate of Disappearance of Phenanthrenequinone as a Function of I_{abs}

The rate of disappearance of phenanthrenequinone was found to be directly proportional to the absorbed intensity over 80-90% of the reaction. A representative plot of the quantity log $(I_o/I-1 + a \log (I/I_o + a)$ *vs.* time (cf. Equation 3, Appendix A) appears in Figure 2.

3. Quantum Yields of the Photoreduction (Φ_{PAQ}) as a Function of 2-Propanol Concentration

The results of a series of experiments performed in increasingly dilute 2-propanol/benzene solutions is presented in Figure 3 and Table 1. A slow but definite decrease in Φ_{PAQ} is apparent with decreasing 2-propanol concentration. Plots of several variables, e.g. Figure 4 succeed only in revealing the dependency of Φ_{PAQ} upon 2-propanol concentration to be a complex one.

It should be noted here that the quantum yields for all of the phenanthrenequinone photoreductions were determined from the slopes of plots of the function illustrated in Figure 2 (cf. Appendix A). The time-consuming nature of these calculations was mitigated in this case by

FIGURE 2

PLOT OF EQUATION (3) APPENDIX A FOR THE PHOTOREDUCTION OF PHENANTHRENEQUINONE

$\lambda = 435\ m\mu$

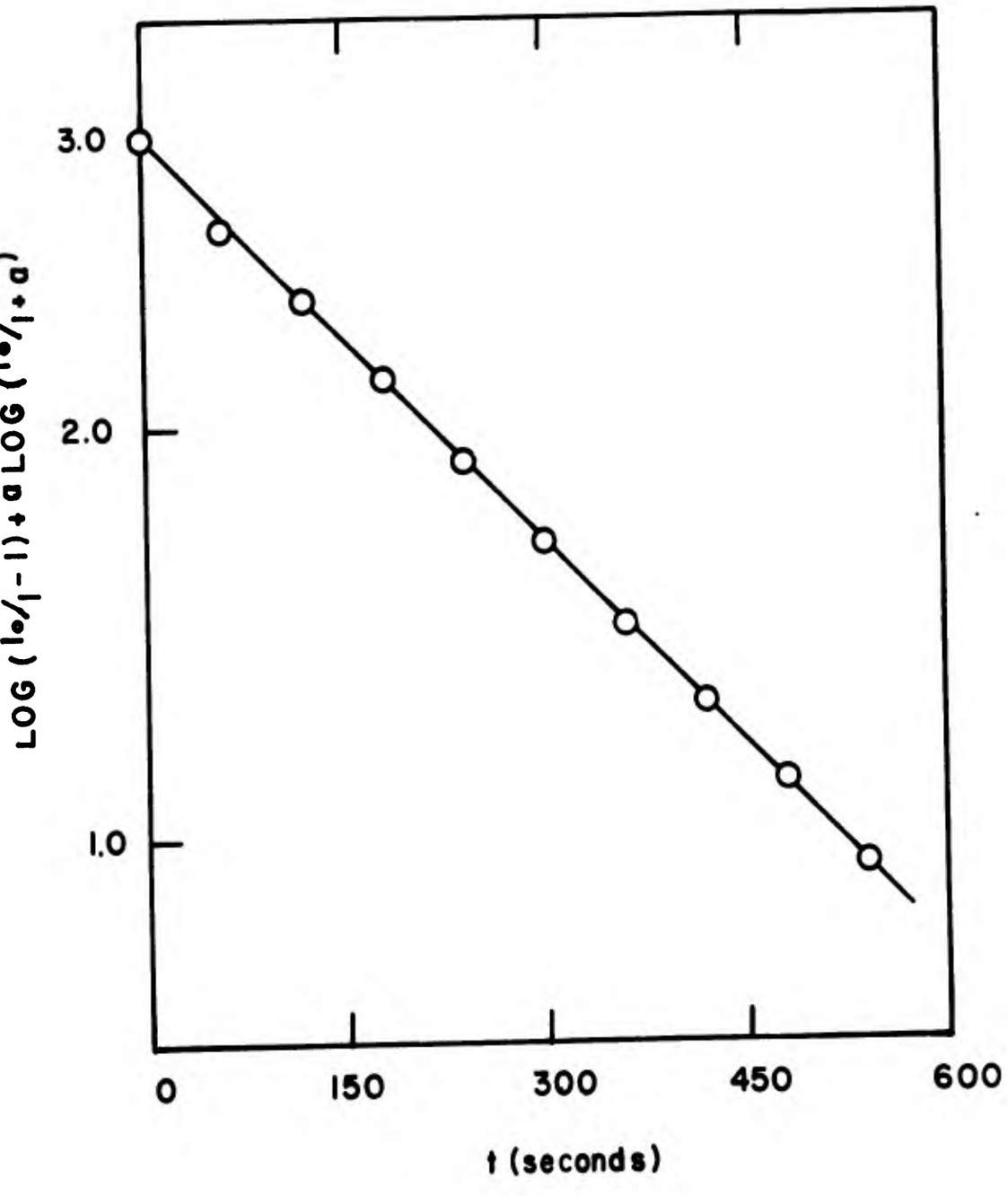

FIGURE 3

Φ_{PAQ} VS. 2-PROPANOL CONC'N. M., $\lambda = 435\ m\mu$

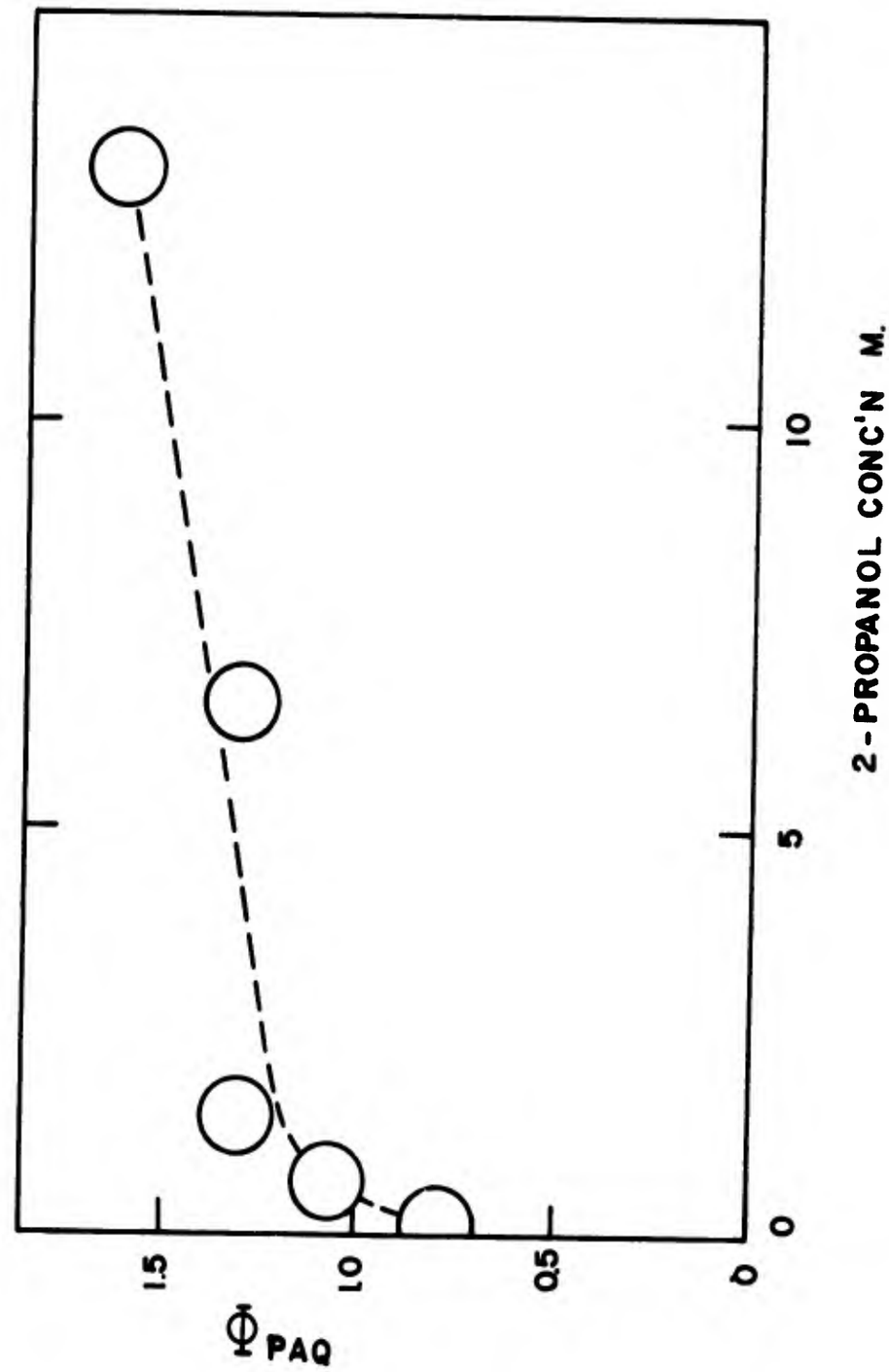

TABLE 1

Φ_{PAQ} AS A FUNCTION OF 2-PROPANOL CONCENTRATION

λ: 435 mμ

Conc. of 2-Propanol M	Φ_{PAQ}	# Runs
13.07[a]	1.62 (0.07)	2
6.54[b]	1.35	1
1.31[b]	1.33 (0.05)	6
0.65[b]	1.07 (0.03)	3
0.131[b]	0.79 (0.05)	2

a. 7.63×10^{-4} M pheranthrenequinone

b. 4.83×10^{-4} M phenanthrenequinone

FIGURE 4

$1/\Phi_{PAQ}$ VS. 1/[2-PROPANOL] M. $\lambda = 435\ m\mu$

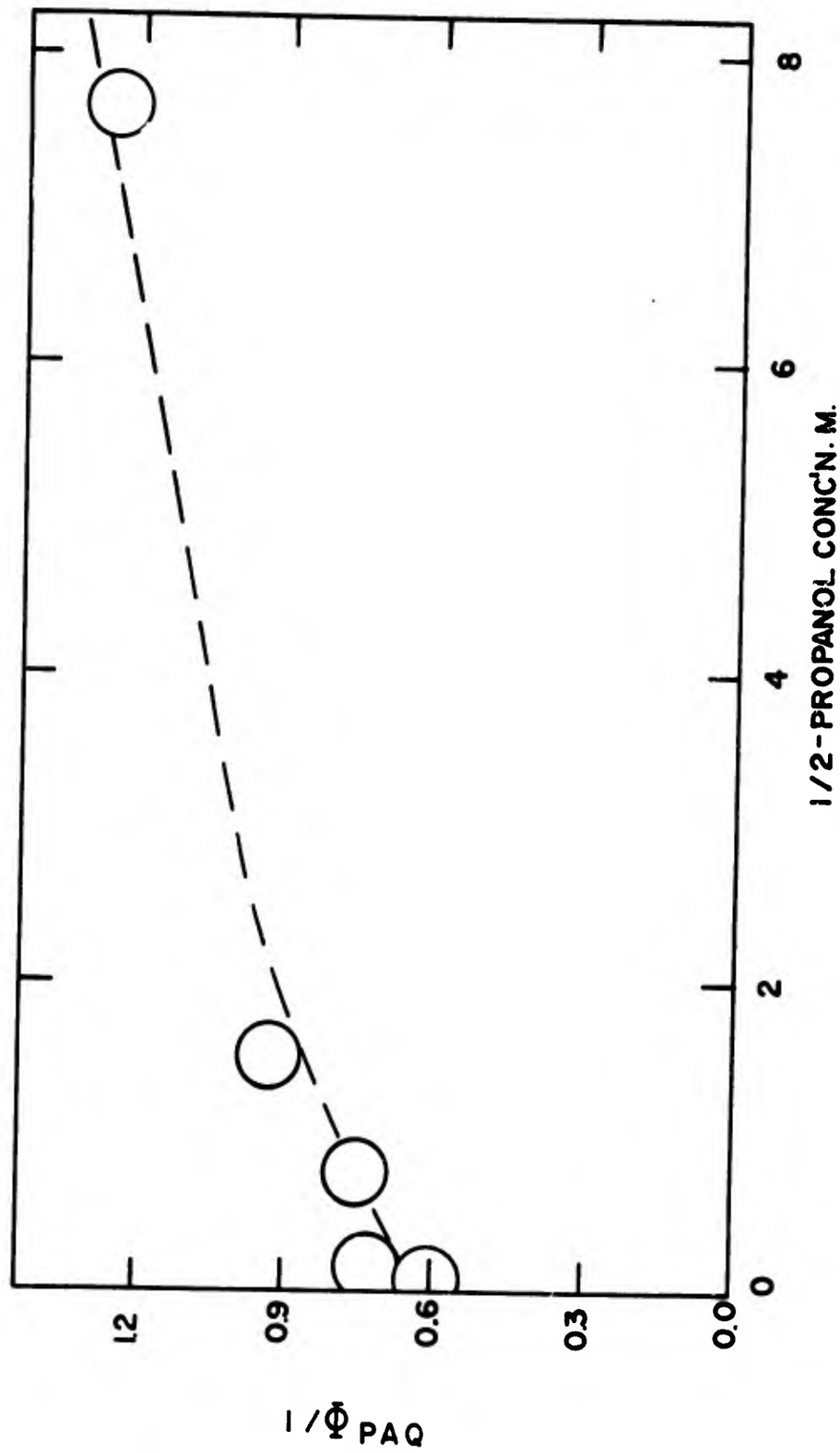

computer-programming of the functions leading to the plots.*

4. Quenching of Phenanthrenequinone (PAQ) Reduction

Quantum yields of photoreduction are presented for experiments run in the presence of the known triplet quencher naphthalene,[26,27] and some disulfides in Table 2. The results indicate that naphthalene has little or no effect, while among the disulfides tested *t*-butyl disulfide and phenyl disulfide are the most effective quenchers.

The results of several experiments performed at various concentrations of *t*-butyl disulfide are presented in Table 3. A plot of $\Phi_{PAQ}/\Phi^{B}_{PAQ}$, the ratio of unquenched quantum yield to the quenched quantum yield *vs.* the *t*-butyl disulfide concentration is presented in Figure 5. The linearity of this plot implies the action of *t*-butyl disulfide in a collisional quenching of the excited state involved in the disappearance of phenanthrenequinone.

5. Thiol Determination in Quenched Reactions

No evidence for the formation of titratable thiol as a product could be found in any of the quenching experiments where spectral overlap with phenanthrenequinone was

---

*This programming was performed by Mr. J. Keffer, under the auspices of the Northeastern University Work-Study Program. The calculations were carried out at the Northeastern University Computation Center.

TABLE 2

Φ_{PAQ} , THE EFFECT OF NAPHTHALENE AND SOME DISULFIDES

λ: 435 mμ

Compound[a]	Conc. M	Φ_{PAQ}
napthalene	9.41×10^{-3}	1.50
phenyl disulfide	1.12×10^{-2}	1.16
mesityl disulfide	6.49×10^{-3}	1.43
	3.50×10^{-3}	1.54
t-butyl disulfide	5.00×10^{-2}	0.65
	2.46×10^{-2}	0.87
		1.62

a. 2-propanol

TABLE 3

Φ_{PAQ} AS A FUNCTION OF *t*-BUTYL DISULFIDE CONCENTRATION

λ: 435 mμ

Conc. of *t*-Butyl Disulfide x 10^2 M [a]	Φ_{PAQ}	# Runs
20.3	0.23 (0.02)	3
10.0	0.45 (0.02)	3
1.99	0.96 (0.11)	2
0.995	1.23 (0.11)	4
0	1.33 (0.05)	6

a. $4.79 \pm 0.04 \times 10^{-4}$ M phenanthrenequinone in 1.31 M 2-propanol/benzene

FIGURE 5

$\Phi_{PAQ} / \Phi^{B}_{PAQ}$ VS. THE CONCENTRATION OF t-BUTYL DISULFIDE, λ435mμ

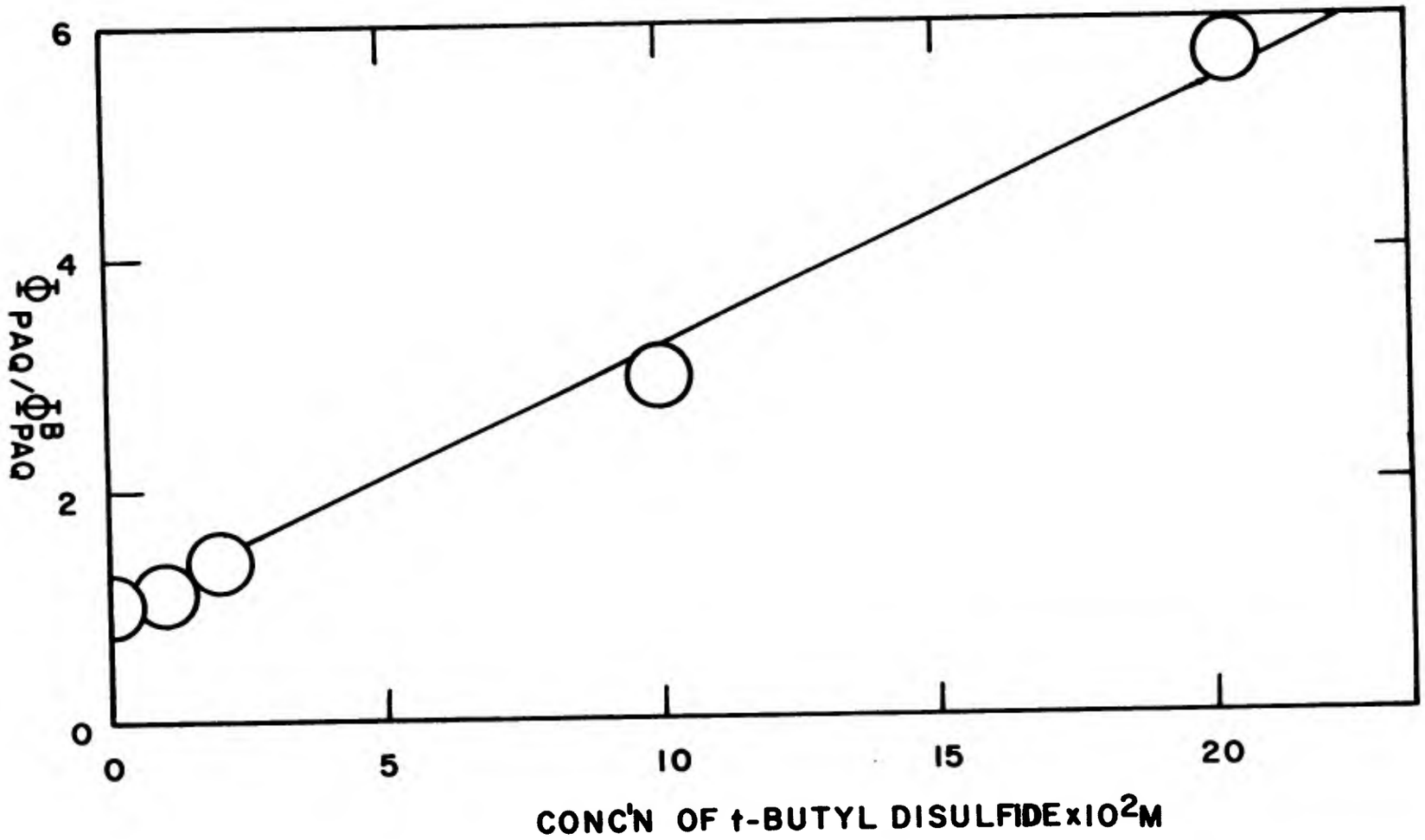

negligible or absent at the wavelength of irradiation. These experiments included irradiation in the presence of *t*-butyl disulfide at 435 mμ and thioctic acid at 405 mμ. The latter experiment, which utilized a solution which was 10^{-2} M in thioctic acid and 3.8×10^{-4} M in phenanthrenequinone, demonstrated a smooth photoreduction to 9,10-phenanthrenediol and a negligible thiol titer. The Φ_{PAQ} calculated by integration of the absorbed intensity *vs.* time and the amount of phenanthrenequinone which was consumed, was *ca.* 0.44. This result is indicative of substantial quenching, relative to $\Phi_{PAQ} = 1.25$ measured in 6.535 M 2-propanol/benzene at 405 mμ.

Discussion - Investigation of the inhibiting effect of added disulfides and mercaptans on the benzophenone photoreducing system have led to the postulation of hydrogen transfer between hydroxydiphenylmethyl radicals disulfides.[15]

Our observations indicate that radicals generated in the phenanthrenequinone/2-propanol reducing system do not transfer hydrogen to the several disulfides examined. Thus PAQ is not a practical sensitizer for the photoreduction of thioctic acid. Furthermore, in the case of *t*-butyl disulfide, where

spectral overlap with phenanthrenequinone is absent at the wavelength of irradiation, we detect no production of thiol in spite of the substantial collisional quenching indicated (cf. Stern-Vollmer plot, Figure 5). As inferred by recent work in these laboratories, we assume the quantum yield of intersystem crossing to be *ca.* unity for phenanthrenequinone. Spectroscopic information places this triplet energy level at 48.8 kcals./mole.[28]

The main features of the mechanism proposed to account for the observed behavior of the phenanthrenequinone photoreducing system follow.

1. We postulate the efficiently populated triplet state of phenanthrenequinone as the chemically reactive state.
2. The observation of Φ_{PAQ} values approaching 2 indicates the significance of the bimolecular step of Equation 8 (*vide infra*), in which ground state quinone abstracts a hydrogen from the 2-hydroxy-2-propyl radical (RH·).
3. The direct proportionality of the rate of quinone disappearance to the absorbed intensity (Figure 2) leads us to postulate the bimolecular disappearance of the 10-hydroxy-9-phenanthryloxyl radical (QH·) to furnish a dimeric species ($[QH]_2$) similar to quinhydrone. A possible structure of $(QH)_2$ is given in Figure 6. This species, which is postulated to have finite lifetime, partitions its disappearance between decomposition to 9,10-phenanthrenediol (QH_2) and phenanthrenequinone (Q), and reaction with 2-propanol (RH_2) to yield two molecules of 9,10-phenanthrenediol (QH_2) and acetone (R). The latter process

FIGURE 6

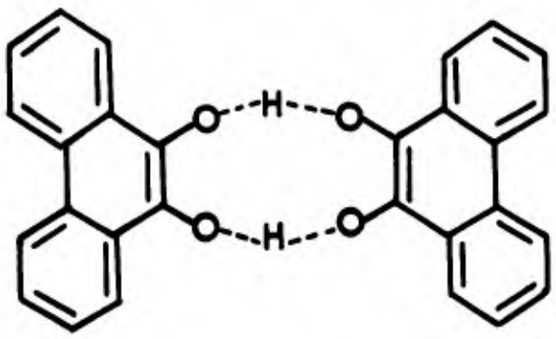

Structure of Intermediate $[QH]_2$

is formulated in a single step, Equation 11 below, in preference to the sequence

$$[QH]_2 + RH_2 \rightarrow QH_2 + RH\cdot + QH\cdot$$

$$QH\cdot + RH\cdot \rightarrow QH_2 + R$$

on the basis of the anticipated speed of the reaction of QH· and RH· generated in close proximity to one another. The detailed mechanism, then, is as follows:*

$$Q \xrightarrow{k_1 I_{abs}} Q^* \qquad \ldots\ldots\ldots (3)$$

$$Q^* \xrightarrow{k_2} Q \qquad \ldots\ldots\ldots (4)$$

$$Q^* \xrightarrow{k_3} Q' \qquad \ldots\ldots\ldots (5)$$

$$Q' \xrightarrow{k_4} Q \qquad \ldots\ldots\ldots (6)$$

$$Q' + RH_2 \xrightarrow{k_5} QH\cdot + RH\cdot \qquad \ldots\ldots\ldots (7)$$

$$Q + RH\cdot \xrightarrow{k_6} QH\cdot + R \qquad \ldots\ldots\ldots (8)$$

$$2QH\cdot \xrightarrow{k_7} [QH]_2 \qquad \ldots\ldots\ldots (9)$$

$$[QH]_2 \xrightarrow{k_8} QH_2 + Q \qquad \ldots\ldots\ldots (10)$$

$$[QH]_2 + RH_2 \xrightarrow{k_9} 2QH_2 + R \qquad \ldots\ldots\ldots (11)$$

---

* Q^* and Q' are respectively the singlet and triplet excited states of the quinone.

Application of the steady state treatment to Q^* and Q' affords.

$$(Q^*) = \frac{k_1 I_{abs.}}{k_2+k_3} \quad \ldots\ldots\ldots (12)$$

$$(Q') = \frac{k_1 k_3 I_{abs.}}{(k_4+k_5(RH_2))(k_2+k_3)} \quad \ldots\ldots\ldots (13)$$

and for QH· , RH· and $[QH]_2$ we obtain

$$k_5(Q')(RH_2) + k_6(Q)(RH\cdot) = 2k_7(QH\cdot)^2 \quad \ldots\ldots\ldots (14)$$

$$k_5(Q')(RH_2) = k_6(Q)(RH\cdot) \quad \ldots\ldots\ldots (15)$$

$$k_7(QH\cdot)^2 = k_8([QH]_2) + k_9([QH]_2)(RH_2) \quad \ldots\ldots\ldots (16)$$

Substitution of Equation 15 into Equation 14 yields the expression

$$k_5(Q')(RH_2) = k_7(QH\cdot)^2 \quad \ldots\ldots\ldots (17)$$

then, substitution of Equation 17 into Equation 16 affords

$$([QH]_2) = \frac{k_5(RH_2)(Q')}{k_8+k_9(RH_2)} \quad \ldots\ldots\ldots (18)$$

Now, the disappearance of phenanthrenequinone is given by

$$-\frac{dQ}{dt} = k_1 I_{abs.} - k_2(Q^*) - k_4(Q') - k_6(Q)(RH\cdot) - k_8([QH]_2) \quad \ldots\ldots\ldots (19)$$

Substitution of Equations 15 and 18 in 19 yields

$$-\frac{dQ}{dt} = k_1 I_{abs.} - k_2 Q^* - k_4 Q' + k_5 (Q') - \frac{k_5 k_8 (RH_2)(Q')}{k_8 + k_9 (RH_2)}$$

. . . . . (20)

If we then introduce Equation 13 for Q' we obtain

$$-\frac{dQ}{dt} = k_1 I_{abs.} - \frac{k_1 k_2 I_{abs.}}{(k_2+k_3)} - \frac{k_1 k_3 k_4 I_{abs.}}{(k_2+k_3)\ (k_4+k_5(RH_2))} +$$

$$\frac{k_1 k_3 k_5 (RH_2)\ I_{abs.}}{(k_2+k_3)\ (k_4+k_5(RH_2))} - \frac{k_1 k_3 k_5 k_8 (RH_2)\ I_{abs.}}{(k_2+k_3)\ (k_4+k_5(RH_2))\ (k_8+k_9(RH_2))}$$

. . . . . (21)

or

$$-\frac{dQ}{dt} = \frac{k_1 k_3\ I_{abs.}}{k_2+k_3} \left[1 - \frac{k_4}{k_4+k_5(RH_2)} + \frac{k_5 (RH_2)}{k_4+k_5(RH_2)} - \frac{k_5 k_8 (RH_2)}{(k_4+k_5(RH_2))\ (k_8+k_9(RH_2))} \right]$$

. . . . . (22)

If we let $k_1 = 1$ (mole/Einstein) and define $K_3 = k_3/k_2+k_3$, we obtain

$$-\frac{dQ}{dt} = \frac{K_3\ I_{abs.}}{k_4+k_5(RH_2)} \left[2k_5 (RH_2) - \frac{k_5 k_8 (RH_2)}{k_8+k_9(RH_2)} \right]$$

. . . . . (23)

or

$$-\frac{dQ}{dt} = \frac{K_3 k_5 I_{abs.}}{k_4+k_5(RH_2)}\left[2 - \frac{k_8}{k_8+k_9(RH_2)}\right] \quad \ldots\ldots\ldots (24)$$

Rearranging the terms in the brackets and dividing through by $I_{abs.}$ yields the expression for Φ_{PAQ}

$$\frac{-\frac{d(Q)}{dt}}{I_{abs.}} = \Phi_{PAQ} = \frac{K_3 k_5 (RH_2)}{k_4+k_5(RH_2)}\left[\frac{k_8+2k_9(RH_2)}{k_8+k_9(RH_2)}\right] \quad \ldots\ldots\ldots (25)$$

or

$$\frac{1}{\Phi_{PAQ}} = \frac{k_4+k_5(RH_2)}{K_3 k_5 (RH_2)}\left[\frac{k_8+k_9(RH_2)}{k_8+2k_9(RH_2)}\right] \quad \ldots\ldots\ldots (26)$$

It can be seen that the mechanism predicts a complex dependence of Φ_{PAQ} on the RH_2 concentration and that neither of the plots illustrated in Figures 3 and 4 is expected to be linear. This is indeed found to be the case. Qualitatively, however, we see that the mechanism predicts $\Phi_{PAQ} = 0$ when $(RH_2) = 0$ and Φ_{PAQ} approaches the limit 2 if (RH_2) becomes large, but no constants or ratio of constants can be deduced.

We should note that a very slow photoreaction of an as yet unspecified nature occurs in pure benzene. We assume that this is suppressed by the very rapid reaction with alcohol.*

---

*Similar assumptions were made in the study of a slower reaction (cf.) J.J. Bohning, Ph.D. dissertation, Northeastern University, Boston (1965).

The observation of quenching or the reduction of phenanthrenequinone by disulfides (cf. Table 4), coupled with the linearity of the plot of $\Phi_{PAQ}/\Phi^{B}_{PAQ}$ *vs.* concentration for *t*-butyl disulfide, Figure 5, suggests collisional quenching by the disulfide. Note that there is no significant quenching by naphthalene, as is to be expected in view of its triplet energy of 61 kcal./mole. The addition of the step

$$Q' + B \xrightarrow{k'} Q + B \qquad \ldots\ldots\ldots (27)$$

to the mechanism described by Equations 3 to 11 furnishes the expression

$$\Phi^{B}_{PAQ} = \frac{K_3 k_5 (RH_2)}{k_4 + k'(B) + k_5 (RH_2)} \left[\frac{k_8 + 2k_9 (RH_2)}{k_8 + k_9 (RH_2)} \right] \qquad \ldots\ldots\ldots (28)$$

which, when combined with the expression for Φ_{PAQ} previously derived for the unquenched case yields the relationship

$$\frac{\Phi_{PAQ}}{\Phi^{B}_{PAQ}} = 1 + k' \frac{(B)}{k_4 + k_5 (RH_2)} \qquad \ldots\ldots\ldots (29)$$

The slope of the plot (Figure 5) of the ratio of quantum yields against the *t*-butyl disulfide concentration yields

$$\frac{k'}{k_4 + k_5 (RH_2)} = 0.22$$

from which, unfortunately, no ratio of rate constants can be obtained.

It is concluded that these considerations tend to confirm the suggestion that the triplet state of alkyl disulfides is not photochemically active. This proposition needs confirmation, however, for other systems.

References

(1) P. A. Leermakers and G. F. Vesley, J. Am. Chem. Soc., 85, 3776 (1963).

(2) *ibid.*, 86, 1768 (1964).

(3) E. S. Huyser and D. C. Neckers, J. Org. Chem., 29, 276 (1964).

(4) W. H. Urry and D. J. Trecker, J. Am. Chem. Soc., 84, 118 (1962).

(5) A. Schonberg and A. Mustafa, Chem. Rev., 40, 181 (1947).

(6) A. Schonberg, "Preparative Organische Photochemie," Springer-Verlag, Berlin, 1958.

(7) M. B. Rubin and P. Zwitkowits, J. Org. Chem., 29, 2362 (1964).

(8) M. B. Rubin, J. Org. Chem., 29, 3333 (1964).

(9) R. F. Moore and W. A. Waters, J. Chem. Soc., 3405 (1953).

(10) P. Walker, J. Chem. Soc., 5545 (1963).

(11) A. Mustafa, Nature, 162, 85t (1948).

(12) G. R. Seely, U. S. Atomic Energy Commission UCRL, 2417, 120 (1953).

(13) H. Brockmann, and R. Muhlmann, Ber., 82, 348 (1949).

(14) J. J. Bohning, "A Kinetic Study of the Photochemical Addition of Phenanthrenequinone to Olefins," Scientific Report No. 1, AFCRL 65-714, July 1965.

(15) S. G. Cohen and S. J. Aktipis, J. Am. Chem. Soc., 88, 3587 (1966).

(16) S. G. Cohen and W. V. Sherman, J. Phys. Chem., 70, 178 (1966).

(17) G. S. Hammond and W. M. Moore, J. Am. Chem. Soc., 81, 6334 (1959).

(18) J. N. Pitts, *et al.*, *ibid.*, 81, 1068 (1959).

(19) W. M. Moore and M. D. Ketchum, J. Phys. Chem., 68, 214 (1964).

(20) J. H. Sharp, T. Kuwana, and J. N. Pitts, J. Chem. & Ind., 508, (1962).

(21) J. Sidman, D. S. McClure, J. Chem. Phys., 24, 757 (1955).

(22) H. L. J. Backstrom and K. Sandros, Acta. Chem. Scand., 12, 3 (1958).

(23) J. T. Dubois, J. Chem. Phys., 37, 4041 (1962).

(24) G. S. Hammond, *et al.*, J. Am. Chem. Soc., 86, 3196 (1964).

(25) "Organic Synthesis," Collective Vol. IV, John Wiley, Inc., New York, 1963, p. 757.

(26) H. L. J. Backstrom and K. Sandros, Acta. Chem. Scand., 16, 958 (1962).

(27) G. Porter and Wilkinson, Proc. Roy. Soc., A264, 1 (1961).

(28) N. A. Scheglova, D. N. Shigovin, and M. V. Gorelik, Zh. Fiz. Khim., 39 (4), 893 (1965).

4. The Unsensitized and Sensitized Photoreduction of Disulfides

by H. P. Wolf and K. Weiss.

Introduction

A. Disulfide Photochemistry

It is well known that disulfides are readily reduced to thiols by irradiation in suitable solvents.[1-5] The quantum yield depends on the structure of the disulfide; a summary of literature values appears in Table 1. Kharasch *et al.* have shown that in the presence of disulfides, light initiates the co-polymerization of butadiene and styrene.[6] This may be taken as evidence that radicals are generated. Lewis and Lipkin have photolyzed phenyl disulfide at liquid air temperature and have noted the reversible formation of a new optical

TABLE 1

PHOTOLYSIS OF DISULFIDES

Disulfide	Solvent	λ (mμ)	Φ_{RSH}
phenyl 2-methyl phenyl 4-methyl phenyl	alcohol hexane ether	> 300	0.046 (0.003)[1]
Cystine	aqueous HCl	> 300	0.02[1]
Trimethylene	3×10^{-3} M HCl in 95% ethanol	366	~0.4[17]
		313	~0.7[17]
Thioctic Acid	95% ethanol	366	~0.4[17]

absorption[7]. These authors found one band in this absorption spectrum which appears to be identical with that observed in solutions of phenyl disulfide in ethyl benzoate at 210°C, and with a band found in long-path measurements of ethanol solutions of the disulfide near room temperature. On this basis, they suggest that this common band should be assigned to the arylsulfenyl (thiyl) radical RS·. A number of studies assign the electron spin resonance absorption generated by thermolysis and photolysis of disulfides to an unpaired non-bonding electron localized on a sulfur atom[8-11]. All these findings support the premise that, under certain conditions, homolysis of the sulfur-sulfur bond is a major consequence of the absorption of light by disulfides. Much of the recent work concerning organic sulfur compounds is related to their role in biological systems. The macro structure of proteins and the function of certain enzymes and hormones have been discussed in terms of the reactivity of the sulfur-sulfur bond in relation to its scission and formation[12-15].

Thioctic acid, Figure 1, is of particular interest. Calvin has suggested that the photosensitized reduction of this compound and the re-oxidation of its product in the dark constitute a light-activated "valve" between the photosynthetic and respiratory cycles[16]. The photochemical reduction of cyclic disulfides appears to be relatively efficient. Calvin has reported that the quantum yield for photolysis of thioctic acid and for 1,2-dithiolane in 95% ethanol is of the order of unity (cf. Table 1)[17]. McGlynn *et al.* have studied the spectroscopy and photolysis of a number of sulfur compounds including some cyclic disulfides[19]. It appears to be generall accepted that, at least for

FIGURE 1

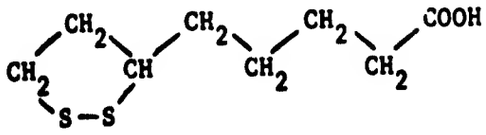

THIOCTIC ACID[a]

a. 3-(4-carboxybutyl)-1,2-dithiolane

the small ring cyclic disulfides, the excitation achieved by irradiation in the longest wavelength absorption band is of the $n \rightarrow \sigma^*$ type, and that the resulting excited state is dissociative.

B. Photosensitization

From the operational point of view, photosensitization is the enhancement of a photochemical reaction by an added substance which absorbs light. Although this definition says nothing about mechanism, it does imply that the energy absorbed by the sensitizer is directly or indirectly transferred to the reactant. Direct energy transfer, atom transfer, and electron transfer constitute possible mechanistic modes of sensitization. The rate of electron transfer and of a subsequent proton transfer are probably so rapid that a discrimination between electron transfer and atom transfer is usually not feasible.

Both direct energy transfer and atom transfer are of interest with reference to disulfide photochemistry. The former mode may provide a means of populating the dissociative excited state of disulfides by a route other than direct absorption. The greater lifetime of a triplet excited state relative to that of a singlet excited state has prompted frequent postulation of the role of the triplet state in direct energy transfer. Examples of triplet-triplet energy transfer with aromatic ketones (notably benzophenone) are numerous and experimentally well characterized[20-22]. Hydrocarbons such as phenanthrene, naphthalene, and biphenyl also sensitize the phosphorescence of biacetyl[23]. Flash photolysis provides the most direct evidence of the transfer of triplet excitation energy from donors such as triphenylene, phenanthrene and anthracene to suitable acceptors[24]. In all of these cases, efficient

transfer is predicated on the existence of an acceptor triplet energy level lower than that of the donor. Hammond and co-workers have taken advantage of this observation to estimate the triplet levels of compounds whose phosphorescence spectra have not yet been determined.[25]

Previous attempts to achieve the sensitized reduction of disulfides have not been crowned with unqualified success. Thus, the observation that the quantum yield of *iso*butyl mercaptan formation during the photolysis of *iso*butyl disulfide in cumene is independent of the concentration of the disulfide has been interpreted as indicative of photosensitization by cumene.[5] However, experimental complexities due to side reactions render the conclusion uncertain. In a more pertinent, direct sensitization attempt Calvin reported that light absorbed by zinc tetraphenylporphyrin causes the polymerization of 1,2-dithiolane.[16] A later communication, however, indicated that neither chlorophyll nor the metal tetraphenylporphyrins induce polymerization with irradiation at 5600 Å or 6700 Å.[18] As far as we have been able to ascertain, no further reports on the sensitization of disulfide reduction have appeared.

C. Plan of Research

The object of the research described is twofold: i) To secure quantitative data on the direct photoreduction of disulfides, and ii) to study the possibility of the sensitized reduction of disulfides.

A number of considerations entered into the choice of thioctic acid as the primary compound for detailed study. Firstly, there is some preliminary information available about its photochemical behavior. Secondly, thioctic acid, as a cyclic disulfide, represents the most reactive class of disulfides. The last, but by no means least, consideration was its ready availability in pure form.

The selection of a reducing agent was based primarily on the lack of absorption of the energies chosen for irradiation, the rate of reduction, and freedom from involvement in side reactions.

In addition to considerations of chemical and photochemical behavior, solubility, availability, etc., there are some specific limitations imposed upon the selection of sensitizer candidates by the nature of the experimental methods employed. Ideally, there should be no overlap of the absorption bands of the sensitizer and the material whose reaction is to be sensitizer (substrate). In cases of spectral overlap it becomes necessary to determine, with meaningful precision, the fraction of the observed change attributable to the action of the sensitizer.

Results

A. Analysis of Thiols

There are available several methods for the determination of thiols in solution. The application of iodometry is based on the relative ease with which thiols are oxidized to their corresponding disulfides by the triiodide ion.[26] This rapid, reproducible method suffers from a lack of selectivity, since compounds other than thiols may be oxidized. The reaction with soluble heavy metal salts is the basis for other, more selective determinations, which use, in the main, electronic endpoints. Of these, the most widely employed is the amperometric titration with silver nitrate.[27] In view of the great range of chemical behavior presented by the sensitizer candidates, the latter method seemed preferable.

During the course of this work, both direct addition of standard silver nitrate solution and back titration of excess silver nitrate with a standardized thiol solution were employed.[28] Figure 2 illustrates the results obtained by each mode of addition. The results of the direct titration of a typical photolysis mixture appear in Figure 3. Note the large negative current which disappears with the

FIGURE 2

A COMPARISON OF DIRECT AND BACK TITRATION METHODS

SAMPLE: SYNTHETIC DITHIOL SOLUTION

DIRECT TITRATION, (A) 2.07 N_{SH}
BACK TITRATION, (B) 2.58 N_{SH}

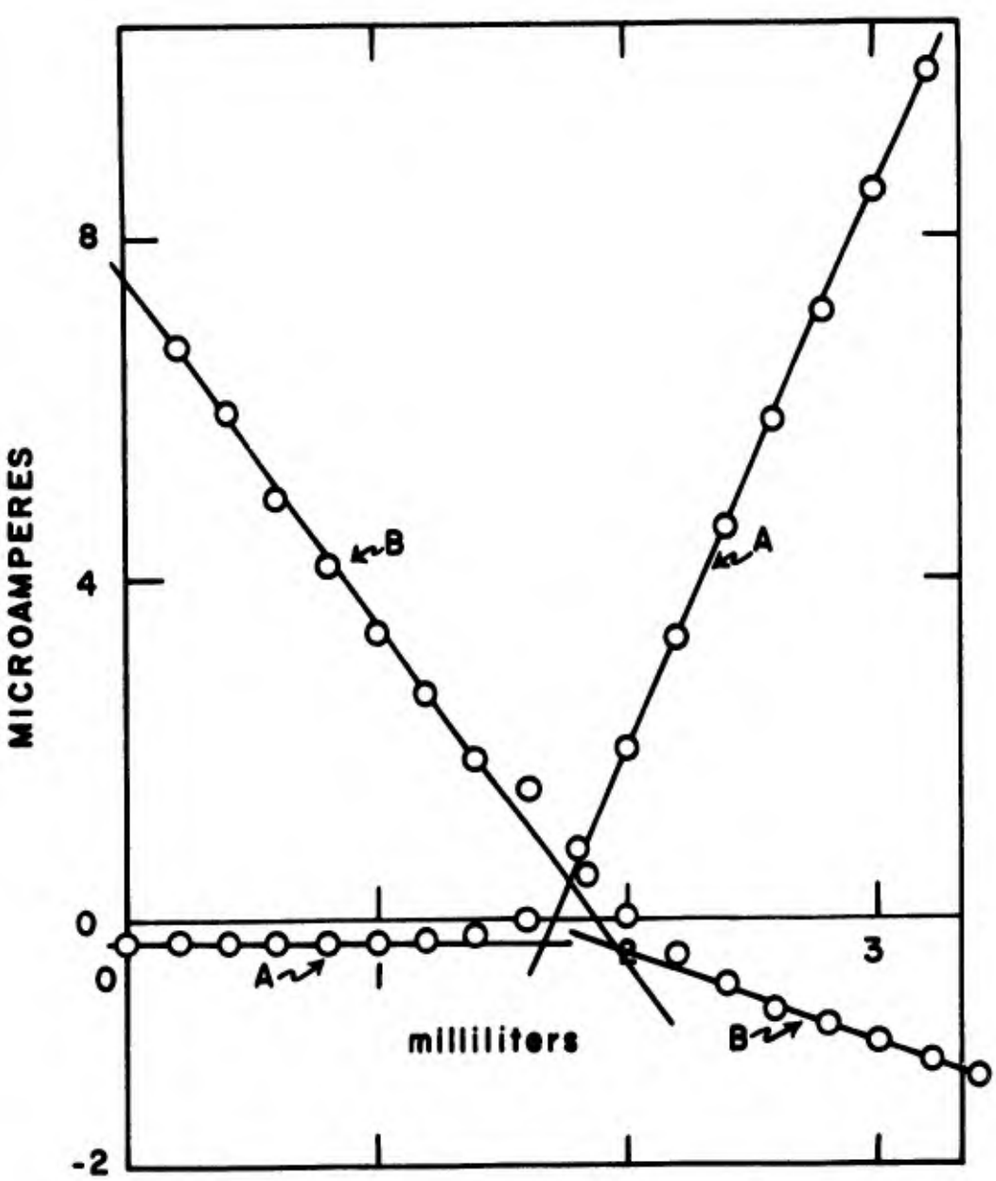

FIGURE 3

DIRECT TITRATION OF A PHOTOLYZED SAMPLE OF THIOCTIC ACID

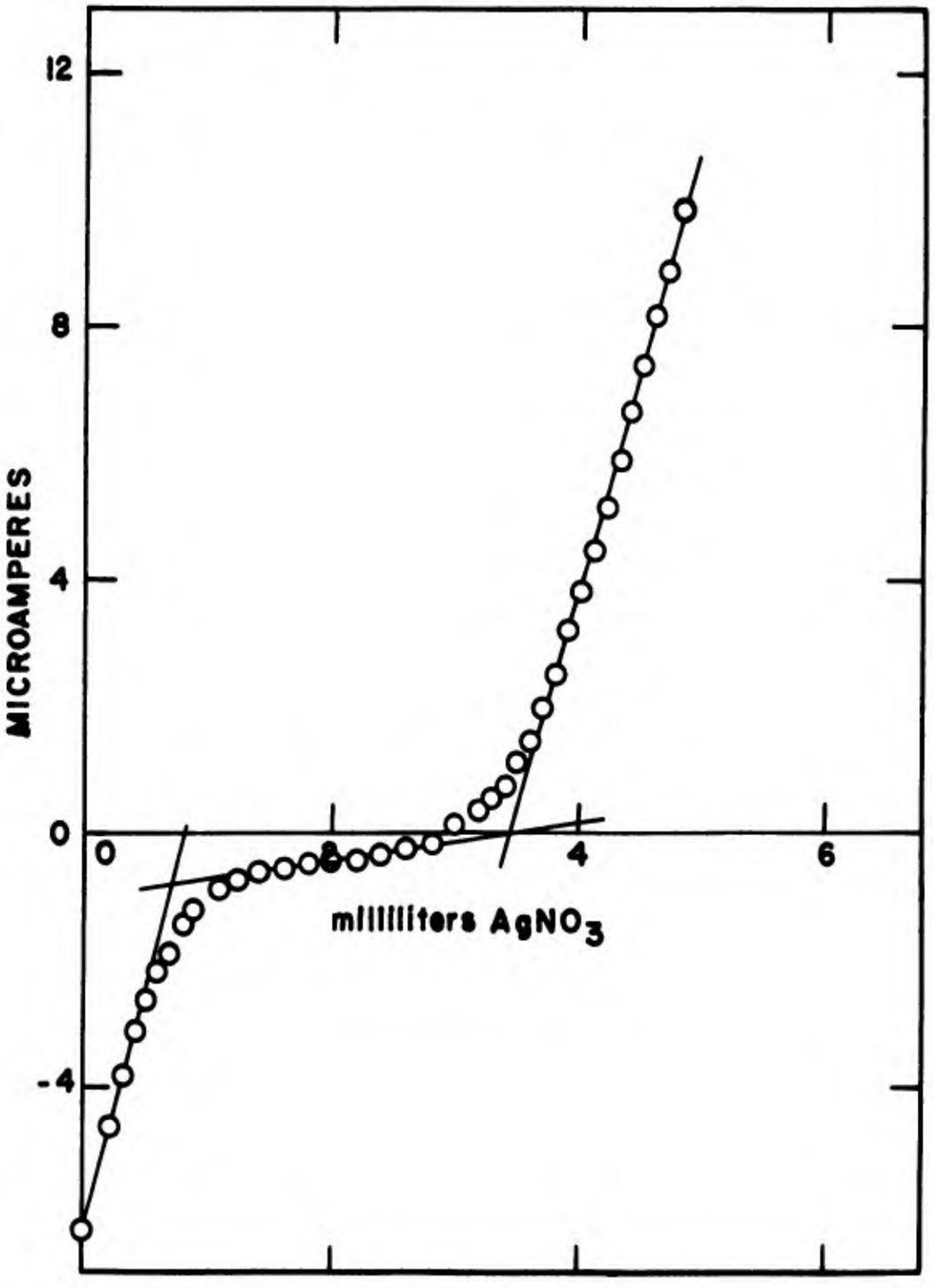

addition of a small amount of titrant. Ideally, this determination should indicate negligible current until the stoichiometric point is reached where a current proportional to excess silver ion concentration should become evident. This current is due to the reduction of silver ion under the applied potential (*ca.* -0.2 volt) at the rotating platinum electrode. The initial negative current might then be considered indicative of the oxidation of some species at the platinum electrode. Several blanks were run with simulated product mixtures which could reasonably be expected to arise from the photolysis of thioctic acid. The results of the direct titration of a sample of synthetic dithiol and then dithiol plus a dilute hydrogen sulfide solution are indicated in Figures 4 and 5. From these results, we conclude that the negative current is due to the presence of a small amount of hydrogen sulfide. If the first "break" is utilized as a crude endpoint, one estimates a hydrogen sulfide content *ca.* 10% of the amount of dithiol indicated.

The difference between the direct and back titration cannot be rationalized at present. We have opted to accept the results of the direct titration. Therefore, all results obtained by the back titration were adjusted by a factor of 1.2 to relate them to those obtained by the direct method. The factor 1.2 represents the average ratio between the direct and indirect titration for fourteen runs.

B. Direct Photolysis

At the outset, the behavior of several disulfides was surveyed to obtain order-of-magnitude quantum yields under various conditions.

FIGURE 4

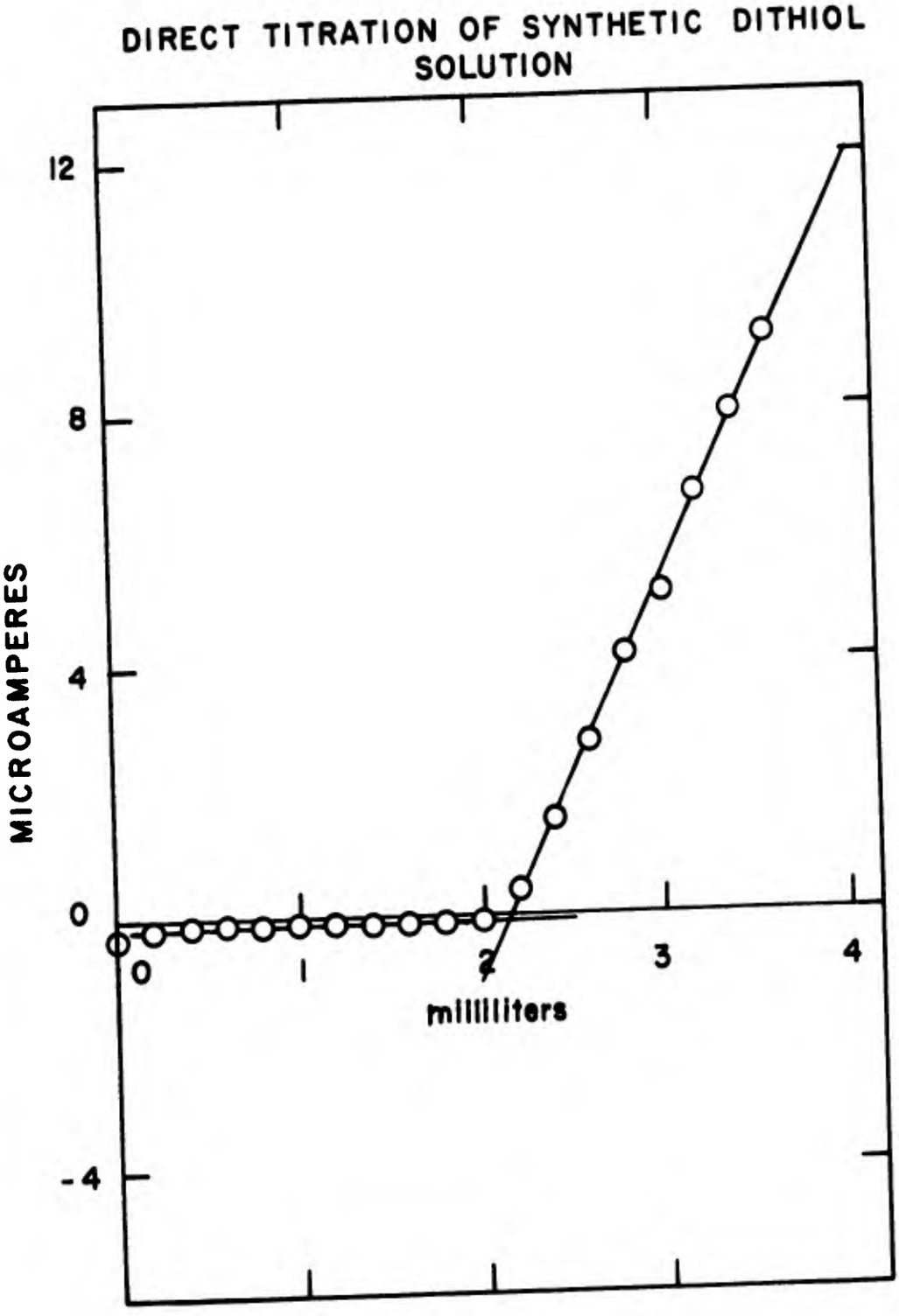
DIRECT TITRATION OF SYNTHETIC DITHIOL SOLUTION
MICROAMPERES
12
8
4
0
-4
0
1
2
3
4
milliliters

FIGURE 5

DIRECT TITRATION OF SYNTHETIC DITHIOL, H_2S MIXTURE

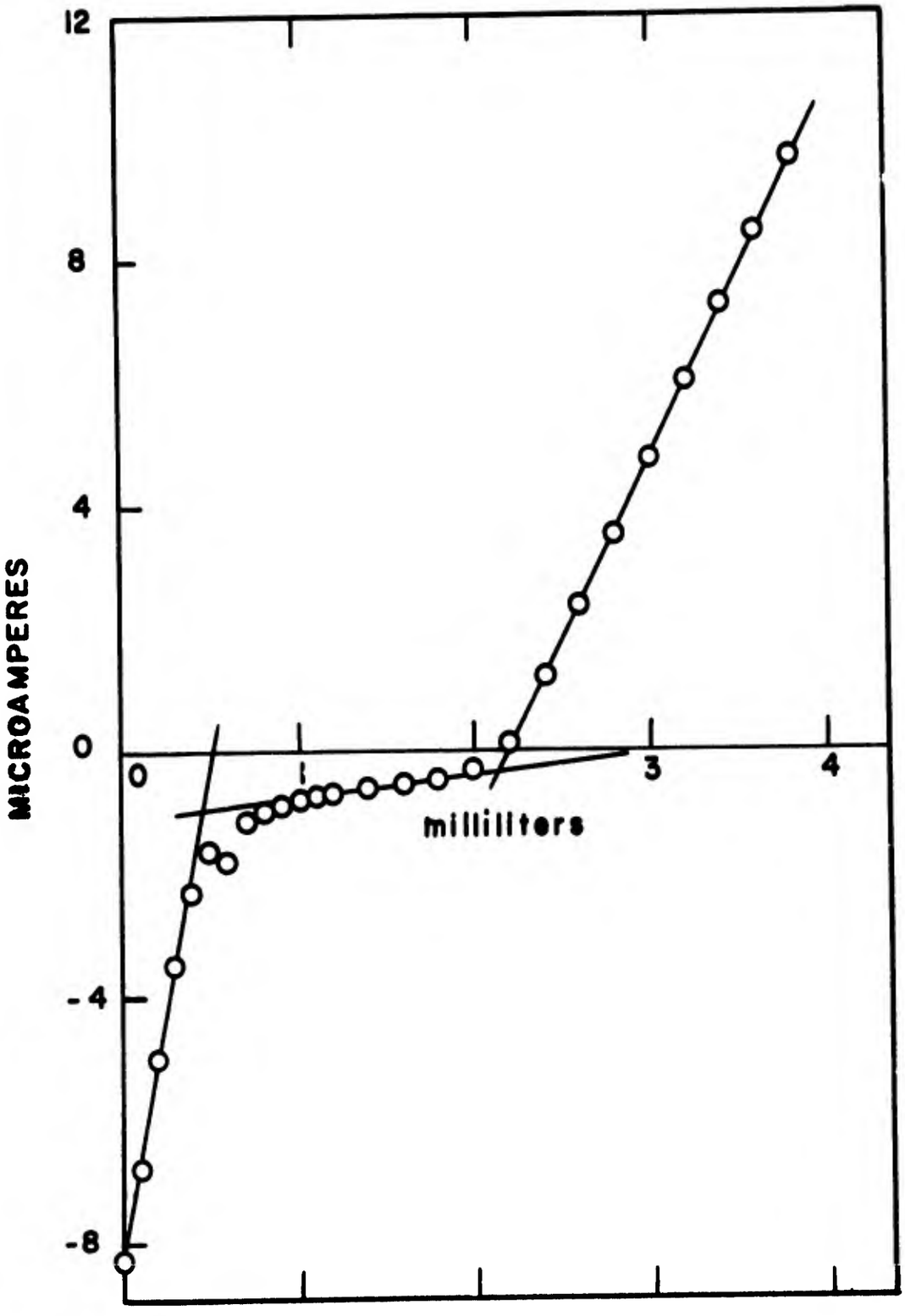

The results of this survey are listed in Table 2. Clearly, thioctic acid is the most reactive disulfide. The n-butyl disulfide-cumene system undergoes complex reactions which generate absorbing products of a deep yellow color. Further, phenyl disulfide in 2-propanol develops scattering and opalescence upon irradiation with 366 mμ light. This behavior suggests the formation of insoluble materials and a complicated reaction path.

Thioctic acid was therefore chosen for detailed study. Its behavior is similar to that of structurally simpler trimethylene disulfide, but it is more stable, and is readily obtained in pure form. In addition, there exists a body of prior information on aspects of its chemical and biochemical behavior and significance[14].

1. Photolysis of Thioctic Acid

Photolyses of thioctic acid were performed at 25°C largely in neat (13.07 M) 2-propanol and in 6.535 M 2-propanol in benzene. A series of photolyses in varying dilutions of 2-propanol in benzene was also run. The general behavior on photolysis is illustrated in Figure 6, which features an isosbestic point at 282 mμ.

Since on prolonged photolysis the 333 mμ absorption band disappears essentially completely, the decrease in the density of this band, particularly at 366 mμ and 405 mμ, may be used as a measure of the disulfide consumption. The thiol produced is then measured by titration (*vide infra*), thus providing a means for establishing the relationship between the disappearance of the disulfide and the appearance of the thiol.

TABLE 2

THE PHOTOLYSIS OF SEVERAL DISULFIDES

Disulfide	Conc. M	Solvent	λ (mμ)	Φ_{RSH}
Mesityl	1.00×10^{-3}	2-propanol	366	≤ 0.05
	1.51×10^{-2}	6.535 M 2-propanol/ benzene	405	≤ 0.02
Phenyl	6.00×10^{-3}	2-propanol	366	≤ 0.08
n-Butyl	3.00×10^{-2}	1.2 M cumene/ benzene	313	0.55 ± 0.03
Thioctic Acid	3.88×10^{-3}	2-propanol	366	0.71

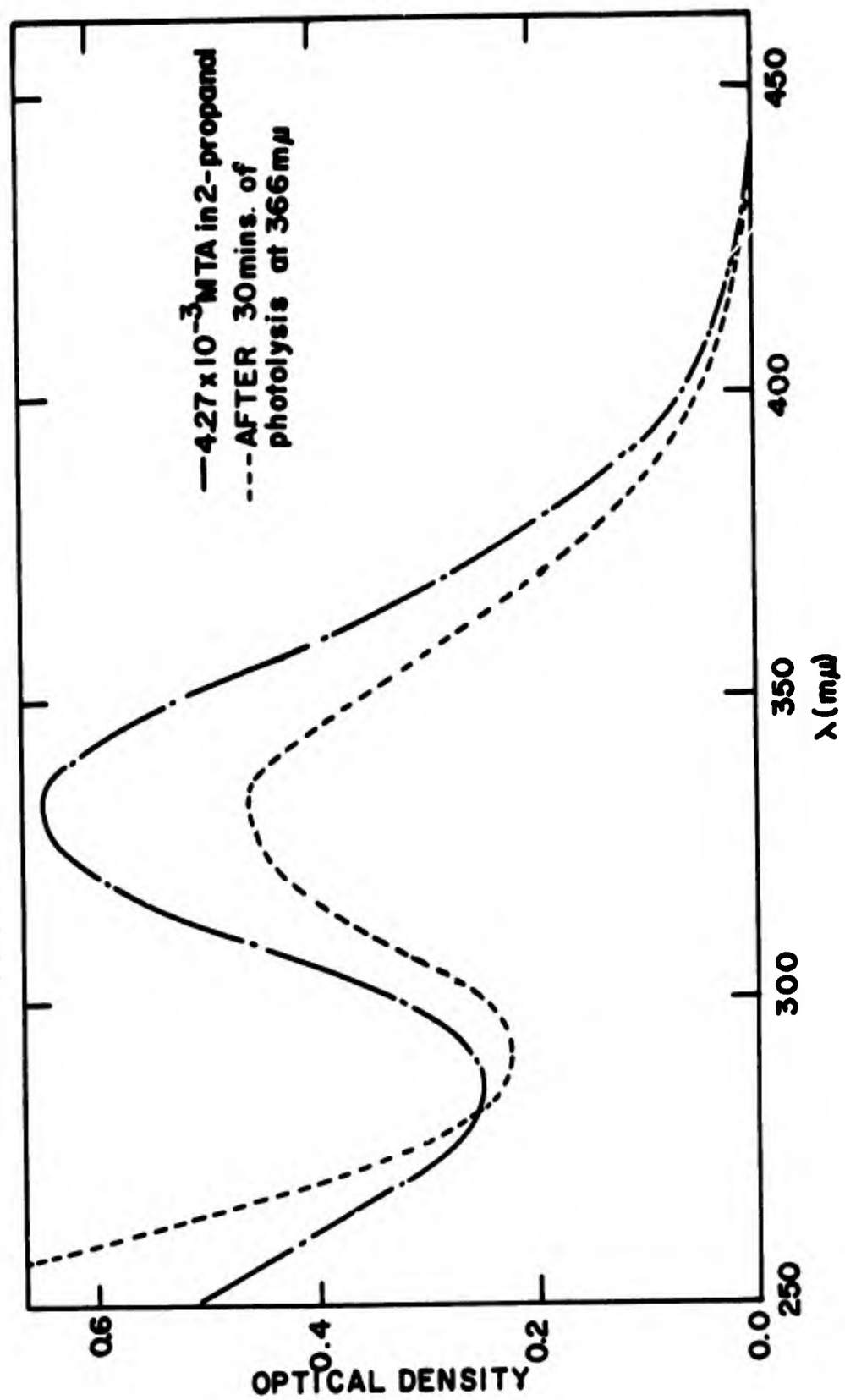

FIGURE 6

PHOTOLYSIS OF THIOCTIC ACID

The kinetic law for the photolysis is:

$$-\frac{d\,RSSR}{dt} = \Phi\, I_{abs.} \qquad \ldots\ldots\ldots (1)$$

for which the relationship

$$\log\,[(1/T_s) - 1] + a \log\,[(1/T_s) + a] = -\frac{(1+a)\,\varepsilon\, A\, I_o\, \Phi\, t}{1-R} \qquad \ldots\ldots\ldots (2)$$

holds (full details including the derivation of this expression are given in Appendix A).

A plot of Equation (2) for a typical photolysis is shown in Figure 7. The quantum yield obtained from the slope ($\Phi_{RSSR} = 0.33$) is in exact agreement with that obtained by integration of I_{abs} *vs* time. This equivalency has been established for a large number of runs. However, since the integration proves less time consuming, the results here and in the remainder of this section were obtained in this manner.

The quantum yield of disappearance of thioctic acid (Φ_{RSSR}) as a function of thioctic acid concentration for irradiation in 13.07 M (neat) 2-propanol and in 6.535 M 2-propanol in benzene at 405 mμ is presented in Table 3. It is clear that, within the sizeable experimental uncertainties, no trend is apparent. We therefore conclude that Φ_{RSSR} is independent of the concentration of thioctic acid.

The scatter in these measurements deserves comment at this point. Initially, we note that the ratio of the yield of titratable

FIGURE 7

PLOT OF EQUATION (2) FOR THE PHOTOLYSIS OF THIOCTIC ACID[a]

(a) 4.27×10^{-3} M/2-propanol at 366 mμ

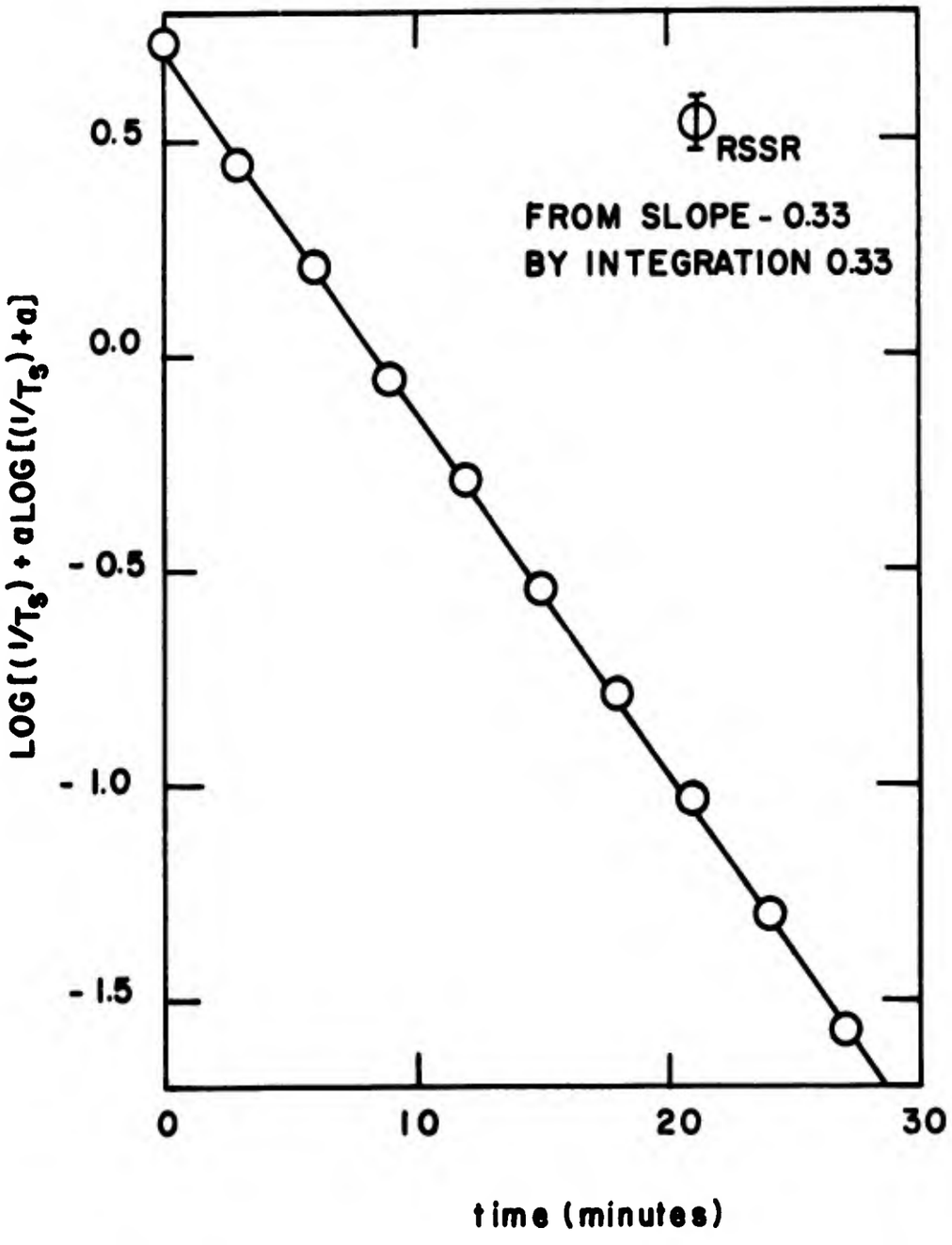

TABLE 3

QUANTUM YIELDS AS A FUNCTION OF THIOCTIC ACID CONCENTRATION

Intensity Quanta/Sec x 10^{15}	Thioctic Acid M	Φ_{RSSR}	Φ_{RSH}	RSH / RSSR	# Runs
	λ = 366 mμ		2-Propanol 13.07 M		
7.0 (0.1)[a]	1.01×10^{-1}		0.65 (0.04)		4
6.8 (0.1)	2.03×10^{-2}		0.61 (0.04)		4
7.9 (0.4)	4.0×10^{-3}	0.34 (0.02)	0.71 (0.04)	2.12 (0.19)	27
13.2 (0.6)	1.3×10^{-3}	0.32 (0.02)	0.69 (0.04)	2.11 (0.03)	2
14.0 (0.4)	4.8×10^{-3}	0.33 (0.03)	0.69 (0.03)	2.10 (0.16)	4
13.7	2.4×10^{-3}	0.40	0.74	1.90	1
	λ = 405 mμ		2-Propanol 6.545 M[b]		
12.7 (0.2)	1.01×10^{-1}		0.27 (0.01)		2
12.5 (0.2)	2.00×10^{-2}		0.26 (0.01)		5

a. numbers in () indicate average deviation from mean

b. diluant is benzene

thiol to that of disulfide disappearance is, in all but one case, greater than two. This condition could only arise as the result of the generation of a species able to remove more silver ion from solution than a thiol is capable of removing. Our prior observations on the amperometric titration for thiols led us to conclude that hydrogen sulfide is present in the products of photolysis. Blank experiments with hydrogen sulfide dilutions indicate the use of the first "break" in the titration curve to be an unreliable endpoint. As a consequence, the indication of a hydrogen sulfide level of *ca.* 10% thiol content must be regarded only as an estimate. Attempts at identification and detection of H_2S in photolyzed samples *via* gas liquid chromatography were thwarted by the relatively low sensitivity of the thermal conductivity detector. Lead acetate test paper did prove sufficiently sensitive to demonstrate the presence of hydrogen sulfide by blackening in the vapor over the photolyzed solution and on contact with the solution. The concentrations of H_2S solution which simulated the titration behavior of a photolyzed solution demonstrated essentially identical behavior with the lead acetate paper. Finally, no effect was observed upon contact with either the synthetic dithiol solution or its vapor.

2. Products of the Photolysis of Thioctic Acid

The results obtained from the photolysis of a 0.100 M thioctic acid sample in 6.535 M 2-propanol in benzene appear in Table 4. These data indicate the production of pinacol as the primary oxidation product of 2-propanol in a ratio of *ca.* one mole for every two moles of titratable thiol groups detected.

TABLE 4

PRODUCTS OF PHOTOLYSIS OF THIOCTIC ACID

0.100 M thioctic acid 6.54 M 2-propanol/benzene
photolyzed for 30 mins. at 405 mμ.

RSH, M	Pinacol, M	Acetone, M
$(3.55 \pm 0.36) \times 10^{-3}$	$(1.73 \pm 0.15) \times 10^{-3}$	$(0.0 \pm 0.2) \times 10^{-4}$

Results obtained from oxidative regeneration of photolyzed thioctic acid samples are indicated in Table 5. This information confirms that *ca.* 20% of the disulfide is consumed in side reactions not leading to dithiol formation. These results do, however, also confirm that the dithiol is the main product of photolysis.

3. Φ_{RSH} as a Function of Intensity

The results of photolyses carried out at different intensities of radiation are presented in Table 6. It can readily be seen that, over the intensity range employed, Φ_{RSH} and Φ_{RSSR} are independent of intensity.

4. Φ_{RSH} as a Function of 2-Propanol Concentration

A summary of the results of experiments performed at different concentrations of 2-propanol in benzene is shown in Table 7. A plot of $1/\Phi_{RSH}$ *versus* the reciprocal of the 2-propanol concentration, as shown in Figure 8, is linear over the range *ca.* 2 to 13 M 2-propanol. At lower concentrations a change in the slope suggests a change in behavior of the system. The results of further experiments performed at still lower concentrations and at zero concentration of 2-propanol are summarized in Table 8. Points of significance are the decrease in Φ_{RSH}/Φ_{RSSR} and the fact that photolysis still gives rise to a measurable, albeit reduced, Φ_{RSH} in benzene alone. Both spectrophotometry and visual observation indicated the development of a scattering phenomenon in the samples photolyzed in benzene. Upon opening the samples, a small amount of an insoluble colorless deposit could be rinsed from the walls of the irradiation cell. There also appears to be a slight trend in Φ_{RSH} with the concentration

FIGURE 8

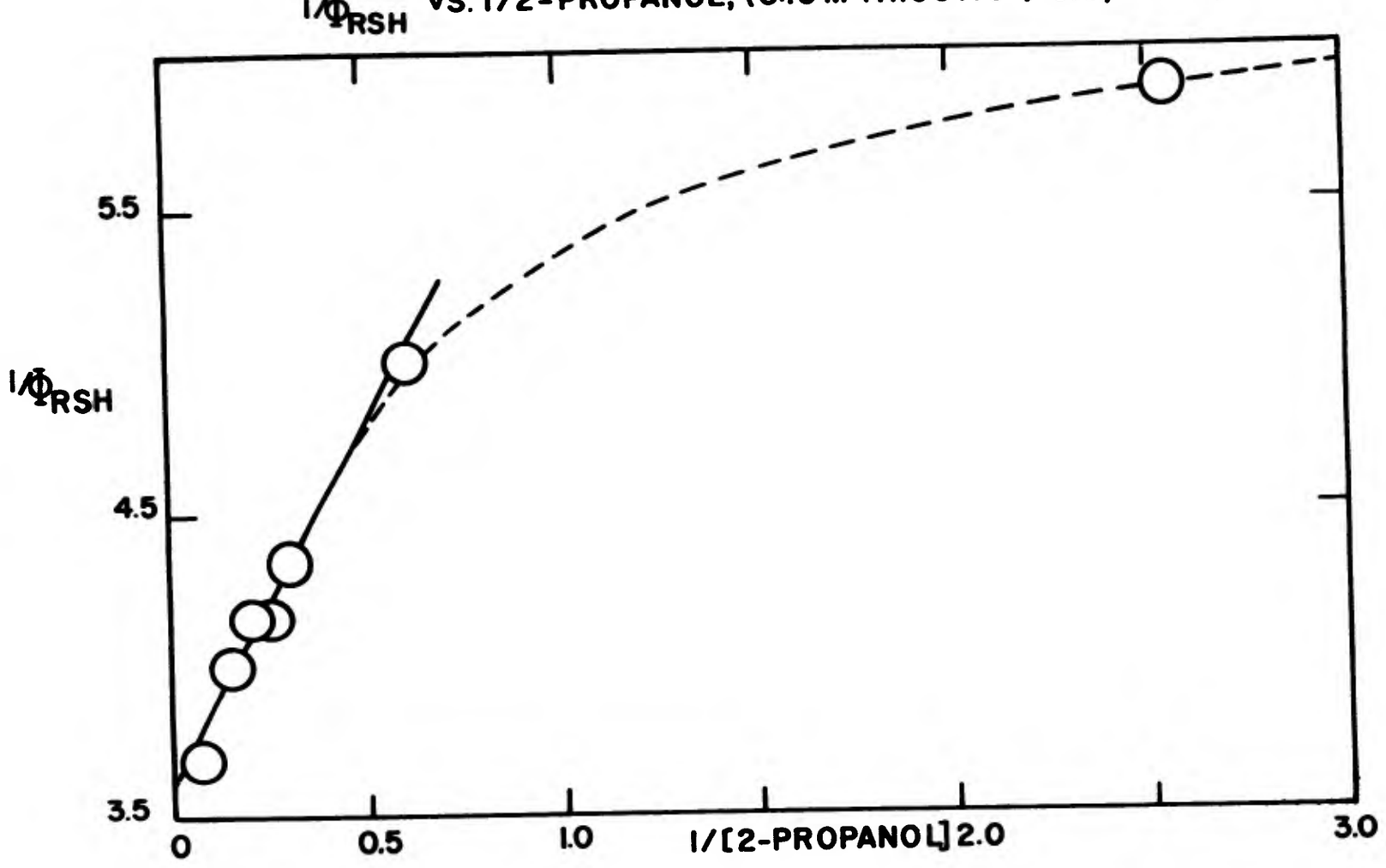
1/Φ RSH VS. 1/2-PROPANOL, (0.10 M THIOCTIC ACID, 405 mμ)
1/Φ RSH
5.5
4.5
3.5
0
0.5
1.0
1/[2-PROPANOL]
2.0
3.0

TABLE 5

OXIDATIVE REGENERATION OF THIOCTIC ACID

Solvent	Thioctic Acid M	Decrease in A_{333} on photolysis	Increase in A_{333} on Oxidation	% Regeneration
2-propanol	8.0×10^{-3}	0.460	0.330	72
6.54 M 2-propanol/ benzene	8.0×10^{-3}	0.404	0.362	90

TABLE 6

QUANTUM YIELDS AS A FUNCTION OF INTENSITY

2-Propanol M	Intensity Quanta/Sec x 10^{15}	Φ_{RSSR}	Φ_{RSH}	$\frac{RSH}{RSSR}$	# Runs
13.07[a]	13.7 (0.6)	0.35 (0.04)	0.71 (0.03)	2.04 (0.17)	10
13.07[a]	7.9 (0.4)	0.34 (0.02)	0.71 (0.04)	2.12 (0.19)	27
6.54[a]	6.5 (0.1)	0.29 (0.01)	0.60 (0.01)	2.08 (0.02)	2
6.54[a]	18.6 (0.1)	0.28 (0.01)	0.67 (0.03)	2.40 (0.05)	4
6.54[b]	3.5 (0.3)	0.25 (0.04)			7
6.54[b]	4.9 (0.3)	0.25 (0.01)			18
6.54[b]	12.7 (0.2)	0.27 (0.01)			2

a. λ:366 mμ thioctic acid: 3.88 - 4.85 x 10^{-3} M

b. λ:405 mμ thioctic acid: 0.10 M

TABLE 7

QUANTUM YIELDS AS A FUNCTION OF 2-PROPANOL CONCENTRATION

λ, mμ	2-Propanol M	Φ_{RSSR}	Φ_{RSH}	$\frac{RSH}{RSSR}$	# Runs
366	13.07	0.34 (0.03)	0.70 (0.05)	2.09 (0.19)	40
	6.54	0.28 (0.04)	0.65 (0.03)	2.30 (0.18)	6
405	13.07		0.27 (0.02)		6
	6.54		0.25 (0.02)		32
	4.90		0.24 (0.02)		7
	4.08		0.24 (0.02)		2
	3.27		0.23 (0.01)		2
	1.63		0.20 (0.01)		3
	0.39		0.17 (0.01)		3

TABLE 8

QUANTUM YIELDS AT LOW 2-PROPANOL CONCENTRATION

λ: 366 mμ

2-Propanol M	Thioctic Acid M	μ Einsteins absorbed	Φ_{RSSR}	Φ_{RSH}	RSH / RSSR	# Runs
9.8×10^{-3}	4.0×10^{-3}	21.2	0.26	0.27	1.04	1
9.8×10^{-3}	4.0×10^{-3}	28.7	0.22	0.35	1.56	1
0	1.0×10^{-1}	27.5		0.35 (0.01)		2
0	2.0×10^{-2}	22.3		0.31 (0.01)		2
0	5.0×10^{-3}	27.8	0.21	0.30 (0.01)	1.42 (0.01)	2

λ: 405 mμ

0	1.0×10^{-1}	40.1		0.13 (0.01)		5

of thioctic acid for photolysis in pure benzene solution, although this cannot be considered certain.

5. Φ_{RSH} as a Function of λ

The data presented in Table 9 indicate that the quantum efficiency of the photolysis of thioctic acid increases with decreasing wavelength of excitation. A probable explanation suggests that reaction proceeds from a very short-lived, vibrationally excited state of the electronically excited molecule. One must assume that only one electronic transition is involved at all of these wavelengths.

C. Sensitized Photolysis

Since, in most cases, both the sersitizer candidate (SC) and thioctic acid (TA) contribute to the total absorption at the wavelength of irradiation, it becomes necessary to measure the fraction of this total absorption due to thioctic acid. It is convenient to define the term F as the fraction of absorbed light attributable to thioctic acid.

$$F = \frac{D^{TA}}{D^{TOTAL}} = \frac{D^{TA}}{D^{SC} + D^{TA}} \qquad \ldots\ldots\ldots (3)$$

Calculation of F by means of (3) may be accomplished by the substitution of i) directly measured densities, ii) densities measured for known dilutions of the sample, iii) densities calculated from the measured concentration and the extinction coefficients, or iv) densities from a calibration curve (Beer's Law plot).

The first method, (i), is the most desirable and involves only the approximation that ground state interactions between the two components do not appreciably alter the apparent total density. The second and

TABLE 9

WAVELENGTH DEPENDENCE OF QUANTUM YIELD IN 2-PROPANOL

λ (mμ)	Φ_{RSSR}	Φ_{RSH}	$\frac{RSH}{RSSR}$	# Runs
313	0.45 (0.01)	1.03 (0.04)	2.28 (0.02)	2
333[a]	0.45 (0.04)	0.86 (0.03)	1.91 (0.12)	2
366	0.34 (0.03)	0.70 (0.05)	2.09 (0.18)	40
405		0.27 (0.02)		6

a. 6.54 M 2-propanol in benzene

third methods, (ii, iii), must assume the validity of Beer's Law. If Beer's Law is not obeyed, correction can be made by constructing a density *vs.* concentration curve (method iv) from which densities may be obtained for any concentration (*vide infra*).

1. Screening Experiments

In this context, the screening experiments fall into two general categories; those experiments in which $D^{SC} >> D^{TA}$, and those experiments in which $D^{SC} \sim D^{TA}$.

In the former case, the total densities are all directly measurable on the irradiation apparatus. F was therefore calculated from the available densities and the Beer's Law plot data for thioctic acid at 405 mμ and 366 mμ. Calculations for the single experiment at 313 mμ and the five at 435 mμ were made using $\epsilon_{313} = 120$ and $\epsilon_{435} = 2.9$, values which were obtained by the measurement with the DK-1 Spectrophotometer. A further consideration arises in the case of measurable changes in density of the reaction mixture during the irradiation. In this case the change in density is attributed to the photolysis of thioctic acid on the basis of the assumed or demonstrated photostability of the sensitizer candidate and the average value of F throughout the run is computed and employed.

Calculation of F in the case of $D^{SC} >> D^{TA}$, in which experiments the total density is far greater than unity, forces the assumption of Beer's Law or the construction of a suitable calibration curve. In the initial screening experiments Beer's Law was assumed to hold. Calculation of F then proceeded from the calibration curves

for thioctic acid and measurements of known dilutions of sample and sensitizer stock solutions. Since, in these experiments, the largest part of the incident light is always absorbed by the sensitizer, ($D^{SC} \gtrsim 15$-60, $D^{TA} \approx 1.5$) and in view of the approximations involved, only a large enhancement (*ca.* 4-fold) of Φ_{RSH}/F over Φ_{RSH} for the corresponding direct photolysis could be considered a meaningful indication of activity.

The results of these experiments are presented in Tables 10 and 11. The five experiments performed at 435 mμ do not strictly fall into the category $D^{SC} \gtrsim D^{TA}$ as $D^{TA} \lesssim 0.029$. However, these systems absorbed no less than 27 μ Einsteins of energy and within the limits of analysis (*ca.* ± 1 μ mole of thiol) demonstrated no activity. Activity is indicated on the part of Rhodamine B, Rose Bengal, and fluorenone in the low density experiments, and for 1,2:3,4-dibenzopyrene and 3,4-benzopyrene in the high density set. Fluorenone did not appear active in the high density experiments. The solution spectrum of Rose Bengal underwent radical alteration upon the addition of a thioctic acid solution, thus rendering that result ambiguous.

It should be noted that the concentrations of sensitizers indicated for these screening experiments are approximate to the extent that they have been computed from literature extinction coefficients (when available) or measured extinction coefficients and optical density data (DK-1 Spectrophotometer).

A large number of sensitizer candidates and the lengthy nature of the experimentation made this approximate screening approach advisable.

TABLE 10

SCREENING EXPERIMENTS IN 2-PROPANOL, $D^{SC} \sim D^{TA}$

Sensitizer Candidate	Conc. M	Thioctic Acid Conc. M	λ (mμ)	Φ_{RSH}	F	$\Phi_{RSH/F}$
Fluoranthene	1.4×10^{-4}	4.80×10^{-3}	366	0.15	0.38	0.40
			366	0.70	1.00	0.70[a]
Fluorenone	3.99×10^{-3}	1.05×10^{-2}	405	0.29	0.20	1.50
Rose Bengal		6.00×10^{-3}	405	0.52	0.17	2.17
Rhodamine B	6.2×10^{-5}	9.49×10^{-3}	405	0.37	0.17	1.97
Perylene	2.3×10^{-5}	9.60×10^{-3}	405	0.07	0.24	0.28
			405	0.27 (0.01)	1.00	0.27 (0.01)[a]
Azulene	2.3×10^{-3}	4.80×10^{-3}	546	0.0	0	

a. blank corresponds to preceding experiments

TABLE 10 (continued)

SCREENING EXPERIMENTS IN 2-PROPANOL, $D^{SC} \sim D^{TA}$

Sensitizer Candidate	Conc. M	Thioctic Acid Conc. M	λ (mμ)	Φ_{RSH}	F	$\Phi_{RSH/F}$
Anthracene	1.4×10^{-4}	4.69×10^{-3}	366	0.41	0.47	0.86
AAQX[a]	1.9×10^{-5}	4.80×10^{-3}	366	0.41	0.49	0.83
3,4-Benzo-pyrene	2.5×10^{-5}	4.80×10^{-3}	366	0.31	0.48	0.64
1,2:3,4-Di-benzopyrene	6.7×10^{-5}	4.80×10^{-3}	366	0.32	0.37	0.86
	3.7×10^{-5}	4.14×10^{-3}	366	0.39 (0.03)	0.50 (0.05)	0.78 (0.07)[b]
	1.7×10^{-5}	4.14×10^{-3}	366	0.28	0.69	0.41
1,2:4,5-Di-benzopyrene	$2.7 - 4.7 \times 10^{-5}$	$3.8 - 4.8 \times 10^{-3}$	366	0.39 (0.04)	0.44 (0.04)	0.85 (0.06)[b]

a. 2,3-(1-acianthrylene)-quinoxaline

b. average of 3 runs

TABLE 10 (continued)

SCREENING EXPERIMENTS IN 2-PROPANOL, $D^{SC} \sim D^{TA}$

Sensitizer Candidate	Conc. M	Thioctic Acid Conc. M	λ (mμ)	Φ_{RSH}	F	$\Phi_{RSH/F}$
Triphenylene	3.1×10^{-4}	4.14×10^{-3}	313	0.78	0.64	1.22
		4.14×10^{-3}	313	1.03 (0.04)	1.00	1.03 (0.04)[a,b]
1,5-Dihydroxy-anthraquinone	8.9×10^{-5}	4.80×10^{-3}	435	0.0	0.04	0.0
Benzanthrone	3.6×10^{-3}	9.60×10^{-3}	435	0.0	0.04	0.0
1,2:3,4-Di-benzopyrene	1.2×10^{-4}	9.60×10^{-3}	435	0.0	0.04	0.0
Perylene	6.0×10^{-5}	9.60×10^{-3}	435	0.0	0.03	0.0
AAQX	9.2×10^{-5}	9.60×10^{-3}	435	0.0	0.03	0.0
		9.60×10^{-3}	435	0.0	1.00	0.0[a]

a. blank corresponds to preceding experiments

b. average of two experiments

TABLE 11

SCREENING EXPERIMENTS IN 6.54 M 2-PROPANOL/BENZENE, $D^{SC}>>D^{TA}$ [a]

Sensitizer Candidate	Conc. M	Φ_{RSH}	F	Φ_{RSH}/F
Fluorenone	0.500	0.027	0.03	0.75
	0.500	0.034	0.03	0.94
Perylene	1.0×10^{-3}	0.074	0.05	1.2
	1.0×10^{-3}	0.067	0.05	1.1
3,4-benzopyrene	2.13×10^{-2}	0.160	0.04	3.3
	2.13×10^{-2}	0.182	0.04	3.7

a. 0.0999 M Thioctic Acid, 405 mμ

TABLE 11 (continued)

SCREENING EXPERIMENTS IN 6.54 M 2-PROPANOL/BENZENE, $D^{SC}>>D^{TA}$[a]

Sensitizer Candidate	Conc. M	Φ_{RSH}	F	Φ_{RSH}/F
1,2:3,4-Dibenzo-pyrene	2.2×10^{-3}	0.371	0.05	6.2
	2.2×10^{-3}	0.315	0.05	5.3
		0.27	1.00	0.27[b]

a. 0.0999 M Thioctic Acid, 405 mμ

b. blanks corresponding to the preceding experiments

The selection of 3,4-benzopyrene, (3,4-BP) Figure 9, for further study was based on several factors. The compound is free of complicated, labile functional groups and has been shown to be photo-stable on irradiation in degassed solution. There is evidence of its stability in the presence of sulphenyl radicals.[29] The absence of ground state interaction is confirmed by the additivity of the spectra of 3,4-benzopyrene and thioctic acid. Furthermore, 3,4-benzopyrene is noticeably more soluble in 6.54 M 2-propanol/benzene than either of the dibenzopyrenes. The repetitions of experiments involving the dibenzopyrenes were prompted by the problem of precipitation during the "wall rinsing" procedure and subsequent difficulties in redissolving the material. This solubility of 3,4-benzopyrene coupled with its moderate to high extinction in the region 300 mμ to 405 mμ affords considerable latitude in the selection of experimental conditions. By no means the least significant factor was the availability of useful literature concerning 3,4-benzopyrene. In addition to extensive documentation of its carcinogenic nature there is a considerable body of useful spectroscopic data.[30]

2. 3,4-Benzopyrene, (3,4-BP) as a Sensitizer Candidate at 405 mμ

The absorption and the emission spectra of 3,4-benzopyrene (9.51×10^{-6} M in 6.54 M 2-propanol/benzene) are shown in Figure 10. The results of Beer's Law measurements are presented (cf. Experimental Section) in Table 21 and the corresponding Figure 25.

The large discrepancy between measurements made for 3,4-benzopyrene on the DK-1 spectrophotometer and the irradiation apparatus

FIGURE 9

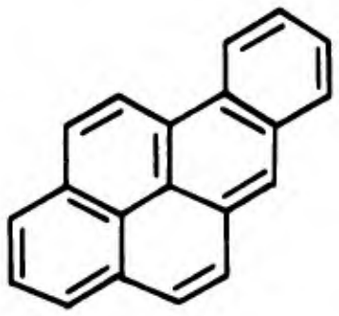

3,4-BENZOPYRENE[a]

III

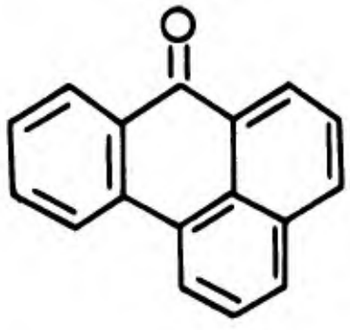

BENZANTHRONE[b]

IV

(a) benz.[α]-pyrene. (b)7-H-benz[d,e]anthracen-7-one

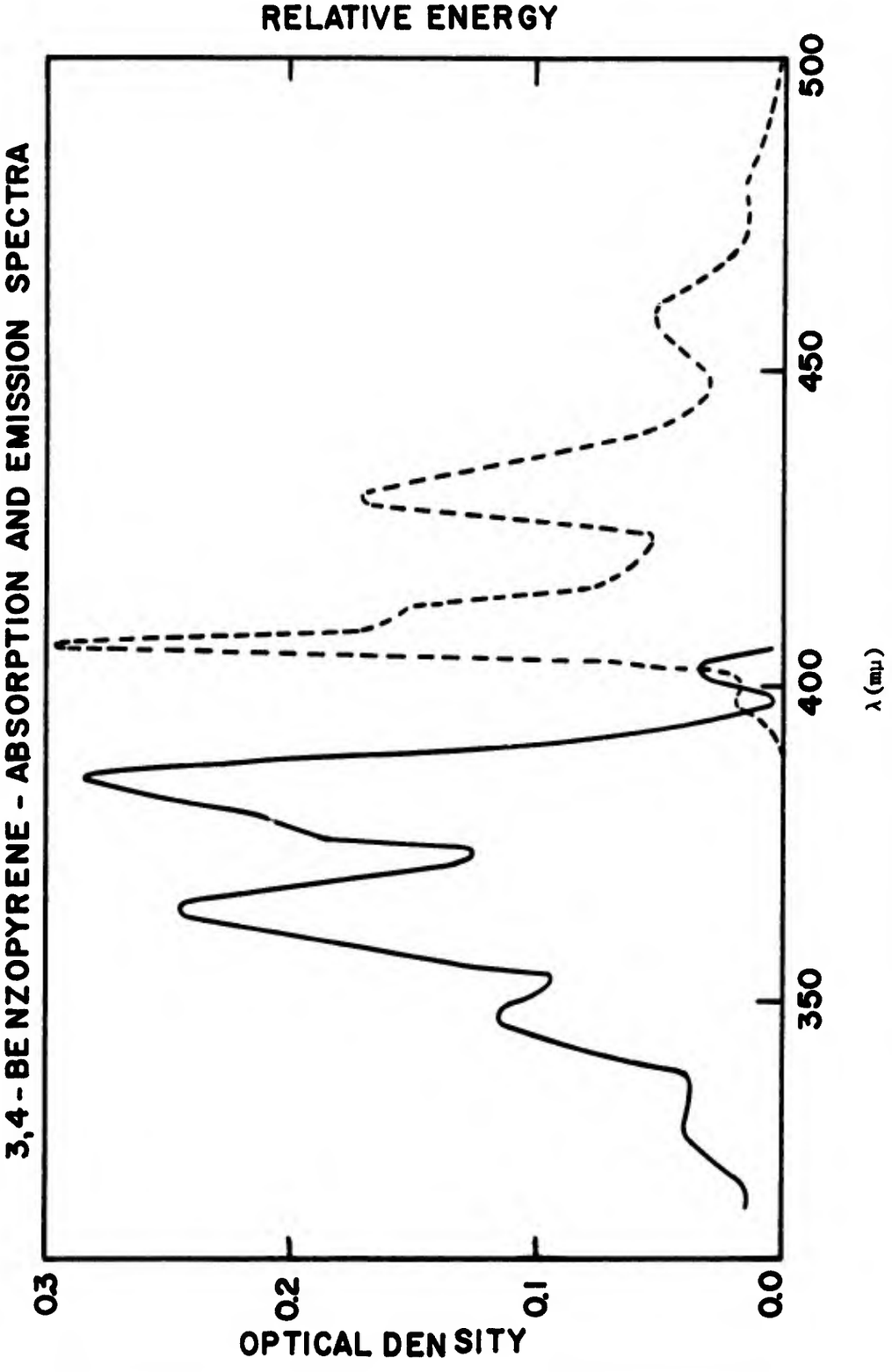
RELATIVE ENERGY
3,4-BENZOPYRENE - ABSORPTION AND EMISSION SPECTRA
OPTICAL DENSITY
0.3
0.2
0.1
0.0
350
400
450
500
λ (mμ)

FIGURE 10

are to be expected. In the case of a significant variation of ε over the bandpass of the instrument employed, the definition of F necessarily becomes[31]

$$F = \frac{\log I_o - \log \int_{\nu_1}^{\nu_2} I_\nu \, d\nu}{n_i \log I_o - \log \sum_i \log \int_{\nu_1}^{\nu_2} I_\nu^i \, d\nu}$$

Calculations of F were therefore made by determining the contribution of 3,4-benzopyrene to the absorption directly from the Beer's Law calibration plot made on the irradiation apparatus (cf. Experimental Section), Figure 25, with a correction for cell thickness.

3. Benzanthrone as a Non-Sensitizer at 405 mμ

In order to demonstrate the behavior of a non-sensitizer, benzanthrone, Figure 9 , was selected from among the inactive candidates. The absorption spectrum of benzanthrone appears in Figure 11. A plot of its Beer's Law behavior is presented in Figure 32 (cf. Experimental Section). Prior information shows this compound to be a photo-stable material of good solubility in 6.54 M 2-propanol/benzene.[32]

A series of measurements of Φ_{RSH} as a function of F were made at constant thioctic acid concentration (cf. Table 12). The behavior demonstrated, Figure 12, is in good agreement with that which would result if the only effect were attenuation of the absorbed light, i.e. an "inner filter" effect.

FIGURE II

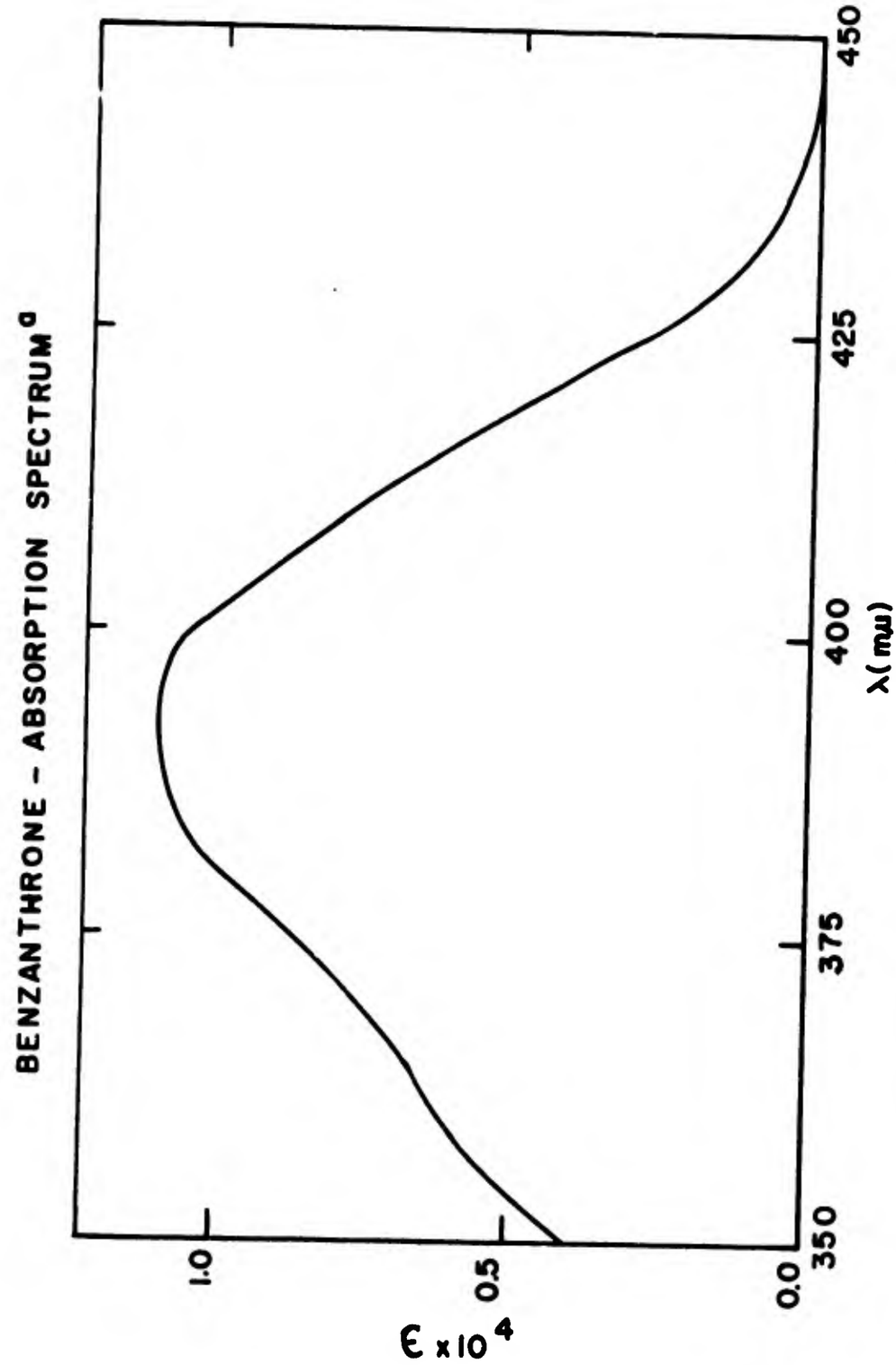
BENZANTHRONE - ABSORPTION SPECTRUM[a]
1.0
0.5
0.0
ε x 10^4
350
375
400
425
450
λ (mμ)

TABLE 12

BENZANTHRONE, Φ_{RSH} AS A FUNCTION OF F

0.100 M thioctic acid in 6.54 M 2-propanol/benzene

λ: 405 mμ

Benzanthrone Conc. M	F	Φ_{RSH}
5.53×10^{-3}	0.032	0.019 (0.002)
1.65×10^{-3}	0.098	0.042 (0.001)
4.98×10^{-4}	0.27	0.082 (0.011)
1.66×10^{-4}	0.52	0.151 (0.007)
4.98×10^{-5}	0.79	0.214 (0.009)
0	1.00	0.25 (0.02)

FIGURE 12

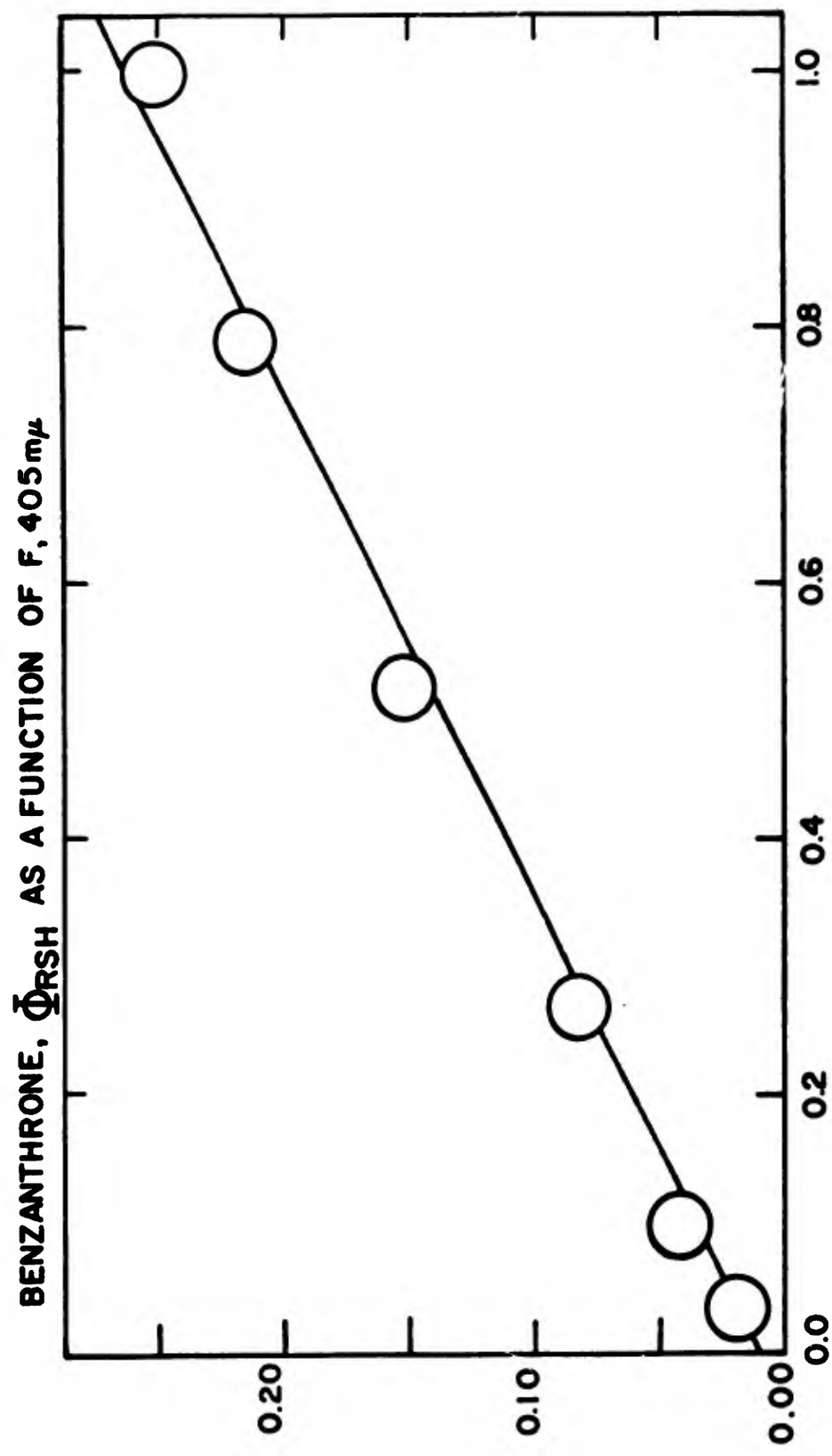
BENZANTHRONE, Φ_{RSH} AS A FUNCTION OF F, 405mμ
0.20
0.10
0.00
0.0
0.2
0.4
0.6
0.8
1.0

4. Φ_{RSH} as a Function of F for 3,4-Benzopyrene at 405 mμ

Table 13 and Figure 13 display the results of a series of experiments with 3,4-benzopyrene in which F is varied at constant thioctic acid concentration.

The plot indicates very slow initial decrease of Φ_{RSH} with decreasing F above the value F$\sim$0.5, after which the quantum yield drops off more and more rapidly toward zero. Sensitization of the reaction is clearly evident but seems to be complicated by inefficiencies at increasing sensitizer concentration.

5. Φ_{RSH} as a Function of Thioctic Acid Concentration at Constant F

In this series of experiments the concentration ratio of sensitizer candidate to thioctic acid was maintained constant through a series of dilutions. The results are presented in TAble 14. A slight dependence of Φ_{RSH} on thioctic acid concentration is indicated, Figure 14, from the highest concentrations down to *ca.* 20×10^{-3} M, followed by a rapid decline with further decrease in concentration. The concentration dependency exhibited here is clearly not a simple one.

6. Φ_{RSH} as a Function of F at 366 mμ

The results of few irradiation experiments performed at three values of F are indicated in Table 15. The behavior, Figure 15, appears to be similar to that observed at 405 mμ this conclusion can only be regarded as tentative.

TABLE 13

3,4-BENZOPYRENE, Φ_{RSH} AS A FUNCTION OF F

0.100 M thioctic acid in 6.54 M 2-propanol/benzene

λ: 405 mμ

3,4-Benzopyrene Conc. M	F	Φ_{RSH}
3.99×10^{-2}	0,024	0.11 (0.01)
2.30×10^{-2}	0.034	0.13 (0.01)
1.91×10^{-2}	0.038	0.13 (0.01)
1.08×10^{-2}	0.063	0.18 (0.01)
$6.11 \times 10^{-}$	0.10	0.19 (0.01)
4.58×10^{-3}	0.13	0.18 (0.01)
2.29×10^{-3}	0.23	0.20 (0.01)
1.15×10^{-3}	0.36	0.20 (0.01)
7.56×10^{-4}	0.43	0.24 (0.01)
5.73×10^{-4}	0.50	0.25 (0.01)
1.43×10^{-4}	0.76	0.27 (0.01)
0	1.00	0.25 (0.02)

FIGURE 13

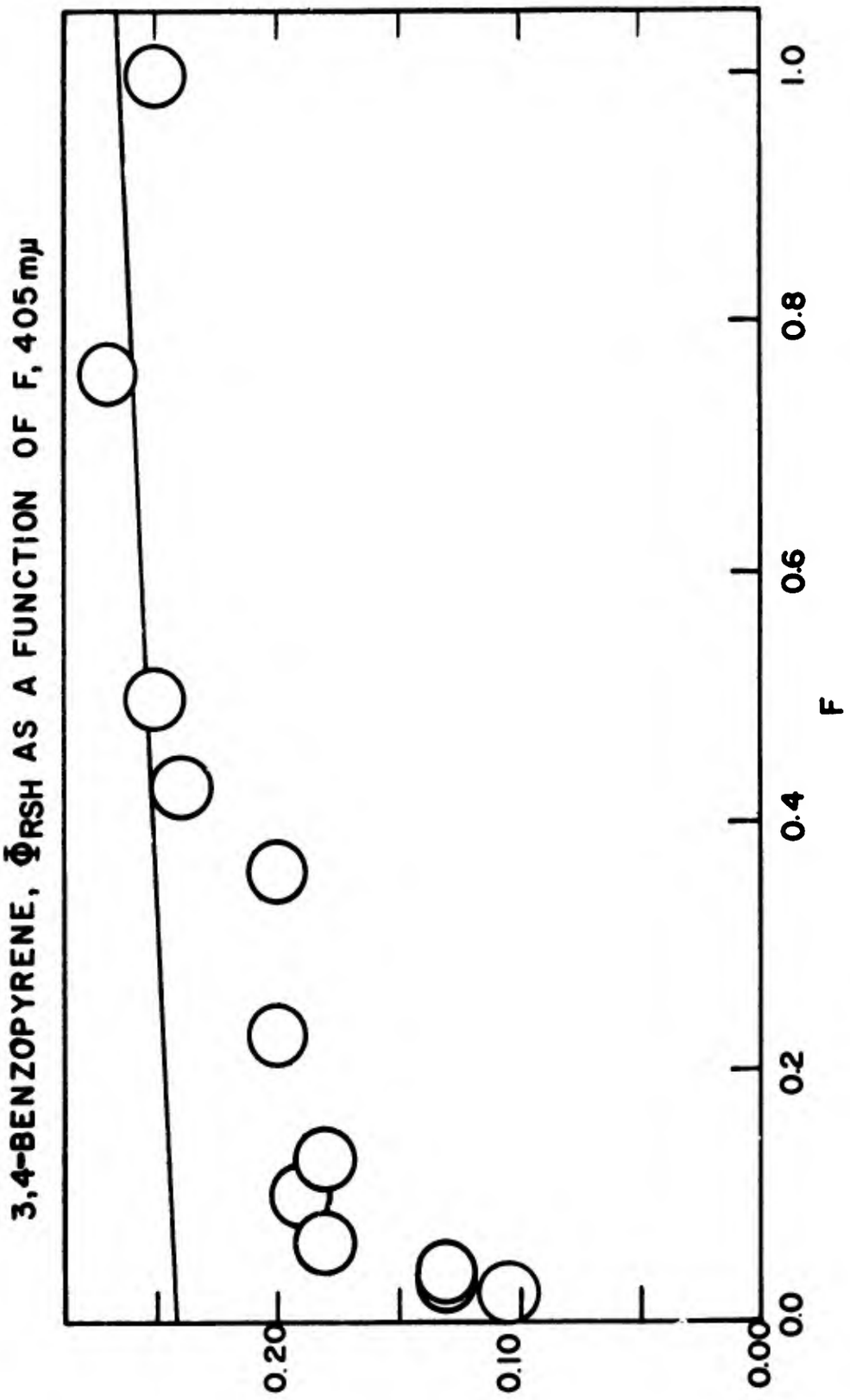
3,4-BENZOPYRENE, ΦRSH AS A FUNCTION OF F, 405mμ
0.20
0.10
0.00
0.0
0.2
0.4
0.6
0.8
1.0
F

TABLE 14

3,4-BENZOPYRENE - 405 mμ

Φ_{RSH} AS A FUNCTION OF THIOCTIC ACID CONCENTRATION

F = 0.028 (0.003)

Thioctic Acid Conc. M[a]	Φ_{RSH}
2.74×10^{-3}	0.058 (0.01)
9.13×10^{-3}	0.096 (0.01)
1.05×10^{-2}	0.107 (0.01)
2.63×10^{-2}	0.116 (0.01)
3.04×10^{-2}	0.110 (0.01)
5.25×10^{-2}	0.122 (0.01)
1.01×10^{-1}	0.112 (0.01)

a. 6.54 M 2-propanol/benzene

FIGURE 14

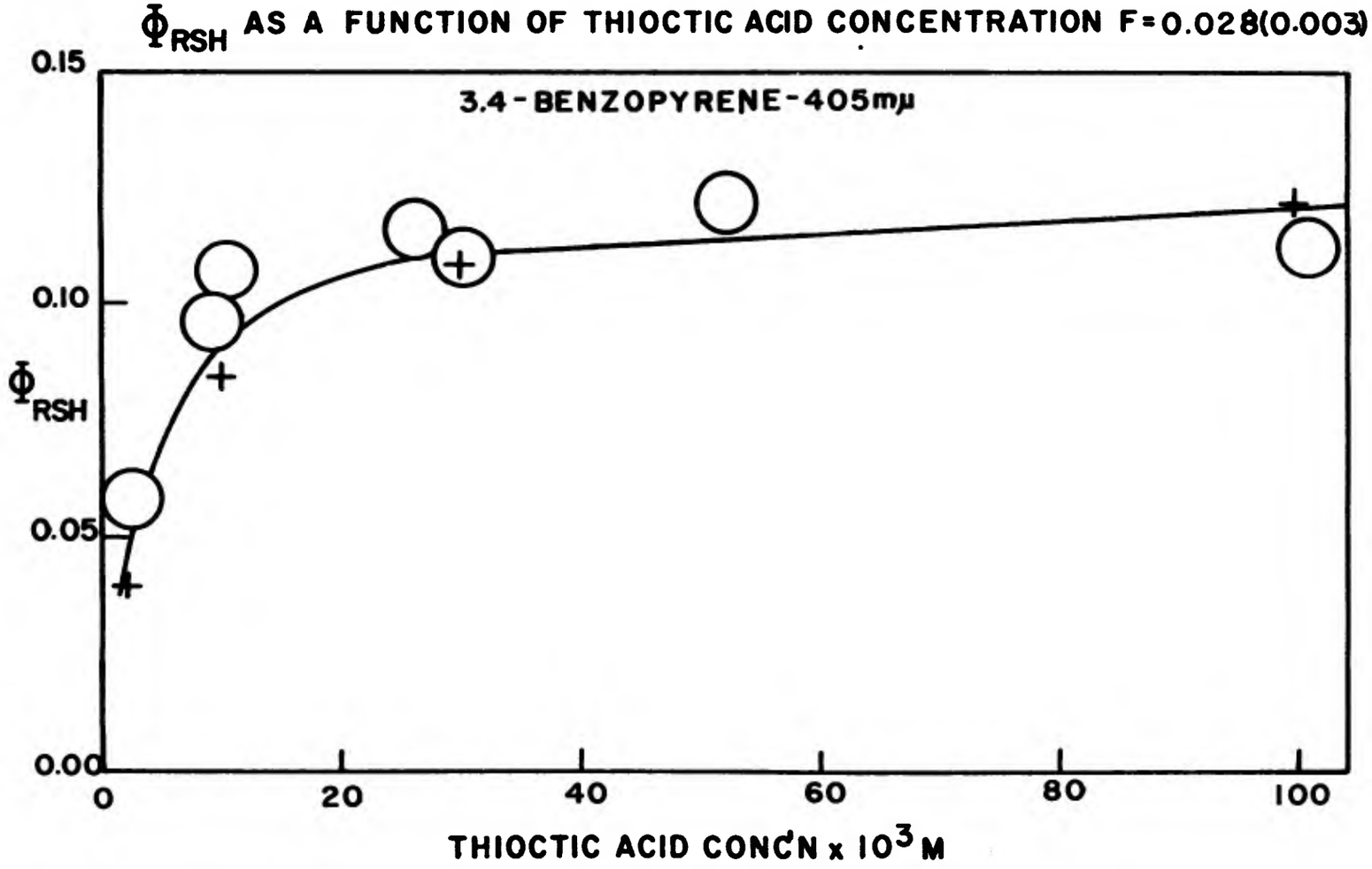
Φ_{RSH} AS A FUNCTION OF THIOCTIC ACID CONCENTRATION F=0.028(0.003)
3.4-BENZOPYRENE-405mμ
0.15
0.10
0.05
0.00
Φ_{RSH}
0
20
40
60
80
100
THIOCTIC ACID CONC'N x 10^3 M

TABLE 15

3,4-BENZOPYRENE

Φ_{RSH} AS A FUNCTION OF F AT 366 mμ

F	Φ_{RSH}
0.02	0.123 (0.007)
0.50	0.418 (0.039)
1.00	0.65 (0.03)

FIGURE 15

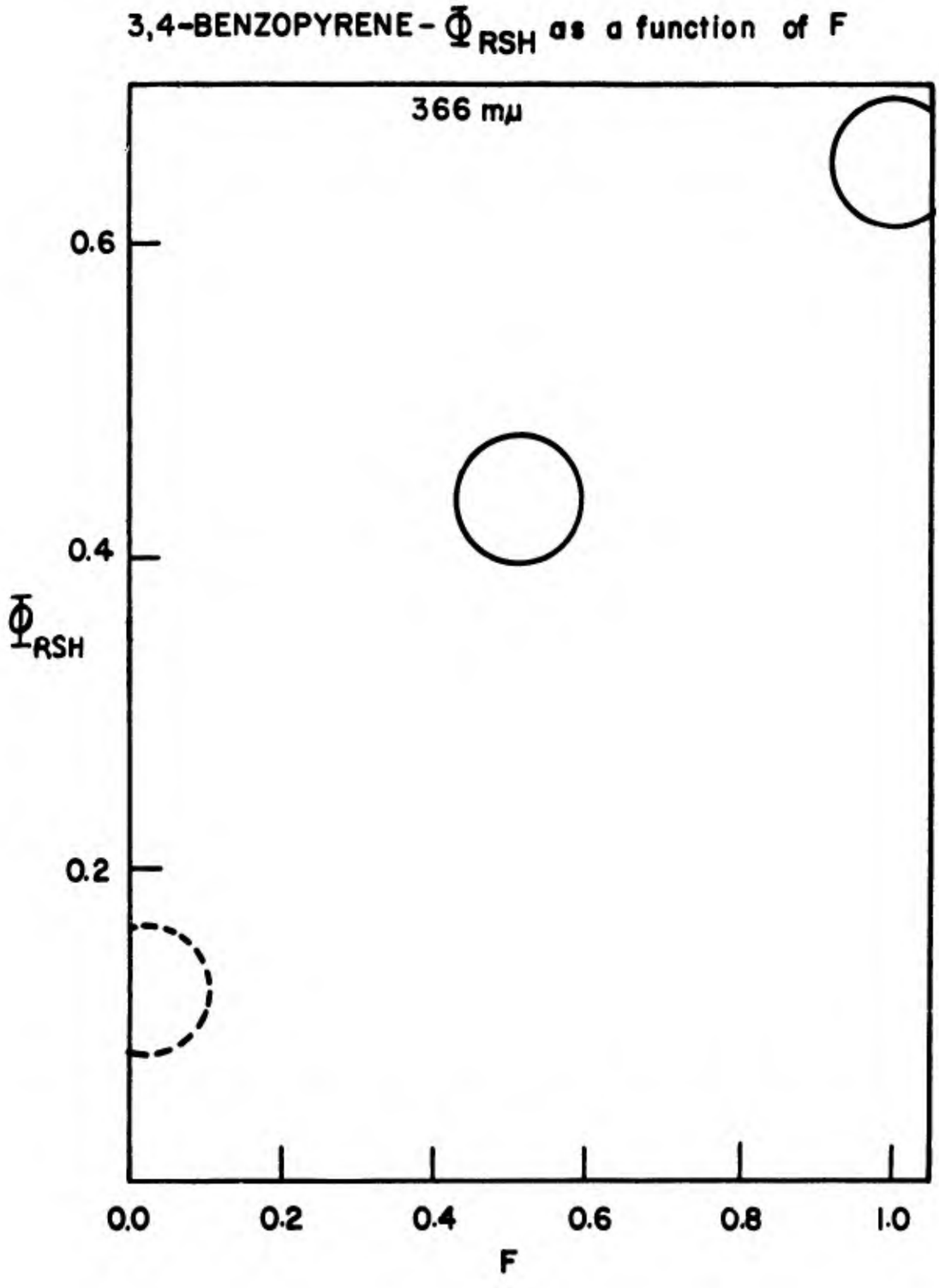
3,4-BENZOPYRENE - $\bar{\Phi}_{RSH}$ as a function of F
366 mμ
0.6
0.4
$\bar{\Phi}_{RSH}$
0.2
0.0
0.2
0.4
0.6
0.8
1.0
F

absorption[7]. These authors found one band in this absorption spectrum which appears to be identical with that observed in solutions of phenyl disulfide in ethyl benzoate at 210°C, and with a band found in long-path measurements of ethanol solutions of the disulfide near room temperature. On this basis, they suggest that this common band should be assigned to the arylsulfenyl (thiyl) radical RS·. A number of studies assign the electron spin resonance absorption generated by thermolysis and photolysis of disulfides to an unpaired non-bonding electron localized on a sulfur atom[8-11]. All these findings support the premise that, under certain conditions, homolysis of the sulfur-sulfur bond is a major consequence of the absorption of light by disulfides. Much of the recent work concerning organic sulfur compounds is related to their role in biological systems. The macro structure of proteins and the function of certain enzymes and hormones have been discussed in terms of the reactivity of the sulfur-sulfur bond in relation to its scission and formation[12-15].

Thioctic acid, Figure 1, is of particular interest. Calvin has suggested that the photosensitized reduction of this compound and the re-oxidation of its product in the dark constitute a light-activated "valve" between the photosynthetic and respiratory cycles[16]. The photochemical reduction of cyclic disulfides appears to be relatively efficient. Calvin has reported that the quantum yield for photolysis of thioctic acid and for 1,2-dithiolane in 95% ethanol is of the order of unity (cf. Table 1)[17]. McGlynn *et al.* have studied the spectroscopy and photolysis of a number of sulfur compounds including some cyclic disulfides[19]. It appears to be generally accepted that, at least for

7. Fluorescence Measurements

The results of the determination of fluorescence quantum yields of anthracene and 3,4-benzopyrene are summarized in Table 16. The value obtained for the ratio of the quantum yields of fluorescence of anthracene and quinine sulfate (used as reference standard) is in excellent agreement with that obtained by Parker and Rees.[33]

It is significant that the value obtained for the quantum yield of fluorescene of 3,4-benzopyrene at 313 mμ is larger than the value at 366 mμ. Further, the 313 mμ yield is greater than unity. This result suggests that the Φ_f cited for quinine sulfate is too high. This observation has already been made by other workers,[34] who have reported the Φ_f of 2-aminopurine to be *ca.* 1.0 at room temperature and 1.2-1.5 at 160°K, when based on $\Phi_f = 0.55$ for quinine sulfate. A fluorescence quantum yield greater than unity is viewed as highly unlikely.

8. Fluorescence Quenching

The results of a series of measurements of the effect of thioctic acid on the Φ_f of 3,4-benzopyrene are summarized in Table 17. The thioctic acid concentrations used are such that absorption in the emission region is negligibly small. The data indicate that thioctic acid is indeed quenching the emission from the excited singlet state of 3,4-benzopyrene.

A Stern-Vollmer plot of the data is presented in Figure 16, which indicates the operation of a collisional quenching mechanism. Significantly, spontaneous decay modes appear to be more important at 313 mμ than at 366 mμ.

TABLE 16

FLUORESCENCE QUANTUM YIELDS [a]

Compound	Φ_F		
	313 mμ	366 mμ	Lit. Values [c] 366 mμ
Anthracene [b]	0.28 (0.02)	0.30 (0.01)	0.26[c]
			0.28[c]
3,4-Benzopyrene	1.10 (0.05)	0.80 (0.04)	

a. In 6.54 M 2-propanol/benzene, relative to Φ_f = 0.55 for quinine sulfate

b. In ethanol

c. C.A. Parker and W.T. Rees, Analyst, 85, 587 (1960).

TABLE 17

QUENCHING OF 3,4-BENZOPYRENE FLUORESCENCE

BY THIOCTIC ACID

Thioctic Acid M	Φ_F [a] 313 mμ	Φ_F [a] 366 mμ
0	1.10	0.80
0.100×10^{-3}	1.05	0.63
1.00×10^{-3}	0.90	0.51
2.00×10^{-3}	0.77	0.39
5.00×10^{-3}	0.46	0.22

a. 9.51×10^{-6} M 3,4-benzopyrene in 6.54 M 2-propanol/benzene

FIGURE 16

STERN–VOLLMER PLOT - QUENCHING OF THE FLUORESCENCE OF 3,4-BENZOPYRENE[a] WITH THIOCTIC ACID

a. 9.51×10^{-6} M, 6.54M 2-PROPANOL/BENZENE

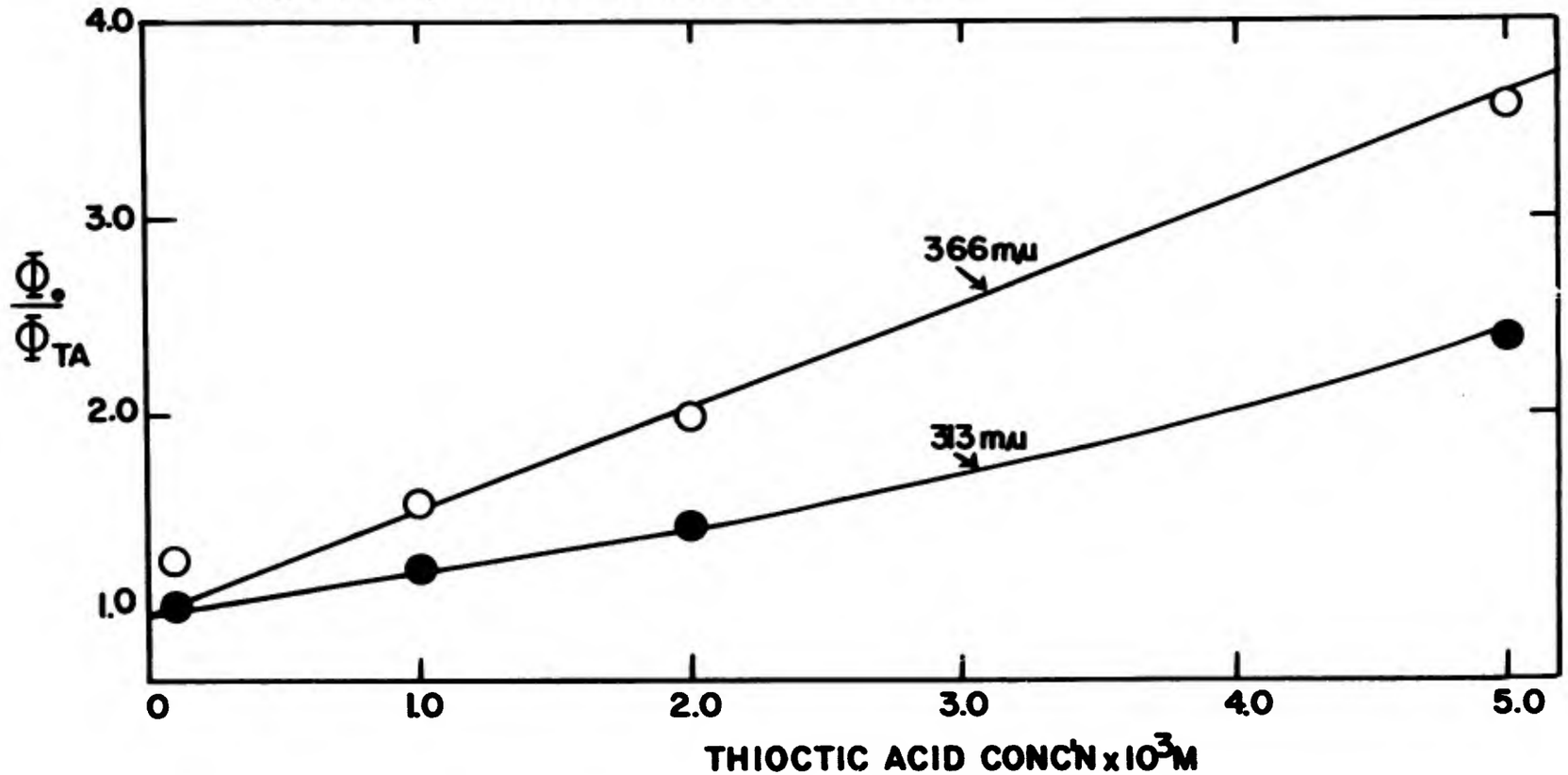

Discussion

The relationship between the structure of disulfides and their properties, particularly those related to the absorption of light, has been the subject of a number of investigations into the nature of the sulfur-sulfur bond. With sixteen electrons, sulfur has the structure

$$1s^2 \quad 2s^2 \quad 2p^6 \quad 3s^2 \quad 3p^4$$

The sulfur-sulfur bond thus would be expected to be primarily p-p in character. The associated C-S bond may be considered p^3-p in character. Of the two remaining pairs of non-bonding electrons, $3s^2$, $3p^2$, the $3p^2$ electrons are less tightly bound and more available for interaction. Bergson has considered the S-S bond as an isolated system and attributes its absorption to transition from the non-bonding 3p-π level to a non-bonding 3p-σ level.[35] The structure of a typical dialkyl disulfide is represented in Figure 17, along with the associated energy levels. In simple disulfide the angle θ between the adjacent sulfur p-π orbitals is *ca.* 90°, and interaction between these non-bonding orbitals is at a minimum.[36] Calvin has utilized these ideas to rationalize the increase in the wavelength of absorption in cyclic disulfides with decrease in ring size (Figure 18).[17] He suggests that decrease of the dihedral angle θ raises the energy of the ground state due to increased interaction of the 3pπ non-bonding orbitals. Since the 3pσ^* orbital is symmetrical about the S-S bond axis, such torsional movements should have little or no effect upon its energy. The net result would then be a decrease in the required energy of transition

FIGURE 17
THE STRUCTURE OF A SIMPLE DISULFIDE
AND ASSOCIATED ENERGY LEVELS

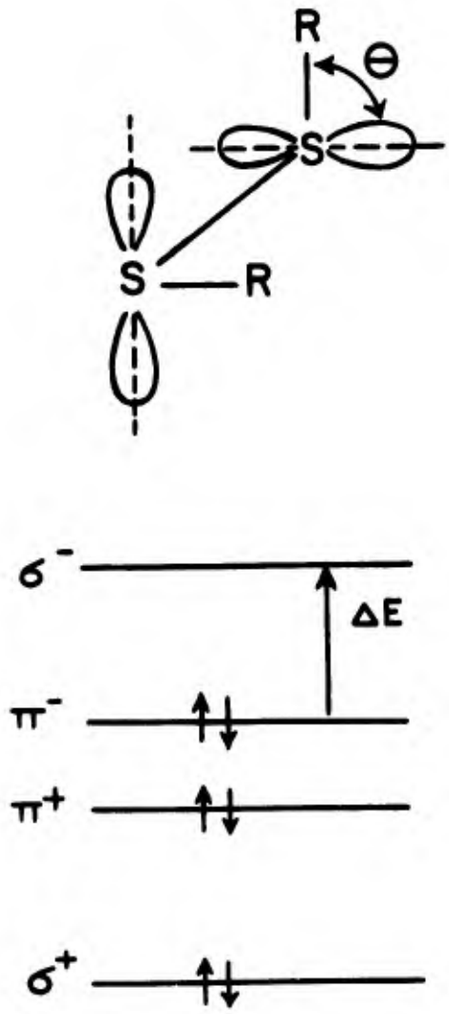

FIGURE 18

ABSORPTION SPECTRA & STRUCTURE OF DISULFIDES

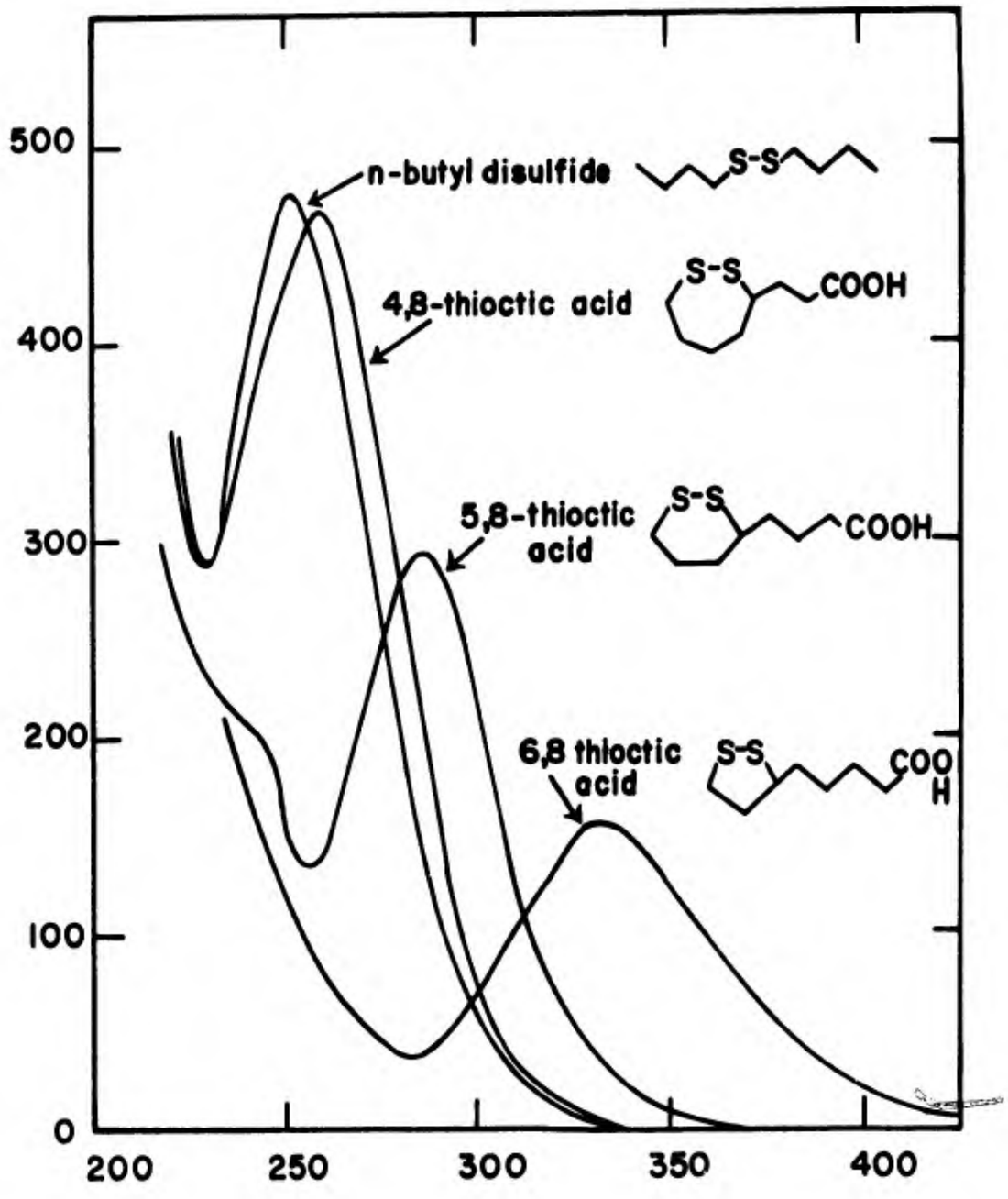

(Figure 19) related to the decrease in θ. Calvin proposes that this wavelength shift, corresponding to some 25 to 30 kcals. of energy in the case of the five-membered ring, directly reflects the strain energy of the disulfide ring structure. The reported sulfur-sulfur bond dissociation energies in dialkyl disulfides are in the range 50 - 70 kcals./mole.[37-39] which places the five-membered disulfide ring sulfur-sulfur bond dissociation energy in the range 30 - 50 kcals./mole. These considerations seem consistant with the observed behavior of disulfides (cf. Introduction, Table 1) in that the pentacyclic disulfides utilize absorbed light far more efficiently than do other structural types. All of the transitions considered here are between singlet states. No spectroscopic observations have yet been presented as evidence for the existence of triplet states in disulfides.

The energetics of the reaction of a disulfide with a secondary alcohol can be estimated as being endothermic or thermoneutral. Taking values of 98, 110, 82, and 76 kcals./mole for the bond energies of C-H, O-H, S-H and π C-O respectively along with a value of 73 kcal./mole for the S-S bond[38] we find the reaction

$$RSSR + R_2CH - OH \rightarrow 2RSH + R_2C = O$$

to be endothermic by *ca.* 40 kcals./mole.

No consideration is given here to the order of bond breakage. Thus the energy of dissociation for the O-H bond in $R_2\dot{C}OH$ has been estimated as 26 kcal./mole.[39] On this basis, the reaction of a disulfide with an alcohol becomes exothermic. This is indeed true for thioctic acid if the strain energy estimated by Calvin is considered.

FIGURE 19

SCHEMATIC

POTENTIAL ENERGY VS. S-S DISTANCE

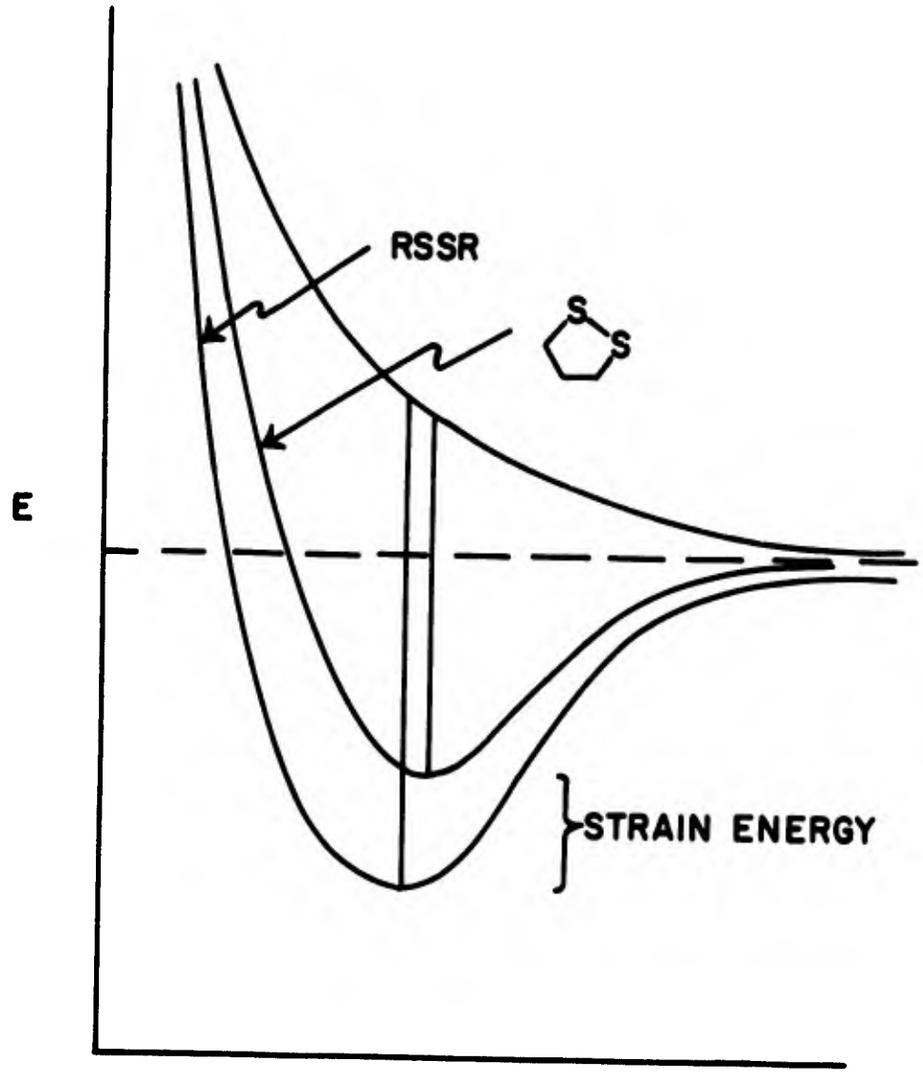

The transfer of energy to the disulfide bond from a suitable sensitizer may be envisioned as occurring by several possible routes. Some of these sequences are indicated below (with S = sensitizer $R'H_2$ = hydrogen donating solvent).

$$S \xrightarrow{h\nu} S_1^* \longrightarrow S_3^* \qquad \ldots\ldots\ldots (4)$$

$$RSSR + S^*_{1 \text{ or } 3} \longrightarrow S + RSSR^* \qquad \ldots\ldots\ldots (5)$$

$$RSSR^* + R'H_2 \longrightarrow 2RSH + R' \qquad \ldots\ldots\ldots (6)$$

$$RSSR^* \longrightarrow 2RS\cdot \qquad \ldots\ldots\ldots (7)$$

$$RS\cdot + R'H_2 \longrightarrow RSH + R'H\cdot \qquad \ldots\ldots\ldots (8)$$

$$S^* + R'H_2 \longrightarrow SH\cdot + R'H\cdot \qquad \ldots\ldots\ldots (9)$$

$$RSSR + SH(\text{or } R'H\cdot) \longrightarrow RSH + S(\text{or } R') + RS\cdot \qquad \ldots\ldots\ldots (10)$$

These mechanisms fall immediately into two categories, those which require an energy transfer step (Equations 4-8), and those which involve hydrogen transfer by the sensitizer (Equations 9&10).

The former class is most generally written with involvement of the triplet state (S_3^*). The basis of this preference lies in the greater probability that the longer-lived triplet will encounter an energy acceptor. However, these considerations by no means preclude the agency of the singlet state in energy transfer.

Atom transfer mechanisms (Equations 9&10) constitute the second

category of sensitization mechanisms which is considered with reference to the phenanthrenequinone photoreduction system (Section 4).

A. Direct Photolysis of Thioctic Acid: A Summary of Observations

Any mechanism which may be proposed must account for the following observations:

1. The quantum yields Φ^{366}_{RSSR}, Φ^{366}_{RSH} and Φ^{405}_{RSH} are independent of the thioctic acid concentration.

2. These same quantum yields are independent of the intensity of illumination.

3. The rate of photolysis of thioctic acid is directly proportional to the absorbed intensity.

4. Φ^{405}_{RSH} *vs.* 1/[2-propanol] is approximately linear at [2-propanol] > 2M.

5. Changes occur in the behavior of the system at very low or zero 2-propanol concentration.

6. Thiol is formed in a mole ratio of *ca.* 2:1 relative to the disappearance of disulfide. About one mole of pinacol appears for each two moles of titratable thiol. However, side reactions consume *ca.* 20% of the disulfide in reactions not leading to dithiol.

The following mechanism is offered to account for the behavior observed upon the photolysis of thioctic acid in solutions of 2-propanol greater than 2 M in concentration.

$$D \xrightarrow[k_1 \; I^D_{abs.}]{h\nu} D^* \qquad \ldots\ldots\ldots (11)$$

$$D^* \xrightarrow{k_2} D \qquad \ldots\ldots\ldots (12)$$

$$D^* \xrightarrow{k_3} D' \qquad \ldots\ldots\ldots (13)$$

$$D' \xrightarrow{k_4} D \qquad \ldots\ldots\ldots (14)$$

$$D' + RH_2 \xrightarrow{k_5} \cdot SRSH + \cdot RH \qquad \ldots\ldots\ldots (15)$$

$$\cdot SRSH + RH_2 \xrightarrow{k_6} HSRSH + \cdot RH \qquad \ldots\ldots\ldots (16)$$

$$2RH\cdot \longrightarrow HRRH \qquad \ldots\ldots\ldots (17)$$

Here D is the disulfide, thioctic acid and D^* is the excited state of the disulfide. D' is the state responsible for the initiation of chemical reaction. The intermediate produced by hydrogen abstraction is represented by ·SRSH (IV, Figure 20), and the dithiol product is HSRSH (V, Figure 20). RH_2 corresponds to 2-propanol, while RH· is the semipinacol or 2-hydroxy-2-propyl radical, and HRRH represents pinacol. $I^D_{abs.}$ is the intensity of the irradiation absorbed by thioctic acid.

Application of the steady-state treatment to D^*, D' and ·SRSH yields

$$(D^*) = \frac{k_1 \, I^D_{abs.}}{k_2 + k_3} \qquad \ldots\ldots\ldots (18)$$

$$(D') = \frac{k_1 \, k_3 \, I^D_{abs.}}{(k_2+k_3)\ (k_4+k_5(RH_2))} \qquad \ldots\ldots\ldots (19)$$

$$[\cdot SRSH] = \frac{k_1 \, k_3 \, k_5 \, I^D_{abs.}}{k_6\ (k_2+k_3)\ (k_4+k_5(RH_2))} \qquad \ldots\ldots\ldots (20)$$

FIGURE 20

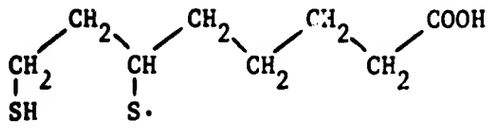

A STRUCTURE FOR INTERMEDIATE ·SRSH

IV

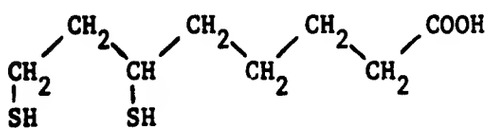

6,8-DITHIOLOCTANOIC ACID

V

The rate of appearance of dithiol is then

$$\frac{d(HSRSH)}{dt} = \frac{k_1 k_3 k_5 \, I^{D}_{abs.} \, (RH_2)}{(k_2+k_3)\ (k_4+k_5(RH_2))} \qquad \ldots\ldots\ldots (21)$$

or, the rate of formation of thiol (SH) groups is

$$\frac{d(RSH)}{dt} = \frac{2k_1 k_3 k_5 \, I^{D}_{abs.} \, (RH_2)}{(k_2+k_3)\ (k_4+k_5(RH_2))} \qquad \ldots\ldots\ldots (22)$$

By letting $k_1 = 1$ (mole/Einstein) as is conventional, we obtain

$$\phi^{o}_{RSH} = \frac{\frac{dRSH}{dt}}{I_{abs.}} = \frac{2k_1 k_3 k_5 \ (RH_2)}{(k_2+k_3)\ (k_4+k_5(RH_2))} \qquad \ldots\ldots\ldots (23)$$

This mechanism therefore satisfies the requirements that Φ_{RSSR} and Φ_{RSH} be independent of the intensity of illumination and that $-\frac{dRSSR}{dt}$ be directly proportional to $I_{abs.}$ Further, the expression (23) does not exhibit a dependency on thioctic acid concentration in agreement with observations.

Inversion of (23) and substitution of the rate constant ratio

$$K_3 = \frac{k_3}{k_2+k_3} \qquad \ldots\ldots\ldots (24)$$

yields

$$\frac{1}{\Phi_{RSH}} = \frac{1}{2K_3} + \frac{k_4}{2K_3 k_5} \left(\frac{1}{(RH_2)}\right) \qquad \ldots\ldots\ldots (25)$$

If we now consider the plot at 405 mμ of $^{1}/_{\Phi_{RSH}}$ *vs.* $^{1}/(RH_2)$, (cf. Figure 8) we obtain from the linear portion a slope of 2.4 and an

intercept of 3.6. Hence

$$1/2K_3 = 3.6$$

or

$$K_3 = 0.14$$

then

$$k_2/k_3 = 6.1$$

Thus, even for the pentacyclic disulfide thioctic acid deactivation is *ca.* six times more important than transition to the reactive species. The observation that the quantum yield increases with the energy of the exciting light most probably reflects an increase in the ratio k_3/k_2+k_3

Providing that excitation takes place in the same electronic transition (the spectrum certainly suggests this to be the case) the implication is that the formation of the reactive intermediate D' takes place from a higher vibrational level of the electronically excited state. The presence of additional vibrational energy in the excited disulfide might be expected to facilitate biradical formation relative to reformation of the sulfur-sulfur bond.

The substitution of the value of K_3 into the expression (25) and solution for the slope of the plot of $1/\Phi_{RSH}$ *vs.* $1/[RH_2]$ (Figure 8) affords,

$$\text{Slope} = \frac{k_4}{0.28\ k_5}$$

Substitution of the value of the slope (slope = 2.4) yields

$$k_4/k_5 = 0.67 \left(\frac{m}{\ell}\right)$$

In pure 2-propanol, at 405 mμ, $[RH_2] = 13.07$ M which provides $\frac{k_4}{k_5(RH_2)} = 0.05$; thus hydrogen abstraction is the important decay mode for D'.

A lower limit estimate of the lifetime of D' can be made by assuming the diffusion controlled rate constant of 1×10^{10} ℓ/mole-sec. for k_5. This leads to a $k_4 = 6.7 \times 10^9$ sec^{-1} or a lifetime, $\tau_{D'} \geq 0.2$ nanoseconds. This value might be expected of an excited singlet rather than a chemically reactive state and renders the assumption of diffusion control for the hydrogen abstraction step (Equation 15) unlikely.

There is no direct evidence for the structure of species D', but the diradical VI, Figure 21, is put forward as a likely possibility. An electron spin resonance signal obtained on the photolysis of concentrated solutions of thioctic acid has been assigned to this structure.[40]

The formation of a long-lived transient ($\tau_{1/2}$ *ca.* 350 μsec. at 500 mμ and 700 mμ) upon the flash photolysis of thioctic acid in benzene has been detected in these laboratories.[41]

It is conceivable that such a species might generate hydrogen sulfide by an inter- or intramolecular abstraction-elimination mechanism. Inspection of molecular models indicates that intramolecular hydrogen abstraction is sterically feasible from several sites on the molecule. Lacking additional knowledge of the side products, further speculation along these lines seems fruitless at this time.

FIGURE 21

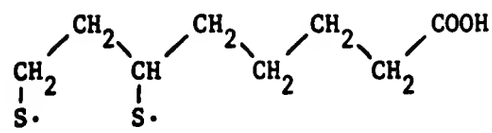

STRUCTURE OF THE BIRADICAL

VI

B. Sensitized Photolysis: A Summary of Observations

Any sensitization mechanism offered must accommodate the following observations:

1. There is an essentially linear decrease of ϕ_{RSH}^{405} with F (the fraction of the total absorbed light absorbed by thioctic acid) with $\phi_{RSH}^{400} \simeq 0$ when F=0 for benzanthrone.
2. In the case of 3,4-benzopyrene, the ϕ_{RSH}^{405} decreases initially more slowly than in the case of benzanthrone, then finally quite rapidly with decreasing F values.
3. At an approximately constant and small F value, the ϕ_{RSH}^{405} decreases with thioctic acid concentration in a slow and approximately linear fashion, and then rolls off steeply toward zero.

Extension of the mechanism proposed for direct photolysis of thioctic acid to account for observations in the presence of 3,4-benzopyrene and benzanthrone results in the following steps:

$$S \xrightarrow[k_1' \; I_{abs.}^{s}]{h\nu} S^* \qquad \ldots\ldots\ldots (26)$$

$$S^* \xrightarrow{k_a} S \qquad \ldots\ldots\ldots (27)$$

$$S + S^* \xrightarrow{k_b} 2S \qquad \ldots\ldots\ldots (28)$$

$$S^* + D \xrightarrow{k_c} S + D^* \qquad \ldots\ldots\ldots (29)$$

then, as before

$$D \xrightarrow[k_1 \; I_{abs.}^{D}]{h\nu} D^* \qquad \ldots\ldots\ldots (30)$$

$$D^* \xrightarrow{k_2} D \qquad \ldots\ldots\ldots (31)$$

$$D^* \xrightarrow{k_3} D' \qquad \ldots\ldots\ldots (32)$$

$$D' \xrightarrow{k_4} D \qquad \ldots\ldots\ldots (33)$$

$$D' + RH_2 \xrightarrow{k_5} \cdot SRSH + \cdot RH \qquad \ldots\ldots\ldots (34)$$

$$\cdot SRSH + RH_2 \xrightarrow{k_6} HSRSH + \cdot RH \qquad \ldots\ldots\ldots (35)$$

$$2 \cdot RH \xrightarrow{k_7} HRRH \qquad \ldots\ldots\ldots (36)$$

Here S is the sensitizer and S^* is its excited singlet state, the decay of which is partitioned between spontaneous decay (Equation 27), concentration quenching (Equation 28), and transfer to D (Equation 29).

Application of the steady state approximation to S^*, D^*, D' and ·SRSH of this scheme yields

$$(S^*) = \frac{k_1' \; I_{abs.}^{S}}{k_a + k_b S + k_c (D)} \qquad \ldots\ldots\ldots (37)$$

$$(D^*) = \frac{k_1 \; I_{abs.}^{D} (k_a + k_b (S) + k_c D) + k_1' \; I_{abs.}^{S} \; k_c (D)}{(k_2 + k_3) \; (k_a + k_b (S) + k_c (D))} \qquad \ldots\ldots\ldots (38)$$

$$(D') = \frac{k_3\,[k_1\,I^{D}_{abs.}(k_a+k_b(S)+k_c(D))+k_1'\,I^{S}_{abs.}\,k_c(D)]}{(k_2+k_3)\,(k_4+k_5(RH_2))\,(k_a+k_b(S)+k_c(D))} \qquad \ldots\ldots\ldots (39)$$

$$(\cdot SRSH) = \frac{k_3k_5\,[k_1\,I^{D}_{abs.}(k_a+k_b(S)+k_c(D))+k_1'\,I^{S}_{abs.}\,k_c(D)]}{k_6\,(k_2+k_3)\,(k_4+k_5(RH_2))\,(k_a+k_b(S)+k_c(D))} \qquad \ldots\ldots\ldots (40)$$

The rate of dithiol formation now becomes

$$\frac{d(HSRSH)}{dt} = \frac{k_3k_5(RH_2)[k_1I^{D}_{abs.}(k_a+k_b(S)+k_c(D))+k_1'\,I^{S}_{abs.}\,k_c(D)]}{(k_2+k_3)\,(k_4+k_5(RH_2))\,(k_a+k_b(S)+k_c(D))}\;\frac{1}{2}\;\frac{d(RSH)}{dt} \qquad \ldots\ldots\ldots (41)$$

If F is now defined as that fraction of all the absorbed light which is absorbed by thioctic acid (D) and 1-F as the fraction absorbed by the sensitizer (S), we may write

$$I_{abs.} = I^{D}_{abs.} + I^{S}_{abs.} = FI_{abs.} + (1-F)I_{abs.}$$

or

$$I^{D}_{abs.} = FI_{abs.}$$

and

$$I^{S}_{abs.} = (1-F)I_{abs.}$$

Substitution of these expressions into Equation 41, and setting $k_1 = k_1' = 1$ affords

$$\frac{d(RSH)}{dt} = \frac{2k_3k_5(RH_2)I_{abs.}\ [F(k_a+k_b(S)+k_c(D))+ (1-F)k_c(D)]}{(k_2+k_3)\ (k_4+k_5(RH_2))\ (k_a+k_b(S)+k_c(D))} \quad \ldots\ldots\ldots (42)$$

Substitution of Equation 23, the expression derived for ϕ^o_{RSH} on direct photolysis, and division by $I_{abs.}$ results in

$$\frac{d(RSH)}{dt}/I_{abs.} = \phi_{RSH} = \phi^o_{RSH} \left[\frac{F(k_a+k_b(S)+k_c(D)) + (1-F)k_c(D)}{k_a+k_b(S)+k_c(D)}\right] \quad \ldots\ldots\ldots (43)$$

or

$$\phi_{RSH} = \phi^o_{RSH} \left[\frac{F(k_a+k_b(S))+k_c(D)}{k_a+k_b(S)+k_c(D)}\right] \quad \ldots\ldots\ldots (44)$$

which becomes

$$\phi_{RSH} = \phi^o_{RSH} \left[\left(\frac{k_cD}{k_a+k_b(S)+k_c(D)}\right) + \left(\frac{k_a+k_b(S)}{k_a+k_b(S)+k_c(D)}\right) F\right] \quad \ldots\ldots\ldots (45)$$

Now, in the case of an absorbing non-sensitizer $k_c = 0$ and the expression (Equation 45) reduces to

$$\phi_{RSH} = \phi^o_{RSH}\ F \quad \ldots\ldots\ldots (46)$$

The plot of ϕ_{RSH}^{405} against F for benzanthrone, Figure 12, conforms to this prediction very well. The slope is 0.26, which is the value of ϕ_{RSH}^{o} within experimental error, and the intercept is *ca.* 0.01 which is zero within the same certainty. It appears that benzanthrone behaves as a simple "inner filter."

In the case of 3,4-benzopyrene the plot ϕ_{RSH}^{405} *vs.* F (Figure 13) presents a very slow initial decrease with decreasing F which, below F=0.5, becomes steadily more significant until, below F=0.15 the function drops off sharply. According to Equation 45, the slope is represented by

$$\text{slope} = \frac{(k_a+k_b(S))}{k_a+k_b(S)+k_cD}\ \phi_{RSH}^{o} \qquad \ldots\ldots\ldots (47)$$

However, the concentration of sensitizer is not constant; it increases as F decreases. If we take the limiting slope of the plot with $F \to 1$ and $(S) \to 0$ as equal to 0.026 we obtain

$$0.026 = \frac{k_a}{k_a+k_c(D)}\ \phi_{RSH}^{o}$$

Substituting $\phi_{RSH}^{o} = 0.25$ and $(D) = 0.10$ M we obtain

$$\frac{k_c}{k_a} \simeq 90$$

Assumption of a diffusion controlled limit for k_c (10^{10} ℓ./mole sec.) then gives

$$k_a \approx 10^8$$

TABLE 18

Φ_{RSH}^{405} CALCULATED FOR VARIOUS THIOCTIC ACID CONCENTRATIONS ASSUMING $k_{b/k_c} = 4$ IN EQUATION 49

Conc. of Thioctic Acid M	Calculated Φ_{RSH}^{405}
0.10	0.122
0.03	0.109
0.01	0.085
0.002	0.039

or a lower limit to the lifetime of S^* of

$$\tau_{S^*} \gtrsim 10 \text{ nanoseconds.}$$

Further information can be obtained by consideration of the plot of Φ_{RSH} *versus* concentration of thioctic acid at constant F (Figure 14). In these experiments, the ratio of the concentration of D to that of S is 4.0 (i.e. [D] = 4[S]), and F=0.028 (0.003). Substitution in Equation 45 yields

$$\Phi_{RSH} = \Phi^{o}_{RSH} \left[\frac{k_c(D)}{k_a + 0.25\, k_b(D) + k_c(D)} + 0.028 \left(\frac{k_a + 0.25\, k_b(D)}{k_a + 0.25\, k_b(D) + k_c(D)} \right) \right] \quad \ldots\ldots\ldots (48)$$

If we substitute $k_c/k_a = 90$, several trials indicate that a ratio of $k_b/k_c = 4$ matches the experimental curve quite well, yielding the relation

$$\Phi_{RSH} = \Phi^{o}_{RSH} \left[\frac{0.028 + 92.5\,(D)}{1 + 180\,(D)} \right] \quad \ldots\ldots\ldots (49)$$

Some points calculated with this equation are given in Table 18 and are indicated by the crosses on Figure 14 (cf. Results Section).

The behavior of the quantum yield Φ^{405}_{RSH} for the sensitized system at high F values can be rationalized on the basis of the increased significance of self quenching modes (Equation 28 of mechanism). Birks and Christophorou[42] have indicated that the fluorescence spectrum of increasing concentrations of 3,4-benzopyrene exhibits effects attributable to the formation of S^*S dimers which are termed excimers. It may be significant that the effect causes a general shift of the

intensity of fluorescence to longer wavelengths.

The fluorescence quenching data affords another means for determining the ratio k_c/k_a. For these experiments we can write the following steps:

$$S \xrightarrow{k_1' I_{abs.}} S^* \qquad \ldots\ldots\ldots (50)$$

$$S^* \xrightarrow{k_a} S \qquad \ldots\ldots\ldots (51)$$

$$S^* + D \longrightarrow S + D^* \qquad \ldots\ldots\ldots (52)$$

Self-quenching is neglected in this case since the concentration in the experiments was *ca.* 10^{-4} M. It should be noted that both radiationless and radiant modes of decay are considered in Equation 51. Therefore, k_a is actually a sum of the constants for both modes of decay. For the quenched system we write

$$\frac{d(S^*)}{dt} = I_{abs.} - k_a(S^*) - k_c(S^*)(D) \qquad \ldots\ldots\ldots (53)$$

in the absence of quencher we have

$$\frac{d(S^*)}{dt} = I_{abs.} - k_a(S^*) \qquad \ldots\ldots\ldots (54)$$

It follows from the relation

$$\phi_F = \frac{\frac{d(S^*)}{dt}}{I_{abs.}} \qquad \ldots\ldots\ldots (55)$$

that the ratio of ϕ_F^o , the unquenched fluorescence quantum yield to ϕ_F^D , the yield in presence of quencher is

$$\frac{\phi_F^o}{\phi_F^D} = 1 + \frac{k_c}{k_a}[D] \qquad \ldots\ldots\ldots (56)$$

From the quenching plot, Figure 16, we can obtain the slope for 366 mμ excitation as 530. Again assuming the diffusion-controlled rate constant for k_c we have

$$\frac{k_c}{k_a} = 530$$

and

$$k_a = \frac{10^{10}}{530} \text{ or } \approx 2 \times 10^7$$

This corresponds to a lifetime for S^* of $\tau_S^* \approx 50$ nanoseconds. This value is in fair agreement with the lifetime obtained from the sensitization experiments. It should be pointed out in this connection that this comparison is based on the assumption that the fluorescence behavior of 3,4-benzopyrene is the same at 366 mμ, where the emission was measured, and at 405 mμ, where the photolyses were performed. A direct comparison of 405 mμ was not possible owing to an overlap of the exciting light and the emission. Further, inspection of Figure 13 clearly shows that the limiting slope, on which the photochemically derived lifetime estimate of $\tau_S^* = 10$ nanoseconds is based, is subject to a large uncertainty.

At this point, the possibility of another mechanism, that of photolysis *via* absorption of the fluorescence emission of the sensitizer, deserves comment. As previously mentioned, this effect is not significant in the fluorescence quenching experiments because of the minimal overlap of disulfide absorption with the emission of the benzopyrene. In photolysis experiments it is more difficult to rule 3,4-benzopyrene solutions emit from a very thin front layer of solution means that *ca.* one-half of the emitted light is lost for reabsorption purposes. In addition, it can be assumed that the Φ_{RSSR} is decreasing at longer wavelength (cf. Results Section, Table 9). These facts combined with the rapidly decreasing absorption of the disulfide with increasing wavelength through the emission region mitigate against the involvement of this process. There is no a priori reason to assume that the photochemistry and quenching are independent processes in this system--in fact, it is our position, implicit in the mechanism offered, that the same states and processes are involved in both cases.

A. Instrumental and Analytical Techniques

1. Spectrophotometry

All spectral measurements were performed with a Beckmann Model DK-1 spectrophotometer. The photometric accuracy of this instrument was checked according to the procedure cited by the National Bureau of Standards; the wavelength accuracy was checked with a mercury arc lamp.

2. Fluorescence Measurements

The method and instrumentation employed for the fluorescence measurements are described in Section 2 of this report. Sample preparation was essentially identical with that used for the photolysis solutions. The cell assemblies (cf. Figure 22) were modified for use with the fluorescence apparatus by lengthening the cell attachment stem and turning the cell 90° around the stem axis.

3. Gas-Liquid Chromatography (GLC)

Gas-liquid chromatography was performed with the F & M model 720 dual column, temperature-programmed chromatograph (F & M Scientific Corp., Avondale, Pa.). This unit was used primarily to check the purity of solvents. The columns utilized were 20% Triton X-305 (Rohm and Haas). 6' x 0.25" dia., and 20% Silicon Gum Rubber (F & M), 4' x 0.25" dia., both supported on a 60-80 mech Chromasorb P (Fisher Scientific Co.). Pinacol analysis was performed with an F & M model 402 flame ionization detector, using a 5' x 0.25" dia. column of 10% Triton X-305 on 80-100 mech Teflon.

4. Thin Layer Chromatography (TLC)

Thin layer chromatography was used to check the purity of sensitizer candidates. Silica gel-coated films (chromatosheets, Eastman Kodak, Inc.) and "Desaga" apparatus (Brinkmann, Inc.) was employed. Silica gel castings cast from slurries (Silica gel G, Merck) were dried at *ca.* 120°C for a minimum of two hours. Solvent mixtures of n-hexane and benzene and 4:1 benzene and ethyl acetate were employed for the elution.

5. Thiol Analysis

The procedure utilized is essentially that of Kolthoff and Harris[27] as modified by Grimes *et al.* [28] A micro volt-ammeter with an impedance *ca.* 100 ohms over the measured current range (Hewlett Packard, Inc. #412 A) was used in conjunction with a large area mercury, mercuric iodide, potassium iodide half cell fitted with a one-meter salt bridge, and a rotating platinum electrode assembly, (E.H. Sargent & Co. # S-76485). In the modified method, back titration of excess silver ion is effected with a solution of n-dodecyl thiol (*ca.* 5×10^{-3} M) which was freshly standardized against silver nitrate for each set of determinations. Blank titrations on unirradiated samples were performed periodically; no corrections of this nature were required.

B. Materials

1. General

The fractional distillation of liquid reagents was performed with a "Podbielniak" 90-cm. long spinning band column or with a 4' "Podbielniak" "Heligrid"-packed column. The selection of

useful fractions from the distillations was made on the basis of GLC analysis.

2. Solvents

*Iso*propanol (Fisher Scientific Company, # A 416) was refluxed over, and distilled from calcium hydride. This method is preferred over purification with magnesium ribbon because impurities are more readily and completely removed. Particularly, a small, persistent, impurity of *ca.* 0.1 mole percent revealed by GLC (Triton X 305, 70°C.) was removed by the calcium hydride method.

Benzene (Fisher Scientific Company, # B 245) was very slowly fractionated on the spinning band column. GLC analysis (Triton X 305, 70°C.) of material boiling 80-81°C. revealed the absence of all impurities indicated in the undistilled solvent.

Cumene (Matheson, Coleman, and Bell, # CX 2105) of boiling point 151-153°C. was distilled under nitrogen on the spinning band column. Unidentified impurities estimated at 0.3 mole percent could not be removed.

Acetone (Mallinckrodt, C.P.) was used for GLC calibration as such. Drum acetone (Fisher Scientific Co., # A-18) was found to be suitable as a solvent in the thiol analysis without further treatment.

Hexane (Fisher H 291) and petroleum ether (Baker # 9273) of boiling range 60-110°C were redistilled before use.

3. Reagents

Disulfides - Both n-butyl disulfide (Eastman Kodak # 1826) of boiling range 110-112°C at 13 mm. and *t*-butyl disulfide (Eastman

Kodak # P 5683) of boiling range 198-204°C were purified by shaking first with 0.1 N iodine in potassium iodide solution, then briefly and rapidly with 0.1 N sodium thiosulfate solution and finally with several portions of water. Drying with anhydrous sodium sulfate was followed by fractional distillation under nitrogen on the spinning band column. GLC analysis (Silicon Gum Rubber, 170°C, 60 ml/min.) revealed a distillate free of resolvable impurities. Mesityl disulfide was prepared by Mr. Barry Cogan. One sample had m.p. 123-124°C (lit. 124°C)[43], and was used without further purification. Phenyl disulfide (Eastman Kodak, # 1500) was recrystallized repeatedly from ethanol to a m.p. of 59-60°C (lit. 59-60°C).[4]

Thioctic acid was obtained in high purity (Sigma Chemical Co. lot# 75B-1760). On the basis of its m.p. 60-61°C (lit. 61-61.5)[44] extinction coefficient ε, 154 in 2-propanol (lit. ε, 154 in 95% ethanol)[17], and TLC (no impurities resolved under several conditions) it was used without further purification.

A sample of 6,8-dithiol octanoic acid was obtained in a sealed vial under nitrogen (Sigma Chemical Co. lot 36B-0450) and was used in simulation titration experiments without further treatment.

N-dodecyl thiol, (Matheson, Coleman, and Bell # DX 2425) was used as obtained. Standardization against silver nitrate

indicated a thiol content of *ca.* 95+%.

Hydrogen sulfide gas was obtained in a lecture bottle (J.T. Baker and Co.). The purity indicated was 98.5% with principle impurities of CO_2, N_2, and O_2.

Pinacol was obtained as a previously purified sample (D.Lambert) and was azeotropically dried with benzene and simply distilled under dry N_2 (b.p. 171-172°C. lit. b.p. 174-176°C[45]).

4. Compounds for Use in Screening Experiments

The following compounds were obtained in the highest commercially available state of purity and were used without further purification.

1,8-dihydroxyanthraquinone (Eastman Kodak, P 6557)

Rhodamine B (Eastman Kodak, P 4453)

phenazine (Matheson, Coleman, and Bell, PX 470)

Rose Bengal (Allied Chemical Corp., # 665)

fluorenone (Matheson, Coleman, and Bell, FX 315)

The following compounds were commercially obtained in a high state of purity, (Rutgerswerks, A.G., Henley and Co., Inc., 202 E. 44th Street, N.Y., N.Y.). Their spectra and m.p. corresponded with or exceeded the specification of Clar.[46] They were used without further treatment.*

fluoranthrene (m.p. 110-110.5°C lit. 110°C[46a])

1,2:3,4-dibenzopyrene (m.p. 228-229°C lit. 224-226°C[46b])

perylene (m.p. 278-279°C lit. 273-274°C[46c])

---

*It should be noted that the literature m.p. cited for the dibenzopyrenes shows a progressive increase with the year of publication of the source, probably due to the advent of more efficient methods of separation (cf. references 46 and 47 and citations therein).

1,2:4,5-dibenzopyrene (m.p. 244.5-245°C lit. 233-234°C[46d], 241-242°C[47])

azulene (m.p. 95-97°C lit. 97-98°C[48])

3,4-benzopyrene (m.p. 176-177.0°C lit. 176.5-177.5°C[46e])

2,3-(1-aci-anthrylene) quinoxaline (m.p. 248-248.5 lit. 237°C[49], 248-249°C[50]) was obtained in a high state of purity and used as such.

Several other hydrocarbons were obtained commercially and were further purified by recrystallization from ethanol, and, in one case, by vacuum sublimation. These were

napthalene (m.p. 80.5-81.0°C lit. 80°C[46f])

triphenylene (m.p. 197.5-198.5°C, lit. 196.5°C[46g])

anthracene (m.p. 217.5-218°C lit. 218°C[46h])

Benzanthrone had been prepared for an earlier investigation by the condensation of anthrone and acrolein, (H_2SO_4, 120°C). Extraction with and recrystallization from benzene followed by recrystallization from 2-propanol yielded yellow crystals of m.p. 171-172°C. (lit. m.p. 168-170°C[51])

5. 3,4-Benzopyrene

Since the original sample of 3,4-benzopyrene was exhausted in the screening experiments and convenience required replacement from another source, Aldrich Chemical Co. material (B 1008) was selected for the detailed investigation. A TLC analysis of this material with n-hexane on a silica gel "chromatosheet" (Eastman Kodak) afforded evidence of a small amount of a slow moving impurity. Thrice-repeated column chromatography on a silica gel

(Merck 7734, 0.05-0.20 mm.) column (3.0 cm. x 20.0 cm.) removed all detectable traces of this impurity by the completion of the second pass. Elution was accomplished by the use of 1:1 n-hexane benzene on the first column and n-hexane alone on the second and third columns. The 3,4-benzopyrene was eluted before the impurity. Because of the efficiency of the separation, column loading was high (*ca.* 0.4 weight % of gel.). The 3,4-benzopyrene thus obtained was carefully recrystallized from 1:12 benzene, petroleum ether and collected on a new clear fritted glass filter (m.p. 178.5-178.7°C, lit. 176.5-177.5°C[46b]).

C. Irradiation Apparatus and Procedures

1. Irradiation Apparatus

The apparatus for the measurement of quantum yields and rates of photochemical reactions is discussed in Section 2 of this report. A detailed description of the apparatus and its applications is given in Appendix A.

2. Sample Preparation

Sample solutions prepared for irradiation were pipetted directly into the test tube-ended sidearm of a "Y" shaped cell assembly, Figure 22. A glass-enclosed micro-stirrer bar was added and degassing was carried out by five or more freeze-pump-thaw cycles involving liquid nitrogen as the low temperature source and a vacuum of *ca.* 5×10^{-5} mm. The sample assembly was then sealed off below the joint. A procedure termed "wall-rinsing" was developed to ensure that no deposition of solids in the side arm (a phenomenon sometimes noticed on the transfer of concentrated solutions) lowered the concentration of reactants in the irradiation

FIGURE 22

IRRADIATION CELL ASSEMBLY

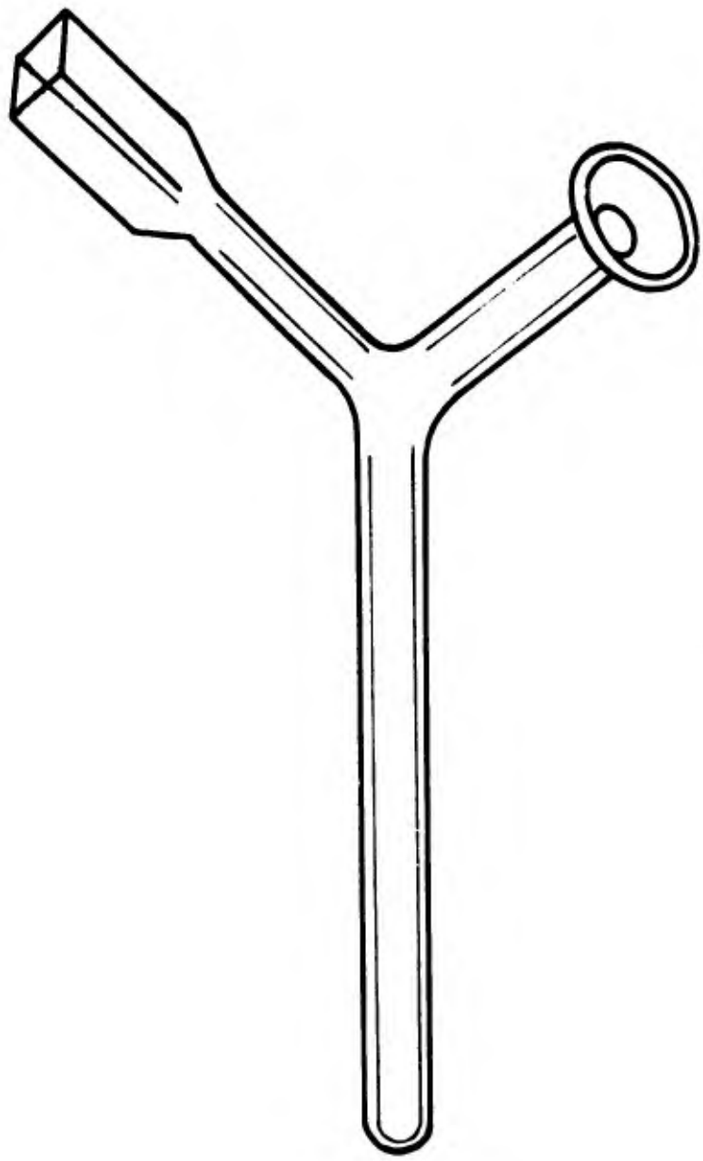

cell. The procedure consisted of fitting a drilled and split cork stopper around the necks of the irradiation cells (1.0 x 1.0 x 4.5 cm. Beckmann silica cells fitted with necks and graded seals). The cork was then pressed into the mouth of a Dewar flask containing water at 26°-30°C such that the irradiation cells containing the transferred sample were immersed. The whole assembly was loosely covered with a black cloth and placed in the refrigerator for a period of 3/4 of an hour to two hours. The net effect is a complete rinsing of the walls of the "Y" tube into the irradiation cell with slowly refluxing solvent without heating of the solution above 30°C. In view of the possibility of thermolysis of the S-S bond, this restriction seemed advisable. Sample preparation was concluded by allowing the sample to come to thermal equilibrium in the irradiation apparatus sample holder. Early in this work, some of the cemented edges of the Beckmann silica cell were found to leak. This problem was overcome by having the edges of the cells carefully fused. This was accomplished without degrading the optical properties of the cells.

D. Beer's Law - Thioctic Acid

1. Thioctic Acid at 366 mμ - See Table 19 and Figure 23 .

2. Thioctic Acid at 405 mμ - See Table 20 and Figure 24.

E. Beer's Law Data - 3,4-Benzopyrene and Benzanthrone at 405 mμ.

In order to compute the fraction of light absorbed by the disulfide in sensitization experiments, it is necessary to measure the density of very concentrated solutions of 3,4-benzopyrene. These measurements were made using a calibrated short path length cell (American Instrument, Co., # 51422) see Table 21 and Figure 25 . Similar measurements were

TABLE 19

BEER'S LAW PLOT - THIOCTIC ACID

366 mμ

Thioctic Acid[a] Conc. X 10	Optical Density	
	Type D	DK-1
15.00	1.260	1.396
12.00	1.034	1.109
7.50	0.635	0.663
4.50	0.385	0.396
3.01	0.262	0.268

a. Solutions in 6.535 M 2-propanol/benzene @ 25°C

FIGURE 23

BEER'S LAW PLOT-THIOCTIC ACID AT 405 mμ

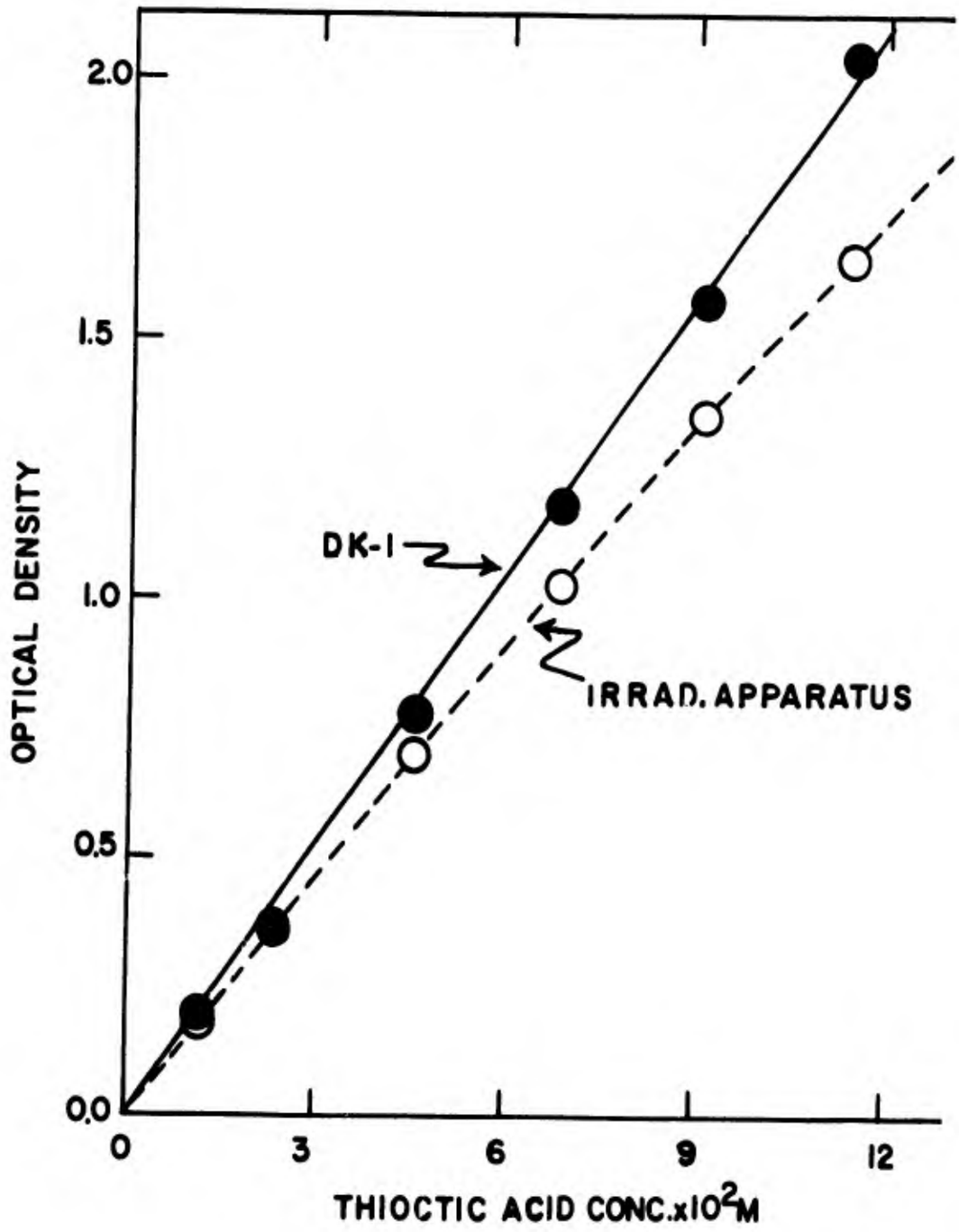

TABLE 20

BEER S LAW PLOT - THIOCTIC ACID

405 mμ

Thioctic Acid[a] Conc. X 10^2	Optical Density	
	Type D	DK-1
11.42	1.657	2.041
9.13	1.359	1.576
6.85	1.027	1.178
4.57	0.699	0.777
2.28	0.366	0.368
1.14	0.180	0.194

a. Solutions in 6.535 M 2-propanol/benzene @ 25°C

FIGURE 24

BEER'S LAW PLOT- THIOCTIC ACID AT 366 mμ

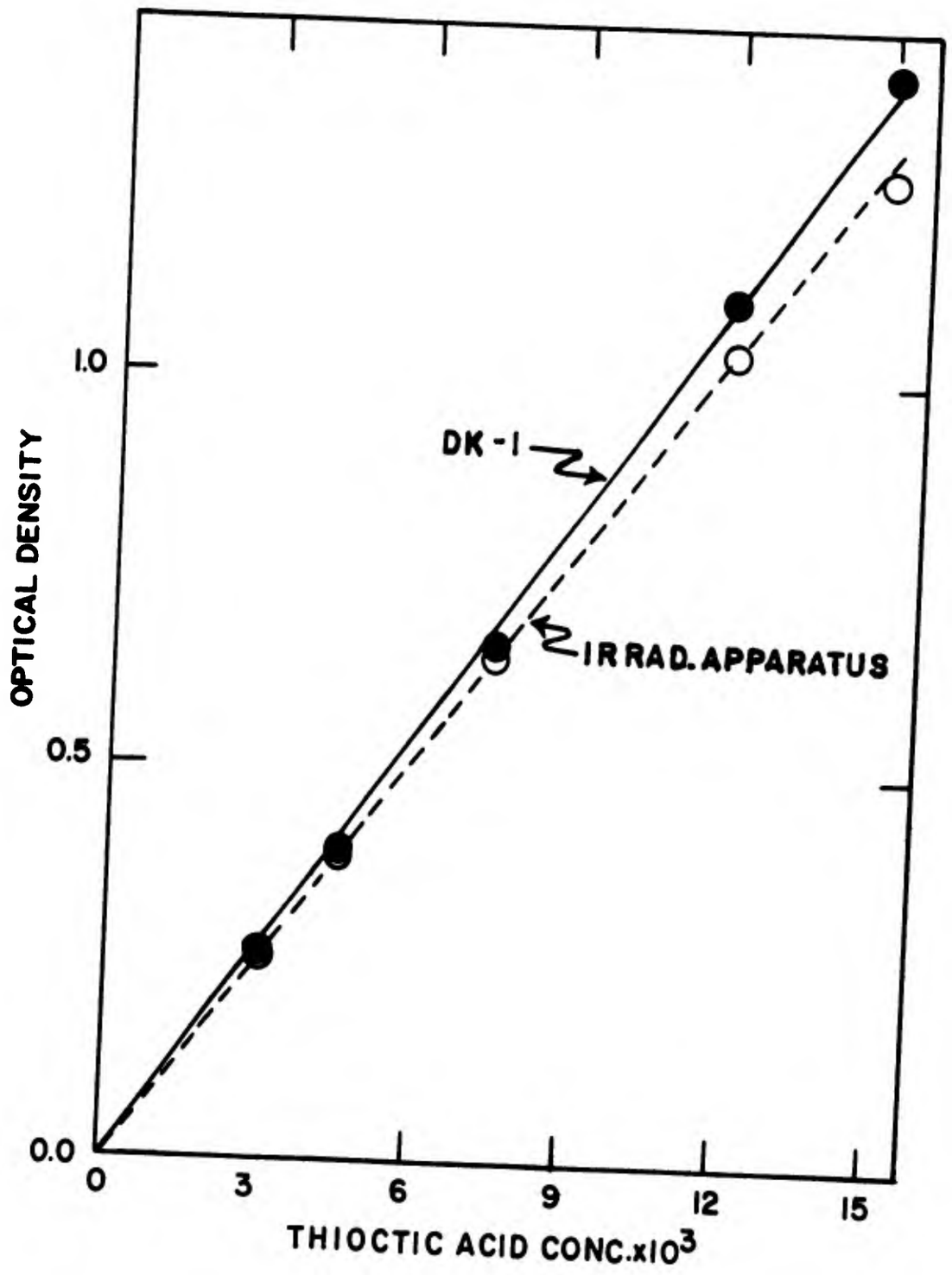

TABLE 21

BEER'S LAW PLOT - 3,4-BENZOPYRENE

405 mμ

3,4-Benzopyrene Conc. X 10^3	Optical Density	
	Type D	DK-1
41.38	0.696	1.38
33.10	0.590	1.05
26.48	0.505	0.828
21.18	0.424	0.689
16.95	0.349	0.567
13.56	0.282	0.442
8.13	0.181	0.250
4.07	0.100	0.130

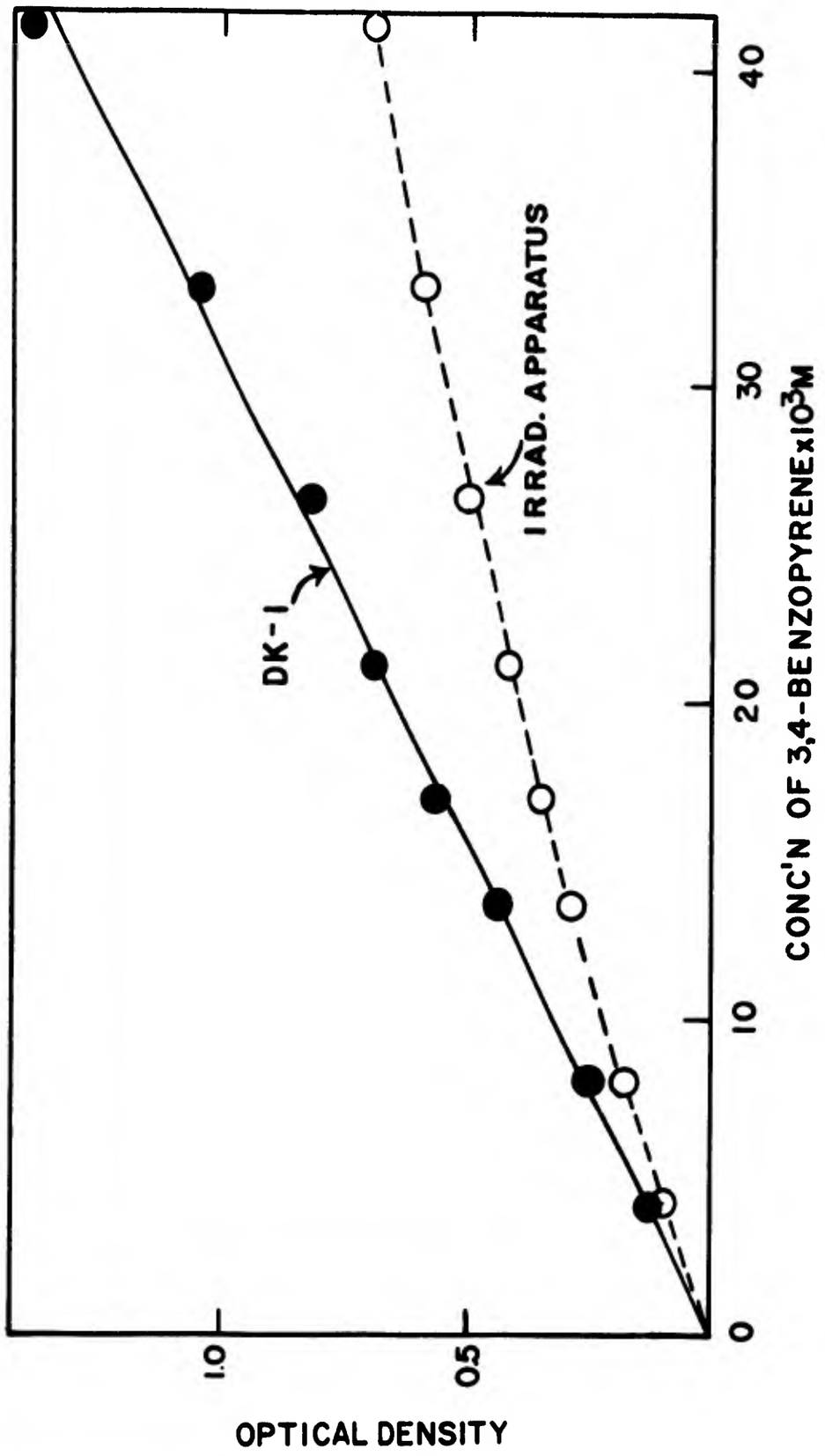
BEER'S LAW 3,4 - BENZOPYRENE, 405mμ
DK-1
IRRAD. APPARATUS
OPTICAL DENSITY
1.0
0.5
0
10
20
30
40
CONC'N OF 3,4-BENZOPYRENE x 10³M

FIGURE 25

made for benzanthrone (Table 22 and Figure 26).

F. Regeneration of Thioctic Acid from Photolyzed Solutions

Regeneration of thioctic acid from photolyzed solutions was accomplished by titration of the photolyzed solution with a *ca.* 3.2×10^{-3} M solution of iodine in benzene. The slight excess of iodine was discharged by the addition of a microdrop of n-dodecyl thiol. The regeneration could therefore be followed spectrophotometrically to its conclusion.

G. The Oxidation Product from 2-Propanol in the Thioctic Acid Photoreduction

GLC on Triton X 305/Chromasorb P at 70°C, 20-60 ml./min. on the Model 720 (F & M Scientific) failed to give evidence for the formation of acetone in the photolysis of thioctic acid. Considering the sensitivity of the detection, an upper limit of 5×10^{-3} M. acetone is inferred. The use of the Silicon Gum Rubber column at 100°C, 60 ml/min. indicated the pressure of a material in low concentration with retention behavior identical to that of pinacol (from pinacol/2-propanol standard solutions).

This identification was further confirmed by the identity of the behavior of this material with that of pinacol on a 10% Triton x 305 column/"Teflon". The greater sensitivity of the flame ionization detector of the chromatograph (F & M, Model 402) to which this column was fitted made possible the quantitative estimation of pinacol in the photolyzed solution.

Accordingly, conditions were determined for the rapid separation of pinacol from the photolyzed solution and the inclusion of a convenient internal standard. Conditions were set as follows: Flash heater, 190°C; detector, 215°C; oven, 114°C; carrier gas flow, 50 ml./min.; the internal standard was 2-octanol in 2-propanol.

TABLE 22

BEER'S LAW PLOT - BENZANTHRONE

405 mμ

Benzanthrone Conc. X 10^3 M	Optical Density: Irradiation Apparatus	Optical Density: DK-1
8.40	0.728	0.885
6.72	0.603	0.702
5.38	0.489	0.569
3.23	0.289	0.337
1.94	0.171	0.201
0.97	--	0.100

FIGURE 26

BEER'S LAW - BENZANTHRONE, 405 mμ

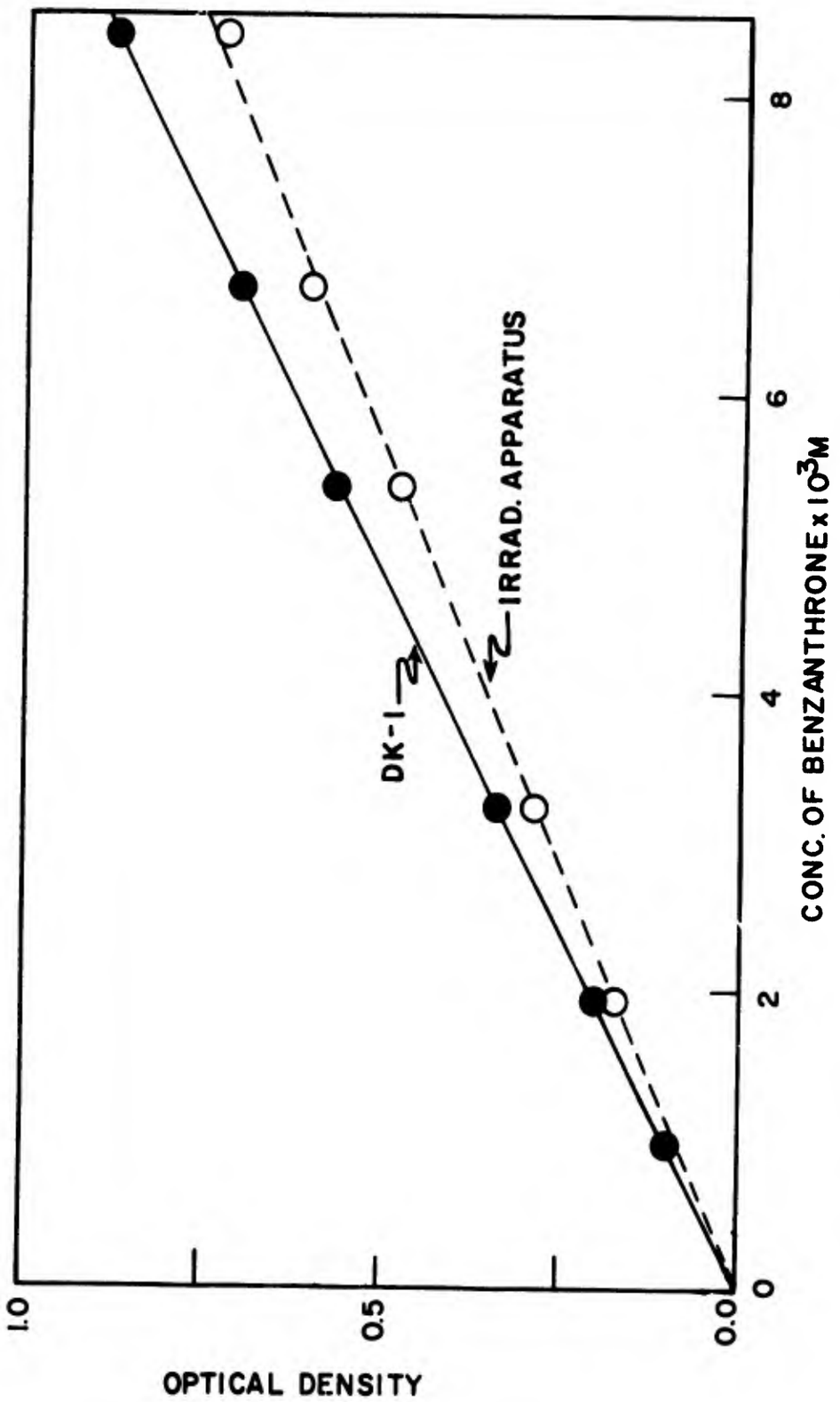

A series of dilutions of a stock solution of anhydrous pinacol (4.14×10^{-2} M) in 2-propanol was prepared. A 30 µℓ. sample of each of the stock dilutions (new, clean, dry 50 µℓ Hamilton syringe) was transferred to an analytically clean serum-capped round bottomed glass vial and a 40 µℓ volume of the 2-octanol/2-propanol solution was added. After thorough and careful mixing, a 4 µℓ sample was withdrawn and injected on the column. The identical procedure was followed with the other dilutions. A 300 ml. sample of 0.10 M thioctic acid in 6.54 M 2-propanol/benzene was photolyzed for 30.0 mins. at 405 mµ in the irradiation apparatus. The identical sample handling procedure as was used for the pinacol standards was followed. The remainder of the sample was rinsed into a titration medium containing a known aliquot of standard silver nitrate solution for the purpose of thiol analysis. The ratio of the area of the pinacol peak (planimeter measurement) to that of the 2-octanol peak afforded a calibration curve (averages of three injections), and thus a means for the quantitative estimation of pinacol.

H. The Photostability of Sensitizer Candidates

The photostability of sensitizer candidates was investigated where appropriate by irradiating a degassed solution of the candidate which absorbed *ca.* one half of the incident light for a period equal to or in excess of that employed in the sensitization experiments performed. The absence of a change in density and spectral structure was taken as an indication of photostability. Both 3,4-benzopyrene and 1,2:4,5-dibenzopyrene appeared to be photostable in high concentrations of 2-propanol at 405 mµ and 366 mµ. Irradiation of

2,3-(1-aci-anthrylene)-quinoxaline (AAQX) in 2-propanol at 366 mμ indicated a slight increase in optical density (*ca.* 0.01 units) after 40 minutes. Anthracene showed a definite decrease in density on irradiation at 366 mμ

References

(1) W. E. Lyons, Nature, 162, 1-04 (1948).

(2) A. F. Bickel and E. C. Kooyman, Nature, 170, 211 (1952).

(3) M. Nakasaki, J. Chem. Soc. Japan, Pure Chem. Sect., 74, 403, 518 (1953).

(4) S. G. Cohen and C. H. Wang, J. Am. Chem. Soc., 77, 211 (1952).

(5) C. Walling and R. Rabinowitz, *ibid.* 81, 1137 (1959).

(6) M. S. Kharasch, W. Nudenberg, and T. H. Meltzer, J. Org. Chem., 18, 1233 (1953).

(7) G. N. Lewis and D. Lipkin, J. Am. Chem. Soc., 64, 2801 (1942).

(8) P. J. Zandstra and J. D. Michaelsen, J. Chem. Phys., 39, 933 (1963).

(9) J. J. Windle, A. K. Wiersema, and A. L. Tappel, J. Chem. Phys., 41, 1996 (1964).

(10) K. Akasaka, J. Chem. Phys., 43, 1182 (1965).

(11) H. C. Box, H. G. Freund, and E. E. Budziuski, J. Chem. Phys., 45, 809 (1966).

(12) V. Du Vigneaud, *et al.*, J. Am. Chem. Soc., 75, 4879 (1953).

(13) A. P. Ryle and F. Sanger, Biochem. J., 60, 535 (1955).

(14) U. Schmidt, P. Grafen, and H. W. Goedde, Angew. Chem. Internat. Edit., 4, 846 (1965).

(15) L. J. Reed, "The Enzymes," Acad. Press, New York, 1960.

(16) M. Calvin and J. A. Barltrop, J. Am. Chem. Soc., 74, 6153 (1952).

(17) J. A. Barltrop, P. M. Hayes, and M. Calvin, *ibid.*, 76, 4348 (1954).

(18) R. B. Whitney, University of California Radiation Laboratory Report, UCRL-2755, Oct. 22, 1954; R. B. Whitney and Calvin, J. Chem. Phys., 23, 1750 (1955).

(19) V. Ramakrishnan, S. D. Thompson, and S. P. McGlynn, Photochem. Photobiol., 4, 907 (1965).

(20) A. M. Terenin and V. L. Ermolaev, Bull. Acad. Sci. U.S.S.R., Phys. Ser. 20, 471 (1956).

(21) S. Lipsky, J. Chem. Phys., 38, 2786 (1963).

(22) H. L. J. Backstrom and K. Sandros, Acta Chem. Scand., 14, 48 (1960)

(23) G. Porter and F. Wilkinson, Proc. Roy. Soc., A264, 1 (1961).

(24) G. Porter and F. Wilkinson, in "Luminescence of Organic and Inorganic Materials," Wiley, New York, 1962, p. 132.

(25) G. S. Hammond, *et al.*, J. Am. Chem. Soc., 86, 3196 (1964).

(26) J. R. Sampey and E. E. Reid, J. Am. Chem. Soc., 54, 3483 (1932).

(27) I. M. Kolthoff, W. E. Harris, Anal. Chem., 21, 963 (1949).

(28) M. D. Grimes, J. E. Puckett, B. J. Newby, and B. J. Heinrich, Anal. Chem., 27, 152 (1955).

(29) W. Conway and D. S. Tarbell, J. Am. Chem. Soc., 78, 2228 (1956).

(30) B. Muel and M. Hubert-Habart, J. Chim. Phys., 55, 377 (1958).

(31) W. A. Noyes and P. A. Leighton, "Photochemistry of Gases," Rheinhold Publishing Corp., New York, 1941, p. 77.

(32) G. P. Rabold, Air Force Cambridge Research Laboratories Report, Bedford, Massachusetts, AFCRL 65-715, July 1965.

(33) C. A. Parker and W. T. Rees, Analyst, 85, 587 (1960).

(34) J. Drobnik and E. Yeargers, J. Mol. Spectros., 19, 454 (1966).

(35) G. Bergson, Ark. Kemi, 18, 409 (1962).

(36) S. C. Abrahams, Quart. Revs., (London), 10, 407 (1952).

(37) A. H. Sehon, J. Am. Chem. Soc., 74, 4722 (1952).

(38) M. L. Huggins, J. Am. Chem. Soc., 75, 4123 (1953).

(39) T. L. Cottrell, "The Strength of Chemical Bonds," Butterworth's Scientific Publications, London, 1954.

(40) E. E. Smissman, and J. R. J. Sorenson, J. Org. Chem., 30, 4008 (1965).

(41) Unpublished results, W. M. Moreau, 1966.

(42) J. B. Birks and L. G. Christophorou, Spectrochimica Acta, 194, 406 (1963).

(43) H. J. Backer and Westerhuis, Rec. Trav. Chim., 71, 1065 (1952). C. A. 47 9898.

(44) M. W. Bullock, J. A. Brockman, Jr., E. L. Patterson, J. V. Pierce, M. H. von Saltza, F. Saunders, and E. L. R. Stokstad, J. Am. Chem. Soc., 76, 1828 (1954).

(45) C. E. Wilson and H. J. Lucas, J. Am. Chem. Soc., 58, 2396 (1936).

(46a) E. J. Clar, in "Polycyclic Hydrocarbons," Vol. 2, Academic Press, Inc., New York, 1964, p. 299.

(b) *Ibid.*, p. 143.

(c) *Ibid.*, p. 27.

(d) *Ibid.*, p. 146.

(e) *Ibid.*, p. 134.

(f) *Ibid.*, Vol. 1, p. 211.

(g) *Ibid.*, Vol. 1, p. 241.

(h) *Ibid.*, Vol. 1, p. 290.

(47) "Dictionary of Organic Compounds," Vol. 2, Oxford University Press, New York, 1965, p. 899.

(48) A. G. Anderson, Jr. and J. A. Nelson, J. Am. Chem. Soc., 73, 1232 (1951).

(49) C. Leikermann and M. Zsulfa, Berichte., 44, 210 (1911).

(50) R. Scholl and C. Seer, Ann., 394, 143 (1912).

5. The Photochemistry of 1,3,5-Trinitrobenzene

by W. M. Moreau and K. Weiss.

Introduction

The mono-, di-, and trinitroderivatives of benzene are a reactive class of compounds. The nitro groups are easily reduced and their presence on the ring enhances electrochemical reduction and displacement by nucleophillic reagents. The nitro group is resistant to further oxidation. Chemical reduction usually leads to a mixture of monomolecular and bimolecular products due to the high reactivity of the intermediate products.

By the use of powerful reducing agents such as stannous chloride in hydrochloric acid, nitrobenzene can be converted in high yield into aniline. By the use of milder reagents, and by the control of the pH of the reaction mixture, it is possible to generate the products of the intermediate stages of reduction. Haber[1] performed comprehensive studies on the electrolytic reduction of nitrobenzene, and his results demonstrated the primary sequences and side products resulting from the coupling of intermediates.

$$C_6H_5NO_2 \xrightarrow{2H} C_6H_5NO \xrightarrow{2H} C_6H_5NHOH \xrightarrow{2H} C_6H_5NH_2$$

$$C_6H_5NO + C_6H_5NHOH \xrightarrow{-H_2O} C_6H_5N{=}NC_6H_5{\scriptstyle O}$$

$$C_6H_5N{=}NC_6H_5 \xrightarrow{2H} C_6H_5\overset{H}{N}-\overset{H}{N}C_6H_5 \xrightarrow{2H} C_6H_5NH_2$$

Nitrosobenzene and phenylhydroxylamine are themselves very reactive substances which are susceptible to air oxidation, condensation, or reduction. In the case of 1,3-dinitrobenzene (DNB) and 1,3,5-trinitrobenzene (TNB), the monomolecular reduction products are very difficult to prepare and the bimolecular azoxy compound predominates in most attempted syntheses. In the case of TNB, only 3,5-dinitrophenyldroxylamine[2] (DNPH) and 3,3';5,5'-tetranitroazoxybenzene[3] (TNAB) have been reported.

Nitrobenzenes also function as Lewis acids and form many charge-transfer complexes.[4] Nucleophillic anions, such as the ethoxide ion,

form ionic addition compounds with TNB. Meisenheimer[5], on the basis of extensive studies of these compounds, postulated their structure as

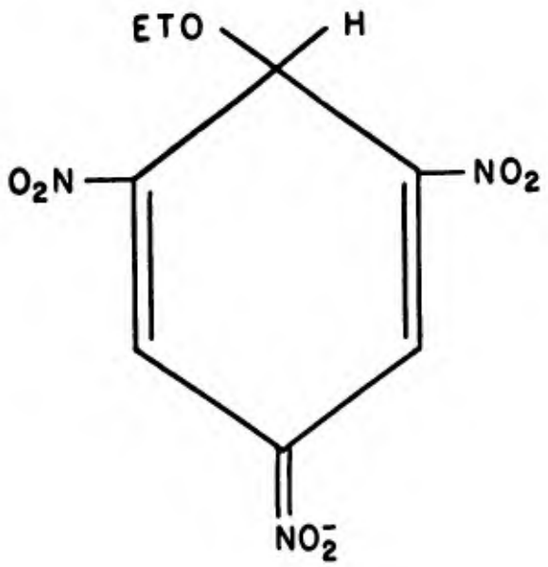

This structure is supported by recent ultraviolet[6] (UV), infrared[7] (IR), nuclear magnetic resonance[8] (NMR), and kinetic studies.[9]

The spectroscopy and excited state chemistry of nitrobenzenes has received limited attention. The lowest lying singlet and triplet states of aromatic nitro compounds have been assigned to originate from the n-Π^* transition of the nitro group.[10] The triplet state of nitrobenzene lies at 60.0 Kcal. above the ground state.[10] The excited states of other nitroaromatics have not been investigated. Trinitrobenzene shows no fluorescence or phosphorescence under any conditions. One can infer by analogy to ketonic chromophores, that the weak long wavelength band

(300 - 360 mμ) is associated with the forbidden n-Π^* transition. TNB also exhibits a broad high intensity band with absorption maximum at 245mμ which most probably represents the intramolecular charge-transfer transition between the benzene ring and the nitro group.[13] The continuous photolysis of gaseous nitrobenzene produces nitrosobenzene and p-nitrophenol as the major products[11], while photolysis in isopropanol produces phenylhydroxylamine.[12] The continuous photolysis of TNB in alcohols produces TNAB as the major product.[3] Gold and Rochester[6] have studied the photolysis of TNB in basic solutions and have demonstrated the displacement of one of the nitro groups. Radicals have been detected and characterized in the photolysis of nitro-aromatics in tetrahydrofuran[14] and in basic solutions.[15] Photochromic nitro compounds have been investigated by flash photolysis[16] and their behavior has been interpreted in terms of intramolecular hydrogen abstraction to form aci-nitro compounds.

In summary, the spectroscopic knowledge of the nitrobenzenes is sparse. Research efforts thus far have heavily emphasized the synthetic aspects and the ESR of radical anions. Detailed knowledge of the photochemistry of these compounds, particularly the dynamic aspects, is lacking.

The purpose of this research is to establish detailed mechanisms for the photochemical reactions of the nitrobenzenes. The techniques employed are continuous photolysis, flash photolysis, and ESR spectroscopy. Data are presented on the photoreactivity under a wide variety of conditions, and the mechanistic implications are summarized in terms of reaction schemes.

EXPERIMENTAL

A. Solvents

1. Methanol

Vogel's[26] method was used for the purification of this solvent. Methanol (Baker's Reagent) was refluxed with 2-furfural and sodium hydroxide, followed by fractional distillation from magnesium turnings using a 100-cm. long Podbielniak "Heligrid"-packed column. Gas chromatography (GC) (10% "Triton" x-305, 80°C) showed an unidentified impurity concentration of ca. 10^{-4}M.

2. Ethanol

Absolute ethanol (United States Industrial) was distilled from magnesium turnings using a 100-cm. long Podbielniak "Heligrid"-packed column. No impurities were detected by GC (10% "Triton" x-305, 85°C).

3. 1-Propanol

The solvent (Fisher Scientific) was distilled through a 90-cm. long "Mini-cal" Podbielniak spinning band column at a reflux ratio of 100 to 1. The material was free of impurities as indicated by GC (10% "Triton" x-305, 90°C).

4. Hexane

Hexane (Phillips Research Grade) was passed through a short silica gel column and was distilled from sodium wire. GC (20% silicone gum rubber, 75°C) revealed ca. 10^{-3}M of unidentified impurities to be present.

5. Tetrahydrofuran (THF)

Tetrahydrofuran (Fisher Reagent) was distilled from lithium aluminum hydride. The material was found to contain ca. 10^{-4}M of unidentified impurities by GC analysis (10% "Triton" x-305, 80°C).

6. 1,2-Dimethoxyethane

Dimethoxyethane (Matheson, Coleman, and Bell) was distilled from lithium aluminum hydride.

7. Miscellaneous Solvents

The following reagent grade solvents were used without further purifications: N,N'-dimethylformamide, benzene, acetonitrile, ethyl acetate, methylene chloride, carbon tetrachloride, and acetone. For systems involving aqueous solvents, distilled water was used.

8. Buffered Water-Ethanol Solutions

Alcohol-water solution (50/50) was buffered at pH 2.0, 7.0, and 9.0 using the buffer of Clark and Lubs.[27] The pH of the solution was checked against a pH 7.0 (buffered aqueous reference solution) using a Beckman Model G pH meter.

B. Materials

1. 1,3,5-Trinitrobenzene (TNB)

This compound was prepared by the method of Vogel.[17] After three recrystallizations from ethanol, it had m.p. 122-123°C (lit.[18] 122-123°C). TLC (benzene, hexane (2/8), silica gel) revealed no impurities in this material.

2. 1,3,-Dinitrobenzene (DNB)

Dinitrobenzene (Fisher Scientific) was thrice recrystallized from ethanol. No foreign material was detected by TLC (benzene, silica gel).

3. Nitrobenzene (NB)

Nitrobenzene (Baker Chem., 500 ml.) was shaken three times with 100 ml. of 40% sodium hydroxide solution and was washed with water. The material was then steam distilled, dried over anhydrous calcium sulfate, and was finally distilled in vacuum to yield a faintly yellow liquid, b.p. 53°C (0.8 mm. Hg.). The pure compound is reported to be colorless.[19]

4. 3,3',5,5'-Tetranitroazoxybenzene (TNAB)

The method of Stenberg and Holter[3] was used to prepare TNAB in very low yield (5%). A facile preparation was found based on the Caro's acid oxidation of 3,5-dinitroaniline:

Into a three-necked 500-ml. round bottom flask equipped with stirrer, thermometer, and immersed in a water bath, was placed 20-ml. of concentrated sulfuric acid and 5 ml. of

water. 3,5-Dinitroaniline (5.0g.) was slowly dissolved in the solution. Caro's acid was prepared by mixing 20 ml. of concentrated sulfuric acid and 30g. of finely ground potassium persulfate with cooling in an ice bath. The Caro's acid solution was added to the mixture followed by ice (100g.), and the mixture was kept at 52°C for 4 hours. At that time, 10g. of potassium persulfate was added and the solution was stirred overnight for 12 hours. The yellow slurry was poured into 500 ml. of ice water, filtered, and vacuum dried. The yellow precipitate was thrice recrystallized from glacial acetic acid. It was characterized by comparison with an authentic sample of TNAB (m.p., IR, UV, and TLC). The material had m.p. 185-186°C (lit.[3] 185-186°C).

5. 3,5-Dinitroaniline (DNA)

This compound (Aldrich Chemical) was thrice recrystallized from ethanol. No impurities were detected by TLC (benzene, silica gel).

6. 3,5-Dinitrophenylhydroxylamine (DNPH)

The method of Cohen and Daken[2] was employed with some modifications. TNB (9.0g.) was suspended in 100 ml. of ethanol and 0.5 ml. of 3.7% aqueous ammonia solution was added. Hydrogen sulfide was bubbled through this solution for exactly 10.0 minutes. The solids were precipitated with water, filtered, and recrystallized five times from benzene to yield 1.0g. of crude product. The material was chromatographed on 200g. of

alumina (Woelm, neutral grade) to separate the sought compound from TNB and DNA. The yield of 3,5-dinitrophenylhydroxylamine was 100 mg., m.p. 135-136°C (lit.[2] 135-137°C). A positive test was noted with Tollen's Reagent.[2] The material is susceptible to air oxidation and was stored in vacuum.

7. 3,5-Dinitronitrosobenzene

Unsuccessful attempts to prepare this compound involved the following methods:

(a) Oxidation of 3,5-dinitroaniline with:

Caro's acid[20]

Peracetic acid[21]

Nitric acid

Hydrogen peroxide (30%)[22]

Chromium trioxide

Acidic potassium dichromate

(b) Oxidation of 3,5-dinitrophenylhydroxylamine with:

Chromium trioxide[23]

Peracetic acid (30%)

Acidic potassium dichromate

(c) Reduction of TNB with:

Zinc (followed by potassium dichromate oxidation)[24]

Hydrogen and palladium catalyst (followed by potassium dichromate oxidation)[24]

Lithium aluminum hydride

In each case, no evidence could be obtained for the presence of a nitroso compound, and 3,3',5,5'-tetranitroazoxybenzene was the main product.

An impure sample of 3,5-dinitronitrosobenzene was obtained by oxidizing DNA with hydrogen peroxide as follows:

3,5-Dinitroaniline (1.0g.) was dissolved in 50 ml. of methylene chloride and the solution was added to a mixture of 4 ml. of formic acid, 1 ml. of 90% hydrogen peroxide, and 10 ml. of methylene chloride. The mixture was refluxed for 5 hours, and another 11 ml. of hydrogen peroxide was added, followed by refluxing for an additional 2 hours. The green methylene chloride layer was separated, dried over anhydrous calcium sulfate, and was concentrated at room temperature. TLC (benzene/acetonitrile (2/8) silica gel) examination showed at least five products in the residue.

This solid was steam distilled and sublimed (40°C, 1 mm.) to yield 50 mg. of pale yellow product, m.p. 125-129°C. Examination on TLC (benzene/ethyl acetate (2/8), silica gel) showed one major product with ca. 10% impurities. The visible spectrum in ethanol revealed a broad absorption band with a maximum at 760 mμ (cf., Fig. 1). Further recrystallization from benzene did not remove the impurities. A sample in benzene which had stood for 24 hours in the dark was examined on TLC and revealed several new impurities.

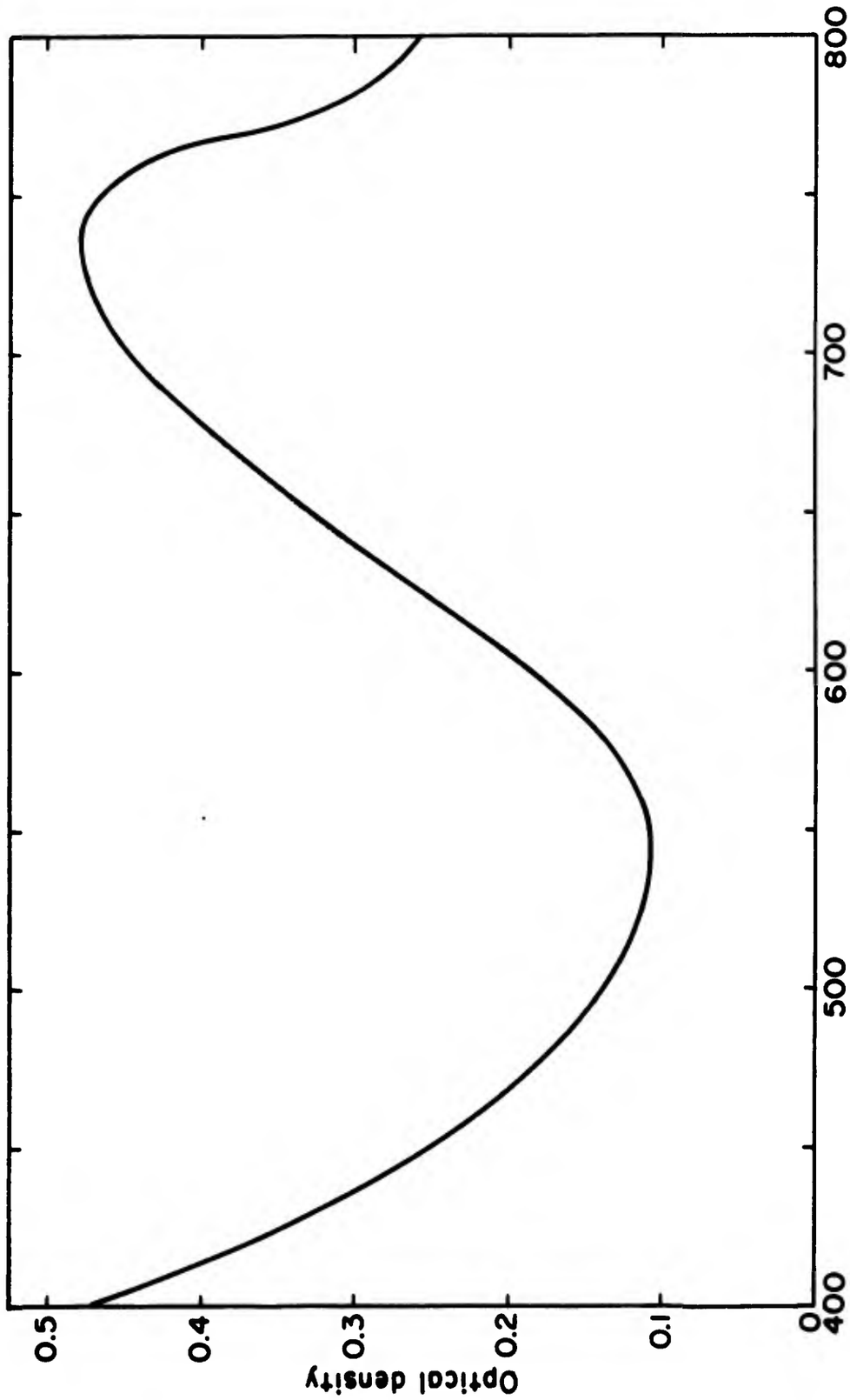

Figure 1 - Absorption Spectrum of the Product of the Oxidation of DNA in Ethanol

8. Identification of Stenberg Reaction Product II

Stenberg and Holter[3] isolated two major products from the continuous irradiation of a suspension of TNB in ethanol and identified one of them as TNAB. A sample of the unknown product was received from Dr. Stenberg and identified on the basis of its UV and IR spectra, TLC, and mixed melting point as 3,5-dinitroaniline.

9. Reaction of TNB with Lithium Aluminum Hydride

TNB (0.01M in anhydrous diethyl ether) was added dropwise to an ether solution of 0.01M lithium aluminum hydride. The unreacted hydride was destroyed with an excess of water after the mixture had stood for one hour at room temperature. The ether layer was separated, dried over calcium sulfate, and concentrated to 1 ml. on a rotary evaporator. TLC (acetonitrile, silica gel) revealed DNA and two other major products. The red solution decolorizes upon standing in the dark. The following properties of a thoroughly degassed solution of the reduction product were observed.

(a) Immediate decolorization with gaseous nitric oxide, dilute nitric acid, and slowly decolorization (12 hours) with gaseous oxygen.

(b) Irradiation of a degassed ethanol solution with 546 mμ light (Osram 500-watt high pressure mercury lamp, Bausch and Lomb Monochromator) resulted in the disappearance of the visible bands.

(c) No ESR absorption was observed at low temperature (-135°C) or at room temperature with a fresh solution prepared by mixing degassed solutions of 0.01M lithium aluminum hydride and 0.01M TNB in ether.

10. Trinitrobenzene Radical Anion

The TNB radical anion was generated according to Ward[25] by the reaction of sodium metal with a degassed solution of TNB in 1,2-dimethoxyethane. The solvent was dried over lithium aluminum hydride and degassed on a high vacuum rack. The solvent was distilled sodium and TNB. The vessel was then sealed and the ultraviolet spectrum was recorded. The ESR spectrum of the anion checked with the spectrum observed by Ward.

C. Apparatus and Methods

1. Gas Chromatography (GC)

The gas chromatographic analyses were performed with a F & M Model 720 temperature programmed dual column instrument. The thermal conductivity detector was maintained at 300°C, and all analyses were performed at least in duplicate. The columns employed were 10% "Triton" x-305 on "Chromosorb" (8 ft. of 8 mm. diameter) for polar materials and 20% silicone gum rubber on "Chromosorb" (6 ft. of 8 mm. diameter) for non-polar materials. Helium (60 ml./min. was used as the carrier gas.

2. Infrared (IR) and Ultraviolet Spectra (UV)

The infrared spectra were recorded on a Beckman IR-5 spectophotometer equipped with sodium chloride optics. Samples were run in pressed potassium bromide discs.

A Beckman DK-1 spectrophotometer was used to record the ultraviolet spectra. The instrument is equipped with a constant temperature block. Spectra were recorded in 1.0-cm. cells unless otherwise noted.

3. Melting Points

All melting points and boiling points recorded are uncorrected.

4. Thin Layer Chromatography (TLC)

A slurry of 30g. of Woelm silica gel G or 32g. of Woelm aluminum oxide G in 45 ml. of distilled water was used to coat glass plates to a thickness of ca. 275μ. The plates were dried for 2 hours at 110°C prior to use. Eastman Kodak "Chromogram" TLC plates (silica gel (70μ) on polyvinyl alcohol sheets) were also employed. The TLC technique was used for the examination of photolyzed solutions and for the check of the purity of materials. The eluting solvents employed were indicated in each application.

5. Continuous Photolysis Apparatus

This apparatus (type A) which has been previously described[28], accomodates test tube-size samples or samples in rectangular (1 cm. × 1 cm. × 46 mm.) spectrophotometer cells. It consists

of a Phillips (HPK) 125-watt high pressure mercury lamp whose arc is focused onto the sample by means of a simple optical system. The sample is held in a constant temperature water-cooled block.

An immersion-type B apparatus, which has also been previously described[29], was used. A General Electric high pressure mercury lamp (100-400 watt) whose outer glass envelope has been removed is concentrically surrounded by a water-cooled jacket, filter solution, and an annular reaction zone. Constant temperature is maintained by passage of cooling water through a water jacket adjacent to the lamp. The apparatus is provided with means of stirring and degassing the solution. Samples can be removed through sampling stopcocks without introduction of air. Depending on the size of the outer vessel, 200 to 500 ml. of photolysis solution can be accommodated.

6. Irradiations with ESR Measurements

Since short-lived radicals are involved in these studies, the irradiations were performed directly in the ESR cavity. A 150-watt medium pressure mercury lamp (Hanovia, no. 30600) was used for this purpose. The arc was focused on the sample with a quartz lens.

7. Low Temperature Irradiations

The assembly for low temperature irradiations was designed to fit in the small cell compartment of the Beckman DK-1

spectrophotometer. The apparatus shown in Figure 2 represents a dual beam modification of a design by Nelson.[30] Two cylindrical (1.0 cm. path length) quartz cells (sample and reference) with evacuated quartz windows are located in a rectangular insulating "Styrofoam" box. The box was glued together with a special rubber cement (3M Co., no. EC 801) which retains its adhesive properties at liquid nitrogen temperature. A side arm is provided for degassing the samples. During an operation, dry air is blown over the protruding evacuated windows to prevent moisture condensation. This design allows for dual beam spectrophotometry of samples using pure solvent glass in the reference cell. The irradiation is also accomplished without passage of light through the coolant.

In working with ethanol solutions at liquid nitrogen temperatures it was found that thorough drying of the solvent and slow cooling of the vessel was necessary to prevent the ethanol glass from cracking. Best results were obtained by initially precooling the vessel with solid dry ice before proceeding to lower temperatures.

8. Flash Photolysis Apparatus

The flash unit is described in Section 2 of this report and in Appendix B. It was used with photoelectric detection (EMI 9558 B and DuMont 6911 photomultiplier tubes). The spectrograph was fitted with an exit slit of 1 mm. width, corresponding to a band pass of 10Å. Liquid samples were flashed in cylindrical "Pyrex" vessels which are symmetrically surrounded by the four flash tubes. To assure reasonably uniform irradiation of the samples, the optical density of the solution

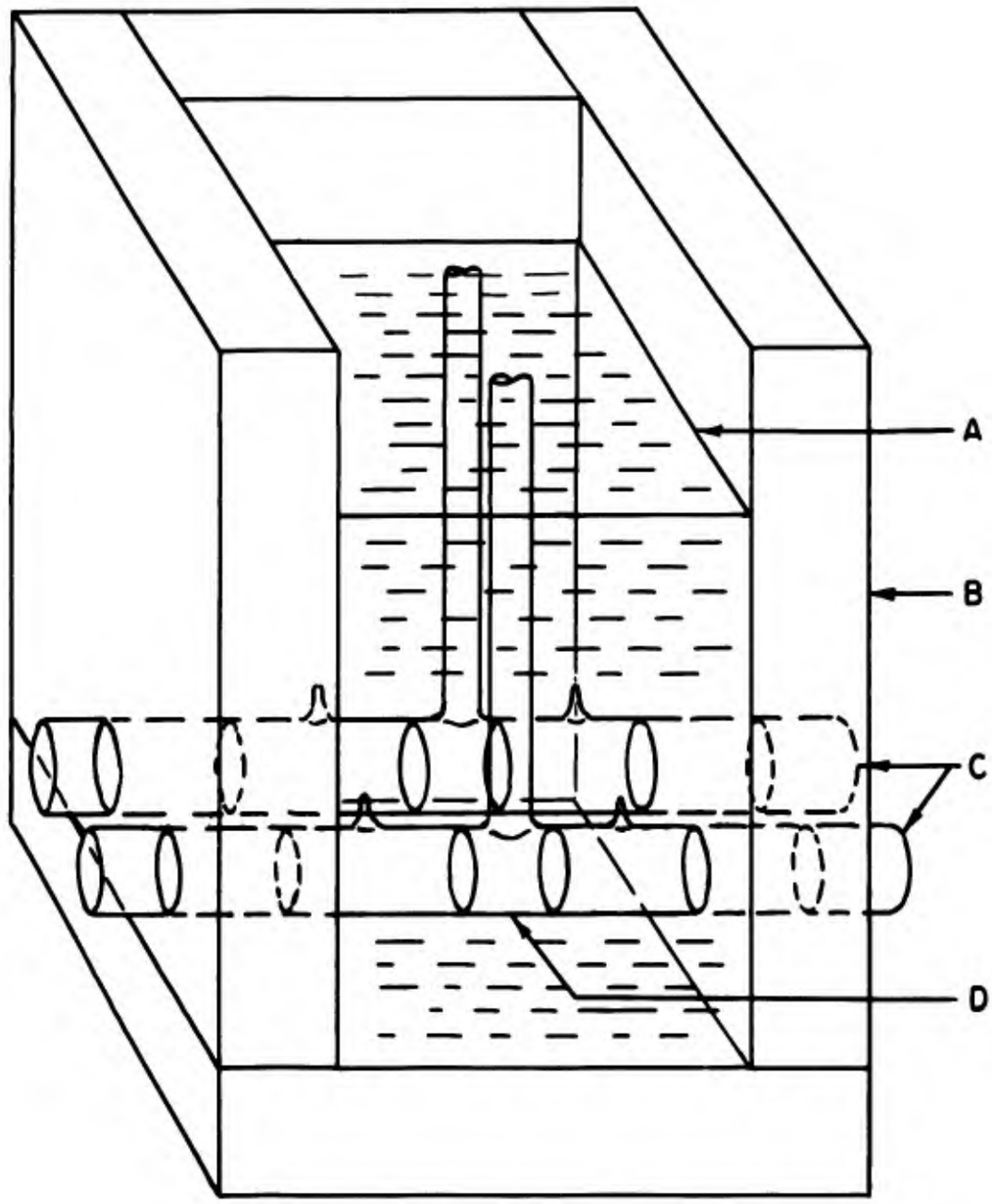

Figure 2 - Low Temperature Photolysis Cell

A. Refrigerant
B. "Styrofoam" (1/2" thick)
C. Evacuated outer quartz windows
D. Quartz absorption cell (1-cm. path)

is adjusted so that a maximum of ca. 30% of the light is absorbed in the cross-section diameter of the tube. The sample cell is protected against continuous photolysis by a suitable filter. For the nitroaromatics the filter solution was a 1.0-cm. path length of saturated sodium nitrite which absorbs all light below 400 mμ. The total length of exposure to the filtered monitoring light was limited to 30 secs., and tests established that under these conditions the deterioration of flashed and fresh sample is not measurable.

In the specific case of the flash photolysis of TNB in alcohol with the flash intensity and TNB concentration employed, a permanent light-sensitive product is formed. Ordinarily this will necessitate the separate degassing of a fresh sample for each run. A simple arrangement was designed to provide fresh samples for each flash without a separate degassing procedure (Appendix C). In this apparatus, ca. 500 ml. of degassed solution provided 20 fresh samples for flashing. In some instances a special filter-jacketed cell was used. It consists of a 12-cm. x 2-cm. "Pyrex" tube with an outside annular filter jacket of 0.76-cm. path length. This cell was used to reduce the scattered light when the kinetics of formation was sought. In the case of TNB, the "Pyrex" glass cutoff at 290 mμ confined the absorption of exciting radiation to the band region from 290-400 mμ. The transient absorption is recorded at wavelengths above 420 mμ. A cobalt chloride filter solution,[31] which transmits from 290 to 360 mμ and absorbs strongly from 360 to 600 mμ was employed in this instance. Ideally, this technique makes it possible to flash with essentially monochromatic light and to record the transient kinetics with minimal background correction for scattered light from the flash.

For flashing the nitroaromatics an input energy of 450 joules/tube was normally used. This unit is capable of a maximum output energy of 1400 joules/tube with a flash duration of 40 μsecs (1/e) value. The flash intensity was varied by changing the input energy voltage (6-12 kv) or by using only two flash lamps. The samples were flashed at room temperature (ca. 24°C). New flash tubes were used at the first sign of tube deterioration (ca. 1000 flashes). A complete transient spectrum was always completed in a daily run to minimize the discrepancy in data obtained in subsequent experiments due to intensity changes. The amount of transient (optical density) formed is proportional to the flash intensity. While the light output decreases slowly with use, steps were taken to assure that there were no significant intensity variations in a series of measurements such as those used for the construction of transient spectra.

The oscilloscope display is recorded photographically ("Polaroid" type 47A film) and a typical record is shown in Figure 3. The light intensities are proportional to the output voltage as follows:

$$I \propto V_o \qquad \ldots\ldots (1)$$

$$I' \propto V_t, V_t', \text{ or } V_{oo} \qquad \ldots\ldots (2)$$

where I' is the intensity attenuated by the transient, and I is the unattenuated intensity. With the monitoring light off, V_{off} is set at the top of the oscilloscope grid. With the sample in place and the light on, the oscilloscope is triggered prior to the flash initiation and the transient display is recorded. The oscilloscope time axis can be varied in the range from 1 μsec./cm. to 10 sec./cm. The volt

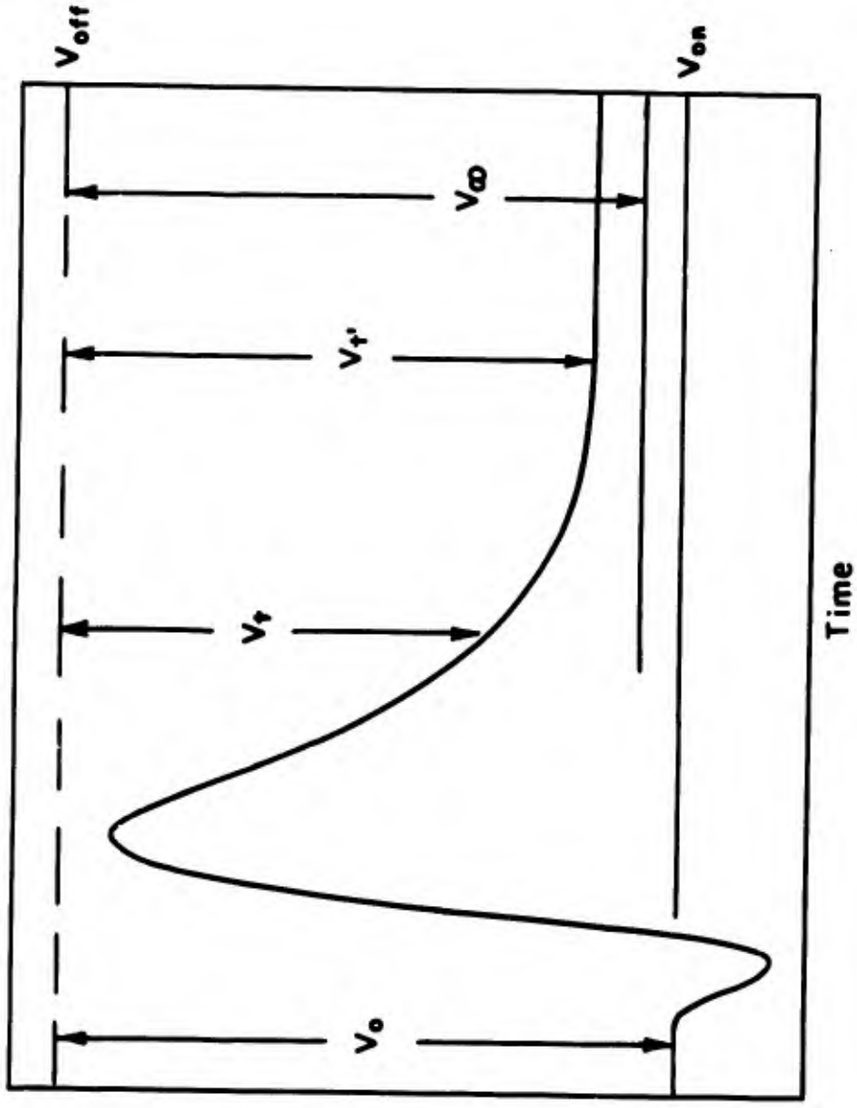

FIGURE 3: Diagram of an Oscilloscope Display Record

(signal) axis can be varied with the scope gain or by amplification of the phototube output. In classic flash photolysis studies (cf., G. Porter[32]) the system is reversible and the transient trace returns to the base line (V_{on}). In the case of TNB a permanent absorbing product is formed and a trace (V_{∞}) is recorded by manually triggering the scope trace 4 minutes after the flash.

The optical densities (D) are defined by

$$D_o = \log \frac{I_o}{I} \qquad \ldots(3)$$

$$D' = \log \frac{I_o}{I'} , \qquad \ldots(4)$$

where I_o is the intensity of the monitoring light incident on the sample. The difference in optical density is

$$\Delta D = \log \frac{V_o}{V_o - Vt} = D' - D_o . \qquad \ldots(5)$$

The transient spectrum of the solution is obtained by adding D_o, the optical density of the original solution (obtained by separate measurement with a spectrophotometer) to ΔD. The transient spectrum is obtained by flashing fresh samples with constant flash intensity at a series of wavelength increments.

The "Polaroid" records were converted from analog to digital form with the aid of a Gerber Digital Reduction System. The digital readout was punched on IBM cards for use with a computer program which tests the basic rate laws.

The program was written in Fortran language , and was executed on an IBM 7094 computer at the M.I.T. Computation Center.

9. Preparation of Samples for Flash and ESR Experiments

Sample solutions were, in all cases, degassed by repeated freeze-pump-thaw cycles operating between liquid nitrogen and room temperature. These operations were performed on a high vacuum line ($< 10^{-5}$ mm. Hg pressure). An argon gas (Med-Tech. Gas, 99.9% purity) overpressure of 1-2 atmospheres was used with all solvents except absolute alcohol and alcohol/water solutions. For the ESR experiments, the samples were degassed inside arms of the apparatus and were examined in 3-mm. diameter quartz tubes or in flat 1-mm. quartz cells. Breakseals were used to add degassed reagent solutions or gases to the photolyzed solutions.

10. ESR Measurements

A Varian V-4500 spectrometer with 100-kc field modulation and a six-inch magnet was employed. The standard Varian variable temperature accessory, in which cooling is effected by the passage of dry nitrogen through a coil immersed in a liquid nitrogen bath, provided temperature control. Temperatures were measured with a copper-constantin thermocouple, and the magnetic field was calibrated with a Fremy's salt solution in 10% sodium bicarbonate.

Kinetic measurements were performed by riding a major peak of the first derivative curve; a blank correction was made for thermal effects due to the irradiating light.

11. Continuous Photolysis of TNB in Ethanol

A 5 ml. sample of 1.0×10^{-3}M TNB in degassed ethanol was irradiated in the apparatus described in Section A. The irradiation was carried out in a 1.0-cm. Pyrex absorption cell. The solution was concentrated to 0.1 ml. and examined by TLC (benzene/hexane (9/1), silica gel). The results are tabulated below to show the comparison with known compounds.

Spot	Rf.	Compound	Rf.
1	0.2	TNAB	0.2
2 (trace)	0.8	DNA	0.8
3	0.95	TNB	0.95

A similar photolysis was performed with 4.0×10^{-4}M TNB and the ultraviolet spectrum was recorded (cf., Fig. 4). Only TNAB was found as a product.

A preparative-scale photolysis was performing using a 500 ml. of 1.0×10^{-3}M TNB in degassed ethanol in the apparatus described in Section B. The sample was irradiated (200 watt lamp) for 14 hours at 20°C and the yellow solution was evaporated to dryness and chromatographed on 150g. of alumina (Woelm, neutral grade). The fractions and their

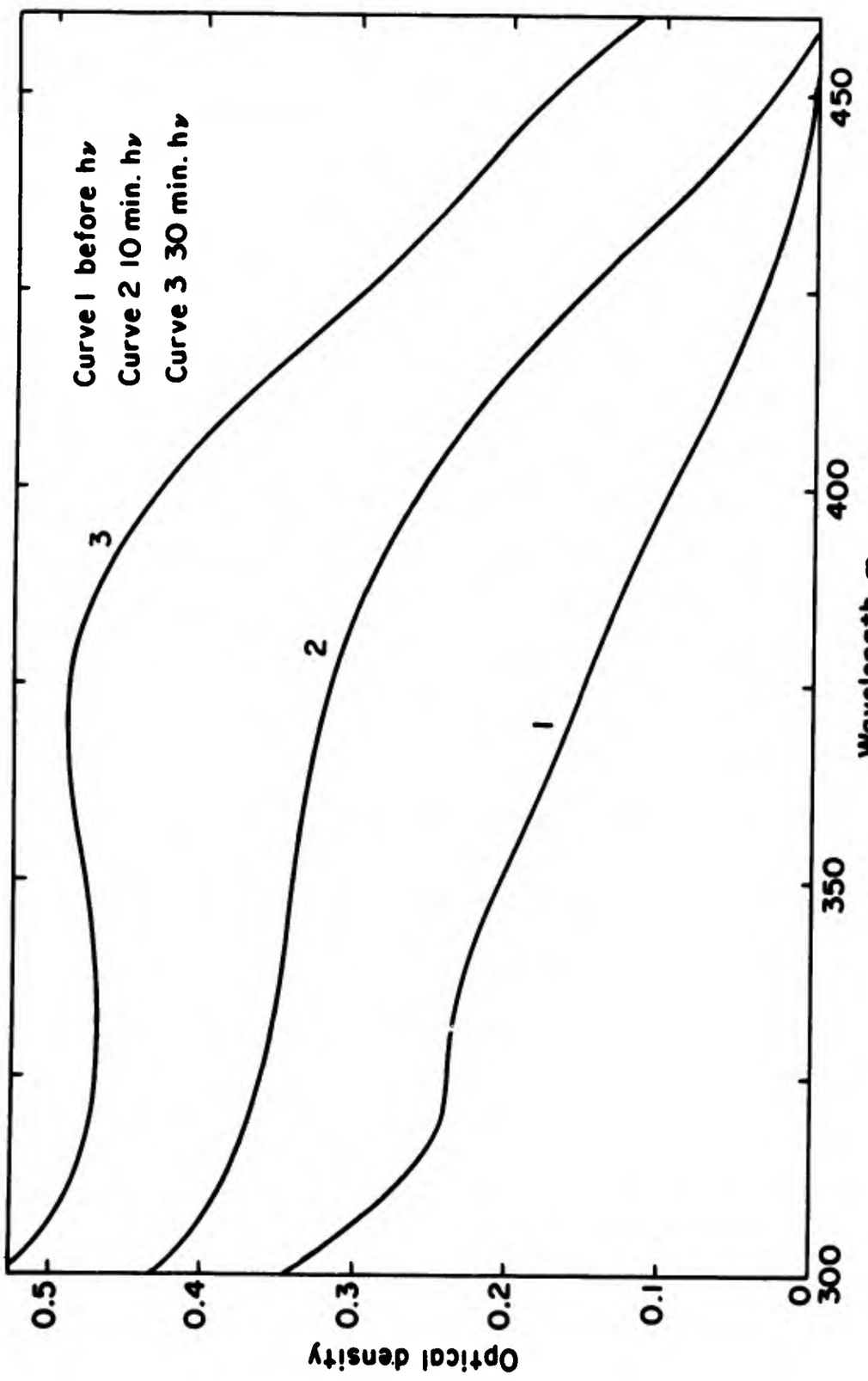

FIGURE 4: Absorption Spectrum of 1.0×10^{-3} M TNB in Ethanol after Photolysis

identity as established by TLC and IR were

Elutant	Compound	% Recovery
Benzene/hexane (2/8)	93 mg. of TNB	93
Benzene/acetonitrile (9/1)	5 mg. of TNAB	5

A solution of 500 ml. of 1.0×10^{-3}M TNB in ethanol was irradiated 14 hours in the above apparatus. Presaturated (ethanol) argon was continuously bubbled through the solution and the exit argon gas was bubbled through a solution of 2,4-dinitrophenylhydrazine to trap any acetaldehyde. Crystals were collected and identified as the acetaldehyde derivative by comparison with an authentic sample, m.p. 164-166°C (lit.[33] 168°C).

12. Continuous Photolysis of TNB in Methanol

A degassed solution of 1.0×10^{-3}M TNB was irradiated in a 1.0-cm. Pyrex cell in the Type A apparatus. The resultant ultraviolet spectrum is shown in Figure 5. TLC (acetonitrile, silica gel) of the red solution gave the following Rf values: 0.2, 0.6 (TNAB), 0.9 (DNA), 1.0 (TNB). The 0.2 spot was scraped off and redissolved in methanol and the visible bands of the solution are attributed to this compound.

13. Continuous Photolysis of TNB in Miscellaneous Solvents

4.0×10^{-4}M TNB in degassed solvents was photolyzed in various solvents in the Type A apparatus and the ultraviolet

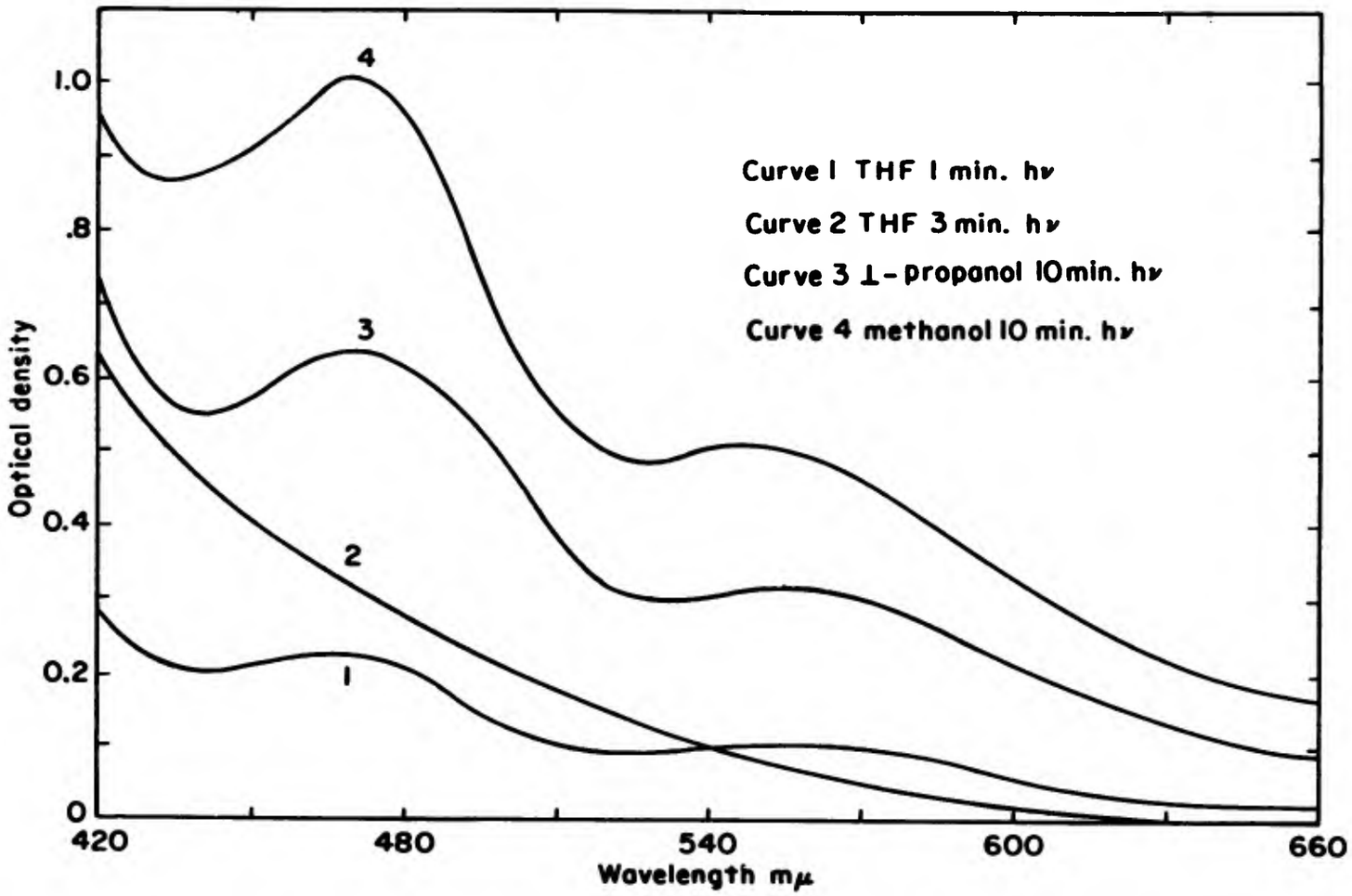

FIGURE 5: Absorption Spectrum of 4.0×10^{-4}M TNB after Photolysis in Various Solvents

spectrum was examined for product formation (cf. Fig. 5). Irradiation of TNB in 1-propanol and in THF with short exposure produces a red solution with a visible absorption spectrum identical to that of the flash product. Irradiation in 2-propanol, benzene/hexane, and cyclohexane induces a yellow color with no defined visible bands. TNB in water or in 1M sulfuric acid appears to be very stable to continuous irradiation.

14. Isolation of Flash Product of TNB in Ethanol

When a degassed (4.0×10^{-4}M) solution of TNB in methanol, ethanol, 1-propanol, 2-propanol, or tetrahydrofuran is flashed, a product is formed which absorbs in the visible region (cf. Fig. 15). The visible band is light-sensitive and bleaches upon further irradiation with filtered light (wavelengths above 410 mμ). No flash product is formed when TNB is flashed in benzene, water, dichloromethane, acetonitrile, or cyclohexane with comparable flash conditions. The flash product is also formed in air-saturated solutions and in buffered water-ethanol mixture of pH 2.0, 7.0, and 9.0.

The product of the flash photolysis of 1.0×10^{-3}M TNB was isolated by column chromatography on silica gel. A 500 ml. solution of 1.0×10^{-3}M TNB in ethanol was degassed in the transfer apparatus and each of the fresh solutions were flashed in a 14-cm. Pyrex cell at ca. 3500 joules. The flashed solution which accumulated in the waste reservoir was vacuum

distilled intc the sample reservoir until a solid film of product remained. The apparatus was open to air and the solid product was dissolved in a minimum volume of acetonitrile and applied to a prepared column of silica gel. The above procedure was repeated with seven 500-ml. solutions and the accumulated sample was chromatographed on silca gel. A short column was prepared from a slurry of 50g. of silica gel (Woelm) and benzene. The solution of flash product was added to the column and the column was eluted with benzene. The benzene removed the unreacted TNB and the red-brown band of flash product remained. The flash product was displaced from the column with acetonitrile.

The solvent was evaporated by vacuum distillation and the solid sample was transferred to a sample tube. The sample was dried by vacuum pumping for three hours. The tube was sealed and the sample (ca. 4 mg.) was sent out for molecular weight analysis.* TLC (silica gel, acetonitrile) revealed only one spot (Rf. 0.2) due to the flash product and no other impurity. No TNAB was detected as a product of the flash photolysis of TNB in ethanol. The flashed solution gave a negative test for nitrite ion using the method recommended by Gold and Rochester.[6]

---

*Chemical analyses indicated a molecular weight of 110, but the sample was contaiminated with impurities. The results were considered as negative.

Several chemical tests were performed on the flash product to obtain more structural information. The addition of hot, dilute nitric acid to a water solution of the isolated flash product resulted (TLC analysis) in the clean formation of TNB. Several agents (oxygen gas, nitric oxide gas and dilute hydrochloric acid were added to a flashed TNB (1.0×10^{-3}M) ethanol solution and the ultraviolet spectra revealed the disappearance of the red visible bands. The solution was quickly decolorized with nitric oxide and hydrochloric acid but was slowly discolored with oxygen over a period of twelve hours. No change was visible in a flashed TNB (1.0×10^{-3}M) solution after 48 hours in the dark.

15. Irradiation of the Flash Product

The effect of 546 mμ irradiation on the flash product was further investigated. A solution (300 ml.) of TNB (1.0×10^{-3}M) in degassed ethanol was flashed at ca. 3500 joules in the transfer apparatus. The solution was concentrated by vacuum distillation to (ca. 30 ml.) fill an attached (10.0-cm. path length) spectrophotometer cell. The sample was irradiated for 1.5 hours with 546 mμ irradiation (Bausch & Lomp monochromator, 500-watt. Osram high pressure mercury lamp) until the visible bands disappeared.

The solution was evaporated to dryness by vacuum distillation and the solid product was chromatographed on silica gel.

A 3 × 50 cm. column was packed with 50g. of silica gel and the column was eluted with benzene/petroleum ether (50/50) mixture. TNB (69 mg., 98% recovery) was eluted with this solvent. The yellow band at the top of the column was displaced with methanol and the eluted compound was identified on the basis of TLC and IR as TNAB (ca. 2 mg., 1% yield).

A previous chromatographic separation of the irradiated flash product had used aluminum oxide (Woelm) as the adsorbent material. A larger yield of TNAB (ca. 4%) was found and a subsequent "blank" experiment on the same column with unirradiated flash product revealed the formulation of TNAB apparently caused by contact of the flash product with aluminum oxide.

RESULTS

1. General Plan of the Experiments

Although a study of nitrobenzene would perhaps appear to be the most fruitful approach to the photochemistry of nitro compounds, consideration of its purification, stability, and prior photochemical studies[11,12] indicated that trinitrobenzene is a better candidate. This path was followed, although some pertinent data about nitrobenzene and DNB was also gathered. The experimental work was directed to the investigation of the primary photochemical processes by the flash photolysis technique. Supporting information was obtained from three sources: continuous photolysis studies, ESR spectroscopy, and identification of the photochemical products. In all cases, TNB was excited with light above 300 mμ.

The flash photolysis experiments were designed to yield information about the rates and mechanisms of the primary processes and about the identity of the intermediates involved. Conditions such as the TNB concentration, the pH, solvent systems, and flash intensity were varied.

Continuous photolysis experiments were performed to confirm the results reported by Stenberg and to generate radicals detectable by ESR. Optical studies were carried out at room temperature in a variety of solvents and in a rigid matrix at low temperature.

Attempts were made to isolate and identify the flash photolysis product. The structures of the continuous photolysis products were

established by comparison with known compounds. A number of derivatives of TNB were synthesized and examined as candidates for the flash product (X) and its transient precursor.

2. The Continuous Photolysis of TNB

Although Stenberg and Holter[3] have studied the photolysis of TNB in ethanol and tetrahydrofuran on a preparative scale, it was felt that a repetition of their experiment was in order to establish the validity of their results and to characterize an unidentified product isolated by them.

TNB in ethanol obeys Beer's Law; its absorption spectrum is shown in Figure 6. When a 1.0×10^{-3}M solution of TNB is continuously irradiated (cf. Expt. sec. 11), spectral changes are immediately evident upon short exposure to intense light. Bands appear at 470 and 540 mμ with optical densities in the ratio of 2 to 1 (cf. Fig. 7). It is pertinent to note that these spectral features also appear after a single flash (cf. Fig. 8) TLC analysis of the solution immediately after this exposure detected the presence of TNAB as well as the "red" flash product. The visible peaks disappear with continued exposure and TNAB is preferentially produced. A kinetic investigation of the disappearance of TNB or of the generation of TNAB or the flash product was not feasible due to the overlapping absorptions of these components.

The quantitative preparative-scale photolysis of TNB (1.0×10^{-3}M) in ethanol (cf. Expt. sec. 11) produced a ca. 5% yield of TNAB and a trace of 3,5-dinitroaniline. Qualitative experiments under the same

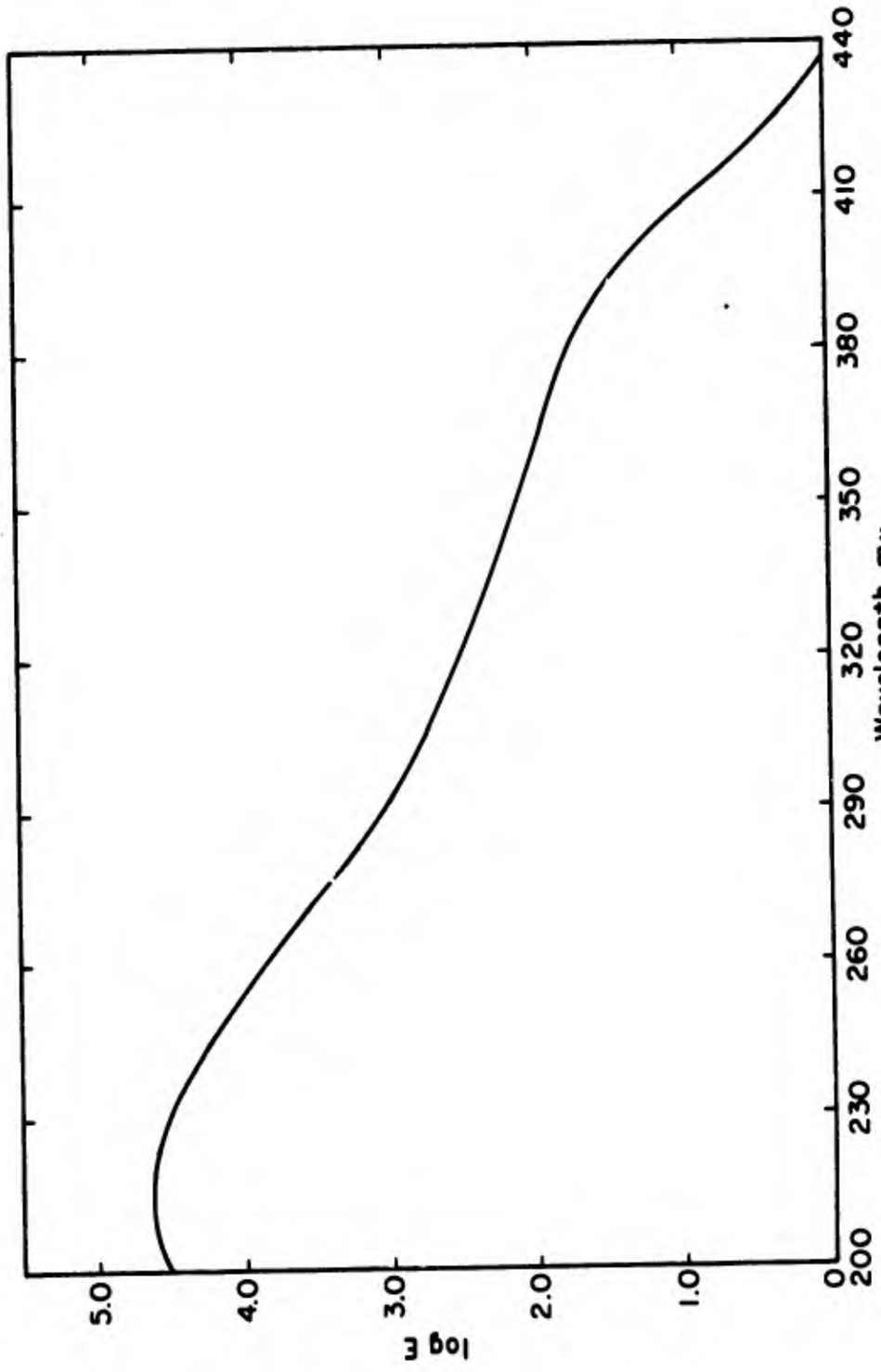

FIGURE 6: Absorption Spectrum of TNB in Ethanol

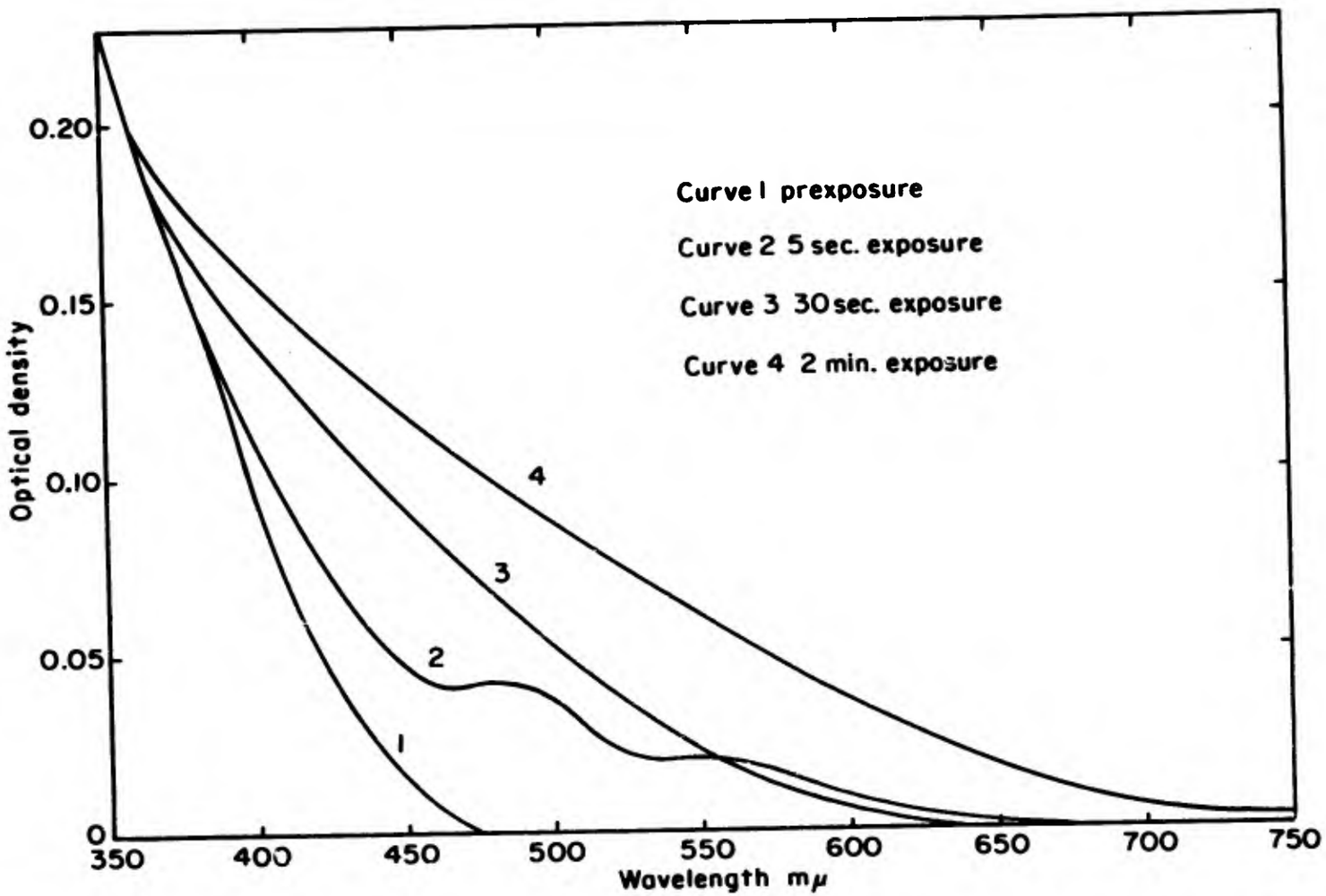

FIGURE 7: Absorption Spectrum in 10-cm Cell of 4.0×10^{-4}M TNB in Ethanol after Photolysis

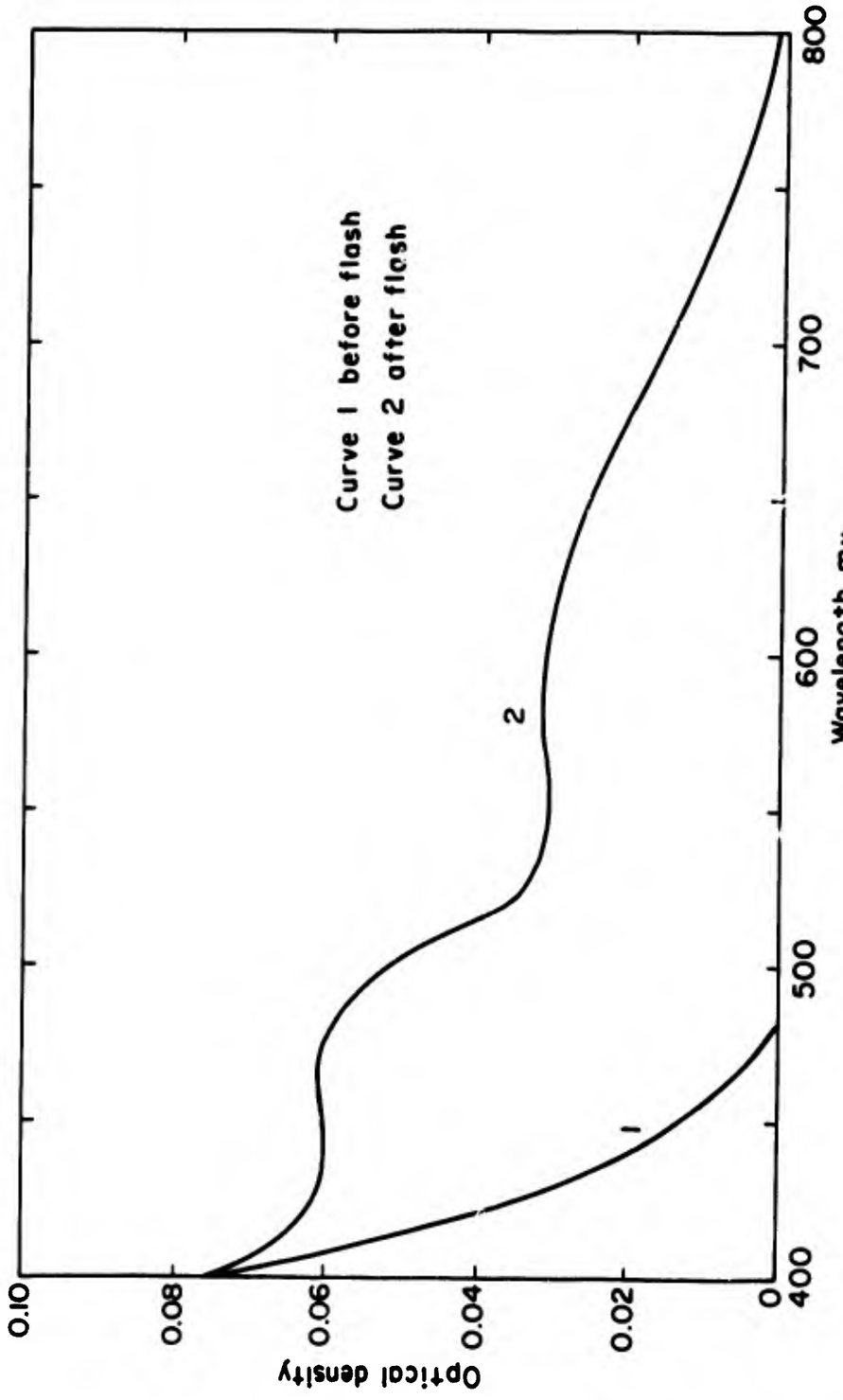

FIGURE 8: Absorption Spectrum in 10-cm Cell of 1.0×10^{-3}M TNB in Ethanol after 1800 Joule Flash

conditions confirmed the earlier report[3] that acetaldehyde is also formed. By contrast, Stenberg and Holter photolyzed under heterogeneous conditions. These authors irradiated a slurry of TNB in 95% ethanol for 36 hours and isolated TNAB and an unidentified product. Working with a sample kindly supplied by these workers, we were able to identify it as 3,5-dinitroaniline.

The photolysis of TNB was also examined in other solvents such as methanol, THF and 1-propanol and in undegassed ethanol solution.

These experiments were more qualitative than the one conducted in ethanol. In all cases with the aforementioned solvents, the same visible bands of (X) were observed (cf. Fig. 5). TLC examination of the methanol photolysis revealed that the red product had the same Rf. value (0.2) as (X). Appreciable quantities of TNAB and DNA were also detected. TNB was found to be light sensitive in benzene and hexane, but an aqueous solution was stable to 24 hours of irradiation. Oxygen exerts a significant effect on the amount of TNAB produced. In comparison with a degassed ethanol solution under duplicate photolyses times and conditions, a smaller yield of TNAB (ca. 30%) results. The growth of the initial visible peaks (vide infra) is significantly faster in degassed solutions.

3. The Low Temperature Photolysis of TNB

TNB (4.0×10^{-4}M) in a rigid ethanol glass was photolyzed at -196°C and the recorded spectrum is shown in Figure 9 . The spectrum measured resembles (cf. Fig. 18) the transient spectrum of the flash photolysis

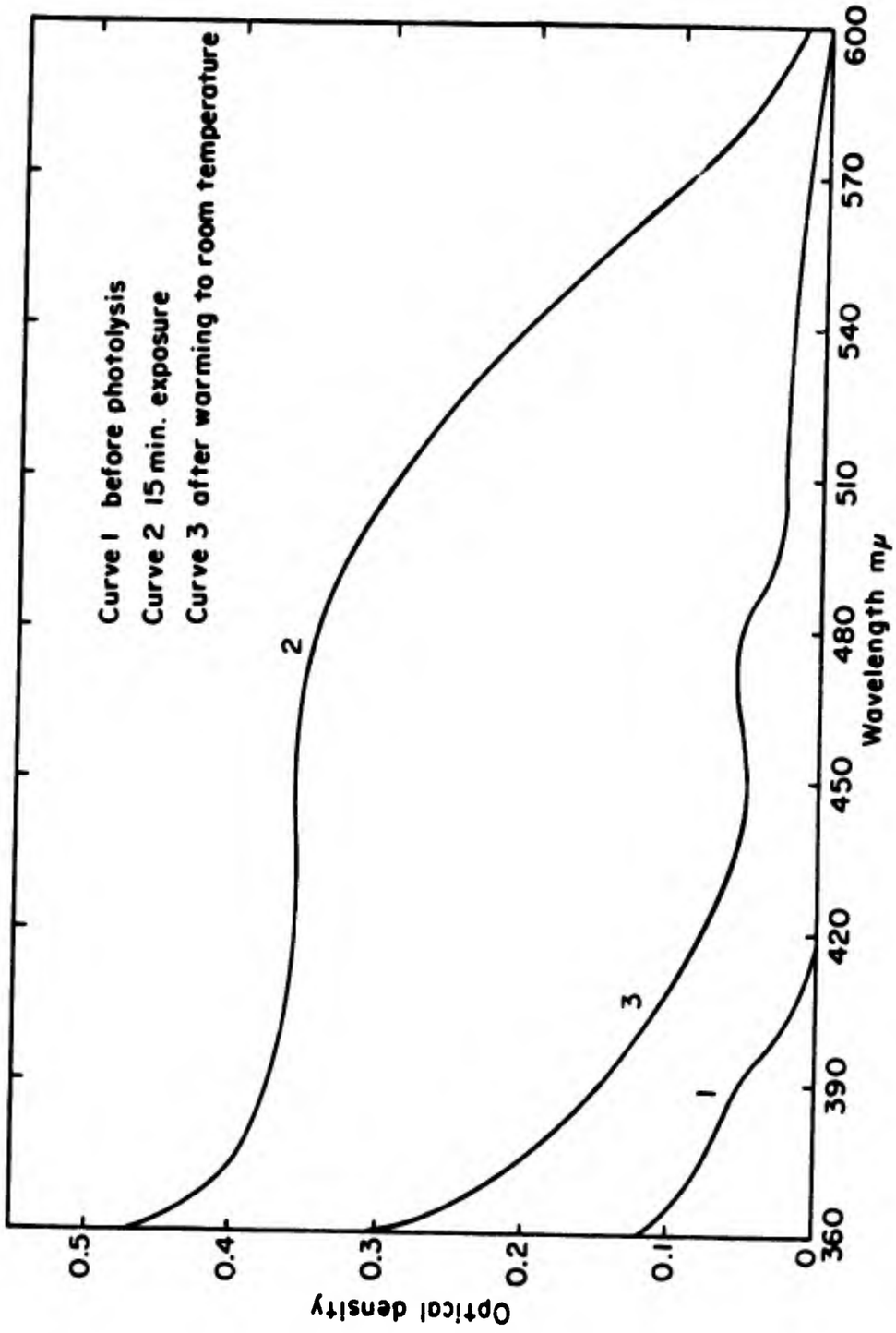

FIGURE 9: Absorption Spectrum at -196°C of the 330 mμ Photolysis of 4.0 x 10^{-4}M TNB in Ethanol

of TNB in ethanol. When the red colored glass was allowed to warm to room temperature, the absorption in the visible region decreases. Finally at room temperature in the now fluid solution, a spectrum closely resembling that of (X) remains. The results substantiate the production of a transient which precedes (X).

4. Isolation and Properties of the Flash Product (X)

The flash photolysis of low concentration solutions at input energies in the range 200 - 3000 joules generates small amounts of a permanent product. This product exhibits distinct maxima at 470 and 570 mμ in the density ratio of 2 to 1 (cf. Fig. 8). The flash product is generated in degassed as well as in oxygen-saturated solutions of TNB. Flashing in aerated ethanol decreases the yield by about 10%. A ca. 1800 joule flash produces small quantities of (X) and no detectable traces of TNAB. The same species is produced by flashing buffered ethanol (pH 2.0, 7.0, and 9.0) solutions and in other solvents such as methanol, l-propanol, and THF. No traces of (X) is evident in flashed benzene, hexane, or aqueous solutions of TNB. The product (X) itself is light-sensitive (cf. Fig. 10).

It seemed likely that this species, which appears to be stable indefinitely in the absence of air, is the precursor of the products of the continuous photolysis and thus represents the key to any mechanistic scheme. A great deal of effort was expended in the isolation of minute (mg.) quantities of this material. For this purpose it was necessary to flash a large number of samples (ca. four

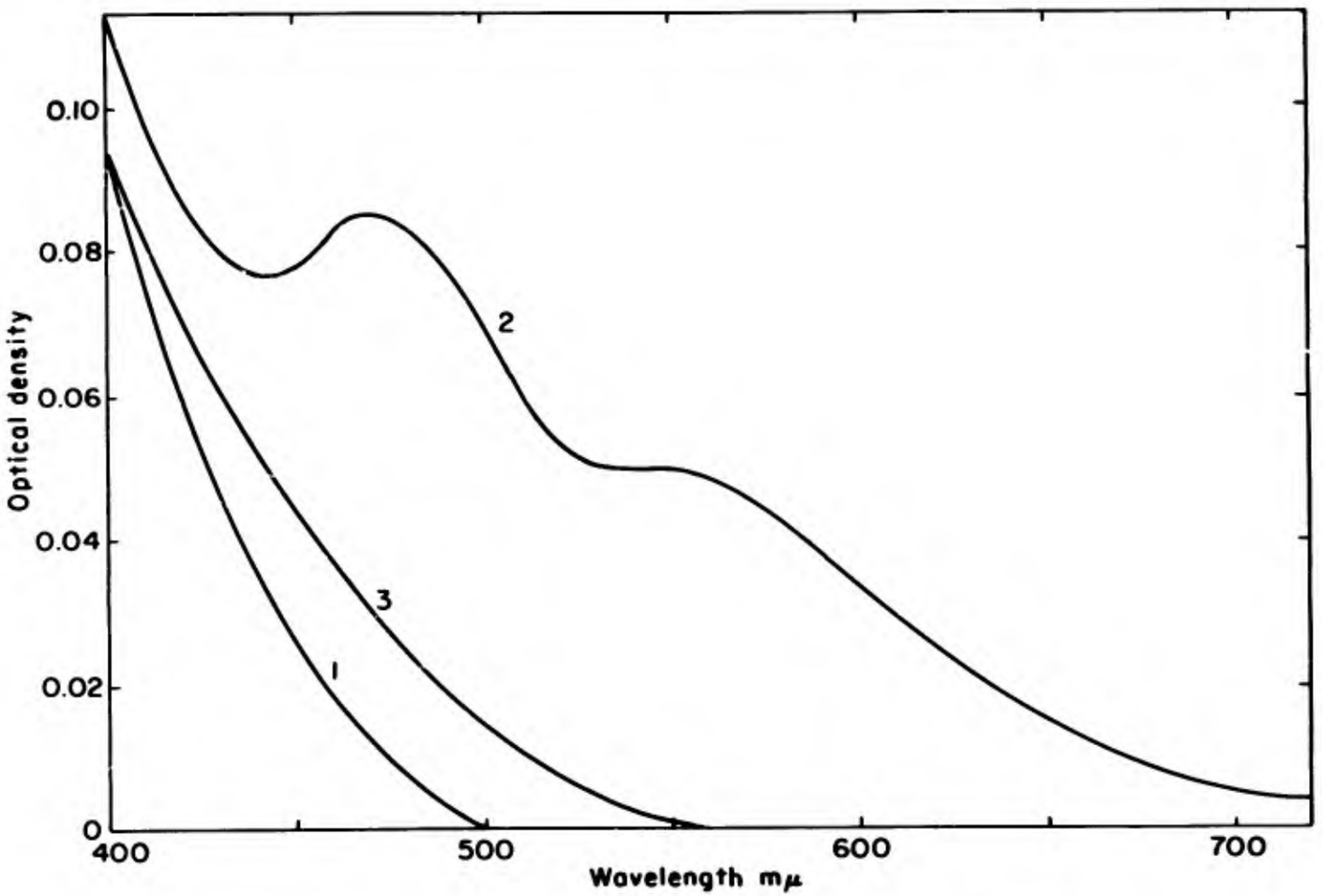

FIGURE 10: Effect of 546 mμ Photolysis on the Flash Product of 1.0×10^{-3}M TNB in Ethanol in 10-cm Cell

liters of solution). Several milligrams of product was finally isolated by chromatography, but subsequent analyses implied that the sample was of questionable purity. Our valient effort ended in vain. Unfortunately, therefore, with respect to the chemical and photochemical properties of this product, conclusions had to be drawn from experiments which contained a very large (100-fold or more) excess of unreacted TNB.

As previously mentioned, the physical and chemical properties of the flash product were determined with flashed solutions or with minute amounts of isolated material of doubtful purity. The product is soluble only in polar solvents such as water or alcohols. No ESR absorption was detectable in a concentrated solution of flashed TNB. The low Rf. value (0.2 acetonitrile) on silica gel-coated or (0.0, acetonitrile) on aluminum oxide-coated TLC plates is indicative of a high molecular weight and/or the presence of polar groups. Chemical agents such as nitric oxide, mineral acids and nitric acid rapidly decolorize a flashed solution. The effect of added nitric oxide is shown in Figure 11. TLC examination of a flashed solution after addition of dilute nitric acid revealed that the flash product is probably oxidized to TNB.

5. Attempted Identification of the Flash Product

The flash product exhibits a structured band system with peaks at 470 and 540 mμ (cf. Fig. 8) and it was considered profitable to attempt an identification by spectral comparison with compounds which chemical reasoning indicated could be formed. Compounds acquired from commercial

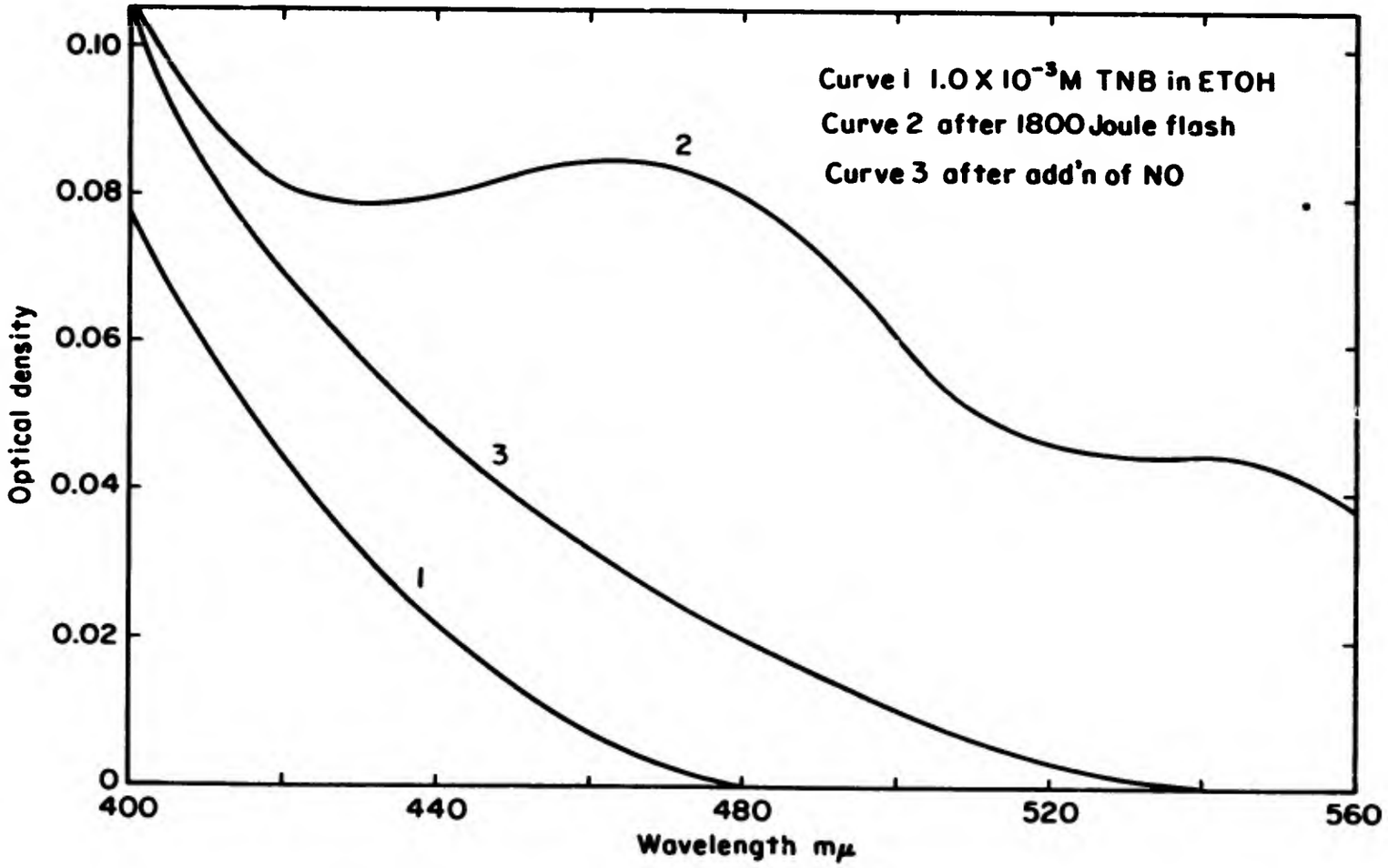

FIGURE 11: Absorption Spectrum of the Flashed Solution of 1.0×10^{-3}M TNB in Ethanol and after the addition of NO in 10-cm Cell

sources or synthesized for this purpose, together with their spectral characteristics, are listed in Table 1. Any compound which can arise from the reduction of one or more of the nitro groups is a potential flash product, and from this point of view, the list is rather limited for obvious reasons. The results of this endeavor are readily summarized: No spectral correlation was found with one possible exception. The spectrum of the adduct formed from TNB and acetone in the presence of base[8] matches the wavelength maxima and the ratio of optical densities of the flash product spectrum.

An attempt was made to generate the product by chemical means by the lithium aluminum hydride reduction of TNB. The absorption spectrum (cf. Fig. 13) of the reaction mixture resembles the product spectrum and several other observations made with this material (cf. Expt. sec. 14) parallel those made with the flash product. Irradiation at 546 mμ bleaches the visible bands (cf. Fig. 13) and chemical agents such as nitric oxide, hydrochloric acid and nitric acid destroy the visible color. Unfortunately, the reaction of TNB with the hydride furnishes a complex array of products. Further the hydride has to be destroyed by water, which results in a basic medium in which further reactions of TNB can proceed. For these reasons no attempt was made to isolate the red material from this mixture.

Several other reducing agents as tin and hydrochloric acid, zinc dust in acetic acid, hydrogen in the presence of palladium, and mercury-sodium amalgam were examined for synthetic possibilities, but no other system was found. In all the cases no red product was formed and DNA and

TABLE 1

SPECTRAL PROPERTIES OF FLASH PRODUCT CANDIDATES

Compound	λ_{max} [a]	ϵ_{max} [b]	Ref.
1. TNAB	328	14,300	c
2. DNPH	358	2,200	c
3. DNA	354	1,985	c
4. DNNB	Fig. 1		c
5. Picric Acid	370	14,500	c
6. Isopicramic Acid	305	12,200	d
7. 3,5-Dinitroethoxybenzene	290	10,050	c
8. TNB + Acetone + Base	470;540	15,000;9,500	e
9. TNB + Sodium Ethoxide	Fig. 12		c
10. NA^+ - TNB^- in DME	Fig. 12		c
11. C-T of TNB with 1-4	f		
12. TNB + Base + Ethanol	Fig. 12		c

a. Longest wavelength bands in mμ.
b. Measured in ethanol.
c. This work.
d. A Meldola and W. Hewitt, J. Chem. Soc. 103, 876 (1912).
e. R. Foster, J. Chem. Soc., A, 53 (1966).
f. No charge-transfer (C-T) bands were found.

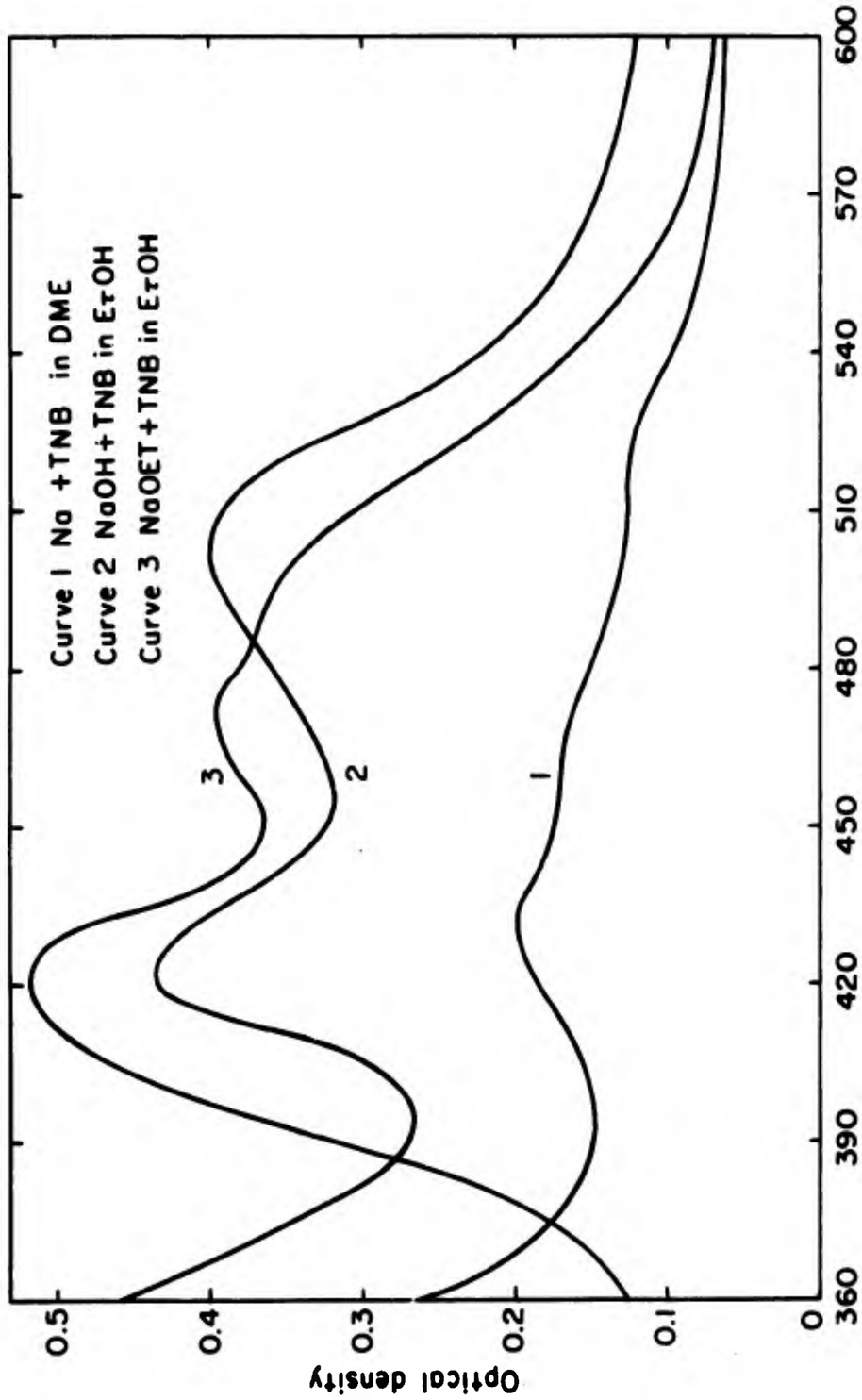

FIGURE 12: Absorption Spectrum of Possible Flash Products

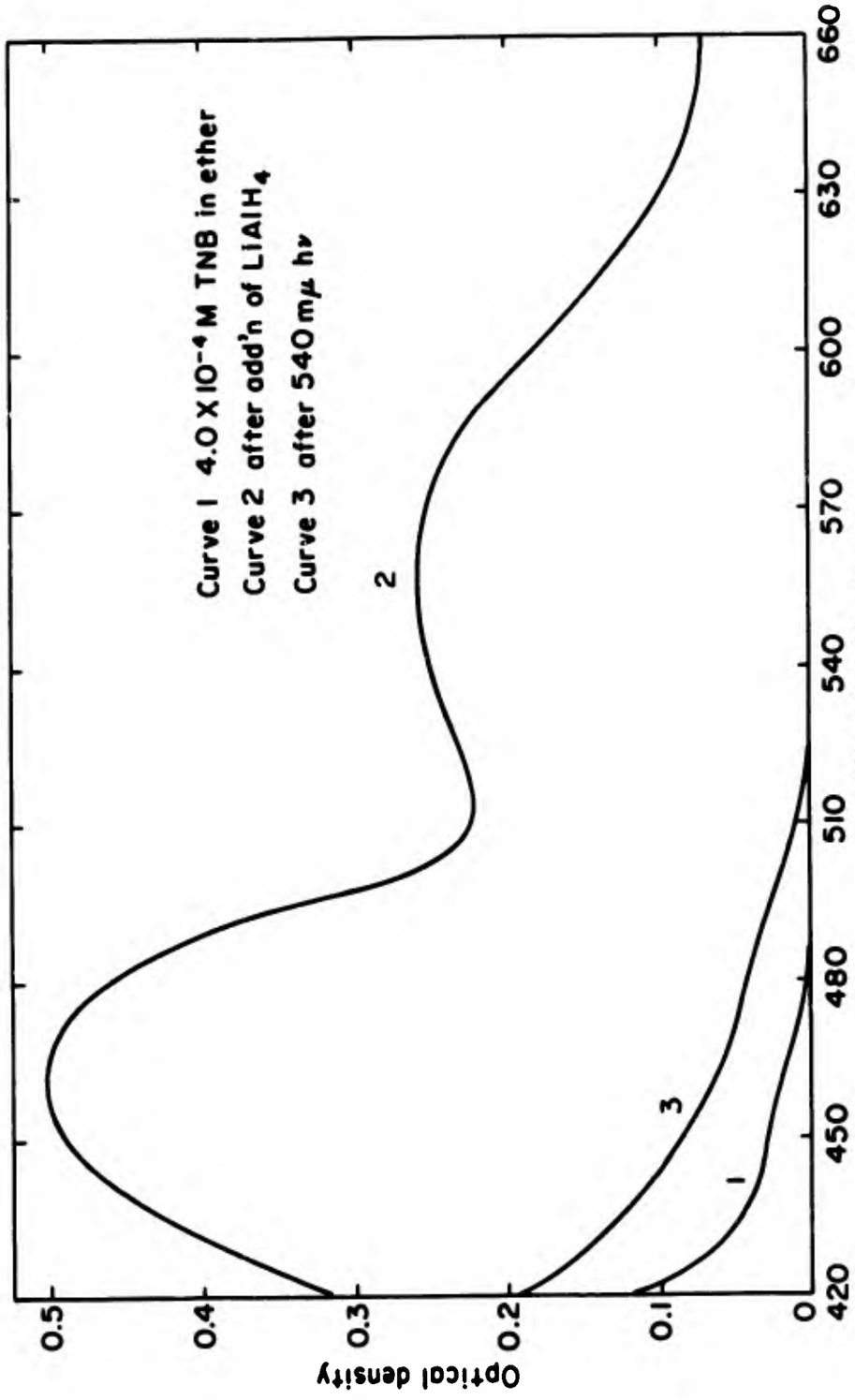

FIGURE 13: Absorption Spectrum of the Product of the Reaction of TNB with Lithium Aluminum Hydride

TNAB predominated as the major reduction products.

6. Photolysis of the Flash Product

Photolysis of the flashed solution at 546 mμ, where only (X) absorbs causes disappearance of the band structure (cf. Fig. 10). The formation of TNAB could be demonstrated by TLC. Further, it was isolated in ca. 1% yield from a 1.0×10^{-3}M TNB solution which was first flashed and then irradiated. In the initial experiments chromatographic separation of the mixture was achieved on an aluminum oxide column. However, a blank experiment without subsequent continuous irradiation also yielded TNAB, apparently due to the action of the column material. For the definitive experiment, silica gel was employed for the separation. Under these conditions, the unirradiated solution gave no TNAB.

7. Electron Spin Resonance Experiments

ESR evidence was sought for radical intermediates in the photolysis of TNB in several solvents. Degassed samples were irradiated in the ESR spectrometer cavity. Using "pyrex" or quartz sample tubes, irradiation at room temperature produced no signal even at the highest instrument sensitivity. Irradiation of 10^{-2}M TNB in frozen ethanol glass at -155°C produced the spectrum shown in Figure 14. At -75°C an eight line spectrum was observed (cf. Fig. 15), while a twelve line spectrum consisting of three quartets with intensities in the ratio 1:3:3:1 was obtained from a 5.0×10^{-2}M solution at -35°C (cf. Fig. 16). In all these experiments the signal reaches an maximum intensity and then diminishes with continued irradiation. No signal was obtained

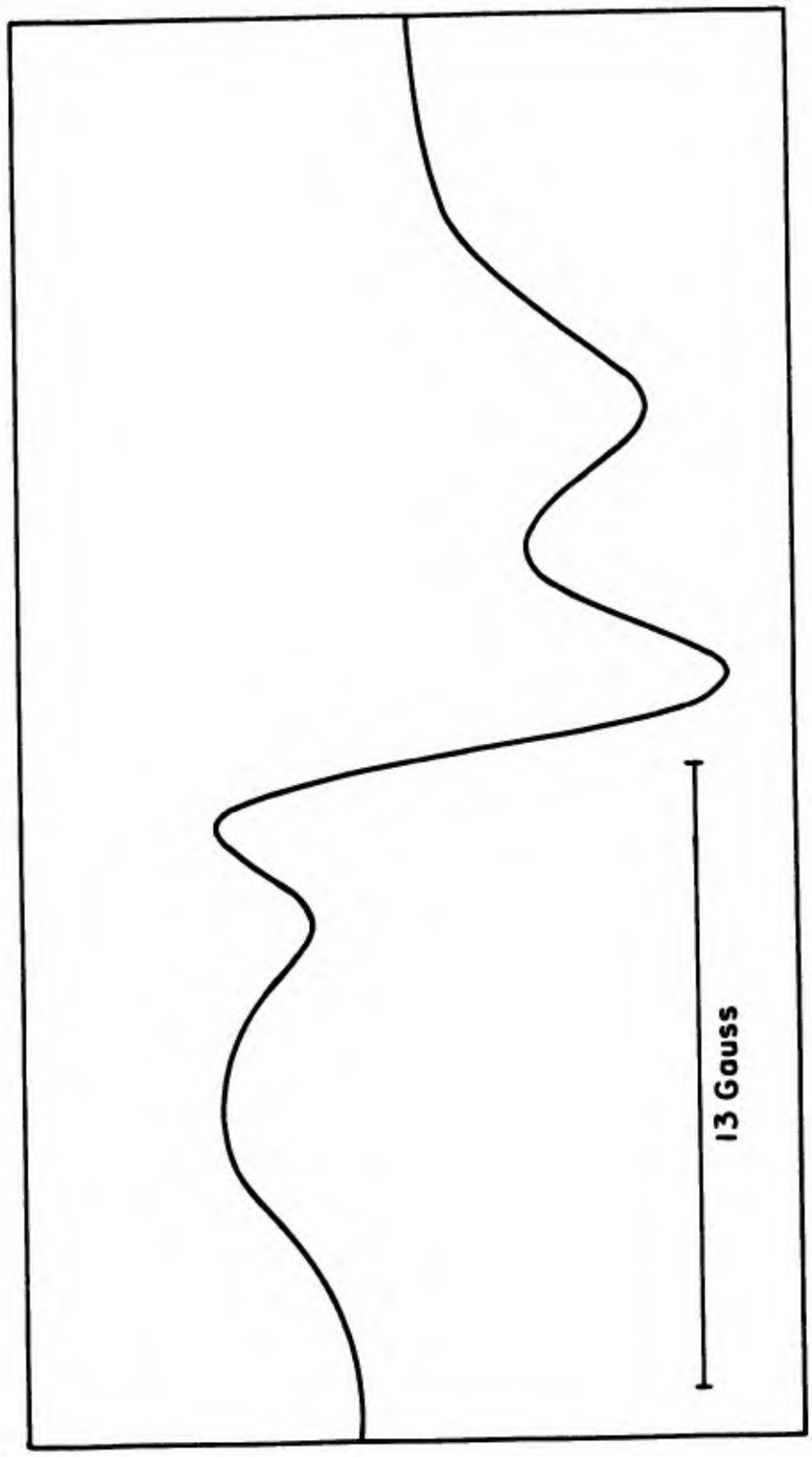

FIGURE 14: ESR Spectrum from the Photolysis of 0.1M TNB in Ethanol at -155°C

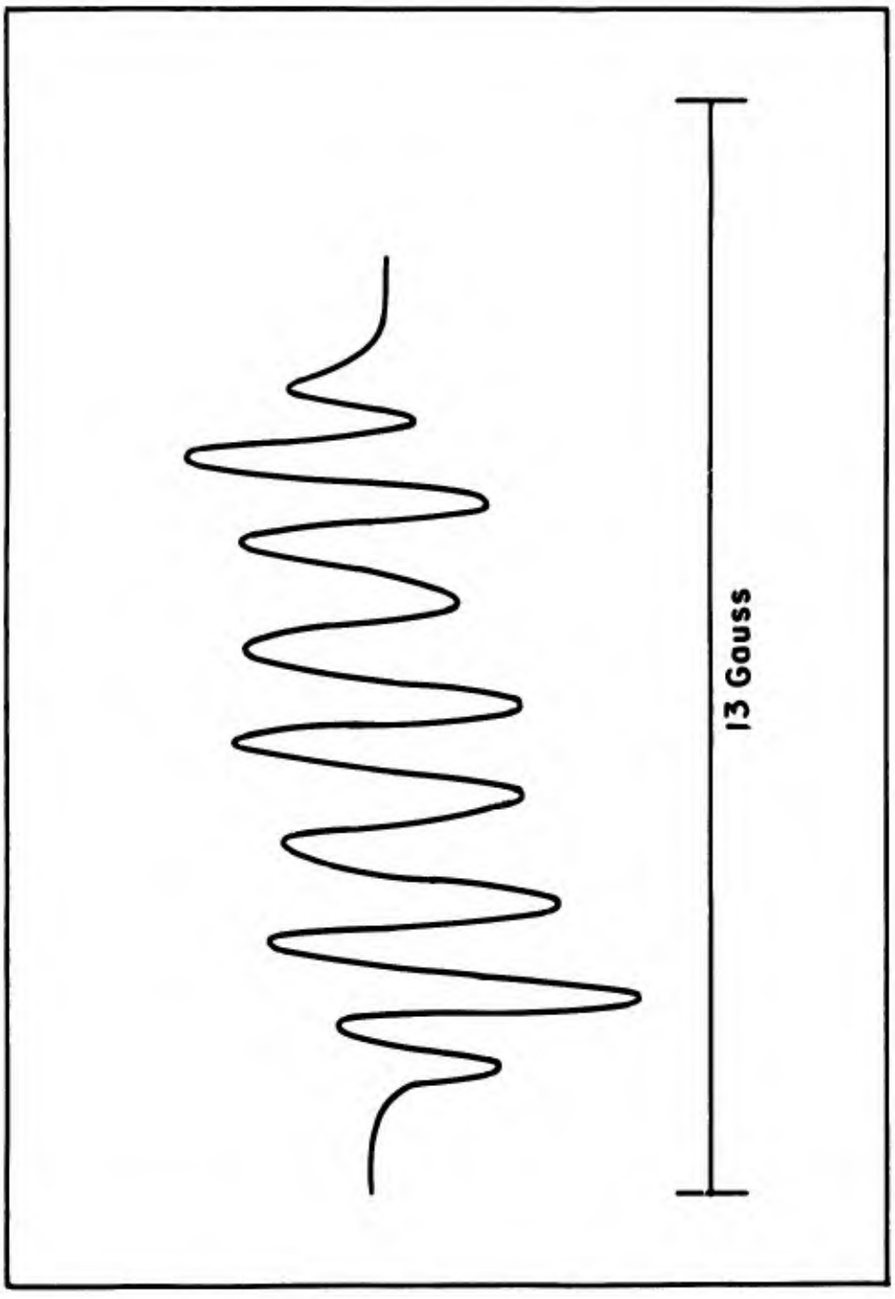

FIGURE 15: ESR Spectrum from the Photolysis of 0.1M TNB in Ethanol at -75°C

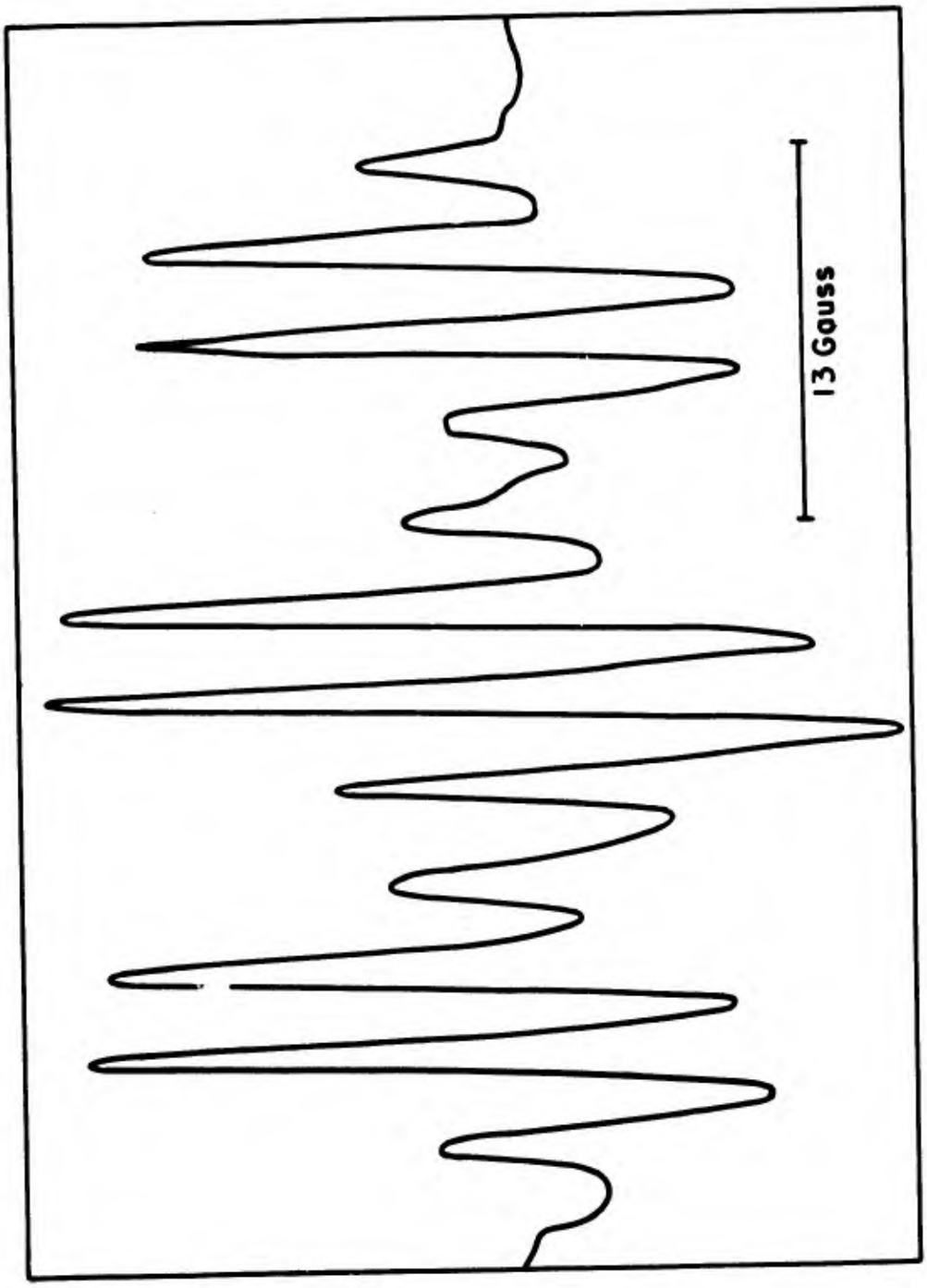

FIGURE 16: ESR Spectrum from the Photolysis of 5.0×10^{-2} M TNB in Ethanol at -35°C

from the photolysis of 1.0×10^{-2}M TNB in hexane at -50°C.

The radical generated at -35°C is assigned to the following species:

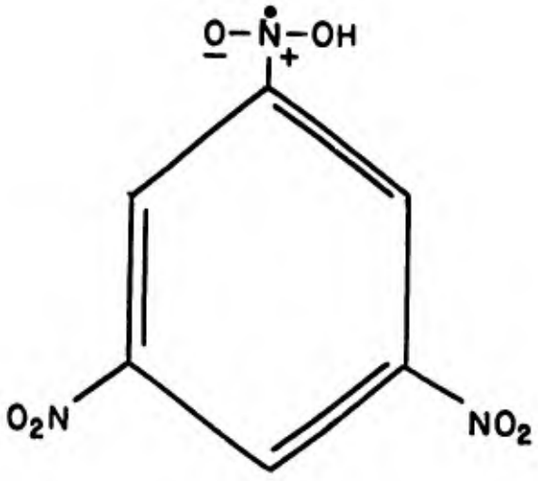

The isotropic coupling constants of the photoradical are A_N(13 gauss) and A_H(3.4 gauss). The spectrum is consistent with the interaction of the unpaired electron with one nitrogen atom and three equivalent protons. A similar structure has been assigned to[14,15] the radical generated photolytically from TNB in THF (cf. Fig. 17). There is little doubt that the same radical is generated in alcohol and in THF, but presently for undeterminate reasons the radical is considerably more stable in the latter solvent.

The spectrum of the solid solution at -155°C (cf. Fig. 14) consists of an assymetric triplet of unequal intensities. Here anisotropic terms apparently come into play, and no interpretation will be offered here.

The other nitro compounds and the flash product were examined for generated radicals. DNB and NB in ethanol did not give rise to ESR signals at room temperature or at low temperature. Similarily, the

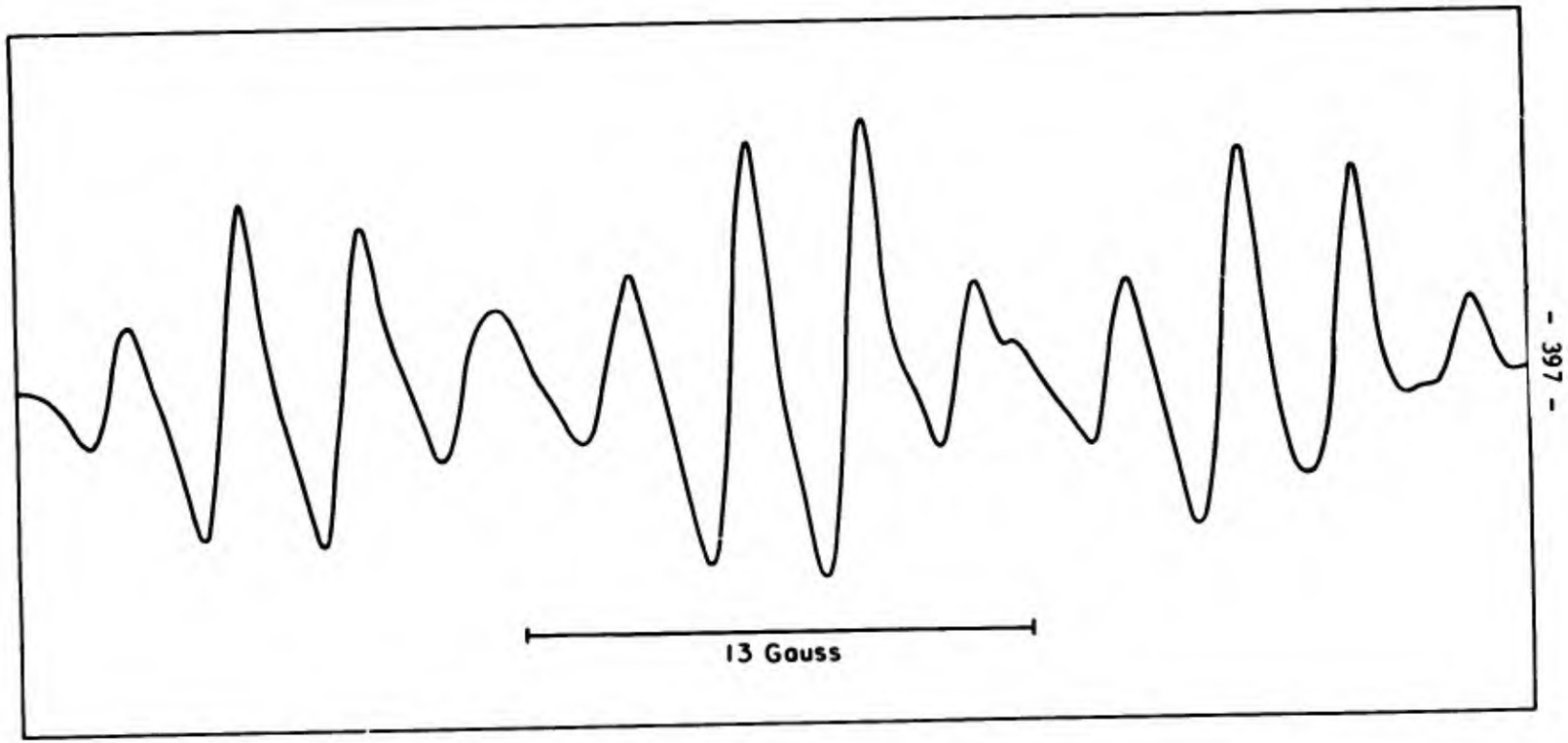

FIGURE 17: ESR Spectrum from the Photolysis of 0.01M TNB in THF at 25°C

same compounds in THF produced radicals which are observable at room temperature. No ESR signal is associated with the permanent flash product or the simulated product generated by lithium aluminum hydride reduction. This is based on the room temperature and low temperature examinations of dilute and concentrated flash solutions. In one experiment, concentrated sodium hydroxide was added to the flashed solution in order to ascertain whether the base would cause a scission into radical products. The result was again negative; no ESR signal was detected.

The decay kinetics of the photoinduced radicals were examined at various temperatures in ethanol and in THF. The half life of the photo-induced radical in ethanol is ca. 3 seconds at -35°C and ca. 2 minutes at -155°C. By contrast the half life of the photoinduced radical in THF at room temperature is ca. 0.5 minutes. The radical in THF decays by a first order process with a rate constant of 2.5×10^{-2} sec^{-1}. The DNB derived radical in THF decays by a faster first order rate of 11.7×10^{-2} sec^{-1}. We were also able to detect the optical decay of a species generated by photolysis of TNB in THF at room temperature. Decay was monitored in the spectrophotometer at 460 mμ; the process is approximately first order with a half-life of 0.4 minutes. Presumably the optical and ESR decay is due to the same species, the photoradical.

Attempts to obtain meaningful decay kinetics in ethanol were hindered by the response of the recorder and by inefficient temperature control. At the higher temperature (-35°C), the radical was decayed beyond one half-life before the recorder can respond to the rapidly

diminishing signal. At the lower temperature in a now rigid matrix the radical has a sufficient lifetime to be measured, but the output signal is not solely due to the decaying radical. When the decay signal was examined at an off-resonance point (no radical absorption and hence no radical signal), a significant signal drift was found which amounted to about one-half of the apparent signal. The cause of this spurious signal was traced to the heating of the sample cavity by the irradiation light. Isothermal conditions exist during measurements under photolyses conditions since the secondary heating effect of the lamp is compensated by the coolant. During decay measurements the lamp is turned off and the compartment is cooled to a new equilibrium temperature. After applying the temperature correction factor to the data, the decay kinetics could only be followed over a small range (20% decay). Therefore, no meaningful decay kinetics could be assessed from the ethanol data.

8. Flash Experiments

Preliminary studies were conducted in a variety of solvents and over a range of flash intensities to establish a suitable set of conditions for more detailed investigation. It was observed that transients were formed in solvents such as primary alcohols, and in THF, but none were formed in water. In hexane, transient absorption is barely detectable. The largest amount of transient was observed in THF. Ethanol was chosen as the standard solvent for the following practical reasons: (1) the availability of large quantities of the pure solvent, (2) a

reasonable amount of measurable transient decay, and (3) freedom from a physical artifact (bubble formation in the reaction vessel induced by the flash) coincidental with the transient decay. Further, there are results from earlier work with this solvent using continuous photolysis.

The majority of the flash work was concerned with pure ethanol, although a water-ethanol system at different pH values was studied. Other parameters, such as the TNB concentration, the alcohol concentration, the flash intensity, the effect of dissolved oxygen, and the temperature were also varied. Transient spectra were obtained in ethanol and were compared with the spectra obtained at various pH values. After examination of the transient spectra, several key wavelengths which showed maximum changes in optical density were chosen and the transient behavior was recorded over a range of time scales.

A. Pure Ethanol and Ethanol/Hexane Mixtures

1. Transient Spectra

The transient spectra in degassed ethanol after four time intervals and at infinite time after the flash are shown in Figure 25. The absorption curve at time infinity matches the spectrum recorded on the Beckman DK-1 spectrophotometer. The transient spectra in undegassed ethanol are identical in gross features. Transient absorption was noted up to 650 mμ, but the weak absorption in this region demanded a high amplifier gain with a consequent signal-to-noise ratio of close to 1. For this reason, no data beyond 600 mμ are presented. At wavelengths

below 420 mμ, the absorption of TNB in the 14-cm. flash cell was very high (> 1). For this region, several runs were made with a shorter 3-cm cell. No bleaching of TNB from 330 mμ to 400 mμ was evident, the transient growth and decay being similar to that at the longer wavelengths.

Inspection of Figure 18 shows that at least two transients are generated. This is evident from the cross-over of the 100 μsecs. and 200 μsecs. spectra. There is initial growth below ca. 530 mμ, while above this wavelength decay is already in progress. There is an isosbestic point near 530 mμ. In Figure 19, the traces of the oscilloscope records taken on 40 μsec./cm. scales illustrate the changes at different wavelengths. At 440 mμ there is clearly a growth which continues after the decay of the flash, while at 570 mμ the growth terminates with the flash. The smallness of the signal beyond 550 mμ made it difficult to obtain quantitative decay information in this region. However, it is to be noted that the flash product produced with these flash intensity employed in this experiment (450 joules/lamp) has negligible absorption beyond 550 mμ.

On the basis of the product isolation it can be estimated that a maximum of 1% of the TNB is converted into the flash product. This corresponds to a product concentration of 2×10^{-6}M based on the assumption (cf., discussion section) that the product is dimeric with respect to TNB.

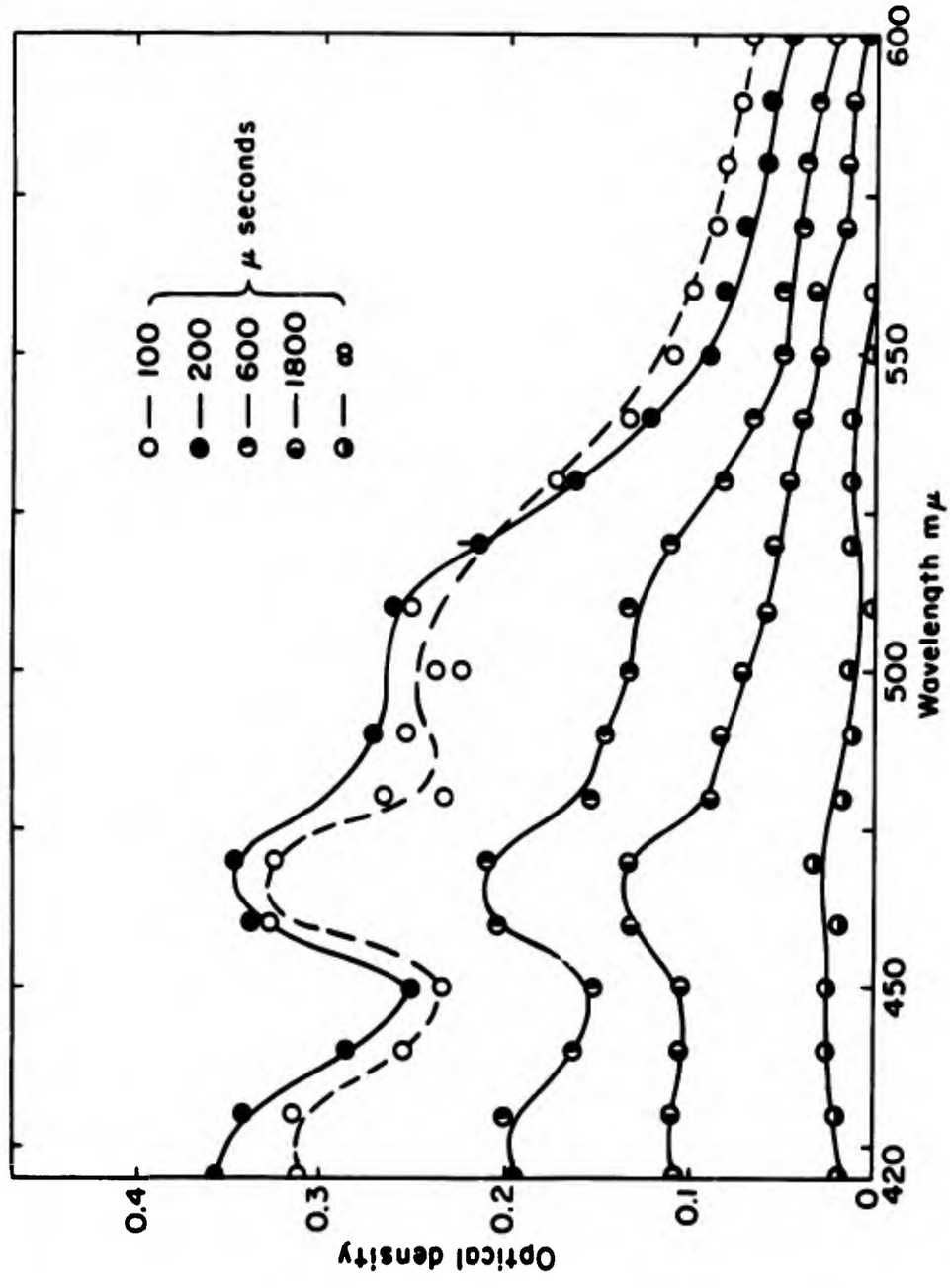

FIGURE 18: Transient Spectra of 4.0×10^{-4}M TNB in Ethanol - The Time is given in μseconds after a Flash of 450 Joules/Lamp

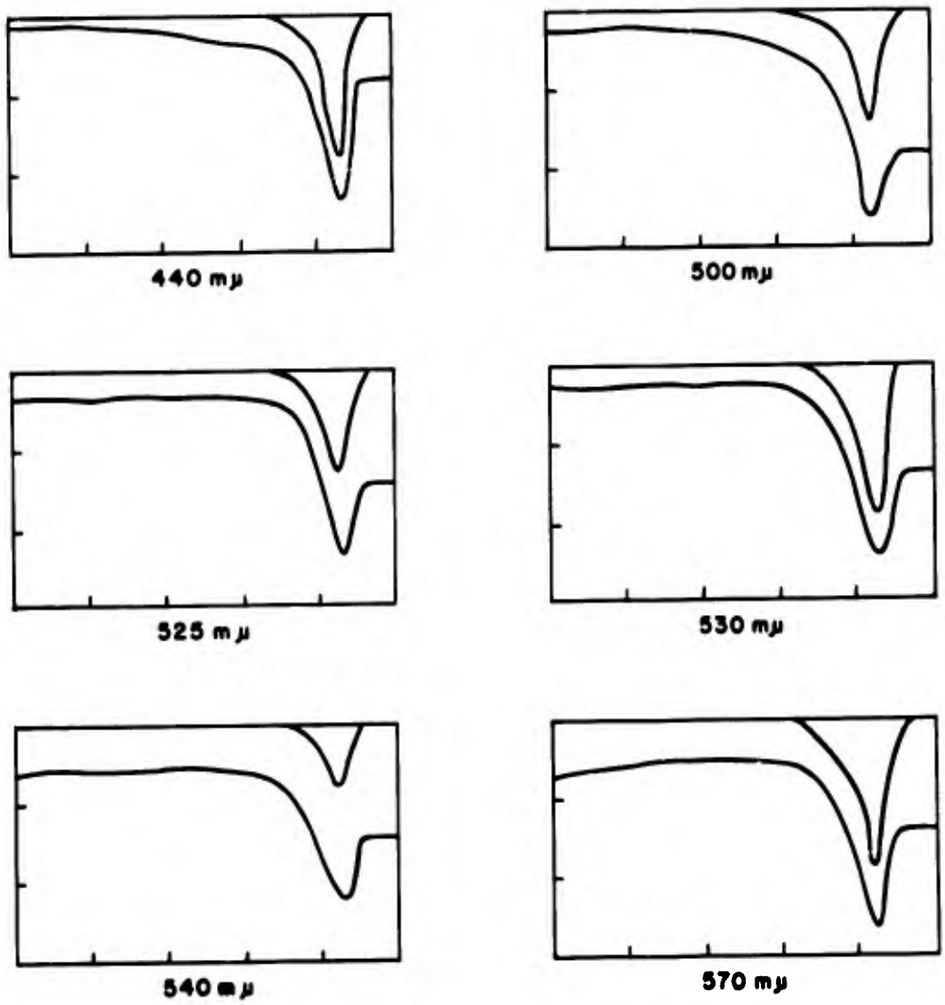

FIGURE 19: Oscilloscope Records of the Initial Transient from 4.0×10^{-4} M TNB in Ethanol - The trace on the top of the 40 μsec./mark scale is the flash profile with the monitoring light off. The lower trace on the voltage scale is with the monitoring light on. The voltage axis is 2.0 volt/division. The horizontal scale is 40 μsec/division.

With ΔD equal to 0.03 at 470 mμ (cf., Fig. 18), this furnishes $1.07 \times 10^{+3}$ as the lower limit of the extinction coefficient.

2. Formation and Decay Kinetics

The initial kinetic analyses of the decay were perform with the aid of a computer program which tested the decay for adherence to a simple first order on a second order rate law. Beer's law is presumed to hold for the transient species and the observed optical densities are proportional to the concentration by the expression

$$\Delta D = \sum_{n} \epsilon_n C_n \ell - \epsilon_A C_A \ell - \epsilon_A C_A^o \ell \qquad \ldots(6)$$

which holds at a constant wavelength and assumes that the starting material (A) is converted into n transient species. In this expression, the symbol ϵ represents the extinction coefficient and the symbol C the concentrations, while C_A^o is the initial concentration of the starting material.

The expression

$$\Delta D = \log \frac{V_o}{V_t} \qquad \ldots(7)$$

has been developed in the experimental section with reference to Figure 3. In the computer evaluation of the transient data, the equation (7) was utilized as well as the functions defined in equations (8) and (9).

$$\Delta D - \Delta D_{\infty} = \log \frac{V_{\infty}}{V_t} \qquad \ldots(8)$$

$$\Delta D - \Delta D' = \log \frac{V_{t'}}{V_t} . \qquad \ldots(9)$$

This first of these equations corrects for the final product absorption. In equation (9) it is assumed that the decay proceeds in two stages, namely a rapid decay over the time range 0-2000 μsecs. followed by a slower decay. The voltage $V_{t'}$ then represents the signal at 2000 μsecs. after the flash. In some cases, where the data indicated this to be appropriate, $V_{t'}$ referred to the signal at a time $t > 2000$ μsecs. The rate laws were tested in terms of the functions $\ell n\ \Delta D$, $\ell n(\Delta D - \Delta D_{\infty})$, and $\ell n(\Delta D - \Delta D')$ for the first order and ΔD^{-1}, $(\Delta D - \Delta D_{\infty})^{-1}$, and $(\Delta D - \Delta D')^{-1}$, which were examined as plots against time.

The results of the initial data evaluation were equivocal. The decay does not follow a simple first order or second order law for any extended time period. Both the first order and the second order plot of the above-mentioned functions show curvature. Inspection of a large number of such plots indicated those based on equation (8) (i.e., $\Delta D - \Delta D_{\infty}$) to be most useful.

In such plots, the decay fits either a first or second order law after ca. 1000 μsecs. This behavior is illustrated for a 4.0×10^{-4}M solution of TNB in ethanol at 420 mμ in Figures 20 and 21. Figure 20 shows the plot of ΔD against time. The time behavior of the pertinent functions of $\Delta D - \Delta D_{\infty}$ is portrayed in Figure 21. The apparent adherence to both rate laws at the longer time is considered to be due to the large experimental errors inherent in the tail portion of the decay, which could rarely be followed more than two half-lives. The first order (k_1) and the apparent second order (k_2) rate constants derived from data at a number of wavelengths are listed in Table 2 . After examination of many plots, it became evident that there was a closer fit to a second order law. The second order decay should be insensitive to changes in the flash intensity and concentration of TNB. In Table 3, the three-fold increase in flash intensity is shown to be without effect within experimental uncertainty. The effect of doubling the TNB concentration (Table 4) is not as clear. At 420 mμ there is an apparent decrease in rate with increasing condentration, while at 480 mμ there is an apparent increase. There is, unfortunately, not enough information to resolve this effect, but it is not unlikely that the figures merely reflect the experimental errors.

Inherent in the treatment applied above to the final portion of the decay is the notion that a single transient is left after t > ca. 1000 μsecs. If this transient arises from the decay of a preceding

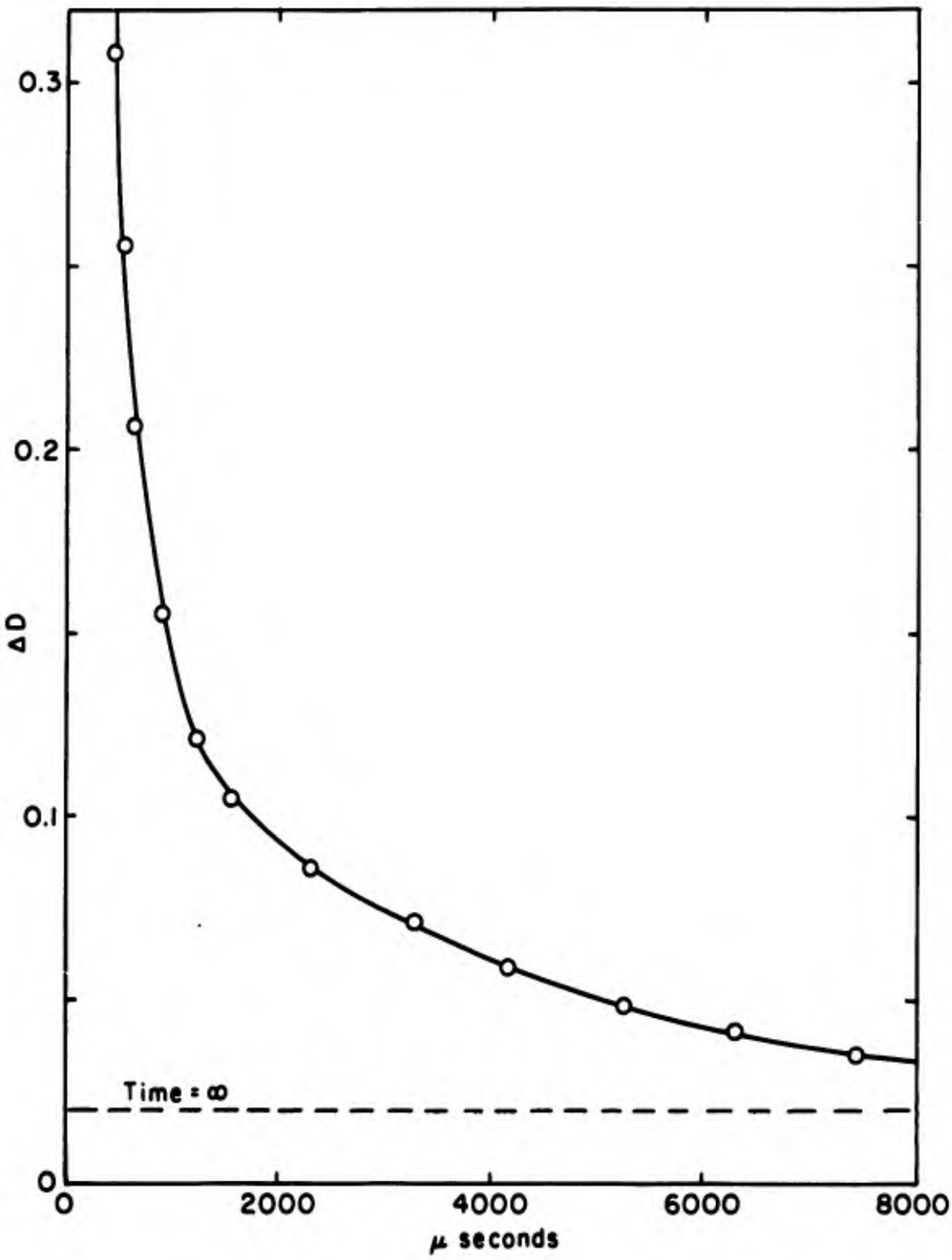

FIGURE 20: Transient Decay at 24°C from 4.0 x 10^{-4}M TNB in Ethanol at 420 mμ

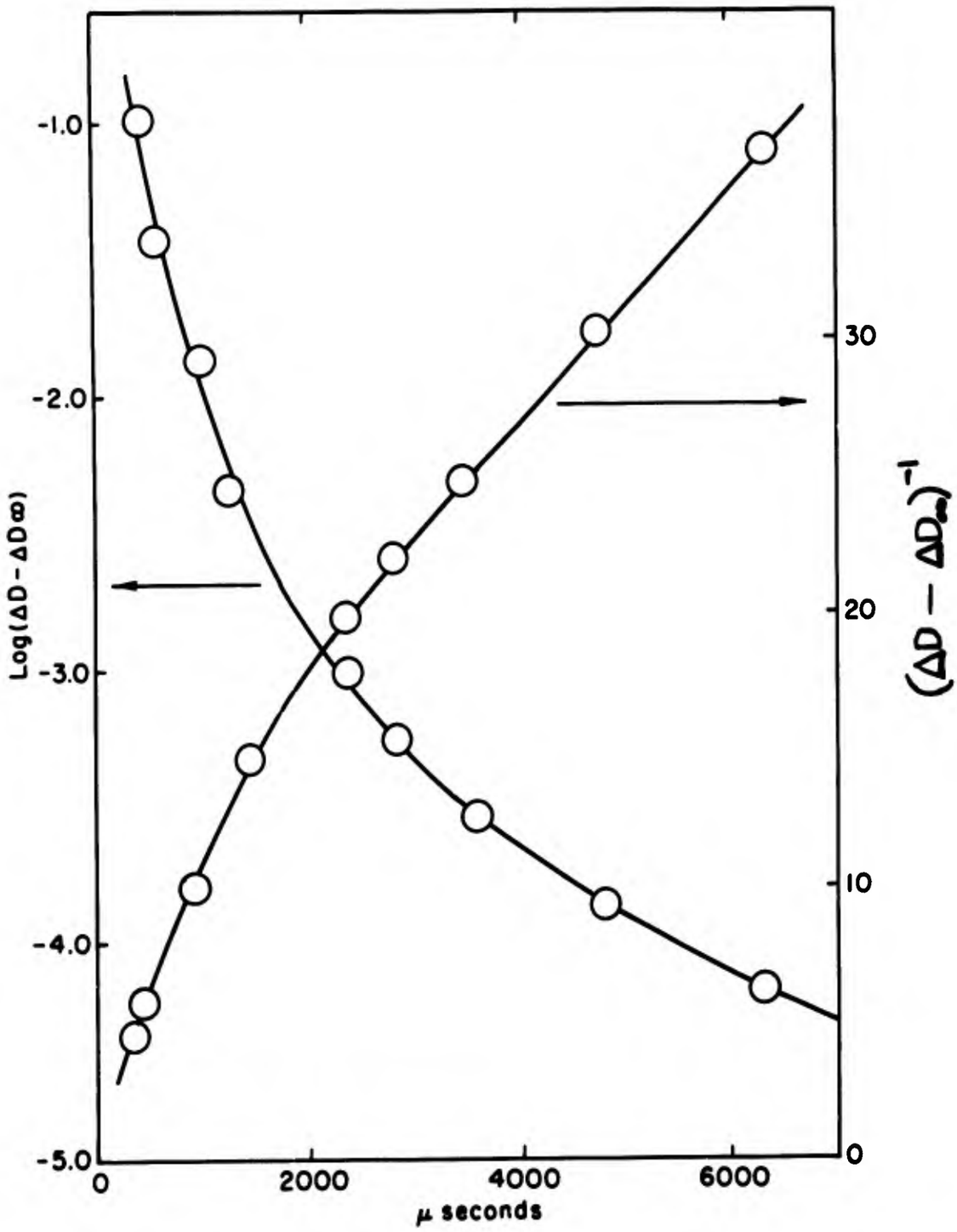

FIGURE 21: First Order and Second Order Plot for the Transient Decay of Figure 20

TABLE 2

FIRST ORDER* RATE CONSTANTS AND THE SECOND ORDER RATE CONSTANTS FOR THE TIME PERIOD AFTER 1000 μsecs

Run	λ(mμ)	$k_1 \times 10^{-2}$ sec^{-1}	$\frac{k_2}{f(\epsilon)}$** $\times 10^{-3}$ sec^{-1}
285-1	420	2.2	5.8
274-1	420	2.2	3.8
-2	420	2.5	5.5
-3	420	2.3	4.5
-4	420	2.8	4.7
-5	420	2.7	3.6
-6	420	2.2	3.0
273-2	420	1.4	4.8
278-2	420	1.9	1.1
273-4	430	1.7	3.3
-23	450	0.6	2.1
278-6	470	1.6	1.7
-7	470	1.4	1.6
273-24	480	1.3	2.6
278-21	480	1.9	3.6
285-3	500	1.6	5.4
273-25	510	1.5	3.8
278-10	520	2.4	6.9
-11	520	2.8	4.9
285-4	540	1.3	7.6
278-16	570	2.9	9.3
285-5	580	4.6	43.5
		AV. $2.1 \pm 0.9 \times 10^{-2}$ sec^{-1}	

*All runs were performed at 24 ± 1°C with 4.0×10^{-4}M TNB except for the 278 series which was carried out with 8.0×10^{-4}M TNB. All runs used a flash energy of 450 joules/lamp except the 274 series which used flash energies which are listed in Table 3.

**$f(\epsilon)$ is an unknown function of extinction coefficient.

TABLE 3

EFFECT* OF FLASH INTENSITY ON THE SECOND ORDER RATE FOR THE TIME PERIOD AFTER 1000 μsecs

Run	λ(mμ)	Joules/Lamp	$\frac{k_2^{**}}{f(\epsilon)} \times 10^{-3} sec^{-1}$
274-1	420	250	3.8
-2	420	340	5.5
-3	420	450	4.5
-4	420	570	4.7
-5	420	700	3.6
-6	420	850	AV. $\frac{3.0}{4.2} \pm 0.9$

*All runs were carried out at 24 ± 1°C with 4.0×10^{-4}M TNB.

**$f(\epsilon)$ is an unknown function of extinction coefficient.

TABLE 4

EFFECT* OF THE CONCENTRATION OF TNB ON THE SECOND ORDER RATE CONSTANT FOR THE TIME PERIOD AFTER 1000 μsecs

Run	λ(mμ)	Conc. × 10^{-4}M	$\frac{k_2^{**}}{f(\epsilon)} \times 10^{-3}$ sec^{-1}
285-1	420	4.0	5.8
274-3	420	4.0	3.8
273-2	420	4.0	4.8
278-1	420	8.0	1.1
273-24	480	4.0	2.6
278-21	480	8.0	3.6

*All runs were carried out at 24 ± 1°C with a flash energy of 450 joules/lamp.

**$f(\epsilon)$ is an unknown function of extinction coefficient.

transient, then behavior in the initial time interval is bound to be complex. In the treatment of the initial transient behavior, it was tacitly assumed that such a consecutive sequence indeed occurs, and it was of interest to examine the initial growth in the period 70-200 μsecs. below 530 mμ and the initial decay in the period 100-300 μsecs. above 530 mμ.

Examination of traces obtained with small oscilloscope time scales (cf., Figure 19) made it quite clear that a reaction order could not be deduced. An assumption, therefore, had to be made to treat the data. It was assumed that the initial decay is primarily first order.

A graphical method was employed to estimate first order rate constants for the initial growth and decay with $t < 500$ μsecs. The changes in optical density (ΔD) at a given wavelength were obtained as usual from the traces, and were plotted on rectilinear coordinate paper as a function of time using scales which are consistent with the precision of the data. A smooth curve, representing the experimentor's best judgement, was drawn with a French curve to average the points. A representative decay of this nature is shown in Figure 22. Tangents to this decay curve were computed at 25 μsecs. intervals by dividing the difference in the ΔD values at 25 μsecs. above and 25 μsecs. below a given ΔD value by 50 μsecs. These tangents $d(\Delta D)/dt$ were then plotted against ΔD as illustrated in Figure 23. The first order rate derived from the slopes of the latter plots are listed in Table 5. The initial decay is seen to be independent of wavelength or the concentration of TMB.

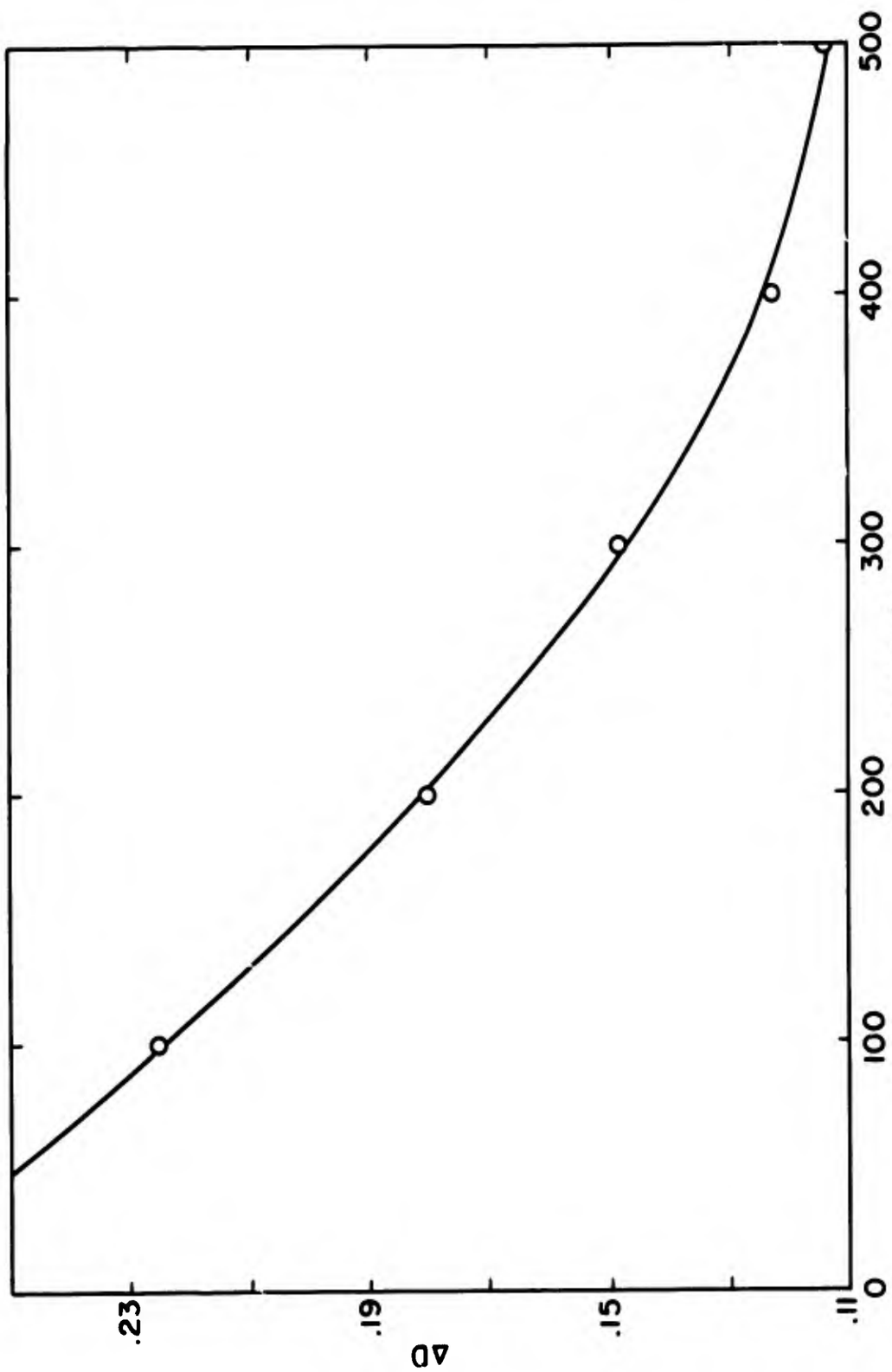

FIGURE 22: Initial Decay Curve from 8.0×10^{-4}M TNB in Ethanol at 570 mμ for run 278-16

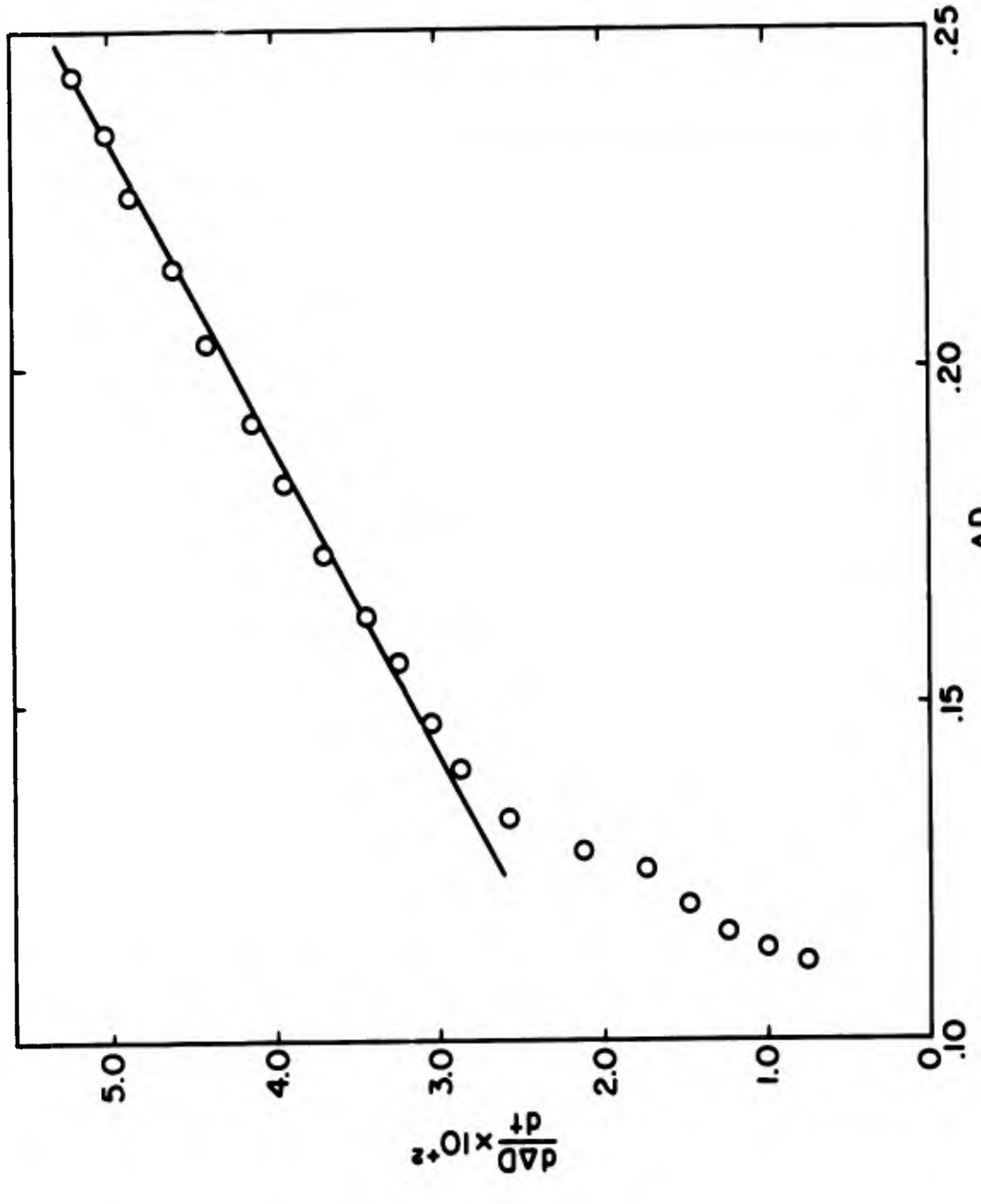

FIGURE 23: First Order Initial Slope Evaluation of the Decay Curve of Figure 29

On the formation side, the slopes of ΔD *versus* time plots were evaluated on the basis of 10 μsec. intervals. Typical examples of this plot and the $d(\Delta D)/dt$ *versus* time plot are reproduced in Figures 24 and 25. The first order formation rate constants are listed in Table 6. Again, the rate as in the decay case, is seen to be essentially independent of the wavelength and the concentration of TNB. It should be pointed out that the uncertainties listed in Tables 5 and 6 do not reflect the intrinsic uncertainty in the rate constant for a given single run. The latter is liable to be quite large. Although the data evaluation involves two subjective steps, the analysis of a single run was reasonably reproducible in the case of the decay. In the formation analysis, however, a basic difficulty is inherent in the slope evaluations. This lies in the inability to reliably estimate the initial slope in the region 70-90 μsecs. where the formation rate is diminishing most rapidly (*cf.*, Figure 24). Furthermore, it is evident that the value of the slope of $d(\Delta D)/dt$ *versus* ΔD plot is based on only a few points (compare Figures 23 and 25). The useful data range in the formation case is limited by the duration of the flash, which, although ostensibly over after *ca.* 60 μsecs., may actually be significantly longer.

3. Ethanol/Hexane Mixtures

It was mentioned earlier that flashing TNB in hexane produces only traces of transient. It is probable that the minute amount of transient observed

TABLE 5

INITIAL* DECAY RATE CONSTANTS IN THE RANGE 550-600 mμ

Run	λ(mμ)	$k_1 \times 10^{-2} sec^{-1}$
273-17	550	21
-18	560	35
-19	570	38
278-13	570	30
-15	570	53
-16	570	24
274-7	570	27
-8	570	27
-9	570	31
-10	570	42
-11	570	63
-12	570	53
288-13	580	46
		AV. $38 \pm 12 \times 10^{-2} sec^{-1}$

*All runs were conducted at 24 ± 1°C with 4.0×10^{-4}M TNB except for the 278 runs which were run with 8.0×10^{-4}M TNB. All runs used a flash energy of 450 joules/lamp except the 274 series whose flash energies are listed in Table 3.

TABLE 6

INITIAL* FORMATION RATE CONSTANTS IN THE RANGE 420-520 mμ

Run	λ(mμ)	$k_1 \times 10^{-2} sec^{-1}$
289-28	420	108
288-3	420	65
275-10	440	157
278-20	480	140
288-6	480	120
275-1	500	120
289-26	500	127
275-17	520	AV. $\frac{120}{120} \pm 16 \times 10^{-2} sec^{-1}$

*All runs were conducted at 25 ± 1°C with 4.0×10^{-4}M TNB except 278-20 which was run with 8.0×10^{-4}M TNB. All runs used a flash energy of 450 joules/lamp.

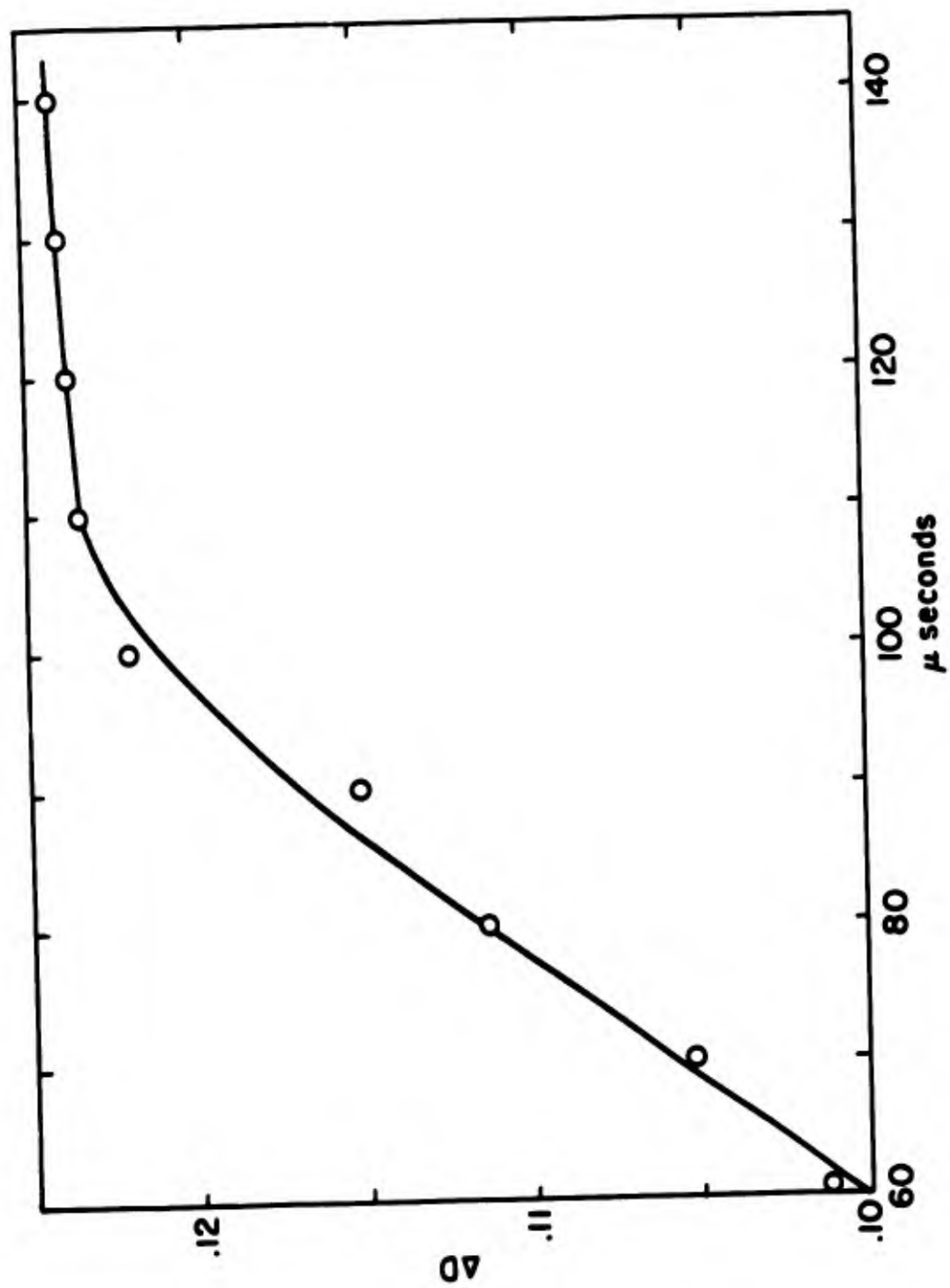

FIGURE 24: Formation Curve from 4.0×10^{-4}M TNB in Ethanol at 420 mμ for Run 275-17

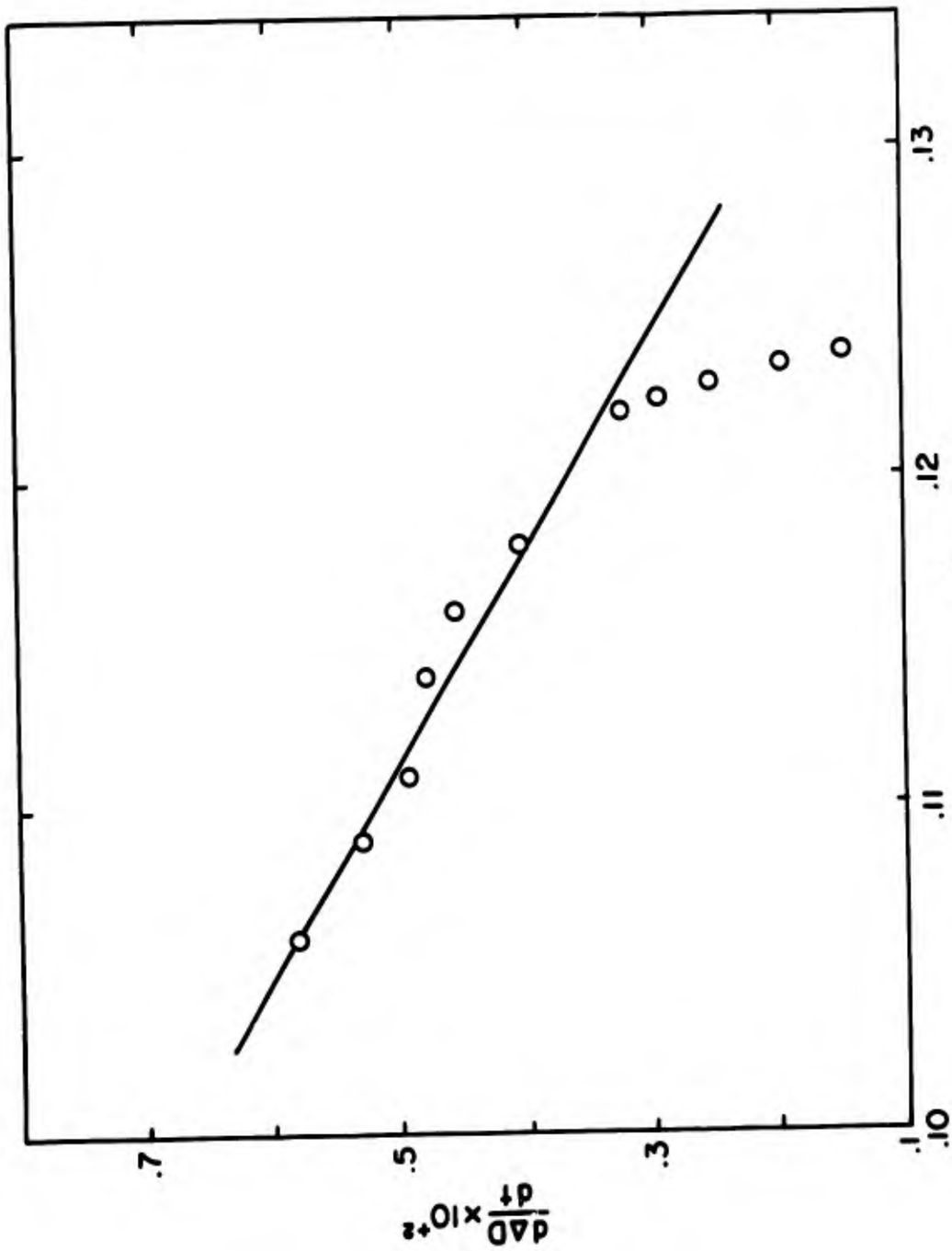

FIGURE 25: First Order Slope Evaluation of the Curve of Figure 31

is due to a slightly active impurity in this solvent. Consequently, hexane was used as a dilutant to study the effect of the alcohol concentration and the transient formation and decay.

The photolysis with diluted ethanol was studied at 570 mμ. The first order rate constants were derived for the initial rapid decay by the method described previously. The initial extent of transient formation, as reflected in values of ΔD at 100 μsecs. after the flash increases with the alcohol concentration. The relation between ΔD_{100} and the concentration is not linear (cf., Figure 26). The first order formation rate constants decrease as the concentration decrease (cf., Table 7). A plot of these rate constants against the alcohol concentration is approximately linear with a slope of 2.0×10^{-2} liters $mole^{-1}$ sec^{-1} and a intercept at, or close to zero (cf., Figure 27).

4. Effect of Air

The transient spectra observed in undegassed ethanol show the same maxima and isosbestic point as in the degassed solvent. Transient formation is less extensive and a smaller amount of product is generated. The initial transient decay was evaluated at 570 and 600 mμ for a

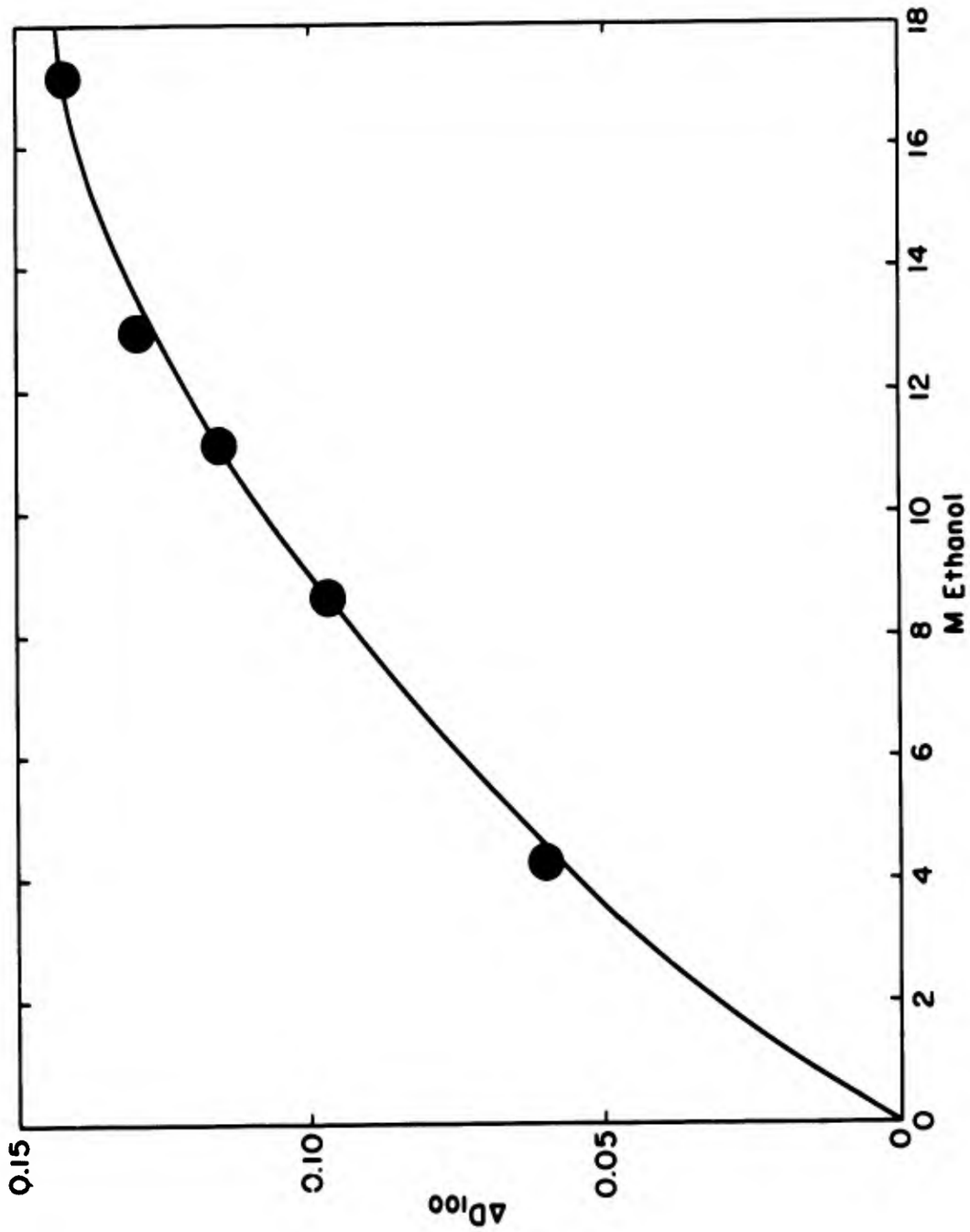

FIGURE 26: Plot of the ΔD at 100 μsecs. from 4.0×10^{-4}M TNB versus the Molarity of Ethanol

TABLE 7

EFFECT* OF THE ETHANOL CONCENTRATION ON THE AMOUNT OF TRANSIENT AND THE INITIAL DECAY AT 570 mμ

Run	M	$k_1 \times 10^{-2} sec^{-1}$	ΔD_{100}**
293-1	17.1	35	0.141
-2	12.9	26	0.129
-5	11.1	23	0.115
-3	8.6	13	0.097
-4	4.3	12	0.060

*All runs were carried out at 24 ± 1°C with a flash energy of 450 joules/lamp.

**ΔD at 100 μsecs. after the flash.

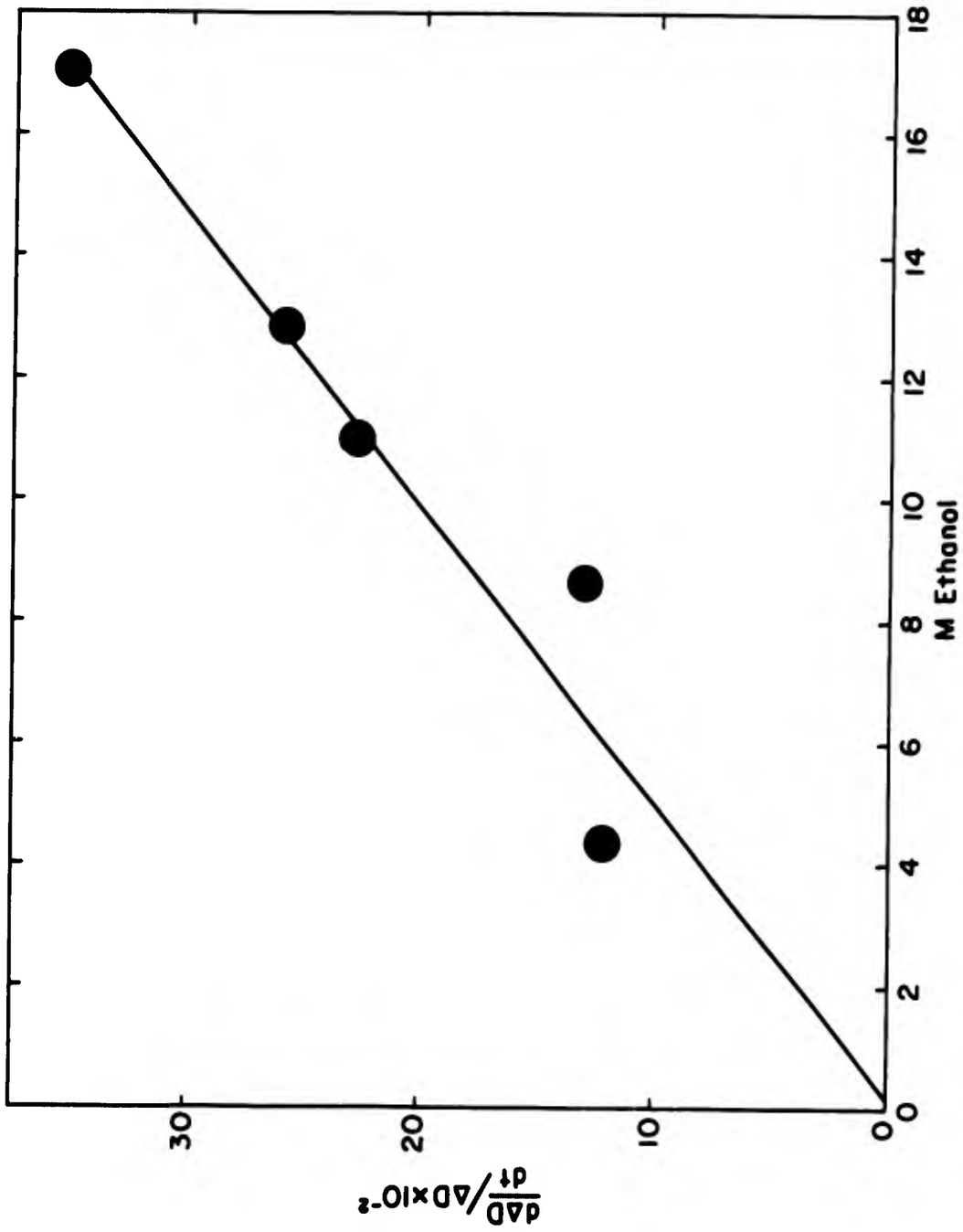

FIGURE 27: Plot of the Initial Decay Rates at 570 mμ from 4.0×10^{-4}M TNB versus the Molarity of Ethanol

1.0×10^{-3}M solution of TNB. The first order rate constants at these two wavelengths were found to be $82 \times 10^{+2}$ sec^{-1} and $86 \times 10^{+2}$ sec^{-1}, respectively. These values may be compared with the value of $36 \times 10^{+2}$ for an 8.0×10^{-4}M degassed solution of TNB. It, therefore, appears probable that both the initially observed transient and its precursor react with oxygen.

Effect of Temperature in Pure Ethanol

Measurements at temperatures other than room temperature were carried out in an all-quartz Dewar vessel with evacuated windows. The samples were cooled with methanol-dry ice slushes and the flash tubes were covered with "Pyrex" glass to confine the light absorption to wavelengths > 300 mμ. The path length of the cell was only 4.5-cm. and the changes in optical density were, therefore, diminished by a factor of about three relative to those observed in the standard length cells. Although it was not possible to obtain reliable rate constants, the following trends were noted at 450 mμ in the temperature range -50°C to +30°C. These were:

(1) The initial formation rate decreases with a decrease in temperature.

(2) The subsequent decay rate also decreases with a decrease in temperature.

If indeed there are two transients showing absorption in this region, as was surmized earlier, and if they decay in consecutive steps, than the temperature behavior indicates that the decays of both transients are activated processes.

B. Unbuffered Water - Ethanol Mixture

Some data were acquired in water/ethanol (50/50) mixtures, but no detailed kinetic analyses were performed. The transient spectrum (cf., Figure 28) is very similar to that observed in pure ethanol (cf., Figure 18). More than one transient species is evident not only from this spectrum, but also from the computer analysis of the decay data. The product formed appears identical to that from pure ethanol. Figure 28 shows an isosbestic point near 520 mμ. Analysis of the initial decay at 570 and 590 mμ gave values of $26 \times 10^{+2}$ sec^{-1} and $36 \times 10^{+2}$ sec^{-1}, respectively for the first order rate constant. In comparing these values with those in Table 7, it is noted that the half-fold dilution of the alcohol with water does not produce the same decrease in the first order rate constant as does dilution with hexane. No transient absorption is evident in pure water under any conditions. Yet it is clear that water is not an inert solvent in the same sense that hexane is.

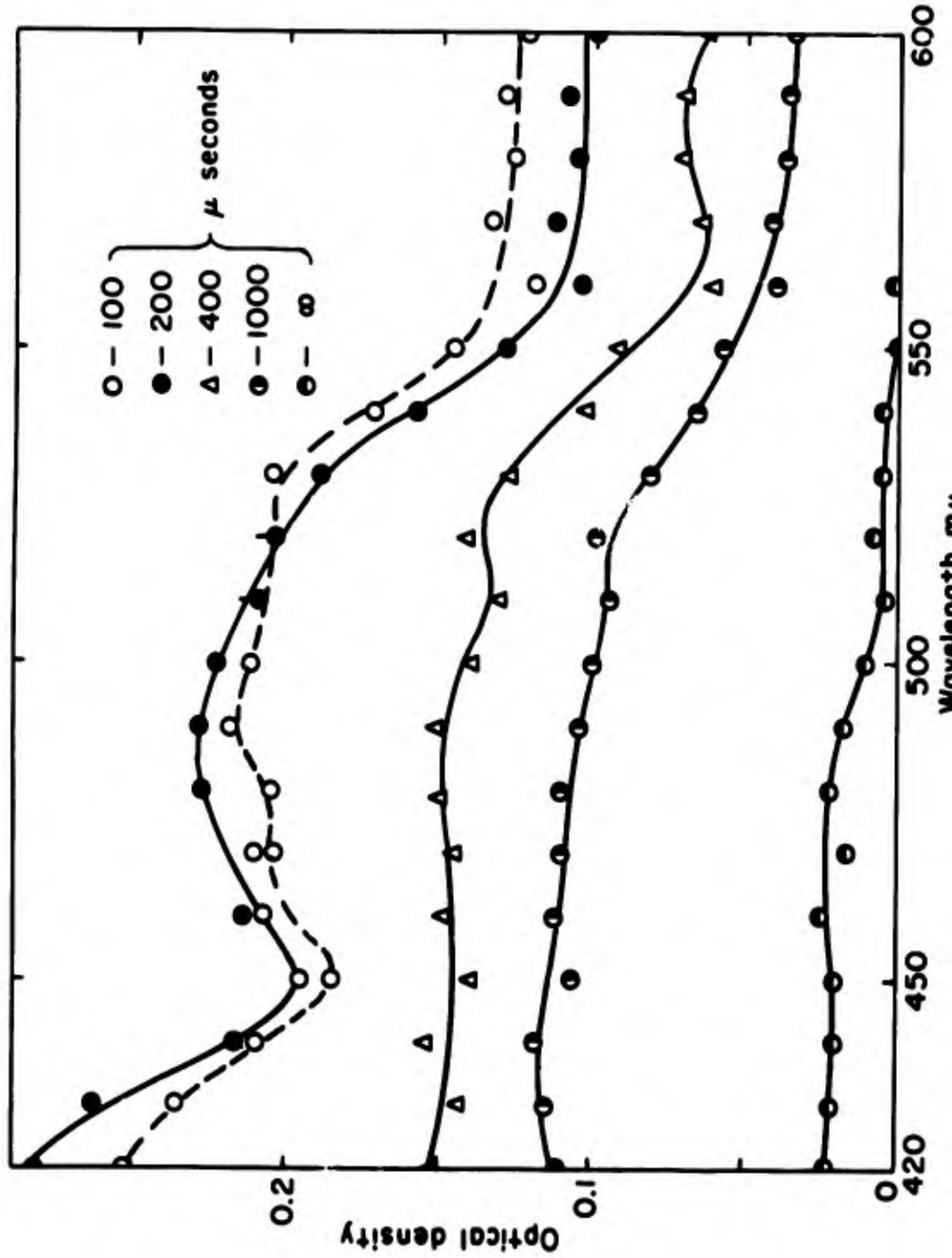

FIGURE 28: Transient Spectra from 4.0×10^{-4}M TNB in (50/50) Water - Ethanol

At long times after the flash (t > 100 μsecs.) the water/ethanol system shows similar kinetic behavior to that of pure ethanol, i.e., no unequivocal distinction can be made between the final first and second order decay modes. The rate constants at four wavelengths are compared with those in pure ethanol in Table 8. The first order constants indicate the decay to be slightly faster in the aqueous medium; with the second order constants any effect could be masked by changes in the extinction coefficient in the two media.

C. Buffered Water - Ethanol Mixture

Buffered solutions of TNB in 1:1 ethanol/water were examined at pH 2 and pH 8.5. The latter value just produces a solution with a spectrum identical with that in neutral solution. At higher pH values, the base addition complex exists in appreciable quantity and there are significant spectral changes in the ground state (cf., Figure 12).

The transient spectrum for the pH 2 solvent is shown in Figure 29. This spectrum is not too dissimilar from those in pure ethanol and in unbuffered ethanol/water mixtures (Figures 18 and 28), except that the absorption near 500 mμ and at ca. 580 mμ is more prominent. There is an isosbestic point near the first peak. Below the

TABLE 9

FIRST ORDER* AND SECOND ORDER RATE CONSTANTS FOR THE TRANSIENT DECAY AFTER 1000 μsecs IN 1:1 ETHANOL/WATER

Run	λ(mμ)	$k_1 \times 10^{-2} sec^{-1}$		$\frac{k_2}{f(\epsilon)}^{**} \times 10^{-3} sec^{-1}$	
		Ethanol/Water	Ethanol	Ethanol/Water	Ethanol
282-3	430	2.8	1.7	1.8	3.3
-4	450	3.5	0.6	3.2	2.1
-5	460	4.0	0.7	3.5	2.6
-7	470	3.6	1.4	3.2	1.6

*All runs were carried out at 25 ± 1°C with 4.0×10^{-4}M TNB. A flash energy of 450 joules/lamp was used.

**$f(\epsilon)$ is an unknown function of the extinction coefficient.

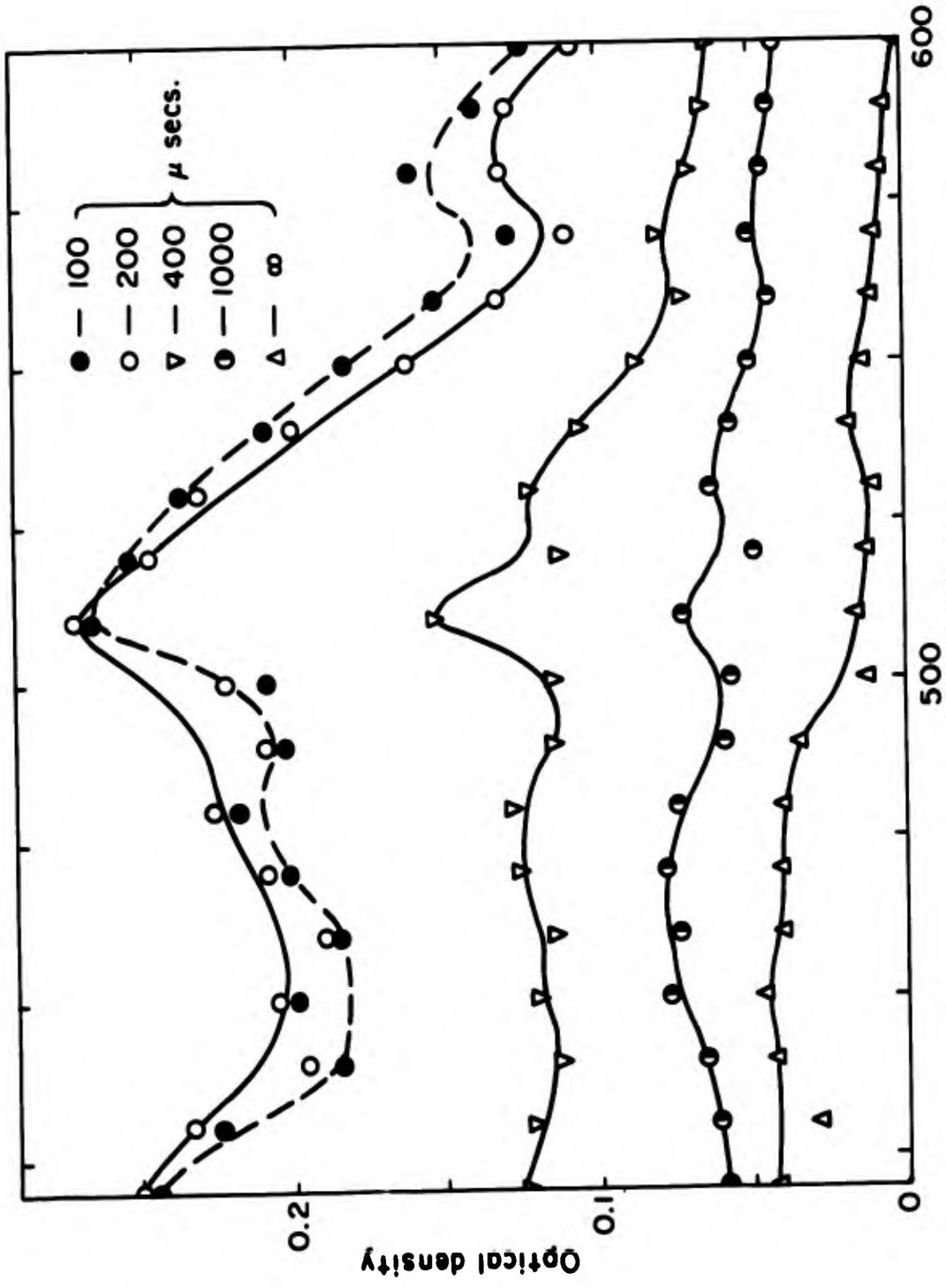

FIGURE 29: Transient Spectra from 4.0×10^{-4}M TNB in pH 2.0 Buffered Water-Ethanol

isosbestic point there is initial growth with simultaneous decay at the longer wavelengths. However, the subsequent decay consists of two distinct processes: A rapid decay which is complete in ca. 1 msec. followed by a very slow decay. This is evident at all wavelengths. The oscilloscope traces at 420 and 580 mμ are reproduced in Figure 30. The transient on the 1 msec. scale is seen to decay to a relatively stable species. On the 200 μsec. scale, initial growth at 420 mμ with concurrent decay at 580 mμ is clearly evident. The close resemblance to the behavior in pure ethanol suggests that the processes occurring in this medium are the same in the initial phases, but that after 1 msec. another intermediate is generated which slowly decays to the same flash product.

The transient spectrum at pH 8.5 is shown in Figure 31. There is an isosbestic point at slightly longer wavelengths (560 mμ) than in the previously described cases. The decay is quite complicated, with a second isosbestic point appearing near 470 mμ after ca. 1800 μsecs. This is good evidence for the inclusion of a third transient. The transient absorption extends to at least 800 mμ. Judging by the spectrum at infinite time, the same flash product is formed as in the other media.

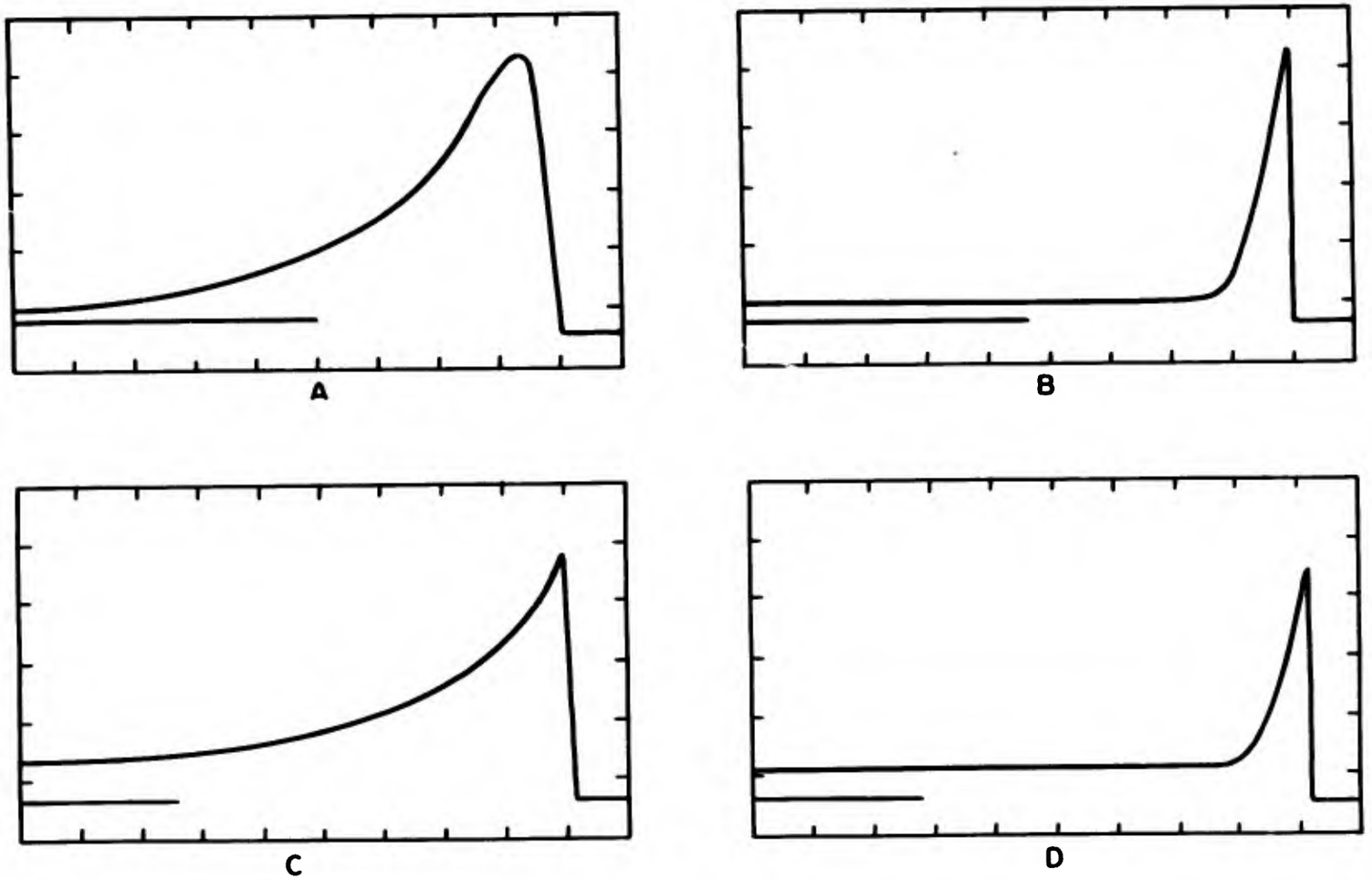

FIGURE 30: Oscilloscope Traces of the Transient Decay at 430 mμ and 580 mμ from 4.0×10^{-4}M TNB in pH 2.0 Water-Ethanol - The left horizontal Trace is the V_{oo} Line.

A. 430 mμ Time - 200 μsec./division
B. 430 mμ Time - 1 msec./division
C. 580 mμ Time - 200 μsec./division
D. 580 mμ Time - 1 msec./division
Vertical Scale - 1.0 volt/division

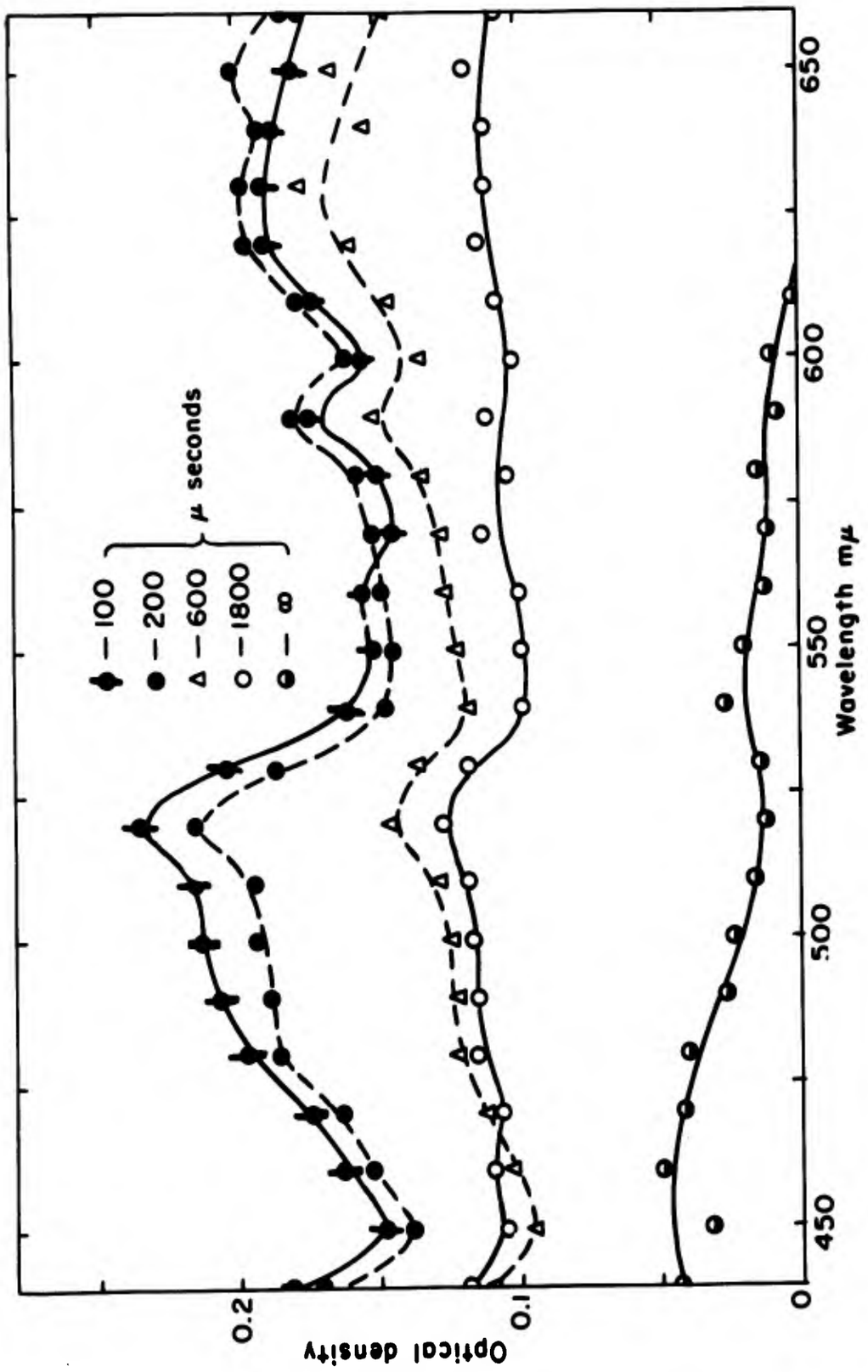

FIGURE 31: Transient Spectra from 4.0×10^{-4}M TNB in pH 8.5 Buffered Water-Ethanol

Between 400 mμ and the isobestic point at 560 mμ, the decay is rapid in the first ca. 600 μsecs. Above ca. 560 mμ the initial decay is considerably more slower. Finally, after about 2000 μsecs. there is an extremely slow decay in evidence at all wavelengths. The second isobestic point is indicative of the slow generation of another transient species. This is clearly shown at the 420 wavelength in the traces of Figure 32. In view of this complex behavior, no quantitative rate data could be obtained for this system. It seems certain that here at least three, and possibly four transients with extensively overlapping absorption are generated.

D. Dinitrobenzene and Nitrobenzene in Ethanol

Only a limited number of flash experiments were performed with DNB and NB. Nitrobenzene in ethanol can be summarized readily: No transient absorption could be detected under the standard conditions employed.

The transient spectra at various times with a 6.0×10^{-4}M solution of DNB in ethanol are shown in Figure 33. Transient formation is considerably less extensive than with TNB as is evident from the small ΔD values. In view of the smallness of the optical density changes, there is no clear indication of an isobestic point. Between 430 and 490 mμ, the 110 μsec, and the 220 μsec. spectra

coincide, but above 550 mμ the decay is monotonic. At infinite time, ΔD returns to zero at all wavelengths; this does not necessarily mean that the product shows no absorption in the visible region. Rather, it is likely that no absorption was detected due to the extensively small extent of conversion. At 1400 μsecs, a new broad peak appears near 500 mμ. This indicates a slower decay in this region than at the higher or lower wavelengths. At least two transients can be inferred from this behavior alone. In view of the small magnitude of the ΔD values, no kinetic evaluation was performed with this system.

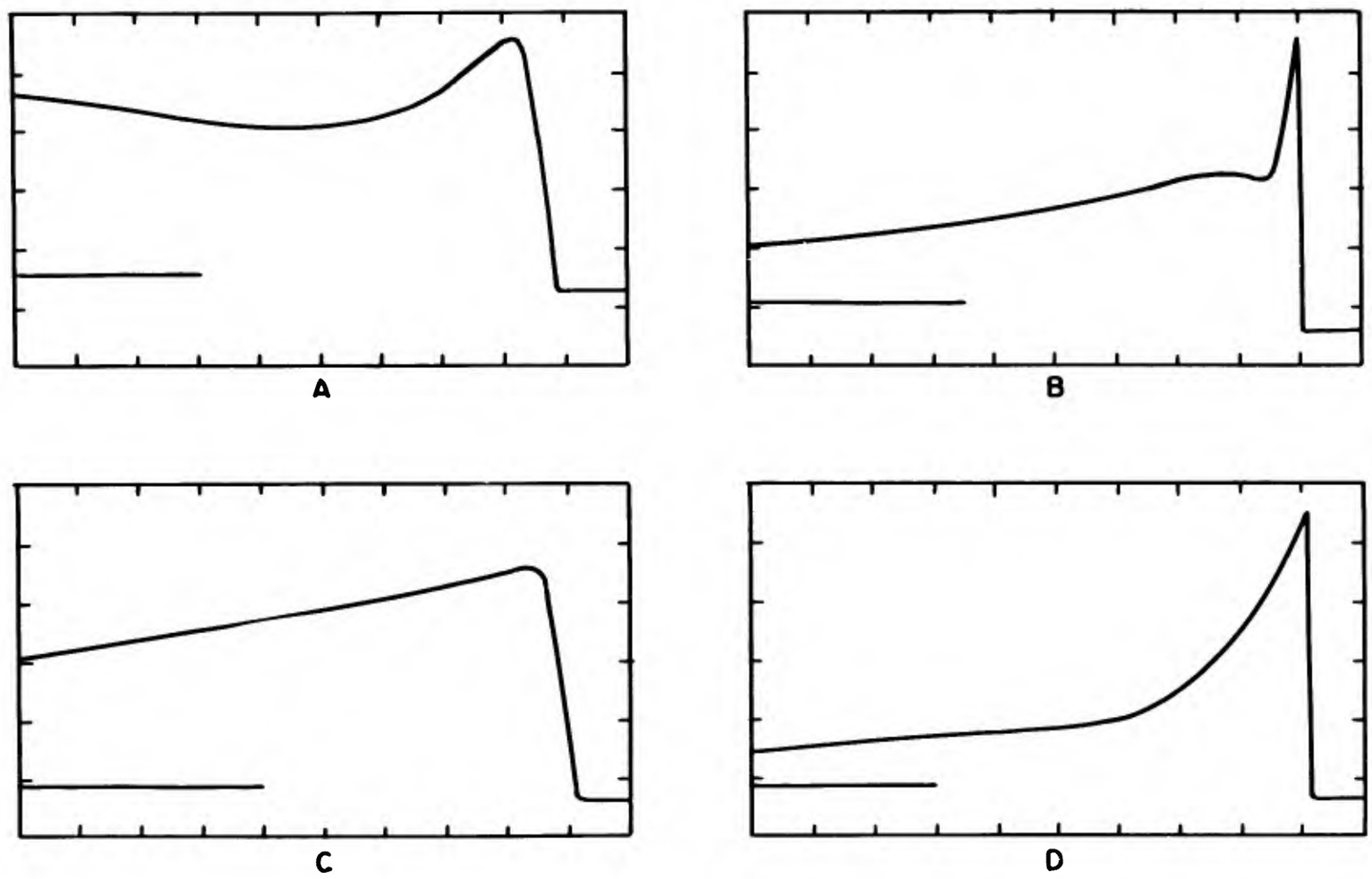

FIGURE 32: Oscilloscope Traces of the Transient Decay at 420 mμ and 580 mμ from 4.0 x 10^{-4}M TNB in pH 8.5 Water-Ethanol - The left Horizontal Trace is the V_{oo} Line.

A. 420 mμ Time - 200 μsec./division
B. 420 mμ Time - 2 msec./division
C. 580 mμ Time - 200 μsec./division
D. 580 mμ Time - 2 msec./division
Vertical Scale - 1 volt/division

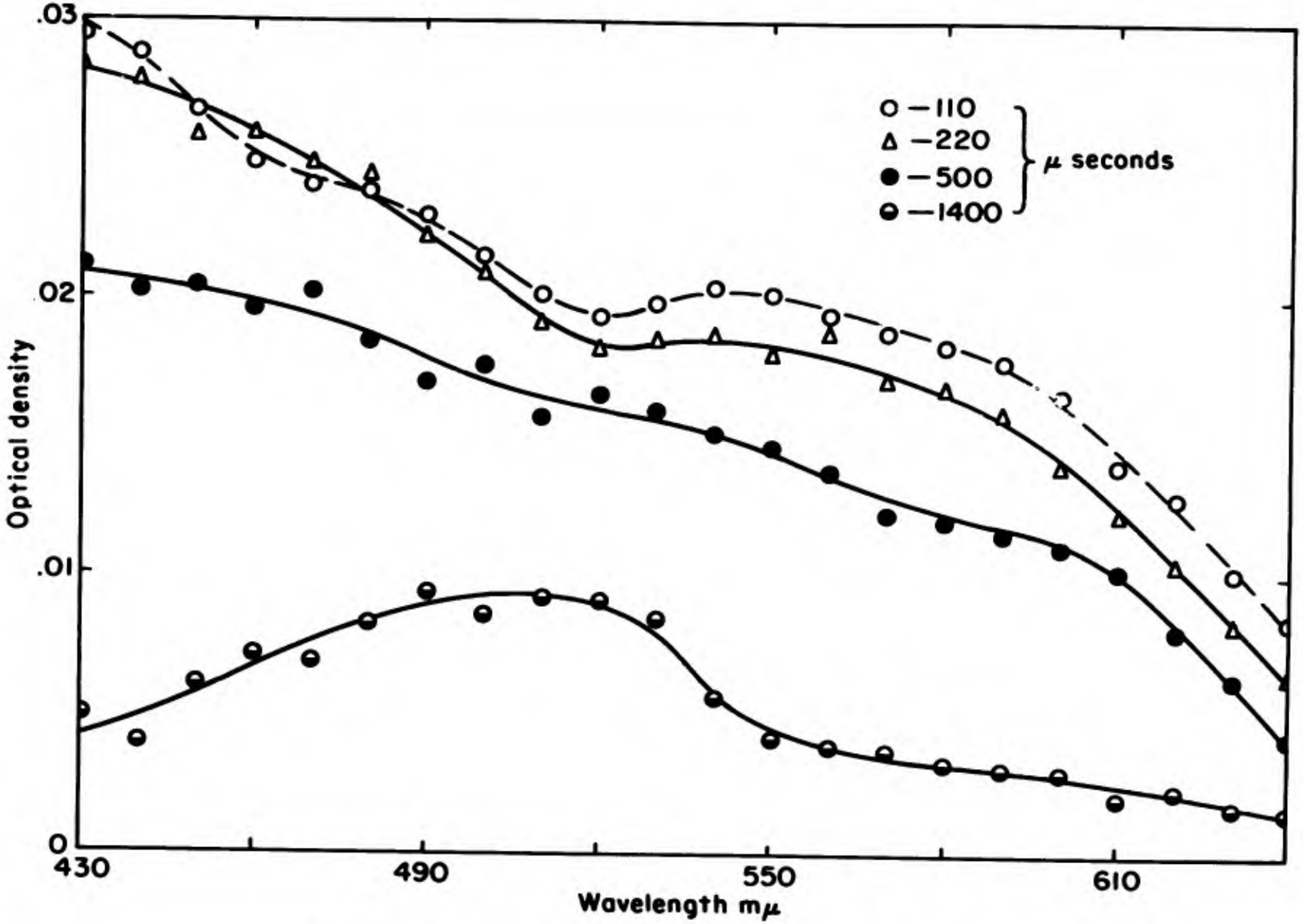

FIGURE 33: Transient Spectra from 6.0×10^{-4}M DNB in Ethanol

Discussion

1. General Considerations

The excitation of TNB was confined to wavelengths above 300 mμ. No unequivocal assignment of the transition corresponding to this tail band (cf., Figure 6) has been reported. There are perhaps only two choices of transitions which are suitable for the assignment of this weak band: An $n \rightarrow \Pi^*$ excitation of the non-bonding electrons of the nitro group or a $\Pi \rightarrow \Pi^*$ transition. The closely analogous compound nitrobenzene has a similar weak band at 330 mμ. The assignment of this transition is still the subject of controversy, but the best evidence for it being $n\text{-}\Pi^*$ in character is the absence of fluorescence from nearly all nitro substituted aromatics.[34] We have similarly observed no fluorescence upon excitation of a degassed solution of TNB in ethanol with 366 mμ light.*

In the case of TNB, McConnell and Lawrey[35] report on oscillator strength of 10^{-3} for the absorption band at 440 mμ and 10^{-2} for the band at 350 mμ. Exact distinction between these bands is obscured by

---

* The fluorescence spectrum was measured with the apparatus described in Section 2 of this report.

their broadness (cf., Figure 6) but, nevertheless, on the basis of a slight blue shift in polar solvents, it is suggested that the shoulder at 400 mμ represents the n-Π^* transition. Support of this assignment from the theoretical point of view, comes from SCF-MO calculations by Peacock and Wilkinson.[36] Their singlet excited state calculations tend to confirm the experimental assignments by McConnell and Lawrey. The lowest lying triplet state was calculated to be ca. 36 K.cal. (12,500 cm^{-1}) above the ground state, but no phosphorescence has ever been observed[37] from TNB to confirm this assignment. Our inability to detect triplet-triplet or other transient absorption on flash photolysis of solutions of TNB in water or hexane is not surprising in view of the above findings.

With these facts in mind, especially the reported absence of phosphorescence, the lack of triplet-triplet absorption in inert solvents, and the lack of fluorescence from TNB, the photochemically active state must be assigned as the n-Π^* singlet state which does not undergo facile intersystem crossing to the triplet state. Though most singlet excited states result from allowed transitions and have radiative lifetimes of ca. 10^{-9} sec., the singlet state in this case with an oscillator strength of 10^{-2} at 350 mμ has a longer mean lifetime of ca. 10^{-7} sec. The transients and permanent product found upon excitation of TNB in alcohols and other reactive solvents can be expected to be derived from the excited singlet state by hydrogen abstraction from the solvent.

It is pertinent at this point to review the work of Testa and Hurley[12] on the photoreduction of nitrobenzene in isopropanol, which

supports the creation of free radical intermediates. In this recent study, nitrobenzene was excited at 366 mμ and phenylhydroxylamine and acetone were identified as the products. In the presence of dissolved oxygen, phenylhydroxylamine is converted into nitrosobenzene and azoxybenzene. Their proposed mechanism is as follows:

$$ArNO_2(\text{triplet}) + RCHOHR \rightarrow Ar\dot{N}O_2H + R\dot{C}OHR \quad \ldots(10)$$

$$Ar\dot{N}O_2H + R\dot{C}OHR \rightarrow RCOR + Ar\dot{N}(OH)_2 \quad \ldots(11)$$

$$Ar\dot{N}(OH)_2 + RCHOHR \rightarrow Ar\dot{N}OH + R\dot{C}OHR + H_2O \quad \ldots(12)$$

$$Ar\dot{N}OH + R\dot{C}OHR \rightarrow ArNHOH + RCOR \quad \ldots(13)$$

The structure $Ar\dot{N}(OH)_2$ is obviously in error, and should be written as $ArN(OH)_2$. With the inclusion of this correction it is doubtful that phenylhydroxylamine could originate from this sequence of reactions. The radical intermediate $Ar\dot{N}O_2H$ and $ArN(OH)_2$ have been proposed on the basis of pulse radiolysis[38] and electrochemical reduction[39] studies of nitrobenzene in ethanol. The best evidence for a free radical intermediate has eventually evolved from ESR studies of the photolysis of nitrobenzene in THF[14] or in basic ethanol[40] where the respective radicals $Ar\dot{N}O_2H$ and $ArNO_2^-$ are unequivocally identified.

Our low temperature ESR experiments showed that a short-lived radical is formed from TNB in ethanol which is assigned to the $(NO_2)_2Ar\dot{N}O_2H$ radical. This assignment is based on the comparison of a similar ESR spectrum observed in the photolysis of TNB in THF at 25°C. In THF, Ward[14] found splitting constants of A_N = 13.0 gauss and A_H = 3.0 gauss in good agreement with our findings of A_N = 13.0 gauss

and A_H = 3.4 gauss for the photolysis of TNB in ethanol. No further splitting from the interaction of the electron with the two other nitrogen atoms was observed.

The unusual stability of the $(NO_2)_2ArNO_2H$ radical in THF at room temperature relative to that in ethanol at much lower temperatures is somewhat surprising. Lagercrantz[41] has suggested charge-transfer stabilization (THF - $(NO_2)_2ArNO_2H$) or ion-pairing, bit the pressure of such species is without experimental foundation. The first order decay of the radical signal in THF may be attributed to further abstraction from the solvent followed by rapid decay of the solvent-derived radicals. This aspect of the decay will be considered again later in this section.

2. Mechanistic Considerations

In formulating a mechanism for the photoreduction of TNB in ethanol or ethanol/hexane mixtures, the following facts pertaining to the behavior of TNB with flash and continuous radiation must be considered.

1. The transient spectrum shows an isosbestic point near 530 mμ (cf., Figure 18).
2. Below ca. 500 mμ the transient absorption is still growing in the 70-200 μsec. interval after the flash. The growth reaches a maximum optical density in ca. 200 μsecs.
3. Above ca. 550 mμ, the maximum optical density is reached within 100 μsecs. after the onset of the flash. The transient is already decaying in the first 100-200 μsec.

interval after the flash while it is still growing at the shorter wavelengths. The initial decay rate at these wavelengths is about the same as the initial formation rate at wavelengths below 500 mμ.

4. The decay at all wavelengths over the time range 0-8000 μsecs. does not follow a simple rate law, such as first order, second order, or combined first and second orders.
5. In the range 1000-8000 μsecs. appropriate plots of the decay indicate reasonable adherence to a second order law. However, since the optical density differences in this time range are quite small, a final first order decay cannot be ruled out.
6. The initial decay at all wavelengths in the first 300 μsecs. is definitely more rapid than the final decay.
7. On the basis of the observation of an isosbestic point and the obvious difference in the rate of the decay at one wavelength over successive time intervals, at least two transients along with the flash product are absorbing at all wavelengths.
8. No transient is evident in solvents such as hexane, benzene, or water. TNB in water exhibits no photoreactivity with continuous exposure over long periods of time. Transients are formed only in hydrogen - donating solvent such as alcohols or THF.
9. In ethanol/hexane mixtures the maximum optical density change produced increases with increasing alcohol concentration at constant flash intensity, though not linearily.

10. Upon photolysis in a rigid ethanolic glass at liquid nitrogen temperatures, a species absorbing in the visible region is formed. After warming to room temperature, a spectrum identical with that of the flash product is observed. Further, at low temperatures in ethanol, the ESR spectrum can unequivocally be assigned to $(NO_2)_2ArNO_2H$ radical.

11. A single flash (450 joules/lamp) produces a single permanent product. The continuous photolysis product, TNAB, was not detected by TLC analysis.

12. On the basis of isolation experiments, the upper limit of the conversion of TNB into photoproduct is ca. 1%/flash.

13. Since the analysis of the actual flash product generated in ethanol was impractical, a sample of the product was generated by the short continuous photolysis in methanol (cf., Figure 5). The mass spectrum* indicates a molecular weight of 446, corresponding to a combination of two molecules of TNB, two hydrogen atoms, and one molecule of water.

14. Acetaldehyde and TNAB were identified as photoproducts from the continuous photolysis of 10^{-3}M TNB in ethanol. As the concentration of TNB is increased, 3,5-dinitroaniline is formed in minor amount. Photolysis at the 546 mμ band of the flash product converts this material into TNAB.

---

*The mass spectral analysis was performed by the West Coast Analytical Service, San Gabriel, California.

From the above considerations several conclusions can be drawn. These points are as follows:

1. It is highly unlikely that the photochemically reactive state is the triplet state of TNB.
2. Since there is no evidence to the contrary, it may be assumed that only two transients are observed in this solvent system.
3. Since the initial absorption after the flash is not due to the triplet, the first rapidly decaying transient is probably the free radical (TNBH·) formed by a hydrogen abstraction step.
4. The photoreduction of TNB is assumed to involve the participation of only one nitro group. This assumption is supported by the electrochemical evidence[42] that the reduction of TNB proceeds by four one-electron steps to 3,5-dinitroaniline.
5. The key chemical step in the photoreduction is the hydrogen abstraction from the solvent to form TNBH· . The evidence suggests that this radical is formed during the lifetime of the flash.
6. There is no evidence that the solvent-derived radical (RH·) does react further with TNB. The pathway for the disappearance of this radical is presumably a bimolecular dismutation step:

$$2RH\cdot \rightarrow R + RH_2 \; . \qquad \ldots(14)$$

In this connection it is noted that the ethanol derived radical, CH_3CHOH, is apparently not a good hydrogen donor since the limiting quantum yield for the photoreduction of benzophenone in ethanol is unity.[43] However, the limiting quantum yield in isopropanol is 2, which indicates a reaction between RH· and the ground state ketone.

R in the above equation corresponds to acetaldehyde, which was isolated in the continuous photolysis experiment. This gas would be extremely difficult to detect in a flashed solution of TNB in ethanol owing to the maximum conversion of ca. 1%. The disappearance of RH· would be diffusion-controlled with an approximate rate constant of 10^9 liter $mole^{-1}$ sec^{-1}. Taub and Dorfman[44] have demonstrated this mode of disappearance for the radical in the pulse radiolysis of ethanol. Further, the dimerization and/or disproportionation of the solvent-derived radical has been proposed by Ward[14] for the photochemical generation of TNBH· in THF.

3. Mechanism of the Photoreduction of TNB

With all these facts and assumptions in mind, and after careful consideration of many alternatives, two simple mechanisms are proposed which are based on two transient species.

A. Reaction Scheme I

$$TNB \xrightarrow{h\nu} TNB^* \quad \ldots(15)$$

$$TNB^* \longrightarrow TNB \quad \ldots(16)$$

$$TNB^* + RH_2 \longrightarrow \dot{T}NBH + RH\cdot \quad \ldots(17)$$

$$\dot{T}NBH + RH_2 \xrightarrow{k_1} TNBH_2 + RH\cdot \quad \ldots(18)$$

$$TNBH_2 + TNB \xrightarrow{k_2} (TNBH)_2 \quad \ldots(19)$$

$$2RH\cdot \xrightarrow{k_3} R + RH_2 \quad \ldots(20)$$

The reactions of equations (15) through (17) are considered to occur during the flash. Identifying A with TNB, B with $\dot{T}NBH$, C with $TNBH_2$, the product P with $(TNBH)_2$, RH· with $CH_3\dot{C}HOH$, R with CH_3CHO, and RH_2 with ethano, the differential equations for the reactions after the end of the flash are:

$$\frac{dA}{dt} = - k_2AC \quad \ldots(21)$$

$$\frac{dB}{dt} = - k_1B(RH_2) \quad \ldots(22)$$

$$\frac{dC}{dt} = k_1B(RH_2) - k_2AC \quad \ldots(23)$$

$$\frac{dP}{dt} = k_2AC. \quad \ldots(24)$$

In these, and in subsequent equations, the capital letters A, B, C, P, and RH_2 represent the concentrations of the species designated above.

The material balance easily follows:

$$A + B + C + 2P = A^{o} = A^{\infty} + 2P^{\infty}, \qquad \ldots(25)$$

where the superscripts refer to the initial time ($t = 0$) and at infinity ($t = \infty$). The measured optical density, ΔD, is comprised of transient species by the basic Beer's law definition

$$\Delta D = \epsilon_A A + \epsilon_B B + \epsilon_C C + \epsilon_P P - \epsilon_A A^{o} \qquad \ldots(26)$$

$$\Delta D_{\infty} = \epsilon_A A^{\infty} + \epsilon_P P^{\infty} - \epsilon_A A^{o} . \qquad \ldots(27)$$

In the initial decay region ($t = 0$-300 μsecs.) the decay of C can be ignored and the ΔD expression is reduced after substitution for A^{o} to

$$\Delta D = B(\epsilon_B - \epsilon_A) + C(\epsilon_C - \epsilon_A). \qquad \ldots(28)$$

Further, if the decay of C is assumed to be unimportant initially, the differential equations (22) and (23) can be solved for C in terms of B.

$$C = B_o' - B, \qquad \ldots(29)$$

where B_o' is the concentration of species B at the end of the flash and the beginning of the decay. After substitution for C in the expression for the rate of change of ΔD, i.e.,

$$\frac{d(\Delta D)}{dt} = (\epsilon_B - \epsilon_A)\frac{dB}{dt} + (\epsilon_C - \epsilon_A)\frac{dC}{dt} \qquad \ldots(30)$$

The initial decay equation which follows predicts a plot of $d(\Delta D)/dt$ <u>versus</u> ΔD is linear with a slope of $k_1(RH_2)$

$$\frac{d(\Delta D)}{dt} = -k_1(RH_2)\ [\Delta D - \Delta D'].\qquad ...(31)$$

Here $\Delta D'$ is a constant term equal to $B_o^1(\epsilon_C - \epsilon_A)$, which represents the maximum optical density change due to C which can be expected in the absence of the decay of C.

In the final region ($t > 1000$ μsecs.) the decay of B is assumed to be completed ($dB/dt = 0$) and the optical density change reflects the decay of C into P. Here, the optical density change must be corrected for absorption due to P. With transient B absent, material balance gives

$$C = (A - A^{\infty})\qquad ...(32)$$

$$C = -(P - P^{\infty})\qquad ...(33)$$

and the substitution, $dC/dt = -k_2AC$, yields

$$\frac{d(\Delta D)}{dt} = -(\epsilon_A + \epsilon_C - \epsilon_P)\ k_2AC.\qquad ...(34)$$

If it can be assumed that the consumption of A is negligible (based on the low conversion yield of the reaction) it follows that $A \approx A^{\infty} \approx A^{o} >> C$. This assumption leads to the integrated first order law

$$\ell n(\Delta D - \Delta D_{\infty}) = -k_2A^{o}t + \text{Const.}\qquad ...(35)$$

If the assumption A >> C is not valid, the following expression containing first and second order terms is obtained.

$$\frac{d(\Delta D)}{dt} = \frac{-k_2}{\epsilon_A + \epsilon_C - \epsilon_P} (\Delta D - \Delta D_\infty)^2 - k_2 A^\infty (\Delta D - \Delta D_\infty) \quad \ldots(36)$$

This equation predicts that a plot of

$$(\Delta D - \Delta D_\infty) \text{ versus } \frac{d\Delta D}{dt}\left(\frac{1}{\Delta D - \Delta D_\infty}\right)$$

should, for the region t > 1000 μsec., have a slope of $\frac{k_2}{\epsilon_A + \epsilon_C - \epsilon_P}$ and the intercept $k_2 A^\infty$. With the approximation $A^\infty \approx A^o$, k_2 can be calculated. This equation appears not to hold, as illustrated in Figure 35 , which represents the experimental data of Figure 34 , in the time range from 1500-8000 μsecs. However, the "snaking" of the plot may be due to the smallness of the change in optical density and a consequent large error. Averaging the points provides a second order slope, which may have validity.

For the initial decay, the equation (31) describes a dependence on the alcohol concentration. This dependence was born out experimentally.

It is considered unlikely that a second order decay of species B would involve the alcohol concentration. Thus the decay of B by the reaction with a molecule of alcohol seems entirely reasonable. In this connection it should be recalled that the decay of the $(NO_2)_2ArNO_2H$ radical, which we have identified with transient B, shows first order decay in THF, although the absolute rate is much slower. From the slope of Figure 23 in which $k_{expt} = k_1(RH_2)$ derived from the

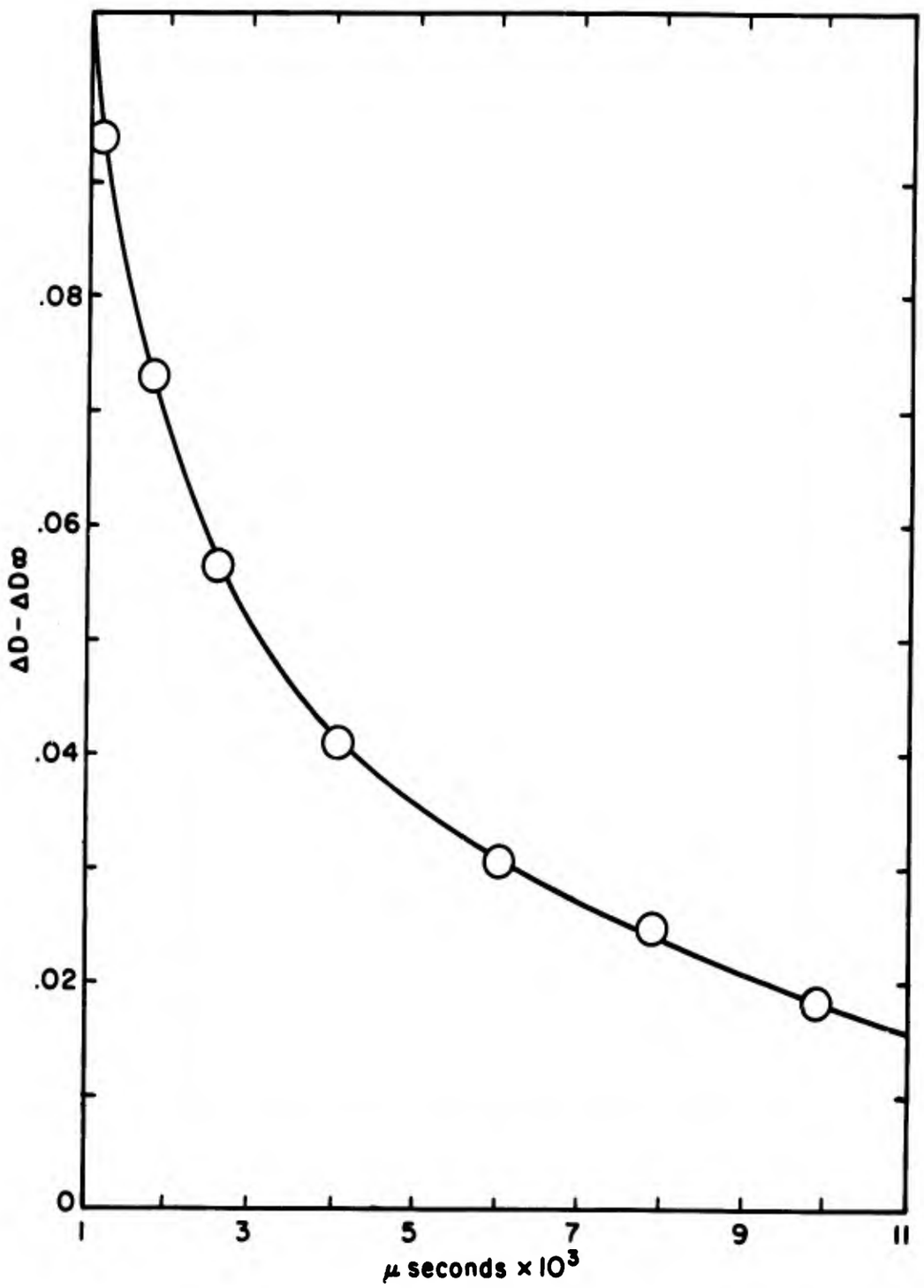

FIGURE 34: Transient Decay Curve from 4.0×10^{-4}M TNB in Ethanol at 420 mμ

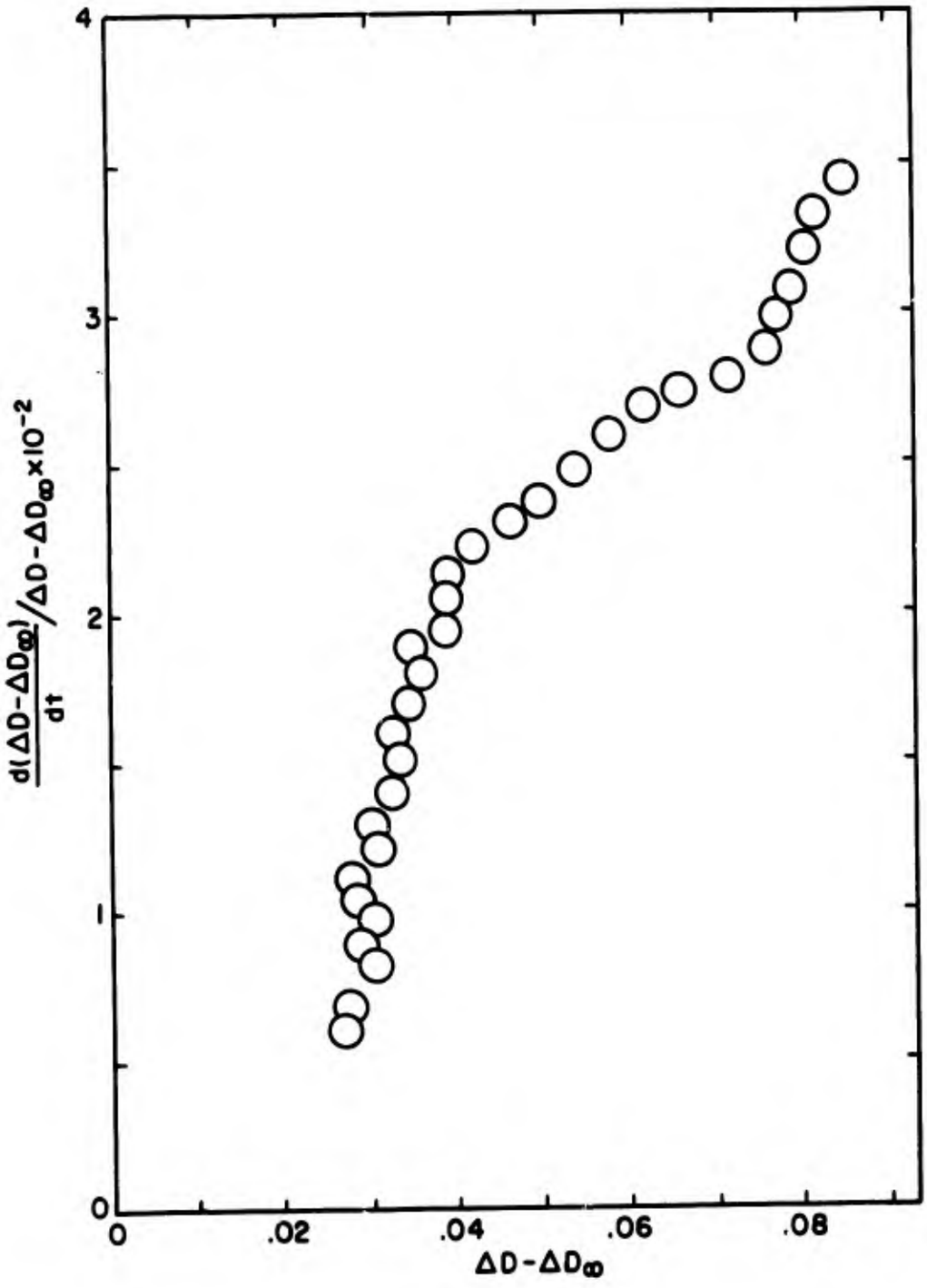

FIGURE 35: Experimental Test of the Decay Curve of Figure 33 to fit Equation 36

initial decay at 570 mμ is plotted against the alcohol concentration, the value $k_1 = 1.4 \times 10^{+2}$ liter $mole^{-1}$ sec^{-1} for the decay of B and the formation of C is obtained. It can be readily shown that the equation for the initial rate of change of ΔD with time is the same for all processes

$$RH_2 + B \rightarrow nC, \qquad \ldots(37)$$

where n = 1,2,3,...,n. The inability to distinguish between the cases n = 1, and n = 2, in particular, open up the possibility that B is a radical involving 2 molecules of TNB. Reactions scheme based on this possibility have been examined. They are, however, considered unlikely inasmuch as the ESR measurements reveal only one radical, namely $(NO_2)_2Ar\dot{N}O_2H$.

B. Reaction Scheme II

The formation of radical B during the lifetime of the flash is formulated as in Reaction Scheme I (equations (15) to (17)). The decay steps are then proposed to be

$$B + RH_2 \xrightarrow{k_1} C + RH\cdot \qquad \ldots(38)$$

$$2C \xrightarrow{k_3} P'. \qquad \ldots(39)$$

Here P' corresponds to the bimolecular product $(TNBH_2)_2$ which is now comprised of two TNB molecules and four hydrogen atoms. This is two more hydrogen atoms than the molecular weight of 446 found for the methanol photolysis product, which corresponds to two molecules of TNB,

two hydrogen atoms, and one molecule of water. However, it must be realized that this product was not produced under flash conditions, and that it was isolated and handled in air. Thus, if this material and the flash product are indeed the same, it is possible for the loss of two hydrogen atoms and the gain of water to occur during handling. The more limited conclusion that the flash product incorporates two molecules of TNB is considered to be correct.

Proceeding as for Reaction Scheme I in the initial time period leads to the same equation for $d(\Delta D)/dt$, namely equation (31). At longer times ($t > 1000$ μsecs.), where the decay of B is complete, a simple second order expression is obtained, i.e.,

$$\frac{d(\Delta D)}{dt} = \frac{-k_2}{\epsilon_C - \frac{\epsilon_{P'}}{2}} (\Delta D - \Delta D_\infty)^2 \qquad \ldots(40)$$

which integrates to

$$\frac{1}{\Delta D - \Delta D_\infty} = \frac{k_2}{\epsilon_C - \frac{\epsilon_{P'}}{2}} + \text{constant.} \qquad \ldots(41)$$

Our cumulative observations in this time period support a reasonable experimental fit to a second order behavior. It should be noted again that, in the initial time period, this mechanistic scheme is not distinguishable from Scheme I.

4. Aqueous Solvent Systems

In aqueous solution at pH 2.0 (acidic), water/ethanol (neutral), and pH 8.5 (basic) two common features are to be noted in the transient spectra. These are an isosbestic point near 530 mμ in the initial 300 μsecs., and the production of the same flash product in all three cases. The last point suggests that the product is not easily protonated or converted into an anionic form. In view of the spectral changes which are evident, it is certain that water exerts an effect even in an unbuffered system. At pH 2 the final decay is distinctly slower than in pure ethanol, which may be indicative of the generation of a protonated form of transient C, or a species derived from transient C by protonation and loss of one molecule of water. If Scheme II indeed applies, this species could be $(NO_2)_2Ar\dot{\overset{+}{N}}OH$. In any case product formation from such charged species can be expected to be slower.

Under basic conditions it is likely that both transients B and C ionize. For transient B this may be formulated as

$$(NO_2)_2Ar\dot{N}O_2H \rightleftharpoons (NO_2)_2Ar\dot{N}O_2^- + H^+ \qquad \ldots(42)$$

Leading to an appreciable concentration of the anion-radical. An atom transfer step is energetically more favored than an electron transfer,[45] and consequently it is probable that radical B is the initial transient even in basic medium and that ionization follows. The slow appearance of a third transient in the basic solution (cf., Figure 31),

may be due to such an ionization process. In this connection some early work of Porter[45] on the photoreduction of duroquinone in ethanol may be cited. Porter observed the neutral semiquinone radical $HOAr(CH_3)_4O\cdot$ in acid solution and the $^-OAr(CH_3)_4O\cdot$ semiquinone radical ion in basic solution. At a intermediate pH value, both species were observed. The concentration of the radical anion immediately after the flash was observed to be nearly zero and to increase, with a simultaneous decrease of the neutral radical. The primary reaction of the excited state of the quinone with the alcohol is postulated to be hydrogen abstraction rather than electron transfer, even when the equilibrium favors the radical anion.

In lieu of the obviously complex nature of the changes in the basic solution, no meaningful kinetic analysis could be accomplished.

5. The Photolysis of m-Dinitrobenzene and Nitrobenzene

Insufficient data, both flash and ESR, are at hand to provide interpretation of the photolysis of dinitrobenzene and nitrobenzene. It has been reported that the continued photolysis[3] of dinitrobenzene in ethanol, produces the corresponding 3,3'-dinitroazoxybenzene; however, a monomeric product, phenylhydroxylamine, was found by Testa with nitrobenzene in isopropanol (vide infra). This difference in behavior may reflect the additional nitro group in dinitrobenzene. It is more likely, though, that isopropanol is more reactive as a hydrogen donor and leads to a more highly reduced product.

If the photochemistry of dinitrobenzene and nitrobenzene in ethanol follows one of the mechanisms presented for TNB (Scheme I or Scheme II), the intermediates equivalent to B and C are considerably more short-lived than with TNB. In the ESR studies with dinitrobenzene it was found that the photoinduced radical, NO_2ArNO_2H, in THF does indeed have a shorter lifetime (6 secs.) than the TNB-derived radical from nitrobenzene in THF was found by Ward[14] to have an even shorter lifetime of ca. 2 secs.

6. Structure of the Flash Product from TNB

The evidence collected supports mechanistic Scheme II for the photoreduction of TNB in ethanol. On the basis of this mechanism, the flash product is formulated as $(TNBH_2)_2$ Or $C_{12}H_{10}N_6O_{12}$. The data do not permit a more detailed formulation. The further reduction of this product to 3,3',5,5'-tetranitroazoxybenzene, $(NO_2)_2ArNNOA_r(NO_2)_2$, disproves the proposal of Stenberg[3] that the azoxy compound is a primary photoreduction product of TNB in ethanol, i.e., that an excited TNB molecule produces the azoxy compound by a sequence of dark reactions alone. The conversion of the flash product by further photolysis to the azoxy compound must involve a number of steps, and speculations regarding their nature is considered pointless in the absence of knowledge of the exact structure of the flash product.

References

(1) F. Haber and G. Schmidt, Z. Physik. Chem., 32, 271 (1900).

(2) J. Cohen and D. McCandlish, J. Chem. Soc., 87, 1257 (1905).

(3) V. Stenberg and D. Holter, J. Org. Chem., 29, 3420 (1964).

(4) G. Briegleb, Elektronen-Donator-Acceptor Komplexes, Springer-Verlag, Berlin, 1961.

(5) J. Meisenheimer, Liebigs Ann. Chem., 323, 219 (1902).

(6) V. Gold and C. Rochester, J. Chem. Soc., 1687 (1964).

(7) L. Dyall, J. Chem. Soc., 5160 (1960).

(8) R. Foster and C. Fyfe, J. Chem. Soc., B, 53 (1966).

(9) J. Ainscough and E. Caldin, Proc. Roy. Soc., A, 228, 263 (1955).

(10) G. Lewis and M. Kasha, J. Am. Chem. Soc., 67, 994 (1945).

(11) S. Hastings and F. Matsen, J. Am. Chem. Soc., 70, 3514 (1948).

(12) R. Hurley and A. Testa, J. Am. Chem. Soc., 88, 4330 (1966).

(13) S. Nagakura and J. Tanaka, Bull. Chem. Soc. Japan, 23, 1441 (1955).

(14) R. Ward, J. Chem. Phys., 38, 2588 (1963); J. Chem. Phys., 39, 852 (1963).

(15) W. Fox, J. Gross, and M. Symons, J. Chem. Soc., A, 448 (1966).

(16) G. Wettermark, Photochem. and Photobiol., 4, 229 (1965).

(17) A. Vogel, Textbook of Practical Organic Chemistry, hongrams, London, 1958, p. 965.

(18) R. Jones, J. Am. Chem. Soc., 66, 1499 (1944).

(19) A. Vogel, loc. cit., p. 963.

(20) Organic Synthesis, John Wiley, New York, 1955, Vol. 3, p. 334.

(21) R. Holmes and R. Bayer, J. Am. Chem. Soc., 82, 3456 (1960).

(22) J. Castellano, J. Kauffman, J. Green, J. Org. Chem., 30, 822 (1966).

(23) W. Borsche, Chem. Ber., 56B, 1494 (1923).

(24) A. Vogel, loc. cit., p. 624.

(25) R. Ward, J. Am. Chem. Soc., 83, 1296 (1961).

(26) A. Vogel, loc. cit., p. 650.

(27) W. Clark and H. Lubs, J. Biol. Chem., 25, 479 (1916).

(28) W. Moreau, Master of Science Thesis, Northeastern University, 1964, p. 60.

(29) W. Moreau, ibid., p. 59.

(30) L. Nelson, Rev. Sci. Instr., 33, 655 (1956).

(31) W. Wladmiroff, Photochem. and Photobiol., 5, 243 (1966).

(32) G. Porter, Proc. Roy. Soc., A200, 284 (1950).

(33) R. Shriner, R. Fuson, and D. Curtin, Systematic Identification of Organic Compounds, John Wiley, New York, 1956, p. 283.

(34) J. Murrell, The Theory of the Electronic Spectra of Organic Molecules, John Wiley, New York, 1963, p. 184.

(35) D. Lawrey and H. McConnell, J. Am. Chem. Soc., 74, 1221 (1952).

(36) T. Peacock and P. Wilkinson, Proc. Phys. Soc., 83, 335 (1964).

(37) J. Czekalla, G. Briegleb, W. Herre, and H. Vahlensieck, Z. Elektrochem., 63, 715 (1959).

(38) K. Asmus, A. Wigger, and A. Henglein, Z. Physik. Chem., 70, 862 (1966).

(39) A. Maki and D. Gesks, J. Chem. Phys., 33, 825 (1960).

(40) P. Ayscough, F. Sargent, and R. Wilson, J. Chem. Soc., 1963, 5418. G. Russell and E. Geels, Tet. Let., 1333 (1963).

(41) C. Lagercrantz and M. Yhland, Acta. Chem. Scand., 16, 1043 (1962).

(42) R. Glicksman and C. Morehouse, J. Electrochem. Soc., 105, 299 (1958).

(43) A. Beckett and G. Porter, Trans. Far. Soc., 59, 2038 (1963).

(44) I. Taub and L. Dorfman, J. Am. Chem. Soc., 84, 4053 (1962).

(45) N. Bridge and G. Porter, Proc. Roy. Soc., 245, 276 (1958).

6. Studies of Charge Transfer Systems

by K. Weiss, W. M. Moreau, A. M. Halpern, and Y. P. Pilette.

Charge transfer complex formation between electron donors and acceptors is the subject of numerous experimental and theoretical investigations. Its role in photochemical transformations has not been extensively explored. The potential significance of charge transfer interactions in photochemistry lies in the possibility of bringing about new reactions which are different from those of the separated components. The participation of complex formation in energy transfer and sensitized reactions has been postulated. Further, the complexation of intermediates such as radicals can affect their lifetimes and reactivities.

The studies reported here deal with several aspects of charge transfer systems. The complexation of organic disulfides was of interest as a possible means of achieving the indirect scission of the S-S bond. The photochemical behavior of amine-iodine systems is the subject of another study. In conjunction with this investigation, a method has been developed for determination of the association constants of bifunctional amines. Finally, some results are presented from a continuing study of the photolysis of complexes derived from hydrocarbon donors.

(a) The Charge Transfer Properties of Disulfides

Disulfides (RSSR) act as donors with electron acceptor molecules. For the complexes of simple aliphatic disulfides with iodine, which have been reported by other investigators,[1] the position of the charge transfer band is almost invariant with different alkyl groups. We have found that alkyl, aryl, and cyclic disulfides form stable

complexes with tetracyanoethylene (TCNE) (cf. Appendix F). With this acceptor, the charge transfer absorption appears in the visible region and its position clearly reflects the nature of the organic groups attached to the sulfur atom.

The association constants and extinction coefficients of the disulfide-TCNE complexes were measured by the Benesi-Hildebrand method. The complex with the cyclic disulfide thioctic acid* is significantly stronger than those involving aliphatic disulfides. The charge transfer transition becomes progressively less energetic in the series methyl, ethyl, n-butyl, t-butyl disulfides, and thioctic acid. Apart from the charge transfer band, the complexes show absorption which may be assigned to the complexed components. For the thioctic acid-TCNE system it was possible to show that complexation shifts the disulfide band to lower wavelengths. With the ethyl disulfide-TCNE complex, the component absorptions overlap and bands due to complexed disulfide and complexed TCNE cannot be unequivocally assigned.

The results summarized above have been interpreted in terms of a semi-empirical, one-electron MO model. This approach involves calculation of the energy levels of the disulfide and of TCNE, and their computing the energies of the mixed orbitals constructed from those molecular of the donor and the acceptor for which interaction is allowed by spatial and symmetry considerations, The charge transfer transition is considered to occur between the highest occupied, and the lowest unoccupied, mixed orbital. Bonds in the

---

*The structure of this compound is given in Section 5

disulfides are considered to involve only the sulfur 3p orbitals. In simple disulfides, the dihedral angle (θ) is approximately 90°, and the decrease in the charge transfer transition energies is considered to reflect a change in this angle. By considering the requirement for maximum orbital overlap we were able to assign, with reasonable confidence, structures to the complexes of the simple alkyl and cyclic disulfides, which have C_2 and C_S symmetry, respectively. Ethyl disulfide and thioctic acid have $\theta \approx 90°$ and 0°, respectively, and using spectral data for these donors in conjunction with values of the ionization potentials, the orbital energies for their TCNE complexes were calculated. The calculated and observed spectral transitions showed gratifying agreement.

The treatment described here differs from the simpler and widely applied molecular orbital treatment developed by Dewar[2] in that it specifically includes the mutual perturbation of the donor and acceptor orbitals. Application of our more sophisticated approach to other systems, for which the structure of the complexes is known or can be reasonably assigned, is considered to be a highly worthwhile endeavor.

The publications collected in Appendix F have been very popular. Almost 200 requests for reprints have been received.

The photolysis of the disulfide-TCNE complexes has been examined.[3] The changes which occur even on prolonged photolysis are quite small. Thin layer chromatographic examination of photolyzed solutions showed that, if new products are formed, they appear in amounts below the detection limit. The complexes used in these

experiments involved TCNE and n-butyl disulfide, t-butyl disulfide, phenyl disulfide, 1,2-dithiane, and thioctic acid. The irradiations were carried out with a filtered light source which confined light absorption to the charge transfer band. In every case the photolysis resulted in a small change in the optical density of charge transfer band. In the dark, the optical density slowly reverts to its original value. The absorption change occurs only in degassed solutions; in the presence of air, irradiation produces no change. Of the complexes examined, those of t-butyl disulfide and thioctic acid are most sensitive to light. Flash photolysis of solutions of the TCNE-disulfide complexes produces barely detectable transient absorption under even the most energetic flash conditions.

The experiments performed were rather limited in scope, and no clear-cut conclusions regarding the significance of the results could be reached. Two explanations for the photochemical change have been considered. One is that isomeric configurations of the complex exist, and that photolysis favors the formation of higher energy forms. Alternatively, photolysis may generate complexes involving more than one donor or acceptor molecule. Only further work can establish the applicability of these and of other, as yet unformulated, concepts.

(b) Amine-Iodine Charge Transfer Complexes

The complexes of amines with iodine are relatively strong compared with those involving aromatic donors. The spectra of solutions of these complexes show charge transfer bands near 300 mμ

as well as bands in the visible region due to free and complexed iodine. Selective excitation in these bands can be expected to lead to different photochemical consequences. Irradiation in the charge transfer region may result in dissociation of the complex or radical-ion pair formation. Iodine is known to dissociate into atoms on photolysis; the recombination rates have been measured by other investigators. In the presence of strong acceptors such as amines, it is anticipated that the iodine atoms will be complexed, and that consequantly their lifetime will be significantly affected. Photolysis in the complexed molecular iodine band should generate complexed atoms directly, whereas with photolysis in the free iodine band complexation would follow dissociation.

Since meaningful photochemical work with the complexes requires knowledge of the composition of the solutions employed, we concerned ourselves first with measuring the stabilities and spectral characteristics. This phase of the work proved to be extremely interesting. Since diamines were included amongst the donors chosen, we were faced with the problem of determining two association constants, corresponding to the formation of complexes involving one and two molecules of iodine.

The gross spectral features of the amine-iodine complexes are summarized in Table 1 together with the ionization potentials of the amines. Triethylenediamine (I) is seen to have a significantly lower ionization potential than the other amines.

TABLE 1

Spectral Characteristics of Amine-Iodine Complexes and Ionization Potentials of Amines

Amine	Ionization Potential, eV	Complex, λ_{max}, mμ [a]	
		CT band	Shifted I_2 band
Triethylamine	7.5[b]	278	414
N,N,N',N'-Tetramethylethylene-diamine	7.3[c]	280	410
1,4-Diazabicyclo-(2,2,2)octane (triethylenediamine, I)	~ 7[c,d]	310	395
Azabicyclo(2,2,2)octane (quinyclidine, II)	7.6[c]	272	400

(a) In n-heptane or methylcyclohexane. The free iodine band is at 520 mμ.
(b) Reference 4
(c) Estimated from position of CT band.
(d) Photoionization measurement indicates this value or less.

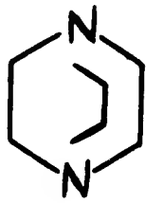

I

II

The method of determining the formation constants of the 1:1 and 1:2 diamine-iodine complexes is based on the following development.

Let D and A represent the donor and acceptor (iodine), respectively. The two equilibria may then be formulated as

$$D + A \rightleftharpoons DA \qquad K_1 = C_1/(C_A C_D) \qquad \ldots\ldots (1)$$

$$DA + A \rightleftharpoons DA_2 \qquad K_2 = C_2/(C_1 C_A) \qquad \ldots\ldots (2)$$

The concentrations are designated by the symbol C, with C_1 and C_2 representing the 1:1 complex (DA) and 1:2 complex (DA_2), respectively. The initial concentrations of donor and acceptor are

$$C_D^\circ = C_D + C_1 + C_2 \qquad \ldots\ldots (3)$$

$$C_A^\circ = C_A + C_1 + 2C_2 \qquad \ldots\ldots (4)$$

and the change in acceptor concentration due to complex formation is $\Delta C_A = C_A^\circ - C_A$. Incorporating equations (3) and (4) in equations 1 and 2 furnishes the relation

$$\frac{\Delta C_A}{C_D^\circ} = \frac{K_1 C_A + 2K_1 K_2 C_A^2}{1 + K_1 C_A + K_1 K_2 C_A^2} \qquad \ldots\ldots (5)$$

It is to be noted that equation (5) contains only the measurable parameters C_D°, C_A, and ΔC_A. C_D° is known from the preparation of the solution, and the other concentrations are available from the optical density of A at its maximum. Since the complexed iodine band near 400 mμ tails to longer wavelengths, it is necessary to apply a correction for absorption due to the complex. Thus

$$\Delta C_A = \frac{D^\circ - D}{(\varepsilon_{I_2} - \varepsilon^*_{I_2})\ell} \qquad \ldots\ldots (6)$$

where D° and D are the initial and equilibrium optical densities, respectively, of free iodine at 520 mμ, ε_{I_2} and $\varepsilon^*_{I_2}$ are the corresponding extinciton coefficients, and ℓ is the path-length. The extinction coefficient $\varepsilon^*_{I_2}$ is determined by converting all the iodine into the complexed form with a large excess of amine.

If we let $\phi = \Delta C_A/C_D^\circ$ and define two new variables

$\alpha = (1-\phi)/(C_A(2-\phi))$ and $\beta = \phi/(C_A^2(2-\phi))$,

equation (5) assumes the simple form

$$\alpha = (\beta/K_1) - K_2 \qquad \ldots\ldots (7)$$

Values of K_1 and K_2 are obtained from the slope and intercept, respectively, of plots of α against β. The plot for tetramethyl-1,6-hexanediamine is shown in Figure 1.

Measurements were made with a series of diamines of structure III with n = 1,2,3,4, and 6, and with diamines I and II. The results are listed in Table 2. To check this method of determining

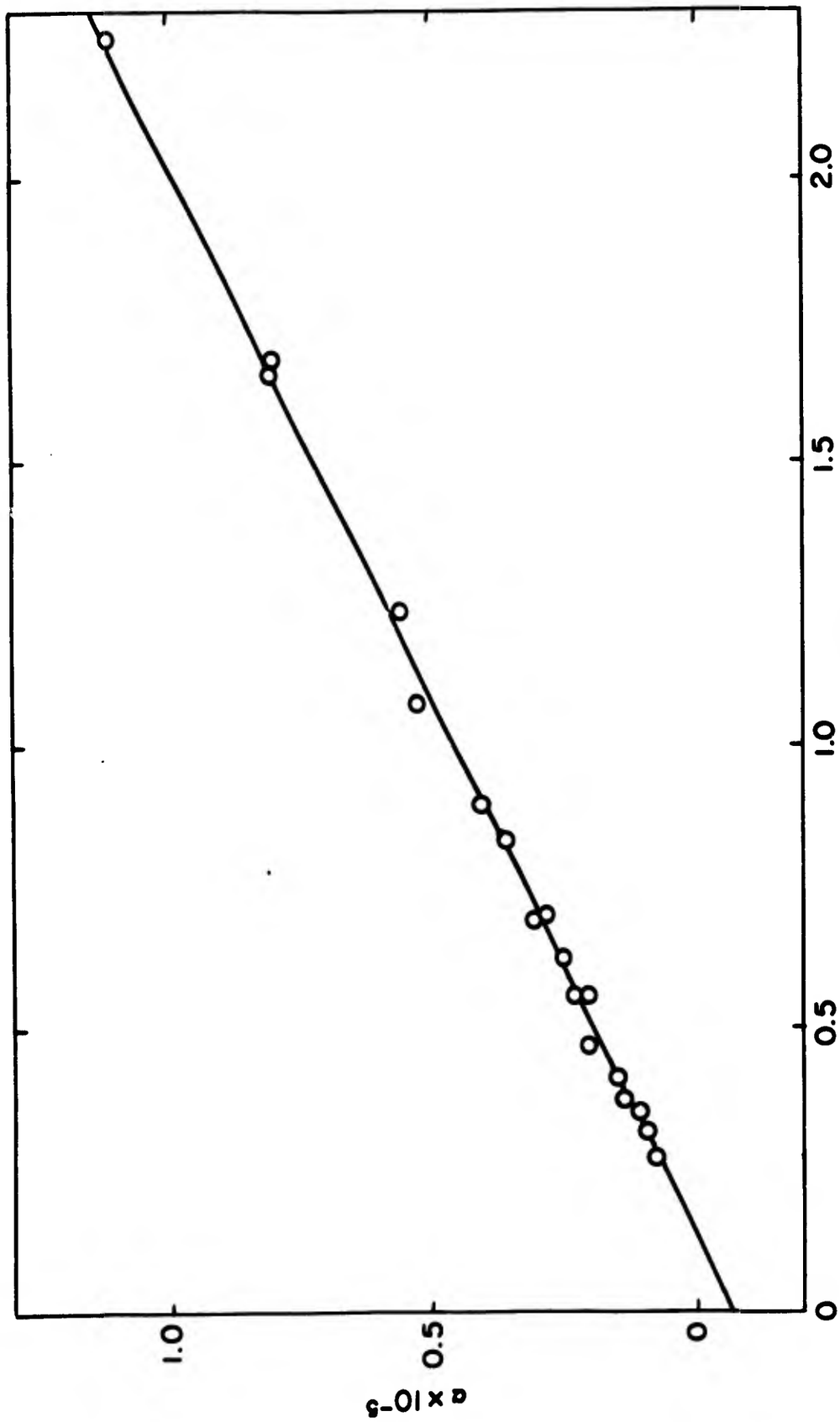

FIGURE 1: Plot of Equation 7 for the tetramethyl-1,6-hexanediamine-iodine complex

$(CH_3)_2N(CH_2)_nN(CH_3)_2$

III

equilibrium constants, measurements were made with triethylamine. In this case the α *versus* β plot passed through the origin, corresponding to $K_2 = 0$ as expected. The value of K_1 afforded by this method (4.9×10^3, methylcyclohexane, 25°) is in good agreement with the value obtained by the Benesi-Hildebrand method[5] (4.7×10^3, n-heptane, 25°).

The K_1 values given in Table 2 are estimated to have an error ± 10%. The K_2 values are inherently less reliable. This limitation of the method arises in part from the instability of the amine-iodine systems in non-polar solvents with respect to precipitation. The solutions invariably become turbid after some time, and consequently the spectral measurements are made during a metastable interval. A solid complex was prepared from diamine I which contains amine and iodine in the ratio 1:2, regardless of whether an excess of donor or acceptor was used.

The data in Table 2 clearly show that intramolecular perturbations are operative which cause the complexed donor site to influence the complexing ability of the uncomplexed site. K_1 is seen to increase as the CH_2-chain between the nitrogen atoms is lengthened. The values for tetramethyl-1,4-butanediamine (III, n = 4) are only appropriate since the solutions containing this donor are particularly unstable. No clear trend is evident in the K_2 values. If the two

TABLE 2

Equilibrium Constants for Diamine-Iodine Complexes[a]

Diamine	Formula	$K_1 \times 10^{-4}$	$K_2 \times 10^{-3}$	K_{1/K_2}
Tetramethylmethanediamine	III, n=1	0.1	$\leq$ 0.5	$\geq$ 2
Tetramethyl-1,2-ethanediamine	III, n=2	1.1	1	11
Tetramethyl-1,3-propanediamine	III, =n=3	1.7	$\leq$ 0.5	$\geq$ 34
Tetramethyl-1,6-butanediamine	III, n=4	(1.9)[d]	(5)[d]	4
Tetramethyl-1,6-hexanediamine	III, n=6	1.7	8	2
Triethylenediamine[b]	I	9.0	2	45
Quinuclidine[c]	II	40	0	∞

(a) In methylcyclohexane at 27°C unless otherwise indicated.
(b) In n-heptane at 26°C.
(c) In methyl cyclohexane at 23°
(d) Approximate values - see text.

donor sites act independently, the ratio K_1/K_2 should be 2 if the statistical factor for the symmetry of the diamine is considered. This limiting value is, within experimental error. attained by the henaxediamine (III, n = 6) system. With the propane- and methanediamine systems, the value $K_2 = 500$ is an upper limit and consequently the ratios listed for these compounds represent lower limits. The strongest intramolecular perturbation effect is shown by triethylenediamine (I). The monoamine quinuclidine (II) with $K_1 = 4 \times 10^5$ is clearly the strongest donor examined; its association constant is larger than that for triethylamine by a factor of almost 100. The magnitude of the perturbation effect is evident from a comparison of triethylenediamine (I) and quinuclidine, which can be expected to be subject to similar steric influences. With diamines III, both steric and electronic factors may be operative.

Qualitatively, the perturbation effect can be rationalized in terms of the transmission of charge from the polarized $\overset{\delta+}{N} - \overset{\delta-}{I_2}$ moiety through the methylene chains. A similar explanation has been advanced for the transmission of spin density in the triethylenediamine (I) cation radical, in which the nitrogen atoms are equivalent.[6] The quantum mechanical treatment of the perturbation effect, even with the aid of semi-empirical theory, represents a formidable problem. No theoretical work along these lines has been attempted.

Only a few preliminary photochemical experiments have been carried out with the triethylamine-iodine complex. Using the unfiltered radiation from a mercury lamp which, with "Pyrex" vessels, was confined to the region above 300 mμ, it was found that the solutions rapidly

become colorless and deposit a white solid. This solid is soluble in polar solvents and it appears to contain iodine ions, but not I_3^- ions. The identification of this solid, as well as further photochemical experiments using continuous and flash irradiation, are still in progress.

(c) The Photochemistry of Complexes Derived from Hydrocarbon Donors

The charge transfer complexes of hydrocarbons, particularly aromatic compounds, have received more detailed attention than any other class of complex.[7] There is a wide variety of systems suitable for photochemical experimentations. Absorption characteristics and other properties can be chosen on a tailor-made basis. For the experiments described here we sought systems which show well-separated charge transfer absorption so that selective excitation can be achieved.

The earliest, and least fruitful experiments were carried out with TCNE complexes.[3] On continuous photolysis in the charge transfer band, the complexes of diphenylacetylene, *cis*- and *trans*- stilbene, and 2-iodonaphthalene show similar behavior to that of the disulfide-TCNE complexes. There is a small increase in absorption in the charge transfer region which is slowly reversed in the dark. There appears to be no detectable chemical consequence of the irradiation. Thus gas chromatographic examination of irradiated solutions of the stilbene complexes indicated that no *cis-trans* isomerization occurs. This result tends to support the proposal that, with TCNE complexes, the absorption changes are due to a structural isomerization as a whole.

Flash experiments were performed with the *trans*-stilbene TCNE complex in dichloramethane solution, using a filter which cuts off light below 490 mμ. It was found that even with very large input energies, the extent of change of absorbance is quite small. Under such high energy conditions, stray light is troublesome, and, owing to the necessity of using high oscilloscope gains, there is much noise in the decay traces. Flashing increases the optical density at all wavelengths between 360 mμ and the charge transfer maximum at 590 mμ. The transient absorption decays rapidly ($t_{1/2}$ 300 μsecs) to an optical density about 5% higher than that of the original solution. Further decay is extremely slow and similar to that observed with continuous photolysis. The data were not suitable for a meaningful kinetic analysis. The decay rates appeared to depend on the TCNE: stilbene ratio of the solution. Flashing undegassed solutions of the complex produced no transient changes whatever. It therefore appears that the transient absorption is due to a triplet state or a radical, or possible both. In view of the smallness of the transient change and other experimental difficulties, the study of the TCNE: stilbene system was abandoned.

A search for other hydrocarbon donor systems produced pyromellitic anhydride (PMA) as a suitable acceptor. The triphenylene, anthracene, stilbene, and pyrene complexes of this compound show well-defined charge transfer absorption bands near 450 mμ. Filter solutions have been developed to confine the absorption of flash irradiation to these bands.

To date, most of the experiments have been carried out with the triphenylene complex. This complex can be obtained as a crystalline solid; its temperature-composition phase diagram indicates a 1:1 complex exists in solution. On continuous irradiation of the complex in dichloromethane solution no detectable changes occur.

Flash photolysis of the triphenylene-PMA complex in dichloromethane solution produces transient absorption in the 500 mμ to 720 mμ region. The transient spectra at various times after the flash are shown in Figure 2, which also shows the ground state absorption of the complex. Conversion into transient species is extensive even with moderate flash energies. Transient maxima appear at 620 mμ and at 675 mμ. The decay rates seem to be the same at all wavelengths, and it is doubtful that more than one species is absorbing. It is certain, however, that the transient absorption is not due to the triplet state of triphenylene. The latter has been reported to have maxima at 428 mμ, 404 mμ, and 346 mμ, with no absorption above 460 mμ.[8] This result has been confirmed by measurements in our laboratory. When the same filter solution is used which confines light absorption to the charge transfer band of the complex, flashing solutions which contain only triphenylene or PMA produces no transient absorption. The new transients are therefore uniquely associated with the complex.

The decay of the triphenylene-PMA transient absorption is complex. Neither first order nor second order rate laws apply. In the initial *ca.* 500 μsecs, the decay is very rapid. A slower

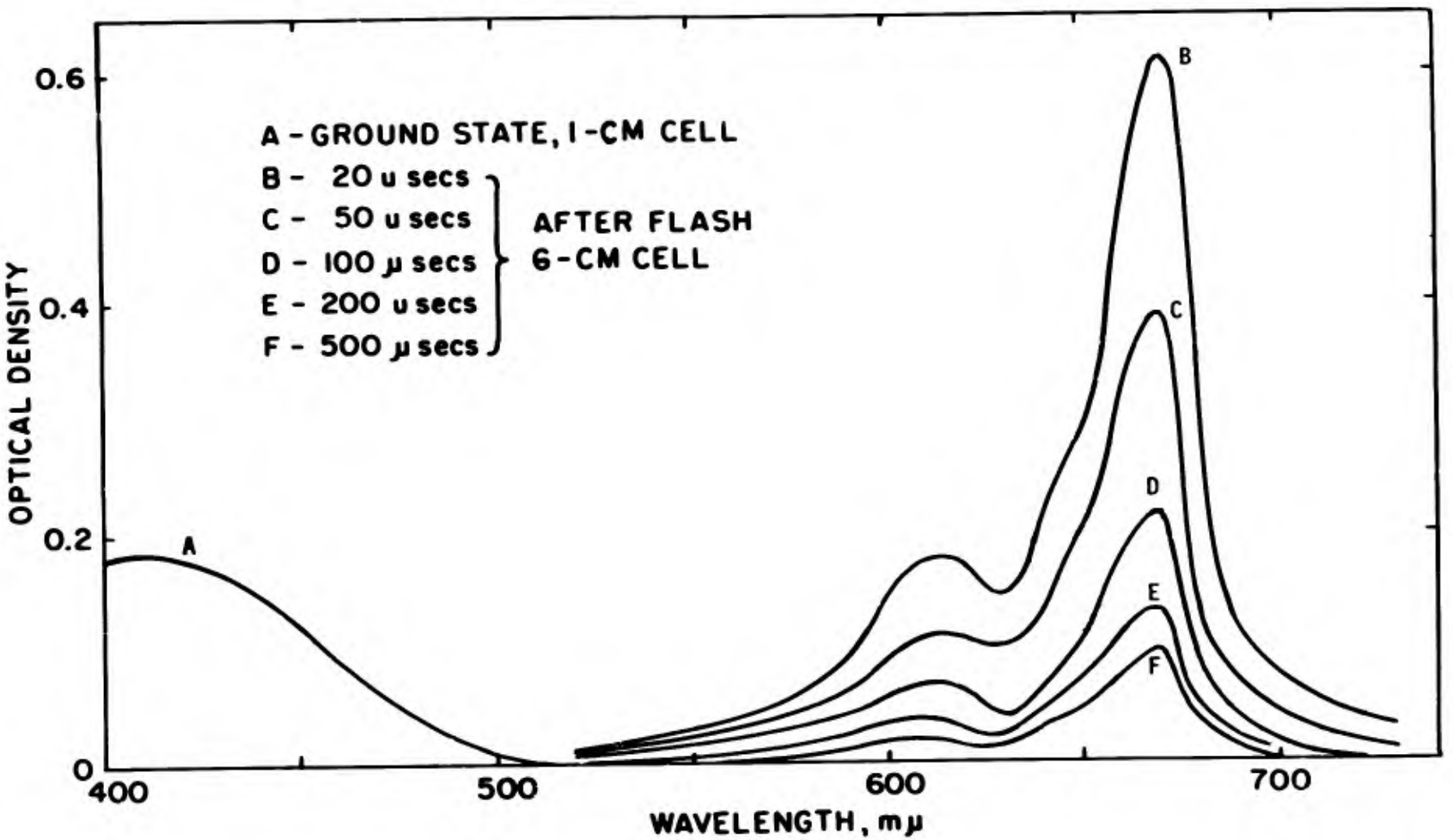

FIGURE 2: Transient Spectra of Flashed Triphenylene (5×10^{-3} M)-Pyromellitic Anhydride (5×10^{-3} M) in Dichloromethane

stage follows, and the decay is essentially complete after 5 milliseconds. The transient change is completely reversible. These results pertain in thoroughly degassed solution. In the presence of air, the transient spectrum is the same, but less of the species are produced. Their decay is more rapid than in the absence of air.

Some preliminary results are also available for flash experiments with the anthracene-PMA complex, the spectrum of which is quite similar to that of the triphenylene complex. Conversion into transients is also quite extensive, and absorption appears in the same 500 mμ to 700 mμ region. The transient maxima are close to those of the triphenylene system. This result suggests that the transient might be derived fro the acceptor.

The nature of the transients generated from these PMA complexes remains to be established. To this end, efforts are continuing on this problem. This further work involves elucidation of the kinetic behavior of the transients, quenching experiments, emission and ESR measurements, and spectral comparisons with radical ions derived from the components of the complexes.

References

(1) S. P. McGlynn, J. Nag-Chandhuri, and M. Good, J. Am. Chem. Soc., 84, 9 (1962), and earlier references cited therein.

(2) M. J. S. Dewar and H. Rogers, J. Am. Chem. Soc., 84, 395 (1962).

(3) W. M. Moreau, M.S. Thesis, Northeastern University, June 1964.

(4) K. Watanabe, T. Nakayama, and J. Mottl, J. Quant. Spectrosc. Radiat. Transfer, 2, 369 (1962).

(5) S. Nagakura, J. Am. Chem. Soc., 80, 520 (1958).

(6) T. M. McKinney and D. H. Geske, J. Am. Chem. Soc., 87, 3013 (1965).

(7) G. Briegleb, Elektronen-Donator-Acceptor Komplexe, Springer-Verlag, Berlin, 1961.

(8) G. Porter and M. W. Windsor, Proc. Royal Soc., 245A, 238 (1958).

7. Laser Photochemistry*

by K. Weiss, R. M. Danziger, and K. H. Bar-Eli.

A pulsed laser represents an ideal photolysis source. It provides strictly monochromatic irradiation and, under special conditions, pulses in the nanosecond range can be obtained. For photochemical work, the ruby laser is most suitable primarily because of the relatively advanced state of the technology of this particular device. The ruby laser flash photolysis apparatus we have developed is described in Section 2 of this report, entitled "Apparatus for Photochemical Investigations."

The systems we have studied with the ruby laser fall into two categories: Those which show substantial absorption at the laser emission wavelength (6943Å), and those which indicate the absence of absorption at that wavelength at normal intensities.

A large number of compounds absorb light in the 7000Å region. Among these are many dyes including chlorophyll, hydrocarbons such as azulene, and charge-transfer complexes. However, photochemical information is available for only a limited number of these systems. Methylene blue was chosen for detailed investigation because its continuous irradiation behavior had been investigated in some detail and some preliminary conventional flash results have been reported.

For the second class of compounds only multiphoton absorption can produce excited states and photochemical consequences. This process has

---

*This study was only partially supported by this contract. Main support was by the U. S. Public Health Service, Division of Radiological Health, Grant RH00302.

been detected by emission measurements. Here we report some preliminary experiments on the multiphoton-generation of transients and their detection by absorption spectroscopy. Compounds for study were chosen on the basis of their spectral properties, transient information from conventional flash experiments, and reported multiphoton behavior.

(a) The Laser Photolysis of Methylene Blue

This study is described in detail in the publication reproduced in Appendix G.

Several aspects of the results of this study deserve special comment. Firstly, the laser photolysis of plain, aqueous methylene blue solution revealed a transient with a half-life of *ca.* 2μsecs., which is not detectable under ordinary flash conditions. It was also found that with a dye solution having an optical density of *ca.* 0.1 at the laser wavelength, a 0.5 joule laser pulse suffices to convert the ground state dye almost completely into transients. There was evidence that absorption saturation with respect to the singlet-singlet occurs, and that initial conversion to the singlet excited state is essentially complete even in very concentrated dye solutions. Consequently, since Beer's law does not hold under these conditions, the laser can penetrate optically dense media which transmit no light at low intensity.

The photochemical results are significant in that they indicate that both the monomeric and dimeric forms of the dye give rise to transients by separate excitation. The participation of polymeric dye forms has been largely overlooked by other investigators. It may have important implications in the photochemistry of dyes. The

kinetic results also indicate that the attainment of the ground state monomer-dimer equilibrium is slow relative to the transient decays. The slowest of these corresponds to a half-life of 140 μsecs.

The longest-lived transient ($t1/_2$ = 140 μsecs) is assigned as a dimeric charge transfer state which is considered to result from an intramolecular electron transfer in the dimeric triplet. This concept may have general validity, and species of this nature may not be confined to dye systems. For instance, the excimers of polynuclear unclear hydrocarbons may decay *via* this type of intermediate.

(b) Multiphoton Experiments

General Considerations

The theoretical ground work for multiphoton processes was laid by Göppert-Mayer in 1931[1]. More recently a discussion applying specifically to ruby lasers was published by Kleinman[2]. The theory of three-photon absorption has been developed in detail by Hameka[3]. A prime criterion for the occurrence of a multiphoton process appears to be that there is significant absorption at multiples of the laser frequency.[2,4] However, for solutions the requirements have not been rigorously delineated.

The solution experiments described here are of an exploratory nature. They primarily involve compounds for which emission ascribed to either a two-photon or a three-photon process had been reported. The experiments were designed to create the first excited singlet *via* a multiphoton process, which is then anticipated to undergo a radiationless (forbidden) transition to the lowest triplet state. The continuous light source (monitoring light) then

permits observation of the allowed $T_1 \rightarrow T_2$ or T_3 transitions. In some systems it is conceivable that population of the triplet state can occur by direct absorption from the ground state, a process which is rendered relatively probable by the high intensity of the laser emission.

The initial experiments were performed in dilute solutions, under experimental conditions similar to those reported by Porter and co-workers[5,6] for the observation of the triplet state in fluid media. In later experiments, solutions of higher concentration and longer pathlength were used in order to optimize the conditions necessary for observation of the phenomenon. In some case, the optical train of the laser photolysis apparatus had to be modified to accommidate the longer cells. The solutions were thoroughly degassed by the freeze-thaw-pump method. The anticipated triplet-triplet absorption was well within the response of the detection circuit.

The compounds studied were benzophenone, naphthalene, biphenyl, 3,4 benzopyrene, and anthracene.

Results

(a) Benzophenone - Table 1 summarizes the conditions used in the individual experiments with benzophenone. The extinction coefficient at 3471Å is equal to approximately 150.[7] The quantum yield of intersystem crossing from the excited singlet to the triplet state has been reported as *ca.* 1.0. The $T_1 \rightarrow T_2$ absorption, according to Porter and Wilkinson,[6] is at 5450Å. A considerable body of information on the transient behavior of benzophenone is available from conventional flash photolysis work.[8-11]

TABLE 1

Experiments with Benzophenone

Experiment Number	Solvent	Concentration ($M \times 10^2$)	Path Length (cm.)
1	Benzene	9.9	1.0
2	*Iso*propanol	55.0	1.0
3	*Iso*propanol	66.0	10.0
4	*Iso*propanol	85.0	14.0

In the four experiments listed in the table, no transient formation was observed at 5450Å. However, after repeated flashing of the 55 x 10^{-2} M solution with the un-Q-switched laser a white precipitate was formed, which may have been benzpinacol.

(b) Naphthalene - The optical density, at 28,800 cm^{-1}, of a 2.49 M solution of naphthalene in benzene is approximately 1.0. At three times the laser frequency, 43,200 cm^{-1}, the extinction coefficient is approximately 1500.[7] The triplet-triplet absorption is as 4103Å.

The data for the experiments performed with naphthalene appear in Table 2. As in the case of benzophenone, the initial experiments were performed at lower concentrations and with a short path length cell. In experiment 3, a high concentration and a 50-cm. path length cell was used. However, the results were negative, there being no transient absorption at several wavelengths in the region where the naphthalene T → T absorption has been reported to occur. It was felt that impurities in the solvent might contribute to quenching of the triplet.

For experiments 4 and 5, solutions of zone-refined naphthalene were prepared in redistilled benzene, and in a highly purified grade of benzene, respectively. The latter experiment was performed in a 14-cm cell, and substantial transient formation was observed. According to Porter and Windsor, there is no triplet-triplet absorption at wavelengths longer than 4650Å.[5] However, transient absorption was observed at 600 mμ; consequently, the transient is not the triplet of naphthalene. Decay measurements at 413 mμ and 550 mμ indicated adherence to a first order law with $k_1 \approx 10^4$ sec^{-1}, corresponding to a half-life of ~100 μsecs. When the contents of the thoroughly degassed cell were

TABLE 2

Experiments with Naphthalene

Experiment Number	Solvent	Concentration ($M \times 10^3$)	Path Length (cm.)
1	n-hexane	4.79[c]	1.0
2	Benzene	107.1[c]	1.0
3	Benzene	1500	50.0
4	Benzene[a]	2050[c]	1.0
5	Benzene[b]	2490[c]	14.0
6	Benzene	2880	14.0
7	Benzene	2880	14.0[d]
8	Benzene[b]	2490[c]	10.0

(*a*) Redistilled benzene; fraction at 80.1°C
(*b*) 99% minumim purity; obtained from Chemical Samples Co., Inc., used directly.
(*c*) Fisher zone-refined reagent, Cat. No. N-128
(*d*) Undegassed

exposed to air, the transient was still observed, although in reduced quantity.

Attempts were made in experiments 6, 7 and 8 to repeat these results, but without success. In experiment 6 an even more concentrated, thoroughly degassed solution of recrystallized naphthalene was flashed in a different 14-cm cell. In experiment 7 the undegassed 2.88 M solution was lased in the same 14-cm cell in which the transients were previously observed. In experiment 8, the same 2.49 M solution that had shown the transient formation in experiment 5 was degassed and flashed in a 10-cm cell. Again no transient formation could be detected. The absorption spectrum of the 2.49 M solution was measured on the DK-1 spectrophotometer, and the absorbance at 6943Å was found to be less than 0.01. This value is well within the limit of the sensitivity of the instrument. It must be concluded that the transient observed in experiment 5 was not due to an impurity which absorbs at the laser wavelength.

The results described here are inconclusive, yet tantalizing. Clearly, much further experimentation is called for.

(c) Biphenyl - Eisenthal and co-workers,[12] observed a luminescence with an intensity proportional to either the second or third power of the laser intensity, which is linearly dependent on the molecular concentration, when biphenyl was irradiated with an un-Q-spoiled ruby laser. The emission could not be correlated with the normal fluorescence or phosphorescence of biphenyl either in the crystalline or the liquid state. There is essentially no absorption of the ground state molecule at twice the laser frequency; however, there is an extremely strong band

with an extinction coefficient of approximately 2.0×10^5 at three times the laser frequency.[7] The wavelength of the triplet-triplet absorption maximum is 3685Å.[6]

In the experiments described here it was hoped to observe either the formation of the triplet in the three-photon process or the absorption due to the products formed by the multiphoton vibrational dissociation of biphenyl.[12] Two experiments were performed using a 1.32 M solution of biphenyl in xylene. The samples were flashed in 1.0-cm and 14.0-cm cells, respectively. No triplet absorption was observed at 3685Å, and no transient absorption was discernible at 50-mμ intervals throughous the visible region.

(d) 3,4 Benzpyrene - Only one experiment was performed with 3,4 benzpyrene, which is another likely candidate for two-photon absorption. It has an extinction coefficient of *ca.* 2.0×10^5 at twice the laser frequency.[7] Double photon emission was observed in dilute solutions of this compound in α-methylnaphthalene.[13] Benzpyrene is only sparingly soluble in most organic solvents, and the concentration of the sample prepared in this experiment was 2.14×10^{-3} M in n-hexane. The triplet-triplet absorption has not been reported for this compound. No transient absorption was observed in the flash experiments at several wavelengths throughout the visible region.

(e) Anthracene - There has been a considerable amount of work reported on the two-photon emission of crystalline anthracene, but no results have been reported for solutions.[14,15] The triplet-triplet absorption maximum was reported[5,16] to be at 4240Å. The extinction coefficient for the band at twice the laser frequency is approximately 2.4×10^4.[7]

The initial two experiments with anthracene were carried out under conditions similar to those reported for conventional flash photolysis. The solutions had concentrations of 1.526×10^{-3} M and 1.313×10^{-3} M in paraffin oil and n-hexane, respectively. Both samples were flashed in 1.0-cm cells, with negative results.

For another experiment, an 8.6×10^{-2} M solution of blue-violet fluorescence-grade anthracene in extremely pure benzene was used in a 14-cm cell. Transient absorption was observed at 4240Å, the maximum of the absorption ascribed to the triplet-triplet transient. This transient had a lifetime of *ca.* 400 μsecs.

Discussion

The results indicate that multiphoton processes may have occured with benzophenone, naphthalene, and anthracene. This in itself satisfies the limited objectives of this study, which were to explore the possibility of observing multiphoton-generated transients by kinetic spectroscopy.

With benzophenone, the evidence for a two-photon process was least convincing. The only suggestion for the operation of this mechanism was the appearance of a white precipitate which may have been benzpinacol. This product is generally considered to arise from the reaction of triplet ketone with the *iso*propanol to produce ketyl radicals which dimerize.[9]

With naphthalene, the observed transient cannot be associated with reported triplet-triplet absorption.[6] It is possible that the observed transient absorption is due to a dimer or higher polymeric ground state form of naphthalene which exists in concentrated solution. In this connection it may be noted that the lifetime of delayed fluorescence from excited dimers of naphthalene has been reported as 0.018 seconds

at 22°C,[17] and that this species may be generated from either the ground state dimer or from reactions involving a monomeric excited state. The possibility that impurities are responsible for the transient is unlikely because of the absence of appreciable absorption of the ground state material at 6943Å. Another, though relatively unlikely possibility, lies in the generation of the second and third harmonics of the laser frequency at quartz surface imperfections. Very weak second harmonic generation in quartz has been reported.[18]

The experiment with anthracene showed a transient in the triplet-triplet absorption region. However, it remains to be established whether this is indeed the triplet, and if it is, whether this state is populated directly or by a 2-photon process.

References

(1) M. Göppert-Mayer, Ann. Physik., 273 (1931).

(2) D. A. Kleinman, Phys. Rev., 125, 87 (1962).

(3) H. F. Hameka, Physica, 32, 779 (1966).

(4) S. Singh and L. T. Bradley, Phys. Rev. Letters, 12, 612 (1966).

(5) G. Porter and W. M. Windsor, Proc. Roy. Soc. A., 245, 238 (1958).

(6) G. Porter and F. Wilkinson, Trans. Faraday Soc., 57, 1686 (1961).

(7) R. A. Friedel and M. Orchin, Ultraviolet Spectra of Aromatic Compounds, John Wiley & Sons, Inc., N.Y.

(8) J. N. Pitts, Jr., R. L. Letsinger, R. P. Taylor, J. M. Patterson, G. Recktenwald and R. B. Martin, J. Am. Chem. Soc., 80, 1068 (1959).

(9) W. M. Moore and M. D. Ketchum, J. Phys. Chem., 68, 214 (1964).

(10) W. V. Sherman and S. G. Cohen, J. Phys. Chem., 70, 179 (1966).

(11) J. A. Bell and H. Linschitz, J. Am. Chem. Soc., 85, 528 (1963).

(12) K. B. Eisenthal, W. L. Peticolas and K. E. Rieckhoff, J. Chem. Phys., 44, 4492 (1966).

(13) W. L. Peticolas and K. F. Rieckhoff, J. Chem. Phys., 39, 1347 (1963).

(14) S. Singh and B. P. Stoicheff, J. Chem. Phys., 38, 2032 (1963).

(15) S. Singh, W. J. Jones, W. Siebrand, B. P. Stoicheff, and W. G. Schneider, J. Chem. Phys., 42, 330 (1965).

(16) G. Porter and M. W. Windsor, Disc. Faraday Soc., 17, 178 (1954).

(17) W. A. Noyes, Jr., Advances in Photochemistry, Vol. 2, P. 361, John Wiley & Sons, N. Y. (1964).

(18) P. A. Franken, A. E. Hill, C. W. Peters and G. Weinrich, Phys. Rev. Letters, 7, 118 (1961).

8. Diphenylpionyhydrazyl as a Calibration Standard in Electron Spin Resonance Spectroscopy

by K. Weiss and K. H. Bar-Eli.

1,1-Diphenyl-2-pionylhydrazyl (DPPH) is widely used as a standard in ESR spectroscopy. For the estimation of the number of spins in solution, DPPH dissolved in an appropriate solvent such as chloroform or benzene is employed. While such solutions deteriorate on prolonged standing, they are generally useful when freshly prepared. Spin concentrations determined with their aid are estimated to be reliable to $\pm$ 25% when the spectrometer is operated under carefully controlled, optimized conditions.

For the determination of spins in solid materials, DPPH admixed with inert solids is used. We have found that a loss of spins can occur in such standard mixtures. The extent of spin loss depends on the nature of the inert material and on the method of mixing. The details of our findings are reported in the publication reproduced in Appendix H.

The inert materials examined were calcium carbonate, magnesium carbonate, and potassium chloride. Homogeneous mixtures with DPPH were prepared by two methods: (1) shaking the components together, and (2) grinding the mixture under standard conditions. The unground mixtures generally showed no spin loss when the DPPH concentration is varied over three orders of magnitude. Of the ground mixtures, only those with potassium chloride showed this stability. With the ground carbonates, there is a substantial loss of spins with increasing dilution. This effect is enhanced on aging. By contrast, ground and aged potassium chloride mixtures are stable with weight fractions of DPPH > 7×10^{-3}. It is

concluded that ground mixtures of DPPH with potassium-chloride are useful standards over a wide composition range.

The deterioration on grinding is tentatively ascribed to a reaction between DPPH and water, which occurs on the surface of the solid diluent particles.

Acknowledgements

The laser photolysis study (Section 7) received its main support from the U. S. Public Health Service, Division of Radiological Health, Grant RH 00302. The electron spin resonance measurements were carried out with the Varian spectrometer in the Energetics Branch, Space Physics Laboratory, Air Force Cambridge Research Laboratories. We are grateful to Dr. N. Yannoni for permission to use this instrument, and to Drs. A. Golubovic and S. Chatterjee for aiding with the measurements.

The contributions made by the following individuals are also gratefully acknowledged: Many valuable discussions were held with Drs. J. L. Roebber and R. N. Wiener; Dr. A. Lander participated in the early work on the amine-iodine systems; Mr. William Hall helped to develop the emission measurement apparatus; Mr. D. Furman constructed some of the specialized equipment; Dr. V. Stenberg, University of North Dakota, provided samples of compounds and information about the photolysis of trinitrobenzene; Drs. S. Chatterjee and A. Golubovic supplied samples and information about some potential sensitizers; Mrs. M. Weiss and Mr. W. Goddard prepared the drawings for this report and for the publications collected in the appendices.

C. INVESTIGATIONS OF NITROGEN-SULFUR SYSTEMS

Abstract

Investigation of Nitrogen-Sulfur Systems
by R. N. Wiener, L. I. Rubin, and S. N. Singh

Tetrasulfurtetranitride and octatomic sulfur were examined spectroscopically, principally in the vacuum ultraviolet region of the spectrum. They were found to possess rather dissimilar spectra. The molecular exciton model was used in the interpretation of the data; delocalizaiton of electrons was assumed to be relatively unimportant. In terms of the model employed, the differemces in the spectra were to be anticipated. Energy level diagrams for both systems, as well as wave functions for the excited states, are presented. Intensities and transition frequencies were found in good agreement with the data. Although not investigated for the systems in this study, the polarization properties for the eigenstates were predicted by the exciton model.

Disulfur dinitride was examined in the ordinary ultraviolet, and the vibrational fine structure of the $B_{2\mu} \leftarrow A_g$ transition was assigned based on progressions of two vibrational frequencies in the upper state. The thermodynamically determined N·S bond energy, in N_2S_2 is reported and is compared to the N·S bond energy in N_4S_4.

Investigation of Nitrogen-Sulfur Systems

by R. N. Wiener, L. I. Rubin, and S. N. Singh

Introduction

The chemistry of nitrogen-sulfur systems has excited interest ever since tetrasulfurtetranitride (N_4S_4) was synthesized in 1835.[1] A prima facie view of these compounds leads one to contrast them with nitrogen-oxygen systems. However, any comparisons one might wish to make between these two apparently similar binary series is totally absent. This may be ascribed to the fact that in the former substances nitrogen is the more electronegative partner whereas oxygen occupies this role in the latter materials. This fact is also reflected in the naming of the compounds as nitrides.

The bonding in N_4S_4 does not follow conventional theories of valence and its nature is uncertain. Although the material is extremely stable at room temperature, when struck, a sample might explode. It is used as a starting material in the synthesis of disulfurdinitride (N_2S_2) which polymerizes upon standing at room temperature to a black powdery polymer, with an empirical formula given by $(NS)_x$. This latter substance has the interesting property of both being a semiconductor and being sublimable, albeit with difficulty. Neither N_4S_4 nor N_2S_2 have this electrical property. The sublimation of $(NS)_x$ results in a rich blue transparent film, which becomes golden upon further heating and finally yields a black film on which oblong crystals grow. These features just described illustrate some of the general characteristics of nitrogen-sulfur compounds, i.e., stability of bonds, tendency to form rings, and polymerization.

The geometrical structure of N_4S_4 had been under discussion for a long while and, in fact, only within the past five years has a definitive analysis (X-ray) been made.[2] It is described as a slightly distorted bisphenoid, with D_{2d} symmetry, and is illustrated in a later chapter (Figure 13). The bond distances are all equal (1.63Å) and intermediate between a "double bond" length of 1.54Å and a "single bond" distance of 1.74Å. The intramolecular sulfur-sulfur distance between atoms on the same side of the nitrogen plane is longer than the sulfur-sulfur bond length of 2.05Å in S_8 but considerably less than the van der Waals radii.

Attempts to explain these parameters have occupied investigators for some time. Becke-Goehring made an early study of the basic hydrolysis of N_4S_4[3] and concluded that this molecule must have sulfur-sulfur rather than nitrogen-nitrogen bonds. This deduction was based on the hydrolysis product analysis which showed that all the nitrogen present was converted into ammonia, rather than hydrazine, and the remaining products all contained sulfur-sulfur bonds. Craig and Paddock[4] proposed a delocalized cyclic model, for N_4S_4, involving $p\pi$ orbitals on the nitrogen atoms and $d\pi$ orbitals on the sulfur atoms. The greater electronegativity of nitrogen was argued to cause a contraction of sulfur d orbitals to such an extent that the orbitals overlapped. A quantitative approach was made by Chapman and Waddington[5]. They approximated the behavior of π electrons by a free electron on a sphere. Their calculations predicted the 2500Å band but was inconsistent with the observed dipole moment and, more importantly, allowed for both sulfur-sulfur and nitrogen-nitrogen bonds. In the light of this it is quite likely the spectral agreement they reported was

fortuitous. Braterman[6] applied Craig's formalism to a study of the electronic structure of N_4S_4. An energy level scheme resulting from the Huckel Molecular Orbital calculation was employed in interpreting the visible and ultraviolet spectrum. His assignments lend support to the sulfur-sulfur bond.

Confronted with this history of the exploration of the nature of the bonding in N_4S_4, the author undertook a spectroscopic investigation of the vacuum ultraviolet region in an attempt to add light to a still hazy situation. A simple model, the Molecular Exciton Model, was chosen as an instrument in this study by making a prior assumption that the spectrum could be accounted for without recourse to delocalization. While the success of such a model is not conclusive, it would be at least consistent with a localized picture.

A second material was chosen for spectroscopic examination, and analysis by the Molecular Exciton Model. Octatomic sulfur (S_8) has a geometrical structure quite similar to that of N_4S_4. An illustration of its geometry appears in a later chapter (Figure 16). It may be described as a puckered octagonal crown, possessing D_{4d} symmetry. Although decided differences between N_4S_4 and S_8 do exist, they are both eight-membered rings, possess significant symmetry, are low vapor pressure solids at room temperature, sublime readily, and both contain sulfur. The heteronuclear bonds of N_4S_4 are polar while the bonds of S_8 are not and it should not be surprising if as many differences as similarities in the spectra develop between the two substances.

The question of delocalization is again of concern in this molecule, as it was for N_4S_4. The possibility of $d\pi$-$d\pi$ overlap of neighboring atoms looms large and because of the multidirectional nature of the d orbitals molecular planarity is certainly not a prerequisite for delocalization to occur. Again, the Molecular Exciton Model cannot unequivocally answer this question but it may offer additional evidence consonant with localization.

The third molecule under consideration in this report is Disulfur Dinitride. Its spectrum is reported along with an assignment of its principal features. Because the structure is probably planar, electron delocalization is likely and conventional Molecular Orbital calculations were used in preference to a Molecular Exciton Model. These calculations were reported in earlier Quarterly Status Reports.

Included as well are brief discussions of the thermodynamic properties of Disulfur Dinitride and of the black polymeric solid formed in its decomposition.

Experimental

A. Spectrometers

The basic instrument employed in gathering the spectroscopic data was a Baird one meter radius mount near normal incidence grating vacuum monochromator which has been described previously.[10] The grating was a Bausch and Lomb magnesium fluoride coated concave grating ruled with 600 grooves/mm and blazed at 1500Å. Fixed entrance and exit slits of 50 microns resulted in an experimental half width of 1Å (resolving power given by $\lambda/\Delta\lambda$, or in this particular instance simply by λ, the wavelength in Angstrom units). This unit had a "light gathering" designation of $^{f}/10$. The hydrogen light source emitted a continuum between approximately 3000Å and 1675Å and a many-lined spectral distribution below 1675Å. A D.C. cold cathode discharge tube based on a design by Hunter[11] was used. The power supply for this source was a voltage regulated Kepco Labs unit, Model 1250, operated at 1000 volts with a power of 300 watts. The detection system consisted of a 1.5 inch diameter x 1 mm quartz disc scintillator coated with a 1.3 mg/cm^2 film of sodium salicylate and cemented into the far end of the cell compartment with Apiezon W. Its fluorescence was measured by a 9514S EMI photomultiplier tube. Depending on the spectral region of the source, the tube was operated over a voltage (D.C.) range between 1000 and 1550 volts. The power to operate this tube was furnished by a regulated high voltage power supply, Model RE2006, manufactured by Northeast Scientific Corporation. The voltage generated by the photomultiplier was further amplified

by a 610A Keithley Instruments electrometer and its output was recorded by a Leeds and Northrup Speedomax W recorder. The entire unit just described was affectionately known as "Dumbo" by all who used it. (The vacuum tank was appropriately painted elephant grey). A block diagram for Dumbo is given in Figure 1.

In addition to this spectrometer, a recording Beckman DK-1 instrument was employed both for many survey runs and in obtaining the spectrum of N_4S_4 at wavelengths above 3000Å.

A third instrument was employed in examining the spectrum of N_4S_4 between 3000Å and 2000Å. It may be described as follows: A one-half meter Jarrell-Ash Model 82000 monochromator was equipped with a 2" x 2" 30000 grooves/inch plane grating blazed at 3000Å and an adjustable bilateral slit assembly opened to 10 microns. Between 3000Å and 2000Å a continuum was furnished by an Hanovia Xenon thousand watt D.C. compact arc lamp, powered by a current regulated Hanovia power system, catalogue number 27801. The exciting radiation was detected by a 6256B EMI photomultiplier tube powered by a 412A John Fluke high voltage D.C. supply operated at 1200 volts. This output was further amplified by a VTE 1 Victoreen Instrument Company electrometer and the signal was recorded by a Leeds and Northrup Speedomax G. This package had an experimental half-width of 0.1 Å, which is a resolving power of 10λ, where again λ is the wavelength of the radiation in angstrom units. The instrument was moderately "fast", having a light gathering designation of $^f/9$. Figure 2 shows a block diagram for this spectrophotometer.

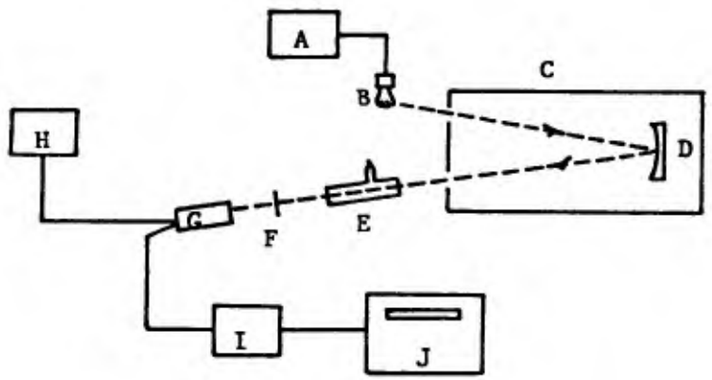

· Kepco power supply; B - Hydrogen source; C - vacuum monochromator; D - concave grating; E - sample cell; F - scintillator; G - photomultiplier; H - Northeast power supply; I - electrometer; J - recorder

FIGURE 1: Vacuum Grating Spectrophotometer (Dumbo)

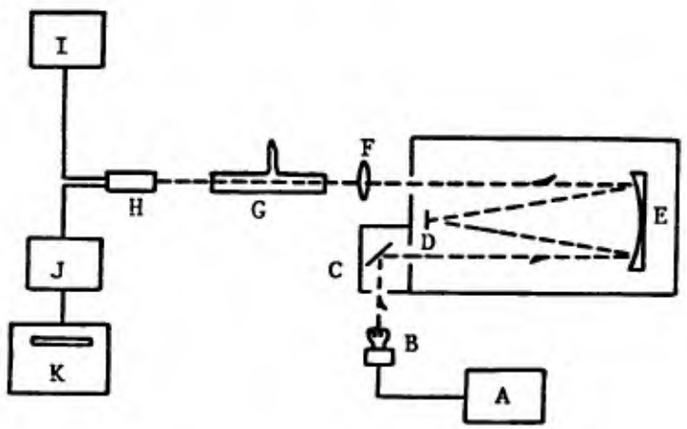

A - Hanovia power supply; B - Xenon lamp; C - plane mirror; D - grating;

E - concave mirror; F - plane-convex 24 cm focal length Suprasil lens;

G - sample cell; H - photomultiplier; I - Fluke power supply; J - electrometer;

K - recorder

FIGURE 2: Jarrell-Ash Spectrophotometer

B. Sample Cells

Three different cells were employed in obtaining the spectral data. In the region between 3000Å and 2000Å the N_4S_4 was examined in a 0.41 meter path length cell constructed of heavy walled Pyrex tubing with o-ring grooved flanges on either end. Ground and polished G.E. type 101 quartz glass discs, 2-1/4" x 1/4", were sandwiched between the end flange of the cell and an identical supporting flange, with Viton A o-rings on either side of the window. In operation, a side arm, used for sample introduction and vacuum evacuation, was sealed off and the cell wrapped with two separate heating tapes, one about the windows and the other around the body. The windows were maintained at a higher temperature than the body to prevent N_4S_4 from condensing on them. The temperature was regulated by a Variac controlled by a Yellow Springs Instrument Company Model RA63 thermistor. A Chromel-Alumel thermocouple was attached to the cell body and the voltage generated determined by means of a Model 2730 Honeywell potentiometer. The temperature accuracy and regulation of this control assembly was $\pm$ 1°C. In Figure 3, the system is illustrated diagrammatically.

The second cell was a 9.2 cm path length Pyrex cell with 20 mm x 1 mm vacuum ultraviolet sapphire windows, supplied by Stanley Scientific Glass Company, Perkasie, Pa. An off-centered side arm was used for introducing the samples of either N_4S_4 or S_8 and for evacuating the cell and filling with helium, the reasons for which will be discussed presently. Two pieces of Pyrex tubing, sized and shaped to slip over

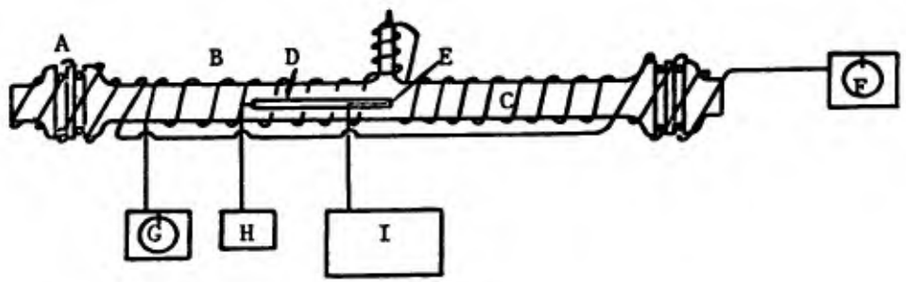

A - window heating tape; B - body heating tape; C - cell; D - thermistor probe (sensor);

E - thermocouple; F - end heating tape variac; G - body heating tape variac;

H - thermistor control; I - potentiometer

FIGURE 3: 0.41 m Cell and Temperature Regulation

the cell and meet at a line bisecting the stem, and to overhang the ends of the cell by approximately 2 mm were wound with Hoskins Chromel A resistance wire supplied by the Malin Company, Cleveland, Ohio. The spacing of the windings was such that for a given current in the wire, the ends were hotter than the body, again to prevent window condensation. A Pyrex tube wound with resistance wire, making a circuit separate from the end heaters, was placed over the side arm to control its temperature. The wire leads to the heaters were insulated from one another by cutting short sections of 3 mm glass tubing and stringing these "beads" on the wire. This allowed the cell and heaters to be moved around in the cell compartment without danger of shorting the circuits to a metal wall. The heaters were operated by independent variacs and the temperature measured by monitoring the absorption of a well-known band. (Discussed in a later section). Figure 4 is a representation of the cell and heater assembly just described.

The third cell was similar to the above described sapphire windowed cell, but has a quartz body with 20 mm x 1 mm suprasil windows, and an 8.7 cm path length. Similar heaters to the above were also constructed for this cell.

The short wavelength transmission cut-off for sapphire is approximately 1400Å and for suprasil approximately 1600Å, while lithium fluoride transmits to 1050Å. Many attempts were made at constructing a silver chloride seal between lithium fluoride and glass.[12] Table I gives the thermal coefficients of expansion of

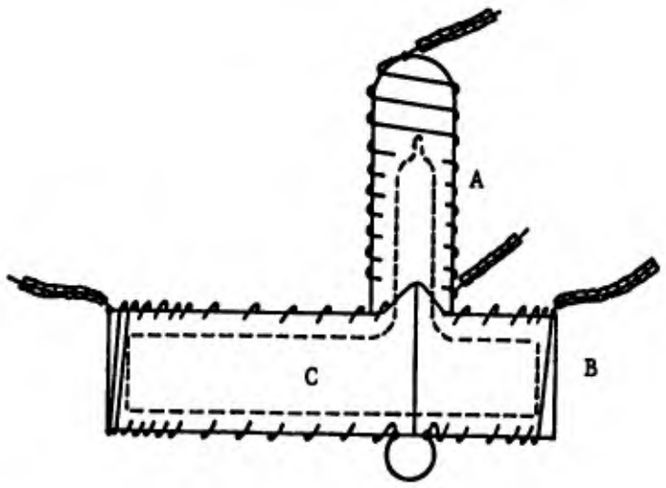

A - side arm heater assembly; B - body heater assembly;

C - cell (dotted line)

FIGURE 4: Sapphire Windowed Cell and Heater Assembly

TABLE I[13]

Thermal Coefficients of Expansion.

Material	Expansion
Lithium Fluoride	3.4
Pyrex	3.2
Quartz	0.5-1.0
Soft Glass	8.5

lithium fluoride and various glasses, in the same units. It will be immediately noticed that if lithium fluoride is bonded to the above listed substances, the cementing medium must possess the ability to absorb the stress generated by the greatly differing rates of expansion when the cell is heated. Of all the vacuum-tight high-melting sealing materials, only silver chloride is sufficiently plastic to dissipate the strain. Attempts with epoxides resulted in shattered LiF plates. Varying cell designs and techniques were employed with equally varying degrees of success, mostly centered about its absence. One approach involved dipping the cell end into molten silver chloride and cooling, repeatedly, until a layer of 1.5 mm was deposited, then annealing the cell end from 450°C to room temperature over a period of 4 hours. The hardened layer of silver chloride was trimmed with a sharp blade until a smooth and flat washer 1 mm thick resulted. A prepared cleaved window of lithium fluoride was placed on the washer and the temperature slowly raised to the melting point of silver chloride (455°C). After keeping the cell at this temperature for approximately 1-2 minutes, until a seal had been effected, it was again annealed to room temperature over a 4 hour period. At this point, the procedure was repeated for the opposite end of the cell if no cracks appeared and the seal was vacuum tight. (Prior to the application of silver chloride a thin ring of DuPont conductive silver paint 4887, supplied by the DuPont Electrochemical Division, New York, New York, was baked on the end of the cell and the outer edge of the window to provide a surface wettable by silver chloride.) Two consecutive successful seals on a given cell body

constituted a complete cell. In actual practice one or many cracks usually appeared on at least one of the seals.

Another method was to place a ring of silver chloride between a silvered cell end and a silvered lithium fluoride window. Again, the temperature of the assembly was elevated to 455°C, maintained there for a time and then annealed as before.

In addition to the various procedures described above, various cell end designs were used. In one instance ring seals were constructed at each end of the cell body and the seal attempted with the inner tube. A second design consisted of flattening the ends of a tube to provide more surface area for the seal, at the expense of the inside diameter. A third choice was to seal the window directly to a ground end. Side views of these designs are illustrated in Figure 5.

FIGURE 5

Silver Chloride Seal Cell End Designs

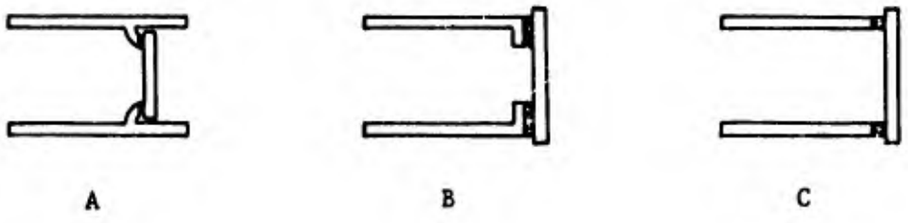

A - ring seal end; B - flattened end; C - ground end

It was felt by the author that a successful lithium fluoride windowed cell could be effected in the relatively near future. With electrodes, the cell could be employed to measure the ionization potential, as well as absorption beyond the sapphire cut-off. However, the timing was such that further attempts had to be abandoned and the highest frequency data was that collected with the sapphire windowed cell.

C. Materials

The spectroscopic investigations of concern deal with vapor phase studies of N_4S_4 and S_8. The latter compound in 99.99% purity was gratefully received from Texas Gulf Sulphur Company, Okotoks, Alberta, and used with no further purification. Prior to actual use, however, each sample was degassed, as described in a later section. N_4S_4 was synthesized by Mr. S. Singh using the following modification of a known recipe[14]: A mixture of 1200 ml of carbon tetrachloride and 75 ml of sulfur dichloride was saturated at room temperature with chlorine and placed in an ice bath to maintain the temperature below 50°C. A fast stream (50 l/hour) of ammonia was passed through the mixture until it was a salmon red color, at which time the mixture was filtered. The solid was wetted with carbon tetrachloride and the mixture slurried with 900 ml of water for 15 minutes. It was again filtered and the residue shaken with 225 ml of ether for one hour and extracted with dioxane in a soxlet extractor. The material was then recrystallized from hot benzene until a "melting point" determination indicated decomposition at 179°C. The purified product was then dissolved in dioxane and placed on a

silica gel plate in an attempt to effect some separation of constituents not removed by the recrystallization process. Benzene, acetone, carbon tetrachloride, and mixtures of benzene-ethylbenzoate were used as elutants. In no instance was any separation observed.

The so-called "melting point" determination mentioned above is not truly a melting phenomenon, but is an extremely sensitive test for the purity of N_4S_4. When a sample of this material is gradually heated, a progression of color changes occurs from its characteristic golden yellow to a reddish brown hue. At 179°C a simultaneous liquefaction and decomposition takes place with the appearance of bubbles. Even the presence of trace amounts of contamination, such as sulfur, produces a marked decrease in the temperature at which this occurs. In fact, to calibrate this method of determining the purity of N_4S_4, trace amounts of sulfur were intentionally introduced into an extremely high purity sample and the "melting point" was observed to drop to around 160°C much more sharply than would be expected from a mixture of two pure materials. Sulfur was chosen as a test contaminant because it is a product of the synthesis of N_4S_4 and might logically be carried through the benzene recrystallization.

D. Sample Handling Techniques

In all instances, a given mass of sample was distilled into an evacuated cell from a bulb attached to the side arm. This was effected by gently heating the sample-containing bulb with a heat gun until sufficient sample had diffused into the cell. This provided the dual advantage of lessening the possibility of sample contamination as

well as the more important benefit of facilitating degassing, since the cell was constantly pumped during this process. Further sublimation of sample within the cell, during evacuation, afforded complete removal of any occluded vapors. The bulb was then sealed off and, in the case of the N_4S_4 spectra taken with the Jarrell-Ash, the side arm was also sealed off under vacuum. For those runs made on "Dumbo", it was found necessary to introduce approximately 13 mm of helium into the cell prior to sealing for the following reason. In the evacuated cell compartment, the only relatively efficient mechanism for heat transfer is radiative. Sapphire transmits the infrared radiation generated by the cell heaters while the Pyrex body absorbs this light with the result that the windows are cooler than the cell body and allow sample condensation to occur. In this situation the helium is a heat exchanger between the walls of the cell, which are infrared heated, and the windows. This problem did not exist in the suprasil windowed cell, nor was it encountered in the unevacuated cell compartment of the Jarrell-Ash instrument. One can derive an expression for the wavelength of maximum illumination, λ_m, at a given temperature by consideration of Planck's distribution law for blackbody radiation. The result[15] is a relationship given by: $\lambda_m T = 2898$ (micron-degree). At 100°C, the wavelength maximum occurs at approximately 7.8 microns. Pyrex transmits to approximately 3.5 microns and sapphire to approximately 7 microns.[13] Hence, our conclusions seem eminently reasonable. They were also verified experimentally, and in fact, the experimental verification occurred

prior to the ratiocination. The helium was introduced by passing this gas through a liquid nitrogen trap filled with Linde Air Products Company type 4A molecular sieves and thence into the vacuum system on which was affixed the cell in question. The pressure was measured with an oil manometer although, prior to the helium introduction, the cell had been checked for leaks by a Consolidated Electrodynamics Corporation type 41550 capacitance micromanometer. The filled and sealed cell was placed in its heaters and the entire assembly loaded into the cell compartment. An eight terminal vacuum lead through (multiheader) was used for electrical connections.

E. Temperature Determination and Regulation

Utilizing available vapor pressure data for N_4S_4[16] and S_8[17], shown abridged in Table II, the temperature of the vapor was determined by monitoring the 2535Å maximum of N_4S_4 and the 2550Å maximum of S_8. The first band was investigated using the Jarrell-Ash spectrophotometer and the 0.41 m path length cell described in earlier sections. Many runs made between 60°-70°C yielded precise data on the optical density as a function of temperature for this absorption. The molar extinction coefficient was then determined from this information employing Equation 3. All subsequent extinction coefficients at other wavelengths for N_4S_4 are referenced to this one. The molar extinction coefficient for the S_8 maximum at 2550Å was taken from Bass[18], who assumed the value determined by Baer and Carmack[9] in solution was valid for the vapor. There is no reason to believe this to be so, and in fact, measurements of N_4S_4 in solution and in the vapor are significantly different. All other sulfur extinction coefficients are based on the value used for

TABLE II

Vapor Pressure Data For N_4S_4 and S_8

T, °C	$P_{N_4S_4}$ (mm)	T, °C	P_{S_8} (mm)
37.5	0.00026	120	0.04
50.5	0.0013	130	0.074
59.0	0.0035	140	0.13
70.5	0.0106	150	0.22
		160	0.37

this maximum. This does not effect the relative intensities reported but does introduce a degree of uncertainty in the absoluteness of the tabulated values. Knowing the molar extinction coefficient at these wavelengths for the respective compounds, the ratio of the absolute temperature to the vapor pressure in mm was calculated, and from the graphs of Ln P *vs.* 1/T, the temperature was obtained. The derivation of this calculation is given as follows: from the consideration of the ideal gas relationship one can express the concentration of a vapor in terms of its pressure and temperature:

$$C = \frac{n}{V} = \frac{P}{RT} \qquad \ldots\ldots(1)$$

where C is concentration in moles per liter, n is the number of moles of material, V is the volume in liters occupied by n moles, P is the pressure of vapor in millimeters, T is the absolute temperature and R is the ideal gas constant expressed in terms of ($mm\text{-}l\text{-}mole^{-1}\text{-}deg^{-1}$). Substituting C in the Lambert-Beer law, which is expressed as follows:

$$\log {}^{I_o}/_{I} = \varepsilon_\lambda C\ell = OD \qquad \ldots\ldots(2)$$

where I_o and I are the incident and transmitted light, respectively, ε_λ is the molar extinction coefficient for a given wavelength, C is again the molar concentration, ℓ is the path length, in cm., traversed by the transmitted light, and OD is the optical density, one obtains the following useful relationship:

$$(T/P) = \frac{(\varepsilon_\lambda)(\ell)}{(OD)(62.1)} \qquad \ldots\ldots(3)$$

Then, as mentioned, the ratio obtained from Equation 3 is compared with that determined from the vapor pressure curves and the temperature deduced. In finding the temperature-pressure ratio from the curves the procedure was to arbitrarily select a temperature, calculate the corresponding pressure and take the ratio of the two. When the desired constant was reached, one then had the values sought for.

As mentioned earlier, the temperature control of spectra taken in the near and far ultraviolet with the Jarrell-Ash instrument was governed by a thermistor-regulated variac. It was adjusted so that the heater on-time equalled the heater off-time. In the case of runs made with the vacuum ultraviolet spectrophotometer, the variac was operated from an unregulated voltage source. However, relatively high fluctuations in the line voltage (60 cps) would require a faster response of the vapor system in question to the change than was possible. From observations of the rate of cooling of the heated cell, at the high temperature end, a one degree drop subsequent to turning off the variacs, required 30 seconds. Hence, in one second a temperature change of $1/30^{th}$ of a degree would develop. In this same period, the current would fluctuate 60 times and any change due to this would be undetectable. Low frequency fluctuations (drift) were apparently averaged out by the heat capacity of the helium because once temperature equilibrium had been established the drift in a monitored absorption appeared to be comparable to the drift in the light source itself. (Approximately one percent in one-half hour).

However, it is still meaningful to ask how valid, or accurate, the temperature control was during a run. An answer to this question may be given by considering an analysis of the Clausius-Clapeyron equation, given below:

$$\frac{d \ln P}{dT} = \frac{\Delta H}{RT^2} \qquad \ldots\ldots(4)$$

where P is the vapor pressure, T the absolute temperature, ΔH the heat of sublimation for N_4S_4, and R the ideal gas constant. Integrating this expression and substituting the result into Equation 3 one obtains the following relationship:

$$\frac{T}{P^{\circ} e^{-\Delta H/RT}} = \frac{\epsilon_{\lambda} \ell}{(OD)(62.1)} \qquad \ldots\ldots(5)$$

where P° is a constant of integration determined by the system in question and the other symbols are as previously defined. By taking the natural logarithm of both sides of Equation 5, substituting in the expression for the optical density, given by Equation 2, where appropriate, and differentiating both sides of the resulting equation, one obtains Equation 6:

$$\left[\frac{1}{T} - \frac{\Delta H}{RT^2}\right] dT = \frac{2.303}{OD} \frac{dI}{I} \qquad \ldots\ldots(6)$$

If one chooses a cell length such that at 127°C, the OD is 1, and substitutes 23 kilocalories for ΔH[16] Equation 6 reduces to:

$$0.031\ \Delta T = \frac{\Delta I}{I} \qquad \ldots\ldots(7)$$

It is immediately obvious from Equation 7 that a one degree temperature change will result in a three percent change in the light intensity. However, it has been previously stated that over a one-half hour period the light intensity of a monitored frequency did not change more than one percent. From this the author concludes that the temperature control was good to ± 1 degree, in spite of its apparent crudeness.

F. Spectral Interferences

Several interesting complications manifested themselves in obtaining the spectrum of N_4S_4. In retrospect, this should not have been surprising since N_4S_4 may be used as a starting material for the preparation of all the other known sulfur nitrides. By heating N_4S_4 in the cells, one could identify the spectrum of disulfurdinitride and that of an unknown material, in addition to N_4S_4. The unknown spectrum was compared with the published spectra on materials which might conceivably be present in a sample of N_4S_4, such as water vapor, ammonia, ammonium chloride, sulfur dioxide, and nitrogen oxides. These substances appeared totally absent from the comparisons. At this point, the preliminary investigations of Mr. D. Mitra and Mr. S. Singh on N_2S_2 proved extremely helpful. It was observed that the formation of these contaminating substances was more pronounced in the Sapphire windowed cell than in the Suprasil windowed cell, and in both cells appeared as a function of temperature and duration of heating. The above mentioned experimenters found that the formation of disulfurdinitride was very sensitive to the nature of the surface on which the synthesis was conducted. If a quartz

furnace was employed, the yield of N_2S_2 was ten to fifty times that obtained with a Pyrex furnace. Apparently, Sapphire exhibits a greater catalytic effect than quartz, based on the relative amounts of N_2S_2 observed in the Sapphire and Suprasil windowed cells. It should be mentioned that simultaneous temperature measurements of the cell body and windows showed that the latter portion of the heated cell was almost twice as hot as the coolest portion of the body. At times, therefore, the windows were close to 200°C, not far from the operating temperature of 230°C in the N_2S_2 synthesis. Mitra and Singh further found that upon standing at room temperature the material slowly polymerized to a black solid having an empirical formula given by $(NS)_x$. Singh further obtained the N_2S_2 spectrum around 2500Å and it was this information that enabled the author to identify one of the contaminants. The author was also delighted that the polymerization did not occur on the windows.

Upon standing, a cell previously heated and cooled to room temperature, and containing a mixture of N_2S_2, N_4S_4 and the unknown was observed to have a spectrum that did not alter over a period of months, once the N_2S_2 had polymerized. In addition, the appearance of sulfur was noted upon prolonged heating. The whitish film dissolved readily in carbon disulfide and intense heating of the film converted it into yellow droplets. A comparison run made on sulfur, by vaporizing enough to form a whitish film approximately equal to that found in the N_4S_4, and then heating severely to form yellow droplets and dissolving it in CS_2, indicated that in these respects the film observed in the N_4S_4 behaved as sulfur did. Vaporization of N_4S_4 under similar conditions did not

yield a whitish film.

In order to establish something of the relationship between the unknown material and N_4S_4, the following series of experiments were performed. A sample of N_4S_4 was heated for three hours in an evacuated and sealed cell and its spectrum taken immediately upon cooling to room temperature, and again after standing overnight (a period of approximately 15-20 hours). The spectra taken at these two separate times differed only by the appearance of the N_2S_2 spectrum which developed in the former instance. This could be subtracted out of the first spectrum and the resultant curve was identical with that obtained the following day. As mentioned earlier, upon standing overnight, only the unknown spectrum remained. This procedure was repeated many times, each time evacuating and sealing the cell before heating for three hours. It did not matter whether a new sample of N_4S_4 was used or a single sample was repeatedly heated; the spectrum that appeared was the same and at the same optical density. A sample was then heated repeatedly for three hour periods, spaced approximately twenty four hours apart, without the intervening evacuation, and again the same spectrum at about the same absorbance appeared. Finally, the sealed cell containing the unknown was heated slowly from room temperature to 120°C while monitoring peaks at 2100Å and 2000Å. Although the optical densities at each peak did increase with temperature, the rise was not in keeping with a vapor-condensed phase equilibrium (Clausius-Clapeyron relation) being greater only by a factor of two at 120°C than at room temperature. If one assumes a heat of vaporization of

15 kcal/mole (a nice round number) the ratio of the vapor pressure at the higher temperature to that at room temperature is approximately 300, according to the Clausius-Clapeyron equation. Considering that the optical density is directly proportional to the pressure of the vapor, the observed absorption should have been off the scale of the instrument. Upon cooling to room temperature the spectrum was identical to that observed prior to the heating. These results remain unexplained. The latter test seems to discount the condensed phase-vapor equilibrium suggested by the earlier tests. This system is certainly deserving of further investigation, both because of the perplexing behavior just discussed, and for its interesting spectrum, which will be presented shortly in a separate section.

A possibility to be explored in the future is that the unknown is tetrasulfurdinitride, N_2S_4. Intuitively, one would state that N_4S_4 decomposes to sulfur and nitrogen. In addition, there is direct evidence that sulfur forms upon heating N_4S_4, a fact alluded to earlier. The formation of N_2S_4 from sulfur and N_4S_4 is a well-known recipe[19] and requires heating a carbon disulfide solution of these materials in the ratio of two parts of sulfur to one part N_4S_4, for two hours at 110°C. A thiocyanogen polymer, $(SCN)_x$, is a principal product in solution, indicating that carbon disulfide's role is more than merely that of solvent. While these exact conditions do not prevail in the cell, conditions suitable to a poor yield of this material may be present. The recipe at least lends credence to its possible formation. By all means its mass spectrum should be speedily examined.

Because of the formation of materials alien to the spectrum of N_4S_4, which are apparently generated as functions of heating time, the procedure for obtaining the desired spectrum was modified. The cell was heated for relatively short periods at a time, scanning approximately four hundred angstroms, then opened, evacuated, refilled with helium and resealed. Although this procedure was time consuming, by adhering to it no complicating products could be detected over the running time. This fact was ascertained by rescanning the 2000Å region upon cooling, where the decomposition product(s) had its strongest absorption. No difference was observed in the incident light traces made before and after the run.

G. Data Reduction and Plotting

Traces of incident and transmitted light for each run were reduced by a Gerber Digital Data Reduction System, model GDDRS-3B, coupled to an IBM 26 card punch machine. By means of this combination, values of the traces at emission maxima and at 3-5Å intervals in the continuous region were automatically punched on IBM cards. This information, together with data on scattered light, temperature, pressure and path length for each run was fed into an IBM 7094 computer. A Fortran program, written by Mr. E. Reid, yielded values of optical density and extinction coefficients at each wavelength and frequency. The points were then plotted by a model 565 Calcomp Digital Incremental Plotter. The spectra of N_4S_4 and S_8 are presented in the next chapter, along with those of N_2S_2 and the previously discussed unknown material, for completeness.

It should be noted that the spectra of Figures 6, 7, and 8 are the averages of many runs, and that the actual data were not smooth as illustrated, but possessed random excursions due mainly to an attenuated transmitted light through imperfect Sapphire windows. In the least favorable instances, the signal-to-noise ratio was 4:1. The windows became pitted when the cell side arm was snapped open. Several times while refilling the cell the inrushing air carried tiny glass chips to the windows, pitting them. This procedure of opening the cell under vacuum was revised when it became apparent what was occurring, although not in time to prevent a cell which scattered light according to the fourth power of the wavelength. Nevertheless, in favorable regions of the spectrum, the signal-to-noise ratio was in excess of 250:1. Since no periodicity was observed (such as vibrational structure of the bands) the best curves possible, consistent with reality, were drawn.

The precisely known wavelengths of the hydrogen emission maxima, first and second order, were fitted to a least squares plot and the wavelength linearity of Dumbo determined. Hence, wavelength data in the regions investigated are accurate to 0.1Å. Since the instrument was not linear with frequency, the wavenumber error will depend on the angstrom region involved.

The molar extinction coefficients are given by Equation 3. Because of the uncertainty in temperature and pressure, the error in the calculated extinction coefficients is estimated at 20%.

Spectra and Interpretation

A. Spectra

The spectra of N_4S_4 and S_8 are shown in Figures 6, 7, 8 and 9,[18] and will shortly be examined further. The curves for N_2S_2 and the unknown material, discussed in the previous chapter, are also presented here in Figures 10 and 11, respectively. Beyond their display at this point, nothing more will be mentioned about them than was discussed earlier.

To facilitate the review of the data, Table III lists the molar extinction coefficients at the various maxima and minima for the substances in question. They are relative to an experimentally determined value of 11500 for N_4S_4 at 39500 cm^{-1} and, in the case of S_8, to a literature value of 3980 [9,18] at 39200 cm^{-1}. The details of the calculation have been presented in an earlier chapter.

In both spectra, very intense absorption occurs at approximately 62000 cm^{-1}, although the relative shapes of this band differs; i.e., the S_8 maximum appears as a possibly unresolved doublet while the N_4S_4 band is broad and symmetrical. The differences in the two curves are quite pronounced, a minimum appearing at approximately 48000 cm^{-1} for the N_4S_4 while a maximum develops at about the same frequency for the S_8. In addition, there is at least a shoulder, if not a definite band, at 54000cm^{-1} in the S_8 spectrum, whereas this feature is totally absent from the N_4S_4 spectrum. Furthermore, N_4S_4 exhibits a pronounced band at 39000 cm^{-1} while a maximum at this same frequency in S_8 appears

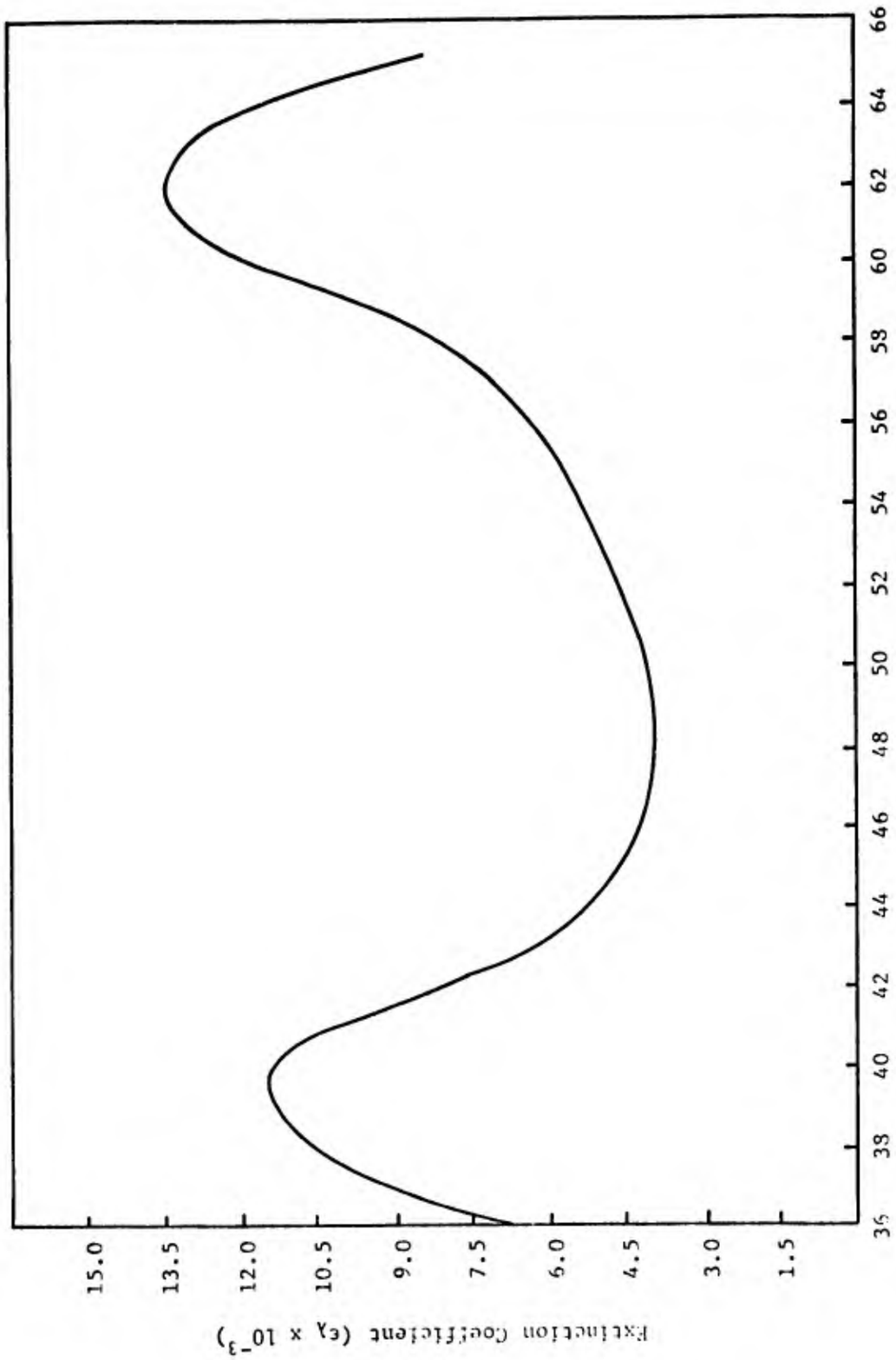

FIGURE 6: N_4S_4 Spectrum (A)

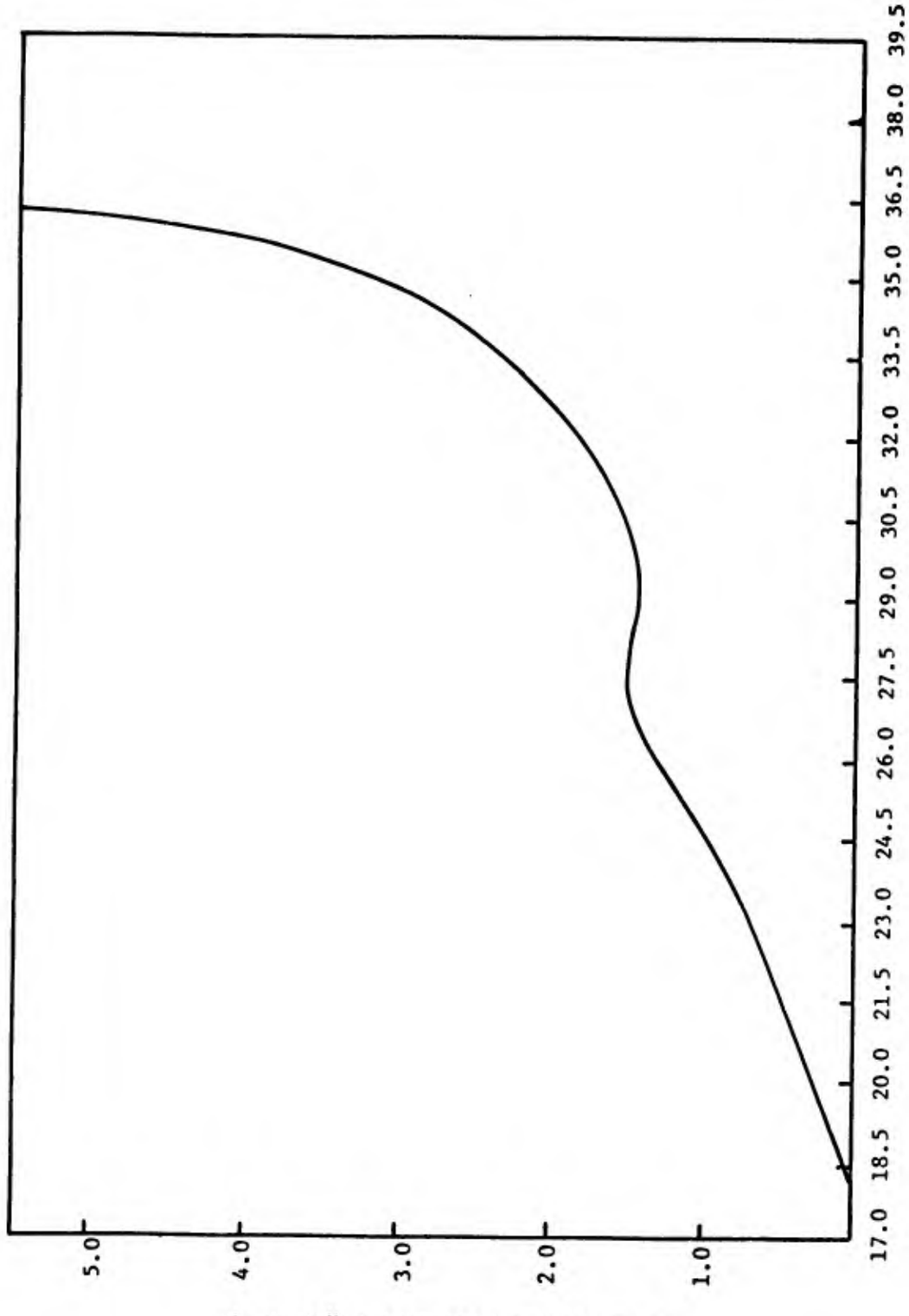

FIGURE 7: N_4S_4 Spectrum (B)

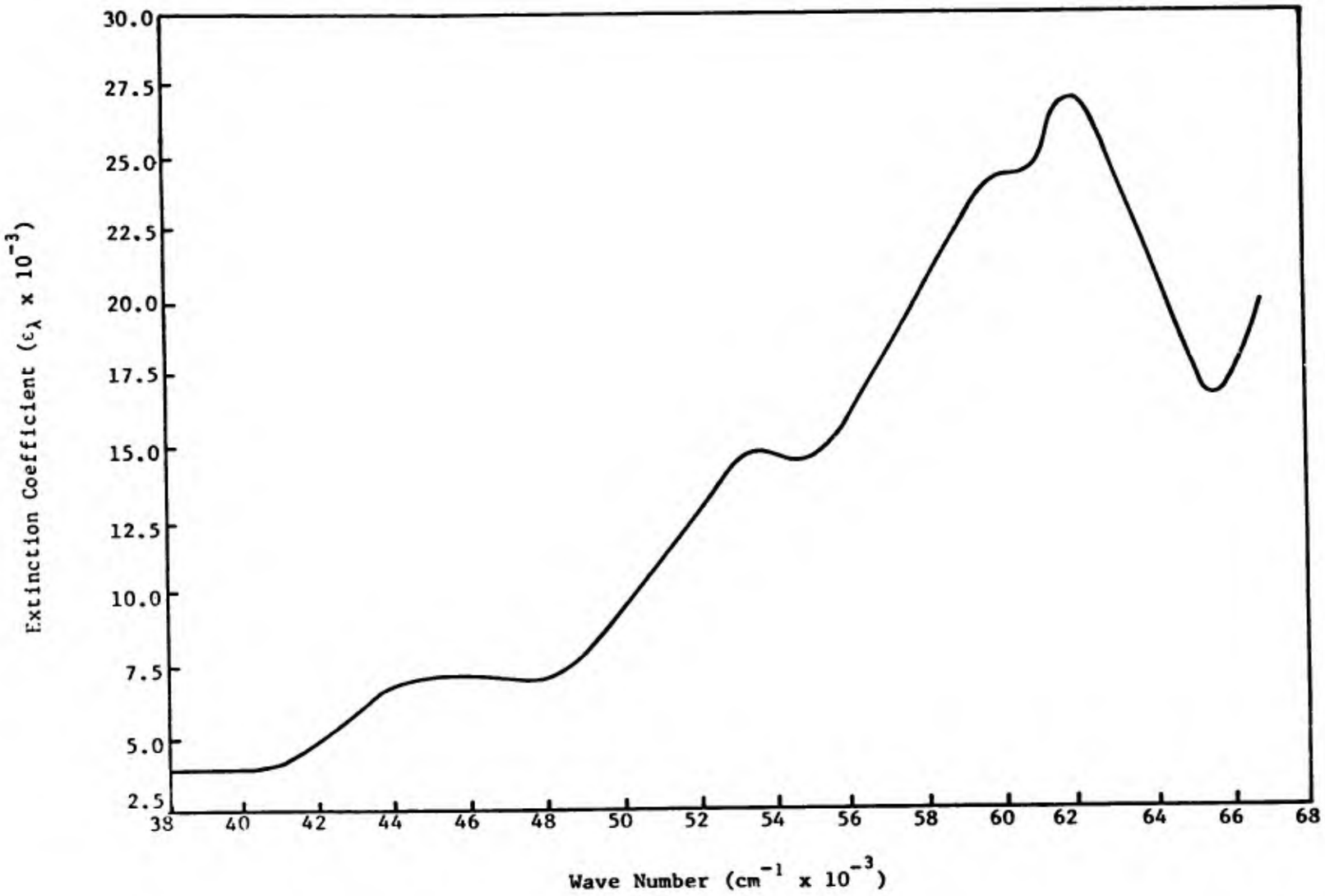

FIGURE 8: S_8 Spectrum (A)

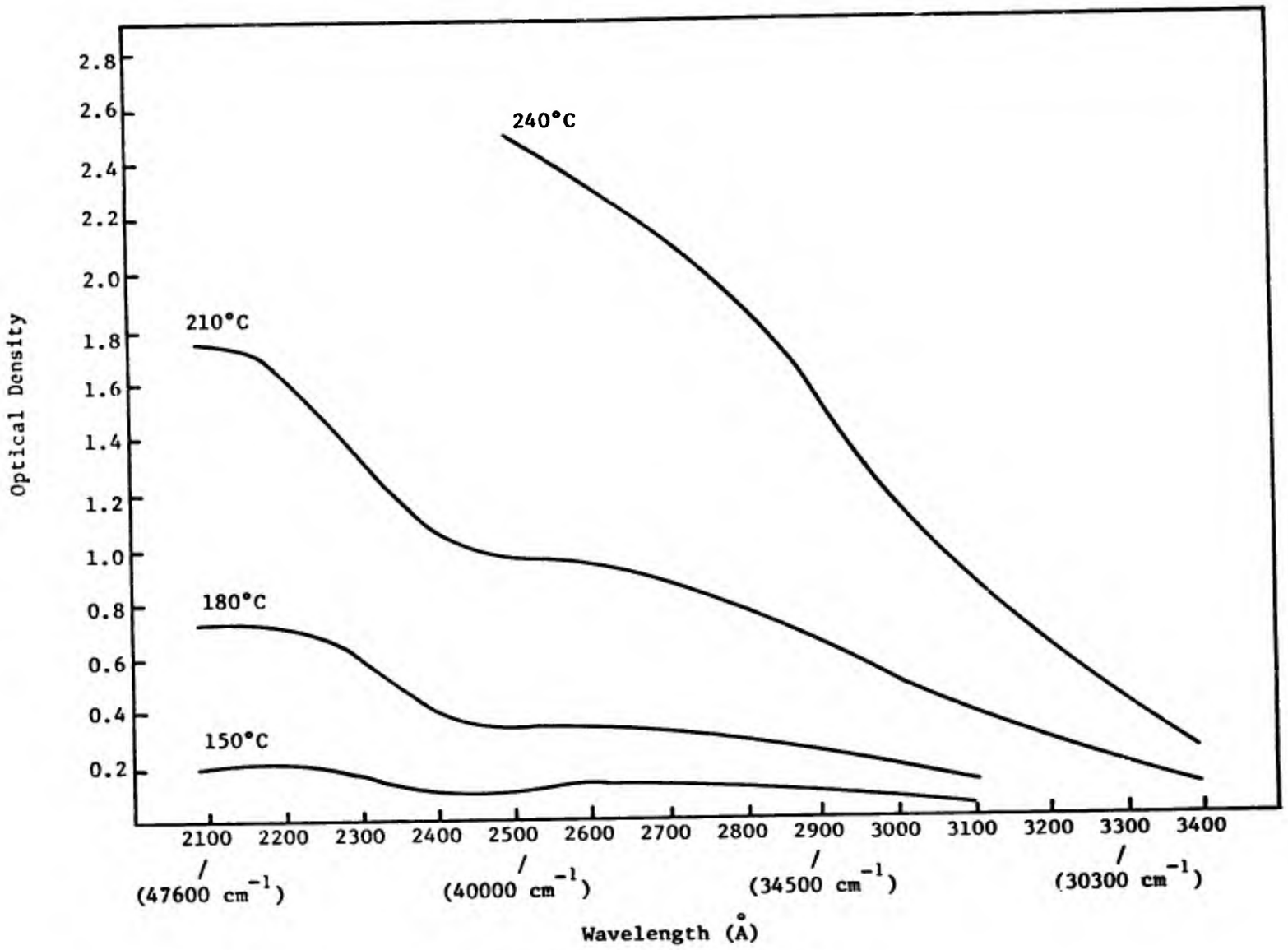

FIGURE 9: S_8 Spectrum (B)

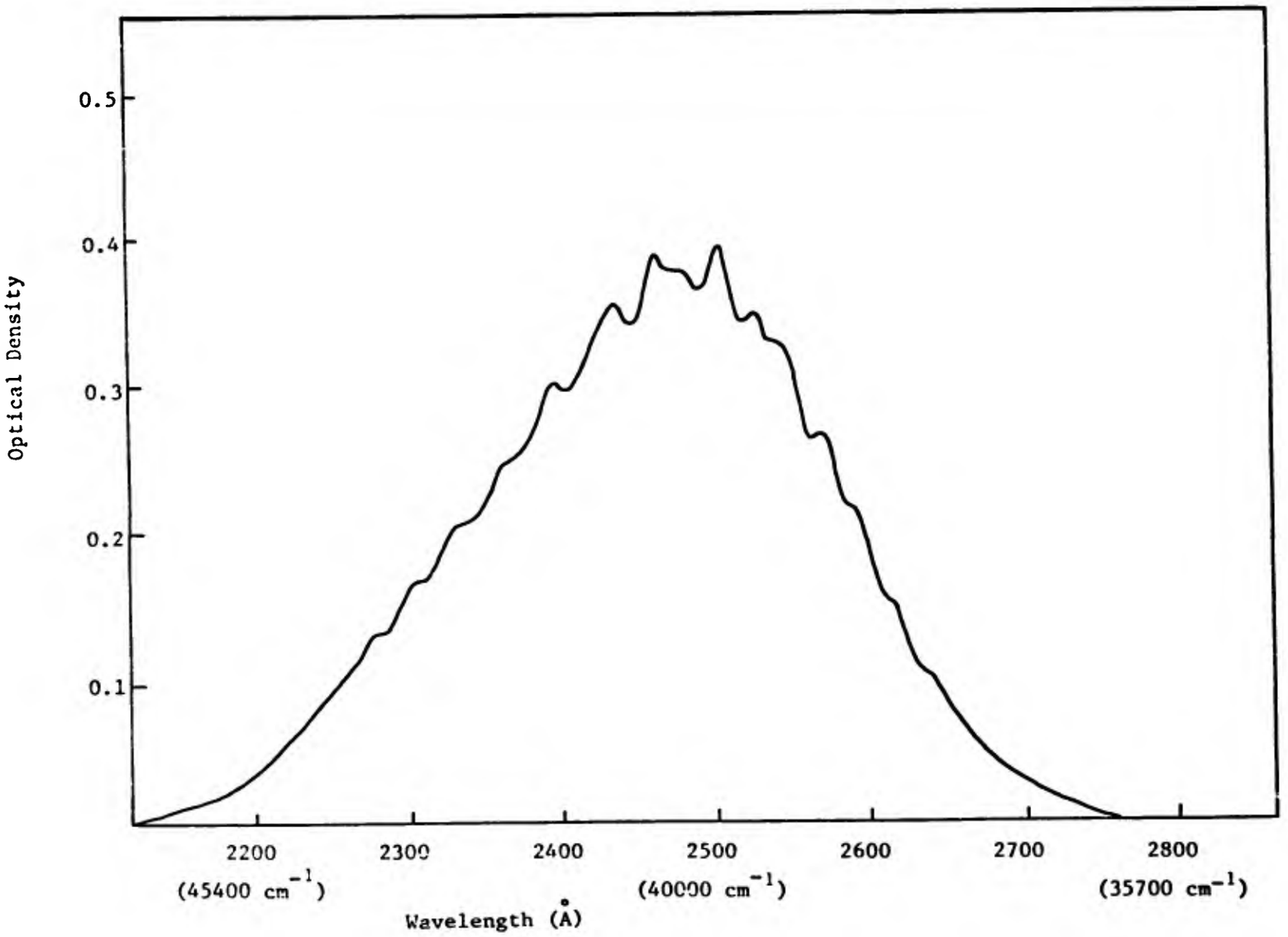

FIGURE 10: N_2S_2 Spectrum

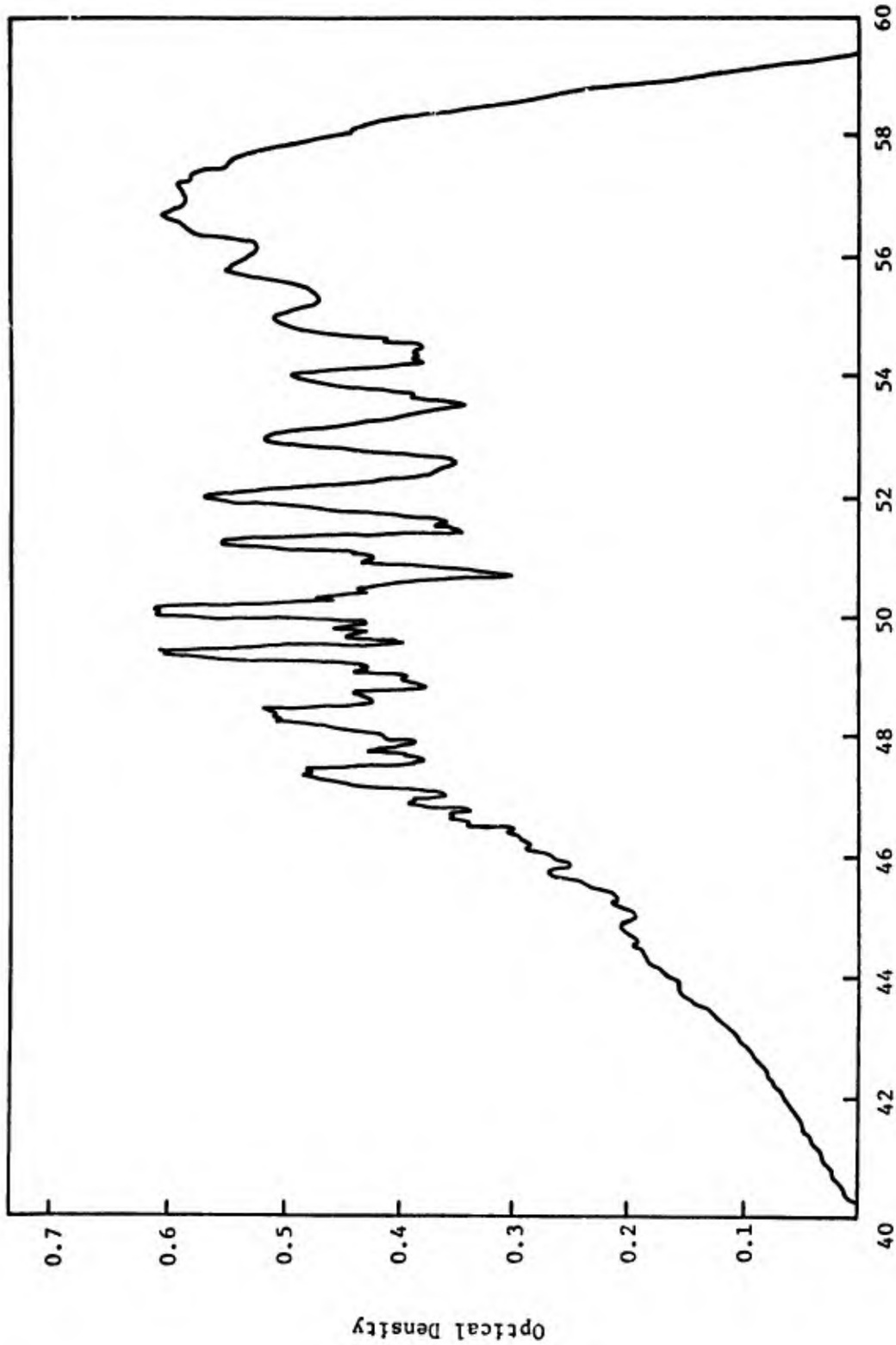

FIGURE 11: Unknown Spectrum

TABLE III

Molar Extinction Coefficients for N_4S_4 and S_8

N_4S_4			S_8		
Frequency (cm^{-1})	Extinction Coefficient	Extremum	Frequency (cm^{-1})	Extinction Coefficient	Extremum
27000 (3700Å)	1500	max	39200 (2550Å)	3940	max
29000 (3450Å)	1360	min	46000 (2170Å)	7290	max
39500 (2535Å)	11500	max	47800 (2090Å)	6950	min
48000 (2080Å)	3890	min	53500 (1870Å)	15250	max
62000 (1612Å)	13600	max	54800 (1825Å)	14300	min
			60200 (1660Å)	24700	shoulder
			61800 (1618Å)	27200	max
			65400 (1530Å)	16500	min

as a plateau. Finally, N_4S_4 shows a very long tail into the red with a possible hint of a maximum at 27000 cm^{-1} and S_8 presents a similar maximum [18] at 35000 cm^{-1}.

At this point, it becomes necessary to briefly compare the overlap region of the S_8 spectrum of Bass [18] and the author. Although in both cases there is general agreement on the spectra, the author feels that gracing the long tail extending toward the red below 40000 cm^{-1} with the appellation of a broad, unresolved band, as Bass does, is quite presumptuous. By increasing the temperature to 240°C, where an appreciable amount of S_8 dissociation exists, strong absorption does indeed appear in this region. However, on the same scale, the 46000 cm^{-1} band becomes gigantic and is not even indicated in the curves. This behavior is exactly analogous to Figure 8 where the author purposefully developed the tail at high temperature (120°C) to indicate the shape of the 27000 cm^{-1} absorption. In addition, it is quite unclear how Bass was able to separate out the absorption due to dissociation products, such as S_2, S_4, S_6, etc. The author did not encounter this problem because all S_8 traces were made below 140°C, where the dissociation of sulfur vapor is small.

B. Molecular Exciton Model

In interpreting the molecular spectra of immediate concern, the Molecular Exciton Model will be adopted. Its use is suggested by a conclusion based on an Hückel Molecular Orbital calculation [6] that delocalization effects are relatively unimportant in interpreting the electronic spectrum of N_4S_4. This model has been described

by several authors [20,21,22] and, although less familiar than the more commonly employed molecular orbital and valence bond techniques, has application to many systems.

In the present application of the model, we shall consider that the spectral transitions develop from excitations of a group of independent entities (bonds), consisting of a pair of optical electrons localized between two positively charged centers. All bonds in the molecules are equivalent, and the non-bonding electrons are localized on the atoms of the molecule and do not contribute to the spectrum. Describing our actual systems more concretely, the s electrons are localized on the respective atoms, S or N, and the pσ electrons are being promoted to excited states. Justification for this approximation is afforded by the spectrum of $S_4(NH)_4$, reported by Braterman [6]. The addition of hydrogen-nitrogen bonds to N_4S_4 ties up a lone 2p electron and leaves the nitrogen with a lone pair, as well as two lone pairs centered on the sulfur atoms. That these electrons are tightly bound is indicated by the appearance of the first absorption band at 46000 cm^{-1}. In this simple model, we are neglecting overlap and electron exchange between bonds. This is an obviously gross approximation, and its validity will depend on the actual bonding in the molecule. As we go to shorter wavelength transitions, such as $\sigma \rightarrow \sigma^*$ found in molecules with only sigma bonds, the approximation becomes more accurate. However, it has also been used with success on such non-total sigma systems as azo dyes,[23] polyenes [24] (such as butadiene, hexatriene, etc.) and carotenoid pigments.[25] At this point, the theory will be unfolded briefly to

introduce the notation and nurture the discussion.

We shall consider the Hamiltonian for the systems in question to be expressible as a sum of two parts:

$$H = \sum_k H_k + \sum_{k<\ell} V_{k\ell} \qquad \ldots\ldots (8)$$

where the first term on the right is the Hamiltonian operator for each of the individual bonds, and obeys the following energy eigenvalue equation:

$$H_k \phi_k = \varepsilon_k \phi_k \qquad \ldots\ldots (9)$$

and the second term of Equation 8 is the electrostatic interaction operator involving bonds k and ℓ. If we consider each bond as a quasi-diatomic molecule, a representative bond Hamiltonian could be expressed in atomic units as:

$$-H_k = {}^1/_2 \nabla_1^2 + {}^1/_2 \nabla_2^2 + \sum \frac{e^2}{r_{ij}} - \frac{e^2}{r_{12}} \qquad \ldots\ldots (10)$$

where the fourth term on the right of Equation 10 is the electron-electron repulsion. The exact form of this Hamiltonian is not of concern in this approximation because the model assumes that the solution of Equation 9 is available. The ϕ_k's of Equation 9 are the normalized ground state wave functions for the component bonds, and may be considered as constructed from one electron hydrogenic type

orbitals. They combine to yield the zeroth order approximation to the singlet ground state of the molecule (all bonds together):

$$\Phi_G = \prod_k \phi_k \qquad \ldots\ldots (11)$$

Since the model assumes the absence of electron exchange between bonds, the anti-symmetrization of Φ_G with respect to interchange of electrons between bonds is meaningless. This is not a violation of the Pauli principle. Our wave functions do not have to reflect the indistinguishability of the electrons while maintaining an overall probability distribution because of our initial assumption. For a system of n component bonds, the zeroth order approximation of the first singlet state is n-fold degenerate. One of the manifold of excited state wave functions is given by:

$$\phi_k^+ = \phi_k^+ \prod_{\ell \neq k} \phi_\ell \qquad \ldots\ldots (12)$$

where ϕ_k^+ is the normalized wave function for excitation of bond K and obeys the following relationship:

$$H_k \phi_k^+ = \varepsilon_k^+ \phi_k^+ \qquad \ldots\ldots (13)$$

The electrostatic interaction potential, $\sum_{k<\ell} V_{k\ell}$, lifts the excited state degeneracy, partially or completely, and we are thus able to obtain correct first order excited state energies and corresponding zeroth order wave functions by enlisting degenerate perturbation theory.[26] At this point, one might reasonably ask if

the perturbation is sufficiently small to allow the use of this method. In an attempt to answer this question, the classical energy of interaction between two dipoles will be calculated and compared to ar estimated value for the ionization potential. The ionization potential of N_2S_2 is 10.5 eV.[27] Assuming the value for N_4S_4 is in this region, we proceed to calculate the interaction energy between two dipoles, head to tail, situated on two adjacent N-S bonds and centered at their midpoint, with each having a dipole moment of 1 Debye (10^{-18} e.s.u.). It can be shown from classical electrostatics that such an energy of interaction is given by:

$$E_{12} = \frac{\vec{\mu}_1 \cdot \vec{\mu}_2 - 3[(\vec{n} \cdot \vec{\mu}_1)(\vec{n} \cdot \vec{\mu}_2)]}{r^3} \qquad \ldots\ldots (14)$$

where $\vec{\mu}_1$ and $\vec{\mu}_2$ are the dipole moments in question, $\vec{n}$ is a unit vector lying along the projection of each dipole moment, and r is the separation between dipoles (considered as points). The result is that the energy of interaction is less than 10^{-5} eV, which is certainly small relative to the energy of the most loosely bound electron in the molecule. The interaction for S_8 will be even less than this because there is no permanent dipole in any bond. Secure in our application of degenerate perturbation theory, one forms the matrix elements $V_{k\ell}$ and solves the n x n secular determinant, which in the present instance is 8 x 8. The solution of this determinant is facilitated by symmetry factoring and ignoring interactions more distant than nearest neighbors.

Let us consider the off-diagonal elements, $V_{k\ell}$, $k \neq \ell$, since the energy levels of our system are determined by them. These elements have the form given by Equation 15:

$$\beta_{k\ell} = \langle \phi_k^+ \left| \sum_{k \neq \ell} V_{k\ell} \right| \phi_\ell^+ \rangle \qquad \ldots\ldots (15)$$

The integrals are formed with the excited state wave functions, even though the excitation occurs in a given bond, because we desire to lift the degeneracy between the states. Equation 15 can be reduced to a form more amenable to physical interpretation in the following manner: we recall that the interaction is between neighboring bonds, and that the bond functions are normalized. It then follows that

$$\begin{aligned} \beta_{k\ell} &= \langle \phi_k^+ \phi_\ell \prod_{m \neq k,\ell} \phi_m \Big| \sum_{k,\ell} V_{k\ell} \Big| \phi_k \phi_\ell^+ \prod_{n \neq k,\ell} \phi_n \rangle \\ &= \langle \phi_k^+ \phi_\ell \left| V_{k\ell} \right| \phi_k \phi_\ell^+ \rangle \langle \prod_{m \neq k,\ell} \phi_m \Big| \prod_{n \neq k,\ell} \phi_n \rangle \\ &= \langle \phi_k^+ \phi_\ell \left| V_{k\ell} \right| \phi_k \phi_\ell^+ \rangle \end{aligned} \qquad \ldots\ldots (16)$$

Because V contains $1/r_{k\ell}$ terms, where $r_{k\ell}$ is the $k\ell$ bond distance, a variable difficult to define and evaluate, a point-multipole expansion is substituted for the electrostatic interaction potential. There are no monopoles (charges) in our systems, since the bonds are electrically neutral, and because all higher interactions than dipole-dipole fall off so rapidly with separation they may be ignored, the

substitution reduces solely to dipole-dipole effects. Although the interaction between dipoles is a three-dimensional function, let us assume for simplicity that the effects occur in one dimension, along a line joining the dipoles. The interaction potential along the Z axis assumes the form:[21]

$$V_{k\ell} = -\frac{e^2 Z_k Z_\ell}{r^3} \qquad \ldots\ldots (17)$$

where r is the distance between dipoles k and ℓ, and the Z's refer to the separation of the electron from its vacancy in the exciton, in local coordinate systems. Before proceeding further with the analysis of Equation 16, one must consider whether more than one r distance exists in the molecule, a condition which would necessitate separate β's. By examination of scale models of N_4S_4 and S_8 it is found that, if the point dipole in the former is located slightly off-center toward the nitrogen atoms and in the latter midway between the bonded atoms, there is only one r value. All other interaction distances are greater. These conclusions are reasonable in the light of the relative electronegativities of the constituent atoms. Returning to Equation 16, we substitute Equation 17 for the value of $V_{k\ell}$ and obtain:

$$\beta_{k\ell} = \langle \phi_k^+ \phi_\ell \left| -\frac{e^2 Z_k Z_\ell}{r^3} \right| \phi_k \phi_\ell^+ \rangle$$

$$= -\,{}^1/_{r^3} \{ \langle \phi_k^+ \left| eZ_k \right| \phi_k \rangle \langle \phi_\ell \left| eZ_\ell \right| \phi_\ell^+ \rangle \}$$

$$\ldots\ldots (18)$$

From Equation 18 we are now able to interpret our β's. We recognize that each of the integrals is precisely the transition moment integral for the excitation of the individual bonds, k and ℓ. Hence, we may consider the β's as the interaction energy between neighboring excitations. $\beta_{k\ell}$ has two components, one depending on the geometry of the molecules and the other depending on the intensity of the absorption.

The correct zeroth order wave functions for the excited states in question may now be formed by a linear combination of the normalized basis wave functions of Equation 12.

$$\Psi_j = \sum_i c_{ji} \phi_i^+ \qquad \ldots\ldots (19)$$

Each of these wave functions corresponds to an eigenvalue λ_j of the secular equation. The square of each coefficient, $|c_{ji}|^2$, gives the probability that the excitation of state Ψ_j will be found in bond i, and the sign of c_{ji} may be associated with the relative phase of the transition moment induced in the bond by the exciting light. If an arrow is used as a designation for the induced transition moment with a direction governed by c_{ji}, one may determine the relative magnitude of the electrostatic energy of interaction between neighboring transition electric dipoles (excitations) by inspection. If the arrows are head to head, a high energy interaction ($\beta>o$) is indicated. If the arrows are head to tail, the interaction is a stabilizing one of low energy ($\beta<o$). The initial assignment is arbitrary and all

subsequent assignments must be consistent with the first. The overall transition is the vector sum of arrow alignment pairs, by considering the arrows as vectors. Before proceeding to the application of the model, an a priori estimate of the direction of the change in β between molecules will be made. Since each N-S bond would be expected to possess a small permanent dipole due to the polarization of the bonding electrons by the more electronegative nitrogen, and because the longer homonuclear S-S bond does not possess a permanent dipole moment and would adhere to a dipole-induced dipole force field decaying as r^{-6}, one would expect the energy splitting (β) in the former to be greater than for the latter molecule. Furthermore, a quantitative measure of this difference is given by the interaction energy of Equation 18: one compares the square of the transition moment integral divided by the cube of the dipole separation, in each instance.

C. Application of the Model

The Molecular Exciton Model just described will first be applied to N_4S_4 and then to S_8. In both instances, the form of the secular determinant is the same. As mentioned earlier, the treatment of this determinant is vastly simplified since all matrix elements other than those formed between neighboring bonds vanish. The result is a specialized instance of a cyclic determinant and is presented by Equation 20:

$$\begin{vmatrix} -X & 1 & 0 & 0 & 0 & 0 & 0 & 1 \\ 1 & -X & 1 & 0 & 0 & 0 & 0 & 0 \\ 0 & 1 & -X & 1 & 0 & 0 & 0 & 0 \\ 0 & 0 & 1 & -X & 1 & 0 & 0 & 0 \\ 0 & 0 & 0 & 1 & -X & -1 & 0 & 0 \\ 0 & 0 & 0 & 0 & 1 & -X & 1 & 0 \\ 0 & 0 & 0 & 0 & 0 & 1 & -X & 1 \\ 1 & 0 & 0 & 0 & 0 & 0 & 1 & -X \end{vmatrix} = 0 \qquad \ldots\ldots (20)$$

where $X = \lambda/_{\beta}$. The solution to this problem is given by Equation 21: [28]

$$X = -2 \cos (2\pi\ k/n) \qquad \ldots\ldots (21)$$

where k = 1,2,3, ... , n and n is the order of the determinant. The eight resulting roots could then be substituted into the secular equations which give rise to Equation 20, and together with the normalization condition, the correct zeroth order wave functions could be obtained.

In practice, group theoretic methods were employed to generate and match the correct linear combinations with the roots. Since we are dealing solely with coulomb interactions between bonds, the group of the Hamiltonian is the group of the equilibrium nuclear positions, which is $V_d \equiv D_{2d}$. It may be noted here that the value of β is unique only if the exciton is at one particular position, slightly to the nitrogen side of the bond midpoint, as previously mentioned. Except for locations near either atom, geometry shows that the

symmetry is only slightly broken at most positions along the bond. Experience has indicated that the use of a larger group where the symmetry breaking is small is usually warranted.[29] The character table of V_d and the classification of linear forms is given in Figure 12. The molecular configuration and the axial directions are shown in Figure 13. The direction of the bond moment is chosen from sulfur to nitrogen, from consideration of the relative electronegativities. The characters of the reducible representation of the basis set are:

	E	$2S_4(Z)$	$S_4^2 \equiv C_2'$	$2C_2$	$2\sigma_d$
Γ	8	0	0	0	0

This result is expected since no exciton lies on a symmetry element of N_4S_4. The basis belongs to the regular representation of V_d, and each irreducible representation in its direct sum appears a number of times equal to its dimensionality.[30] Therefore:

$$\Gamma = A_1 + A_2 + B_1 + B_2 + 2E$$

To generate a set of eigenfunctions with the correct transformation properties, the Van Vleck basis generation machine was used.[31] The projections of elements 1 and 2 (Figure 13) are:

	E	$2S_4(Z)$	$S_4^2 = C_2'$	$2C_2$	$2\sigma_d$
1	1	3,7	5	2,6	4,8
2	2	4,8	6	1,5	3,7

V_d	E	$2S_4(Z)$	$S_4^2 \equiv C_2''$	$2C_2$	$2\sigma_d$	
A_1	1	1	1	1	1	
A_2	1	1	1	-1	-1	
B_1	1	-1	1	1	-1	
B_2	1	-1	1	-1	1	Z
E	2	0	-2	0	0	(X,Y)

FIGURE 12: D_{2_d} Character Table

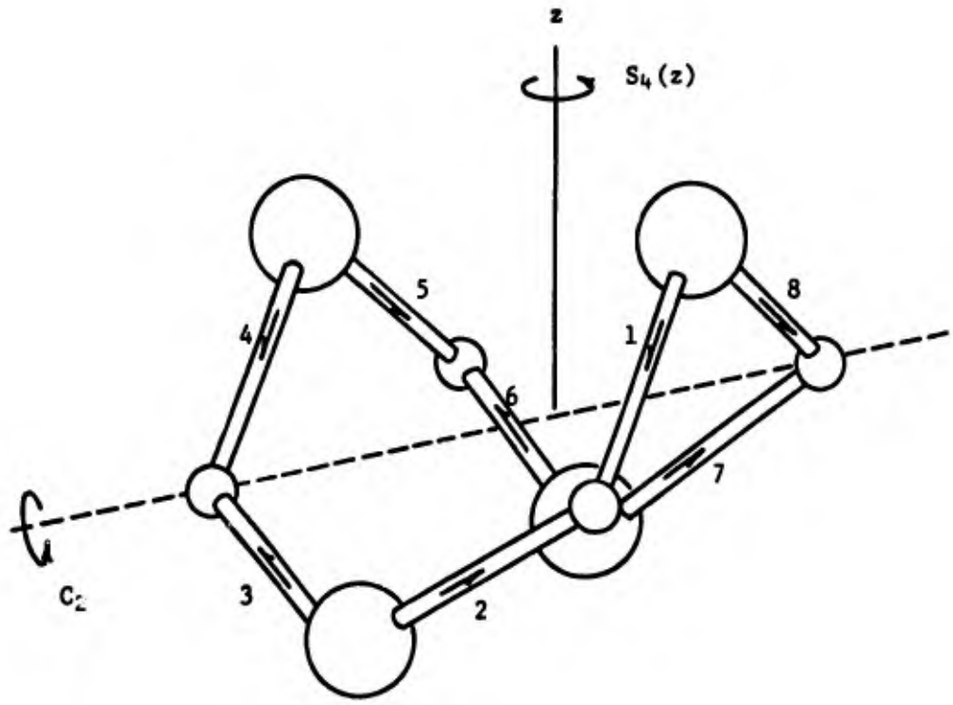

FIGURE 13: Shape of N_4S_4 Molecule

The nondegenerate eigenvectors may be written immediately:

$$\Psi_1\ (a_1) = \frac{1}{\sqrt{8}}\ (\Phi_1 + \Phi_2 + \Phi_3 + \Phi_4 + \Phi_5 + \Phi_6 + \Phi_7 + \Phi_8)$$

$$\Psi_2\ (a_2) = \frac{1}{\sqrt{8}}\ (\Phi_1 - \Phi_2 + \Phi_3 - \Phi_4 + \Phi_5 - \Phi_6 + \Phi_7 - \Phi_8)$$

$$\Psi_3\ (b_1) = \frac{1}{\sqrt{8}}\ (\Phi_1 + \Phi_2 - \Phi_3 - \Phi_4 + \Phi_5 + \Phi_6 - \Phi_7 - \Phi_8)$$

$$\Psi_4\ (b_2) = \frac{1}{\sqrt{8}}\ (\Phi_1 - \Phi_2 - \Phi_3 + \Phi_4 + \Phi_5 - \Phi_6 - \Phi_7 + \Phi_8)$$

Since all H_{ii} are 0 and $H_{ij} = \beta$ only when i and j are consecutive, one may compute the eigenvalues of these linear combinations by inspection:

$$\varepsilon_{\Psi_1(a_1)} = 2\beta$$

$$\varepsilon_{\Psi_2(a_2)} = -2\beta$$

$$\varepsilon_{\Psi_3(b_1)} = \varepsilon_{\Psi_4(b_2)} = 0$$

Although Ψ_3 and Ψ_4 are accidentally degenerate, this does not create an assignment problem.

In order to generate more than one set of doubly degenerate eigenvectors by the Van Vleck machine, one must take a properly oriented set of the basis. The choice of this set is neither obvious nor unique. The first sets chosen for projection are $\Phi_1 + \sqrt{2}\ \Phi_2 + \Phi_3$, a clockwise turn around the Z axis, and $\Phi_1 + \sqrt{2}\ \Phi_8 + \Phi_7$, a counter-clockwise turn. Application of the characters of V_d to the projections

of these sets yields the following pair of wave functions:

$$\Psi_{5,6}(e) = \frac{1}{\sqrt{8}} \left(\Phi_1 + \sqrt{2}\ \Phi_2 + \Phi_3 - \Phi_5 - \sqrt{2}\ \Phi_6 - \Phi_7\right)$$

and

$$\Psi'_{5,6}(e) = \frac{1}{\sqrt{8}} \left(\Phi_1 - \Phi_3 - \sqrt{2}\ \Phi_4 - \Phi_5 + \Phi_7 + \sqrt{2}\ \Phi_8\right)$$

The eigenvalues of this doubly degenerate set is $\sqrt{2}\beta$. The final pair of properly oriented bases are $\Phi_1 + \sqrt{2}\ \Phi_4 + \Phi_7$ in a clockwise direction, and $\Phi_1 + \sqrt{2}\ \Phi_6 + \Phi_3$ in a counterclockwise direction. Basis generation yields:

$$\Psi_{7,8}(e) = \frac{1}{\sqrt{8}} \left(\Phi_1 - \Phi_3 + \sqrt{2}\ \Phi_4 - \Phi_5 + \Phi_7 - \sqrt{2}\ \Phi_8\right)$$

$$\Psi'_{7,8}(e) = \frac{1}{\sqrt{8}} \left(\Phi_1 - \sqrt{2}\ \Phi_2 + \Phi_3 - \Phi_5 + \sqrt{2}\ \Phi_6 - \Phi_7\right)$$

This doubly degenerate set has an eigenvalue $-\sqrt{2}\beta$.

At this juncture the graphical treatment of N_4S_4 will be considered. N_4S_4 is described as a slightly distorted bisphenoid with the following angles: N-S-N (104°), N-N-N (90°), S-N-S (113°).[2] In accordance with the model, one assigns a vector direction to each bond with a magnitude given by the appropriate coefficient in the wave function. Then, by use of vector addition and subtraction, resultant vectors for that function are obtained which are correlated with the intensity of a given transition. This information is presented in Figure 14. The vector diagrams shown in this figure were obtained from the three-dimensional structure by assigning the proper direction to each bond and folding the top opposing N-S-N planes inward and the corresponding

Wave Function	Vector Projection ($\|\rightarrow\|=1$; $\|\Rightarrow\|=\sqrt{2}$)	Resultant
$\Psi_1(a_1)$		$\begin{pmatrix}0\\0\\0\end{pmatrix}$
$\Psi_2(a_2)$	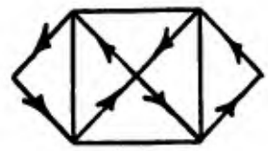	$\begin{pmatrix}0\\0\\0\end{pmatrix}$
$\Psi_3(b_1)$		$\begin{pmatrix}0\\0\\0\end{pmatrix}$
$\Psi_4(b_2)$	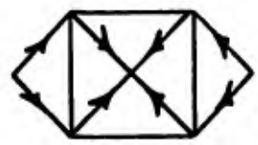	$\begin{pmatrix}0\\0\\4.9\end{pmatrix}$

FIGURE 14: N_4S_4 Vector Projections

Wave Function	Vector Projection ($\|\rightarrow\|=1$; $\|\Rightarrow\|=\sqrt{2}$)	Resultant
$\Psi_{5,6}(e)$		$\begin{pmatrix}3.8\\1.6\\0\end{pmatrix}$
$\Psi'_{5,6}(e)$	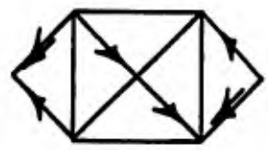	$\begin{pmatrix}1.6\\3.8\\0\end{pmatrix}$
$\Psi_{7,8}(e)$	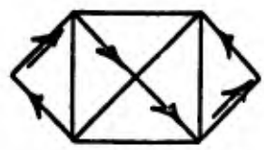	$\begin{pmatrix}1.6\\0.7\\0\end{pmatrix}$
$\Psi'_{7,8}(e)$	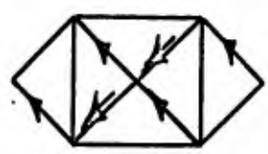	$\begin{pmatrix}0.7\\1.6\\0\end{pmatrix}$

FIGURE 14: N_4S_4 Vector Projections (cont.)

bottom opposing planes outward. We see that transitions to $\Psi_1(a_1)$, $\Psi_2(a_2)$, and $\Psi_3(b_1)$ are forbidden because the transition moment vectors add to zero. We further note that transition $\Psi_4(b_2)$ is polarized along the Z axis while transitions to both of the remaining doubly degenerate levels have components polarized along the X and Y directions. The relative intensity for one transition against another is found by taking the ratio of the squares of the respective products of the intensity factor and the normalization constant for the given wave function.

We are now in a position to analyze the spectrum of N_4S_4. Figure 15 presents the energy levels for the excited states in question, in terms of $\beta<o$. The ground state level appears in this figure, but is some unspecified distance below Ψ_1. This scheme predicts three allowed transitions from the ground singlet state. Transition to Ψ_1 is forbidden and hence would appear very weakly, if observed at all. If present, it should be found at relatively low frequency. Transition to Ψ_2 is also forbidden, and hence if such an absorption manifests itself at high frequencies, it should likewise be very weak. Transitions to $\Psi_{5,6}$, Ψ_4, and $\Psi_{7,8}$, are allowed and the relative intensities are 6:8:1. This may be shown by referring to Figure 14, and considering the intensities for the levels in question. The ratios are obtained as follows:

$$\Psi_{5,6} = \frac{(3.8)^2 + (1.6)^2}{8} = \frac{17}{8}$$

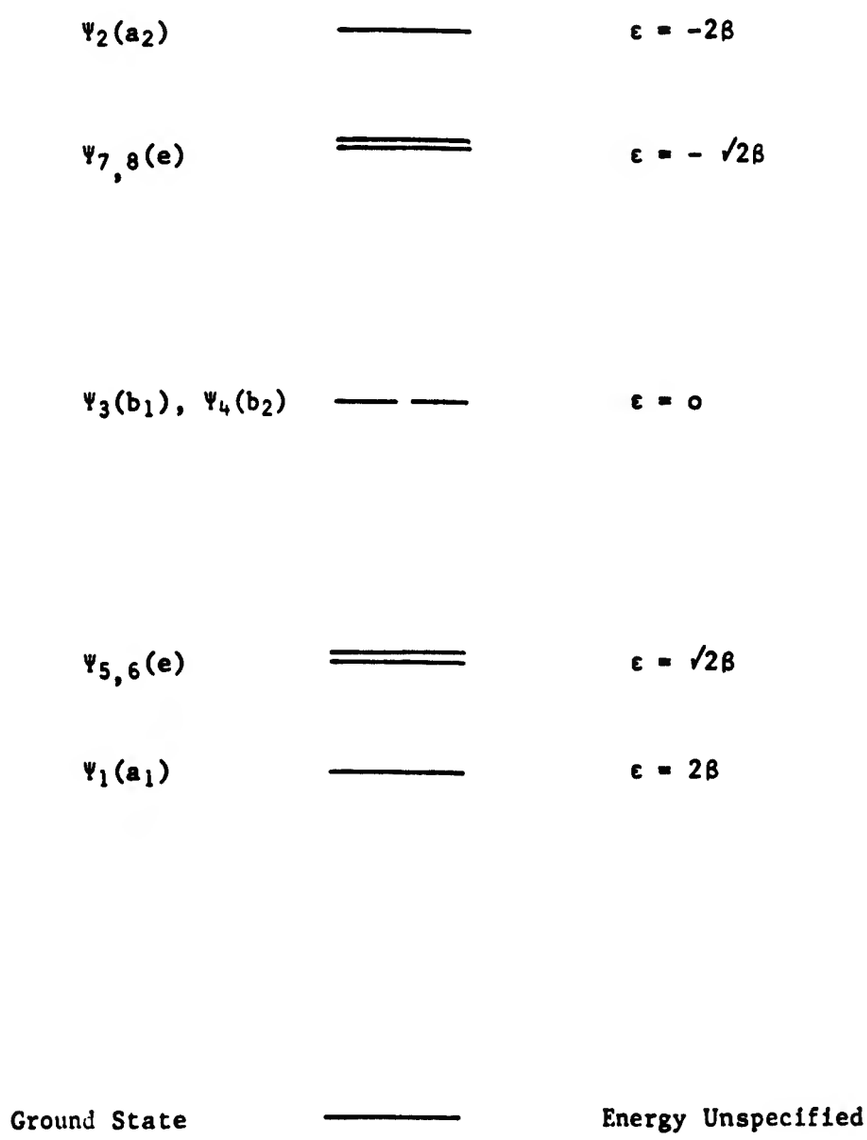

FIGURE 15: N_4S_4 Energy Level Diagram

$$\Psi_4 = \frac{(4.9)^2}{8} = \frac{24}{8}$$

$$\Psi_{7,8} = \frac{(1.6)^2 + (0.67)^2}{8} = \frac{3}{8}$$

$$\Psi_{5,6}:\Psi_4 :\Psi_{7,8} = 17:24:3 \sim 6:8:1$$

We further note that the calculated transition moment vectors are in agreement with the group theoretical prediction. Since the ground state is of representation a_1, the representations of linear forms show that transitions to b_2 levels are Z polarized and those to e levels are (X,Y) polarized. The vector diagram confirms this. A comment made earlier that the accidental degeneracy of $\Psi_3(b_1)$ and $\Psi_4(b_2)$ would pose no assignment problem can now readily be justified. Only the b_2 transition is allowed. If we ascribe the observed low frequency transition at 27000 cm^{-1} to the first forbidden transition and the transition at 39000 cm^{-1} to the second in our scheme we have in effect assigned a value to β; i.e. the energy difference between the first two observed transitions is 12000 cm^{-1}, which is thus equivalent to 0.6β. Our unit of energy becomes β=20,000 cm^{-1} On the basis of the first two bands of the N_4S_4 spectrum, one would predict a third absorption maximum at 67000 cm^{-1} and a fourth at 95000 cm^{-1} with relative intensities for the second, third, and fourth bands in the ratio of 6:8:1. A fifth weak absorption (forbidden) is predicted as possible at 107000 cm^{-1}. Unfortunately, the data did not extend to high enough frequencies to allow corroboration of the fourth

and fifth transitions, but a strong band was found at 62000 cm^{-1}. (At this point, and for the remainder of the N_4S_4 discussion, it would be well to have the data of Table III in mind). Furthermore, since the quantitative measure of absorption intensity is given by the oscillator strength, which is the integrated absorption coefficient over the frequency range of the absorption, we may use a comparison of the molar extinction coefficients* for each band as a qualitative measure of the relative intensities. Taking into account the relative broadness of the two bands, a rough measure of the band half-width, we found that the intensity ratio is 1:1.2, in very good agreement with the prediction. Hence, this simple model we have constructed is consistent with the available experimental data. The band predicted at 95000 cm^{-1} is just within the lithium fluoride transmission limit, and could be detected if such a windowed cell were used.

Perhaps the most edifying aspect of this treatment of N_4S_4 is the apparent unimportance of π delocalization in contributing to the electronic spectrum. Implicit in the fact of a single nitrogen-sulfur distance in N_4S_4 is that all such bonds in the molecule are equivalent. Furthermore, the bond distance of 1.63Å is intermediate between a "single bond" length of 1.74Å, obtained by applying the

---

*The molar extinction coefficients, ε, were calculated using the relationship: $\varepsilon = \frac{1}{c\ell} \log I_o/I$, where c is molar concentration, ℓ is the path length in centimeters, I_o and I are incident and transmitted light, respectively.

Pauling radii to nitrogen and sulfur, and a "double bond" length of 1.54Å. Table IV lists bond lengths and angles reported for several molecules containing N-S bonds. These observations have caused investigators to speculate that delocalization of electronic charge in $p\pi - d\pi$ orbitals may be significant. As mentioned, the present treatment discounts this, a conclusion also reached on the basis of an Hückel Molecular Orbital calculation.[6]

Before analyzing the S_8 spectrum, the work of Braterman[8] should be considered in some detail. A vapor phase spectrum of N_4S_4 was photographed, but other than the band at 39000 cm^{-1}, no additional information was obtained. However, runs in different solvents at various temperatures were made and the observed maxima tabulated. A clear curve of the data was not presented, and it was difficult to determine, independent of his tabulated results, just where and how intensely the maxima did appear. In the absence of such a separate check, it can only be concluded that the spectrum reported by Braterman and that presented by the author are vastly different. One might expect frequency shifts to occur in solvent, but in the region of comparison, 24000 cm^{-1} to 50,000 cm^{-1}, two shoulders were detected not found in the present investigation. In fact, a maximum was reported in a region (49000 cm^{-1}) where a minimum was observed by the author. In addition, the extinction coefficient calculated by Braterman for the 39000 cm^{-1} band was a factor of two greater than that found in this present study. Without more information than was presented, further comment on the spectral comparison is meaningless.

TABLE IV

Distances and Angles in NS Compounds

Molecule	S-N length (Å)	N-S-N angle	Reference
KO_3SNH_2	1.57	106-107	(32)
$KO_3SN_2O_2$	1.63	106-108	(33)
$K(O_3S)_2 \cdot NH$	1.66	103-107	(34)
$O_2S(NH_2)_2$	1.60	106-107	(35)
$S_4N_4H_4$	1.67	108-109	(36)
O_3SNH_3	1.76	103	(37)
N_4S_4	1.63	104	(38)

Some slight detail on the spectrum of $S_4(NH)_4$ was also presented, but it was insufficient for an analysis.

The second system to be treated by this work is octatomic sulfur. This molecule possesses D_{4d} symmetry and has a staggered eight-membered ring structure, illustrated in Figure 16, with bond angles of 105° and dihedral angle of 102°.[39] As in the case of N_4S_4 we may find the eigenvectors of the cyclic determinant by a basis function generation. The character table for D_{4d} appears in Figure 17. The characters of the reducible representation of the basis in D_{4d} are:

	E	$2S_8$	$2C_4$	$2S_8^3$	C_2	$4C'_2$	$4\sigma_d$
Γ	8	0	0	0	0	-2	0

This is decomposed as

$$\Gamma = A_2 + B_2 + E_1 + E_2 + E_3$$

From the geometry of S_8, we can tabulate the projections of 1 and 2 under the group elements.

	E	$2S_8$	$2C_4$	$2S_8^3$	C_2	$4C_2^1$	$4\sigma_d$
1	1	2	3	4	5	-1	-2
		8	7	6		-3	-4
						-5	-6
						-7	-8
2	2	1	4	5	6	-2	-1
		3	8	7		-4	-3
						-6	-5
						-8	-7

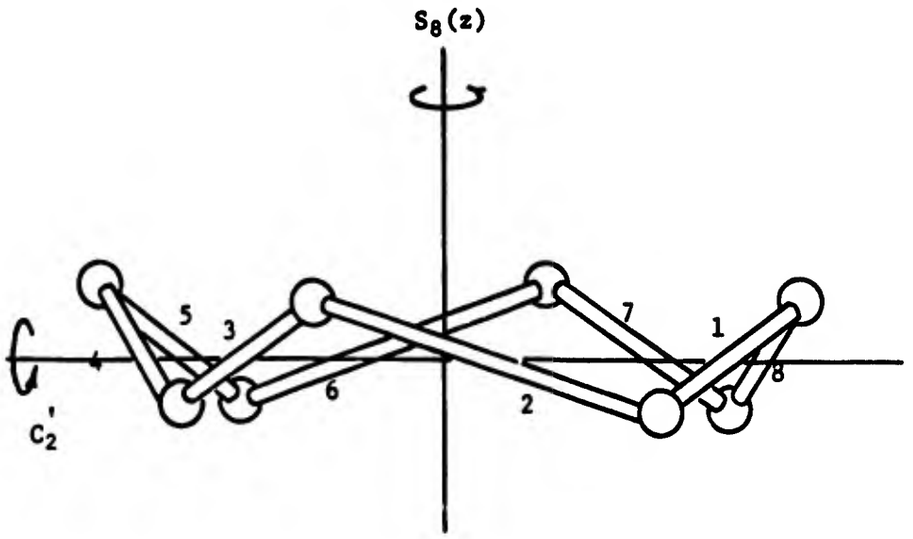

FIGURE 16: Shape of S_8 Molecule

D_{4d}	E	$2S_8$	$2C_4$	$2S_8^3$	C_2	$4C'_2$	$4\sigma_d$	
A_1	1	1	1	1	1	1	1	
A_2	1	1	1	1	1	-1	-1	
B_1	1	-1	1	-1	1	1	-1	
B_2	1	-1	1	-1	1	-1	1	z
E_1	2	$\sqrt{2}$	0	$-\sqrt{2}$	-2	0	0	(x,y)
E_2	2	0	-2	0	2	0	0	
E_3	2	$-\sqrt{2}$	0	$\sqrt{2}$	-2	0	0	

FIGURE 17: D_{4_d} Character Table

The product of the projection and the character under that class in a given representation then provides the wave function.

$$\Psi_1(a_2) = \frac{1}{\sqrt{8}} \ (\phi_1 + \phi_2 + \phi_3 + \phi_4 + \phi_5 + \phi_6 + \phi_7 + \phi_8)$$

its eigenvalue is 2β. The wave function with eigenvalue -2β is given as:

$$\Psi_2(b_2) = \frac{1}{\sqrt{8}} \ (\phi_1 - \phi_2 + \phi_3 - \phi_4 + \phi_5 - \phi_6 + \phi_7 - \phi_8)$$

The doubly degenerate sets are obtained by Schmidt orthogonalization of the projection of adjacent pairs. The wave function pair with an eigenvalue of $\sqrt{2}\beta$ is:

$$\Psi_{3,4}(e_1) = \frac{1}{(16+8\sqrt{2})^{1/2}} [(1+\sqrt{2})\phi_1+(1+\sqrt{2})\phi_2+\phi_3-\phi_4-(1+\sqrt{2})\phi_5-(1+\sqrt{2})\phi_6-\phi_7+\phi_8]$$

and

$$\Psi'_{3,4}(e_1) = \frac{1}{(16-8\sqrt{2})^{1/2}} [(1-\sqrt{2})\phi_1-(1-\sqrt{2})\phi_2-\phi_3-\phi_4-(1-\sqrt{2})\phi_5+(1-\sqrt{2})\phi_6+\phi_7+\phi_8]$$

The degenerate set with eigenvalue 0β is:

$$\Psi_{5,6}(e_2) = \frac{1}{\sqrt{8}} \ (\phi_1 + \phi_2 - \phi_3 - \phi_4 + \phi_5 + \phi_6 - \phi_7 - \phi_8)$$

and

$$\Psi'_{5,6}(e_2) = \frac{1}{\sqrt{8}} \ (\phi_1 - \phi_2 - \phi_3 + \phi_4 + \phi_5 - \phi_6 - \phi_7 + \phi_8)$$

The set with eigenvalue of $-\sqrt{2}\beta$ is:

$$\Psi_{7,8}(e_3) = \frac{1}{(16-8\sqrt{2})^{1/2}} [(\sqrt{2}-1)\Phi_1+(\sqrt{2}-1)\Phi_2-\Phi_3+\Phi_4-(\sqrt{2}-1)\Phi_5-(\sqrt{2}-1)\Phi_6+\Phi_7-\Phi_8]$$

and

$$\Psi'_{7,8}(e_3) = \frac{1}{(16+8\sqrt{2})^{1/2}} [(\sqrt{2}+1)\Phi_1-(\sqrt{2}+1)\Phi_2+\Phi_3+\Phi_4-(\sqrt{2}+1)\Phi_5+(\sqrt{2}+1)\Phi_6-\Phi_7-\Phi_8]$$

In drawing the vector components of the wave functions, a different and more convenient projection may be employed than was used for N_4S_4. The excitons lie on the vertices of a regular octagon. To ascertain components perpendicular to the plane of the projection, the signs must be considered. In all such diagrams, Φ_1 is at "approximately 3:30" and the enumeration is clockwise, but sign alternation must be used because of the direction from which the point dipole enters the projection. Representative calculations are shown for the less obvious states of $\Psi_{3,4}(e_1)$ and $\Psi_{7,8}(e_3)$. The vector projections and the relative magnitudes of the resultant appear in Figure 18. The vector components conform to our expectations based on the irreducible representations to which the linear forms belong. $\Psi_2(b_2)$ is seen to be Z polarized, and $\Psi_{3,4}(e_1)$ and $\Psi'_{3,4}(e_1)$ are (X,Y) polarized. According to the character table, Z belongs to B_2 and (X,Y) to E_1.

An energy level diagram for this system appears in Figure 19. It predicts two allowed transitions with a spacing of $(2+\sqrt{2})\beta$, and the remaining transitions are forbidden. If one chooses the transition at 46000 cm^{-1} to be $\Psi_{3,4}(e_1)$ and the peak at 61800 cm^{-1} to be $\Psi_2(b_2)$, the value of β can be fixed at 4650 cm^{-1}. The model predicts a forbidden transition at $(2-\sqrt{2})\beta$, from ground to the forbidden $\Psi_{7,8}(e_3)$ state, to occur at 59000 cm^{-1}. There is a

Wave Function	Vector Projection	Resultant
$\Psi_1(a_2)$	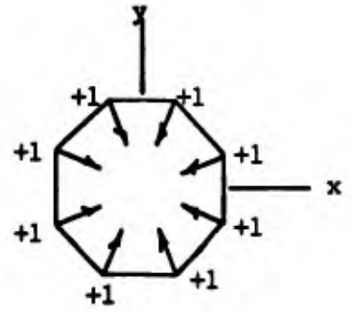	$\begin{pmatrix}0\\0\\0\end{pmatrix}$
$\Psi_2(b_2)$	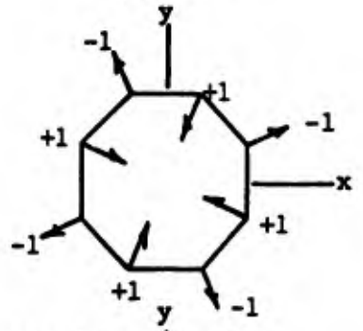	$\begin{pmatrix}0\\0\\8\end{pmatrix}$
$\Psi_{3,4}(e_1)$	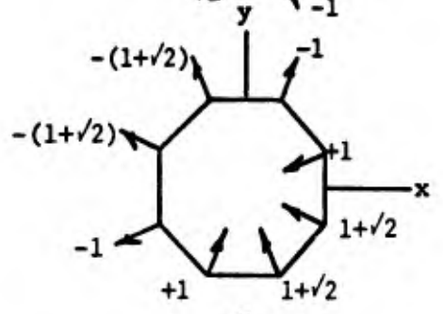	$\begin{pmatrix}0\\8\\0\end{pmatrix}$
$\Psi'_{3,4}(e_1)$	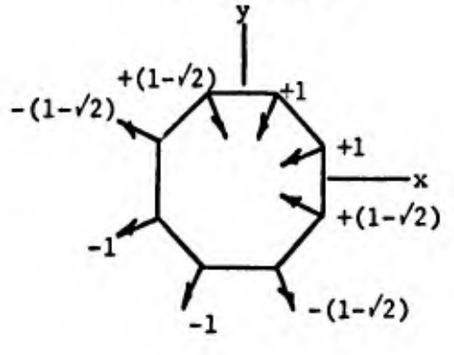	$\begin{pmatrix}8\\0\\0\end{pmatrix}$

FIGURE 18: S_8 Vector Projections

Wave Function	Vector Projection	Resultant
$\Psi_{5,6}(e_2)$	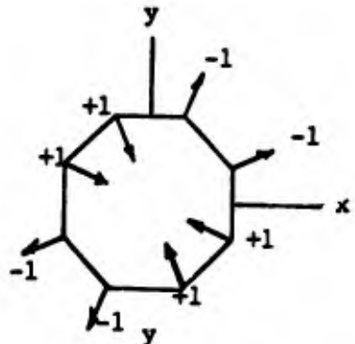	$\begin{pmatrix}0\\0\\0\end{pmatrix}$
$\Psi'_{5,6}(e_2)$	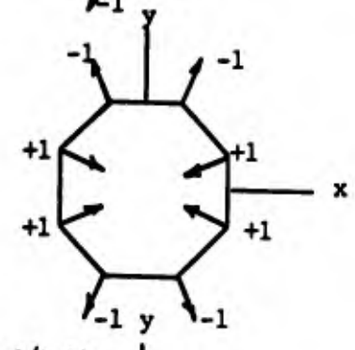	$\begin{pmatrix}0\\0\\0\end{pmatrix}$
$\Psi_{7,8}(e_3)$	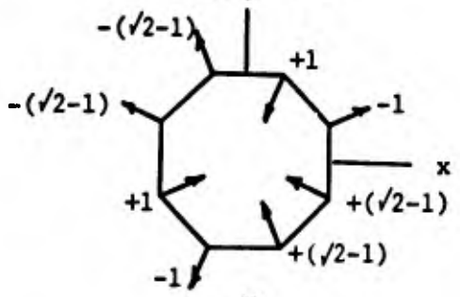	$\begin{pmatrix}0\\0\\0\end{pmatrix}$
$\Psi'_{7,8}(e_3)$	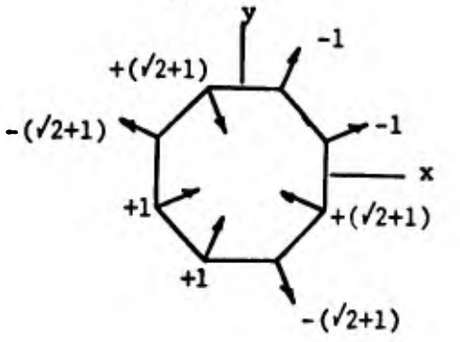	$\begin{pmatrix}0\\0\\0\end{pmatrix}$

FIGURE 18: S_8 Vector Projections (cont.)

Sample Vector Projection Resultant Calculations

$\Psi'_{3,4}(e_1)$: The x component is determined by moving clockwise around the octagon and resolving the vectors:

$$x = 2(1+\sqrt{2}) \cos \frac{\pi}{8} + 2(1+\sqrt{2}) \cos \frac{3\pi}{8} + 2 \cos \frac{\pi}{8} - 2 \cos \frac{3\pi}{8} = 8$$

The y and z components are 0 by an analogous calculation.

$\Psi'_{7,8}(e_3)$: The x component is again determined as above:

$$x = 2 \cos \frac{\pi}{8} + 2 \cos \frac{3\pi}{8} + 2(\sqrt{2}+1) \cos \frac{3\pi}{8} - 2(\sqrt{2}+1) \cos \frac{\pi}{8} = 0$$

Similarly for the y and z components.

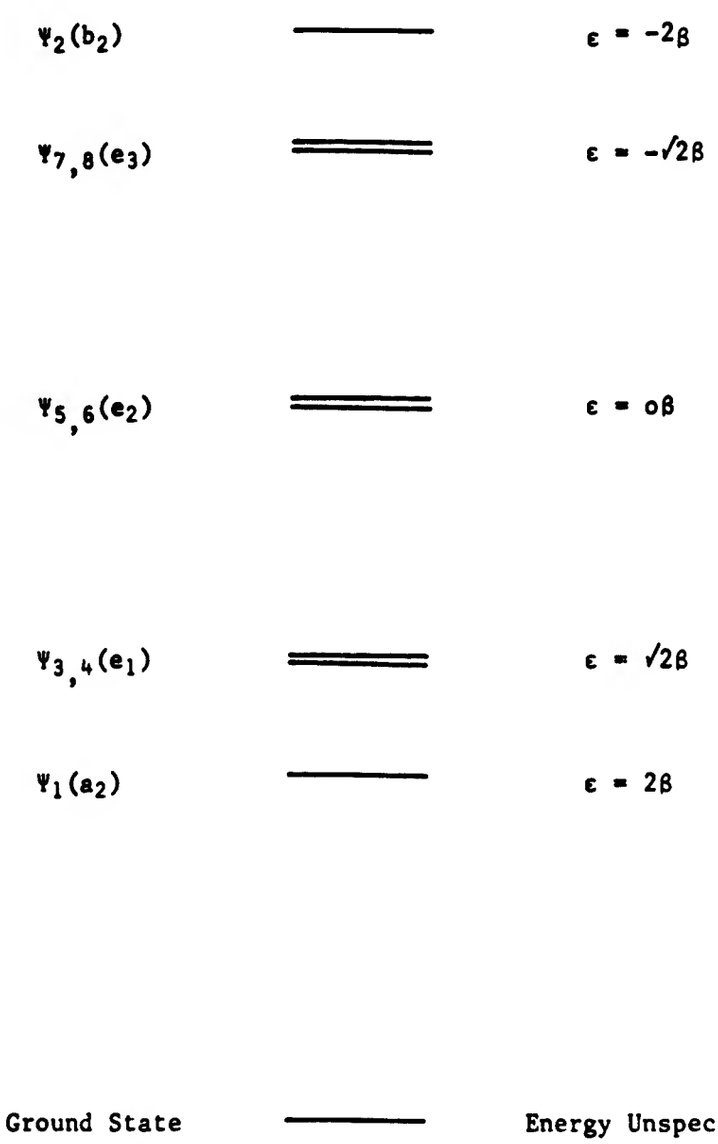

FIGURE 19: S_8 Energy Level Diagram

shoulder at 60200 cm^{-1} which could be this transition. A forbidden transition, to $\Psi_1(a_2)$, is predicted at 43200 cm^{-1}. There is a weak suggestion of a maximum at 39200 cm^{-1}. This association is somewhat tenuous. Finally, the model predicts a level at 52500 cm^{-1}, corresponding to the forbidden ground to $\Psi_{5,6}(e_2)$ state. There is a peak at 53500 cm^{-1}.

The final prediction of the exciton model is that the allowed transitions are of equal intensity. The extinction coefficients are clearly not equal, but the short wavelength band is relatively narrow whereas the transition in the ordinary ultraviolet is very broad so that the oscillator strengths of these transitions may indeed be comparable. The 53500 cm^{-1} transition, lying near the probable intersection of the two bands may well draw most of its intensity from the two overlapping tails and in truth be very weak.

One might reasonably ask two related questions at this point: is the magnitude of the change in β between N_4S_4 and S_8 expected, given the similarity between the two substances; and is the direction of the change correct? The latter question has already been answered when the splitting for the heteronuclear system was predicted to be larger than that for the homonuclear molecule. The answer to the first question is found with more difficulty. Without actually evaluating the transition moment integrals, and without having a series of homologous systems to study, the author would answer this question by again referring to the answer to question two. The interaction between induced dipole moments is far less than between

permanent dipoles, going in the former case as $1/r^6$ as contrasted with $1/r^3$ for the latter. Hence, the author concludes that, in spite of the apparent geometrical similarity between the two molecules under investigation, the large magnitude of the difference in the β's is not surprising.

In order to fairly evaluate the worth of the molecular exciton model in the light of its application to the spectra of N_4S_4 and S_8, it is important to realize the essence of this model lies in the localization of the optical electrons. When excitation delocalization is accompanied by extensive charge delocalization, electron overlap and exchange will be present, and the model is less physically reasonable. Even so, with exchange and overlap present, a large part of the total energy of interaction may be deduced if the localized electrons make a significant contribution.

D. Future Exploration

In the present instance, there are many desiderata; obviously necessary is more quantitative data as well as spectra to higher frequencies. In addition, the literature fortunately provides recipes for a series of nitrogen-sulfur binary compounds and their spectra should be examined in the light of the molecular exciton model. Although the bonding in these compounds obviously differs from that in N_4S_4, the extent to which this model has application may be elucidated by a spectral comparison. For example, one would not expect N_2S_4 to have solely N-S bonds. N_2S_2 is believed to possess a planar structure, and $p\pi$-$d\pi$ bonding is quite probable. It is already

known (Figure 10) that the 2500Å band of this material is structured. However, a vibronic analysis could supplement the electronic transition analysis afforded by the exciton approach. The appearance of molecular Rydberg transitions of non-bonded electrons would afford an opportunity to determine the contribution of bonding electrons to the remaining absorption in terms of the exciton model.

In addition to the binary N-S systems available, other ring structures of the N_4S_4 parent are known. A preliminary spectrum of $S_4(NH)_4$, in the ordinary ultraviolet, has been presented by Braterman,[6] as mentioned earlier. An obvious extension to the vacuum ultraviolet should be made. The reaction of N_4S_4 with chlorine, in carbon disulfide, yields a yellow crystalline tetrachloride, $N_4S_4Cl_4$; with bromine, the compounds $N_4S_4Br_4$ (bronze) and $N_4S_4Br_6$ (red) have been obtained.[40] The treatment of N_4S_4 with cold sulfur monochloride gives black, crystalline $N_4S_6Cl_2$; with acetyl chloride, or sulfur monochloride at elevated temperatures, one obtains yellow N_3S_4Cl.[41,42] Not to lose sight of materials generated in this work, the unknown material, whose spectrum is presented in Figure 11, should be investigated, as mentioned several times earlier.

In closing, the author wishes to remind one that the suggested spectroscopic investigations need not be restricted to interpretation by the molecular exciton model. As stated previously, it was adopted for this work because it was believed to be possibly germane to the systems involved. Other theories, of course, remain quite respectable, and in any given situation may well prove much superior to the model used here.

The Absorption Spectrum of S_2N_2 in the Ordinary Ultraviolet

The spectrum of N_2S_2 vapor was measured on the Jarrell-Ash 500 mm spectrometer described in Figure 2. It was taken in a 42 cm cell with Supersil windows filled with gas whose pressure ranged from 50 microns Hg to 210 microns. This latter value is its room temperature vapor pressure. The gas was stored on an external vacuum rack and could be pumped in and out through a vacuum passthrough. During a single record, the gas was pumped out and readmitted periodically as a check against decomposition and polymerization. The spectrum recorded through this region appears on Figure 10.

The band is too complex to assign as a progression of one vibration. Wave number separation of maxima range from 233 to 480 cm^{-1} in that portion of the spectrum where the maxima and their frequencies are ambiguous.

One can invoke symmetry arguments to explain the observed behavior. The group of the Schrödinger Equation of N_4S_4 is V_h if one assumes a square planar configuration, and C_{2v} if one assumes a puckered ring structure. Inasmuch as both V_h and C_{2v} are abelian and N_2S_2 has an even number of electrons, the ground state is necessarily A_{1g} (or A_1). For the planar structure the highest filled and the lowest unfilled orbitals must be $g \longleftrightarrow \mu$ for allowedness since displacement in V_h is always μ. The magnitude of the oscillator strength certainly indicates that this is the case. Thus, the vibrations that combine with the transition would be even. The resolution of vibration in V_h is

$$\Gamma = 2ag + b_{1g} + b_{1\mu} + b_{2\mu} + b_{3\mu}$$

and the symmetry coordinates are diagrammatically represented in Figure 20.

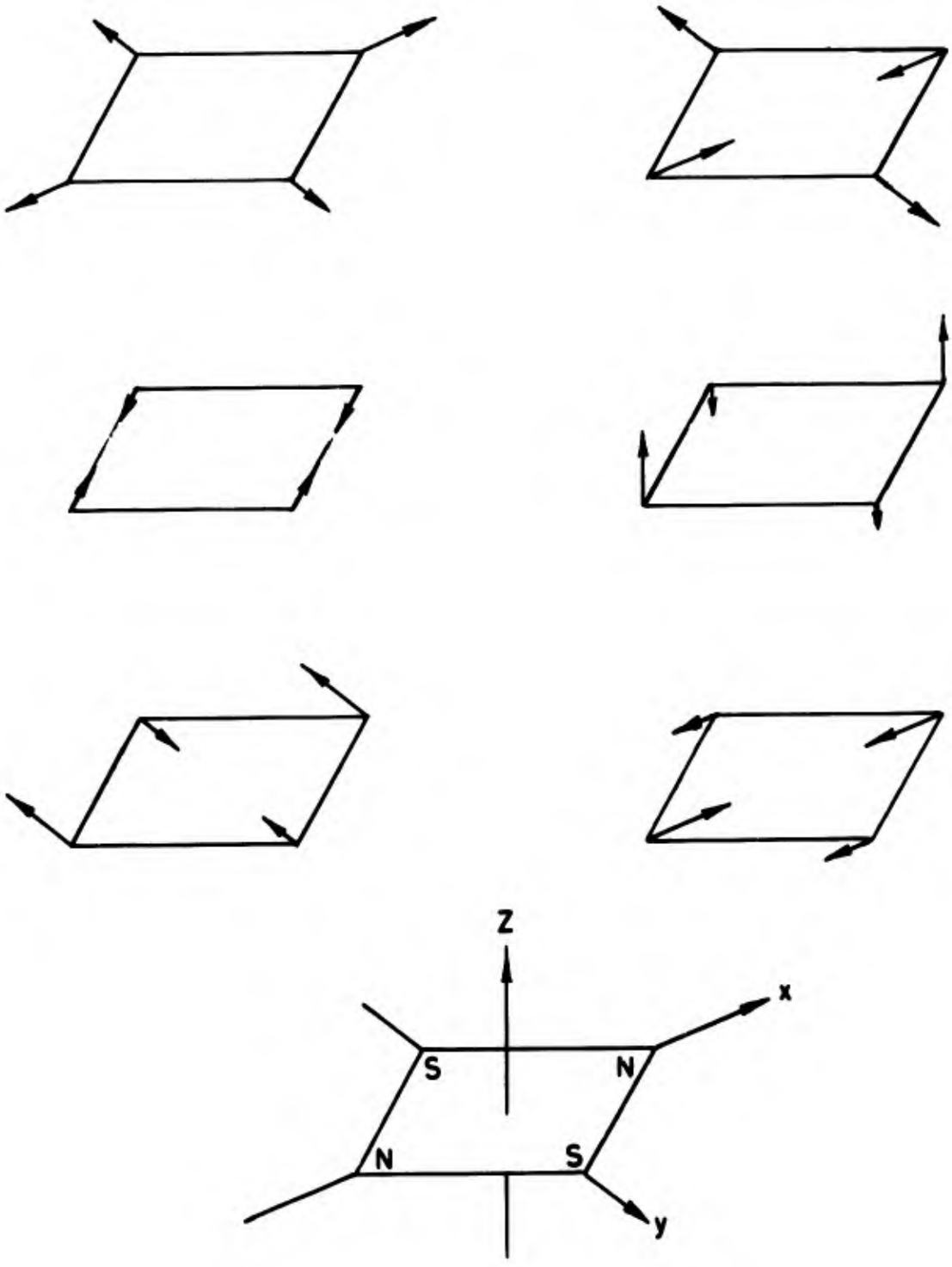

FIGURE 20: Symmetry Coordinates of N_2S_2

The correlation to C_{2v} is shown in Figure 21. For a postulated planar configuration therefore, either the two a_{1g} or the b_{1g} vibrations combine with the electronic transition. Since the spectrum appears to be based on a progression of more than one vibration, the choice of the two a_{1g}, the completely symmetric vibrations seem more likely. Both a_g vibrations would, of course be forbidden in the absorption spectrum of the ground state.

Designating the two frequencies upon which progressions may be built as ν_1^* and ν_2^*, it is found that the best fit to the data is obtained when ν_{oo} is taken as 37705 cm^{-1} and ν_1^* and ν_2^* are 766 cm^{-1} and 525 cm^{-1}, respectively. The assignments appear on Table V.

Other combinations tried gave comparable wave length agreement, but were seriously inconsistant in relative intensity or provided missing frequencies. In order to qualify as "consistant" in intensity, the peak heights must vary smoothly as the vibrational quantum number increases and peak at some particular value. The intensity curves are shown in Figure 22.

Inasmuch as the vibration peaks were not separated by a return to the base line, but rather that the peak-valley separation represented only about 20% of the optical density, two presentations are included. In one optical density is plotted against v as they appear on the spectra; in the other, an envelope was drawn which most smoothly connected the valleys. This is an attempt to subtract out the continuum. Where peaks overlapped, at 42,328 cm^{-1}, 39,994 cm^{-1}, and 39,227 cm^{-1}, the total optical density was proportioned in a way to make the envelopes most regular.

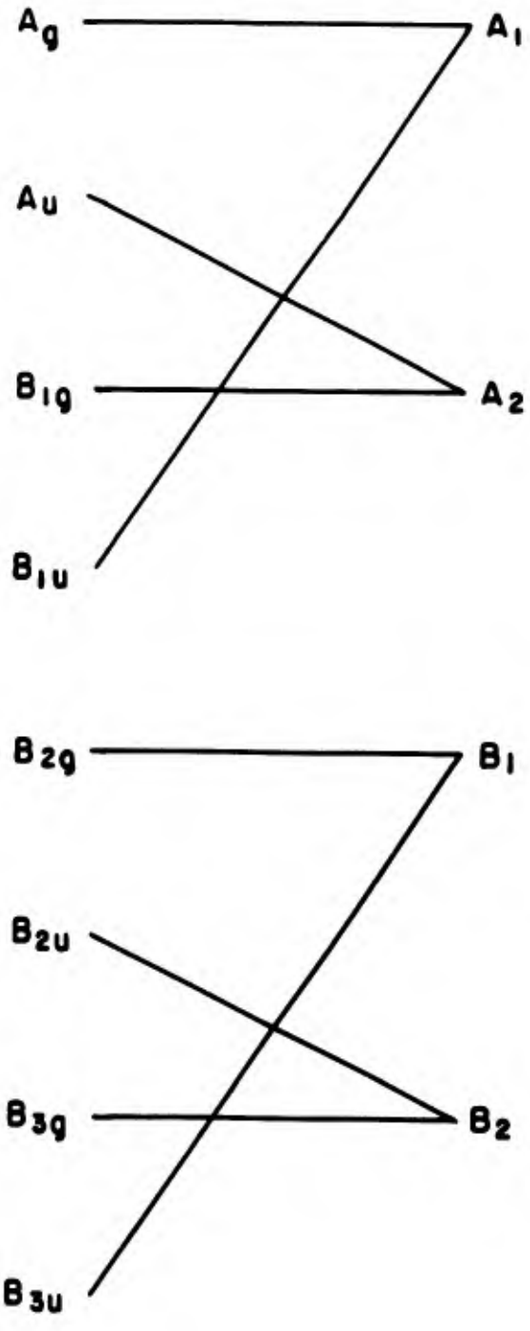

FIGURE 21: Correlation between V_h and C_{2v}

TABLE V

Frequency Assignment

Band Center (in cm^{-1})	Assignment	Calculated (in cm^{-1})	Discrepancy (calc-obs)	Discrepancy ÷ V
43,437	$\nu_{oo} + 11\nu_2^*$	43,480	+ 43	+ 4
42,875	$\nu_{oo} + 10\nu_2^*$	42,955	+ 80	+ 8
42,328	$\nu_{oo} + 6\nu_1^*$	42,301	- 27	- 5
	$\nu_{oo} + 9\nu_2^*$	42,420	+ 92	+ 10
41,892	$\nu_{oo} + 8\nu_2^*$	41,905	+ 13	+ 2
41,513	$\nu_{oo} + 5\nu_1^*$	41,535	+ 22	+ 4
41, 339	$\nu_{oo} + 7\nu_2^*$	41,380	+ 41	+ 6
40,857	$\nu_{oo} + 6\nu_2^*$	40,869	+ 12	+ 2
40,716	$\nu_{oo} + 4\nu_1^*$	40,769	+ 53	+ 13
40,282	$\nu_{oo} + 5\nu_2^*$	40,330	+ 48	+ 10
	$\nu_{oo} + 2\nu_2^* + 2\ _1^*$	40,292	+ 10	+ 3

TABLE V (continued)

Band Center (in cm^{-1})	Assignment	Calculated (in cm^{-1})	Discrepancy (calc-obs)	Discrepancy ÷ V
	$\nu_{oo} + 3\nu_2^* + \nu_1^*$	40,045	+ 51	+ 13
39,994	$\nu_{oo} + 3\nu_1^*$	40,005	+ 11	+ 4
	$\nu_{oo} + 4\nu_2^*$	39,905	- 89	- 22
39,510	$\nu_{oo} + 2\nu_2^* + \nu_1^*$	35,522	+ 12	+ 4
39,277	$\nu_{oo} + 3\nu_2^*$	39,280	+ 3	+ 1
	$\nu_{oo} + 2\nu_1^*$	39,237	- 40	- 20
38,797	$\nu_{oo} + 2\nu_2^*$	38,755	- 42	- 21
38,521	$\nu_{oo} + \nu_1^*$	38,471	- 50	- 50
38,226	$\nu_{oo} + \nu_2^*$	38,230	+ 4	+ 4
37,807	$\nu_{oo} + \nu_1^* - \nu_2$	37,835	+ 28	+ 14
37,488	$\nu_{oo} + \nu_2^* - \nu_1$	37,405	- 83	- 42
37,175	$\nu_{oo} - \nu_2$	37,180	+ 5	+ 5

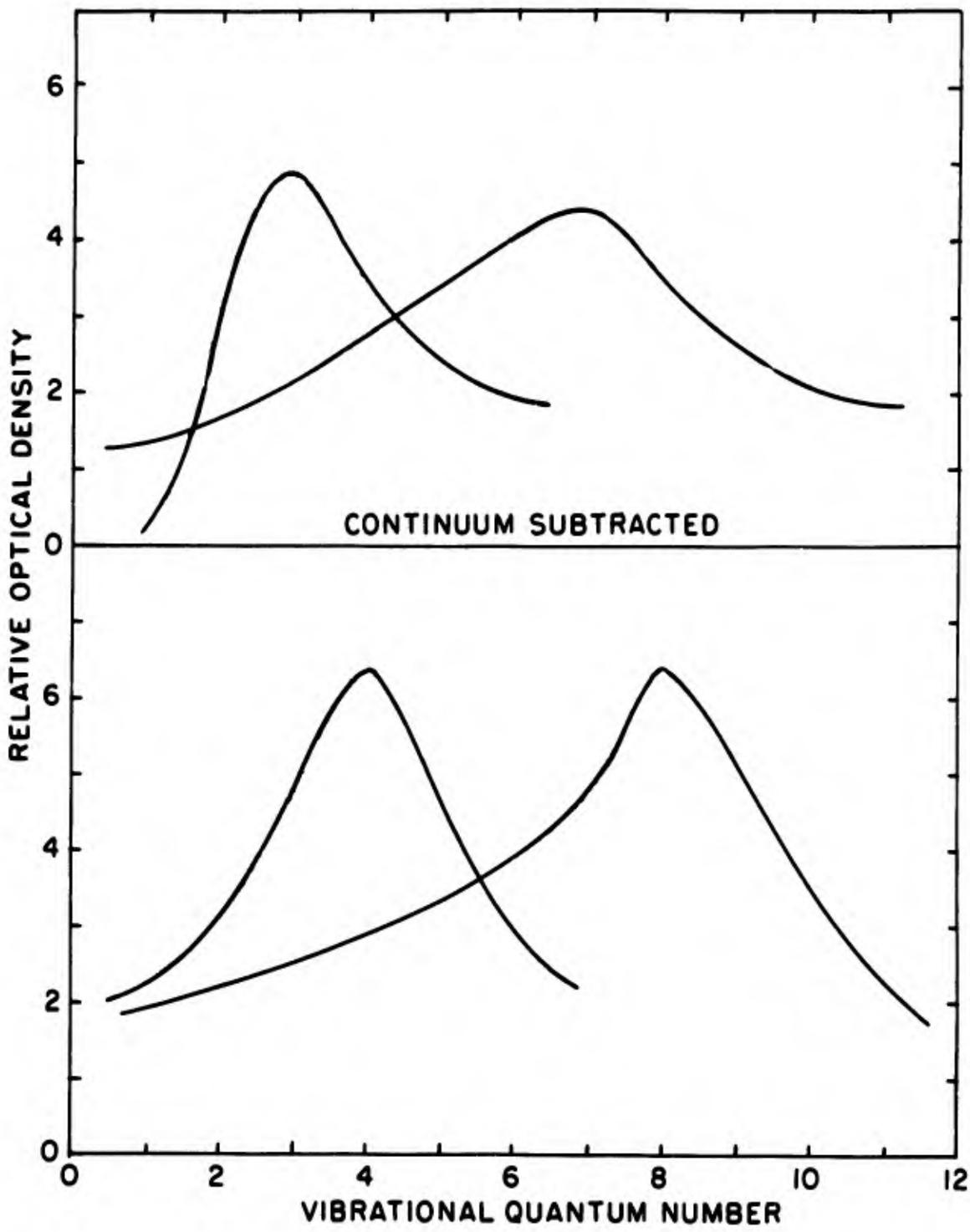

FIGURE 22: Relative Optical Density vs. Vibrational Quantum Number

Having generated the numbers 766 cm^{-1} and 525 cm^{-1} by a best fit to the observed spectrum, one can compare these to vibrational frequencies in the ground state for comparison.

The a_{1g} frequencies are not infrared active but may be computed, in part from those frequencies which are active and from the infrared spectrum of N_4S_4. A normal coordinate calculation was undertaken based on the assignment of 787 cm^{-1} as ν_6 ($b_{3\mu}$) and 477 cm^{-1} as ν_5 ($b_{2\mu}$). This latter assignment is in conflict with that of Warn and Chapman[43] who assign the 477 cm^{-1} band as ν_4 ($b_{1\mu}$).

The most naive force constant calculation places the inactive ν_2 (a_{1g}) at 613 cm^{-1}. This computation was carried out assuming a simple bending force constant for both SNS and NSN bends and no interaction. It likewise assumed no mixing between ν_1 (a_g) and ν_2 (a_g). There are no bands between 750 and 500 cm^{-1} in either the gas phase or in solution, but in the infrared spectrum of a sublimed polycrystalline film at 70°K, a band of strong intensity appears at 670 cm^{-1}. In a Nujol Mull at room temperature, twin peaks appear at 654 and 649 cm^{-1}. The allowedness of the forbidden ν_2 (a_g) could easily be explained on the basis of site symmetry perturbation. This argument would be more convincing if ν_1 (a_{1g}) was also made allowed but such is unfortunately not the case. Warn and Chapman assign the 474 cm^{-1} band as the out of plane mode and the 650 cm^{-1} band as ν_6 ($b_{3\mu}$).

The estimation of the stretching frequencies ν_1 (a_{1g}) and ν_3 (b_{1g}) were made based on a single N-S stretching force constant which was that taken from N_4S_4, namely 2.82 m d/Å. Further, one assumes no mixing in

a_{1g} and no interaction. This oversimplified calculation yields the result ν_1 (a_{1g}) = 810 cm^{-1} and ν_3 (b_{1g}) = 905 cm^{-1}. According to these calculations and assumptions, the Raman spectrum would have three scatterings; 905 cm^{-1}, 810 cm^{-1}, and 650 cm^{-1} with the highest frequency shift completely depolarized. Further, a very low frequency infrared band (< 250 cm^{-1}) should be active. We have made repeated attempts to measure the Raman Spectrum of N_2S_2 but these have, as yet, produced no meaningful results. We have no facility to observe infrared spectra below 250 cm^{-1}.

If our assumptions concerning the ground state are correct, then the generation of 766 cm^{-1} with the most intense band as (0-3) and 525 cm^{-1} with the most intense band as (0-7) is understandable. Assume that these correspond to ν_1 (a_g) = 805 cm^{-1} and ν_2 = 650 cm^{-1} in the ground state.

Simple HMO calculations, reported earlier[44] assign the first allowed transition as a non-bonded electron on sulfur into an antibonding π orbital ($A_g \rightarrow B_{2\mu}$). Such an excitation would be expected to lengthen and loosen the N-S bond slightly. The upper state frequency red shifted by 40 cm^{-1} and peaking at the (0-3) transition is consonant with this assignment. Further, the ($A_g \rightarrow B_{2\mu}$) electron promotion would be expected to reduce the NSN angle at the expense of the SNS angle. Such an electronic promotion would also take some of the stiffness toward bending out of the ring. The postulated upper frequency red shifted by 125 cm^{-1} and peaking at (0-7) is consistant with these predictions. The last feature of the gas spectrum is its overall contour. One has neither the continuous band one normally associates with marked change in geometry (or dissociation), nor the very sharp spectra with a very intense ν_{oo} that

one associates with very slight geometric change. Rather one has diffuse vibrational structure, intermediate between these extremes, and again consonant with the assignment.

The Measurement of the Vapor Pressure of N_2S_2

There were two reasons why it was deemed desirable to measure the vapor pressure of N_2S_2 as a function of temperature. First, the room temperature vapor pressure is necessary to compute the extinction coefficient from the spectroscopic optical density. Secondly, to compute the bond energies in N_2S_2, the heat of sublimation must be known.

The measurement itself presents a number of experimental problems. N_2S_2 is not stable, even at ice temperature. At low temperature, N_4S_4 and the black polymer $(NS)_x$ are formed. At higher temperatures, N_2 is produced as well. Due to the rapidity of polymerization and decomposition, it was deemed inadvisable to carry out any measurements above room temperature. Neither the black polymer (vide infra) nor N_4S_4 [16] have appreciable vapor pressures in the temperature range under consideration, but gaseous N_2, even if produced in miniscule amounts, profoundly alters any measurement of a static pressure.

A second consideration is the range of pressure under consideration. Manometric measurement is impossible over a sufficiently wide range with a 25°C upper limit. Any measurement based on effusion would be seriously in error due to the decomposition of N_2S_2 to N_2.

The following procedure was adopted as one which minimized the known sources of error. An ethereal suspension of N_2S_2 was placed in a vacuum system of minimum volume, cooled to 0°C and pumped for several hours to remove the last traces of ether. The sample was brought to its equilibrium temperature and the pressure increase measured as a function of time. This resulted in a rapid rise followed by a very

slow rise. The gas produced by the slow rise is not condensible with liquid N_2 and is assumed to be N_2. Inasmuch as the residual gas pressure on liquid N_2 condensation is quantitatively equal to the extrapolated value of the slow pressure rise, the N_2S_2 pressure can be found. Any possible contribution of $(NS)_x$ or N_4S_4 are disregarded.

At the high temperatures, pressures were measured by both an oil manometer and by an N.R.C. type 520 B alphatron vacuum gauge. At the low temperatures, pressures were measured by the alphatron gauge alone. The oil manometer was filled with degassed Dow-Corning diffusion pump oil of density 1.07 g/cc. The advertised room temperature vapor pressure of this oil is less than 10^{-5} mm of Hg. The oil levels were read on a cathetometer with a 0.01 mm vernier. The alphatron tube is calibrated only for air but, unlike most other presser transducers, it is linear in pressure. In the case of the alphatron, the linearity occurs over six decades of pressure. A single reading of pressure on both an absolute gauge and an alphatron provides a scale response factor. We had two such readings which served as an internal check. The factor was 0.316 in both cases. Low volatility prevented further checks. The data is shown in Table VI. These points each represent an average of six values obtained in three heating and three cooling cycles. In all cases, residual N_2 was pumped out between measurements. The well-known Clapyeron plot yields a reasonably straight line with a heat of sublimation of 23.0 kcal/mole. The uncertainty in this value could be no more than $\pm$ 1.0 kcal; perhaps $\pm$ 0.5 kcal could be justified.

TABLE VI

Vapor Pressure of N_2S_2

mm of oil	Alphatron Readings	Pressure (mm of Hg)	$\ln\left(\frac{P}{1mm}\right)$	Temperature ° Centigrade	$\frac{10^3}{T°\ K}$
2.77	0.66	2.1×10^{-1}	-1.60	24.0	3.36
1.53	0.38	1.2×10^{-1}	-2.29	19.0	3.42
--	0.19	6.0×10^{-2}	-2.82	15.0	3.47
--	0.091	2.8×10^{-2}	-3.58	9.0	3.53
--	0.032	9.4×10^{-3}	-4.68	0.0	3.66
--	0.0080	2.5×10^{-3}	-6.00	- 5.0	3.73
--	0.0022	6.1×10^{-4}	-7.44	-14.0	3.86

The Heat of Combustion and the Bond Energy of N_2S_2

The measurement of the heat of combustion of N_2S_2 has proven to be a persistent disappointment. The combustion of N_4S_4[16] was a clean quantitative reaction which gave a reproducible ΔH and an analysis of products. The combustion of N_2S_2 was explosive, unpredictable, and not terribly reproducible. In many attempts, the sample prematurely exploded in the process of filling. In a number of attempts, doubt could be cast on sample purity as revealed in product analysis. The details of experimental procedure were those described eralier. In all, the average of thirteen measurements was $\Delta H = -160 \pm 5$kcal. for the reaction

$$N_2S_2\ (S) + 3O_2(g) \rightarrow N_2(g) + 2SO_3(g)$$

Combining this with known heats of formation[45]

	ΔH(kcal)
$N_2S_2(S) + 3O_2(g) \rightarrow N_2(g) + 2SO_2\ g)$	-160 ± 5
$N_2S_2(g) \rightarrow N_2S_2(S)$	-23 ± 1
$2SO_3(g) \rightarrow 3O_2(g) + \frac{1}{4} S_8(S)$	+189
$\frac{1}{4} S_8(S) \rightarrow 2S(g)$	+107
$N_2(g) \rightarrow 2N(g)$	+171
$N_2S_2(g) \rightarrow 2N(g) + 2S(g)$	$+284 \pm 6$

The bond energy based on a cyclic structure would be 71 ± 1.5 kcal/N·S bond. This can be compared with a value of 70.0 ± 0.5 kcal/N·S bond for N_4S_4. The rationale for using the syslic structure and the comparison

of the two values appear elsewhere.[16,43] The standard heat of formation of N_2S_2 can be given by

	Δ
$N_2(g) + 2SO_3(g) \rightarrow N_2S_2(S) + 3O_2(g)$	$+160 \pm 5$
$\frac{1}{4} S_8(S) + 3O_2(g) \rightarrow 2SO_3(g)$	-179
$N_2(g) + \frac{1}{4} S_8(S) \rightarrow N_2S_2(S)$	-19 ± 5

This can be compared with a value of -31 ± 2 kcal for N_4S_4. The reaction which forms N_2S_2 from N_4S_4 in the gaseous phase $\frac{1}{2} N_4S_4(g) \rightarrow N_2S_2(g)$ has a ΔH of -3 ± 5 kcal. The dimerization of N_2S_2 to N_4S_4 in the solid phase $N_2S_2(S) \rightarrow \frac{1}{2} N_4S_4(S)$ has a ΔH of $+3.5 \pm 7$ kcal.

There were several attempts to measure the heat of combustion of the black solid. In these, black solid was first ground to a fine powder, extracted with dioxane for several hours, and finally heated under vacuum for several hours at 120°C. This procedure is thought to remove all N_4S_4, N_2S_2, S_8, dioxane, and ether which are the conceivable contaminants.

Unlike N_4S_4 which burns regularly or N_2S_2 which explodes violently, the black solid smolders slowly in the combustion bomb. The temperature rises steadily for a period of 1-3 hours to a reasonably constant value. On opening the bomb, SO_2 fumes, totally absent in both N_4S_4 and N_2S_2 combustions, are present. Furthermore, a white refractory solid remains. N_4S_4 and S_8 liquefy on heating above 170°C. A remote

possibility, NH_4Cl, which is a by-product of the N_4S_4 synthesis is, of course, water soluble. The white refractory solid is not water soluble. The solid is not soluble to any noticeable extent in benzene, chloroform, or carbon disulfide. The emasurement was repeated several times with the same result and the matter dropped.

The Volatility of the Black Solid

Throughout this and other investigations[16,46] it had been assumed that the black solid was a very high polymer in which the 1-1 atom ratio of its precursor was maintained. A series of experiments was undertaken which tends to show that the solid may not be so simple.

Infrared spectra of the black solid were measured by two sampling techniques.[16] The purified black solid was finely ground and mulled with Nujol of pressed into a KBr pellet. The second method was to sublime a thin film of N_2S_2 at liquid N_2 temperature, and allow it to come to room temperature under vacuum. This is essentially an in-situ synthesis of the black solid. The first method, grinding, suffers the disadvantage of scattering light. In the infrared, this poses no serious problem, but in the visible and ultraviolet, the discs and mulls gave no meaningful absorption spectrum. The second method, in situ generation, suffered the disadvantage of impurity. N_4S_4 was generated along with the black solid. It was hoped that the black solid itself might possess sufficient volatility to permit sublimation to a mounting plate suitable for spectroscopic observation.

After several unsuccessful designs, sublimation was achieved in a cell shown in Figure 23. At the bottom of the inner member, a one inch quartz disc is pressed between two o-rings by flanges tightened by bolts. This arrangement was the only one of many tried that combined the capabilities needed. The requirements were:

a) that the window had to be the coldest position of the cell in the vicinity of the heated black solid

b) that the cell was evacuable to at least 10^{-5} mm

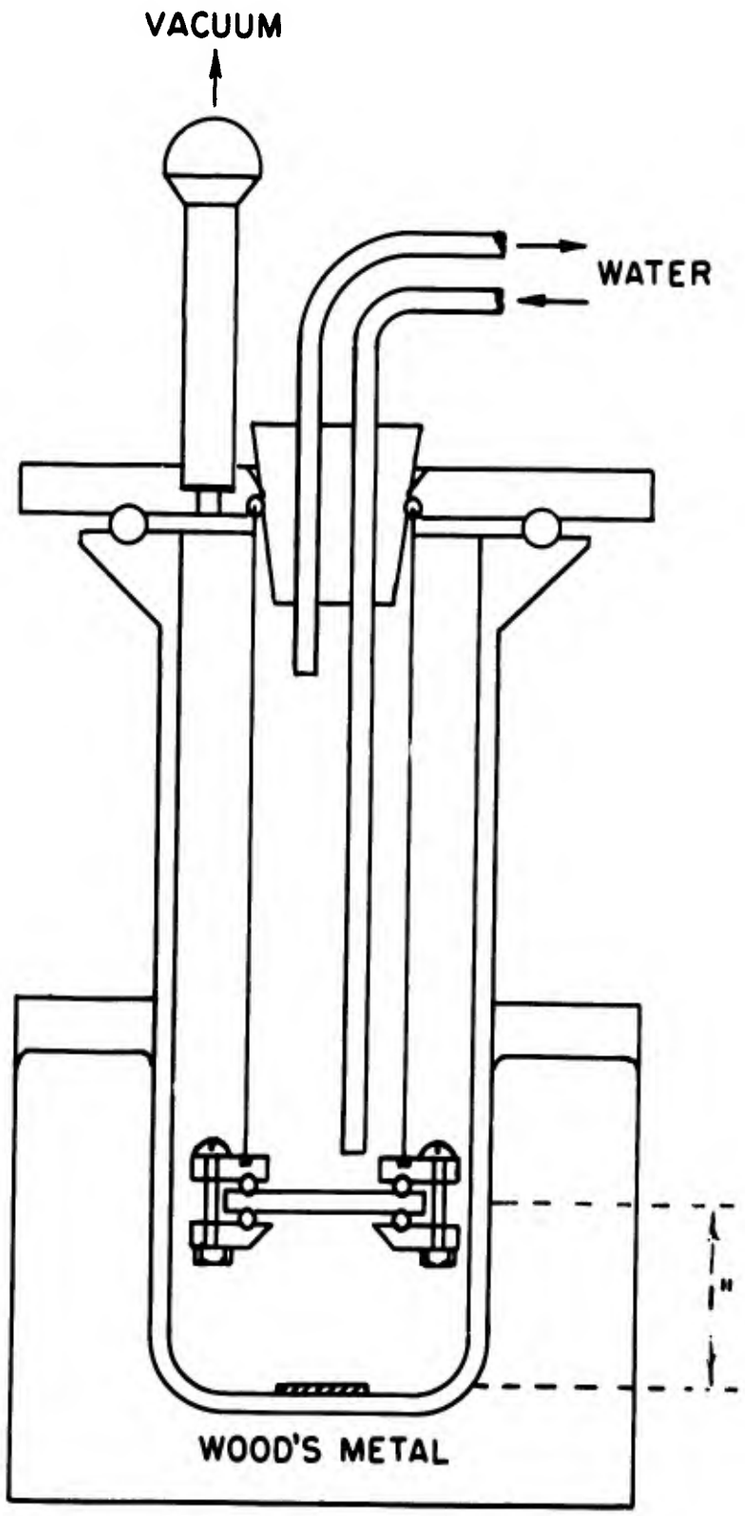

FIGURE 23: Sublimation Cell

c) that the window be demountable without its being handled

d) that the seals hold for prolonged heating at elevated temperatures

In this cell, the window is directly cooled by flowing water. It may be removed by loosening the bolts and lifting by its edges. The o-rings and the epoxide seals showed no sign of deterioration when the Wood's Metal bath was maintained at 250°C for 12 hours.

It was found that when the Wood's Metal bath was maintained below 145°C, no sublimation was detected within an eight hour time period. At 170°C, sublimation for four or five hours produced a deep blue film suitable for spectroscopic observation. If the sublimation is allowed to run for twelve to fourteen hours, the deposit is highly reflective and golden in appearance.

Inasmuch as the sublimation was carried out at the ultimate vacuum of the system which varies markedly from run to run, it was impossible to prepare films of reproducible thickness by merely timing the duration of sublimation.

From these observations, one may conclude that the volatility of the balck solid is very low, but not as low as one would expect for a truly high polymer. To establish a lower limit to the volatility, acid treated Cadmium metal was placed in the cell. At 175°C, the vapor pressure of Cadmium is 0.1 microns of Hg. After eight hours, there was no observable sublimation setting 0.1 microns as a lower limit of vapor pressure at 175°C.

References

(1) M Becke-Goehring, Quart. Rev., 10, 437 (1956).

(2) D. B. Sharma and J. Donohue, Acta. Cryst., 16, 891 (1963).

(3) M Goehring, Chem. Ber., 80, 110 (1947).

(4) D. P. Craig and N. L. Paddock, J. Chem. Soc., 1376 (1962).

(5) D. Chapman and T. C. Waddington, Trans. Faraday Soc., 58, 1679 (1962).

(6) P. S. Braterman, J. Chem. Soc., 2297 (1965).

(7) E. S. Gould, Inorganic Reactions and Structure, Henry Holt, New York, 1955, p. 283.

(8) G. Herzberg and L. G. Mundie, J. Chem. Phys., 8, 263 (1940).

(9) J. E. Baer and M. Carmack, J. Am. Chem. Soc., 71, 1215 (1949).

(10) R. Tousey, F. S. Johnson, J. Richardson and N. Toran, J. Opt. Soc. Am., 41, 696 (1951).

(11) J. A. R. Samson, Geophysics Corporation of America Technical Report 62-9-N, p. 22 (1962).

(12) M. H. Greenblatt, Rev. Sci. Instr., 29, 738 (1958).

(13) American Institute of Physics Handbook, McGraw-Hill, New York, 1957, p. 4-51.

(14) M. H. M. Arnold, J. A. C. Hugill and J. M. Hutson, J. Chem. Soc., 1645 (1936).

(15) J. Strong, Concepts of Classical Optics, W. H. Freeman, San Francisco, 1958, p. 78.

(16) R. N. Wiener, S. M. Smith and D. N. Mitra, Air Force Cambridge Research Laboratory Contract No. AF19(604)-7358 Final Report, November 22, 1963, p. 90.

(17) N. A. Lange, Handbook of Chemistry, Handbook Publishers, Sandusky, Ohio, 1949, p. 1459.

(18) A. M. Bass, J. Chem. Phys., 21, 80 (1953).

(19) M. Becke-Goehring, Inorg. Syntheses, 6, 128 (1960).

(20) E. G. McRae and M. Kasha, Physical Processes in Radiation Biology, Academic Press, New York, 1964, p. 23-42.

(21) W. T. Simpson, Theories of Electrons in Molecules, Prentice-Hall, New Jersey, 1962, Chapter 4.

(22) J. Raymonda, Doctoral Dissertation, University of Washington, 1966.

(23) M. B. Robin and W. T. Simpson, J. Chem. Phys., 36, 580 (1962).

(24) W. T. Simpson, J. Am. Chem. Soc., 73, 5363 (1951).

(25) W. T. Simpson, J. Am. Chem. Soc., 77, 6164 (1955).

(26) L. D. Landau and E. M. Lifshitz, Quantum Mechanics, Pergamon Press, Oxford, 1965, p. 133.

(27) R. N. Wiener, private communication

(28) W. Kauzmann, Quantum Chemistry, Academic Press, New York, 1957, p. 49.

(29) R. N. Wiener, private communication

(30) H. Weyl, The Theory of Groups and Quantum Mechanics, Dover Publications, New York, 1950, p. 316.

(31) M. Tinkham, Group Theory and Quantum Mechanics, McGraw-Hill, New York, 1964, p. 40.

(32) C. J. Brown and E. G. Cox, J. Chem. Soc., 1 (1940).

(33) K. N. Trueblood and J. W. Mayer, Acta Cryst., 9, 628 (1956).

(34) D. N. Sharma, Crystal and Molecular Structural Studies of Various Inorganic Compounds with Unusual Element to Element Bonding, University Microfilms, Inc., Ann Arbor, Michigan, 1961.

(35) D. Clark, J. Chem. Soc., 1615 (1952).

(36) G. A. Jeffrey and D. W. Jones, Acta Cryst., 9, 283 (1956).

(37) R. L. Sass and J. Donohue, Acta. Cryst., 11, 497 (1958).

(38) R. L. Sass, Acta Cryst., 13, 321 (1960).

(39) C. Lu and J. Donohue, J. Am. Chem. Soc., 66, 818 (1944).

(40) T. Moeller, Inorganic Chemistry, John Wiley and Sons, New York, 1952, p. 548.

(41) W. Muthmann and E. Seitter, Ber., 30, 627 (1897).

(42) A. Muewsen, Ber., 65B, 1724 (1932).

(43) J. R. W. Warn and D. Chapman, Spectrochimica Acta, 22, 1371 (1966).

(44) Quarterly Report, January 1965.

(45) Rossini et al., Selected Values of Chemical Thermodynamic Properties, Circular of the National Bureau of Standards, 500, United States Government Printing Office (Washington, 1952).

(46) Goehring, Progress in Inorganic Chemistry, ed. Cotton., Interscience Publishers, Inc., New York, (1961), p. 3.

PUBLICATIONS

Scientific Reports

#1: "A Kinetic Study of the Photochemical Addition of Phenanthrenequinone with Olefins" by James J. Bohning, AFCRL 65-714, AD 629 478, July 1965.

#2: "An Investigation of Photochemically Generated Free Radicals From Perinaphthenones" by Gary P. Raboldm AFCRL 65-715, AD 629 479, July 1965.

#3: "Apparatus for Flash Photolysis" by Peter A. Schnieper, AFCRL 65-716, AD 627 533, July 1965.

#4: "Charge Transfer Properties of Disulfides" by Wayne M. Moreau and Karl Weiss, AFCRL 66-197, AD 632 719, March 1966.

#5 "Literature Survey on the Surface Structures of Refractory Metals with Reference of Thermionic Emission and Energy Converters" by Welville B. Nowak and Jacob Babakian, AFCRL 66-362, AD 636 954, June 1966.

Dissertations

Master of Science:

Raymond J. Sonoff, "The Transient Photoresponse of a P-N Homojunction and the Relationship of this Response to the Overall Photovoltaic Energy Conversion Efficiency," June 1966.

Donald H. Lambert, "Photochemical Studies of Some Organic Disulfides," June 1964.

Wayne M. Moreau, "Charge Transfer Properties of Disulfides," June 1964.

Doctor of Philosophy:

Gary Paul Rabold, "An Investigation of Photochemically Generated Free Radicals from Perinaphthenones," June 1965.

James J. Bohning, "A Kinetic Study of the Photochemical Addition of Phenanthrenequinone to Olefins," June 1965.

Harold Paul Wolf, "The Sensitized and Unsensitized Photolysis of Some Disulfides," June 1967.

Wayne Martin Moreau, "Photoreduction of 1,3,5-Trinitrobenzene," June 1967.

Doctor of Philosophy: (continued)

Lewis I. Rubin, "The Electronic Spectrum of Tetrasulfurtetranitride and of Octatomic Sulfur," June 1967.

Articles

1. Eleven publications based on the photochemical research - See Appendices A-H.

2. W. B. Nowak, "Thin, Large Crystals of Silicon on Amorphous Quartz," J. of Vac. Sci. and Technol., 2, 276 (A) (1965).

Conferences Attended

W. B. Nowak:

Registration fee to the MIT Physical Electronics Conference, February 1964.

Registration and Report 25th Physical Electronics Conference MIT, January 1965.

Registration fees for Conference & Report of MIT Physical Electronics Conference, January 1966

Registration fee for International Conference on Crystal Growth Boston, Mass., June 20-24, 1966.(April)

Registration fee for AIME meeting August 29-31, 1966 held at Boston, Massachusetts.

Karl Weiss:

ESR Workshop, Varian Associates, Palo Alto, California, October 1964.

Photochemistry Conference, Rensselear Poly. Inst., Troy, N.Y., June 1966.

ACS Meeting, Pittsburgh, Pa., March 1966.

ACS Meeting, New York, N.Y., September 1966.

Conference on "The Organic Solid State," Franklin Institute, Philadelphia, Pa., May 1964.

R. N. Wiener:

Spectroscopy Conference, Columbus, Ohio, June 1964
June 1965
June 1966

Conference of "The ORganic Solid State," Franklin Institute, Philadelphia, Pa., May 1964.

Conference on Photochemistry, Rensselear Poly. Inst., Troy, N.Y., June 1966.

APPENDIX A

Photochemistry and Photobiology. 1967. Vol. 6, pp. 321–329. Pergamon Press Ltd. Printed in Great Britain

APPARATUS FOR THE MEASUREMENT OF QUANTUM YIELDS AND RATES OF PHOTOCHEMICAL REACTIONS

HAROLD P. WOLF, JAMES J. BOHNING, PETER A. SCHNIEPER and KARL WEISS
Photochemistry and Spectroscopy Laboratory, Northeastern University, Boston, Massachusetts 02115

(*Received* 22 *August* 1966; *revised* 17 *November* 1966)

Abstract—A versatile irradiation apparatus for the quantitative study of photochemical reactions is described, which incorporates a commercial monochromator and utilizes a calibrated thermopile for the continuous measurement of light absorption during irradiation. The operating characteristics are discussed, and illustrative applications are cited. Using this apparatus, the quantum yield of the potassium ferrioxalate actinometer at 366 nm and 25°C was determined as 1·27 ± 0·01 for a 6·0 × 10^{-3} M solution, in excellent agreement with reported values of 1·26.

INTRODUCTION

THE EXPERIMENTAL techniques of quantitative photochemistry, which have been summarized and reviewed,[1,2] vary considerably in precision and sophistication. The simplest, though probably not the most accurate, method for the determination of quantum yields utilizes a suitably filtered light source in conjunction with a chemical actinometer.[3,4] Monochromators, whose applications in ultraviolet photochemistry have recently been surveyed,[5] are less frequently employed. The use of the thermopiles appears to be largely confined to the critical examination of actinometric systems.[6–9]

For reactions in which photolysis produces a decrease in the optical density at the irradiating wavelength,[10–12] the most convenient method of determining quantum yields requires continuous measurement of the transmitted intensity during irradiation. The apparatus described in this paper, which is based on a commercial monochromator and calibrated thermopile, was designed for this purpose. Crucial design considerations were: (1) The achievement of a reasonable rate of light absorption (~10^{15} photons/sec), (2) an optical system which provides completely uniform illumination of the sample so that no error is incurred by monitoring only a fraction of the area presented for irradiation, (3) accurate temperature control, and (4) protection of the thermopile against spurious thermal effects. When the reaction rate is proportional solely to the absorbed intensity, the data can be evaluated in terms of a simple integrated rate expression. Under other conditions, graphical integration of the absorbed intensity–time curves is necessary.

THE APPARATUS

A schematic representation of the complete irradiation assembly is shown in Fig. 1. The monochromator is a Bausch and Lomb grating instrument (catalogue No. 33–86–45) with an aperture ratio of f/4·4 and a focal length of 50 cm. The 600 lines/mm grating is blazed for 300 nm and has a dispersion of 0·30 mm/nm. This unit, including the quartz condenser lenses $L_{1,2}$ and slit lenses L_3 and L_4 supplied with it, is used without modification. The light sources and the irradiation train, which terminates with the thermopile, involve critical features; these are discussed in the sections which follow.

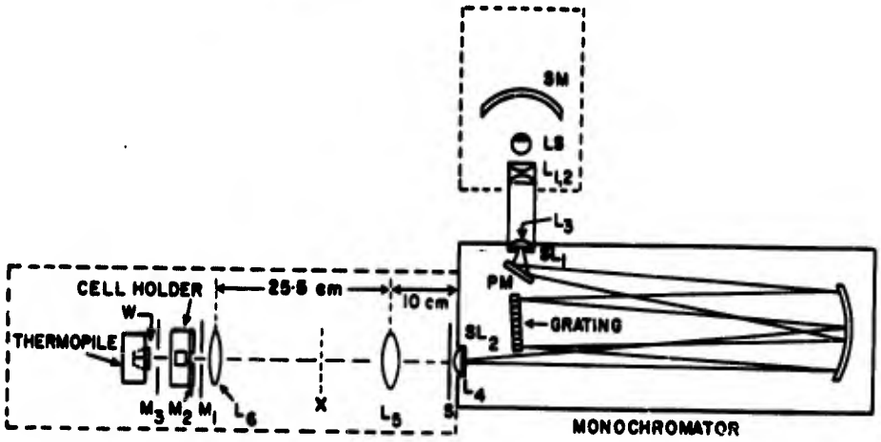

FIG. 1. Diagram of irradiation assembly. See text for explanation of symbols. The dashed lines represent the lamp housing and enclosure for the irradiation train.

Light sources

The key requirement for sources in this application is stability. Two suitable sources are the Osram HBO 500W super-pressure mercury lamp and the General Electric BH-6 1000-W air-cooled high pressure mercury lamp.

With the Osram lamp, the entrance optics provide efficient imaging of the arc on the entrance slit (SL_1, Fig. 1). The lamp (LS) is housed as recommended by the manufacturer.[18] A substantial increase in intensity is achieved by using a 4·5-in. dia., 35-mm focal length front surface-aluminized spherical mirror (SM) which images the arc back onto itself. The lamp is d.c. powered (85 V, 5·7A during operation) with a Gates P-500-D supply and LRK-500 ripple kit. Provided that a warm-up period of at least 1 hr is employed, and that the slits are properly adjusted (*vide infra*), this source is extremely stable. The high frequency noise is less than 0·25 per cent, and the intensity varies by less than 1 per cent over a period of several hours. Alternating-current operation (Osram 1C choke, A-0100 ignition device) is unsatisfactory; not only is the noise greater, but there are also random changes in intensity which can amount to several percent.

The BH-6 lamp is a.c.-operated with an A. 142G2 control unit at an input voltage of 120 V. Imaging of the 25-mm long arc on the entrance slit by condenser $L_{1,2}$ is relatively inefficient, and intensity could be gained with better entrance optics. Since the lamp is started horizontally and operated in the vertical position, use of spherical mirror (SM) is inconvenient. In operation, the intensity of the BH-6 lamp decreases linearly at the rate of 2–3 per cent per hour, for which correction is made.

Irradiation train

As shown in Fig. 1, the thermopile intercepts radiation 6 cm beyond the plane of the cell holder. Consequently, the exit optics must provide uniform intensity over at least this distance. The grating represents the aperture stop of the monochromator, and field lens L_4 (focal length 6 cm) produces a uniformly intense 1·2 cm × 1·2 cm image of this aperture at a distance of about 5 cm from the exit slit SL_2. Lenses L_5 and L_6 have a diameter of 6·3 cm and focal lengths of 5 cm and 15 cm, respectively.* Lens L_5, whose effective aperture is only 2·4 cm × 2·4 cm, furnishes an image of the monochromator aperture (4·5 cm × 4·5 cm) in the plane of lens L_6. The latter serves as a field lens and produces an image (*ca.* 4 cm × 4 cm) of the effective aperture of lens L_5 about 40 cm from L_6. The cross-section of the beam appears constant over this distance, and measurements have shown the intensity to be uniform to ± 1 per cent for six inches beyond L_6 and over a 3·7 × 3·7 cm area. The lenses employed are not achromatic, and the focal positions quoted change somewhat with wavelength. With the given fixed lens positions, no wavelength dependence was observed in the uniformity of intensity in the target zone.

An alternative sample position is 10 cm beyond lens L_5 (X, Fig. 1), where this lens places a 1 : 1 image of the exit slit. Since this is also an image of the arc, the illumination is not entirely even. With a 5-mm slit, the intensity is approximately 25 times that beyond lens L_6. The position is clearly not suitable for continuous intensity measurements, but may be used in conjunction with chemical actinometry.

The cell holder is shown in detail in Fig. 2. It accommodates Beckman standard silica or "Pyrex" rectangular 1-cm spectrophotometer cells in a block which has overall dimensions 9·4 cm × 6·8 cm × 2·5 cm. Good contact with two cell holder walls is accomplished by grinding the non-optical cell faces if necessary. The cells are attached to a Y-shaped glass assembly, one arm of which serves for degassing by the freeze–pump–thaw method. Constant temperature (± 0·1°) is maintained by rapid circulation of water from a thermostatted bath. The solutions (3 ml) are magnetically stirred throughout irradiation with a *ca.* 8 mm long piece of glass-covered steel wire driven by a 600 rev/min motor.† This rate of stirring was found to be complete and rapid enough not to affect rate measurements with systems in which an absorbing reactant disappears during 10–50 min of irradiation.[10] Mask M_1 (10 mm × 28 mm opening) protects the bulk of the cell holder against radiation and confines the light to the opening in mask M_2 (8·50 mm × 26·0 mm, exact) which defines the irradiated area of the solution.

The thermopile is an air-type Eppley instrument with 8 bismuth–silver junctions and a nominal 12/32 in. diameter sensitive surface. Mask M_3 (16 mm dia.) matches the opening in the thermopile; it serves to intercept light reflected from the shiny thermopile exterior. Calibration by the Eppley Laboratory in the range 0·4–2·5 mW/cm² indicates a basic sensitivity of 0·124 mV/mW cm^{-2} with a quartz window. Intensity measurements without the cell holder and masks in place indicate that these elements reduce the sensitivity by a factor of 0·914 without affecting the response time. Attempts to decrease the irradiated portion of the sensitive surface further by reducing the opening in mask M_3 results in sluggish response. The output from the thermopile is amplified (Hewlett Packard 425-A d.c. Microvolt–Ammeter) and divided with a variable resistor chain which can always be adjusted to satisfy the input impedance requirements of the Leeds and Northrup "Speedomax W" Azar recorder. Accurate calibration of the recorder is achieved with reference

*INSACO, Inc., Quakerstown, Pa.

†"Synchron" timing motor, Hansen Mfg. Co., Inc., Princeton, Ind.

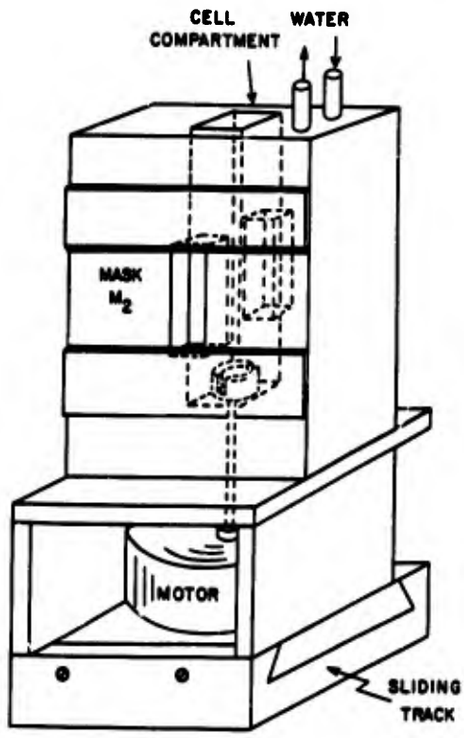

FIG. 2. Detailed view of the constant temperature cell holder. The water circulates beneath the cell compartment to the top of left side of the block, and back. The front face constitutes mask M_2, towards which the light is directed.

signals from a Leeds and Northrup K-3 potentiometer. The amplifier–voltage divider combination provides full scale recorder deflections over a wide range of intensities (10^{-6}–10^{-1} W/cm^2). Since the light beam is uniform, the thermopile is maintained in a fixed horizontal position and the total intensity on the sample is computed from the output and the area of mask M_2.

The irradiations are initiated and terminated with the shutter S. To minimize thermal drifts and scattering effects, it is essential that the irradiation train be enclosed in a light-tight box and that the interior of the box, cell holder, lens mounts, and masks be blackened.

Operation

The monochromator slit widths were chosen so as to maintain the highest possible intensity while not encroaching on neighboring line groups. Considering only the major mercury lines, acceptable band widths are 25 nm, 10 nm, and 5 nm, respectively, for lines in the ranges 366–578 nm, 334–313 nm, and 303–235 nm. The corresponding slit widths are 7·5 mm 3 mm, and 1·5 mm for both entrance and exit slits. An entrance slit of 7·5 mm is not satisfactory with the Osram lamp since the outermost regions of the arc are not stable

and a small overlap with the slit results in considerable noise at the detection end. To overcome this problem, an entrance slit of 10 mm, which is slightly larger than the arc image at the slit, is employed in conjunction with a 5-mm exit slit in the 366–578 nm region.

TABLE 1. INTENSITIES AT THE SAMPLE POSITION, $\lambda > 310$ nm

Wavelength (nm*)	Intensity (quanta/cm² sec × 10^{-15})		
	Osram 500 Hg Lamp		BH-6 Hg Lamp
	New apparatus	After 3 years operation	After 3 years operation
313		0·33	0·42
334		0·28	0·37
366	5·7	2·9	2·0
405	3·9	2·3	2·0
435	5·8	3·7	3·0
500	0·88	0·69	0·51
546	5·4	5·2	3·7
578	5·8	6·0	2·0
650		0·69	0·43
546†		~0	~0

*Wavelength set to maximize the output for each line group. Slit widths: 10 mm entrance and 5 mm exit for 366–650 nm; 3 mm for entrance and exit at 313 and 334 nm.
†Corning 7–51 filter (absorbs completely at 546 nm, transmits 300–400 nm) behind cell holder.

TABLE 2. INTENSITIES AT THE SAMPLE POSITION, $\lambda < 320$ nm

Wavelength (nm†)	Intensity (quanta/cm² sec × 10^{-15}*)	
	Osram 500 W Hg Lamp	BH-6 Hg Lamp
313	0·41	0·62
303	0·21	0·41
297	0·12	0·37
289	0·03	0·20
280	0·01	0·16
275	0	0·11
265	0	0·03
254	0·006	0·01
248	0·003	0·05
240	0·006	0·02
235	0	0

*With new monochromator entrance mirror (PM, Fig. 1).
†1·5 mm entrance and exit slits; wavelength set to maximize output for each line group.

Typical intensity values are presented in Tables 1 and 2. There is some variation with individual lamps, and optimal output requires critical optical alignment. Points to be noted are:

(1) The BH-6 lamp provides substantially more intensity below 366 nm than the Osram lamp.

(2) The intensities at all wavelengths decrease with prolonged use (*cf.* the two columns for the Osram lamp, Table 1), primarily due to the reflection losses at the monochromator

entrance mirror (PM, Fig. 1). The data of Table 2 were obtained with a new entrance mirror, and comparison of the values at 313 nm with those listed in Table 1 indicate enhancement by a factor of about 3.

(3) The stray light level is low. There is none detectable at 546 nm due to the 313 nm and 366 nm lines (line 10, Table 1). Tests with a 1 cm "Pyrex" filter indicate < 0·5 per cent scattered radiation below 300 nm.

(4) There is a significant contribution from the continuum. Photon fluxes measured at 500 nm and 650 nm, wavelengths which are remote from intense spectral lines, are 10–20 per cent of the values for line positions in the 366–578 nm region. The loss of spectral purity due to the continuum contribution, which varies with wavelength and slit parameters, is difficult to specify. For the visible region, 20 per cent probably represents a lower limit.

With the BH-6 lamp operated as specified, new entrance mirror, and 5 nm band pass, the total photon flux is $1{\cdot}2 \times 10^{16}$ quanta/sec at 313 nm and $1{\cdot}0 \times 10^{15}$ quanta/sec at 248 nm. By way of comparison, Johns and Rauth[5], using a Bausch and Lomb monochromator with 0·62 mm/nm dispersion and a 2·4 nm band pass in conjunction with a 500 W mercury lamp, obtained a flux of 7×10^{15} quanta/sec at 313 nm.

APPLICATIONS

A typical experimental record for a reaction in which the light absorbed during photolysis decreases is shown in Fig. 3. The intensity incident on the reaction cell is designated as I_t, and the intensities transmitted by the cell and solution, and by the cell filled with pure solvent are given as I and I_o, respectively. Reflections occur at the cell faces, at the thermopile window (W, Fig. 1), and at the lenses, for which allowance has to be made in computing the absorbed intensity, I_{abs}. This problem has been considered in detail.[14–16] Comparison of measured transmittancies with calculated values based on Fresnel's equation indicates that, at wavelengths greater than 300 nm, light attentuation by the cell faces and thermopile window is almost entirely due to reflection. For solvents such as water, propanol, and benzene, reflections at the quartz–solvent interface are negligible experimentally and by calculation. Since the values of the reflectances at the quartz–air interfaces are small (~0·05), secondary reflections of reflected light may be neglected and the total absorbed intensity is

$$I_{abs} = \frac{AI_o}{(1-R)}(1-T_s)(1+aT_s) \qquad (1)$$

In this equation A is the area of the solution which receives radiation and $a = R + fR'(1\text{-}R)^2$, where R and R' are the reflectances of the cell faces and thermopile window, respectively, and f is the fraction of A which receives reflected light from the thermopile window. In this approximation, the transmittance of the solution is $T_s = I/I_o$ and $I_o = I_t(1-R)^2$.

As a check on the performance of the apparatus, the quantum yield for the potassium ferrioxalate actinometer has been redetermined following the directions of Hatchard and Parker[7]. The measurements were made with $6{\cdot}0 \times 10^{-3}$ M solution of the oxalate at 366 nm and 25°C. Exactly 3 ml portions of this solution were irradiated for 600 ± 0·1 sec. For spectrophotometric analysis, the photolyzed samples were diluted to 25 ml. The calibration graph provided $\epsilon = 1{\cdot}11 \times 10^4$ for the ferrous phenanthroline complex, which may be compared with $\epsilon = 1{\cdot}105 \times 10^4$ calculated from Hatchard and Parker's data.

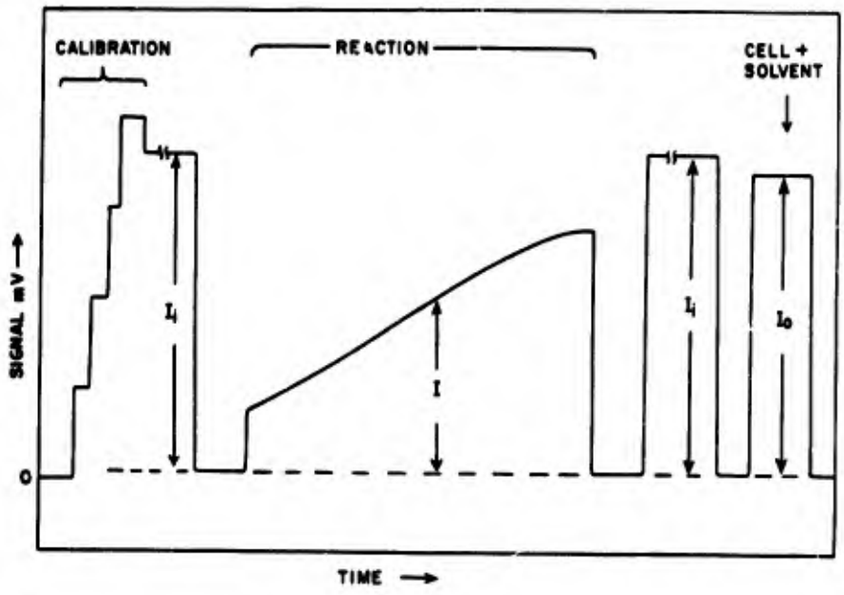

FIG. 3. Typical experimental record for a reaction in which the light absorption changes with time. I_t is the intensity incident on the sample cell.

Under the conditions employed, $T_s = 0$ and equation (2) is applicable in its simplest form. The results are compared with previous determinations in Table 3.

In many photochemical reactions, the disappearance of a reactant X follows the rate expression

$$-\mathrm{d}\,[X]/\mathrm{d}t = \phi_{abs} \qquad (2)$$

where ϕ is the quantum yield which is independent of the incident intensity. Incorporating equation (1) and the definition $T_s = \exp(-2{\cdot}303\ \epsilon\ [X]\ d)$, where ϵ is the molar extinction coefficient at the wavelength of irradiation and d is the path-length in cm, and integrating yields

$$\log[(1/T_s) - 1] + a \log[(1/T_s) + a] = -\frac{(1 + a)\,\epsilon\, A\, I_0\, \phi\, t}{(1 - R)} + \text{constant} \qquad (3)$$

TABLE 3. QUANTUM YIELD OF POTASSIUM FERRIOXALATE ACTINOMETER ($6{\cdot}0 \times 10^{-3}$ M) AT 366 nm AND 25°C

Investigators	ϕ
Hatchard and Parker[7]	$1{\cdot}26 \pm 0{\cdot}02$*
Lee and Selinger[8]	$1{\cdot}26 \pm 0{\cdot}03$
This study	$1{\cdot}27 \pm 0{\cdot}01$

*Based on measurements using a thermopile. Value based on comparison with uranyl oxalate actinometer is lower.

To obtain the quantum yield from the slope of plots of equation (3), I_0 must be expressed in photons/l.sec cm². A number of systems which allow use of equation (3) have been investigated, amongst them the reaction of phenanthrenequinone with olefins,[16] and the reduction of thioctic acid and of phenanthrenequinone in 2-propanol.[17] Figure 4 represents an illustrative result from the phenanthrenequinone reduction study. The slope corresponds to $\phi = 1{\cdot}55$ for the disappearance of quinone by photolysis at 435 nm. Figure 4 includes the plot of log $[(1/T_s)-1]$ against time (curve B), which is seen to be linear also but with a smaller slope. The fact that the slopes differ by a constant factor arises

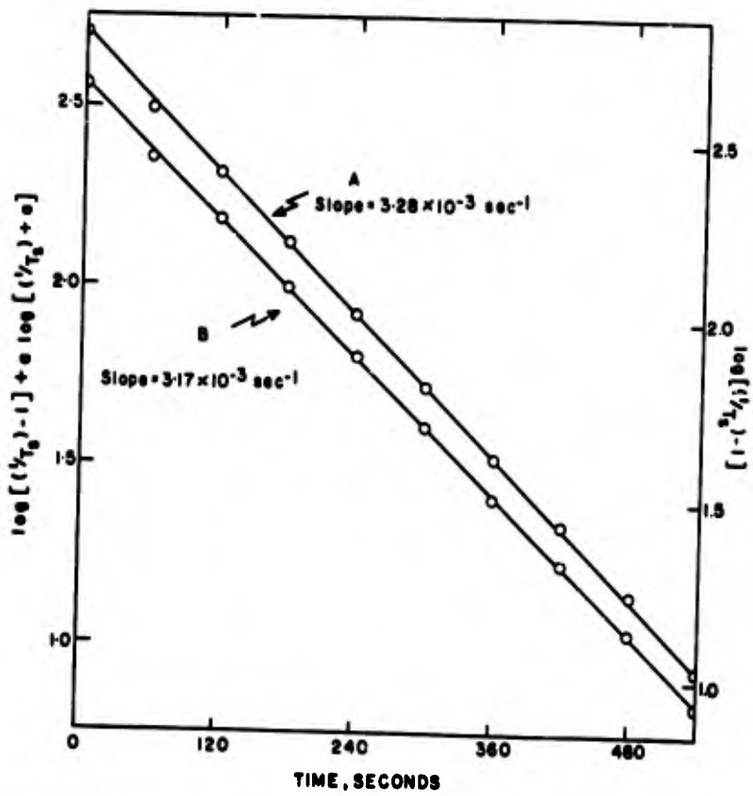

FIG. 4. Photolysis of 7·63 × 10⁻⁴M phenanthrenequinone in 2-propanol at 435 nm and 25°. A—Equation (3), left ordinate; B—log $[(1/T_s)-1]$ alone, right ordinate.

from the small magnitude of the reflection corrections ($a \sim 0{\cdot}07$). Empirically it was found that for the integration of equation (2) the time variable factor $(1 + a\,T_s)$ of equation (1) can, to a very close approximation, be replaced by the constant factor $(1 + 0{\cdot}5a)$. Quantum yields can then be obtained from the simpler plot. This approach was utilized in the phenanthrenequinone–olefin study.[16]

Measuring spectral changes at wavelengths other than the exciting wavelength may be accomplished by monitoring with an analyzing beam at right angles to the exciting

beam. We have adapted a Beckman model B spectrophotometer for this purpose by building a constant temperature cell holder similar to that shown in Fig. 2 into its sample compartment. Filters in front of the detector eliminate stray exciting light. This unit has proven its utility in rate measurements of the formation and decay of the long-lived intermediate (λ_{max} 650 nm) which is generated by 366 nm photolysis of perinaphthenone in various solvents.[18]

Acknowledgements—This work was supported by the U.S. Air Force Cambridge Laboratories, Office of Aerospace Research, under contracts AF19(604)-7358 and AF19(628)-3836). We gratefully acknowledge the contributions of Mr. Michael Doyle in the construction of the apparatus, and the help of Mr. Leonard Gosule with some quantum yield measurements. The crossed beam monitoring modification was developed by Dr. Gary P. Rabold.

REFERENCES

1. W. A. Noyes, Jr. and P. A. Leighton, *The Photochemistry of Gases*, Chapter 2. Reinhold New York (1941).
2. J. G. Calvert and J. N. Pitts, Jr., *Photochemistry*, Chapter 7. John Wiley, New York (1966).
3. W. M. Moore, G. S. Hammond and R. P. Foss, *J. Am. Chem. Soc.* **83**, 2789 (1961).
4. D. J. Trecker and J. P. Henry, *Anal. Chem.* **35**, 1882 (1963).
5. H. E. Johns and A. M. Rauth, *Photochem. Photobiol.* **4**, 673, 693 (1965).
6. W. G. Leighton and G. S. Forbes, *J. Am. Chem. Soc.* **52**, 3139 (1930).
7. C. G. Hatchard and C. A. Parker, *Proc. Roy. Soc., London* **A235**, 518 (1956).
8. J. Lee and H. H. Selinger, *J. Chem. Phys.* **40**, 519 (1964).
9. C. A. Discher, P. F. Smith, I. Lippman and R. Turse, *J. Phys. Chem.* **67**, 2501 (1963).
10. J. J. Bohning and K. Weiss, *J. Am. Chem. Soc.* **88**, 2893 (1966).
11. P. Smith and A. M. Rosenberg, *J. Am. Chem. Soc.* **81**, 2037 (1959).
12. M. Pestemer, *Z. Elektrochem.* **58**, 121 (1954).
13. Osram bulletin entitled *Hints for Designing Devices for Super Pressure Mercury Lamps HBO*, (1961).
14. R. E. Hunt and T. L. Hill, *J. Chem. Phys.* **15**, 111 (1947).
15. J. A. Davies and P. P. Manning, *J. Am. Chem. Soc.* **79**, 5148 (1957).
16. J. Lee and H. H. Selinger, *Photochem. Photobiol.* **4**, 1015 (1965).
17. H. P. Wolf and K. Weiss, unpublished results.
18. H. Köller, G. P. Rabold, K. Weiss and T. K. Mukherjee, *Proc. Chem. Soc.* 332 (1964).

APPENDIX B

REPRINTED BY NEREM FROM THE NEREM RECORD 1965, A DIGEST OF PAPERS PRESENTED AT THE NORTHEAST ELECTRONICS RESEARCH AND ENGINEERING MEETING ON NOVEMBER 3, 4 and 5, 1965

SESSION: Biological Effects of Laser Radiation II

Co-sponsored by the U.S. Army Medical Research and Development Command

TPM-2: Flash Photolysis—An Application of Electrical Engineering in Chemical Research

P. A. Schnieper

Northeastern University

Boston, Mass.

FLASH PHOTOLYSIS is a method used for the study of interaction of light with matter.[1] It serves to detect and characterize short-lived intermediates (lifetimes $<10^{-4}$ sec.) which play an important role in photochemical reactions. A sample of a gas or solution is excited with an intense flash of light to produce chemical transients, the complete absorption spectrum of which is then obtained by allowing a second, delayed flash to pass through the sample into a spectrograph. Alternatively, a continuous monitoring light beam passes through the sample into a monochromator which is coupled to a photoelectric detector. This method provides information at a single wavelength.

Our photochemical research program utilizes two photolysis units: a conventional flash apparatus based on xenon-filled lamps (Figure 1), and a laser flash apparatus[2] (Figure 2). To obtain maximum information about the chemical transients, the photolytic flash must be as short as possible. To prolong the flash tube lifetime, the discharge circuit should be critically damped ($R/2L = (LC)^{-1/2}$). For a fixed capacitance and a given discharge energy ($E = \frac{1}{2}CV^2$), critical damping is achieved by minimizing the circuit inductance and modifying the length and cross-section of the flash tube. The flash tubes, designed by Dr. Edward Wall, incorporate expansion chambers as suggested by Claesson and Lindqvist.[3] Each tube can discharge 2000 joules in 20 μseconds, and has a breakdown voltage of 3.5kvolt at 100 mm xenon pressure. Each capacitor services two tubes (Figure 3). Four flash tubes and the reaction cell are located in a cylindrical aluminum cavity which serves as a light reflector as well as the high voltage terminal of the trigger circuit. Above the breakdown voltage, triggering the "Ignitron" initiates the flash, while at lower voltages the tubes are ionized by a 35,000 volt pulse applied to the aluminum cavity. The combination of external trigger and "Ignitron" allows the tubes to be reliably fired over a wide range (1-20kvolt).

A 150-watt xenon arc or a 70-watt tungsten filament serve as monitoring source for single wavelength photoelectric detection. The spectroscopic flash (50-150 joules, 20 μseconds) for photographic detection is provided by a small xenon flash lamp. Waveform and pulse generators are used to delay the spectral flash relative to the photolytic flash. The delay time is accurately measured with a photo-diode which samples the light from both flashes. The circuits for the photomultiplier tubes include a variable load resistance (1-1000kohm) to allow control of the transient signal amplitude. The signal shape constitutes important information concerning the chemical transients. Consequently the circuit time constant must be significantly less than the lifetime of these transients.

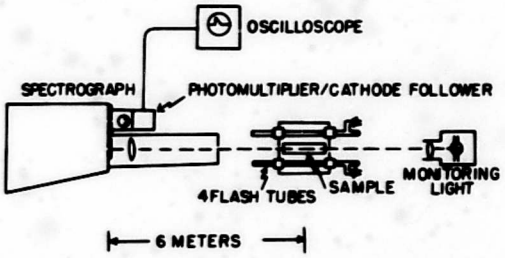

FIGURE 1—**Physical arrangement of conventional flash photolysis apparatus with photoelectric detection.**

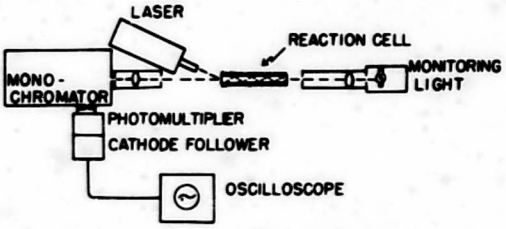

FIGURE 2—**Physical arrangement of laser photolysis assembly. The reaction cell is externally silvered to allow multiple internal reflection of the laser beam.**

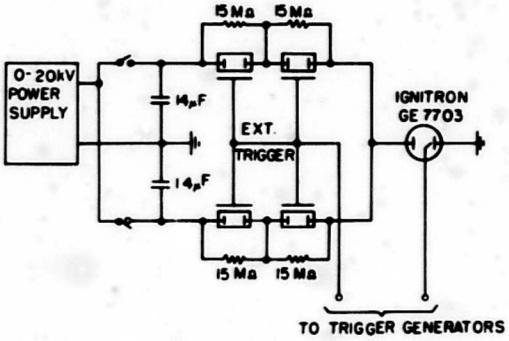

FIGURE 3—**Main discharge circuit for flash photolysis apparatus.**

1) R. G. W. Norrish, American Scientist, *50*, 131 (March 1962).

2) K. Weiss, K. Bar-Eli, P. Schnieper, and R. Danziger, Abstracts, IEEE Laser Conference, Boston, August 1964.

3) S. Claesson and L. Lindqvist, Arkiv Kemi, *11*, 60 (December, 1957).

4) B. H. Soffer, J. Appl. Phys., 35, 8 (August, 1964).

5) P. Graceffa, paper at Northeastern Section of American Chemical Society—Sponsored Student Research Symposium, MIT, May 1965.

Saturation of the photomultiplier tube by stray photolytic light can be suppressed by temporarily rendering the tube inoperative (Figure 4). With photographic detection stray light is not troublesome due to the high intensity of the monitoring spectral flash.

In the laser apparatus a 100-joules pulsed ruby laser replaces the flash lamps. Single giant pulses are obtained by passive Q-spoiling with cryptocyanine in methanol.[4] At an input energy of 6700 joules, the 0.5 joule pulse duration is of the order of 50 nanoseconds. Since the Q-spoiled flash appears about one millisecond after activation of the laser pump tube, it is necessary to delay the oscilloscope sweep with respect to the firing of the flash tube. Since the photolysis light obtained from the laser is monochromatic, there is complete absence of stray light except at the laser wavelength. The extremely short pulses which can be achieved allow the study of very short-lived transients.

A typical decay of transient absorption is shown in Figure 5. The light intensities are proportional to the output voltages, which are related to the optical densities ($D' = D_o + \log \frac{V_o}{V_t}$; D_o = optical density of the original solution and D' = optical density at time t). Complete transient spectra[5] are reproduced in Figure 6. Such data allow decay rate laws to be formulated and the transients to be identified.

This research is sponsored by the U. S. Air Force Cambridge Research Laboratories, Office of Aerospace Research, Contracts AF19(604)-7358 and AF19(628)-3836, and by the U. S. Public Health Service, Grant RH00302-02.

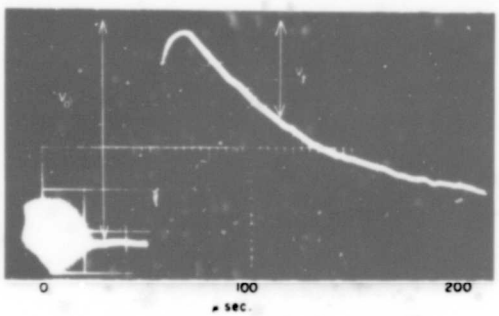

FIGURE 5—Transient decay in laser-flashed aqueous Methylene Blue at 400mμ. The decay is exponential with a half-life of 43 μseconds.

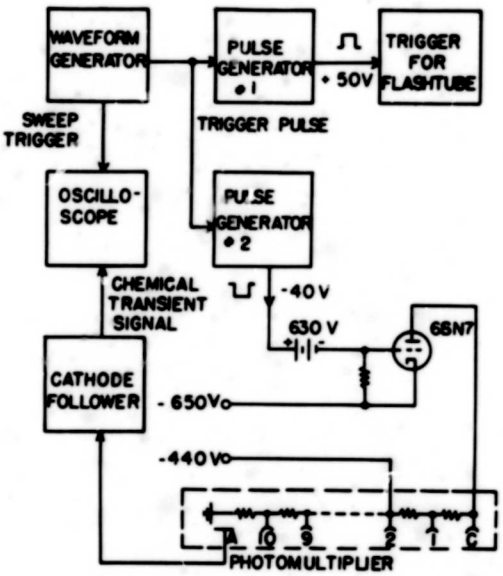

FIGURE 4—Circuit for turning off the photomultiplier tube during the photolytic flash. Application of negative pulse drives the triode into cut-off region.

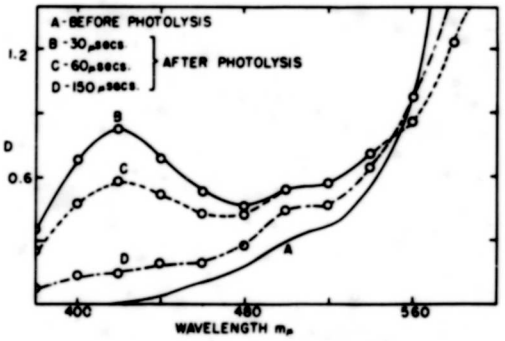

FIGURE 6—Transient spectra of aqueous Methylene Blue at various times after conventional photolytic flashes. Photoelectric detection at single wavelengths was used.

APPENDIX C

[Reprinted from Journal of Chemical Education, Vol. 43, Page 435, August, 1966.]

Wayne M. Moreau,
Theodore A. Tyler, and **Karl Weiss**
Northeastern University
Boston, Massachusetts

Transfer Apparatus for Degassed Solutions

In many liquid phase photochemical experiments, the rigorous exclusion of oxygen is necessary. This is usually accomplished by subjecting solutions to repetitive liquid nitrogen freeze-thaw cycles on a high vacuum line. When the photochemical change is completely reversible in the dark, a given sample may be used for many experiments. However, most photochemical reactions are irreversible, and in these cases repetitive experiments require the preparation of many individual samples. This is extremely time-consuming. Also, if a number of different sample cells are employed, slight differences between them and non-uniform solvent loss lead to poor reproducibility of results. We have developed a sampling apparatus which overcomes these problems, and which has been successfully used in flash photolysis and spectrophotometric kinetic studies. All glass construction is preferred since the greaseless O-ring seals recommended by Hanrahan[1] are susceptible to slow attack by solvents such as tetrahydrofuran.

The degassing bulb[2] *A* (see figure) is filled with solution by means of a narrow funnel which is inserted into the ring-sealed tube *D*. The assembly is connected to an "L"-shaped arm of the vacuum line (ball and socket joints), so that bulb *A* is held in a vertical position for efficient freezing. Degassing is carried out in the usual manner with magnetic stirring during the thawing cycles. If desirable, the solvent can be trap-to-trap distilled between flasks *A* and *B*. After degassing, the assembly is sealed at *E*, and solution is poured into the reaction vessel *C* by tipping. After the experiment, the contents of *C* are transferred, again by tipping, into the waste reservoir *B*. The reaction vessel is then rinsed with a small quantity of fresh solution and is refilled for the next run.

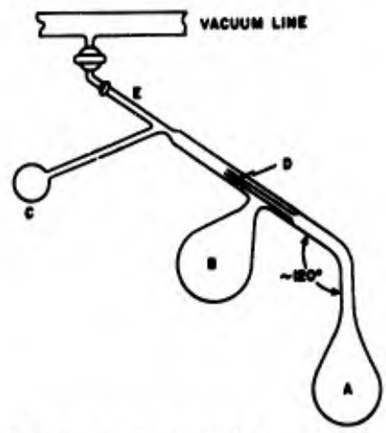

Transfer assembly attached to vacuum line.

In one application of the apparatus, *C* is a cylindrical flash photolysis cell (14.0 cm path length, 25 ml capacity), and vessels *A* and *B* can each accommodate 500 ml of solution. This quantity suffices for 22 flash experiments, which would have required the same number of sample preparations. A smaller version of the assembly is suitable for repetitive photochemical electron spin resonance experiments.[3]

This apparatus was developed in the course of research sponsored by the U. S. Air Force Cambridge Research Laboratories, Office of Aerospace Research (Contract AF19(628)-3836), and by the Department of Health, Education, and Welfare, Public Health Service (Grant RH00302-02).

[1] Hanrahan, R. J., *J. Chem. Educ.*, 41, 623 (1964).
[2] "Pyrex" Kjeldahl flasks make reliable degassing bulbs.

[3] Rabold, G. P., Bar-Eli, K. H., Reid, E., and Weiss, K., *J. Chem. Phys.*, 42, 2438 (1965).

APPENDIX D

BLANK PAGE

Reprinted from Proceedings of the Chemical Society, October, 1964, page 332

The Photochemistry of Phenalen-1-one

By H. Köller, G. P. Rabold, K. Weiss*, and T. K. Mukherjee†

Irradiation of aromatic ketones generally gives bimolecular reduction products,[1] whereas $\alpha\beta$-unsaturated ketones dimerise to cyclobutanes.[2] Dimerisation is still the preferred reaction if the double bond is conjugated with an aromatic ring. The combination of these structural features in phenalen-1-one (I) leads to unique behaviour.

Although irradiation of ketone (I) in outgassed benzene, methylcyclohexane, or carbon tetrachloride (100-w mercury lamp, 20—75 hr.) results in only slight change, the solution in propan-2-ol becomes deep green after a few minutes (see Figure). Identical

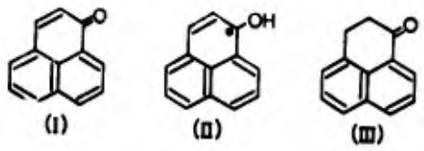

(I) (II) (III)

absorption bands are produced in methanol, ethanol, ethyl acetate, and acetone. In propan-2-ol, the colour shows first-order decay in the dark ($k = 4{\cdot}1 \times 10^{-3}$ min.$^{-1}$ at 25°); in the other solvents, the decay is more complex. Oxygen or iodine immediately discharges the colour. In basic solution a deep orange-red colour is produced (see Figure), which is also oxygen-sensitive and decays more slowly ($k = 3{\cdot}2 \times 10^{-3}$ min.$^{-1}$ at 25°). Strong electron spin resonance (e.s.r.) signals are associated with the coloured solutions: a 24-line spectrum of six quartets (neutral) and a six-line spectrum (basic). We assign these spectra to the 1-hydroxyphenalen-1-yl radical (II) and its anion, respectively,[3] which have been previously detected by polarography.[4] However, the optical spectra shown in the Figure are not due to these radicals. This conclusion is based on (1) a faster e.s.r. signal decay ($k = 0{\cdot}18$ min.$^{-1}$)[3] than optical decay, (2) the absence of transient colour in diphenylmethane solutions which show the 24-line e.s.r. spectrum, and (3) the approximate equality of the rate of colour formation observed by flash technique and the rate of radical decay.

In propan-2-ol and methanol, irradiation produces at least six compounds. 2,3-Dihydrophenalen-1-one (III) as isolated in both solvents in 13% yield [based on converted ketone (I)]. In diphenylmethane, the ketone (III) is the major product. This direct photochemical reduction of a double bond appears to be without precedent, although a sensitised reduction has been reported.[5] The propanol reaction also furnished two yellow compounds, which have analytical and spectral data consistent with their being diketonic dimers of ketone (I). No acetone was detected, and an attempt to trap

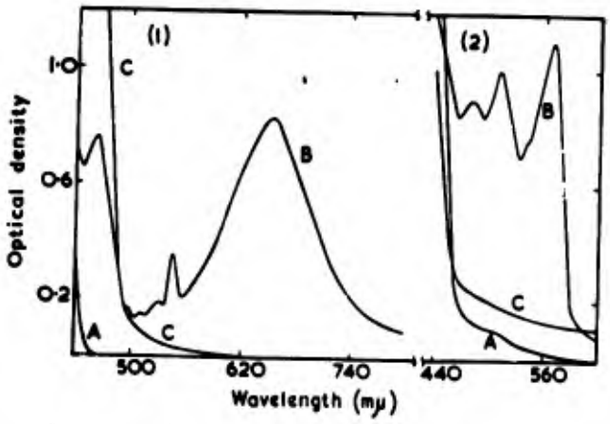

Spectra of intermediates from 1×10^{-3}M-*phenalen-1-one in* (1) *propan-2-ol, and* (2) 0·1M-*NaOH* (2·3 : 1 *propan-2-ol–water*: (*A*) *before*, (*B*) *immediately after irradiation*, (*C*) *after admission of oxygen.*

* Department of Chemistry, Northeastern University, Boston 15, Mass., U.S.A.
† Energetics Branch, Air Force Cambridge Research Laboratories, Bedford, Mass., U.S.A.

[1] G. Porter and P. Suppan, *Proc. Chem. Soc.*, 1964, 191; J. N. Pitts, Jr., H. W. Johnson, Jr., and T. Kuwana, *J. Phys. Chem.*, 1962, **66**, 2456, and references cited therein.
[2] P. E. Eaton, *J. Amer. Chem. Soc.*, 1962, **84**, 2344; A. Mustafa, *Chem. Rev.*, 1952, **51**, 1.
[3] G. P. Rabold and K. Weiss, manuscript in preparation.
[4] H. Berg, Preprints Fifth Internat. Symp. on Free Radicals, Uppsala, 1961, paper 8; H. Beckmann, *Austral. J. Chem.*, 1961, **14**, 229; H. Beckmann and P. Silberman, *Chem. and Ind.*, 1955, 1635.
[5] G. W. Griffin and E. J. O'Connell, *J. Amer. Chem. Soc.*, 1962, **84**, 4148.

$HO{\cdot}CMe_2{\cdot}$ radicals as terebinic acid by the addition of maleic acid[6] failed.

The transient colours are reminiscent of the intermediate in the photo-reduction of benzophenone in propan-2-ol, for which radical structures could not be confirmed by e.s.r. measurements.[7] Our results leave little doubt that the radicals generated by reaction of excited ketone with solvent are precursors of the coloured diamagnetic intermediates. The latter appear to incorporate the solvent or a solvent-derived oxidation product. Significantly, solvents in which colour is observed either bear carbonyl groups or can give rise to them by oxidation. Although the sensitivity to oxygen and iodine may be an intrinsic property of the intermediate, it is more likely to be due to an equilibrium with radicals in which the diamagnetic molecule is heavily favoured.

(*Received, August 5th*, 1964.)

[6] Cf. G. O. Schenck, G. Koltzenburg, and H. Grossmann, *Angew. Chem.*, 1957, **69**, 177.
[7] G. O. Schenck, W. Meder, and M. Pape, Proc. Internat. Conf. Peaceful Uses At. Energy, Geneva, 1958, **29**, 352; J. H. Sharp, T. Kuwana, A. Osborne, and J. N. Pitts, Jr., *Chem. and Ind.*, 1962, 508; J. N. Pitts, Jr., R. L. Letsinger, R. P. Taylor, J. M. Patterson, G. Recktenwald, and R. B. Martin, *J. Amer. Chem. Soc.*, 1959, **81**, 1068.

Paramagnetic Hyperfine Splitting by Hydroxylic Hydrogen

BY

G. P. RABOLD, K. H. BAR-ELI, and K. WEISS

Reprinted from CHEMICAL COMMUNICATIONS, No. 3,
10 February, 1965, Page 33.

LONDON:
THE CHEMICAL SOCIETY
BURLINGTON HOUSE, W.1

Paramagnetic Hyperfine Splitting by Hydroxylic Hydrogen

By G. P. Rabold, K. H. Bar-Eli, and K. Weiss

(*Department of Chemistry, Northeastern University, Boston, 15, Mass., U.S.A.*)

Hyperfine interaction between an electron spin and the nuclear spin of a proton attached to oxygen in an organic radical has been observed in only a few instances.[1] We now report the high resolution electron spin resonance spectrum of the 1-hydroxyphenalen-1-yl radical (I) and its interpretation on the basis of McLachlan MO-SCF theory,[2] which allow an estimate to be made of Q_{OH}, the spin density transmission parameter for the OH σ-bond.

The irradiation of phenalen-1-one in propan-2-ol gives rise to a dark green solution which is paramagnetic.[3] At moderate modulation amplitude the spectrum consists of six quartets with splitting

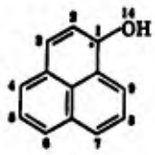

(I)

constants (6·21 and 1·68 gauss) and intensities which clearly show them to arise from groups of protons at positions 3, 4, 6, 7, and 9 and at positions 2, 5, and 8, respectively, of radical (I). Under optimized irradiation and resolution conditions,

E.s.r. spectrum of radical (I) from the photolysis of 1×10^{-3}M-*phenalen-1-one in propan-2-ol.*

the spectrum is further resolved into 100 lines (see Figure). Splitting by hydrogen on oxygen is reflected in the terminal doublets of equal intensity. The inner multiplets are due to small differences within the two groups of ring protons which are satisfactorily predicted by the McLachlan calculation (see Table), but not by Hückel MO theory. The spin density distribution is compatible with a six-constant model with CH splittings of 6·40, 6·26, 6·12, 1·73, and 1·58 gauss, and an OH splitting of 0·14 gauss, which accurately reproduce the spectrum. If McConnell's equation[4] is applicable in the form $a_{OH} = Q_{OH}\rho_{OH}$, the results furnish $Q_{OH}/Q_{CH} = 0{\cdot}29$. With $|Q_{CH}| = 24{\cdot}2$ gauss,[5] this gives $|Q_{OH}| \approx 7$ gauss. Actually better agreement between the observed and calculated spin densities is obtained with $|Q_{CH}| = 27$ gauss, which raises $|Q_{OH}|$ to about 8 gauss.

The configuration interaction model developed by McConnell[4,5] can be used to provide an independent estimate of Q_{OH}. If it is assumed that an odd electron localized on the oxygen atom can be represented by a neutral hydroxyl radical, this approach leads to the equation

$$\frac{Q_{OH}}{Q_{CH}} = \frac{(J_{p_z p_z} - J_{p_z s})_{OH}\,(1 - S_C{}^4)\,\Delta E_{21}^{CH}}{(J_{p_z h} - J_{p_z s})_{CH}\,(1 - S_O{}^4)\,\Delta E_{21}^{OH}}$$

Values for the exchange integrals, J, between the indicated orbitals ($h = sp^2$), and for the overlap integrals S_O and S_C ($<p/s>$ and $<h/s>$ for OH and CH, respectively) were obtained from published data. The ratio of the energy differences (ΔE_{21}) between the doublet ground and excited states was taken as equal to the ratio of the lowest transitions of CH and OH radicals. The calculation[6] yields $Q_{OH}/Q_{CH} \approx 0{\cdot}3$ and, with $|Q_{CH}| =$

Spin densities in radical (I)

Position	2	5	8	6	4	7	3	9	14
ρ_i (calc.)* ..	−0·058	−0·068	−0·067	0·240	0·230	0·230	0·217	0·219	0·018
ρ_i (obs.)† ..	0·058	⌙ 0·064 ⌚		0·237	⌙ 0·231 ⌚		⌙ 0·226 ⌚		0·017

* $\lambda = 1{\cdot}2$, cf. ref. 2. MO parameters $h = 2{\cdot}0$, $k = 1{\cdot}0$ in $\alpha_O = \alpha + h\beta$ and $\beta_{OC} = k\beta$ (α's coulomb integrals, β's exchange integrals) give best fit within narrow limits.

† $\rho_i = a_i/27$ for positions 2—9; $\rho_{14} = a_{OH}/8$.

[1] W. T. Dixon and R. O. C. Norman, *J.*, 1963, 3119; J. R. Bolton, A. Carrington, and J. dos Santos-Veiga, *Mol. Phys.*, 1962, **5**, 465; L. H. Piette, G. Bulow, and K. Loeffler, Preprints, Symposium on the Use of e.s.r. in the Elucidation of Reaction Mechanisms, 1964, **9**, No. 2C, p. C-9.

[2] A. D. McLachlan, *Mol. Phys.*, 1960, **3**, 233.

[3] H. Köller, G. P. Rabold, K. Weiss, and T. K. Mukherjee, *Proc. Chem. Soc.*, 1964, 332.

[4] H. M. McConnell, *J. Chem. Phys.*, 1956, **24**, 632, 764.

[5] H. M. McConnell and D. B. Chesnut, *J. Chem. Phys.*, 1958, **28**, 107.

[6] For details cf. G. P. Rabold, K. H. Bar-Eli, E. Reid, and K. Weiss, *J. Chem. Phys.*, to be published.

24—27 gauss, $|Q_{OH}| \approx 7$—8 gauss, which supports the experimentally derived assignment.

The presence of non-bonding electrons on oxygen and its greater electronegativity may cause hydroxylic proton splitting to be more sensitive to the medium than CH proton splitting. It remains to be established with further experimental examples whether Q_{OH} is as independent of the environment as Q_{CH} appears to be.[7]

(*Received, December 21st*, 1964.)

[7] Cf. J. Gendell, F. H. Freed, and G. K. Fraenkel, *J. Chem. Phys.*, 1962, **37**, 2832.

BLANK PAGE

Reprinted from THE JOURNAL OF CHEMICAL PHYSICS, Vol. 42, No. 7, 2438–2447, 1 April 1965
Printed in U. S. A.

Photochemically Generated Free Radicals. I. The Perinaphthenone System

GARY P. RABOLD,* KEDMA H. BAR-ELI, ERIC REID, AND KARL WEISS
Photochemistry and Spectroscopy Laboratory, Department of Chemistry, Northeastern University, Boston, Massachusetts
(Received 24 November 1964)

The photolysis of perinaphthenones in 2 propanol generates the corresponding hydroxyperinaphthenyl radicals which are relatively stable at room temperature. The electron spin resonance spectra can in most cases be interpreted in terms of splitting by two distinct groups of protons. Under high-resolution conditions small differences within these groups become apparent, and splitting by hydrogen on oxygen is observed. Detailed assignments are made on the basis of McLachlan MO-SCF calculations. The data indicate that $|Q_{OH}| \approx 7$ G. The same value is obtained by a calculation based on the configuration-interaction model of McConnell.

I. INTRODUCTION

FREE radicals are postulated to be intermediates in many photochemical reactions and, in a number of instances, have been detected by direct measurements. Both electron spin resonance and absorption spectroscopy have been used for this purpose. By means of the former it has been possible to identify the radicals in the photolysis of peroxides[1] and in the photolysis of a number of other systems whose photochemistry is less clearly delineated.[2–6] Transient absorptions observed during the flash photolysis of aromatic carbonyl compounds have been assigned to hydroxylic radicals of the type $R_2\dot{C}OH$.[7–9] In the case of benzophenone, the corresponding radical could be observed by ESR measurements at −150°, but not at room temperature.[10] On the other hand, photolysis of aromatic ketones in basic solution furnishes sizable concentrations of radicals even at room temperature.[11,12]

In this paper we describe the radicals obtained during the photolysis of perinaphthenones (Fig. 1). The parent compound, perinaphthenone [Fig. 1(a)], in inert solvents such as benzene or methylcyclohexane undergoes very little change on prolonged photolysis. By contrast, photolysis in hydrogen-donating solvents such as 2-propanol, methanol, ethanol, ethyl acetate, or acetone rapidly produces a deep green color (λ_{max} 650 mμ) which decays slowly in the dark.[13] From the reactions in 2-propanol and methanol, perinaphthanone [Fig. 2(b)] and dimeric products were isolated. The reduced compound is considered to arise from the

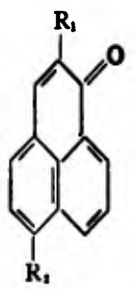

FIG. 1. Structure of perinaphthenones photolyzed: (a) $R_1 = R_2 = H$; (b) $R_1 = H$, $R_2 = OH$; (c) $R_1 = Br$, $R_2 = H$.

hydroxyperinaphthenyl radical [Fig. 2(a)], which is formed via hydrogen abstraction by excited ketone from the alcohol.[13] Indeed, strong electron spin resonance signals are associated with the irradiated solutions. Irradiation in diphenylmethane generates radicals but no transient color. This finding, in conjunction with kinetic measurements and a flash-photolysis experiment, has led us to conclude that the color is not due to the radical. The hydroxyperinaphthenyl radical has previously been reported to be formed by polarographic reduction,[14] and its decay has been measured by flash polarography.[15]

In the evaluation of the spectra we utilize McConnell's relationship between and proton hyperfine splitting (HFS) and the spin density on the carbon atom to

* National Science Foundation Cooperative Research Fellow, 1963–1965.
[1] L. H. Piette and W. C. Landgraf, J. Chem. Phys. **32**, 1107 (1960).
[2] M. C. R. Symons and M. G. Townsend, J. Chem. Soc. **1959**, 263 (peroxides, azobisisobutyronitrile, ethyl iodide).
[3] P. B. Ayscough, F. P. Sargent, and R. Wilson, J. Chem. Soc. **1963**, 5418; C. Lagercrantz and M. Yhland, Acta Chem. Scand. **16**, 1799 (1962); R. L. Ward, J. Chem. Phys. **38**, 2588 (1963) (nitro compounds).
[4] C. Lagercrantz and M. Yhland, Acta Chem. Scand. **16**, 1043 (1962) (*p*-chloranil).
[5] R. L. Ward, J. Chem. Phys. **39**, 852 (1963) (tetracyanoethylene).
[6] C. S. Johnson, Jr., and H. S. Gutowsky, J. Chem. Phys. **39**, 58 (1963); F. Bruin, F. W. Heineken, M. Bruin, and A. Zahlen, *ibid.* **36**, 2783 (1962) (viologens).
[7] A. Becket, A. D. Osborne, and G. Porter, Trans. Faraday Soc. **60**, 873 (1964); A. Becket and G. Porter, *ibid.* **59**, 2038 (1963), and earlier references cited.
[8] J. A. Bell and H. Linschitz, J. Am. Chem. Soc. **85**, 528 (1963).
[9] W. A. Bryce and C. H. J. Wells, Can. J. Chem. **41**, 2722 (1963).
[10] J. H. Sharp, T. Kuwana, A. Osborne, and J. N. Pitts, Jr., Chem. Ind. (London) **1962**, 508.
[11] P. B. Ayscough and F. P. Sargent, Proc. Chem. Soc. **1963**, 94.
[12] G. A. Russell and E. J. Geels, Tetrahedron Letters **1963**, 1333.
[13] H. Köller, G. P. Rabold, K. Weiss, and T. Mukherjee, Proc. Chem. Soc. **1964**, 332.
[14] H. Beckmann, Australian J. Chem. **14**, 229 (1961).
[15] H. Berg, Paper 8, preprints, Fifth International Symposium on Free Radicals, Uppsala, Sweden, 1961.

which it is attached.[16] The latter are calculated from the MO-SCF theory of McLachlan,[17] which has been shown in numerous applications to provide better agreement with experimental results than simple Hückel MO theory. If a reasonable spin density appears on the oxygen atom of the radical of Fig. 2(a), hyperfine splitting by the attached hydrogen atom can be expected. The interpretation based on the MO-SCF method indicates this indeed to be the case.

II. EXPERIMENTAL

Perinaphthenone (from the Aldrich Chemical Company or synthesized[18]) contained perinaphthanone and another impurity. These were removed by careful chromatography on a Merck silica gel column using benzene as eluent. The purified material had mp 154°–155° (reported[18] 154°–155°). 6-Hydroxyperinaphthenone was synthesized[19] and had the reported physical properties. 2-Bromoperinaphthenone was prepared by bromination of perinaphthenone.[20a] Material twice recrystallized from ethanol had mp 152°–152.5° (reported[20a] 152°–152.4°). All solvents were of the best available reagent grade. 2-Propanol was refluxed for several hours over magnesium ribbon and then distilled through a Podbielniak column using a large reflux ratio. Acetone was purified by a similar distillation. Diphenylmethane was recrystallized several times from pentane. Benzene was purified by preparative-scale gas chromatography. All these materials were shown to be pure by gas chromatography. Tetrahydrofuran, previously stored over potassium hydroxide, was distilled from lithium aluminum hydride into a vessel containing fresh hydride. This material was then attached to a vacuum line and distilled trap to trap for subsequent use. 1,2-Dimethoxyethane (DME) was stored over sodium hydroxide and similarly distilled from calcium hydride.

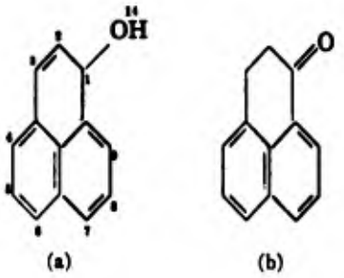

FIG. 2. Structures of (a) the hydroxyperinaphthenyl radical and (b) perinaphthanone.

All samples were thoroughly degassed by the freeze–pump–thaw method using liquid nitrogen as coolant and were sealed under vacuum. The degassing bulb was attached as a sidearm to the reaction vessel, which was either a 1-mm×11mm×44-mm flat Pyrex or quartz cell, or a 4-mm-o.d. Pyrex tube. Because basic solutions of perinaphthenone undergo a slow chemical reaction, it was necessary in these experiments to outgas the base solution and perinaphthenone solution separately and then mix them immediately before the photolysis. The sodium ketyls were prepared by placing solid perinaphthenone in the degassing bulb, triply distilling sodium into a separate sidearm, and then distilling the solvent into the bulb containing the ketone. This solution was then degassed and sealed. Under these conditons the sodium ketyls appear to be stable indefinitely. Dilution studies in the sealed system could be made by distilling solvent from the sidearm into the main tube.

The irradiations were accomplished with a 100-W General Electric H-100 series mercury lamp or a 500-W Osram HBO-500 mercury lamp. Both lamps were focused onto the sample cell in the spectrometer cavity with two double-convex Pyrex lenses. Perinaphthenone has a well-defined absorption band at 359 mμ, and the substituted compounds have similar absorption characteristics. The Pyrex thus serves as a filter for the more energetic mercury lines.

The standard Varian V-4500 spectrometer with 100-kc/sec modulation and a 6-in. magnet was used. The low-temperature spectra were also obtained with the standard Varian attachment. Fremy's salt was used as the calibration standard for determining linewidths and splitting constants. The larger splitting constants are estimated to be reliable to ±0.05 G. Kinetic measurements were carried out by riding a major peak of the first-derivative curve. This allowed both the rate of formation and the rate of decay to be followed.

III. RESULTS

A. Hydroxyperinaphthenyl Radical

The spectra described here were obtained by photolysis of solutions of perinaphthenone in 2-propanol. The same spectra are observed in acetone, methanol, and diphenylmethane as solvents. The HFS constants for this, and for the other radicals discussed below, are summarized in Table I. The numbering system of Fig. 2(a) is used in all cases.

1. Low-Resolution Spectrum

At moderate modulation amplitudes the spectrum consists of six main groups of lines separated by 6.21 G.

[16] H. M. McConnell, J. Chem. Phys. **24**, 632, 764 (1956).
[17] A. D. McLachlan, Mol. Phys. **3**, 233 (1960).
[18] L. F. Fieser and F. B. Hersberg, J. Am. Chem. Soc. **60**, 1658 (1938).
[19] R. G. Cooke, B. L. Johnson, and W. Segal, Australian J. Chem. **11**, 230 (1958).
[20] (a) L. F. Fieser and L. W. Newton, J. Am. Chem. Soc. **64**, 917 (1942); (b) this 24-line spectrum was first observed by A. Golubovic, to whom we are also grateful for assistance with the early spectral measurements.

TABLE I. HFS constants for perinaphthenyl radicals.

Spectrum	Fig.	HFS constants[a,b]								
		$\bar{a}$	$\bar{b}$	a_1	a_2	a_3	b_1	b_2	c	s
Perinaphthenyl[e]		7.3 (5.46)	2.2 (1.66)							
Hydroxyperinaphthenyl	3	6.21 (5.54)	1.68 (1.55)							
Hydroxyperinaphthenyl	4			6.40 (5.81)	6.26 (5.57)	6.12 (5.29)	1.58 (1.41)	1.73 (1.63)	0.14 (0.13)[d]	
Hydroxyperinaphthenyl anion	5	5.62 (5.22)					0.86 (0.80)	1.53 (1.45)		
Sodium ketyl of perinaphthenone (+25°)	6	5.44					0.15	1.36		0.30
Sodium ketyl of perinaphthenone (−94°)	7	5.38						1.28		
Dihydroxyperinaphthenyl (−39°)	8	6.34 (5.37)	1.72 (1.51)				(1.46)[e]	(1.61)[e]	(0.16)[d]	
Bromohydroxyperinaphthenyl		6.22	1.60							

[a] Values in brackets are calculated from Eq. (1) with $Q_{CH} = 24.2$ G.
[b] Constants a refer to Positions 3, 4, 6, 7, and 9, Constants b to Positions 2, 5, and 8, Constant c to oxygen, and Constant s to sodium; $\bar{a}$ and $\bar{b}$ are averages of unresolved constants.
[e] Reference 21.
[d] Calculated with $Q_{OH} = 7$ G.
[e] Here b_1 refers to Positions 2 and 5 and b_2 to Position 8.

Each group consists of four lines spaced 1.68 G apart (Fig. 3).[20b] Within each quartet the intensity ratios are approximately 1:3:3:1, while the ratios for the six quartets are 0.94:4.9:10:10:4.9:0.9. Some indication of further splitting is evident in some of the lines. The number of lines and their intensities suggest splitting by a set of five equivalent protons and another set of three equivalent protons. From Fig. 2(a) one can deduce that these sets refer to the protons at Positions 3, 4, 6, 7, and 9 and at Positions 2, 5, and 8, respectively. These sets are designated as α protons and β protons, and the corresponding HFS constants as a and b. The spectrum resembles that of the perinaphthenyl radical described by Sogo, Nakazaki, and Calvin,[21] which shows seven quartets with somewhat larger splitting constants in the expected intensity ratios. It is evident that although introduction of the hydroxyl group in the 1 position destroys the symmetry of the molecule, the spin-density distribution is changed relatively little. This is borne out by the molecular orbital calculations discussed in Sec. IV, which correctly place the highest spin densities in the α positions.

FIG. 3. Hydroxyperinaphthenyl radical from photolysis of $1\times10^{-3}M$ perinaphthenone in 2-propanol.

[21] P. B. Sogo, M. Nakazaki, and M. Calvin, J. Chem. Phys. 26, 1343 (1957).

2. *High-Resolution Spectrum*

By optimizing the irradiation intensity and operating with low modulation amplitude at higher power levels, it was possible to obtain the further resolved spectrum of Fig. 4. The individual members of the quartets are now seen to be split in a regular pattern. The total number of lines is 100, consisting of the sets 2, 3, 3, 2; 4, 5, 5, 4; 5, 6, 6, 5; 5, 6, 6, 5; 4, 5, 5, 4; 2, 3, 3, 2. The pattern is indicative of small differences in the a and b HFS constants, as well as of splitting by the hydroxyl proton which is discussed in detail in Sec. IV. The six HFS constants a_1, a_2, a_3, b_1, b_2, and c(for the oxygen) which are listed in Table I were assigned on the basis of the MO calculations. They reproduce the observed spectrum remarkably well.

B. Hydroxyperinaphthenyl Anion Radical

The optical spectrum of perinaphthenone is changed very little by the addition of aqueous sodium hydroxide to its solution in 2-propanol, but on standing in the dark decomposition slowly occurs. However, by working with freshly prepared solutions (see Sec. II) it was possible to obtain reproducible spectra which are

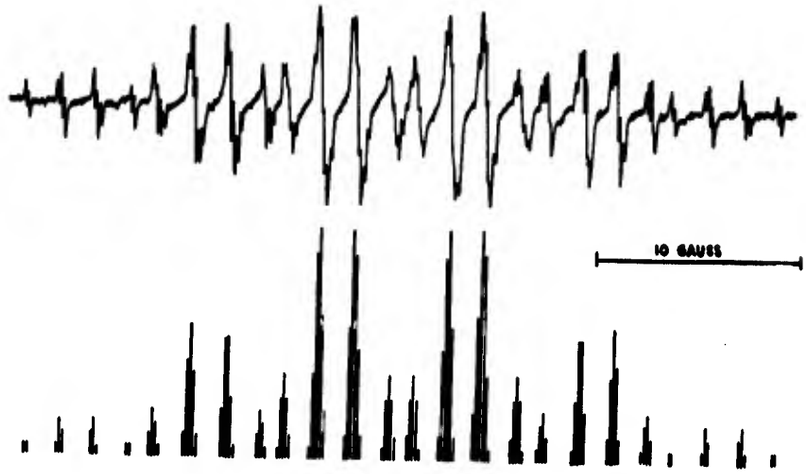

FIG. 4. Hydroxyperinaphthenyl radical from photolysis of $1\times10^{-3}M$ perinaphthenone in 2-propanol at high resolution, and its theoretical reconstruction.

ascribed to the radical anion of perinaphthenone. At the concentration of sodium hydroxide employed ($0.1M$) there can be little doubt that the neutral radical is completely dissociated. The irradiated solution is red, but in view of the properties of irradiated neutral solutions[13] it is not possible to ascribe the color to the anion radical without kinetic experiments.

In concentrated solution, the spectrum consists of six equally spaced lines. In dilute solution, where exchange between the anion radical and the ketone is minimized, the six sextets shown in Fig. 5 are obtained. The intensities for the small sextets are approximately 1:1:2:2:1:1, while for the major sextet they are 1:4.5:9.5:9.5:4.5:1. The high resolution achieved in neutral solution was not attainable. This spectrum is adequately analyzed in terms of three HFS constants, a, b_1, and b_2 (Table I), with the latter in the approximate ratio 1:2. Differences in the a values indicated by the MO calculations remain unresolved. These calculations allow assignment of b_1 to Position 2 and b_2 to Positions 5 and 8.

C. Sodium Ketyl of Perinaphthenone

Ketyls are prepared by addition of the metal to the ketone in an aprotic solvent. These compounds differ from the corresponding radical anions in that there is strong association between the anion and metal ion. It was of interest to compare the spectra of these two species of perinaphthenone. The first preparations were carried out in tetrahydrofuran. However, the spectrum obtained was exceedingly complex and assymmetrical, and no attempt was made to interpret it. Better results were obtained in DME, which also gave a red solution. A typical room-temperature spectrum is shown in Fig. 6. Splitting by sodium is immediately evident, which is no longer the case at $-94°$ (Fig. 7). These spectra are discussed in some detail in Sec. IV, and here it is merely noted that the basic sextet structure is retained (Table I).

D. Dihydroxyperinaphthenyl Radical

This radical [cf. Fig. 1(b)] has C_{2v} symmetry and is thus expected to show a more symmetrical spin-density pattern than the monohydroxy radical. On the basis of one less α position, a spectrum of five quartets is predicted and obtained (Fig. 8). The intensity ratios are 1.1:5.0:5.9:5.0:1.1 (predicted 1:4:6:4:1) for the quintet and about 1:3:3:1 for the quartets. The parent ketone is highly fluorescent, and the quantum yield of the radical is low. Consequently it was necessary to

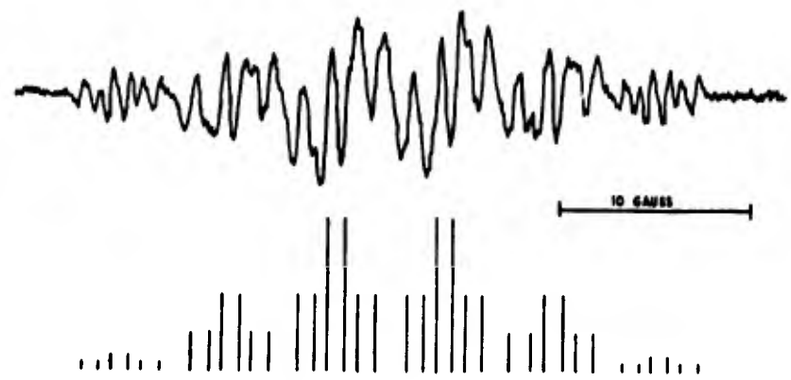

FIG. 5. Hydroxyperinaphthenyl anion radical from photolysis of $1.2\times10^{-3}M$ perinaphthenone in 4:1 2-propanol/water $0.1M$ in NaOH, and its theoretical reconstruction.

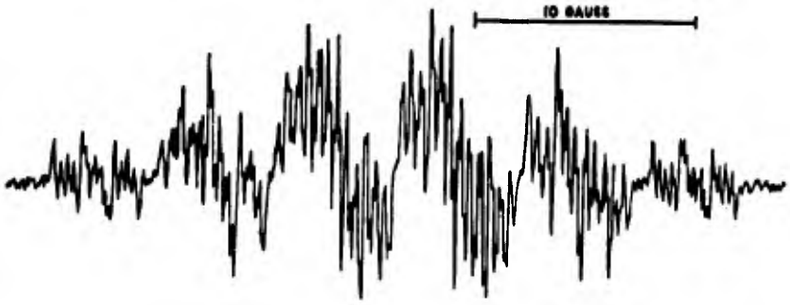

FIG. 6. Sodium ketyl of perinaphthenone in DME at 25°.

work at low temperature (−39°) and at relatively high modulation amplitude and power levels in order to observe the spectrum. Predicted small differences in the b splitting constants were not resolved. The measured constants are quite close to those of the hydroxyperinaphthenyl radical (Table I).

E. Other Perinaphthenyl Radicals

2-Bromoperinaphthenone [Fig. 1(c)] surprisingly showed a six-quartet spectrum which closely resembles that of the monohydroxy radical with respect to HFS constants (Table I) and intensities. Analysis in terms of splitting by bromine leads to unsatisfactory intensity ratios. It is surmized that the excited state of this ketone, or the radical initially formed from it, loses halogen and is converted to perinaphthenone. The spectrum observed would thus be that of the hydroxyperinaphthenyl radical. This point deserves further study from the chemical point of view.

The sodium salt of dicyanomethyleneperinaphthene [perinaphthenone in which C=O is replaced by C=C(CN)$_2$] in tetrahydrofuran gives a spectrum which is similar to that of the sodium ketyl.[22] The basic sextet shows a separation of 6.5 G. Further splitting due to sodium, differences within the α positions and β positions, and possibly nitrogen is evident.

IV. DISCUSSION

A. Molecular Orbital Calculations

Tentative assignments of splitting constants to particular protons could be made from structural considerations alone for the spectra which are only partially resolved. In these cases MO calculations provide meaningful confirmation. These calculations were essential for the interpretation of the further splitting observed under high-resolution conditions. The experimentally measured splitting constants were compared with those calculated from McConnell's equation[16]

$$a_i = Q_{CH}\rho_i, \qquad (1)$$

where a_i is the splitting due to the ith proton and ρ_i is the spin density on the adjacent carbon atom. Various values have been proposed for Q_{CH}.[22,24] We have used the value −24.2 G, which was derived by McLachlan[17] from the spectra of several hydrocarbons by an averaging procedure. The McLachlan MO–SCF theory introduces spin correlation by treating the exchange interactions between the odd electron and electron and electrons having the same spin as the odd electron as small perturbations. Hückel orbitals are

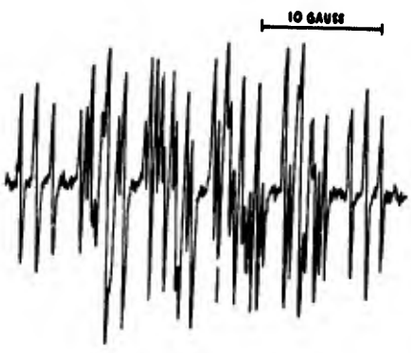

FIG. 7. Sodium ketyl of perinaphthenone in DME at −94°.

FIG. 8. Dihydroxyperinaphthenyl radical from photolysis of $1\times10^{-2}M$ 6-hydroxyperinaphthenone in 2-propanol at −39°.

[22] T. K. Mukherjee and A. Golubovic, Abstracts, 148th National Meeting, American Chemical Society, Chicago, Illinois, 1964, p. 84S.

[22] R. W. Fessenden and S. Ogawa, J. Am. Chem. Soc. **86**, 3591 (1964).

[24] G. Vincow and G. K. Fraenkel, J. Chem. Phys. **34**, 1333 (1961).

used, and the spin densities are given by

$$\rho_i = C_{0i}^2 + \sum_1^n (C_{ni}'^2 - C_{ni}^2), \quad (2)$$

where C_{0i} and C_{ni} are the Hückel coefficients for the odd electron and lower occupied orbitals, respectively. The coefficients C_{ni}' represent orbitals occupied by the spin-correlated electrons, which are obtained by replacing the Hückel Coulomb integral α_i by α_i':

$$\alpha_i' = \alpha_i + 2\lambda C_{0i}^2 \beta. \quad (3)$$

In this equation, β is the bond integral and λ is a constant perturbation parameter. The oxygen atom is accommodated in the usual manner by setting $\alpha_0 = \alpha + h\beta$ and $\beta_{c0} = k\beta$. The calculation of ρ_i thus involves computing orbital coefficients from a Hückel matrix, and using the results to construct a new matrix with the Coulomb integrals of Eq. (3). The Jacobi method,[25] written in a FORTRAN program for the IBM 7094 computer, conveniently solved these matrices.

The parameters h and k were varied over the range 0–2.0. This includes all the values which have been used to modify the oxygen integrals,[26] and the lower limit provides a means of checking the results of each set of calculations. The auxiliary inductive parameter[26] for the carbon atom connected to the carbonyl group was neglected since it introduces only a very small change, and it was preferred to utilize only three empirical constants. The value of λ was taken as 1.2 in all cases.[17] For the neutral radicals (hydroxyperinaphthenyl, dihydroxyperinaphthenyl) in which the oxygen-core potential is +2, a reasonable spin-density pattern was obtained with $h = 2.0$ and $k = 0.8$–1.2. Correlation with the observed splittings showed $k = 1.0$ to be the best value within narrow limits. Similarly, for the hydroxyperinaphthenyl anion with an oxygen-core potential of +1, $h = 1.0$ and $k = 1.0$ gave the best agreement with the experimental data. It may be noted that the application of McLachlan theory to some cyclic ketyls and *o*-semiquinones gave good results $h = 1.5$–1.6 and $k = 1.3$–1.6 when small changes in the carbon–carbonyl and inter-ring carbon-bond integrals were included.[27]

In the ranges of h and k values examined, the relative spin-density variations at the β positions and oxygen are greater than at the α positions. The general trends are: (1) Increasing k at constant h causes the spin densities at the α positions to rise to a shallow maximum, for example, with $h = 1.0$ ρ_6 has a maximum value of 0.229 at $k = 0.6$. With $h = 2$, ρ_3 and ρ_5 decrease continuously, while ρ_4, ρ_6, and ρ_7 show maxima. At Positions 5 and 8, the densities become less negative. This effect is more marked at higher h values. On the other hand, ρ_2 rises to positive values above $k = 1.4$–1.6. On the oxygen atom, the density increases with increasing k. With $h = 1.0$, there is a shallow maximum at $k = 1.6$, which is not shown with $h = 2.0$. (2) Increasing h at constant k causes the densities at the α positions to increase continuously. With $k = 1.0$ this change is from ~0.1 to ~0.24. At Position 2 the values are initially positive, but become negative above $k = 0.6$. At Positions 5 and 8 the densities become uniformly more negative, while on the oxygen atom they are always positive and increase.

B. Analysis of the Results

Spin densities at the pertinent positions [cf. Fig. 2(a)] are shown in Table II. The extra oxygen atom in the dihydroxy radical is assigned Position 15. Perinaphthenyl is included for comparison; the spin densities shown agree closely with those calculated by McLachlan.[17] For this radical, HMO theory predicts zero odd-electron density at Positions 2, 5, and 8. The introduction of the hydroxyl group at Position 1 furnishes some spin density at these positions (<0.01), but this is insufficient to account for the observed splitting. The modified SCF method provides a density distribution quite similar to that of the parent radical, although small differences are seen to exist between the individual α and β positions. Spectra measured at moderate modulation amplitudes therefore show six quartets with the expected intensity ratios.

Under conditions of high resolution the small differences in spin densities become evident as additional components. This explanation of the 100-line spectrum of Fig. 4 parallels that presented by Venkataraman, Segal, and Fraenkel for the spectrum of the *p*-tolusemiquinone ion.[28] However, the spin-density differences alone cannot account for the observed spectrum. Since the position, in gauss, of the jth line from the center of the spectrum is $|\Delta B_j| = \sum_i a_i m_i$, where $m_i = \pm\frac{1}{2}$, it is clear that the separation between the last line and the next-to-last line cannot represent a difference between splitting constants. In Fig. 4 it is seen that the outermost lines of the 24-line spectrum are cleanly split into doublets of equal intensity. This additional splitting is therefore assigned to the only other available proton, namely, that on the oxygen atom. Several alternative interpretations were considered. These were (1) a loose association between the hydroxyperinaphthenyl radical and a 2-propanol fragment such as acetone, and (2) a superposition of two spectra of slightly different g values. The first can be rejected on the basis of the number of lines, and the second would lead to an unsymmetrical composite spectrum. Further the higher basicity of the anion radical than that of

[25] O. Taussky, J. Todd, Math. Mag. **26**, 71 (1952).
[26] A. Streitwieser, Jr., *Molecular Orbital Calculations for Organic Chemists* (John Wiley & Sons, Inc., New York, 1961), Chap. 5.
[27] R. Dehl and G. K. Fraenkel, J. Chem. Phys. **39**, 1793 (1963).
[28] B. Venkataraman, B. G. Segal, and G. K. Fraenkel, J. Chem. Phys. **30**, 1006 (1959); B. Venkataraman and G. K. Fraenkel, *ibid.* **23**, 588 (1955).

TABLE II. Spin densities by the McLachlan HMO-SCF method.

Radical	ρ_1	ρ_2	ρ_5	ρ_8	ρ_6	ρ_4	ρ_7	ρ_3	ρ_9	ρ_{14}	ρ_{15}
Perinaphthenyl[a]	0.226	−0.069	−0.069	−0.069	0.226	0.226	0.226	0.226	0.226		
Hydroxyperinaphthenyl[b]		−0.058	−0.068	−0.067	0.240	0.230	0.230	0.217	0.219	0.018	
Hydroxyperinaphthenyl anion[c]		−0.033	−0.061	−0.059	0.234	0.216	0.219	0.194	0.200	0.069	
Dihydroxyperinaphthenyl[b]		−0.060	−0.060	−0.068		0.222	0.222	0.222	0.222	0.023	0.023

[a] These values agree with those reported in Ref. 17. [b] Calculated with $h=2.0$, $k=1.0$. [c] Calculated with $h=1.0$, $k=1.0$.

the ketone makes it unlikely that significant quantities of the former are present under neutral conditions.

If all the positions in the hydroxyperinaphthenyl radical are associated with significantly different spin densities, 512 lines can be expected. Table II shows the spin densities to be almost identical at Positions 5 and 8, 4 and 7, and 3 and 9. Average values of these pairs were therefore taken, which are designated as $\rho_{5,8}$, $\rho_{4,7}$, and $\rho_{3,9}$, respectively. Further, it is seen that $\rho_{5,8}-\rho_2=\rho_6-\rho_{4,7}\approx\rho_{4,7}-\rho_{3,9}$. This leads to a model with six splitting constants which, according to Eq. (1), are taken as $a_1\propto\rho_6$, $a_2\propto\rho_{4,7}$, $a_3\propto\rho_{3,9}$, $b_1\propto\rho_2$, $b_2\propto\rho_{5,8}$, and $c\propto\rho_{14}$. If cognizance is taken of the approximate nature of the MO-SCF calculations and that $Q_{OH}<Q_{CH}$ (see below), the relation

$$a_1-a_2=a_2-a_3=b_2-b_1=c \qquad (4)$$

is reasonable. The splitting constants listed in Table I and the theoretical reconstruction of Fig. 4 are based on this relation and on the average experimental splitting constants defined as $\bar{a}=\frac{1}{3}(a_1+2a_2+2a_3)$ and $\bar{b}=\frac{1}{2}(b_1+2b_2)$. This model gives the observed number of lines and reproduces the intensities correctly. Since the latter were rather difficult to glean accurately from the spectra, the reconstruction was checked by superposition of Lorentzian derivative curves for several of the multiplets.

Placing a negative charge on oxygen in the anion radical drastically reduces the spin density at Position 2, while the values for the α positions are changed little from those in the neutral radical. This effect evidently results from the decreased electronegativity of the oxygen atom in the anion relative to that in the radical. Differences between the a constants are predicted to be larger, although this could not be experimentally verified. The theoretical reconstruction of Fig. 5 is based on the three constants $\bar{a}$, b_1, and b_2 and is in good agreement with the spectrum.

No complete analysis was attempted for the complex spectra of the sodium ketyl of perinaphthenone. Useful deductions could, however, be made from the terminal members of the sextet. Retention of this basic six-line structure indicates that the largest spin density remains at the α positions. At low temperature, the terminal lines are split into triplets (Fig. 7), indicating that interactions between the radical anion and the metal reduce ρ_2 to an almost negligible value. The separations within the triplets may confidently be assigned to splitting arising from protons at Positions 5 and 8 ($b_2=1.28$ G). At room temperature the triplets are split further (Fig. 6); the outer lines became quartets of approximately equal intensity, while the inner line is resolved into nine components. The quartets are clearly due to sodium (nuclear spin of $\frac{3}{2}$) and give its splitting constant as $s=0.30$ G. This is in good agreement with the value of 0.35 G reported for the sodium ketyl of fluorenone in DME.[29] Differences in the b

[29] P. B. Ayscough and R. Wilson, J. Chem. Soc. 1963, 5412.

TABLE III. HFS constant ratios and total widths.

Radical	Ratios[a]				Width (G)	
	a/b	a/b_2	b_2/b_1	b/c	Obs.	Calc.
Perinaphthenyl	3.32 (3.29)				~49[b]	37.8
Hydroxyperinaphthenyl	3.70 (3.55)		1.09 (1.15)	12.0 (12)	36.4	32.3
Hydroxyperinaphthenyl anion		3.67 (3.60)	1.78 (1.81)		31.9	29.4
Dihydroxyperinaphthenyl	3.69 (3.56)			(9.5)	30.9	26.2

[a] Calculated values in brackets. [b] Reference 21.

splitting constants appear to be responsible for the complexity of the center line of the triplet. Nine lines can be accommodated if $b_1 \ll b_2$ and if there are small differences in b_2 such that $b_2' - b_2 \approx b_1 \approx \frac{1}{2}s$. From the spectrum $b_1 = 0.15$ G and $b_2/b_1 = 9.1$, while $b_2/b_1 = 1.78$ for the anion radical. This assignment is supported by signs of incipient splitting in the terminal quartets. The loss of splitting by sodium at low temperature has been noted previously.[29] It has been suggested to be due to a change in the extent of oscillation of the metal about its mean position, thereby altering the overlap with the π system. The additional complexity of the inner four members of the basic sextet is ascribed to differences in the a constants and has not been further analyzed.

The dihydroxyperinaphthenyl radical has identical spin densities at the four α positions. The simple spectrum of five quartets is adequately accounted for by the calculated average spin densities at the β positions. The spin density on oxygen is calculated to be slightly larger than in the hydroxyperinaphthenyl radical. The absence of splitting by hydrogen at these positions is ascribed to the inability to achieve the necessary high-resolution conditions.

The theoretical HFS constants and total widths are seen to be consistently about 10% lower than the observed values (Tables I and III). Perinaphthenyl shows a larger discrepancy, but for this radical the measurements were probably not as precise as for the others.[21] However, the calculated ratios of the splitting constants, which are independent of Q_{CH}, agree well with the observed ratios (Table III). With the MO-SCF model employed, the calculations show that no reasonable combination of h and k can accommodate the observed widths. The latter are matched better if Q_{CH} is taken as 27 G, which is not an unusually large value.[23]

C. Value of Q_{OH}

Splitting by hydrogen on oxygen has been observed in relatively few cases. Early work with the radicals derived from 2-propanol, ethanol, and methanol showed no evidence of such splitting[30]; in fact, the radicals from ethanol deuterated on the hydroxyl group gave a spectrum identical with that from the nondeuterated alcohol.[31] Recently, Piette and co-workers have observed OH splitting with the radicals from methanol[32a] and from ethanol.[32b] This splitting is also evident with the CH≡CĊHOH radical from propargyl alcohol[33] and with semiquinone cations.[34] Lack of observation of OH splitting was originally ascribed to rapid rotation of the hydroxyl group or to rapid proton exchange with the solvent,[35] but it now appears as if experimental limitations were largely responsible.

If it is assumed that the hydroxyl proton splitting is proportional to the spin density on oxygen, Eq. (1) may be written in the form $a_{OH} = Q_{OH}\rho_{OH}$, and Q_{OH} can be estimated from the hydroxyperinaphthenyl radical spectrum and the MO-SCF calculations. Using an average value for the spin densities at the α positions and ρ_{14} from Table I in conjunction with $a = 6.21$ G and $c = 0.14$ G, Eq. (1) yields $Q_{OH}/Q_{CH} = 0.29$. With $|Q_{CH}| = 24.2$ G, the value of $|Q_{OH}|$ is 7.0 G. Actually, as shown above, the spectra are better accommodated by $|Q_{CH}| = 27$ G, which raises $|Q_{OH}|$ to about 8 G.

The ratio Q_{OH}/Q_{CH} can be estimated independently by the configuration-interaction model used by McConnell[16,36] to compute an order-of-magnitude value

[30] D. J. E. Ingram and M. Fujimoto, Trans. Faraday Soc. **54**, 1304 (1958); J. F. Gibson, M. C. R. Symons, and M. G. Townsend, J. Chem. Soc. **1959**, 269; M. C. R. Symons, *ibid.*, p. 277, and earlier references cited in these papers.

[31] R. S. Alger, T. H. Anderson, and L. A. Webb, J. Chem. Phys. **30**, 695 (1959).

[32] (a) L. H. Piette, G. Bulow, and K. Loeffler, preprints, Symposium on the Use of ESR in the Elucidation of Reaction Mechanisms **9**, No. 2C, p. C-9, 1964; (b) L. H. Piette (private communication).

[33] W. T. Dixon and R. O. C. Norman, J. Chem. Soc. **1963**, 3119.

[34] J. R. Bolton and A. Carrington, Proc. Chem. Soc. **1961**, 385; J. R. Bolton and A. Carrington, Mol. Phys. **5**, 161 (1962); J. R. Bolton, A. Carrington, and J. dos Santos-Veiga, *ibid.*, p. 465; J. R. Bolton, A. Carrington, and P. F. Todd, *ibid.* **6**, 169 (1963).

[35] D. J. E. Ingram, *Free Radicals as Studied by Electron Spin Resonance* (Butterworth's Scientific Publications, Ltd., London, 1958), Chap. 6.

[36] H. M. McConnell and D. B. Chesnut, J. Chem. Phys. **28**, 107 (1958).

of Q_{CH}. It is assumed that an odd electron localized on the oxygen atom can be represented by a neutral hydroxyl radical. For the ground state, only three electrons are considered, one each in the $2p_x$ and $2p_z$ orbitals of oxygen and one in the $1s$ orbital of hydrogen. The latter orbitals constitute the σ bond between the atoms. Actually, this bond has slightly more s character than indicated owing to some contribution by the $2s$ orbital of oxygen. However, this will be neglected in this approximation. The calculation otherwise includes all the assumptions made by McConnell.[16,36] This leads to the expression

$$\frac{Q_{OH}}{Q_{CH}}=\frac{(J_{p_xp_z}-J_{p_xs})_{OH}(1-S_C{}^4)\Delta E_{21}{}^{CH}}{(J_{p_xh}-J_{p_xs})_{CH}(1-S_O{}^4)\Delta E_{21}{}^{OH}}, \qquad (5)$$

in which the J's are the exchange integrals between the indicated orbitals, h is the sp^2 hybrid orbital used by McConnell, and S_O and S_C are the overlap integrals $\langle p/s\rangle$ and $\langle h/s\rangle$ for OH and CH, respectively. The energy differences between the ground and excited doublets whose interaction gives rise to the spin density at the proton are designated as $\Delta E_{21}{}^{CH}$ and $\Delta E_{21}{}^{OH}$. Values for the exchange integrals J_{ps} can be estimated from the tables of Kotani *et al.*[37] to be 0.4 eV for both the CH and OH fragments. The value of J_{ph} is given by Altman[38] to be 1.81 eV for CH, and one can calculate a $J_{pp}=1.30$ eV for OH from his data. The overlap integrals are given by Jarrett[39] for CH and by Mulliken *et al.*[40] for OH. The values are 0.8 and 0.3, respectively. The ratio of the ΔE_{21} values can be estimated by assuming that it is the same as the ratio between the first excitation levels of CH and OH. These are given by Herzberg[41] as 2.78 and 4.03 eV, respectively. Substitution in Eq. (5) gives $Q_{OH}/Q_{CH}=0.3$, and with $|Q_{CH}|=24.2$ G, $|Q_{OH}|=7$ G. This value was used to compute the theoretical HFS constants for the hydroxyl hydrogen which are listed in Table I.

The agreement between these two estimates of Q_{OH} is remarkably good when the small magnitude of the splitting observed in our experiment is considered. It should be noted, however, that owing to the greater electronegativity of oxygen and to the presence of nonbonding electrons on this atom, OH splitting can be expected to be more influenced by the nature of the solvent than CH splitting.[42] Thus the results of Bolton *et al.* with the semiquinone cations generated in concentrated sulfuric acid show that, although the OH splitting increases with increasing spin density on oxygen as calculated by HMO theory, the relationship is not linear.[34]

It is of interest to compare the value of Q_{OH} with ESR data on hydroxyl radicals which have been produced in solid aqueous matrices by ionizing radiation and, in the gas phase, by microwave discharge. Unfortunately, there is considerable disagreement between the results and interpretations by different investigators. Thus, Matheson and Smaller[43] originally ascribed a doublet with a separation of 10 G, observed in ice at 4°K and in ice containing hydrogen peroxide at 77°K, to the hydroxyl radical. This value corresponds well with our estimate of Q_{OH}. Another doublet with a splitting of 30.5 G was attributed to strongly perturbed hydrogen atoms. The latter doublet has also been found by Siegel and co-workers[44] (39.3 G) and by McMillan, Matheson, and Smaller[45] in single ice crystals (41.3-G contact interaction), but was assigned by these authors to the hydroxyl radical. The spectra of irradiated metallic salt hydrates yield contact terms of 10.6–13.3 G.[46] In this case the species considered to be responsible for the absorption is hydrogen bonded to the oxygen of an oxyanion at a distance of about 1.6 Å, which is considerably longer than the normal OH separation of 1 Å.

In the gas phase, the contact term for the hydroxyl radical is 26 Mc/sec,[47] which may be compared with 22 Mc/sec (8 G) for the hydroxyperinaphthenyl radical. It must, however, be borne in mind that the contact interaction for the gaseous radical is modified by spin–orbital coupling, which is essentially quenched in organic free radicals and in the ice matrix.

If the doublet with the 30–40-G splitting constant detected in ice is accepted as due to the hydroxyl radical, it is clear that the resonance arises in part from interactions not encountered with the hydroxyperinaphthenyl radical in solution. The two radicals were generated in vastly different environments, and they differ further in that the organic radical includes a large carbon group. The potential importance of the environment factor is supported by the increase in the doublet splitting observed when the composition and structure of the ice matrix was modified.[42]

D. Stability of the Radicals

Hydroxylic radicals derived from aromatic ketones are generally too unstable to be observed under ordinary conditions.[10] By contrast, the hydroxyperinaphthenyl radical has a relatively high stability at room tem-

[37] M. Kotani, A. Amemiya, E. Ishoguro, and T. Kimura, *Table of Molecular Integrals* (Maruzen Company, Ltd., Tokyo, 1955).
[38] S. L. Altman, Proc. Roy. Soc. (London) **A210**, 327, 343 (1951).
[39] H. S. Jarrett, J. Chem. Phys. **25**, 1289 (1956).
[40] R. S. Mulliken, C. A. Rieke, D. Orloff, and A. Orloff, J. Chem. Phys. **17**, 1248 (1949).
[41] G. Herzberg, *The Spectra of Diatomic Molecules* (D. Van Nostrand Company, Inc., New York, 1950).
[42] Solvent effects on HFS constants are considered to be entirely due to a redistribution of spin density, which arises from the interaction of the solvent with a polar substituent or heteroatom; cf. J. Gendell, J. H. Freed, and G. K. Fraenkel, J. Chem. Phys. **37**, 2832 (1962).
[43] M. S. Matheson and B. Smaller, J. Chem. Phys. **23**, 521 (1955).
[44] S. Siegel, L. H. Baum, S. Skolnik, and J. M. Flourney, J. Chem. Phys. **32**, 1249 (1960).
[45] J. A. McMillan, M. S. Matheson, and B. Smaller, J. Chem. Phys. **33**, 609 (1960).
[46] P. E. Wigen and J. A. Cowen, Phys. Chem. Solids **17**, 26 (1960); cf. also T. E. Gunter and C. D. Jeffries, Bull. Am. Phys. Soc. **9**, 740 (1964).
[47] H. E. Radford, Nuovo Cimento **14**, 245 (1959).

perature. Its decay in 2-propanol is first order, and in a $10^{-3}M$ solution of perinaphthenone at 25°, the half-life is 3.9 min. The anion radical is more stable. The neutral radical can also be generated in benzene by photolysis of a mixture of perinaphthenone and its reduction product, perinaphthanone. By comparison with a standard DPPH solution, the steady-state concentration in a solution which is $10^{-2}M$ in each of these ketones is $\sim 3\times 10^{-5}M$. Here the decay is second order with $k_2 \approx 2\times 10^4$ liter mole^{-1} min^{-1} at 25°. Further kinetic and flash-photolytic studies with these and related radicals are in progress and will be reported elsewhere.

ACKNOWLEDGMENTS

This work was sponsored by the U.S. Air Force Cambridge Research Laboratories, Office of Aerospace Research, under Contracts AF 19(604)-7358 and AF 19(628)-3836. We are very grateful to the staff of the Energetics Branch at AFCRL for use of their ESR spectrometer. The computation work was carried out at the MIT Computation Center and Northeastern University Computation Center. It is a pleasure to acknowledge the aid of Miss Noralie Barnett with the data evaluation and the many helpful discussions held with Dr. John L. Roebber and Dr. Robert N. Wiener.

APPENDIX E

BLANK PAGE

[Reprinted from the Journal of the American Chemical Society, 88, 2893 (1966).]

A Kinetic Study of the Photochemical Reaction of Phenanthrenequinone with Olefins

James J. Bohning and Karl Weiss

Contribution from the Photochemistry and Spectroscopy Laboratory, Northeastern University, Boston, Massachusetts 02115. *Received February 16, 1966*

Abstract: Quantum yields at 405 mμ for the addition of phenanthrenequinone to stilbene, diphenylethylene, and triphenylethylene in benzene solution are independent of the olefin concentration over a wide range but vary with the structure of the olefin. *cis*-Stilbene and *trans*-stilbene react at different rates but give rise to a common product. This reaction is accompanied by *cis–trans* isomerization for which $\Phi_{CS\rightarrow TS} \approx \Phi_{TS\rightarrow CS}$. The system reaches a stationary *trans/cis* isomer ratio of 0.7 ± 0.05, which is close to that reported for some photostable, high-energy sensitizers, but which in this case represents a balance between the rates of isomerization and adduct formation. Measurements with α,α′-stilbene-d_2 indicate a kinetic isotope effect for adduct formation. The results are consistent with the formation of the spectroscopic triplet state of *trans*-stilbene by classical energy transfer and of a short-lived common association complex between triplet quinone and the *cis*- or *trans*-olefin, which is partitioned between decay to a nonspectroscopic excited state and collapse to adduct. The intersystem-crossing efficiency for phenanthrenequinone is inferred to be unity.

Phenanthrenequinone (PAQ) adds photochemically to olefins. This is a general reaction for certain 1,2-diketones which was first reported by Schönberg and Mustafa[1] and which has been carried out on a preparative basis with a large number of olefins. The reaction yields adducts of structure I (eq 1). It was

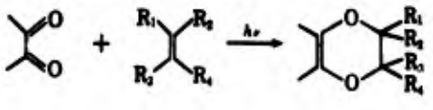

(1)

I

established by Pfundt and Schenck that only excitation of PAQ leads to adduct I; separate excitation of the olefin produces no conversion of PAQ.[2,3] On the basis of limited kinetic measurements, these authors propose a mechanism in which an excited state of PAQ forms a biradical intermediate with the olefin. Adduct is postulated to result from the interaction of this intermediate with a second, ground-state PAQ molecule.[3]

PAQ has a triplet energy of 48.8 kcal/mole,[4] and it was anticipated and found that, with the stilbenes, adduct formation is accompanied by *cis–trans* isomerization. Sensitized olefin isomerization is well documented, but the detailed mechanism of this process can by no means be regarded as established.[5] The question arises as to whether there is a relation between adduct formation and isomerization and whether, in general, olefin-sensitizer intermediates participate in the isomerization brought about by low-energy sensitizers. The detailed kinetic study of the reaction of PAQ with stilbene and with two other phenyl-substituted ethylenes was undertaken to firmly establish a mechanism for the addition reaction and to shed light on the role of

(1) A. Schönberg and A. Mustafa, *J. Chem. Soc.*, 387 (1944).
(2) G. O. Schenck, O. Neumüller, and R. Koch, *Strahlentherapie*, 114, 22 (1961).
(3) G. Pfundt, Doctoral Dissertation, Göttingen, 1962.
(4) This value was obtained from the emission spectra of PAQ in aliphatic hydrocarbons at 77°K; *cf.* N. A. Shcheglova, D. N. Shigorin, and M. V. Gorelik, *Zh. Fiz. Khim.*, 39 (4), 893 (1965).
(5) G. S. Hammond, J. Saltiel, A. A. Lamola, N. J. Turro, J. S. Bradshaw, D. O. Cowan, R. C. Counsell, V. Vogt, and C. Dalton, *J. Am. Chem. Soc.*, 86, 3197 (1964). This paper cites earlier references.

olefin-sensitizer intermediates. Further mechanistic information was sought by measurements with the 1,2-dideuteriostilbenes.

Experimental Section

Materials. Purities were established by gas chromatography (gc) using an F & M Model 720 temperature-programmed instrument with columns packed with appropriate substances (silicon grease, Carbowax 1500, and Triton X-305, 20% on Chromosorb-P, and by thin layer chromatography (tlc) on aluminum oxide coatings.

A. Solvents. Acetone and chlorobenzene were purified by fractional distillation. Ethyl acetate was treated with acetic anhydride prior to distillation, and acetic acid was distilled from phosphorus pentoxide. Carbon tetrachloride and tetrachloroethylene (both spectral grade) were used without further purification. *t*-Butyl alcohol was dried over sodium sulfate, refluxed over sodium, and finally distilled from sodium. Benzene satisfactory for the kinetic experiments was obtained by preparative-scale gas chromatography of CP benzene (16 ft × 1 in. column of 18% Triton X-305 on Chromosorb-P at 70°) and subsequent distillation.

B. Reactants. Commercial PAQ, after initial recrystallization from benzene or ethanol, was chromatographed on silica gel. The PAQ eluted with ethyl acetate and recrystallized from benzene was free of detectable impurities. *trans*-Stilbene (Eastman Kodak) was converted into its dibromide[6] from which it was regenerated by treatment with zinc.[7] Analysis of material prepared in this manner by tlc and gc showed it to be free of the *cis* isomer. In some kinetic experiments scintillation grade *trans*-stilbene containing less than 2% of the *cis* isomer as the sole impurity was used without further purification. *cis*-Stilbene (Eastman Kodak) was freed of the *trans* isomer by chromatography on alumina.[8] Pure samples of 1,1-diphenylethylene were obtained by gc of commercial material (4 ft × 0.25 in. column of 20% silicone grease on Chromosorb-P at 270°). Triphenylethylene (Eastman Kodak) was recrystallized from ethanol. 2-Acetonaphthone and naphthalene from the same source were recrystallized from ligroin and ethanol, respectively.

Deuterated Stilbenes.[9] Diphenylacetylene[10] in hexane was allowed to react with deuterium (99.5% purity) in the presence of 10% palladium-on-charcoal until 1 molar equiv of the gas was absorbed. The *cis*-stilbene-1,2-d_2 was freed from small amounts of the *trans* isomer and diphenylacetylene by chromatography on alumina using hexane as eluent. The fraction used for kinetic work contained at least 99.85% of the *cis* isomer (gc). *trans*-Stilbene-1,2-d_2 was obtained by the iodine-catalyzed photoisomerization, which can be conveniently followed by periodic spectral measurements, of the *cis* compound.[9] The material had mp 122.5–124° after recrystallization from ethanol (lit.[9] 123.8–125°) and contained at least 97% of the *trans* isomer (gc). Analysis by the falling-drop method indicated 16.40 atom % of deuterium[11] (calculated 16.67 atom %).

PAQ–Stilbene Adduct. Preparative-scale irradiations of PAQ were carried out in a modified version of the immersion apparatus described by Schenck.[12] A filter solution (1×10^{-4} *M* naphthalazine in xylene) served to exclude light below 390 mμ. PAQ (0.226 g, 1.09 mmoles) and *trans*-stilbene (1.075 g, 5.96 mmoles) in 280 ml of *t*-butyl alcohol were deoxygenated with a stream of nitrogen in the irradiation assembly, which was maintained at 30° by the circulation of water from a constant-temperature bath. The vigorously agitated suspension of PAQ was irradiated with a 250-w mercury lamp. After 15 min the PAQ had dissolved and a solid began to separate which was filtered after a total of 90 min of irradiation. Recrystallization from ethanol furnished 0.094 g (22%) of colorless adduct, mp 245–247° (lit.[13] 225°).

Similarly, *cis*-stilbene gave an adduct in 9% yield, mp 244–250°, after 45 min of irradiation. Every test applied showed the two adducts to be identical. A mixture melting point showed no depression, and the ultraviolet, infrared,[13] and nmr spectra were indistinguishable. Further, tlc under several conditions failed to effect a separation.

Apparatus and Procedure for the Kinetic Measurements. The monochromatic irradiation assembly[14] consists of a 500-w mercury lamp, a grating monochromator, a shutter, lenses to provide a collimated beam of light, a constant-temperature cell holder (±0.1°), and an Eppley thermopile with a basic sensitivity of 0.124 mv/mw cm^{-2}. These components are linearly arranged in the order given, with the thermopile directly behind the cell holder. The output of the thermopile is recorded on a strip chart recorder which is calibrated with reference signals from a precision potentiometer. At 405 mμ, the wavelength utilized in the kinetic experiments, this apparatus furnishes intensities of about 2 mw/cm^2 (4×10^{15} quanta/cm^2 sec).

The irradiations were carried out in rectangular Pyrex spectrophotometer cells of 1-cm path length. Since only an accurately masked area was illuminated, the solution was agitated throughout the photolysis by means of a magnetic stirrer. Separate tests established that the mixing was complete and rapid enough so as not to affect instantaneous measurements of the transmitted intensity. Solutions for kinetic runs were prepared by introducing aliquots of stock solutions of the reactants into a bulb to which the irradiation cell is attached. The solvent was completely removed on a high-vacuum line; pure, degassed benzene, which was stored over calcium hydride, was distilled into the bulb. The assembly was then sealed under vacuum. The initial concentration of PAQ and the volume of the solution were determined from its optical density at 407 mμ. Data recorded for each experiment were: (1) the dark response (shutter closed) and the intensity of the unattenuated light beam before and immediately after photolysis, (2) the intensity transmitted by the cell and solvent (I_0), and (3) the intensity transmitted by the cell and solution during photolysis (I) as a function of time. It can be readily shown that the total intensity of light absorbed at any time (I_{abs}) is given to a good approximation[14] by

$$I_{abs} = F(I_0 - I) \qquad (2)$$

where F is constant factor which includes the area irradiated, a correction for variations in intensity across the beam, and corrections for reflections from glass–air interfaces. Optical densities ($D = \log I_0/I$) measured with the irradiation apparatus agree to ±0.01 with values obtained with a spectrophotometer. Runs under a given set of conditions were made at least in duplicate. Quantum yields were computed from the least-squares slopes of $\log[(I_0/I) - 1]$ *vs.* time plots (see Results).

Since it was established that at very high olefin-to-PAQ ratios (~100:1) air had a negligible effect on the reaction,[15] the rate of isomerization of the stilbenes was measured in nondegassed solutions. The irradiation cell was provided with a serum-cap-covered opening through which microliter samples were withdrawn periodically during irradiation. The *cis–trans* isomer distribution was determined by gc using a 4 ft × 0.25 in column of 20% silicone grease on Chromosorb-P at 250°. By varying the column temperature it was shown that no thermal isomerization occurs.

Spectral Measurements. These were made with a Beckman DK-1 spectrophotometer using a constant-temperature cell block. Under the conditions of the kinetic experiments (concentrations were PAQ ~ 5×10^{-4} *M* and olefins ~10^{-2} *M*), only the PAQ absorbed light at wavelengths greater than 390 mμ. The adduct spectra in benzene are all very similar and show maxima near 350 and 370 mμ with $\epsilon \approx 1.6 \times 10^3$. The maximum of PAQ at 407 mμ (ϵ 1.86×10^3, benzene) conveniently almost coincides with a mercury emission line. Adherence to Beer's law in the range 1–5 $\times 10^{-4}$ *M* was found for PAQ at 367 and 407 mμ and for the stilbene photoadduct at 367 mμ. It was shown by comparing the calculated and observed densities of mixtures that there is no ground-state complex formation between the quinone and stilbene, and that the spectra of the quinone and its adduct are additive. A degassed solution of PAQ and *trans*-stilbene showed no spectral changes on standing in the dark for 80 days.

(6) "Organic Syntheses," Coll. Vol. 3, E. C. Horning, Ed., John Wiley and Sons, Inc., New York, N. Y., 1955, p 350.
(7) W. M. Schubert, B. S. Rabinovitch, and N. R. Larson, *J. Am. Chem. Soc.*, **74**, 4590 (1952).
(8) M. Calvin and H. W. Alter, *J. Chem. Phys.*, **19**, 765 (1951).
(9) *Cf.* N. Tunkel, Doctoral Dissertation, Rutgers University, 1955.
(10) Reference 6, p 377.
(11) Measured by Josef Nemeth, Urbana, Illinois.
(12) G. Schenck, *Dechema-Monograph.*, **24**, 105 (1955). The modified design, which was suggested by Dr. H. Köller, is described in the M. S. thesis of D. H. Lambert, Northeastern University, 1964.
(13) A. Butenandt, L. Karlson-Poschmann, G. Failer, U. Schiedt, and E. Bickert, *Ann.*, **575**, 123 (1951).
(14) A detailed description of this apparatus will be published (H. P. Wolf, J. J. Bohning, P. A. Schnieper, and K. Weiss).
(15) *Cf.* also S. Malkin and E. Fischer, *J. Phys. Chem.*, **68**, 1153 (1964).

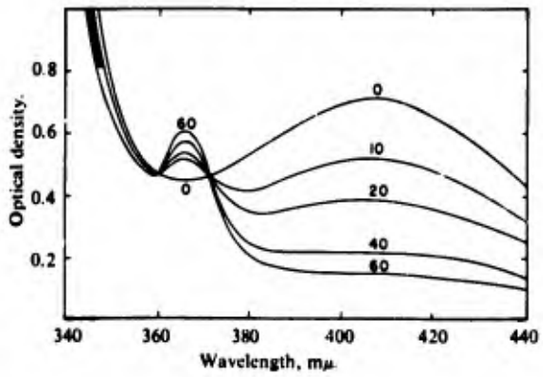

Figure 1. Photolysis of PAQ and *trans*-stilbene in benzene. The initial concentrations were PAQ 4×10^{-4} *M* and *trans*-stilbene 4×10^{-2} *M*. The numbers on the curves represent the irradiation time in minutes.

Results

Addition Reaction. To obtain meaningful rate data, it was first necessary to establish conditions under which adduct formation is the predominant reaction. Under preparative conditions, the isolated yields of adduct were found to be low even when light absorption was confined to the PAQ. The photolysis of PAQ in a number of purified and thoroughly outgassed solvents resulted in its disappearance even in the absence of olefin. In two cases (acetic acid, acetone) about 50% of the PAQ was regenerated when the cells were opened to air. This is indicative of the formation of 9,10-dihydroxyphenanthrene, which is known to undergo rapid air oxidation.[16] With respect to reactivity and the solubility of the reactants, benzene appeared most suitable. Its further purification by preparative-scale gas chromatography provided a solvent which was adopted for the kinetic work in view of the following facts.

1. Irradiation of PAQ in this solvent under standard kinetic conditions results in the disappearance of only 25% in 60 min, and oxygen regenerates 60% of the reacted PAQ. In the presence of 10^{-2} *M* *trans*-stilbene, 86% of the PAQ reacts in the same time and none is re-formed with oxygen.

2. In the absence of olefin, irradiation gives rise to isosbestic points at 354 and 365 mμ and a new peak at 357 mμ. With *trans*-stilbene, isosbestic points appear at 357 and 372 mμ, and the photoadduct peak appears at 367 mμ.[3,17] (Figure 1).

3. Using the decrease in optical density at 407 mμ as a measure of the PAQ which has reacted in conjunction with the extinction coefficients at 367 mμ for PAQ and adduct, 90–95% yields of adduct can be calculated from the optical densities at 367 mμ of stilbene reaction mixtures.

Clearly the olefin almost completely suppresses the side reaction with the solvent, the nature of which remains obscure.

In the presence of an excess of olefin, the disappearance of quinone follows the simple rate law $-d[Q]/dt = \Phi_A I_{abs}$ ([Q] = PAQ concentration, Φ_A = quantum yield) for 75–80% of reaction.[18] Introducing the

(16) P. Ramart-Lucas, J. Matti, T. Guilmart, and M Grumey, *Bull. Soc. Chim. France*, 1215 (1948).

(17) *Cf.* also G. O. Schenck, *Strahlentherapie*, **115**, 597 (1961).

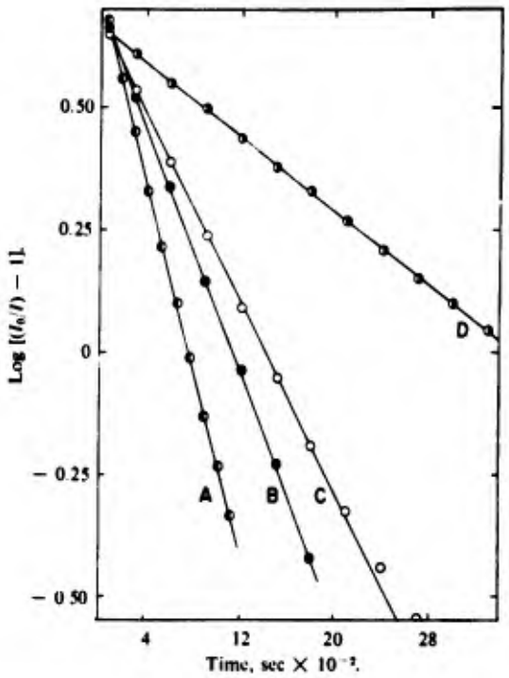

Figure 2. Determination of Φ_A according to eq 3 Initial concentrations were PAQ $\sim 5 \times 10^{-4}$ *M* and olefins $\sim 5 \times 10^{-2}$ *M*: (A) *cis*-stilbene, (B) triphenylethylene, (C) *trans*-stilbene; (D) 1,1-diphenylethylene.

definition $I_{abs} = I_0' - I' = I_0'[1 - \exp(-2.3\epsilon[Q]d)]$, where *d* is the path length in cm, ϵ is the extinction coefficient of PAQ at 405 mμ, and I_0' and I' represent the incident and transmitted light intensities (einsteins/l. sec) corrected according to eq 2, and integrating lead to

$$\log [(I_0/I) - 1] = \log [(I_0/I) - 1]_{initial} - \Phi_A I_0' \epsilon t \quad (3)$$

Some representative plots of eq 3 with PAQ:olefin ratios of 100 are shown in Figure 2, while Table I lists the quantum yields for all the olefins studied.

Table I. Quantum Yields for the Addition of PAQ to Olefins[a]

Olefin	Quantum yield (Φ_A)[b]
trans-Stilbene	0.066 ± 0.002[c]
cis-Stilbene	0.14 ± 0.005
α,α′-*trans*-Stilbene-d_2	0.069 ± 0.002
α,α′-*cis*-Stilbene-d_2	0.17 ± 0.005
Triphenylethylene	0.11 ± 0.004
1,1-Diphenylethylene	0.035 ± 0.001

[a] With 405-mμ light, in benzene at 25°. Initial PAQ and olefin concentrations are $\sim 5 \times 10^{-4}$ and $\sim 5 \times 10^{-2}$ *M*, respectively. [b] Slope (eq 3) divided by $I_0'\epsilon$. [c] Average of ten determinations with intensities in the range 1.5–3.3 × 10^{-6} einstein/l. sec.

At this point it is pertinent to examine why there are deviations from eq 3 toward the end of the photolysis It should be noted that the plots invariably curve upwards; *i.e.*, there is an apparent decrease in quantum yield. The effect is particularly noticeable with *trans*-stilbene, where the appearance of *cis*-stilbene as the reaction proceeds cannot be responsible since this isomer is more reactive. Apart from mechanistic con-

(18) 1,1-Diphenylethylene, the least reactive olefin, was only followed for 60% of reaction.

siderations, other causes to be explored are: (1) the fact that the adduct or a product of side reactions is a more efficient quencher of excited PAQ than stilbene, and (2) the formation of side products which show absorption in the 400-mμ region. With respect to the first possibility it was found that added adduct at twice the PAQ concentration has essentially no effect on the *trans*-stilbene reaction ($\Phi_A = 0.063$). Naphthalene and 2-acetonaphthone, which have been reported to quench benzophenone triplets at close to diffusion-controlled rates,[19] and which seemed to constitute reasonable model quenchers of PAQ in view of an early estimate of its triplet energy as ~65 kcal,[20] produced no change in Φ_A for the *trans*-stilbene reaction.

Case 2 appears to account for the lack of linearity at high conversion. Thus when a second charge of PAQ (as solid) is added to a photolyzed *trans*-stilbene–PAQ (100:1) reaction mixture and the solution is rephotolyzed, the apparent quantum yield is about 20% lower than for the initial photolysis. Subsequent additions of PAQ and photolyses show increasingly smaller decreases in the slopes, as if the component responsible for the change was gradually being eliminated. This behavior is entirely consistent with the appearance of a small amount of absorption in the 400-mμ region which would cause the actual PAQ concentrations to be significantly lower than the apparent concentrations at high conversion.

The quantum yields quoted in Table I are independent of the olefin concentration provided that a reasonable excess of olefin is maintained. With *trans*-stilbene, there is no appreciable decrease in rate until the olefin:PAQ ratio is less than 3:1. Under conditions where the reaction rate is independent of the olefin concentration, it is also insensitive to oxygen. As shown in Table II, the quantum yields for the stilbene reactions show a small temperature dependence.

Table II. Temperature Dependence of the Stilbene–PAQ Reaction[a]

Temp, °C	Φ_A *trans*-Stilbene	Φ_A *cis*-Stilbene
11	0.067 ± 0.002	0.16 ± 0.01
26	0.065	0.14
40	0.061	

[a] Stilbene:PAQ ratio is 100:1.

***cis–trans* Isomerization.** Data for the stilbene reactions in which *ca.* 4×10^{-4} *M* PAQ was photolyzed under standard conditions are presented in Table III. Isomerization quantum yields were determined from the initial rates of light absorption and the initial slopes of the isomerized stilbene concentration *vs.* time curves, in each case starting with the pure isomer (Table IV). The estimated uncertainty of ~5% in the quantum yields leads to the conclusion that $\Phi_{CS \rightarrow TS} \approx \Phi_{TS \rightarrow CS}$ for stilbene.[23]

Table III. PAQ-Sensitized *cis–trans* Isomerization of Stilbenes[a]

Initial concentrations PAQ × 10^4	Total stilbene × 10^2	*trans/cis* ratio Initial	*trans/cis* ratio Final
4.49	4.51	0.054	0.077
4.59	4.61	0.32	0.35
4.06	4.00	1.11	1.02
4.73	4.74	4.26	2.70
4.33	4.32	330	16.2
4.35	4.33[b]	25.9	9.5
4.31	4.30[c]	0.0084	0.039

[a] At 25° in benzene. Solutions were irradiated for 45 min. [b] α,α'-*trans*-Stilbene-d_2. [c] α,α'-*cis*-Stilbene-d_2.

Table IV. Quantum Yields for the PAQ-Sensitized Isomerization of Stilbene[a]

Starting isomer	Quantum yield
cis	0.45 ± 0.03
trans	0.43 ± 0.03

[a] In benzene at 25°, PAQ and stilbene concentrations ~5×10^{-4} and 5×10^{-2} *M*, respectively.

The data of Table III indicate that a stationary *trans*-/*cis*-stilbene ratio (R) is ultimately reached. A series of consecutive PAQ additions and photolyses were carried out with solutions in which the initial values of R were close to 1, and the stationary ratios $R_S = 0.7$ for stilbene and $R_S = 0.8$ for α,α'-stilbene-d_2 were obtained by the extrapolation of plots of R against the reciprocal of the total amount of PAQ reacted. The uncertainty in these values is again large (at least ±0.05). The sensitized isomerization is not quenched by the adduct.

Discussion

Consideration must first be given to the Pfundt–Schenck mechanism,[8] for which the key steps are

$$Q \overset{h\nu}{\rightleftharpoons} Q^* \quad (4)$$

$$Q^* + C{=}C \longrightarrow X \quad (5)$$

$$X + Q \longrightarrow A + Q \quad (6)$$

$$X \longrightarrow C{=}C + Q \quad (7)$$

Here Q and Q* represent ground-state and excited PAQ, respectively, X a "biradical" addition complex,[24] and A the adduct. Even if modified for the occurrence of isomerization by expanding eq 5 and 6 into separate steps for *cis* and *trans* isomers, the mechanism gives $\Phi_A = a[Q]/(b + [Q])$, where a and b are constants if a large excess of olefin is employed. We propose that this mechanism is inapplicable because (1) within the limitations imposed by minor side reactions, Φ_A is independent of the PAQ concentration;[25] (2) the mech-

(19) G. S. Hammond and P. A. Leermakers, *J. Phys. Chem.*, 66, 1148 (1962).

(20) This value was based on the stationary-state *trans/cis* ratio of piperylene achieved by sensitized isomerization.[21] The large discrepancy between this and the spectroscopic value[4] is undoubtedly due to the photochemical addition of PAQ to the 1,3 diene.[22]

(21) G. S. Hammond, N. J. Turro, and P. A. Leermakers, *ibid.*, 66, 1144 (1962).

(22) G. O. Schenck, *Z. Elektrochem.*, 64, 997 (1960).

(23) For stilbene-d_2, $\Phi_{CS \rightarrow TS} > \Phi_{TS \rightarrow CS}$ barely within the error limits. The possible occurrence of an isotope effect in *cis–trans* isomerization is obviously highly pertinent to the mechanism of this process, and to the problem of radiationless transitions in general. Further isomerization experiments with deuterated substrates, unsensitized and sensitized with stable compounds are in progress.

(24) *Cf.* G. O. Schenck, Plenary Lecture, Fifth International Symposium on Free Radicals, Uppsala, Sweden, 1961.

(25) The side reactions could obscure dependence on [Q]. However, since they are small in extent (~5%) we believe that, with b of significant magnitude, dependence on [Q] would lead to lack of linearity in plots of eq 3 at much smaller conversions than is actually the case.

anism ascribes a specific "quenching" role to ground-state PAQ (eq 6) (if participation by a third molecule is necessary, any molecule, *i.e.*, solvent, olefin, or adduct, should be satisfactory); (3) Φ_A being invariant with changes in olefin concentration implies that the reverse step of eq 4 is unimportant. The model then predicts identical Φ_A values for *cis* and *trans* isomers. In fact, it can be readily shown that any mechanism in which a single intermediate is partitioned between decomposition into isomers and formation of adduct leads to Φ_A independent of R.

A meaningful discussion of the kinetic results is possible in terms of a simple mechanism (eq 8 to 17) which includes many of the steps proposed by Hammond and co-workers for sensitized *cis–trans* isomerization.[5] In these equations, the symbols not defined previously have the following significance: Q'', excited singlet state of PAQ; p, a nonspectroscopic excited state of stilbene as defined by Hammond;[5] TS and CS, *trans*- and *cis*-stilbene; Q' and TS', the spectroscopic triplet states. The direct excitation process CS → CS' is not included in view of the sizable energy difference between Q' (48.8 kcal) and CS' (57 kcal).[26,27] The scheme includes a collision complex (X) of finite lifetime between Q' and olefin, which is implied in the original discussion of the p state,[28] and which provides a link between energy transfer and Schenck's "biradical" mechanism.[29] With stable sensitizers (benzophenone, etc.) X decays only to p and ground-state sensitizer. With a reactive sensitizer such as PAQ, X is partitioned between decay to p and collapse to product. We take the physical identity of the products isolated from *cis*- and *trans*-stilbene to be strong evidence for the existence of a common intermediate. It is reasonable to suppose that the change in geometry leading to nonplanar p takes place in the complex X. Freedom of torsional motion in energy-rich X would be expected to furnish the same distribution of adducts Ia and Ib, which differ with respect to geometry about the 2,3 bond of the dioxene ring, from the *cis*- and *trans*-olefins.[30] The energy of TS' (50 kcal)[26] is approximately matched with that of Q'. Classical energy transfer (eq 12) must be invoked, for in its absence the quantum yields of adduct formation become independent of R.

$$Q \underset{k_2}{\overset{h\nu}{\rightleftharpoons}} Q'' \tag{8}$$

$$Q'' \xrightarrow{k_3} Q' \tag{9}$$

$$Q' + TS \xrightarrow{k_4} X \tag{10}$$

$$Q' + CS \xrightarrow{k_5} X \tag{11}$$

$$Q' + TS \underset{k_{-6}}{\overset{k_6}{\rightleftharpoons}} TS'\ Q \tag{12}$$

$$X \xrightarrow{k_7} A \tag{13}$$

$$X \xrightarrow{k_8} p + Q \tag{14}$$

$$TS' \xrightarrow{k_9} p \tag{15}$$

$$p \xrightarrow{k_{10}} TS \tag{16}$$

$$p \xrightarrow{k_{11}} CS \tag{17}$$

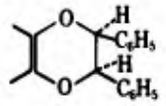

Ia

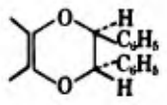

Ib

Application of the steady-state hypothesis to transient species leads to the rate equation

$$-\frac{d[Q]}{dt} = \frac{I_{abs}K_3K_7(k_4R + k_5)}{(k_4 + ak_6)R + k_5} \tag{18}$$

where, for convenience, we have defined $K_3 = k_3/(k_2 + k_3)$, $K_7 = k_7/(k_7 + k_8)$, and $a = k_9/(k_9 + k_{-6}[Q])$. The appearance of a in eq 18 introduces a rate dependence on [Q] such that the quantum yields decrease with increasing conversion. However, we can reason that the extent of transfer between TS' and Q is negligibly small.[31] Thus a can be taken as unity, and we can generate the expressions listed in Table V for the conditions $R >> 1$ and $R << 1$, corresponding to reactions which start with *trans*-stilbene and *cis*-stilbene, respectively. As Table III shows, when these conditions apply initially, they remain unchanged for a significant part of the reaction. Numerical values for ratios of constants were computed from the expressions of Table V and the experimentally determined quantities, and are listed in Table VI. The ratio k_4/k_5 was obtained by applying the stationary-state condition $dR/dt = 0$.[32]

Table V. Expressions for the Quantum Yields Base on Eq 18[a]

	$R_{initial} >> 1$	$R_{initial} << 1$
Φ_A	$\frac{K_3K_7k_4}{k_4 + k_5}$	K_3K_7
$\Phi_{CS\rightarrow TS}$		$K_3K_5K_{10}$
$\Phi_{TS\rightarrow CS}$	$\frac{K_3K_{11}[K_5(k_4 + k_5) + K_7k_5]}{k_4 + k_5}$	

[a] With $a = 1$; $K_8 = 1 - K_7$; $K_{10} = k_{10}/(k_{10} + k_{11})$; $K_{11} = 1 - K_{10}$.

Within experimental error, the intersystem-crossing efficiency for PAQ (K_3) is unity and $k_{10} \approx k_{11}$ for stil-

(26) D. F. Evans, *J. Chem. Soc.*, 1351 (1957).

(27) Only the minimum number of steps required to account for the results are included. Steps such as TS' → TS and TS' → CS, which are potentially significant, are omitted because their inclusion leads to composite constants from which no information can be gleaned which is not also available from the simple scheme. It is obvious that the change TS' → CS requires passage through a nonplanar state such as p.

(28) G. S. Hammond and J. Saltiel, *J. Am. Chem. Soc.*, 85, 2516 (1963).

(29) G. O. Schenck and R. Steinmetz, *Bull. Soc. Chim. Belges*, 71, 781 (1962).

(30) In a private communication, G. O. Schenck and G. Pfundt have indicated that the adduct of mp 245–250° isolated by us from reactions with *cis*- and *trans*-stilbene has the *trans* configuration Ib. The *cis* adduct (structure Ia) melts ~80° lower, and in benzene or *t*-butyl alcohol the isometric adducts are formed in comparable amounts: G. O. Schenck and S. Farid, *Tetrahedron*, in press.

(31) Thus we already know that $k_{-6}[Q] >> k_5$ cannot hold, for then $a \approx 0$ and Φ_A becomes independent of R. The range of [Q] is 5×10^{-4} to 1×10^{-4} M during photolysis. This is about two orders of magnitude lower than the sensitizer concentrations employed in Hammond's extensive study of stilbene isomerization,[5] and on the basis of these data is close to the infinite dilution limit. In fact, the data on quenching by azulene[5] indicate that $k_{-6} \approx 10^2 k_5$ is reasonable. This gives $a \approx 0.95$–0.99 during the decomposition of 4×10^{-4} M of PAQ.

(32) [TS] + [CS] = S_0 − ([Q]$_0$ − [Q]), where S_0 is the total initial substrate concentration. This equation yields $(R_8 + 1)\ d[CS]/dt = d[Q]/dt$ which, with appropriate substitution, affords k_4/k_5 as a function of experimentally measured parameters.

Table VI. Rate Constant Ratios for the PAQ–Stilbene Reaction

System	k_4/k_6	k_4/k_5	$\frac{k_6}{k_4 + k_6}$	K_8	K_7	K_{10}
Stilbene	0.89 ± 0.05	0.7 ± 0.1	0.5 ± 0.1	0.98 ± 0.06	0.14 ± 0.01	0.53 ± 0.03
α,α'-Stilbene-d_2	0.70 ± 0.04				0.17 ± 0.01	

bene. The data further indicate that all the processes which deactivate the PAQ triplet proceed at comparable rates. Since the decay of X is heavily in favor of the formation of the p state ($K_8 = 0.86$), adduct formation can be viewed as a minor deactivating path, and the nonspectroscopic excitation of stilbene occurs at about the same rate as the classical energy transfer. The small temperature dependence of K_7 (*cf.* Table II) indicates that the decay of X to p and Q is favored at higher temperature and hence involves some activation energy. The temperature variation of the ratio $K_7k_4/(k_4 + k_6)$ is in the same direction as that of K_7, but the magnitude is too small to detect a significant influence of $k_4/(k_4 + k_6)$.

The stationary *trans/cis* ratio, $R_S = 0.7$, is close to that reported for high-energy sensitizers.[5] However, in the present case it represents a balance between the rate of isomerization and the rate of addition. Since the addition of PAQ to *cis*-stilbene is faster than to *trans*-stilbene, it is clear that for isomerization only R_S would be much smaller than 0.7.

Since the association complex X resembles the transition state of thermal reactions, the appearance of secondary deuterium isotope effect in adduct formation is not surprising. The formation of X may not only involve the appearance of torsional freedom about the central C–C bond of the olefin, but may also cause the geometry at the central carbon atoms to change from that appropriate for an sp^2 hybridization to a configuration between sp^2 and sp^3. In this case $(k_4)_D > (k_4)_H$ is expected,[33] but the data indicate that $(k_4/k_6)_D < (k_4/k_6)_H$. Consequently there is a strong implication that $(k_6)_D > (k_6)_H$, *i.e.*, that the classical energy transfer occurs at less than the diffusion-controlled rate and is subject to an isotope effect.[34] That $(K_7)_D > (K_7)_H$ can be readily accommodated if the olefinic carbon configuration in X is closer to sp^2 than to sp^3, and if the configuration in X and p are similar. Under these circumstances $(k_8)_D \approx (k_8)_H$ and $(k_7)_D > (k_7)_H$. These arguments imply that an activation energy is involved in the formation of X and in its passage into adduct.

Acknowledgments. This study was supported by the U. S. Air Force Cambridge Research Laboratories, Office of Aerospace Research, under Contracts AF19-(604)-7358 and AF19(628)-3836. We are grateful to Mr. Harold P. Wolf for making some of the isomerization rate measurements, and to Dr. John L. Roebber for helpful discussions. We also wish to thank Professor G. O. Schenck and Dr. G. Pfundt for providing a copy of the latter's dissertation and for informing us about some pertinent results prior to publication.

(33) L. Melander, "Isotope Effects on Reaction Rates," Ronald Press, Co., New York, N. Y., 1960.

(34) G. W. Robinson and R. P. Fosch, *J. Chem. Phys.*, **38**, 1187 (1963), predict on theoretical grounds that only a very small isotope effect can be expected if the energy difference between the initial and final states is small.

APPENDIX F

(*Reprinted from Nature, Vol. 208, No. 5016, p. 1203 only, December 18, 1965*)

Charge Transfer Properties of *dl*-Thioctic Acid and Other Disulphides

THE ability of organic sulphur compounds to act as donors with electron acceptor molecules is well established. As far as disulphides are concerned, previous studies have been limited to simple aliphatic compounds with iodine as the acceptor[1]. In these systems, the charge transfer (CT) band appears between the disulphide absorption and the blue-shifted iodine absorption, and its position appears to be little affected by changing the alkyl groups. We wish to report that alkyl aryl and cyclic disulphides form 1 : 1 complexes in solution with tetracyanoethylene (TCNE), which show well-separated CT bands in the visible region. Further, the position of these bands clearly reflects steric and electronic factors in the disulphide molecule.

The complexes are readily generated by mixing rigorously purified solutions of the donor and acceptor. Special care must be taken to remove thiols, which are the major impurities in disulphides, since these react with TCNE. Table 1 lists some representative spectral data; several sulphides are included for comparison. It is apparent that (1) simple alkyl disulphides show a progressive decrease in CT transition energy with increasing chain length; (2) branched chain complexes absorb at longer wave-lengths than the corresponding straight chain complexes; (3) for disulphides, ring closure has a larger effect on the CT transition than elongation of the alkyl chain, while the opposite is the case for sulphides. The complexes have low formation constants (K_c, l./mole) and molar extinction coefficients (ε). In dichloromethane at 25° typical values are: methyl disulphide $K_c = 0{\cdot}16$, $\varepsilon = 2{,}100$; *tert.*-butyl disulphide $K_c = 0{\cdot}36$, $\varepsilon = 4{,}500$; *dl*-thioctic acid $K_c = 1{\cdot}22$, $\varepsilon = 6{,}500$. The corresponding enthalpies of formation are $-0{\cdot}4$, $-1{\cdot}5$, and $-7{\cdot}2$ kcal/mole. Based on the photoionization value of 8·46 eV for methyl disulphide[2], we estimate the ionization potentials of *tert.*-butyl disulphide and *dl*-thioctic acid to be 7·78 and 7·53 eV, respectively. The general trend of these data may be rationalized in terms of the increased inductive (electron-releasing)-effect of the larger alkyl groups, and the decrease in the dihedral angle between the adjacent sulphur 3-$p\pi$ orbitals which

Table 1. CHARGE TRANSFER MAXIMA OF TCNE-SULPHUR COMPOUND COMPLEXES IN DICHLOROMETHANE SOLUTION

Donor	λ_{max} (mμ)	Donor	λ_{max} (mμ)
Alkyl, aryl disulphides:		Cyclic disulphides:	
Methyl	425	Tetramethylene	535
Ethyl	450	Trimethylene	575
n-Propyl	453	*dl*-Thioctic acid	583
n-Butyl	460	Sulphides:	
iso-Propyl	465	Ethyl	505
tert.-Butyl	530	*n*-Butyl	530
*Cyclo*hexyl	525	Phenyl	590
Phenyl	515	Pentamethylene	495
Mesityl	430	Tetramethylene	515

[Reprinted from the Journal of the American Chemical Society, 88, 204 (1966).]

Charge-Transfer Complexes of Disulfides with Tetracyanoethylene

Wayne M. Moreau and Karl Weiss

Contribution from the Photochemistry and Spectroscopy Laboratory, Northeastern University, Boston, Massachusetts 02115. *Received August 17, 1965*

Abstract: Using the Benesi–Hildebrand procedure, the association constants and extinction coefficients have been measured for a number of disulfide–TCNE complexes. In the series *n*-alkyl disulfides, *t*-butyl disulfide, and thioctic acid, K_c at 25° increases from ~0.1 to 1.2 l./mole and $-\Delta H$ increases from 0.41 to 7.2 kcal./mole in the order given. The charge-transfer transition energies decrease in the same order. It is proposed that these trends reflect the decreasing angle between the doubly occupied 3p orbitals on the adjacent sulfur atoms of the disulfides. Structures are postulated for the alkyl disulfide and cyclic disulfide complexes, which are considered quantitatively with the aid of semiempirical molecular orbital theory. With an empirically derived estimate for the exchange integral between sulfur 3p and carbon 2p orbitals situated in separate planes, the MO model provides very satisfactory agreement with the observed charge-transfer transitions and transitions assigned to the complexed components.

The donor properties of organic sulfur compounds have been the subject of numerous publications.[1,2] Alkyl sulfides and disulfides form charge-transfer complexes with iodine[3-5] which are more stable than those of the corresponding oxygen compounds.[3c,6] Of the two types of sulfur compound, the sulfides are by far the stronger donors. Inductive effects[1,3c] and a smaller overlap integral[3c,4] for the disulfide complex have been considered as explanations for this difference.

Since the interactions in the ground state of weak complexes are small, absorption bands apart from the charge-transfer transition are observed, which may be ascribed to the complexed components. These bands are generally shifted with respect to those of the uncomplexed components. A variety of interpretations have been advanced for the origin of this shift,[7] and the most reasonable ones appear to be the mutual perturbation of the donor and acceptor energy levels[8] and the removal of restrictions on symmetry-forbidden transitions.[9] McGlynn[5] has studied the ethyl disulfide iodine complex from this point of view and found the complexed disulfide to have a smaller transition energy than the free disulfide. Using a simple molecular orbital (MO) description of the disulfide molecule, he proposes that the red shift is due to a change in the dihedral angle between the nonbonding, perpendicular 3p orbitals of the two sulfur atoms.

The point of departure for this study was McGlynn's suggestion[5] that the shift of the -S-S- absorption should

(1) R. J. Niedzielski, R. S. Drago, and R. L. Middaugh, *J. Am. Chem. Soc.*, **86**, 1694 (1964); this paper cites much of the earlier literature.
(2) R. S. Drago, B. Wayland, and R. L. Carlson, *ibid.*, **85**, 3125 (1963).
(3) (a) N. W. Tideswell and J. D. McCullough, *ibid.*, **79**, 1031 (1957); (b) J. D. McCullough and D. Mulvey, *ibid.*, **81**, 1291 (1959); (c) H. Tsubomura and R. P. Lang, *ibid.*, **83**, 2085 (1961); (d) R. P. Lang, *ibid.*, **84**, 4438 (1962).
(4) M. Good, A. Major, J. Nag-Chaudhuri, and S. P. McGlynn, *ibid.*, **83**, 4329 (1961).
(5) S. P. McGlynn, J. Nag-Chaudhuri, and M. Good, *ibid.*, **84**, 9 (1962).
(6) M. Tamres and M. Brandon, *ibid.*, **82**, 2134 (1960).
(7) G. Briegleb, "Elektronen-Donator-Acceptor Komplexe," Springer Verlag, Berlin, 1961, Chapter 5.
(8) S. Nagakura, *J. Am. Chem. Soc.*, **80**, 520 (1958).
(9) J. Czekalla, *Z. Elektrochem.*, **63**, 1157 (1959).

be enhanced with stronger acceptors such as tetracyanoethylene (TCNE). The specific aims of this work were to ascertain the effect of changes in the structure of the disulfide on the charge-transfer and complexed component transitions. It was of particular interest to examine five-membered ring disulfides in which complexation is not likely to bring about marked changes in geometry. The disulfide–TCNE complexes have been briefly described in a preliminary communication.[10] In this paper we report their thermodynamic and spectral properties in detail and present a semiempirical MO model to account for the spectral features.

Experimental Section

Materials. The chemicals employed in this work were in most cases of the highest commercially available quality, which were rigorously further purified. For liquids, the purity was checked by gas chromatography (g.c.) with an F & M Model 720 temperature-programmed dual column instrument. Columns packed with 10% Triton X-305 on Chromosorb P (8 ft. × 0.25 in.) and with 20% silicone gum rubber on Chromosorb P (4 ft. × 0.25 in.) provided satisfactory analyses in all cases. The melting and boiling points given here are uncorrected.

The solvent, dichloromethane (Matheson Coleman and Bell), was washed repeatedly with 5% sodium carbonate solution and finally with water. It was distilled from phosphorus pentoxide under nitrogen with a 100-cm. long Podbielniak Heligrid-packed column using an 18:1 reflux ratio. The material had b.p. 40.0–40.2° (760 mm.) and a minimum purity of 99.9% (g.c.). Dichloromethane has been used in previous spectrophotometric studies with TCNE; complex formation involving this solvent appears to be negligible.[11]

The most critical impurities in the disulfides are the corresponding thiols. These react with TCNE,[4,12] and this probably accounts for the unsuccessful previous attempt to generate a stable disulfide–TCNE complex.[5] Methyl, ethyl, *n*-butyl, and *t*-butyl disulfides (Eastman Kodak Co.) were purified by washing with sodium hydroxide solution (Vogel's method[13]) followed by fractional distillation. The liquids had b.p. 109–110° at 760 mm. (methyl), 151–152° at 760 mm. (ethyl), 90° at 3 mm. (*n*-butyl), and 66° at 4 mm. (*t*-butyl), and had purities of better than 99.9% (g.c.). Samples of butyl disulfide of similar purity were also obtained by the iodine oxidation of 1-butanethiol.[13] Phenyl disulfide was prepared by the ferric chloride oxidation of thiophenol.[14] The recrystallized, vacuum-dried material had m.p. 60–60.5° (lit.[14] 59–60°) and an ultraviolet spectrum in pentane which duplicates the published data.[15] Benzyl disulfide (Eastman Kodak Co.) was recrystallized several times from spectral grade 2-propanol and had m.p. 71–72° (lit.[16] 71°).

Of the cyclic disulfides, *dl*-thioctic acid (Aldrich Chemical Co. or British Drug Houses, Ltd.) was used without further purification. It had m.p. 60–61° (lit.[16] 61–61.5°), and comparison with material which had been recrystallized three times from petroleum ether showed both samples to give quantitatively identical charge-transfer spectra. 1,2-Dithiolane (trimethylene disulfide) was prepared by the iodine or ferric chloride oxidation of 1,3-propanedithiol.[17] The sample employed had m.p. 72.5–74° (lit.[17] 73–74°), and its spectrum in dichloromethane (λ_{max} 330 mμ (ε 142)) compared favorably with the reported spectrum[18] in ethanol (λ_{max} 334 mμ (ε 150)). The method of Barltrop, Hayes, and Calvin[18] was employed to prepare 1,2-dithiane (tetramethylene disulfide), which had the reported physical properties. This disulfide slowly polymerizes at room temperature but could be stored at −80° in dichloromethane solution. Tetrahydrothiophene (Eastman Kodak Co.) was distilled through a Podbielniak spinning-band column, and had b.p. 124.0° (760 mm.) (lit.[16] 121.2° (699 mm.)). High-purity samples of this compound as well as of methyl disulfide and ethyl disulfide were also obtained from the U. S. Bureau of Mines.

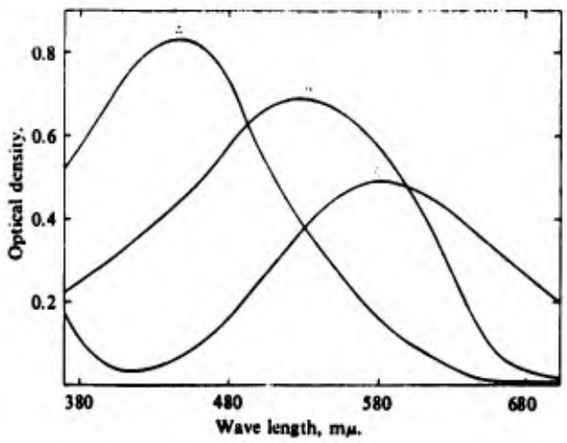

Figure 1. Charge-transfer bands of disulfide–TCNE complexes in dichloromethane (d = 1.00 cm.): A, 0.040 M ethyl disulfide, 0.050 M TCNE; B, 0.00845 M *t*-butyl disulfide, 0.050 M TCNE; C, 0.0279 M thioctic acid, 0.0473 M TCNE.

Tetracyanoethylene (Eastman Kodak Co.) was twice recrystallized from chlorobenzene and twice sublimed at 160° (1 mm.). The melting point (197–198°, sealed tube) and ultraviolet and infrared spectra agreed with published data.[19] The moisture-sensitive material was stored under vacuum over solid sodium hydroxide. Iodine (analytical reagent) and tetracyanoquinodimethane[20] were used without purification, and chloranil (Eastman Kodak Co.) was recrystallized from ethanol.

Measurement Procedures. All the spectra were measured with a Beckman Model DK-1 recording spectrophotometer. The matched 1-cm. or 10-cm. path length stoppered quartz cells were accommodated in a specially constructed aluminum block which fits into the sample compartment, and through which water from a precision constant temperature bath is rapidly circulated. The temperature control was better than ±0.1°. The volumetric ware was calibrated according to accepted procedures, and the solutions were made up to volume after equilibration in the constant-temperature bath. Only freshly distilled solvent was used. For the stability-constant measurements an excess of donor was used with concentrations in the range 0.1–1 M (donor) and 10^{-4}–10^{-3} M (acceptor). It was necessary to employ the 10-cm. spectrophotometer cells with the very weak donors in order to bring the optical density readings into the 0.2–1.5 range. The pure solvent served as the reference in all cases.

With the thioctic acid–TCNE complex spectral measurements in the disulfide absorption region could be made with 1-cm. cells. The weak ethyl disulfide complex, however, required a very short path length. For this purpose a cell was constructed from round, quartz plates which are separated by an annular Teflon shim (0.04–0.15 mm. thick).[21] This assembly is firmly compressed between bolted metal rings. A small off-center hole through one of the quartz plates, which can be closed with a Teflon plug, allows the solution to be introduced with a capillary dropper. With this cell the reference beam passed through air, and it was necessary to make separate measurements with the solution and the solvent.

Results

In contrast with iodine–disulfide complexes in which the charge-transfer band appears between the disulfide and blue-shifted iodine bands, the TCNE complexes show well-separated absorption in the 400–600-mμ region. Some typical curves are shown in Figure 1.

(10) W. M. Moreau and K. Weiss, *Nature*, in press.
(11) R. Merrifield and W. Phillips, *J. Am. Chem. Soc.*, **80**, 2778 (1958).
(12) W. J. Middleton, R. E. Heckert, E. L. Little, and C. G. Krespan, *ibid.*, **80**, 2783 (1958).
(13) A. Vogel, "A Textbook of Practical Organic Chemistry," John Wiley and Sons, Inc., New York, N. Y., 1962, p. 498.
(14) C. Wang and S. G. Cohen, *J. Am. Chem. Soc.*, **79**, 1924 (1957).
(15) R. Friedel and M. Orchin, "Ultraviolet Spectra of Aromatic Compounds," John Wiley and Sons, Inc., New York, N. Y., 1951, spectrum no. 152.
(16) E. E. Reid, "Organic Chemistry of Bivalent Sulfur," Vol. 3, Chemical Publishing Co., Inc., New York, N. Y., 1960, pp. 395–400.
(17) T. J. Wallace, *J. Am. Chem. Soc.*, **86**, 2018 (1964).
(18) J. A. Barltrop, P. M. Hayes, and M. Calvin, *ibid.*, **76**, 4348 (1954).
(19) C. E. Looney and J. R. Downing, *ibid.*, **80**, 2840 (1958).
(20) Kindly supplied by Dr. S. Chatterjee, Air Force Cambridge Research Laboratories.
(21) This versatile design was suggested by Dr. R. N. Wiener.

Table I. Spectral and Thermodynamic Properties of the Disulfide–TCNE Complexes in Dichloromethane Solution

Disulfide	λ_{max},[b] mμ	Temp., °C.	$K_c\epsilon$	$\delta K_c\epsilon$[a]	K_c, l./mole	δK_c	ϵ	$\delta\epsilon$	$-\Delta H$,[d] kcal./mole
Methyl	425	25.0	342	±11	0.16	±0.09	2150	±1200	0.41
[c]		6.0	359	14					
Ethyl	450	25.0	411	4	0.14	0.03	3000	700	
n-Butyl	460	25.0	460	6	0.09	0.01	5200	500	
t-Butyl	530	25.0	1640	9	0.36	0.13	4600	1000	1.5
		14.0	1780	63	0.41	0.06	4300	500	
		5.0	1960	96	0.57	0.18	3450	1100	
Phenyl	510	25.0	448	58	1.5	0.5	290	80	
Benzyl	405	25.0	805	9	2.6	0.2	310	25	
Thioctic acid	583	25.0	7950	290	1.2	0.3	6500	1300	7.2
		5.0	18900	1330	3.1	0.6	6200	1200	
Tetrahydro-thiophene	510	25.0	1140	60	0.60	0.08	1900	250	

[a] The uncertainties, δ, are the standard deviations. [b] Charge-transfer band. The position does not change with temperature. [c] The conditions were such that only $K_c\epsilon$ could be obtained. [d] Computed from the temperature variation of $K_c\epsilon$. The uncertainty in ΔH is estimated as ±0.1 kcal./mole.

The bands are seen to be broad, the half-intensity widths[22] being 7900 cm.$^{-1}$ for the ethyl disulfide complex and 5300 cm.$^{-1}$ for the thioctic acid (I) complex.

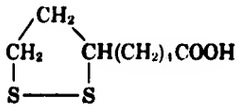

I

The latter value is close to that reported for some weak complexes of iodine with aromatic hydrocarbons.[23]

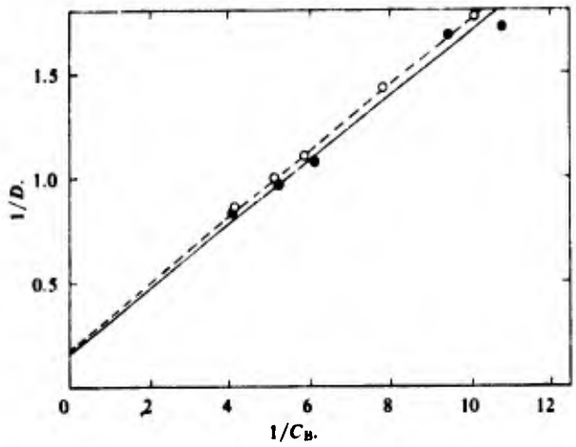

Figure 2. Plots of eq. 1 for the thioctic acid–TCNE complex in dichloromethane at 25.0°, with d = 1.00 cm.: –O–, C_A = 8.29 × 10^{-4} M; –●–, C_A = 7.90 × 10^{-4} M.

The preliminary indications were that the TCNE complexes are quite weak, with association constants (K_c) ~ 1 or less. Indeed, logarithmic plots of the optical density (D) at the charge-transfer maximum against the donor concentration (C_D) for a series of solutions in which the TCNE concentration (C_A) was kept constant had uniform slopes in the range 0.96–1.01 for methyl, ethyl, *n*-butyl, *t*-butyl, and phenyl disulfides. The latter compounds also showed maxima at a mole fraction of 0.5 in continuous variation plots.[24] While neither of these results can be considered to unequivocally establish the stoichiometry of the complexes,[25] a 1:1 association is assumed with reasonable confidence.

Values of K_c and the molar extinction coefficient of the complex (ϵ) were obtained by the analysis of spectral data using the Benesi–Hildebrand procedure.[26] At the charge-transfer maxima, no corrections for donor and acceptor absorption were necessary. In many of the experiments the acceptor concentration was kept constant, thereby allowing use of the modified form of the Benesi–Hildebrand relation (eq. 1, d = path length in cm.) which offers some advantages for weak complexes.[27] Plots of $1/D$ against $1/C_D$ for the thioctic acid complex is shown in Figure 2. The scatter of points is typical of that obtained in all the experiments. By suitable choice of path length and C_A, it was always possible to meet Person's criterion for the significant evaluation of K_c and ϵ, *i.e.*, $(C_D)_{max} > 0.1(1/K_c)$.[28] Slopes and intercepts were obtained by least-squares analysis, and the standard deviations were computed in the usual manner.

$$\frac{d}{D} = \left[\frac{1}{K_c\epsilon C_A}\right]\frac{1}{C_D} + \frac{1}{\epsilon C_A} \qquad (1)$$

Table I presents the results for seven disulfides and one sulfide. The uncertainties, which appear to be realistic, decrease with increasing stability of the complex as predicted.[26,27] The values of K_c and ϵ are probably somewhat more reliable than those reported for some other weak complexes since measurements could be made without spectral interference by the donor or acceptor.[29,30] The differences in K_c for the

(22) Estimated from plots of molar extinction coefficient against the frequency in cm.$^{-1}$.
(23) J. Peters and W. B. Person, *J. Am. Chem. Soc.*, **86**, 10 (1964).
(24) P. Job, *Ann. chim. phys.*, [10] **9**, 113 (1928).
(25) *Cf.* ref. 7, Chapter 12. Perusal of the recent literature indicates that only in a few cases is *any* attempt made to establish the stoichiometry of charge-transfer complexes.
(26) H. A. Benesi and J. H. Hildebrand, *J. Am. Chem. Soc.*, **71**, 2703 (1949).
(27) P. R. Hammond, *J. Chem. Soc.*, 479 (1964).
(28) W. B. Person, *J. Am. Chem. Soc.*, **87**, 167 (1965).
(29) N. B. Jurinski and P. A. D. de Maine, *ibid.*, **86**, 3217 (1964).
(30) For some additional examples, see K. Conrow, G. D. Johnson, and R. E. Bowen, *ibid.*, **86**, 1025 (1964).

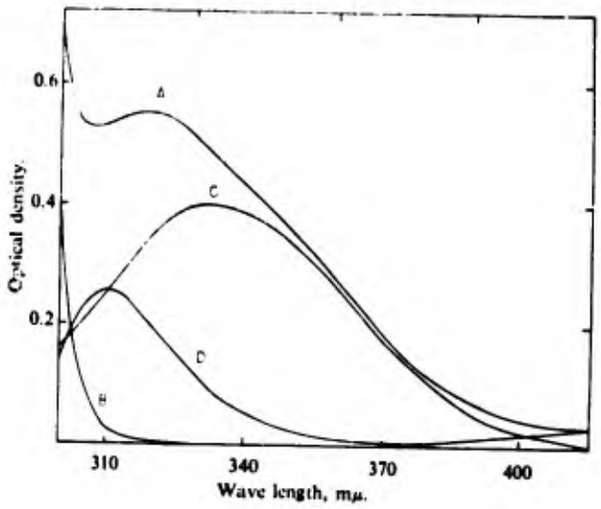

Figure 3. Resolution of the spectrum of a dichloromethane solution 0.0473 *M* in TCNE and 0.0279 *M* in thioctic acid (d = 1.00 cm.): A, solution spectrum; B, free TCNE; C, free -S-S- absorption; D, complexed -S-S- absorption.

three straight-chain alkyl disulfides are obviously not significant, although the increasing trend of $K_c\epsilon$ is clear.

The charge-transfer maxima of some additional disulfide- and sulfide–TCNE complexes are given in the earlier paper,[10] where significant trends are noted. The spectra exhibit a marked solvent dependence. Thus in ethyl acetate the *n*-butyl disulfide complex has a maximum at 410 mμ, compared with 460 mμ in dichloromethane. The spectral characteristics of complexes with some other acceptors are given in Table II.

Table II. Spectral Characteristics of Some Other Disulfide Complexes

Disulfide	λ_{max}, mμ[a] Iodine[b]	Chloranil	TCNQ
Methyl	~300		
Ethyl	302[c]		
n-Amyl	303[c]		
t-Butyl	335	465[d]	510[d]
Tetramethylene	348	465[d]	510[d]
Trimethylene	365		
Thioctic acid	365	550	625

[a] In dichloromethane unless otherwise noted. [b] Iodine in dichloromethane has λ_{max} 500 mμ. Shifted bands, not corrected for uncomplexed iodine, appeared in the region 470–495 mμ. [c] In carbon tetrachloride; *cf.* ref. 4 and 5. [d] These bands appear as barely resolved maxima in the tail of the acceptor absorption.

We note that the maxima for the iodine complexes of the simple alkyl disulfides are very close and are probably identical within experimental error. Thioctic acid is the only compound which shows well-separated charge-transfer absorption with chloranil and tetracyanoquinodimethane (TCNQ).

Figure 3 shows the absorption of a thioctic acid–TCNE solution and its resolution into the component bands due to uncomplexed TCNE and disulfide and complexed disulfide. This was accomplished using K_c and ϵ from Table I in conjunction with the optical density at the charge-transfer maximum. The shift of the -S-S- band is apparent even in the unresolved curve. The resolved shift of 23 mμ is probably reliable to ±3 mμ. With the ethyl disulfide–TCNE complex, the resolution is much less reliable owing to the small magnitudes of K_c and ϵ. Further, with this system the component absorptions overlap considerably, and hence bands due to complexed disulfide and complexed TCNE cannot be unequivocally resolved. Figures 4 and 5 show the curves for two solutions in which the donor:acceptor ratios are 133 and 7, respectively. The complexed component curves (D) are quite similar even though the optical densities of the free TCNE and the free disulfide are inverted in the two cases. The general shape and position of this absorption thus appear to be real, and not due to experimental artifacts. The greater resolution in Figure 4 is not significant and is probably due to the density differences approaching the photometric resolution limit of the instrument. If the two maxima in curve D represent separate species, the implication is that the complexed -S-S- absorption is shifted relative to the free -S-S- absorption either 0·2 mμ to shorter wave lengths or ~6 mμ to longer wave lengths, with complementary conclusions (~9- or ~15-mμ blue shifts) for the TCNE absorption. The significance of

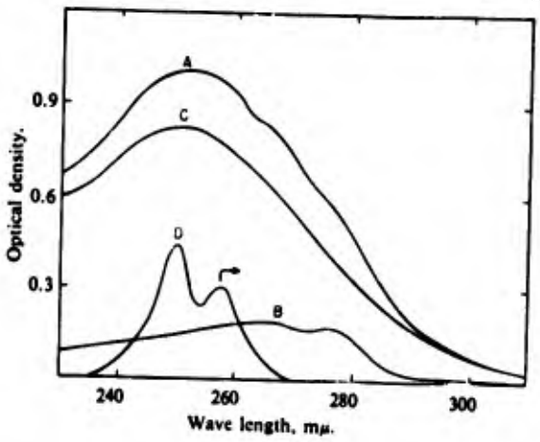

Figure 4. Resolution of the spectrum of a dichloromethane solution 0.232 *M* in ethyl disulfide and 1.74 × 10^{-3} *M* in TCNE (d = 0.075 mm.): A, solution spectrum; B, free TCNE; C, free -S-S- absorption; D, complexed -S-S- and TCNE absorption.

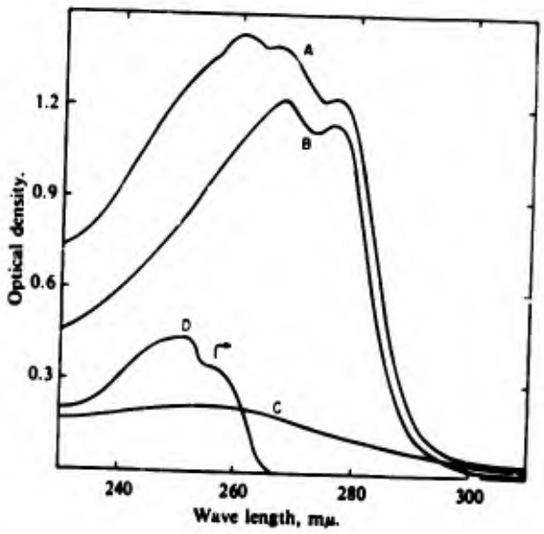

Figure 5. Resolution of the spectrum of a dichloromethane solution 0.0113 *M* in TCNE and 0.0794 *M* in ethyl disulfide (d = 0.075 mm.). The labels are the same as in Figure 4.

such assignments is further obscured by the effect errors in K_c and ϵ (a *minimum* of $\pm 20\%$) have on the resolution of the spectra.

Discussion

Since all the TCNE complexes are weak, the possible contribution of contact charge transfer must be considered.[31] From the most stringent point of view,[27] only six of the K_c values quoted in Table I are significant. Criteria for contact charge transfer are generally the temperature variation of ϵ and decreasing values of ϵ for increasing values of K_c in a series of related complexes. Table I shows that ϵ is temperature independent within experimental error for the two quoted cases. For the series methyl, ethyl, *n*-butyl, *t*-butyl disulfides, and thioctic acid, the ϵ values with one exception (*n*-butyl) increase with K_c. The same trend is shown by the oscillator strengths,[21] which increase from 0.08 for ethyl disulfide to 0.15 for thioctic acid. The enthalpy of formation values for the complexes, obtained from the temperature dependence of $K_c\epsilon$, are clearly in the order methyl disulfide < *t*-butyl disulfide < thioctic acid, and support the trend of K_c. The phenyl and benzyl disulfide complexes have anomalously low extinction coefficients in relation to their stability constants. With these disulfides the aromatic rings may modify the nature of the charge-transfer interaction, perhaps by acting as donor sites or by overlap with the sulfur orbitals (in phenyl disulfide).[32] In limiting further discussion, therefore, to the alkyl disulfide and thioctic acid complexes, we feel justified in assuming that the charge-transfer absorption is predominantly due to complexes of finite stability.

In simple disulfides the dihedral angle (θ) is approximately 90°.[33] *t*-Butyl disulfide has an anomalous absorption spectrum[34] and a smaller dipole moment than other alkyl disulfides[35] which have been ascribed to a larger than normal angle between the bulky *t*-butyl groups. The five-membered ring disulfide, thioctic acid, is generally accepted to have $\theta \approx 0°$.[36,37] From the most elementary point of view, the bonds in divalent sulfur compounds involve only the sulfur 3p orbitals.[36] It is clear that *any* change of θ from 90° (increase or decrease) will *decrease* the angle between the perpendicular 3p orbitals on adjacent sulfur atoms. The data in Table I indicate that the diminution of the charge-transfer transition energy and the growth of K_c and ϵ are associated with a decrease in the sulfur 3p(1)–3p(2) angle. Inductive effects probably play only a very minor role.[38]

In the theoretical treatment, we concern ourselves only with the extreme cases $\theta \approx 90°$ and $\theta \approx 0°$. Pertinent data are available for the ethyl disulfide and thioctic acid complexes. The acid is more stable than trimethylene disulfide, and the spectra of these two cyclic compounds and of their complexes are virtually identical[10,18] (Table II). Of the numerous theoretical approaches[39] we have adopted a modification of the simple, semiempirical, one-electron MO theory developed by Nagakura[40] for intramolecular charge-transfer spectra. The method involves calculation of the energy levels of the disulfide and of TCNE, and then computing the energies of the mixed orbitals constructed from those molecular orbitals of the donor and acceptor for which interaction is allowed by symmetry considerations. The charge-transfer transition is considered to occur between the highest occupied, and the lowest empty, mixed orbital.

In monosulfide–iodine complexes a linear S–I–I arrangement appears to be firmly established,[41] and a perpendicular orientation of the iodine molecule to the S–S bond has been assumed in disulfide complexes. With TCNE we utilize Mulliken's principle of maximum overlap[42] to arrive at the structures shown in Figure 6a and 6b for the alkyl and cyclic disulfide complexes, respectively. Confining symmetry considerations to the disulfide bond region, we may assign symmetry C_2 to the alkyl disulfide ($\theta \approx 90°$) and symmetry C_{2v} ($\theta \approx 0°$) to the cyclic disulfide. Since TCNE belongs to point group D_{2h}, the symmetries of the complexes become C_2 and C_s, respectively.[43] The π molecular orbitals of the disulfide may be expressed as linear combinations of the 3p orbitals (χ_1 and χ_2) on the two sulfur atoms

$$\Phi_\pm = c_\pm(\chi_1 \pm \chi_2) \tag{2}$$

where + and − designate the bonding and antibonding orbitals, respectively.[5,37] When $\theta = 90°$, these become degenerate, perpendicular 3p orbitals. For TCNE, with the ten atoms labeled A through J, the molecular orbitals are expressed as linear combinations of the atomic 2p orbitals.

$$\Phi_i = c_{iA}\chi_A + \ldots + c_{iE}\chi_E + c_{iF}\chi_F + \ldots + c_{iJ}\chi_J \tag{3}$$

Consideration of the dimensions of the donor and acceptor molecules, shown in Figure 7 as a top view of the structures of Figure 6, suggests that as a first approximation the intermolecular interactions involve primarily the orbital pairs χ_1 and χ_F, and χ_2 and χ_E.[44]

For a given pair of donor and acceptor molecular orbitals, Φ_D and Φ_A, two new perturbed wave functions may be specified as[40]

$$\chi_{1,2} = a_{1,2}\Phi_D + b_{1,2}\Phi_A \tag{4}$$

with the definitions, $H_{AA} = \langle\Phi_A|H_{eff}|\Phi_A\rangle$, $H_{DD} = \langle\Phi_D|H_{eff}|\Phi_D\rangle$, and $\beta_{DA} = \langle\Phi_A|H_{eff}|\Phi_D\rangle$, and neglect of

(31) L. E. Orgel and R. S. Mulliken, *J. Am. Chem. Soc.*, 79, 4839 (1957).

(32) Aryl disulfides behave differently from the corresponding hydrocarbons. Thus the TCNE complexes of phenyl disulfide and mesityl disulfide have maxima at 515 and 430 mμ,[10] respectively, while the benzene and mesitylene complexes absorb at 384 and 461 mμ, respectively.[11]

(33) S. C. Abrahams, *Quart. Rev.* (London), 10, 407 (1956).

(34) H. Koch, *J. Chem. Soc.*, 394 (1949).

(35) M. T. Rogers and T. W. Campbell, *J. Am. Chem. Soc.*, 74, 4742 (1952).

(36) G. Bergson, *Arkiv Kemi*, 12, 233 (1958); 18, 409 (1961).

(37) The observed dihedral angle in a related compound, 1,2-dithiolane-4-carboxylic acid is 27°; *cf.* O. Foss and O. Tjomsland, *Acta Chem. Scand.*, 12, 1810 (1958).

(38) The inductive substituent constants, σ_I, for the alkyl groups in Table I are almost identical; *cf.* R. W. Taft, Jr., and I. C. Lewis, *J. Am. Chem. Soc.*, 80, 2436 (1958).

(39) For a recent review, see R. L. Flurry, Jr., *J. Phys. Chem.*, 69, 1927 (1965).

(40) S. Nagakura and J. Tanaka, *J. Chem. Phys.*, 22, 236 (1954); S. Nagakura, *ibid.*, 23, 1441 (1955).

(41) O. Hassel, *Proc. Chem. Soc.*, 250 (1957); G. Y. Chao and J. D. McCullough, *Acta Cryst.*, 13, 727 (1960).

(42) R. S. Mulliken, *Rec. trav. chim.*, 75, 845 (1956).

(43) Even if the lower symmetry C_s is assumed for the cyclic complex, the arguments which follow are not changed.

(44) For the structure of TCNE, *cf.* D. A. Bekoe and K. N. Trueblood, *Z. Krist.*, 113, 1 (1960).

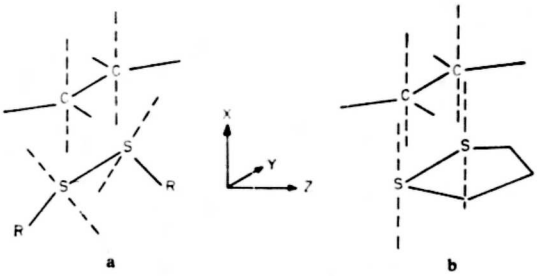

Figure 6. Structures proposed for the TCNE complexes of (a) alkyl disulfides with $\theta \approx 90°$, and (b) cyclic disulfide with $\theta \approx 0°$. The dotted lines represent the long axes of the sulfur 3p and carbon 2p orbitals.

overlap such that $a_{1,2}^2 + b_{1,2}^2 = 1$, solution of the pertinent secular equation yields the energies

$$\epsilon_{1,2} = \frac{1}{2}(H_{AA} + H_{DD}) \pm \frac{1}{2}[(H_{AA} - H_{DD})^2 + 4\beta_{DA}^2]^{1/2} \quad (5)$$

where ϵ_1 corresponds to the $-$ sign and ϵ_2 to the $+$ sign. If the approximation that interaction is confined to χ_1, χ_2, χ_E, and χ_F is now incorporated, β_{DA} may be expressed in terms of the two-center integral $\beta_{SC} = \langle\chi_1|H_{eff}|\chi_F\rangle = \langle\chi_2|H_{eff}|\chi_E\rangle$.

$$\beta_{DA} = c_{\pm}(c_{1E} \pm c_{1F})\beta_{SC} \quad (6)$$

In applying eq. 5 as modified by eq. 6, we identify H_{AA} with the energy of the unperturbed acceptor MO and H_{DD} with the energy of the unperturbed donor MO.[40]

The energies of the disulfide molecular orbitals $\Phi_{\pm}$ are approximately given by[5]

$$\epsilon_{\pm} = (\alpha_S \pm \beta_{SS}\cos\theta)/(1 \pm S\cos\theta) \quad (7)$$

where α_S, β_{SS}, and S represent the Coulomb, exchange, and overlap integrals, respectively. To calculate $\epsilon_{\pm}$, we equate $-\alpha_S$ to the ionization potential of ethyl disulfide (8.5 e.v.[45]). Combined with the difference in the spectral transition energies for ethyl disulfide (4.92 e.v.) and thioctic acid (3.72 e.v.), *i.e.*, 1.20 e.v. $= (\alpha_S S - \beta_{SS})/(1 - S)$ with $S = 0.129$,[48] the value $\beta_{SS} = -2.14$ e.v. is found and $\epsilon_{\pm}$ can be computed as a function of θ.[49] The results are shown in the center of Figure 8.

For TCNE, simple MO calculations were performed with the parameters[50] $\alpha_N = \alpha_C + \beta_{CC}$, $\alpha_{C'} = \alpha_C + 0.1\beta_{CC}$, $\beta_{CN} = 2.0\beta_{CC}$, and $\beta_{CC'} = 0.9\beta_{CC}$, where the subscripts indicate the atoms, with C′ designating the carbon atom bonded to nitrogen. The results pertinent to the present problem are shown in Table III.[51]

(45) An average was taken of the mass spectrometric value (8.85 e.v.[46]) and the photoionization value (8.27 e.v.[47]).

(46) B. G. Gowenlock, J. Kay, and J. R. Majer, *Trans. Faraday Soc.*, 59, 2463 (1963).

(47) K. Watanabe, T. Nakayama, and J. Mottle, *J. Quant. Spectry. Radiative Transfer*, 2, 369 (1962).

(48) The upper σ^- antibonding orbital is taken as independent of θ.[5] The value of S is for an S–S distance of 2.08 Å.

(49) McGlynn[5] attempted to calculate $\epsilon_{\pm}$ from the difference in the transition energies and the rotational barrier about the –S–S– bond (0.52 ± 0.09 e.v.). It can be easily shown that his equations can be rearranged to

$$4S(\alpha_S S - \beta_{SS})/(1 - S) = 4.68S = (1 + S)(0.52 \pm 0.09)$$

which, with $S = 0.129$ become identical and cannot be solved for α_S and β_{SS}.

(50) The relation $\beta_{CN} = 2.0\beta_{CC}$ gave good agreement between the calculated and observed spin densities for a number of cyano radicals; see P. H. Rieger and G. K. Fraenkel, *J. Chem. Phys.*, 37, 2795 (1962).

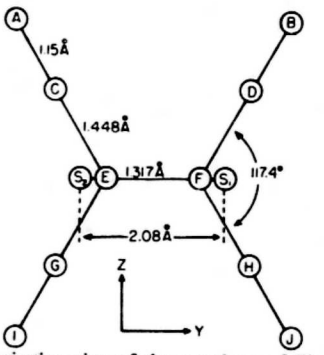

Figure 7. Projection view of the complexes of Figure 6. A–J represent the TCNE molecule, with A, B, I, and J the nitrogen atoms. S_1 and S_2 are the two sulfur atoms of the disulfide.

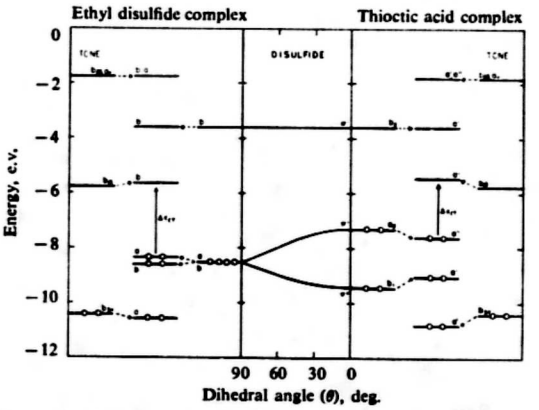

Figure 8. Orbital energies for TCNE, for the disulfide as a function of θ, and for the TCNE complexes of ethyl disulfide and thioctic acid. Labels are the symmetries of the orbitals. The –S–S– absorption of the uncomplexed disulfide corresponds to $\pi^- \rightarrow \sigma^-$ for $\theta < 90°$ and $\pi^* \rightarrow \sigma^-$ for $\theta = 90°$.

To place these levels on an absolute scale, we again equate the energy of the highest-filled MO (b_{3u}) with the ionization potential (I_p) which, in the absence of an experimental value, is estimated as 10.4 e.v.[52] The other levels are located by spectral correlation. TCNE shows a structured band with λ_{max} 266 mμ (ε 13,900) (dichloromethane) which, for present purposes, is assigned to the allowed π–π^* transition $A_{1g} \rightarrow B_{2u}$.[53]

(51) For a previous simple MO calculation, see B. R. Penfold and W. N. Lipscomb, *Acta Cryst.*, 14, 589 (1961). These authors' results were approximately matched with $\beta_{CN} = 1.2\beta_{CC}$, and $\beta_{CC} = -2.55$ e.v. These levels do not, however, yield a satisfactory spectral correlation (see text).

(52) For acrylonitrile the reported ionization potentials are 10.75 e.v. (mass spectrometric value, J. D. Morrison and A. J. C. Nicholson, *J. Chem. Phys.*, 20, 1021 (1952)) and 10.91 e.v. (photoionization value[47]). In arriving at the estimated value for TCNE, it was noted that although the introduction of additional electronegative groups is expected to raise I_p, increased conjugation has the opposite effect.[47]

(53) This band is at 254 mμ for the vapor[54] and thus appears to show the red-shift behavior characteristic of π–π^* (N → V) transitions.[55] However, on the basis of polarized ultraviolet and infrared spectral measurements with crystals of TCNE, this absorption has been ascribed to a Rydberg N → R transition ($A_{1g} \rightarrow B_{3u}$) superimposed on an N → V transition.[54] (Note that owing to a different choice of axes, B_{3u} here corresponds to B_{1u} in ref. 54.) The Rydberg orbital has symmetry a_{1g}, which is not an irreducible representation for the π-MO's of TCNE in D_{2h} and is not amenable to the MO treatment developed here. Vacuum ultraviolet measurements, currently in progress in this laboratory (J. L. Roebber), should clarify the nature of the transition.

(54) J. Prochorow and A. Tramer, *Bull. Acad. Polon. Sci., Ser. Sci. Math. Astron. Phys.*, 12, 429 (1964).

(55) H. McConnell, *J. Chem. Phys.*, 20, 700 (1952).

Table III. Molecular Orbitals and Energy Levels for TCNE

MO[a]	Symmetry	Energy
$\Phi_8 = 0.312(\Phi_A + \Phi_B - \Phi_I - \Phi_J) - 0.390(\Phi_C + \Phi_D - \Phi_G - \Phi_H)$	b_{2g}	$\alpha_C - 1.50\beta_{CC}$
$\Phi_7 = 0.312(\Phi_A - \Phi_B - \Phi_I + \Phi_J) - 0.390(\Phi_C - \Phi_D - \Phi_G + \Phi_H)$	a_u	$\alpha_C - 1.50\beta_{CC}$
$\Phi_6 = 0.278(\Phi_A - \Phi_B + \Phi_I - \Phi_J) - 0.188(\Phi_C - \Phi_D + \Phi_G - \Phi_H) - 0.524(\Phi_E - \Phi_F)$	b_{1g}	$\alpha_C - 0.36\beta_{CC}$
$\Phi_5 = 0.268(\Phi_A + \Phi_B + \Phi_I + \Phi_J) - 0.597(\Phi_E + \Phi_F)$	b_{1u}	$\alpha_C + 1.00\beta_{CC}$

[a] Φ_1 is the lowest and Φ_5 the highest occupied MO. The accidental degeneracy of Φ_7 and Φ_8 was also obtained for the Φ_3 and Φ_4 orbitals which have the same symmetries (a_u and b_{2g}).

Table IV. Calculated and Observed Spectra of Some Cyanoethylenes

Compound	$x_{t+1} - x_t$[a]	Transition energy, e.v. Calcd.	Obsd.	$\epsilon \times 10^3$	Solvent
Acrylonitrile	1.76	6.05	6.11[b]	6.0	Ethanol
1,2-Dicyanoethylene	1.57	5.40	5.58[c]	~13–16	Ethanol
Tricyanoethylene	1.46	5.02	5.23[d]	13.1	Ether
Tetracyanoethylene	1.36	(4.66)	4.66[e]	13.9	Dichloromethane

[a] In units of β_{SS}; $\epsilon_t = \alpha_C + x_t\beta_{SS}$. [b] R. Heilman, J. Bonnier, and G. de Gaudemaris, *Comp. rend.*, **244**, 1787 (1957). [c] The *cis* and *trans* compounds have the same λ_{max}, with the lower ϵ for the *cis* compound: R. L. Webb, S. Frank, and W. C. Schneider, *J. Am. Chem. Soc.*, **77**, 3491 (1955). [d] C. L. Dickinson, D. W. Wiley, and B. C. McKusick, *ibid.*, **82**, 6132 (1960). [e] This study.

This leads to the rather high value $\beta_{CC} = -3.44$ e.v. To check whether this value indeed provides a spectral correlation for cyanoethylenes, MO calculations using the same parameters were performed for three compounds, with the reassuring results given in Table IV.

With $\theta \approx 90°$ in ethyl disulfide, the orbitals on the sulfur atoms are inclined 45° to the plane defined by the long axes of the orbitals (χ_E and χ_F) on the central atoms of TCNE (*cf.* Figure 6a). Let β_{SC} represent the exchange integral for the cyclic disulfide complex in which the orbitals χ_1, χ_2, χ_E, and χ_F are essentially coplanar (Figure 6b). Then, if the intermolecular separation remains constant, the exchange integral (β'_{SC}) for the structure of Figure 6a is, to a good approximation, given by $\beta'_{SC} = \beta_{SC} \cos\theta = 0.707\beta_{SC}$. Using eq. 5 and 6 with $\beta_{SC} = -0.92$ e.v. ($\beta'_{SC} = -0.65$ e.v.), the energy levels shown in Figure 8 were computed. Typical mixing parameters for the new donor levels in the complexes are $\beta_{DA} = -0.73$ e.v., $a_1 = 0.932$, and $b_1 = 0.367$ for b_{1g} and a_2 levels; and $\beta_{DA} = -0.48$ e.v., $a_1 = 0.987$, and $b_1 = 0.168$ for the b_{1g} and b levels.

The calculated and observed spectral data are summarized in Table V. The model predicts a red-shifted –S–S– absorption for the ethyl disulfide complex (second a level → third b level) without recourse to a changed dihedral angle which has been postulated to accompany charge transfer in the ground state.[5] Judging by the mixing parameters quoted above, the extent of ground-state charge transfer is extremely small for this complex. None the less, a slight structural adaptation of the disulfide cannot be excluded, and may well accompany the orbital perturbations. The –S–S– absorption of the complexed cyclic disulfide (lowest a'' level → third a'' level) is predicted to be blue-shifted as observed. For thioctic acid, θ is undoubtedly greater than 0° as we have assumed,[38] but any further diminution would probably be strongly opposed by the geometrical requirements of the ring. Thus in this complex, orbital perturbation is the predominant factor responsible for the absorption shift.

Table V. Calculated and Observed Transitions for Disulfide–TCNE Complexes

Transition	Energy, e.v.[a] Calcd.	Obsd.
Thioctic Acid Complex		
Charge transfer	2.14	2.13
Complexed RSSR	4.01	4.00
Complexed TCNE	5.34	*b*
Ethyl Disulfide Complex		
Charge transfer	2.70	2.76
Complexed RSSR	4.77	4.82, 4.94
Complexed TCNE	4.89	

[a] Observed values for free RSSR are 4.92 (thioctic acid) and 3.72 e.v. (ethyl disulfide). [b] No measurements were made in this spectral region.

The empirical equation of McConnell, Ham, and Platt may be utilized[56] to estimate the ionization potentials of some disulfides which lack experimental values. Based on spectral data from Table I and photoionization potentials of 8.46 and 8.27 e.v.[47] for methyl and ethyl disulfides, respectively, this takes the form[57]

$$h\nu_{CT} = 0.85I_p - 4.3 \text{ e.v.} \qquad (8)$$

Since only two close points were used, the error in this equation could be large. Some illustrative values are 7.78 and 7.57 e.v. for *t*-butyl and trimethylene disulfides, respectively. For the latter compound the estimate is much lower than a previous one of 8.53 e.v.[5]

Acknowledgments. This study was sponsored by the U. S. Air Force Cambridge Research Laboratories, Office of Aerospace Research, under Contracts AF 19(604)-7358 and AF 19(628)-3836. We are grateful to Drs. J. L. Roebber, R. N. Wiener, and K. H. Bar-Eli for many fruitful discussions. Samples of several sulfur compounds were kindly furnished by the U. S. Bureau of Mines, Laramie, Wyo. We also wish to thank Mr. Eric Reid for his aid with the computation work which was carried out at the MIT Computation Center.

(56) H. McConnell, J. S. Ham, and J. R. Platt, *J. Chem. Phys.*, 21, 66 (1953).

(57) This equation is almost identical with the equation given for substituted benzene–TCNE complexes by E. M. Voigt and C. Reid, *J. Am. Chem. Soc.*, 86, 3930 (1964).

APPENDIX G

[Reprinted from the Journal of Physical Chemistry, 71, 2633 (1967).]

The Laser Photolysis of Methylene Blue

by Robert M. Danziger, Kedma H. Bar-Eli, and Karl Weiss

Photochemistry and Spectroscopy Laboratory, Department of Chemistry, Northeastern University, Boston, Massachusetts 02115 *(Received January 30, 1967)*

The giant pulse ruby laser flash photolysis of plain aqueous methylene blue solutions reveals three transient species (A, B, and C) with half-lives of ~2, 30, and 140-μsec, respectively. With a 5.5×10^{-6} *M* dye solution a 0.5-joule, 30-nsec pulse causes almost complete conversion into transients. The photochemical change is completely reversible. Experiments at various concentrations in the range 5.5–294 $\times 10^{-6}$ *M* indicate that transients A and C are derived from the dimeric form of the dye, which exists in equilibrium with the monomer. It is proposed that transients A and B are the triplet states of the dimer and monomer, respectively, and that transient A decays primarily into the longer lived transient C, which is viewed as a charge-transfer state of the dimer. The creation of C by reaction of the monomer triplet (B) with the ground-state monomer is estimated to be slower than diffusion controlled. The establishment of the ground-state monomer–dimer equilibrium appears to be slower than all the transient decay processes. The results obtained by laser photolysis and conventional flash photolysis are compared.

Introduction

The pulsed ruby laser constitutes an ideal flash photolysis source. The output is strictly monochromatic at 6493 A and with Q-spoiling techniques flash durations of 30×10^{-9} sec are readily achieved.[1] These properties have obvious advantages for the study of very short-lived transients.[2] In this paper we report the giant pulse laser flash photolysis of aqueous methylene blue solutions. The dye shows strong absorption in the 5000–7000-A region, which encompasses the ruby laser emission line ($\epsilon_{6943} \sim 1 \times 10^4$ in water). Extensive previous photochemical studies indicate that methylene blue is readily photoreduced[3-5] and conventional flash photolysis has revealed two transient species.[6,7] It was not anticipated that the dye would show markedly different behavior with laser excitation. Rather, this study was designed to develop the tech-

(1) B. A. Lengyel, "Introduction to Laser Physics," John Wiley and Sons, Inc., New York, N. Y., 1966.

(2) Chemical applications of lasers, actual and potential, have recently been reviewed by D. L. Rousseau, *J. Chem. Educ.*, 43, 566 (1966).

(3) M. Koizumi, H. Obata, and S. Hayashi, *Bull. Chem. Soc. Japan*, 37, 108 (1964), and previous papers cited.

(4) G. Oster and N. Wotherspoon, *J. Am. Chem. Soc.*, 79, 4836 (1957).

(5) C. A. Parker, *J. Phys. Chem.*, 63, 26 (1959).

(6) S. Kato, M. Morita, and M. Koizumi, *Bull. Chem. Soc. Japan*, 37, 117 (1964).

(7) S. Matsumoto, *ibid.*, 37, 491 (1964).

nique of laser flash photolysis and to make measurements in the time range not accessible by conventional means.

Experimental Section

Methylene Blue. The dye (Fisher Certified reagent, 88–90% dye content) was purified by the method of Bergmann and O'Konski.[8] The ratio of the optical densities at 6650 and 6200 A was 2.0, indicative of the absence of demethylated forms. Concentrations were computed to ±2% from the reported[8] extinction coefficients. The transient characteristics of the unpurified dye were quite similar to those of the purified dye, although the decay rates were faster.

Apparatus and Procedure. The photolysis apparatus is shown diagramatically in Figure 1. Central to its operation is a Maser Optics, Inc., Model 869 water-cooled laser head which accommodates a $^3/_8$-in. diameter, 6.5-in. long ruby rod. Energy for the two flash tubes is supplied by a circuit consisting of an 8.5-kv power supply, a 1560-μf capacitor bank, and a 400-μhenry inductance. The triggering mode is internal by means of an Atlas Engineering Co. transformer No. 7831, which amplifies an 800-v trigger pulse to 2.4 kv. Q spoiling is accomplished with a methanolic solution of cryptocyanine.[9] Single 30-nsec pulses are obtained by adjusting the concentration of the cryptocyanine solution and the input voltage in the range 2.2–2.9 kv. The energy is 0.5 joule (±5%)/pulse, as measured calorimetrically, corresponding to *ca.* 10^7 w. The operation of the unit is extremely reproducible. Even the scattered laser light is extremely intense and its elimination at the detection end is critically dependent on the placement of the components. It was possible to achieve freedom from stray light below 6500 A.

The laser beam makes an angle of *ca.* 15° to a monitoring beam which originates from a General Electric Type CPR 108-W battery-operated tungsten projection lamp (LS) and terminates in a Bausch and Lomb 250-mm grating monochromator. Masks, which have to be carefully placed so as not to be hit by the *ca.* 12-mm diameter laser beam, serve to confine the monitoring light to the irradiated portion of the reaction cell. Firing of the photolysis unit is accomplished as follows. A wave form and pulse generator (Tektronix Types 162 and 161) actuate the 800-v trigger pulse generator, which causes the flash lamps to fire. The flash duration is *ca.* 2 msec. Scattered light from the Q-spoiled laser flash, which is produced during this interval, is registered on photomultiplier PM 1 (RCA 1P28, emitter follower). The rising current pulse in this tube triggers a Fairchild 777 dual beam oscilloscope which displays the laser spike and the transient absorption changes. The latter are registered on photomultiplier PM 2 (RCA 1P28, EMI 6256B, or DuMont 6911, and cathode follower). After a 1-sec delay, the absorption display is triggered again to provide a base line. Tests established that the position of this trace is the same as before lasing. The time resolution is *ca.* 2 μsec for PM 2 and *ca.* 0.5 μsec for PM 1. The laser pulse is thus partially integrated, but it was shown that the maximum pulse height remains proportional to the energy.

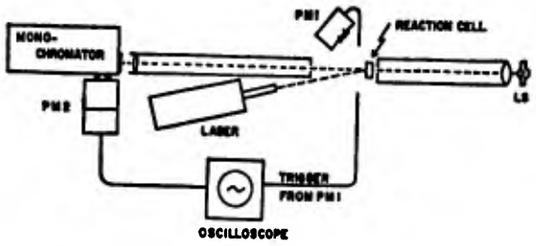

Figure 1. Laser flash photolysis apparatus.

The quartz reaction cells are cylindrical with a 2.5-cm diameter and a 1-cm path length. Dye solutions were prepared in distilled water. Degassing was carried out in bulbs attached to the reaction cell by first expelling dissolved carbon dioxide by bubbling purified nitrogen through the solution followed by freeze-(−200°)-pump-thaw cycles. The photolyses were run at ambient temperature (23 ± 1°) without specific temperature control. A single Q-spoiled pulse produced no measurable temperature change. With cells of longer path length (3–14 cm) the transient decay curves showed a superimposed, high-frequency (100-kc) sinusoidal pattern whose origin remains obscure.

The oscilloscope traces were recorded on Polaroid film and digital information was obtained directly from the photographic record with a Gerber data reduction system. These data were evaluated in terms of ΔD, the change in optical density relative to that of the unexcited solution. Conventional spectrophotometric measurements were made with a Beckman DK-1 spectrophotometer.

For comparison with the laser results and literature reports,[6,7] conventional flash photolysis experiments were conducted under one set of conditions. The apparatus for this purpose, which will be described in detail elsewhere, incorporates xenon-filled flash tubes which provide *ca.* 20-μsec pulses with input energies

(8) K. Bergmann and C. T. O'Konski, *J. Phys. Chem.*, 67, 2169 (1963).

(9) P. Kafalas, J. I. Masters, and E. M. E. Murray, *J. Appl. Phys.*, 35, 2349 (1964).

in the range 100–5600 joules. A 7.0×10^{-6} M solution of methylene blue was used, which was freed of oxygen by bubbling water-saturated, purified nitrogen through it for 45 min. Since the unfiltered flash causes irreversible bleaching of the dye, the cylindrical "Pyrex" reaction cell (14 cm, 2-cm diameter) was covered with a Roscoe No. 809 filter, which confines light to the visible absorption band. The input energy was 250 joules/flash.

Results

1. General Features. Plain aqueous solutions of methylene blue in the concentrated range 294×10^{-6} to 5.5×10^{-6} M were studied. With the most dilute solution employed, the 0.5-joule laser pulse suffices to convert the ground-state dye almost completely into transients. The changes which occur are completely reversible; thus there is no detectable change in optical density after many laser flashes and after prolonged exposure to the glass-filtered monitoring light. From Bergmann and O'Konski's spectral data,[8] a radiative lifetime of 9.8 nsec can be calculated for the methylene blue singlet excited state. The quantum yield of fluorescence is low[10] so that the actual lifetime of this state is at least an order of magnitude smaller. This lifetime, in conjunction with the 30-nsec pulse duration and the high intensity, constitutes the conditions for absorption saturation with respect to the singlet–singlet transition and for the inapplicability of Beer's law.[11] Although no measurements using the split-beam technique[11] were made with methylene blue, there is reason to believe that initial conversion to the singlet excited state was essentially complete even in the most concentrated solution. The number of light quanta is always in excess of the number of molecules in the irradiated volume.

2. Transient Spectra. The general features of the transient spectra are similar at all the concentrations examined. Maxima appear at 420, 520, and in the 700–900-mμ region, which parallels the results obtained by conventional flash photolysis.[6,7]

The transient behavior of the 5.5×10^{-6} M solution is shown in Figures 2–5. Decay at 520 mμ is slower than that at 420 mμ (Figure 2), which is indicative of at least two transients with absorption in this region. The bleaching region (570–695 mμ) is shown in Figure 3. In this case the transient optical density, obtained by adding the ground-state optical density to ΔD, is plotted to portray the extent of bleaching. The 8-μsec curve stops at 660 mμ, since beyond this wavelength a photomultiplier circuit with slower response was used. The ground-state absorption curve of the dye (dotted line) was obtained by spectrophotometer. The curves

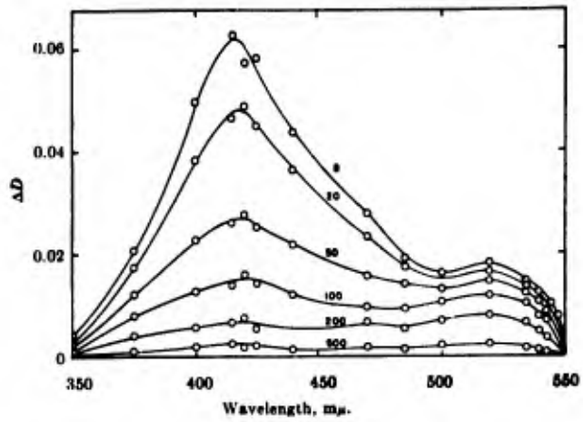

Figure 2. Transient absorption in the 350–550-mμ region, 5.5×10^{-6} M methylene blue. The numbers indicate the time in microseconds after the laser flash.

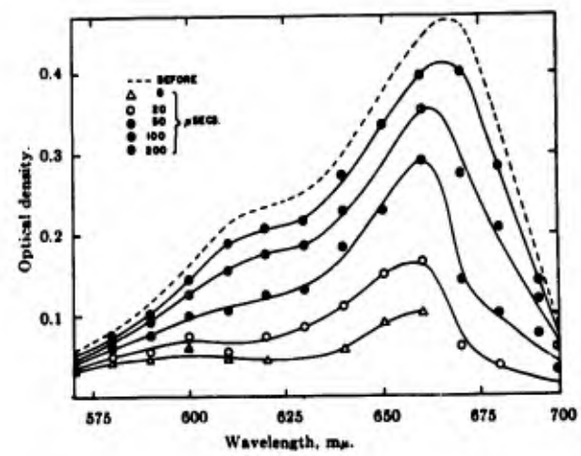

Figure 3. Transient bleaching in the 570–700-mμ region, 5.5×10^{-6} M methylene blue.

corresponding to bleaching resemble the ground-state curve quite closely. The apparent ~5-mμ shift in the maximum is probably due to a calibration discrepancy between the flash apparatus monochromator and the spectrophotometer and it is probable that there is no absorption due to transient species in the 600–680-mμ range. Extrapolation of log ΔD *vs.* time curves to zero time for wavelengths in the vicinity of the maximum indicates at least 90% bleaching. Figure 4 represents

(10) N. Wotherspoon and G. Oster, *J. Am. Chem. Soc.*, **79**, 3992 (1957).

(11) Absorption saturation by laser radiation has been observed with phthalocyanine and cryptocyanine solutions. *Cf.* J. A. Armstrong, *J. Appl. Phys.*, **36**, 471 (1965); F. Gires and F. Combaud, *J. Phys. Radium*, **26**, 325 (1965); F. T. Arecchi, V. Degiorgio, and A. Sona, *Nuovo Cimento*, **38**, 1096 (1965); V. Degiorgio and G. Potenza, *ibid.*, **41**, 254 (1966); C. R. Giuliano and C. D. Hess, *Appl. Phys. Letters*, **9**, 196 (1966).

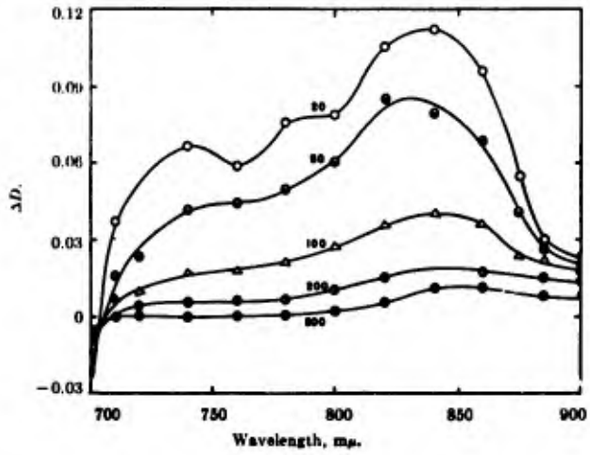

Figure 4. Transient absorption in the 700–900-mμ region, 5.5×10^{-6} *M* methylene blue. The numbers indicate the time in microseconds after the laser flash.

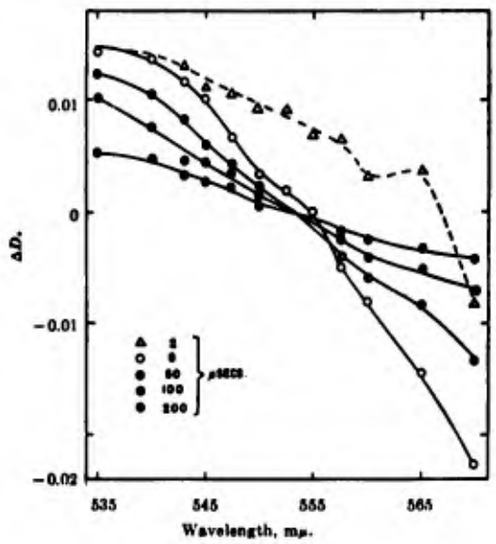

Figure 5. Transient changes in the 535–570-mμ isobestic region, 5.5×10^{-6} *M* methylene blue.

transient absorption in the near-infrared region. Maxima appear at 740, 780, and 840 mμ. The decay is rapid, as it is near 420 mμ, although a slow component is again apparent above 800 mμ. By placing a cryptocyanine filter solution in front of the monochromator entrance slit it was possible to observe methylene blue fluorescence[12] above 720 mμ.

From the shape of the absorption curves, it is clear that isosbestic points appear near the short-wavelength and long-wavelength edges of the ground-state band. In the 540–560-mμ isosbestic region an extremely short-lived transient is apparent (Figure 5)

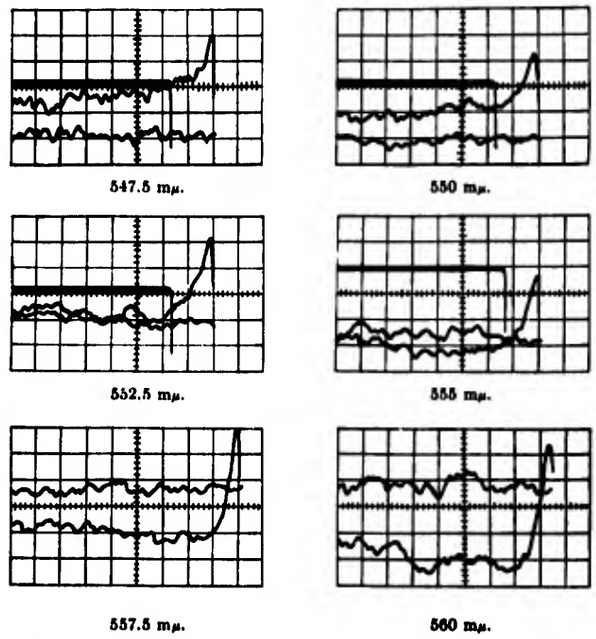

Figure 6. Oscilloscope traces in the isosbestic region. The ordinates are 0.05 v/major division and the abscissas 5 μsec/major division, except at 547.5 mμ where it is 10 μsec/major division. The voltage deflection due to the monitoring light is 8.0 v in all cases. The horizontal traces represent the base lines. For the laser spikes at 547.5–555 mμ, the axes are 2.0 v/cm and 20 μsec/cm.

which is not detectable under ordinary flash conditions. After ~10 μsec an isosbestic point due to the longer lived transients appears at 552.5 mμ. This is shown clearly in the oscilloscope traces of Figure 6, which indicate that the decay of the transient is complete in *ca.* 10 μsec. The apparent half-life is 2 μsec or less, which is just about the time resolution of the measurements. The fast transient is not distinctly manifested in other spectral regions; below 420 mμ, maximum absorption is reached after less than 2 μsec, whereas near 520 mμ it is reached after *ca.* 6 μsec. In the region above 660 mμ, the fast transient is outside the time resolution of detection and consequently an uncomplicated isosbestic point appears at 705 mμ. The lower wavelength isosbestic point with respect to the longer lived species changes regularly with concentration, being 552.5, 550, 546, 544, and 540 mμ at 5.5, 23.8, 55.0, 130, and 294×10^{-6} *M*, respectively.

The relative proportion of the transients changes with the concentration of the dye. At 546 mμ, the isosbestic point for a 55×10^{-6} *M* solution of methylene

(12) G. N. Lewis, O. Goldschmid, T. T. Magel, and J. Biegeleisen, *J. Am. Chem. Soc.*, 65, 1150 (1943).

blue, the maximum ΔD due to the fast transient, is 0.018. For the 5.5×10^{-6} M solution, the fast transient contribution to ΔD is 0.0025 at the same wavelength. Measurements in the ground-state absorption region indicate a maximum of 30% bleaching and conversion into the longer lived transient states for the more concentrated solution. Since conversion is essentially complete in the dilute solution, $\Delta D_{max} \sim 0.08$ is expected for 55×10^{-6} M. The larger than anticipated ΔD_{max} value thus reflects a change in the *composition* of the solution with increasing concentration. Methylene blue exists in monomer–dimer equilibrium in aqueous solution[8,13,14] and the most reliable value of the dissociation constant is $(1.7 \pm 0.2) \times 10^{-4}$ mole/l. at 25°.[8] With this information, one can calculate the fractions of dimer to be 0.30 and 0.055 for the 55×10^{-6} and 5.5×10^{-6} M solutions, respectively. These considerations strongly suggest that the fast transient is derived from the dimeric dye species. The decay kinetics (*vide infra*) indicate that the 400 and 800-mμ regions represent absorption by two components and that a single species absorbs near 500 mμ. The ratio $\Delta D_{max}^{520}/\Delta D_{max}^{820}$ increases with increasing fraction of dimer as shown in Figure 7. This implies that the slow 520-mμ transient is also dimeric and that absorption at 820 mμ is predominantly due to a monomer-derived species. Owing to the slower detection circuit response, the maximum absorption change is observed at a longer time after the flash at 820 mμ than at 520 mμ and this probably accounts for the failure of the plot of Figure 7 to extrapolate to a zero value for the ΔD ratio.

3. Decay Kinetics. A detailed kinetic analysis was made only for the 5.5×10^{-6} M solution, although some results for the 55×10^{-6} M solution will be quoted. Analysis for the more concentrated solutions is complicated by substantial ground-state dye absorption throughout the 350–720-mμ region. Every indication is that, apart from the fast transient, there are two longer lived transients generated. Labeling these A, B, and C in order of increasing lifetime, we have

$$\Delta D = \epsilon_A C_A + \epsilon_B C_B + \epsilon_C C_C + \epsilon_M(C_M - C_M^\circ) + \epsilon_{M_2}(C_{M_2} - C_{M_2}^\circ) \quad (1)$$

where M and M_2 represent the monomeric and dimeric dye, respectively, ϵ the molar extinction coefficients, and C the concentrations. The superscript degree refers to initial concentrations. The expression becomes simpler in different spectral regions for the dilute solution since ϵ_M and ϵ_{M_2} are negligible between 350 and 540 mμ and above 720 mμ and it is assumed that there is no transient absorption between 600 and 680 mμ. Further, $C_A = 0$ after 10 μsec.

In the region 485–540 mμ, the decay of ΔD is strictly first order for at least three half-lives. Rate constants for the decay of the slowest transient (C), to which absorption in this range is ascribed, are quoted in Table I. The tenfold change in concentration is seen to be without effect on the rate.

Table I: Rate Data for Transient C

λ, mμ	$k_C \times 10^{-3}$ sec^{-1} [a]	
	5.5×10^{-6} M	55×10^{-6} M
485	5.2 (3)	
500	4.9 (3)	
520	4.4 (3)	4.9 (2)
535	4.4 (1)	
540	5.7 (1)	5.2 (2)
543	5.5 (1)	5.3 (2)
	Av $k_C = (5.0 \pm 0.5) \times 10^3$ sec^{-1}	

[a] Average value for the number of runs quoted in brackets.

At wavelengths where two transients absorb (below 480 mμ and above 720 mμ), the data were found to fit two concurrent first-order processes. The rate constant for the faster transient (B) was obtained by extrapolation and subtraction of the contribution of the slower transient, as illustrated for decay at 400 mμ in Figure 8. Similar behavior is shown in the bleaching

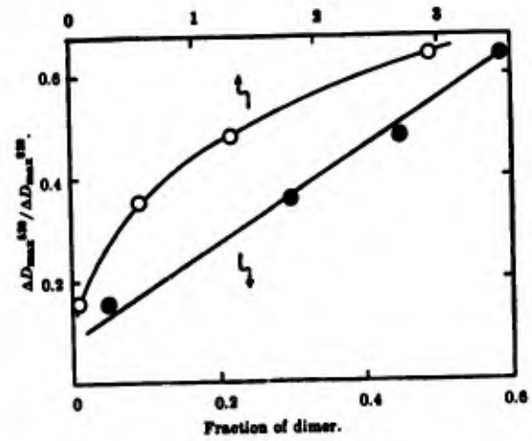

Figure 7. Variation of the relative amounts of transients as a function of the concentration and composition of the solution.

(13) G. Holst, *Z. Physik. Chem.* (Leipsig), A182, 321 (1938).

(14) (a) E. Rabinowitch and L. F. Epstein, *J. Am. Chem. Soc.*, 63, 69 (1941); (b) B. Broyde and G. Oster, *ibid.*, 81, 5099 (1959), report that the irradiation of glasses containing a high concentration of thiazine dyes and a mild reducing agent leaves a species with strong absorption in the 500–600-mμ region which they identify as the entrapped dimer of the dye.

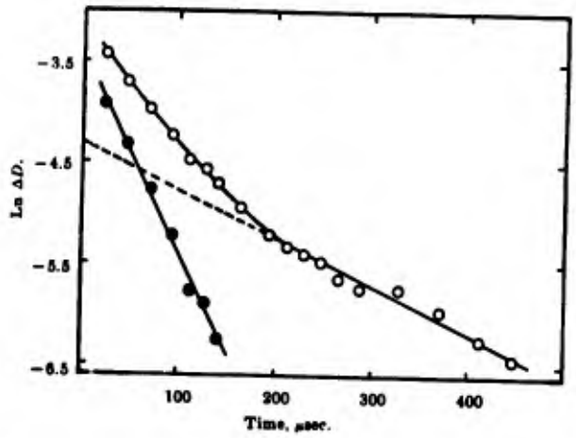

Figure 8. Decay kinetics at 400 mμ, 5.5×10^{-6} *M* methylene blue.

region, where the recovery of absorption mirrors the disappearance of transients B and C. These results are summarized in Table II. The value of k_c given here is in satisfactory agreement with the one listed in Table I. The data in Table II refer to the dilute solution. For the 55×10^{-6} *M* solution, evaluation of the decay at 420 mμ provides the value $k_c = 4.2 \times 10^3$ sec^{-1} for the slow transient, which is comparable to the tabulated values. However, the extracted contribution of transient B does not show first-order behavior, the apparent first-order constant decreasing from $\sim 50 \times 10^3$ sec^{-1} at 20 μsec to $\sim 20 \times 10^3$ sec^{-1} at 100 μsec. Evidently, another decay mode becomes important in concentrated solutions.

Discussion

The results leave little doubt that the monomeric and dimeric forms of methylene blue give rise to transients by separate excitation. The ground-state absorption spectra of the two species indicate an isosbestic point close to the excitation (laser) wavelength at which $\epsilon_{M_2} \approx 2\epsilon_M$.[8] Consequently, the fractions of the total absorbed light which is absorbed by the monomer and dimer are simply α and $1 - \alpha$, respectively, where $\alpha = C_M/(C_M + 2C_{M_2})$. Since the fast transient (A) appears to be derived from the dimer, the excitation processes may be formulated as

$$M_2 \longrightarrow M_2^* \longrightarrow A \qquad (2)$$

$$M \longrightarrow M^* \longrightarrow B \qquad (3)$$

The starred species represent the first excited singlet states and, for reasons set forth below, we assign A and B to the corresponding triplet states.[15] Competing with the rapid conversion to A and B are the processes $M_2^* \rightarrow M_2$ or 2M and $M^* \rightarrow M$. Little can be said about the former reaction other than, reasoning by analogy with the behavior of thionine,[14a] that it is probably entirely radiationless. On the other hand, the competing decay of M^* proceeds with and without emission.[10] On the basis of photochemical reduction studies with methylene blue in dilute aqueous solution (where $C_M >> C_{M_2}$), the quantum yield of the singlet–triplet intersystem crossing has been estimated as 0.2.[4,16] This value renders the observed extensive long-lived depletion of the ground state entirely reasonable. The identification of A and B as triplets is based on their lifetimes ($t_{1/2} \lesssim 2$ and 30 μsec, respectively) and their sensitivity to oxygen. In air, the decay of A is so rapid that its absorption is below the limit of detection. At the same time, the amount of the slowest transient (C) is decreased, but its decay rate is about the same as in the degassed solution. Air causes a decrease in the amount of transient B formed and substantially increases its decay rate. This behavior has already been noted for the 420 and 520-mμ peaks.[6] The lifetime of transient B agrees within a factor of 2 with that obtained by quenching the photoreduction of methylene blue.[4]

The simplified decay scheme is proposed

$$A \xrightarrow{k_A} C \qquad (4)$$

$$A \xrightarrow{k_{A'}} M_2 \text{ (or 2M)} \qquad (5)$$

$$B \xrightarrow{k_B} M \qquad (6)$$

$$B + M \xrightarrow{k_{B'}} C \qquad (7)$$

Table II: Rate Data for Transients B and C in the λ < 480-mμ, Bleaching, and Near-Infrared Regions[a]

λ, mμ	$k_B \times 10^{-3}$ sec^{-1}	$k_C \times 10^{-3}$ sec^{-1}
375	23	5.1
400	20	4.9
420	26	4.3
470	26	5.1
600	25	3.9
610	23	4.2
620	25	4.1
630	25	4.4
820	27	5.0
860	25	3.0
Av	(25 ± 2)	Av (4.4 ± 0.5)

[a] 5.5×10^{-6} *M* methylene blue solution.

(15) Although the lifetime of A is clearly shorter than observed here, a simple calculation based on the response characteristics of the detection circuit shows that A is not likely to be M_2^*.

(16) N. Kosui, K. Uchida, and M. Koisumi, *Bull. Chem. Soc. Japan* 38, 1958 (1965).

$$B + M \xrightarrow{k_B''} 2M \text{ (or } M_2) \quad (8)$$

$$C \xrightarrow{k_C} M_2 \text{ (or } 2M) \quad (9)$$

The decay of A into C (eq 4) is reasonable in view of the dimeric nature of both transients. Further, in the 5.5 $\times 10^{-6}$ M solution, the maximum absorption due to C at 520 mμ appears approximately when the decay of A is complete. The contribution of the competing conversion of A into ground-state molecules (eq 5) cannot be estimated, although the intrinsically short lifetime of A may reflect $k_A >> k_A'$, *i.e.*, $k_A \approx 3 \times 10^5$ sec^{-1}.

The fact that the decays of transients B and C can be treated as first-order processes over a wide spectral range indicates that the bimolecular reactions of eq 7 and 8 are unimportant in the very dilute solution. The rate constants k_B and k_C derived from the bleaching region are the same within experimental error as those from the transient absorption regions (Tables I and II). The ground-state absorption of the dimeric dye is at lower wavelengths than the monomer absorption (λ_{max} 605 and 664 mμ, respectively, with comparable extinction[8]), so that this result suggests that B and C retain their molecular identity on decay, *i.e.*, B → M and C → M_2. A further consequence is that the attainment of the equilibrium is slow relative to the transient

$$M_2 \underset{k_2}{\overset{k_1}{\rightleftharpoons}} 2M \quad (10)$$

decays.[17] Since $k_B > k_C$, the concentration of M is larger than allowed by eq 10 during decay, but little recombination takes place in this metastable interval. Since dimerization involves two large ions with identical charge, a less than diffusion-controlled rate seems reasonable although this cannot be documented with pertinent examples. In view of the experimental uncertainties, the inferences drawn here should be regarded as tentative. The direct measurement of the dimerization rates of dyes is clearly desirable.[18]

In the more concentrated solutions in which the ground-state dye concentration is appreciable at all times, contributions from the bimolecular reactions are evident. These processes afford a qualitative explanation of the behavior of the 55 $\times 10^{-6}$ M solution at 420 mμ. At this concentration, the formation of transient C appears to continue after the decay of A since maximum absorption in the 520–540-mμ region is reached only after *ca.* 30 μsec, compared with 6 μsec in the dilute solution. An estimate of k_B' can be obtained as follows. It is assumed that conversion into transients B and C in the dilute solution is complete after 10 μsec following eq 2–4 and that the decay of B (eq 6) is complete after 200 μsec. This provides $\epsilon_C^{520} = 1.2 \times 10^5$, $\epsilon_C^{420} = 1.0 \times 10^5$, and $\epsilon_B^{420} = 9.0 \times 10^3$ as lower estimates of the extinction coefficients. These values allow calculation of the concentrations of B and C in the 55 $\times 10^{-6}$ M solution at the time of maximum absorption at 520 mμ, when the condition $-dC_c/dt = k_C C_C - k_B' C_B C_M = 0$ is assumed to hold. With $C_M \approx C_M^\circ - C_B$, this gives $k_B' \approx 3 \times 10^7$ l./mole sec, which must be considered an order of magnitude value. The significant point is that k_B' is at least an order of magnitude less than the diffusion-controlled value of 6.6 $\times 10^9$ l./mole sec. With the diffusion-controlled rate, transient C is predicted to be still growing at times when it is observed to be decaying. No information pertaining to the quenching of B according to eq 8 could be extracted from the data; however, $k_B'' = k_B'$ is probably an upper limit.[19]

On the basis of their spectral characteristics and lifetimes, there is little doubt that transients B and C are the same as species generated by a filtered xenon flash (Table III). Kato, Morita, and Koizumi[6] propose that transient C is created solely by the reaction of the monomer triplet with the ground-state monomer (eq 7) and assume that this reaction is diffusion controlled. This has now been shown not to be the case. These authors denote C as "a loosely combined pair (consisting of) semiquinone and a half-oxidized state (of

Table III: Comparison of Laser and Conventional Flash Results

Reference	Transient maxima, mμ	Decay: λ, mμ	Decay: $t_{1/2}$, μsec
6	260–280, 415, 520, ~800	415	60–90
		800	70–90
		520	200–260
7	282, 420, 520, 730, 790, 870	414	~130
This study, conventional flash	420, 520, 750, 850	420	55
		420	10[a]
		520	190
		850	45
This study, laser flash	420, 520, ~550, 740, 780, 840	~550 (A)	~2
		420, 820 (B)	30
		520 (C)	140

[a] In air.

(17) Under these circumstances $C_B = C_M - C_M^\circ$ and $C_C = C_{M_2} - C_{M_2}^\circ$ and according to eq 1 with $\epsilon_A = \epsilon_B = \epsilon_C = 0$, the recovery of absorption parallels the decay of B and C.

(18) A somewhat cryptic footnote in ref 14, p 76, indicates that equilibrium may be established quite slowly.

(19) *Cf.* G. Porter and M. W. Windsor, *Discussions Faraday Soc.*, 17, 178 (1954); H. Linschitz, C. Steel, and J. A. Bell, *J. Am. Chem. Soc.*, 66, 2574 (1962).

the dye)," *i.e.*, $(M^+ \cdots M^-)$ or, more correctly, $(MB^{2+} \cdots MB\cdot)$ if MB^+ represents the dye cation. The results of the present study tend to support this structural assignment. The ground-state dimer is considered to be held together by multipole–multipole interactions of the van der Waals type,[8,14a] a concept which has also been applied to certain types of donor–acceptor complexes.[20]

In relation to the dimer, transient C can then be formulated as a charge-transfer state which results from an internal electron transfer. From this point of view, the binding between dye molecules may well be stronger in transient C than in the ground-state dimer.

Acknowledgments. This investigation was supported by U. S. Public Health Service Research Grant RH 00302, Division of Radiological Health, and in part by the U. S. Air Force Cambridge Research Laboratories, Office of Aerospace Research, under Contract No. AF19(628)-3836. We are grateful to Dr. Edward Wall and Mr. Philip Graceffa for carrying out the conventional flash experiments. Mr. Peter A. Schnieper was responsible for the development of most of the electrical equipment used in this work.

(20) M. J. S. Dewar and C. C. Thompson, *Tetrahedron Suppl.*, 7, 97 (1966).

APPENDIX H

[Reprinted from the Journal of Physical Chemistry, 70, 1677 (1966).]

The Electron Spin Resonance Absorption of Solid 1,1-Diphenyl-2-picrylhydrazyl Mixtures. Surface and Aging Effects

by Kedma H. Bar-Eli and Karl Weiss

Tyco Laboratories, Inc., Waltham, Massachusetts 02154, and Photochemistry and Spectroscopy Laboratory, Northeastern University, Boston, Massachusetts 02115 *(Received October 29, 1965)*

Matsunaga and McDowell[1] have reported that the electron spin resonance spectra of mixtures of 1,1-diphenyl-2-picrylhydrazyl (DPPH) with zinc oxide and with nickel oxide show line broadening and an apparent loss of spins when compared with the spectra of DPPH itself. This effect has been ascribed to a transfer of electrons between DPPH and the oxides. DPPH admixed with inert solids is widely employed as a standard in electron spin resonance spectroscopy.[2] In this note we show that an interaction leading to loss of spins can occur even with materials considered to be inert. The extent of spin loss depends on the nature of the material and on the method of mixing.

The measurements were made with a standard Varian V-4500 spectrometer using a single cavity. DPPH (Aldrich Chemical Co.) was used either as received or after recrystallization,[2b] with identical results. Calcium carbonate (Mallinckrodt Analytical reagent), magnesium carbonate, basic (Fisher Certified), and potassium chloride (Baker Analyzed) were used without further treatment. The mixtures were examined in air as weighed samples of constant volume.

A Wig-L-Bug amalgamator (Crescent Dental Manufacturing Co.) served to prepare mixtures of varying DPPH content. For *unground* mixtures the components were merely shaken until homogeneous. For *ground* mixtures (1-min grinding time), a stainless steel ball was included. Once homogeneity was attained by either method, the esr signal amplitude was independent of further mixing. The average particle diameter of DPPH and mixtures with KCl is $>50\ \mu$ before grinding and $\sim 5\ \mu$ after grinding measured by a Fisher Sub-Sieve Sizer. The particle size of $MgCO_3$ mixtures was determined by the carbonate itself which is $<0.5\ \mu$. Intensities were computed from the amplitude of the derivative curve and the line width, which was found to be invariant within each set of samples.[3]

The results are summarized in Figures 1 and 2 as plots of the specific intensity (I_{sp}, intensity per milligram of DPPH) against the weight fraction of DPPH in the mixture (X_D). The behavior of unground samples is illustrated by magnesium carbonate mixtures, which show the anticipated lack of dependence of I_{sp} on X_D. Fresh, ground mixtures with potassium chloride (Figure 1) also behave as expected. With ground magnesium carbonate and calcium carbonate mixtures, however, there is a marked decrease of I_{sp} with increasing dilution. That a rapid destruction of spins occurs during the grinding process is supported by a corresponding decrease in the apparent extinction coefficient of DPPH at 525 mμ observed in chloroform extracts of the ground magnesium carbonate mixtures.

(1) Y. Matsunaga and C. A. McDowell, *Can. J. Chem.*, **38**, 724 (1960).

(2) (a) D. J. E. Ingram, "Free Radicals as Studied by Electron Spin Resonance," Butterworth and Co. Ltd., London, 1958, Chapter 3; (b) J. J. Lothe and G. Eia, *Acta Chem. Scand.*, **12**, 1535 (1958); (c) L. S. Singer, *J. Appl. Phys.*, **30**, 1463 (1959); (d) J. Zanchetta, A. Marchand, and A. Pacault, *Compt. Rend.*, **258**, 1496 (1964).

(3) *Cf.*, however, F. Bruin and M. Bruin, *Physica*, **22**, 129 (1956).

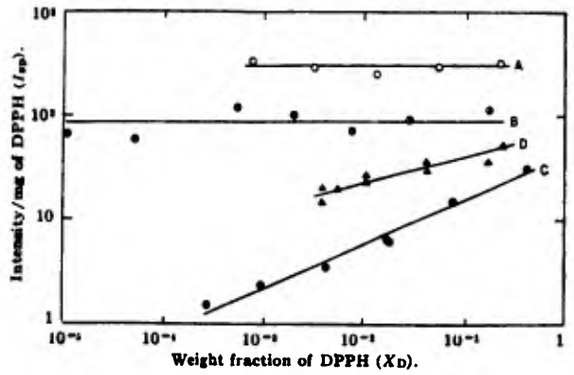

Figure 1. Specific intensity as a function of the weight fraction of DPPH for fresh mixtures: A, magnesium carbonate (unground); B, potassium chloride (ground); C, magnesium carbonate (ground); D, calcium carbonate (ground). I_{sp} is in arbitrary units. Curves coincide, but have been moved apart for clarity.

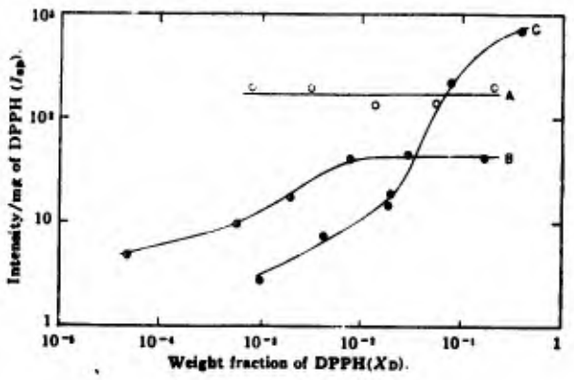

Figure 2. Specific intensity as a function of the weight fraction of DPPH for aged (1 month) mixtures. The labels are the same as in Figure 1. I_{sp} units and vertical positions of curves are arbitrary.

Storage of ground mixtures in air causes further decrease in I_{sp} (Figure 2). Again, the effect is most pronounced with magnesium carbonate. Although no change in line width resulted from the grinding, aging caused an increase from 1.9 gauss[4] to 2.5 gauss.

It has been reported that DPPH in benzene solution reacts with surface-bound water and hydroxyl groups.[5,6] The grinding effect increases in the order potassium chloride < calcium carbonate ≪ magnesium carbonate, which is also the order of increasing water content of these materials. Since grinding can provide the intimate contact necessary for a rapid solid–solid interaction to occur, this sequence suggests that the surface reaction with water is primarily responsible for the permanent loss of spins. The data indicate that freshly prepared, ground mixtures of DPPH with potassium chloride constitute useful standards over a wide range of composition.

Acknowledgments. This work was sponsored by the U. S. Air Force Cambridge Research Laboratories, Office of Aerospace Research, under Contracts AF19-(628)-2845 and AF19(628)-3836.

(4) *Cf.* R. G. Bennett and A. Henglein, *J. Chem. Phys.*, **30**, 1117 (1959).

(5) J. G. Aston and D. N. Mitra, *J. Phys. Chem.*, **69**, 3219 (1965).

(6) T. Laederich and P. Traynard, *Compt. Rend.*, **259**, 1848 (1964).

Unclassified

Security Classification

DOCUMENT CONTROL DATA - R&D

(Security classification of title, body of abstract and indexing annotation must be entered when the overall report is classified)

1. ORIGINATING ACTIVITY *(Corporate author)*
Northeastern University
360 Huntington Avenue
Boston, Massachusetts 02115

2a. REPORT SECURITY CLASSIFICATION
Unclassified

2b. GROUP

3. REPORT TITLE

RESEARCH IN ENERGY CONVERSION

4. DESCRIPTIVE NOTES *(Type of report and inclusive dates)*
Scientific. Final. 1 October 1963-30 September 1966 (Approved 20Sept.'67)

5. AUTHOR(S) *(Last name, first name, initial)*
Welville B. Nowak
Karl Weiss
Robert N. Wiener

6. REPORT DATE
1 September 1967

7a. TOTAL NO. OF PAGES
696

7b. NO. OF REFS
308

8a. CONTRACT OR GRANT NO.
AF19(628)-3836

b. Project, Task, Work Unit Nos.
8659- 01 01

c. DoD Element 61445014

d. DoD Subelement 681308

9a. ORIGINATOR'S REPORT NUMBER(S)

9b. OTHER REPORT NO(S) *(Any other numbers that may be assigned this report)*
AFCRL-67-0512

10. AVAILABILITY/LIMITATION NOTICES
Distribution of this document is unlimited. It may be released to the Clearinghouse, Department of Commerce, for sale to the general public.

11. SUPPLEMENTARY NOTES
Multiple Reprints

12. SPONSORING MILITARY ACTIVITY
Air Force Cambridge Research Laboratories (CRF)
L.G. Hanscom Field
Bedford, Massachusetts 01370

13. ABSTRACT

The results of investigations dealing with a broad spectrum of topics in energy conversion are presented. The individual studies are:

A. Investigations in Thermionic and Photovoltaic Energy Conversion
1. Techniques for Fabrication of Large, Thin Silicon Single Crystals
2. Cathodes for Thermionic Energy Conversion
3. Carnot-Limitation on Efficiency of Photovoltaic Energy-Converters
4. Transient Photoresponse of Solar Cells from Reverse to Zero Bias
5. Electric Field Effects on Diffusion in Silicon
6. Heterojunction Photovoltaic Energy Converters

B. Photochemical Studies of Molecular Systems
1. Apparatus for Photochemical Investigations
2. The Photochemistry of Perinaphthenone
3. The Photochemistry of Phenanthrenequinone
4. The Unsensitized and Sensitized Photoreduction of Disulfides
5. The Photochemistry of 1,3,5-Trinitrobenzene
6. Studies of Charge Transfer Systems
7. Laser Photochemistry
8. Diphenylpicrylhydrazyl as a Calibration Standard in Electron Spin Resonance Spectroscopy

C. Investigation of Nitrogen-Sulfur Systems

DD FORM 1 JAN 64 1473

Unclassified

Security Classification

Unclassified
Security Classification

14. KEY WORDS		LINK A		LINK B		LINK C	
		ROLE	WT	ROLE	WT	ROLE	WT
Silicon	Photochemical Apparatus						
Ketones	Charge Transfer Complexes						
Sulfur	Carnot Efficiency Limit						
Disulfides	Photosensitization						
Bond Energy	Multiphoton processes						
Free Radical	Nitrogen-Sulfur Compounds						
Photochemistry	Molecular Exciton Theory						
Solar Cell	Vacuum Ultraviolet Spectroscopy						
Single Crystal	Thermionic energy conversion						
Nitro Compounds	Photovoltaic energy conversion						
Laser Photolysis	Electron Spin Resonance Spectroscopy						
Flash Photolysis							
Energy Conversion							
Heterojunction diode							
Electric Field Effect							
Cathodes and Anodes							

INSTRUCTIONS

1. ORIGINATING ACTIVITY: Enter the name and address of the contractor, subcontractor, grantee, Department of Defense activity or other organization *(corporate author)* issuing the report.

2a. REPORT SECURITY CLASSIFICATION: Enter the overall security classification of the report. Indicate whether "Restricted Data" is included. Marking is to be in accordance with appropriate security regulations.

2b. GROUP: Automatic downgrading is specified in DoD Directive 5200.10 and Armed Forces Industrial Manual. Enter the group number. Also, when applicable, show that optional markings have been used for Group 3 and Group 4 as authorized.

3. REPORT TITLE: Enter the complete report title in all capital letters. Titles in all cases should be unclassified. If a meaningful title cannot be selected without classification, show title classification in all capitals in parenthesis immediately following the title.

4. DESCRIPTIVE NOTES: If appropriate, enter the type of report, e.g., interim, progress, summary, annual, or final. Give the inclusive dates when a specific reporting period is covered.

5. AUTHOR(S): Enter the name(s) of author(s) as shown on or in the report. Enter last name, first name, middle initial. If military, show rank and branch of service. The name of the principal author is an absolute minimum requirement.

6. REPORT DATE: Enter the date of the report as day, month, year, or month, year. If more than one date appears on the report, use date of publication.

7a. TOTAL NUMBER OF PAGES: The total page count should follow normal pagination procedures, i.e., enter the number of pages containing information.

7b. NUMBER OF REFERENCES: Enter the total number of references cited in the report.

8a. CONTRACT OR GRANT NUMBER: If appropriate, enter the applicable number of the contract or grant under which the report was written.

8b, 8c, & 8d. PROJECT NUMBER: Enter the appropriate military department identification, such as project number, subproject number, system numbers, task number, etc.

9a. ORIGINATOR'S REPORT NUMBER(S): Enter the official report number by which the document will be identified and controlled by the originating activity. This number must be unique to this report.

9b. OTHER REPORT NUMBER(S): If the report has been assigned any other report numbers *(either by the originator or by the sponsor)*, also enter this number(s).

10. AVAILABILITY/LIMITATION NOTICES: Enter any limitations on further dissemination of the report, other than those imposed by security classification, using standard statements such as:

(1) "Qualified requesters may obtain copies of this report from DDC."

(2) "Foreign announcement and dissemination of this report by DDC is not authorized."

(3) "U. S. Government agencies may obtain copies of this report directly from DDC. Other qualified DDC users shall request through _____."

(4) "U. S. military agencies may obtain copies of this report directly from DDC. Other qualified users shall request through _____."

(5) "All distribution of this report is controlled. Qualified DDC users shall request through _____."

If the report has been furnished to the Office of Technical Services, Department of Commerce, for sale to the public, indicate this fact and enter the price, if known.

11. SUPPLEMENTARY NOTES: Use for additional explanatory notes.

12. SPONSORING MILITARY ACTIVITY: Enter the name of the departmental project office or laboratory sponsoring *(paying for)* the research and development. Include address.

13. ABSTRACT: Enter an abstract giving a brief and factual summary of the document indicative of the report, even though it may also appear elsewhere in the body of the technical report. If additional space is required, a continuation sheet shall be attached.

It is highly desirable that the abstract of classified reports be unclassified. Each paragraph of the abstract shall end with an indication of the military security classification of the information in the paragraph, represented as *(TS), (S), (C), or (U).*

There is no limitation on the length of the abstract. However, the suggested length is from 150 to 225 words.

14. KEY WORDS: Key words are technically meaningful terms or short phrases that characterize a report and may be used as index entries for cataloging the report. Key words must be selected so that no security classification is required. Identifiers, such as equipment model designation, trade name, military project code name, geographic location, may be used as key words but will be followed by an indication of technical context. The assignment of links, rules, and weights is optional.

Security Classification